# Hydrocarbon potential characterisation and kinetic models for source rocks in the Bonaparte and Gippsland basins, Australia

Submitted to Macquarie University in fulfillment of the requirements for the degree of

Doctor of Philosophy

October 2014

## Soumaya Abbassi

Macquarie University

Faculty of Sciences

Department of Earth and Planetary Sciences

New South Wales, Australia

## *Statement of Authenticity*

*I hereby declare that this thesis entitled "Hydrocarbon potential characterisation and kinetic models for source rocks in the Bonaparte and Gippsland basins, Australia" has not been submitted for the award of a higher degree at any other university or institution other than Macquarie University. I also certify that this thesis is an original piece of research that has been written by me and that the help in preparing this study and all sources used have been appropriately acknowledged. Four chapters are in the form of a series of either published, submitted or in-preparation papers of which I am the primary author. Information on author and co-authors contribution are clearly stated for each of these chapters.*

*This thesis is a joint study by Macquarie University (Australia) and Helmholtz Centre Potsdam, GFZ - German Research Centre for Geosciences (Germany) under the supervision of Prof. Simon George and Prof. Brian Horsfield, respectively. Dr. Herbert Volk (CSIRO - Australia, currently at BP Exploration Company - UK) and Prof. Rolando di Primio (GFZ) co-supervised this work. This project was sponsored by both Macquarie University and GFZ institute.*

**Soumaya Abbassi**

## *Dedication*

*To my loving family Omi, Baba, Walid, Besma, Soussou, Kawther, Aymen and Sofien for their unwavering support and sacrifices.*

*To my Uncle Youssef for supporting me through all my years at school and university.*

*To Ahmadi for your love: We are just one step away from achieving one of our goals.*

## *Acknowledgments*

# Abstract

A detailed geochemical study was performed on potential source rocks in the Bonaparte Basin (Australian North West Shelf) and the Gippsland Basin (Australian southeastern margin). Both of these basins have been the focus of attention for extensive exploration activity that has led to the discovery of numerous economic gas and oil accumulations. The hydrocarbon generation characteristics of potential source rocks in each of these two basins remain uncertain. This study involved the integration of several techniques and approaches, such as Rock-Eval pyrolysis and open-system pyrolysis-gas chromatography (Py-GC) to assess the petroleum potential and to define petroleum organo-facies. Pyrolysis experiments under open-system conditions were applied to simulate the timing of hydrocarbon formation for a range of source rocks in these Australian basins. The bulk kinetics of petroleum formation were determined by pyrolysis experiments under closed-system conditions to predict and provide insights on phase behaviour and compositional properties of generated hydrocarbons.

Two case studies were carried out within the Bonaparte Basin (the Vulcan Sub-basin and the Laminaria High), from which 61 and 14 source rock samples were analysed, respectively. Py-GC results indicate that the overall molecular compositions of the organic matter preserved in the Bonaparte Basin do not differ significantly between the Upper Jurassic and Lower Cretaceous kerogens. The low abundance of phenolic compounds in these kerogens indicates a contribution from marine material. In contrast, the Middle Jurassic Plover Formation is more enriched in straight chain hydrocarbons with a higher carbon-number range and exhibits higher phenolic and aromatic content, suggesting high input of terrigenous organic matter in the source facies. Additionally, there is a significant variation in petroleum-type organofacies, which ranges from gas/condensates to Paraffinic-Naphthenic-Aromatic. This variability in organic richness, petroleum potential and organic facies type is interpreted to be a direct result of the varied sedimentary environments in which these facies were deposited, reflecting the transition from fluvial-deltaic during the Middle Jurassic, to open marine settings during the Late Jurassic to Early Cretaceous in response to fault activity and regional subsidence. Similarly, bulk and compositional kinetic analyses reveal variable degrees of heterogeneity in thermal stability and composition. The compositional kinetic model predictions also indicate that under geological conditions, a greater proportion (~80%) of the hydrocarbons were generated as oil. Counterintuitively, however, our results indicate that the marine Lower Cretaceous Echuca Shoals Formation has greater ability to form gas (43%) than the other source rocks, due to inertinite dominating its maceral assemblage.

The kinetic dataset developed from the Laminaria High area was incorporated into a 3D petroleum system model using the Schlumberger PetroMod 3D software packages to investigate the hydrocarbon charge history of the Laminaria High-Nancar Trough region. The modelling results indicate that most of the potential structures could have received oil charge from the Nancar Trough kitchen, where the Middle Jurassic source rocks are mature with respect to the oil generation window. When buried deep enough to reach sufficient thermal maturity, the Lower Cretaceous source rocks can provide additional sources for oils with a marine affinity. The onset of hydrocarbon generation in the Nancar Trough commenced during the Early Cretaceous, and during the mid to late Cenozoic for the Laminaria High, in response to elevated heat flow during the syn-rifting phase. The second and main phase of hydrocarbon generation and expulsion occurred in the mid-Eocene and continued until the present day, being controlled by the deposition of the thick Cenozoic carbonate shelf, which resulted in deep burial of Mesozoic source rocks. This latter phase of expulsion coincided with the reactivation of fault-bounded traps, which implies that some or all of the initially trapped hydrocarbons could escape out of charged structures. Having excluded the majority of wells drilled either off structure or with trap integrity issues such as inadequate reservoir and/or seal, vertical leakage from faults that are open at the present-day is the most likely explanation for structures that are now completely or partially emptied of hydrocarbons.

It has been long suggested that the Latrobe Group coals are the main contributors to hydrocarbon accumulations in the Gippsland Basin. Results from the analysis of 91 source rock samples used in this study show that shales and coaly shales, rather than coal, have more potential for liquid hydrocarbon generation. No substantial variability in kinetic parameters was observed in shales and coaly shales containing Type II/III kerogens, which suggests that the Upper Cretaceous to Paleocene source rocks can be considered as a continuous but organically-heterogeneous facies, deposited in fluvio-deltaic to marginal marine settings. However, four representative samples show that there is a noticeable difference in terms of the compositional models that predict variable potential for gas (17-32%) versus oil generation (68-83%). Kinetic differences are also translated into the physical properties, where the highest GORs (213-1443 $Sm^3/Sm^3$) were measured for the Paleocene (*L. Balmei* biozone) carbonaceous shales, and the lowest ratios (120-175$Sm^3/Sm^3$) were measured for the Turonian (*P. Mawsonii* biozone) shales. The incorporation of the developed kinetics into 3D petroleum system models that account for different kinetic characteristics would enable pre-drill prediction of petroleum quality and refinement of the filling history of the Gippsland Basin.

# Table of contents

# List of tables

# List of figures

# Chapter 1. Introduction

Conventional petroleum resources are widespread both onshore and offshore in Australia. These occur in various sedimentary basins, but most of the resources are off the north-west margin in the Bonaparte, Browse, Canning and Carnarvon basins. On the south-east Australian margin, the Gippsland Basin forms another prominent petroleum-producing province where several petroleum discoveries with variable sizes have been made, both onshore and offshore. This PhD thesis involves the Gippsland and Bonaparte basins that have been two of the most actively explored regions in Australia. Results derived from exploration activity indicate that many unsuccessful wells were also drilled in these two basins, for various reasons. For instance, several structures in the Laminaria High area (Bonaparte Basin) were found to be dry, and this was interpreted to be due either to leakage or to a lack of adequate hydrocarbon charge (O'Brien et al., 1999; Brincat et al., 2004; George et al., 2004b; Gartrell et al., 2006; Dyt et al., 2012). Seal breach is also considered to be a key risk causing failures in the Vulcan Sub-basin, located within the Bonaparte Basin (O'Brien and Woods, 1995; Lisk et al., 1998; Lisk, 2012). Risks related to trap identification have been proposed to contribute to some extent to exploration failure in the Gippsland Basin (Thomas et al., 2003).

Since petroleum exploration in the two sedimentary basins started almost 70 years ago, many elements of the petroleum system are now known. Numerous studies have been conducted to gain understanding of the different facets of active petroleum systems and to identify the mechanisms that controlled accumulation and subsequent petroleum preservation in the two basins. Source rock occurrence and facies distribution in the two basins seem to be largely controlled by syn- and post-rift phases. Organic-rich sediments were deposited in complex fluvio-deltaic systems that prevailed during the early syn-rift, and in marine environments during the later syn-rift to early post-rift phases.

In the Gippsland Basin, previous research efforts were directed toward the evaluation of the properties of accumulated oil and gas and their distribution within the basin (e.g. Brooks, 1970; Shanmugam, 1985; Burns et al., 1987; Rahmanian et al., 1990; Moore et al., 1992; Cowley and O'Brien, 2000; Boreham et al., 2001; O'Brien et al., 2008). Coals of the Latrobe Group have been attributed as the dominant source of both gas and liquid hydrocarbons (Smith and Cook, 1984; Stainforth, 1984; Shanmugam, 1985). In addition to coals,

interbedded shaly coals and shales are also present, but these are generally ignored, despite their high petroleum potential. It is more than likely that each of these interbedded facies could have contributed to the overall petroleum accumulations in the basin. Similarly in the Bonaparte Basin, and particularly in the Vulcan Sub-basin and Laminaria High areas investigated in this study, active petroleum systems have been recognised in which Middle Jurassic to Lower Cretaceous shales and to some extent coals have been regarded as potential source rocks (Preston and Edwards, 2000; Edwards et al., 2004; George et al., 2004b).

Despite the mature history of exploration and production in the Gippsland and Bonaparte basins, to a large extent it is the oils, gas-condensates and source rock extracts that have been the topic of research studies, rather than kerogen. These studies, carried out to establish oil-oil and oil-source correlations and to delineate oil families, were mostly based on molecular and isotopic compositional analyses. However, there are still uncertainties regarding the effective source rocks that have contributed to the accumulated gas and oil. Thus, a good definition of the potential source rocks as well as their petroleum generation characteristics within the two investigated basins would lead not only to a better understanding of the active petroleum systems, but would also allow more reliable predictions of the quality of potential accumulations.

## 1.1. Thesis aims

As already mentioned, previous studies have presumed that petroleum accumulations in the Gippsland Basin were generated from a coal facies within the Upper Cretaceous−early Oligocene Latrobe Group, and that the oil versus gas distributions in the basin are the result of differences in thermal maturity and/or the presence of deep unrecognised source rock intervals, rather than facies variation (Rahmanian et al., 1990; Boreham et al., 2001). Shaly coals and shales are also widely distributed across the basin, but it remains unclear to what extent coals, shaly coals and shales differ from each other in terms of petroleum potential and bulk kinetic properties. Using these hypotheses and observations, this study provides new insights into the generation characteristics of five source rocks facies that were defined by palynological zones. Apart from addressing the potential of coals to generate liquid hydrocarbons, compositional kinetic models have been acquired for shales to assess their contribution as active petroleum system in the Gippsland Basin.

Studies based on extensive biomarker, isotopic and fluid inclusion analyses, combined with sedimentological and paleontological data, indicate the occurrence of two main Mesozoic and Paleozoic petroleum systems in the Bonaparte Basin. In the Vulcan Sub-basin and

Laminaria High, various genetic groups of oils and gas-condensates have been distinguished and correlated mainly to fluvio-deltaic to marine Mesozoic petroleum systems (George et al., 1997; 1998b; 2004b; Preston and Edwards, 2000; Edwards et al., 2004; Edwards and Zumberge, 2005). Detailed examination of the delineated petroleum families in the two areas point to mixed sources, and their compositions reflect to variable degrees the impact of secondary alterations processes, such as leakage associated with trap breach during Cenozoic plate margin collision. Hence, there is a need to decipher which of the source rocks have effectively contributed to the generated hydrocarbons. This wouldn't be possible without an understanding of petroleum phase that originally charged the reservoir structures. In addition, for these areas of the Bonaparte Basin, extensive efforts have been made to gain insights into the bulk properties of the source rocks (e.g. Preston and Edwards, 2000; Edwards et al., 2004), whereas the generation characteristics of the source rocks are rather poorly understood.

With this mind, the prime aim of this study is to investigate in detail the quality and petroleum potential of the recognised source rocks in the Gippsland and Bonaparte basins. To achieve this, several techniques have been employed to generate information that can be used not only to characterise the petroleum potential and kerogen type, but also to assist in predicting the petroleum organofacies. The primary cracking of kerogen into petroleum was simulated using artificial maturation experiments that allow estimation of the timing and extent of petroleum formation under geological conditions. Bulk kinetic parameters were combined with data describing the molecular composition of the released fractions using MSSV closed-system pyrolysis to establish compositional kinetic models and predict phase behaviour. The predicted petroleum generation characteristics were checked against those of the naturally occurring fluids and provide a framework for a better understanding of the effective source rocks in the two studied basins.

Although the main focus of this study is to comprehensively evaluate the source rock potential and establish a kinetic dataset describing the petroleum generation characteristics, the investigation of the northern Bonaparte Basin was extended by using these data to constrain a 3D petroleum system model for the Laminaria High and Nancar Trough region. A few commercial discoveries have been made in this region, but several structures that were drilled were dry. The rather low exploration success, and the unusual compositions of the retained reservoired fluids, suggest that either post-filling processes, trap integrity or lack of hydrocarbon charge have acted together or individually to lead to such observations. To shed light on the possible mechanisms that can explain the present-day distribution and

composition of accumulated hydrocarbons, a 3D numerical model integrating several inputs was produced, which aims to describe the region's evolution in terms of burial and maturity history. The developed kinetic models were also implemented into basin simulators, thus serving to understand the fill history of the Laminaria High and Nancar Trough region through geological time and to identify active mature source rock kitchens.

The kinetic data sets acquired in this study to predict the composition and physical properties of generated petroleum, represent valuable inputs for future petroleum system models for both the Gippsland and Bonaparte basins, where complex fill histories are widely reported. In addition, the development of representative kinetic schemes is extremely important for reliable numerical modelling, and these can help unravel mechanisms that can contribute to reducing potential hydrocarbon exploration risk.

## 1.2.    Thesis structure

The thesis is subdivided into seven chapters. This first Chapter 1 is an introductory chapter and the remainder includes two main sections. The first section sets the scene by briefly outlining the geological background and petroleum prospectivity of the Gippsland Basin and Bonaparte Basin, with a special emphasis on the Vulcan Sub-basin and the Laminaria High areas within the latter basin. This section also contains a brief literature review of previous source rock studies conducted in the two basins. As source rocks are the main focus of this study, the second section of Chapter 1 is devoted to introducing the reader to the importance of a good understanding of the source rock component in petroleum exploration, and presents a short overview of the different source rock types with some pioneering worldwide examples. This second section presents an outline of the methods generally employed to characterise and assess directly or indirectly source rocks.

Chapter 2 presents details on the sample dataset and provides a description of the different methods and approaches used to characterise potential source rock units in the two investigated basins.

Chapters 3, 4, 5, 6 are presented as a series of self-contained chapters and they correspond to papers that are either published, or are ready to be submitted. These chapters are organised as follows:

-    Chapter 3 represents a final version of a manuscript that is expected to be submitted to *Organic Geochemistry* in October 2014. This chapter provides new insights into the petroleum potential of coals, shaly coals and shales in the Gippsland Basin. Bulk

kinetic parameters determined for selected shale and coal source rock samples, and compositional models established for shales, are discussed.

- Chapter 4 is a published article in *Organic Geochemistry* (Abbassi et al., 2014b). This chapter characterises the potential source rock units occurring in the Vulcan Sub-basin and presents new bulk and compositional kinetic descriptions of the petroleum generation characteristics. The carbon isotopic compositions of light hydrocarbons generated during thermal cracking of kerogen under microscale sealed vessel (MSSV) experiments are discussed.

- Chapter 5 is a published article in *Marine and Petroleum Geology* (Abbassi et al., 2014a). This chapter characterises the source rocks from the Laminaria High and presents the bulk and compositional kinetic description for the best known and most widely attributed source rocks in the area. The carbon isotopic compositions of light hydrocarbons generated during thermal cracking of kerogen under MSSV experiments are discussed.

- Chapter 6 is a published article in *Marine and Petroleum Geology* (Abbassi et al., 2014c). The chapter presents a 3D petroleum system model constrained for the Laminaria High and Nancar Trough areas of the northern Bonaparte Basin. The model integrates and uses as inputs 3D seismic interpreted data, thermal maturity parameters and the kinetic models developed for source rocks in the Laminaria High and the Plover Formation source rock in the Vulcan Sub-basin. The 3D model is constrained to address the thermal history, to predict the timing of hydrocarbon generation and expulsion, and to highlight possible mechanisms that led to exploration failures in the Laminaria High and Nancar Trough region.

Chapter 7 lists the main conclusions that can be drawn from this study and presents some perspectives on the applicability of the results for further research.

## 1.3. Study areas

### 1.3.1. The Gippsland Basin

#### 1.3.1.1. Geological background

The east-west trending Gippsland Basin **(Figure 1.1)** was developed as a consequence of Gondwana break-up and extension between the Australian and Antarctic continents in the Early Cretaceous (Rahmanian et al., 1990; Norvick and Smith, 2001; Willcox et al., 2001). Several tectonic events are highlighted in the basin's architecture and controlled to a large degree the type and evolution of its sedimentation. Three major events can be distinguished: (1) A first phase of rifting during the Early Cretaceous, which corresponds to a rift valley

complex with multiple half-graben systems (Power et al., 2001), and which was terminated by regional uplift and compression in the Cenomanian due to the separation of Australia from Antarctica (Duddy and Green, 1992). (2) A second phase of rifting in the Late Cretaceous to early Eocene, which occurred mainly as a response to the opening of the Tasman Sea, and which was responsible for the development of the Central Deep as the main depocentre of the basin. Volcanic activity was pronounced during the early Campanian and contributed to an increase in basin subsidence (Megallaa, 1993). (3) A compressional phase during the late Eocene, associated with localised uplift, which spanned from the Eocene to Pliocene-Pleistocene and produced a series of anticlines that trap most of the hydrocarbon accumulations in both the offshore and onshore parts of the basin (Smith, 1988; Dickinson et al., 2002). These tectonic events overprinting the Gippsland Basin were exemplified by a number of unconformities and time-breaks. More details on the stratigraphic and tectonic settings of the basin are presented in **Chapter 3**.

### *1.3.1.2. Petroleum prospectivity and potential source rocks*

The Gippsland Basin has been the subject of extensive oil and gas exploration, both onshore but mainly offshore. The following information is derived from the 2012 Offshore Petroleum Exploration Acreage Release by Geoscience Australia. The history of oil production in the basin dates back to 1924 with the Lake Bunga well, which recorded a 13 m oil column. However, extensive exploration in the Gippsland Basin did not commence until the mid-1960s. The first successful well, East Gippsland Shelf 1, later known as Barracouta 1, was drilled in 1964-1965 and discovered a 102.5m gas column. Following this, a second large gas and condensate accumulation was discovered at Marlin in 1966. Considering these two large gas discoveries, the basin was initially regarded as a significant gas province until 1967, when Kingfish 1 was drilled and encountered a large oil accumulation.

The 1970−1990s is perceived as the most successful phase of the basin's petroleum exploration, when numerous oil and gas discoveries were made. These include the giant Fortescue oil field and Kipper gas field, and the West Tuna, Seahorse and Halibut discoveries. Peak oil production of the Gippsland Basin was reached in 1985 by the end of 1986, the basin had supplied 88% of Australia's cumulative crude oil production and 48% of cumulative natural gas production. Throughout the 1990s, except for the Blackback oil and condensate field, and a few discoveries such as Archer and Anemone, no significant plays were successfully tested. Similarly, only intermittent and generally small new discoveries were made during the last decade. A discovery in 2001 at East Pilchard 1, which is situated south of the Kipper Field (see **Chapter 3** for discovery locations), encountered

100 meters of gross gas pay. Two additional discoveries have been made since then, one the 2006 gas discovery at Longtom, and the second an oil and gas discovery (2010) found on the northern margin of the Central Deep.

On a basin-scale, several regional 2D and 3D seismic surveys have been acquired and cover much of the basin. These surveys help the mapping of potential anticlinal closures and the identification of petroleum prospects. However taken in its entirely, many parts of the Gippsland Basin, especially the southern and eastern parts, are virtually unexplored and poorly understood given the limited number of exploration wells. According to a recent USGS report (USGS, 2012), the undiscovered conventional resource potential of the Gippsland Basin is estimated to be 137 MMbbl of liquids and 283 Bcf of gas. Recent exploration outcomes have suggested the need for further investigation of the remaining petroleum prospectivity in the deep sections of the Latrobe Group. Such plays would rely on the definition of new petroleum systems.

Non-marine organic-rich shales but mainly coals of the Upper Cretaceous-early Cenozoic Latrobe Group are widespread within the offshore part of the Gippsland Basin **(Figure 1.2)**. These sediments were generally deposited in lower coastal plain settings, and have been traditionally viewed to be the main source rocks for both liquid and gaseous hydrocarbons (Brooks and Smith, 1969; Burns et al., 1987; Moore et al., 1992).
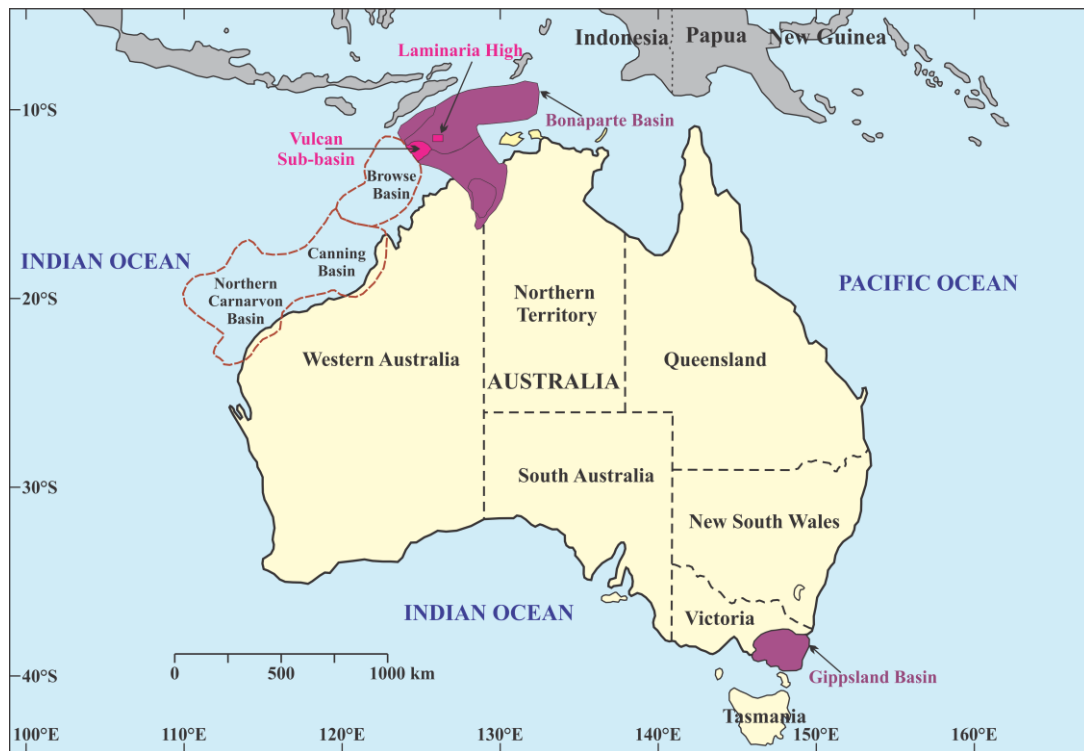
**Figure 1.1. Regional map showing the location of the Gippsland and the Bonaparte basins. Areas that were investigated within the Bonaparte Basin are highlighted in pink.**

In the Central Deep, the organic-rich facies within the Campanian *Tricolporites lilliei* palynological zone is interpreted as having being deposited in transitional marine to lower coastal plain environments, and is also suspected to contribute to some extent to the petroleum accumulations in the basin (Rahmanian et al., 1990; Moore et al., 1992; Chiupka, 1996). Other marine and lacustrine shales (e.g. the Kipper Shale) within the deeper section (Emperor Subgroup) of the Latrobe Group have source rock potential, but are generally classified as poor quality gas sources (Sloan et al., 1992; Megallaa, 1993). Rahmanian et al. (1990) related the occurrence of both oil and gas to varying thermal maturities and not to gross variation in source rock type. Most of the discoveries **(Figure 1.3)** made to data have been found within reservoirs of the Upper Cretaceous to early Cenozoic Latrobe Group. Producing fields are located in the western and northern parts of the Gippsland Basin, and only four discoveries (Angler, Blackback-Terakihi, Archer-Anemone and Gudgeon) have been made in the eastern part of the basin. Despite the significant number of wells drilled in the Gippsland Basin, only a few have penetrated into thermally mature sediments of the Halibut and Golden Beach subgroups, where most of the recognized source rock units occur. As a result, the extension of both the source rocks and the thermally mature kitchens are poorly determined and understood.

Oils in the Gippsland Basin are waxy and are believed to be generated from terrigenous organic matter within coaly facies of the fluvio-deltaic Latrobe Group (Brooks and Smith, 1969; Stainforth, 1984; Shanmugam, 1985). According to Smith and Cook (1984) and Moore et al. (1992), the chemistry of most of the petroleum in the basin is consistent with generation from perhydrous vitrinite and liptinite. While volumetric modelling, and published molecular, biomarker and isotopic data account for oils being generated from coals, no definite conclusion was made regarding the contribution of interbedded shaly coals and shales as sources for petroleum in the basin (Moore et al., 1992; Murray et al., 1998). Nevertheless, Alexander et al. (1987) suggested that some crude oils in the Gippsland Basin show more affinity to organic-rich shales, rather than coals.



**Figure 1.2. Event Chart for the Upper Cretaceous-Cenozoic petroleum system in the Gippsland Basin, after Summons et al. (2002).**

Two geochemically distinct oil families, referred to as the GA and GB families, have been delineated in the Gippsland Basin based on differential input of angiosperm-rich organic matter (Murray et al., 1998). Oils grouped under the GA family were further subdivided into two populations GA1 and GA2, due to the variable impacts of a range of secondary processes, rather than to source rock facies variation. Maturity-dependent parameters indicate that the GA1 oil population, reservoired in the Top Latrobe Group in the south-

eastern extremity of the basin, was uniformly produced at the peak of the oil generation window. In contrast, the GA2 oil population, reservoired in the Intra-Latrobe Group in the northern part of the basin, was described as being generated at variable levels of thermal maturity, with possible additional sourcing from Golden Beach Formation coals. The GB oil family, which occurs in both Top- and Intra-Latrobe Group reservoirs along the western margin of the Gippsland Basin, contains very immature biomarker patterns and variable isotopic signatures. The unusual characteristics of this family are regarded as being acquired during migration of mature oils thought immature to marginally mature sediments that are enriched in soluble bitumen (extractable organic matter). Additionally, for this family as for many of the oils in the Gippsland Basin, the combined effects of biodegradation and maturity differences have been put forward to explain their variable chemical compositions (Burns et al., 1987; Rahmanian et al., 1990; Summons et al., 2002; O'Brien et al., 2008).

### 1.3.2. The Bonaparte Basin
#### 1.3.2.1. Geological background

The Bonaparte Basin is a northeast-southwest sedimentary basin that covers an area of approximately 270,000 km$^2$ of the Australian north-western continental margin, with 250,000 km$^2$ located offshore **(Figure 1.1)**. The formation of the Bonaparte Basin has been attributed to the breakup of Pangaea, which resulted in the opening of the Neotethys Ocean in the Permo-Triassic (Golonka, 2007). The basin developed during two phases of northeast-directed extension in the Paleozoic, followed by Upper Triassic compression (AGSO, 1994), and then further northwest-directed extension in the Mesozoic that culminated in the breakup of Gondwana in the Middle Jurassic (O'Brien, 1993).

The convergence of the Australia-India plate and the Southeast Asian microplates in the Miocene to Pliocene resulted in widespread fault reactivation across the western Bonaparte Basin (Longley et al., 2002). Structurally, the Bonaparte Basin is characterised by a complex history and comprises several Paleozoic and Mesozoic sub-basins and platforms. Detailed structural and stratigraphic evolution of the basin have been described and summarised in numerous papers (MacDaniel, 1988; Mory, 1991; Woods, 1994; Whittam et al., 1996; Labutis et al., 1998; Longley et al., 2002; Cadman and Temple, 2004). Two main structural elements of the Bonaparte Basin were investigated in this study, including the Vulcan Sub-basin and the Laminaria High that are located in the western and northern part of the Bonaparte Basin, respectively **(Figure 1.1)**.
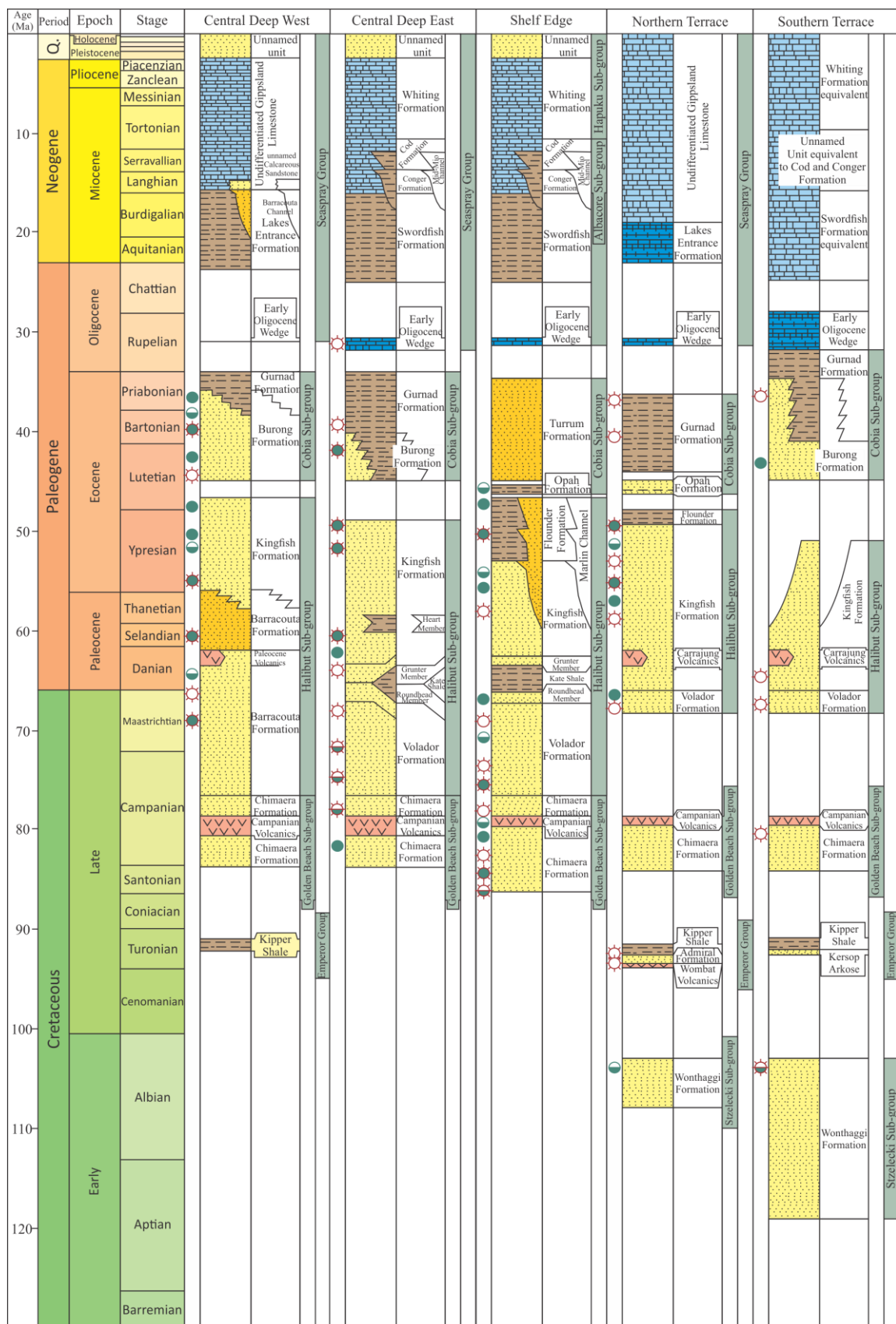
**Figure 1.3. Lithostratigraphic charts of the Central Deep, Shelf Edge, and the Northern and Southern Terraces., showing the petroleum discoveries and lithologies. Geological Time Scale after Gradstein et al. (2012).**

In the following section, only a brief description of the structural and stratigraphic settings of these two areas are presented. Further details are given in the following chapters. The Vulcan Sub-basin is a prominent northeast-southwest trending depocentre that was initiated during the Late Carboniferous to Early Permian rifting event, and subsequently developed as a response to Middle Jurassic to Lower Cretaceous extensional structuring (MacDaniel, 1988; Pattillo and Nicholls, 1990; Baxter et al., 1997; O'Brien et al., 1999). The Vulcan Sub-basin is considered to be a failed rift system (Chen et al., 2002), and consists of a number of complex horsts (e.g. the Jabiru and Challis horsts), graben (e.g. the Swan and Paqualin grabens) and marginal terraces (e.g. the Montara Terrace). The graben structures generally contain thick Jurassic fluvial shales and marine mudstones that include the best potential source rocks for oil and gas accumulations in the sub-basin.

The major Middle Jurassic extensional event, typified by the NE-SW structural trend commonly visible across the North West Shelf, has led locally to the formation of E-W trending structures, as is the case for the Laminaria High (de Ruig et al., 2000; Longley et al., 2002). The Laminaria High is a small east-west oriented platform that is located to the north of the Vulcan Sub-basin (Smith et al., 1996). Structurally, the Laminaria High is composed of a N-S and NNE-SSW-trending Permian block-faulted basement, a Jurassic-Cretaceous horst and graben system, and a series of NNE-SSW trending Cenozoic fault systems (de Ruig et al., 2000; Langhi and Borel, 2008).

### 1.3.2.2. Petroleum prospectivity and potential source rocks

The Bonaparte Basin has been intermittently explored for the last few decades, resulting in the production of oil and gas from several offshore fields. Petroleum exploration commenced in the late 1940s, with reconnaissance work in the onshore area. Exploration in the Vulcan Sub-basin started in the early 1970s after 5 years of offshore exploration in the Bonaparte Basin. Seven wells were drilled in the Vulcan Sub-basin between 1971 and 1975 and in 1983, a commercial oil discovery at Jabiru 1A was made. This discovery simulated further exploration activity in the sub-basin and led to the drilling of approximately 12 wells between 1984 and 1986, resulting in the discovery of the Cassini, Challis and Skua oil accumulations. Following this overall successful phase of exploration, 32 wells were drilled between 1988 and 1990, and this led to several oil and gas discoveries (e.g. Maple, Montara), but no significant or commercial accumulations was found.

In 1992, the focus of offshore exploration in the Bonaparte Basin shifted to the Laminaria High and adjacent areas within the northern part of the basin. Discoveries made in the Laminaria High region include Laminaria 1 (1994), Buffalo 1 and Corallina 1 (1996). During

this time, exploration drilling in the Vulcan Sub-basin identified only one significant oil discovery at Tenacious 1 (1998), and then declined dramatically until 2001, with only minor oil and gas discoveries (e.g. Padthaway 1 and Audacious 1). The last decade has been a period of mainly extension/appraisal and development in both the Vulcan Sub-basin and the Laminaria High, but was highlighted by a number of recent discoveries at Katandra 1A (2004), Vesta 1 (2005) and Swallow 1 (2006) in the Vulcan Sub-basin, and at Karongo 1 and Kasareta 1 (2010) on the Laminaria High. Hydrocarbons within the Bonaparte Basin occur in complex structural traps formed by Jurassic and Cretaceous extensional fault systems that were reactivated in the Neogene. Although the basin has a significant potential for additional hydrocarbon discoveries, the leakage of structural traps, in particular in the northern part of the basin, is a major exploration risk (Castillo et al., 2000; de Ruig et al., 2000; Gartrell et al., 2002; 2006). Oil production from the Vulcan Sub-basin, and from the Laminaria-Corallina fields on the Laminaria High, as well as gas/condensate discoveries at Bayu-Undan, Sunrise and Sunset fields, highlight the continuing prospectivity of the region (Bradshaw et al., 1988; Kopsen, 2002; Cadman and Temple, 2004).

In both the Vulcan Sub-basin and the Laminaria High, recognised potential source rocks are mainly siliciclastics and range from the Middle Jurassic to the Lower Cretaceous (**Figure 1.4**). The Early to Middle Jurassic Plover Formation consists of widespread fluvio-deltaic deposits, with organic-rich sediments in both the Vulcan Sub-basin and the Laminaria High. The fluvio-deltaic sediments were overlaid by shallow marine shelf deposition as a response to increased rifting in the Callovian (Pattillo and Nicholls, 1990). During the syn-rift phase, marine conditions became more widespread in the Vulcan Sub-basin, resulting in the deposition of thick shales of the Oxfordian to mid-Tithonian lower Vulcan formation, and the mid-Tithonian to early Valanginian upper Vulcan formation.

On the Laminaria High, analogues of these shales are the shales of the Oxfordian-Kimmeridgian Frigate Formation, and the Berriasian to early Valanginian Flamingo Formation. These, together with the sandstones and thin shales of the Callovian to mid-Oxfordian Laminaria Formation, form the Flamingo Group. The pre- (Plover Formation) and mainly syn-rift formations (lower Vulcan Formation within the Vulcan Sub-basin; and Flamingo and Frigate formations within the Laminaria High) are of critical importance to both the Vulcan Sub-basin and the Laminaria High as they are thought to contain the source rocks that provide the majority of petroleum charge in these two areas (Preston and Edwards, 2000; Edwards et al., 2004; George et al., 2004b). The upper Vulcan Formation is a lean source rock and is believed to not contribute significantly to hydrocarbons recovered in the Vulcan Sub-basin (Edwards et al., 2004). The Valanginian-Aptian Echuca Shoals Formation

is a marine unit deposited during the early post-rift phase, and also represents a potential source rock in both areas, once sufficient thermal maturity is attained.

Given the occurrence of multiple source rock facies in the Vulcan Sub-basin and Laminaria High, oils and condensates are described as having mixed marine and terrigenous geochemical signatures. It has been also reported that secondary processes, such as water-washing and hydrocarbon leakage, have influenced the composition of oil and gas accumulated in these areas. In both the Laminaria High and the Vulcan Sub-basin, the numerous phases of tectonism have had a major impact on the traps and thus on controlling hydrocarbon retention (O'Brien and Woods, 1995; Lisk, 2012). The most significant event was the collisional event that took place during the Miocene, which led to the reactivation of deeper rift fault systems and the breaching of several traps. This is regarded as a key exploration risk, not only in these two areas but also in several other parts of Australia's North West Shelf (Pattillo and Nicholls, 1990; O'Brien and Woods, 1995; Shuster et al., 1998). Besides trap integrity risk, the petroleum occurrence and distribution in these areas were interpreted to be controlled to a large extent by source rock facies and thermal maturity variations (Preston and Edwards, 2000; Edwards et al., 2004; George et al., 2004b).

Preston and Edwards (2000) investigated the geochemical characteristics of source rock extracts and crude oils in the northern Bonaparte Basin with a special emphasis on those in the Laminaria High and Flamingo High area. Oils and condensates recovered from the Lower Cretaceous reservoir unit display a marine signature and are inferred to be sourced from the marine mudstones of the Lower Cretaceous Echuca Shoals Formation. In contrast, oils recovered from the Middle Jurassic reservoir units were divided into two end-member families, with one having terrigenous source affinity and the other having marine-algal source affinity. The authors suggested that these Jurassic-reservoired oils and condensates were derived from several variable organic-rich facies within the Middle to Upper Jurassic sediments, including the Lower-Middle Jurassic Plover and Laminaria formations, with possible additional contributions from the Middle Jurassic-Lower Cretaceous Frigate and Flamingo formations. Extracts from these source rocks indicate a progressive depletion in terrigenous input from the stratigraphically older (the Frigate Formation) to the younger sediments (the Echuca Shoals Formation). In addition, it has been concluded that the organic-rich sediments within the Plover Formation have provided large amounts of gas and only minor liquid hydrocarbon charge to the fields discovered in the Laminaria High (e.g. Laminaria and Corallina).

As a complementary study to that conducted in the Laminaria High and the Flamingo High of the northern Bonaparte Basin, Edwards et al. (2004) carried out a detailed study on oils

and condensates in the Vulcan Sub-basin, where they identified two major end-member groups: one with a marine source affinity and the other with a terrigenous source affinity **(Figure 1.5)**. Oils and condensates are distributed both north and south within the sub-basin and show, based on their biomarker signatures, variable compositions and a relatively wide range of thermal maturation. With the exception of the Lower Cretaceous Echuca Shoals Formation, similar source rock units to those reported in the Laminaria High have contributed to petroleum accumulations in the Vulcan Sub-basin.

The oils and condensates recovered from the southernmost sub-basin are terrestrially-influenced and support derivation from shales and coals of the Plover Formation. The second end-member group of oils and condensates have a distinct composition and are interpreted to have originated from marine organic-rich sediments within the Oxfordian Lower Vulcan formation.

Broader isotopic variations were observed for the gas accumulations, however, no definite gas-source rock correlation was established due to the interference of thermal maturity effects. In both the Vulcan Sub-basin and the Laminaria High, secondary processes such as water-washing and evaporative-fractionation have altered to varying extents the composition of the reservoired oils. These processes have been largely related to fault seal leakage and gas flushing, and have complicated oil-source rock correlations. For instance, oils occurring in the Laminaria High are light (API>50), have low GOR ratios (<350 SCF/STB) and are depleted in low weight molecular hydrocarbons, such as $C_1$–$C_3$ alkanes, benzene and toluene. Such characteristics have been interpreted to be the result of several processes.

In an attempt to improve understanding of the fill history and to identify the possible mechanisms that lead to the unusual composition of these oils, George et al. (2004b) investigated and compared the geochemistry of oil-bearing fluid inclusions and crude oils recovered from the Laminaria High area. The comparison revealed not only some aspects of the fill history, but also the progressive charge evolution through time in this area. The overall geochemical signatures of oil-bearing fluid inclusions are relatively similar to those of the crude oils produced in the Laminaria High.
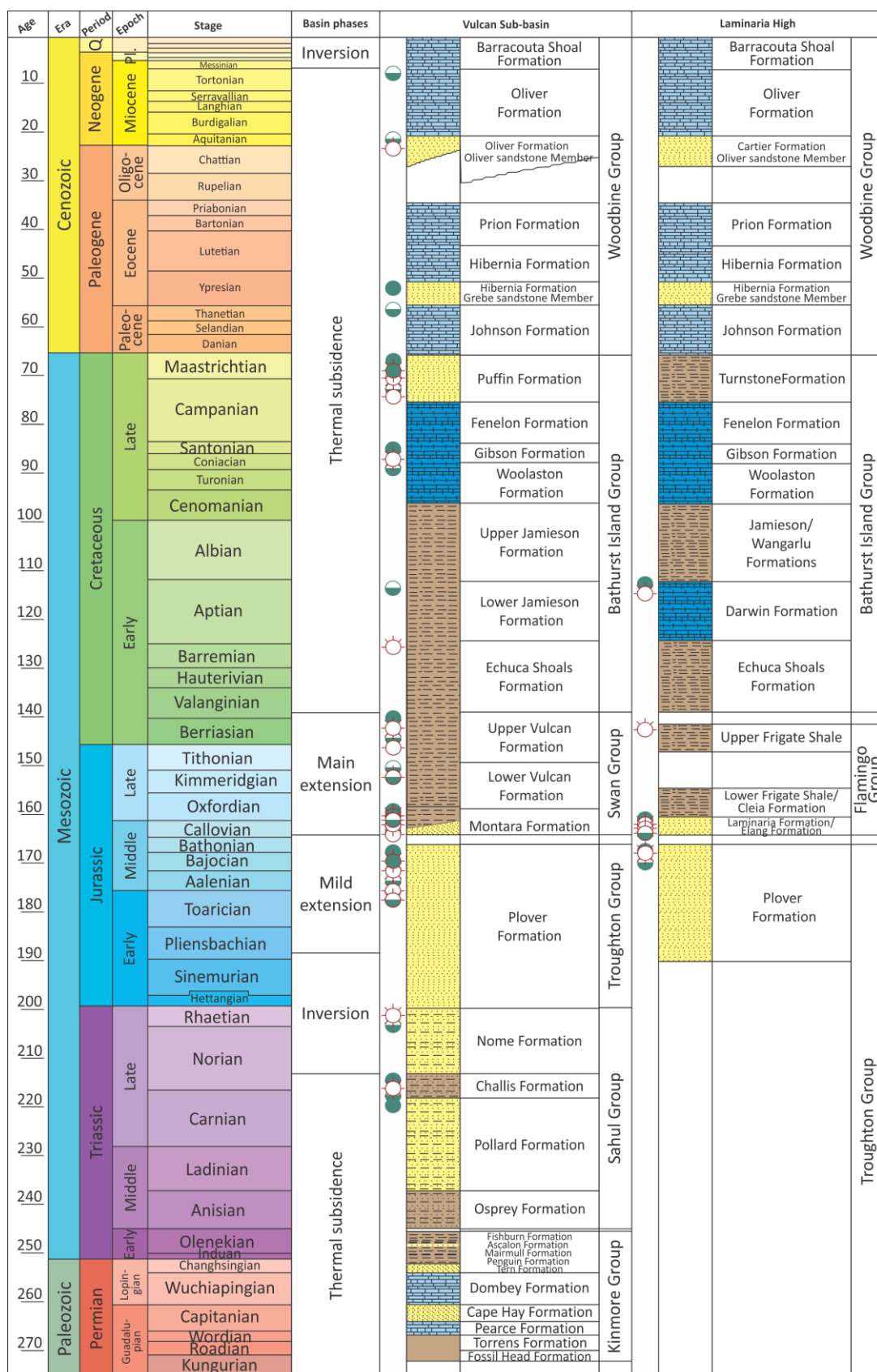
**Figure 1.4. Lithostratigraphic charts of the Vulcan Sub-basin and the Laminaria High, showing the main tectonic events, petroleum discoveries and lithologies (Nicoll et al., 2009). The geological time scale is after Gradstein et al. (2004) and Ogg et al. (2008).**

The crude oil compositions are consistent with those reported by Edwards et al. (2004) and are thought to be derived from terrestrially-influence facies within the Plover and Laminaria

formations. There is also a possibility that traps in the Laminaria High have received an additional charge from the same facies producing the Nancar oil family that was defined by George et al. (2002). However, oil-bearing fluid inclusions are interpreted to have been generated from a slightly less-terrestrially-influenced facies than those generating the present-day reservoired oils.
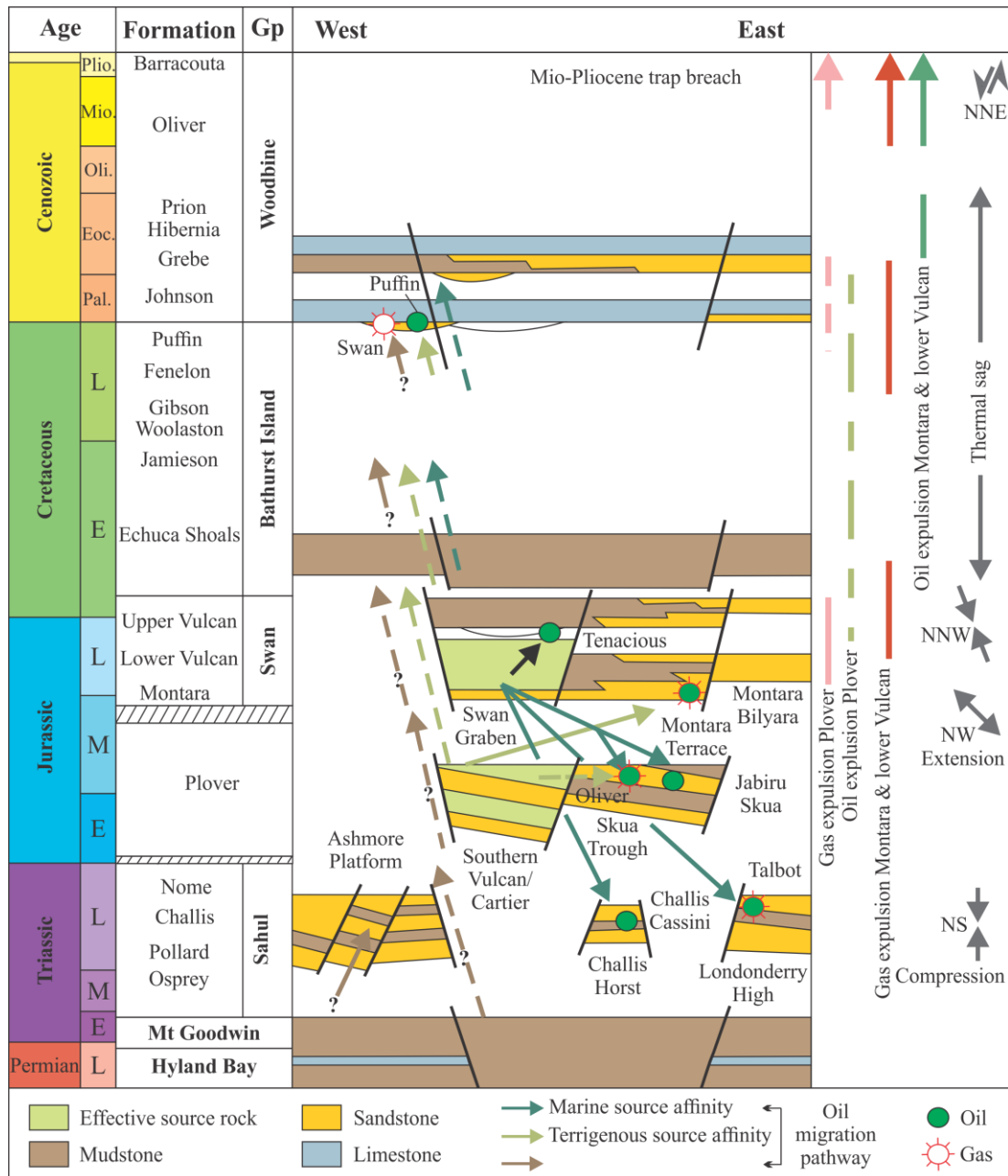


Figure 1.5. Schematic Diagram showing petroleum systems in the Vulcan Sub-basin (Edwards et al., 2004). Hydrocarbons expulsion models are after Kennard et al. (1999).

In addition, the compositions of the hydrocarbon-bearing fluid inclusions suggest that the first charge flowing through the Jurassic sandstone reservoirs was an unaltered oil rather than gas and condensate, as has been previously proposed by Newell (1999). George et al.

(2004b) also concluded that the combined effects of water-washing and fault-seal leakage, postdating the time of oil-bearing fluid inclusion formation, are the main mechanisms leading to the present-day undersaturated structures and the occurrence of unusual light oils in the Laminaria High. These two processes are thought to be related to fault reactivation during Cenozoic times that were responsible for the migration of deep hot brines (Lisk et al., 1998; O'Brien et al., 1999).

## 1.4.    Background information on source rock characterisation

In sedimentary basins, petroleum occurs when at least four components are present: source rock, reservoir, trap structure and seal. These form the elements of a given petroleum system (Magoon, 1988; Magoon and Dow, 1994). While all these elements are necessary for the occurrence of hydrocarbon accumulations that can be economically investigated, the source rock is the primary requisite element, without which all the other elements become irrelevant. A source rock is by definition a fine-grained organic-rich rock that, depending on the abundance and type of organic matter, could generate or has already generated various types of petroleum (Dow, 1978; Arthur et al., 1984; Peters and Cassa, 1994). Organic-rich sediments can occur within a broad range of depositional environments and can be of various lithologies. Stratigraphic, lithological and geochemical data are widely used as tools for distinguishing depositional settings and thus classifying source rocks. Clayton (1988) and Palacas (1988) stated that source rocks fall into two main categories: (1) marine sediments, in which the organic matter originates in a marine environment with or without additional terrigenous and bacterially-reworked input; and (2) non-marine sediments, in which the organic matter derives from terrigenous or freshwater algenan material.

As with marine source rocks, the petroleum potential of non-marine source rocks depends mainly upon their organic facies and preservation conditions, although it is largely accepted that non-marine source rocks are gas-prone rather than oil-prone, while significant liquid potential is generally expected from marine source rocks. Besides these marine and terrigenous depositional environments, intermediate settings such as lacustrine and nearshore brackish are known as sites for both oil- and gas-source rocks. Under these depositional settings, organic-rich sediments may contain variable kerogen types that may range from Type I to Type IV. For example, lacustrine environments are typically known as the most favourable settings for the deposition of oil-prone source rocks (Powell, 1986). These heterogeneities are the result of numerous variables, such as organic matter type (e.g. algae, spores), dilution, preservation (oxic versus anoxic) and physicochemical (e.g. salinity) conditions (Demaison and Moore, 1980).

In addition to this depositional environment-based classification, source rocks are of two types depending on their lithologies: carbonates and siliciclastics. Marine organic-rich carbonate rocks (e.g. limestones) are the source of significant global petroleum reserves (e.g. Palacas, 1988). Prominent examples of worldwide oil accumulations sourced from carbonate rocks include the deep marine Permian Bone Springs Limestone in the Delaware Basin (Wiggins and Harris, 1985; Barker and Halley, 1986), the Jurassic Smackover Formation (Sassen, 1990; Heydari et al., 1997) and the Upper Cretaceous La Luna Formation (Talukdar et al., 1986; James, 1990; Montilla et al., 2013). Siliciclastic source rocks such as shales are also widespread in both time and space, and are recognised as important contributors to the world's discovered oil and gas reserves (Dott and Reynolds, 1969; Jones, 1984). In the Williston Basin, the Bakken Shale is a major source rock that provides ample petroleum charge to both conventional and unconventional plays across the basin (Webster, 1984; Osadetz et al., 1992; Jarvie, 2001). In the Paris Basin and the Lower Saxony Basin of Northern Germany and parts of Western Europe, black Toarcian shales, deposited under anoxic bottom conditions are the source of significant commercial oil fields, but are also considered as having high potential as sources of shale gas, where found at high levels of thermal maturation (Mackenzie et al., 1980; Tissot and Welte, 1984; Horsfield and Dueppenbecker, 1991; Littke et al., 1991; Röhl et al., 2001; Frimmel et al., 2004; Vandenbroucke and Largeau, 2007; Bernard et al., 2012).

Similarly, large reserves of coal were deposited in the Late Carboniferous, Permian, Jurassic and Cenozoic (Hunt, 1991). Such sediments generally accumulated in coastal/delta plain settings prone to periodic marine incursion and are found interbedded with shales and/or shaly coals (McCabe, 1984; Hamilton and Tadros, 1994; Flint et al., 1995; Petersen and Andsbjerg, 1996). Coals are traditionally known as major source rocks for gas, but are also thought to be the probable source of oils in several basins, in Alaska, the Philippines, Indonesia, New Zealand and Australia (Thomas, 1982; Durand and Paratte, 1983; Tissot, 1984; Shanmugam, 1985; Thompson et al., 1985; Alexander et al., 1987; Jones, 1987; van Aarssen et al., 1992; Curry et al., 1994; Killops et al., 1998; Wilkins and George, 2002).

Coals with the potential to generate and expel liquid petroleum are generally humic in character, enriched in long-chain aliphatic hydrocarbons and are of Paleozoic to Cenozoic age (Hedberg, 1968; Curry et al., 1994; Macgregor, 1994; Isaksen et al., 1998). Key examples of oil-prone coals from Australia include Permian coals in the Bowen and Cooper basins (Shibaoka et al., 1978; Thompson et al., 1994; Boreham et al., 1999; Kramer et al., 2001) and Jurassic coals in the Surat Basin (Salehy, 1986; Khavari Khorasani, 1987; Hoffmann et al., 2009). Oils reservoired within these basins have shown significant

signatures of land-plant organic matter with localised contributions from marine source rocks (e.g. Boreham, 1995; Al Arouri et al., 1998).The liquid petroleum potential for coals is related to some extent to their maceral composition, although no direct or clear relationship has been established (Powell et al., 1991). For instance, coals dominated by liptinite (e.g. suberinite, resinite) and certain vitrinite macerals have the potential to generate oils (Horsfield et al., 1988; Hagemann and Pickel, 1991; Teerman and Hwang, 1991; Burnham et al., 1995). However, for most coal types, the process of liquid expulsion and its relative efficiency, due to the high adsorptive effects of coals, remains a major concern (Radke et al., 1980; Given, 1984).

Huc et al. (1986) examined isolated kerogens from coals and interbedded shales in the Mahakam Delta and concluded that there is no evidence favouring shale over coal as potential source rocks. However, concerns arise as to whether coals or associated shales may contribute to liquid petroleum accumulations (Weston et al., 1989; Killops et al., 1994). This confusion comes largely from the inability to easily differentiate between oils generated by coals from those generated by interbedded terrigenous-dominated shales, based on their molecular and bulk compositions (Sun et al., 2000). The Taranaki Basin is one example where coals, coaly shales and carbonaceous mudstones are reported to contribute to accumulations in the basin (Sykes, 2001). A second example is the onshore part of the Mahakam Delta, where waxy oils from the Handil and Nilam fields have been interpreted to be generated from both coals and shales (Peters et al., 2000). Sykes and Snowdon (2002) recommended the analysis of individual lithologies (coal, shaly coal and coaly mudstone) rather than bulk cuttings to better elucidate generation and expulsion characteristics of each component rock type and thus evaluate their individual contributions to the overall hydrocarbon accumulations.

After deposition, the organic matter undergoes substantial changes, being first controlled by physico-chemical and biological processes, followed by thermal processes. The first stage that describes the evolution of the freshly deposited organic matter is referred to as diagenesis, during which time several functional groups and nitrogen- and oxygen-bearing compounds within the organic matter are partially removed (Huc, 1980; Tissot and Welte, 1984). Such reactions generally occur at low temperatures ($< 60°C$), at which temperatures the action of archaea and bacteria are still efficient. A portion of the products resulting from the degradation of original "biopolymers", consisting mainly of amino acids, phenols, sugars, may recondense to form a "geopolymer" (e.g. Welte, 1974; Huc, 1980). However, some organic materials, such as spores and cuticles and microalgae-derived macromolecules show higher resistivity to microbial activity (Philp and Calvin, 1976; Tegelaar et al., 1989;

Vandenbroucke and Largeau, 2007) and are reported to be the precursor of highly aliphatic oils (Largeau et al., 1986). At the end of this evolutionary stage, the organic matter in sedimentary rocks can be present in two main forms: "bitumen" and "kerogen". The former is defined as being the soluble or extractable portion of organic matter in organic solvents, such as benzene, ether and chloroform, while the latter is insoluble in these solvents.

The kerogen may occur in coals, or it may be disseminated organic matter within source rocks, and is the precursor of petroleum (Forsman and Hunt, 1958; Philp and Calvin, 1976; Durand, 1980). It can originate from either marine (e.g. planktonic and bacteria), lacustrine (e.g. algae) or terrigenous-derived material (e.g. residues of lignin). Depending on the origin, different types (I, II, III, and IV) of kerogens and thus variable potential for gas and oil generation were defined, with Type I kerogen being the most oil-prone (Tissot et al., 1974; Espitalié et al., 1977b).

If the organic matter has escaped degradation by archaeal and bacterial processes, and with increasing burial, the organic matter accumulated in the sediments is subjected to a series of complex reactions termed catagenesis (temperatures between 60°C and 150°C) that lead to kerogen conversion and thus hydrocarbon formation (Welte, 1974; Durand and Espitalié, 1976; Dow, 1977). The quantity and quality of petroleum that can be generated from a source rock are a function of a number of variables, such as primary organic productivity (kerogen type), pre- and post-depositional environment conditions, sedimentation rates and the thermal history of the basin in which the source rock was deposited (Didyk et al., 1978; Moldowan et al., 1985; Pedersen and Calvert, 1990; Creaney and Passey, 1993).

In attempts to address and elucidate these variables and controls, significant emphasis was placed on investigating source rock extracts (bitumens), crude oils and kerogens. Accordingly, several analytical techniques and approaches aiming to a large extent at comprehensively deciphering the origin and occurrence of petroleum in sedimentary basins have been developed and employed. Extensive published literature and reviews have described and summarised these techniques (e.g. Eglinton and Murphy, 1969; Hitchon, 1974; Larter and Douglas, 1982; Horsfield, 1984, 1990; Rullkötter and Michaelis, 1990; Larter and Horsfield, 1993; Hunt et al., 2002). Hence, an exhaustive review of the advances in these techniques is beyond the scope of this introductory chapter. However, a brief inventory of the main and commonly used methods and techniques is necessary to justify those employed to characterise the source rocks investigated in this study.

The need to evaluate the type of petroleum that can be generated from one or many potential source rocks in a sedimentary basin is crucial for successful petroleum exploration. Source

rock studies have been shown to be generally more comprehensive when they are based on integrated approaches and techniques (Powell et al., 1991; Peters and Cassa, 1994; Boreham and Summons, 1999). The chemical structure of kerogens was investigated by elemental analyses (C, H, N, O, and S), from which specific ratios have been used to classify the organic matter (Durand and Monin, 1980).

One of the routinely used techniques in source rock evaluation is Rock-Eval pyrolysis that allows a rapid screening and assessment of the quality and thermal maturity of organic matter present within the rock (Espitalié et al., 1977a; Espitalié and Bordenave, 1993). A detailed description of this technique is given in the Methodology **Chapter 2**. In addition to these techniques, parameters derived from optical techniques, such as vitrinite reflectance, maceral composition and thermal alteration index have been employed to obtain further information regarding organic matter and/or kerogen typing and thermal maturity (Staplin, 1969; Stach et al., 1975; Harris, 1979; Peters and Cassa, 1994).

 Isotopic geochemistry produces valuable information on depositional environments and the origin of oils and source rocks, and has helped establish genetic relationships using oil-oil, oil-source rock and source rock-source rock correlations (Silverman and Epstein, 1958; Stahl, 1977; Peters, 1986; Summons et al., 1998; Sauer et al., 2001). Apart from these, stable isotope ratios have been extensively used to distinguish oils from marine and non-marine source rocks, and to differentiate oils sourced by carbonates from those sourced by shales (Schoell, 1984; Sofer, 1984).

Following the development and coupling of gas chromatography (GC) and mass spectrometry (MS) in 1960, a significant number of compounds were discovered and identified in both crude oils and source rock extracts. These compounds correspond to biological markers, also referred to as biomarkers, which are specific organic molecules resistant to alteration processes, such as biodegradation and thermal stress, and thus preserving to a large extent the signatures of their original precursor (Seifert and Moldowan, 1981, 1986). These biomarkers, (e.g. steranes and terpanes) have served as powerful tools to establish correlations between oils and oil-source rock pairs, to delineate oil families, to infer thermal maturation levels, and to interpret the prevailing depositional settings under which these precursors might have been deposited and preserved (Moldowan et al., 1985; Brassell et al., 1986; Peters, 1986; Seifert and Moldowan, 1986; Leenheer and Zumberge, 1987; Feinstein et al., 1988; Price and Clayton, 1992; Picha and Peters, 1998; Zhang et al., 2000; Peters et al., 2005; Gratzer et al., 2011).

In published organic geochemistry literature, only a limited number of studies investigating the analysis of oil-bearing fluid inclusions is available. Although fluid inclusions are found in reservoir units and not in source rocks, they offer great opportunities for reconstructing the filling history of a reservoir and for deciphering the hydrocarbon migration record within a sedimentary basin, especially where a complex charge history is suspected (Horsfield and McLimans, 1984; Eadington et al., 1991; Nedkvitne et al., 1993; George et al., 1996, 1997, 1998, 2001, 2004a, 2004b; Pang et al., 1998; Lisk et al., 2002; Volk et al., 2005; Lisk, 2012).

Most of the previously listed techniques are routinely applied to characterise mainly source rock extracts and crude oils, but for kerogens, these only offer a sound basis for its qualitative and gross chemical properties. Structurally, kerogen is known to be a cross-linked macromolecular system with a highly complex structure that undergoes progressive physical changes with increasing thermal maturation (Béhar and Pelet, 1985; Béhar and Vandenbroucke, 1987). Therefore, efforts were directed towards obtaining a better understanding of the molecular composition of kerogens and monitoring its behaviour under thermal stress (Lewan et al., 1979; Horsfield and Douglas, 1980; Winters et al., 1983; Horsfield, 1984; Larter, 1984). Based on the type of system being used, two categories of pyrolysis methods can be distinguished: (1) a dynamic pyrolysis system, in which kerogen or a whole rock is analysed to gain a succinct perspective of its molecular compositions; and (2) a static pyrolysis system that is used to simulate petroleum formation characteristics that are controlled by a number of first-order and irreversible chemical reactions (Ungerer et al., 1990). For the first category, analytical programmed-temperature pyrolysis are implemented in conjunction with gas chromatography (Py-GC), mass spectrometry (Py-MS) and both (Py-GC-MS) to provide complementary information on the kerogen structure and its degree of evolution (Douglas and Grantham, 1974). The combined Py-GC method is now regarded as a common tool for source rock characterisation and petroleum organofacies typing (Larter, 1984; Horsfield, 1989). It is, however, important to note that this technique, although being used in several studies, is viewed as an addition to other kerogen composition and typing methods (Larter, 1984; Larter and Senftle, 1985; Horsfield, 1989; Horsfield and Dueppenbecker, 1991).

The second category may be described as bulk-flow pyrolysis (e.g. hydrous pyrolysis) and consists of artificial thermal degradation of organic matter under controlled time-temperature laboratory conditions (Horsfield, 1984; Lewan et al., 1985; Cooles et al., 1986; Burnham et al., 1988; Hunt, 1991). The most commonly used experiment is non-isothermal open-system pyrolysis using multiple constant heating rates. This system drives estimation

of the timing and extent of petroleum generation, that are governed by the kinetic parameters of the kerogen in terms of its activation energy distribution and single frequency factor, varying according to bond strength and heterogeneity (Tissot and Welte, 1984; Schaefer et al., 1990; Braun et al., 1992; Schenk and Horsfield, 1993; Tegelaar and Noble, 1994; Schenk and Dieckmann, 2004). Although still a matter of debate, the derived kinetic models based on the calculated kinetic parameters, have been reported to be reliable for petroleum formation predictions in naturally-occurring systems, with the assumption that the same reactions take place whatever the heating rate (Ungerer and Pelet, 1987; Braun and Burnham, 1990; Forbes et al., 1991; Tegelaar and Noble, 1994; Schenk and Horsfield, 1998).

In sedimentary basins where potential source rocks are unrecognized, it becomes generally difficult to ascertain whether the crude oils are sourced from a single rock or are the result of mixing from many source rock units. Crude oils in reservoir units can be subjected to secondary alteration processes, such as secondary cracking, biodegradation and water-washing, rendering the interpretation of their source more intricate, if not impossible. Thus, diagnosing the generated original compositions is fundamental, because the aforementioned processes simply act upon and modify them. To trace the effect of thermal maturation on the composition of fluids generated from kerogens, artificial maturation can be carried out by closed-system pyrolysis, of which MSSV is one of the conveniently designed techniques to carry out such simulation (Horsfield et al., 1989). The fluid composition and especially the gas composition are the main driving force of phase behaviour, along with the pressure and temperature during secondary migration (England et al., 1987; Horsfield and Dueppenbecker, 1991; di Primio et al., 1998). The phase state and physical properties such as gas: oil ratios (GORs) measured by these experiments are generally comparable to those measured for fluids in natural fields (Santamaría and Horsfield, 2003; di Primio and Skeie, 2004; di Primio and Horsfield, 2006; Erdmann and Horsfield, 2006). Sequentially, this closed-system pyrolysis experiment follows and uses as inputs data derived from bulk kinetic measurements. This combined open- and closed-system pyrolysis technique is referred to as PhaseKinetics. Compositional kinetic models can be developed using two or more compounds (Espitalié et al., 1988; Béhar et al., 1997; di Primio et al., 1998; Boreham et al., 1999). However, the most challenging steps have been to determine one or more representative compositional kinetic schemes to incorporate as inputs in petroleum system models.

Two-dimensional (2D) and particularly three-dimensional (3D) petroleum system modelling approaches and tools are seeing dramatic application in the last decade, and provide major

steps forward in petroleum exploration and research (Sachsenhofer, 1994; Rodriguez and Littke, 2001; Carr and Petersen, 2004; Naeth et al., 2005; Allen and Allen, 2013; Bruns et al., 2013). These numerical and integrated modelling approaches are applied as tools to scrutinise in a dynamic way both the geological, geophysical and geochemical processes as a function of geological time (Welte and Yalçin, 1988; Hermanrud, 1993; Littke et al., 1994; Poelchau et al., 1997; Welte et al., 2000).

In petroleum system basin analysis, the most sensitive parameter is the thermal history of the basin (Holmes et al., 1999; He and Middleton, 2002). This is because the degree of accuracy of any prediction of the timing and volumes of petroleum hydrocarbon expulsion and generation are largely dependent on the accuracy of the thermal history model. Besides this application, petroleum system modelling is now widely used to predict the quality of petroleum accumulations, fluid movements and hydrocarbon losses in tectonically-active basins where leakage is likely to occur (Wilkinson et al., 2006; Paton et al., 2007; Hantschel and Kauerauf, 2009). Details of the pyrolysis methods as well as the approaches applied in building, calibration, and simulating the 3D petroleum system models used in the study are presented in **Chapter 2**.

## 1.5. References

Abbassi, S., George, S.C., Edwards, D.S., di Primio, R., Horsfield, B., Volk, H., 2014a. Generation characteristics of Mesozoic syn- and post-rift source rocks, Bonaparte Basin, Australia: New insights from compositional kinetic modelling. Marine and Petroleum Geology 50, 148-165.

Abbassi, S., Horsfield, B., George, S.C., Edwards, D.S., Volk, H., di Primio, R., 2014b. Geochemical characterisation and predicted bulk chemical properties of petroleum generated from Jurassic and Cretaceous source rocks in the Vulcan Sub-basin, Bonaparte Basin, North West Shelf of Australia. Organic Geochemistry 76, 82-103.

Abbassi, S., di Primio, R., Horsfield, B., Edwards, D.S., Volk, H., Anka, Z., George, S.C., 2014c. On the filling and leakage of petroleum from traps in the Laminaria High region of the northern Bonaparte Basin, Australia. Marine and Petroleum Geology 59, 91-113.

AGSO, 1994. Deep reflections on the North West Shelf: changing perceptions of basin formation, in: Purcell, P.G., Purcell, R.R. (Eds.), The Sedimentary Basins of Western Australia: Proceedings of the Petroleum Exploration Society of Australia Symposium, Perth, Western Australia, pp. 63-76.

Al Arouri, K., Boreham, C.J., McKirdy, D.M., Lemon, N.M., 1998. Modeling of thermal maturation and hydrocarbon generation in two petroleum systems of the Taroom Trough, Australia. American Association of Petroleum Geologists Bulletin 82, 1504-1527.

Alexander, R., Noble, R., Kagi, R., 1987. Fossil resin biomarkers and their application in oil to source-rock correlation, Gippsland Basin, Australia. Australian Petroleum Exploration Association Journal 27, 63-72.

Allen, P.A., Allen, J.R., 2013. Basin analysis: Principles and application to petroleum play assessment. Wiley & Sons Ltd., 603 p.

Arthur, M.A., Dean, W.E., Stow, D.A.V., 1984. Models for the deposition of Mesozoic-Cenozoic fine-grained organic-carbon-rich sediment in the deep sea. Geological Society, London, Special Publications 15, 527-560.

Barker, C.E., Halley, R.B., 1986. Fluid inclusion, stable isotope and vitrinite reflectance evidence for the thermal history of the Bone Spring Limestone, southern Guadalupe Mountains, Texas, in: Gautier, D.L. (Ed.), Roles of Organic Matter in Sediment Diagenesis, Society of Economic Paleontologists and Mineralogists. Special Publication, 38, pp. 190-203.

Baxter, K., Cooper, G.T., O'Brien, G.W., Hill, K.C., Sturrock, S., 1997. Flexural isostatic modelling as a constraint on basin evolution, the development of sediment systems and palaeo-heat flow: application to the Vulcan Sub-basin, Timor Sea. Australian Petroleum Production and Exploration Association Journal 37, 136-153.

Béhar, F., Pelet, R., 1985. Pyrolysis-gas chromatography applied to organic geochemistry: Structural similarities between kerogens and asphaltenes from related rock extracts and oils. Journal of Analytical and Applied Pyrolysis 8, 173-187.

Béhar, F., Vandenbroucke, M., 1987. Chemical modelling of kerogens. Organic Geochemistry 11, 15-24.

Béhar, F., Vandenbroucke, M., Tang, Y., Marquis, F., Espitalié, J., 1997. Thermal cracking of kerogen in open and closed systems: determination of kinetic parameters and stoichiometric coefficients for oil and gas generation. Organic Geochemistry 26, 321-339.

Bernard, S., Horsfield, B., Schulz, H.M., Wirth, R., Schreiber, A., Sherwood, N., 2012. Geochemical evolution of organic-rich shales with increasing maturity: A STXM and TEM study of the Posidonia Shale (Lower Toarcian, northern Germany). Marine and Petroleum Geology 31, 70-89.

Boreham, C.J., 1995. Origin of petroleum in the Bowen and Surat Basins: geochemistry revisited. Australian Petroleum Production and Exploration Association Journal 35, 579-579.

Boreham, C.J., Summons, R.E., 1999. Petroleum systems and frontiers-New insights into the active petroleum systems in the Cooper and Eromanga basins, Australia. Australian Petroleum Production and Exploration Association Journal 39, 263-296.

Boreham, C.J., Horsfield, B., Schenk, H.J., 1999. Predicting the quantities of oil and gas generated fromAustralian Permian coals, Bowen Basin using pyrolyticmethods. Marine and Petroleum Geology 16, 165-188.

Boreham, C.J., Hope, J.M., Hartung-Kagi, B., 2001. Understanding source, distribution and preservation of Australian natural gas: a geochemical perspective. Australian Petroleum Production and Exploration Association Journal 41, 523-547.

Bradshaw, M., Yeates, A., Beynon, R., Brakel, A., Langford, R., Totterdell, J., Yeung, M., 1988. Palaeogeographic evolution of the North West Shelf region, in: Purcell, P.G., Purcell, R.R. (Eds.), The North West Shelf, Australia: Proceedings of the Petroleum Exploration Society of Australia Symposium, Perth, Western Australia, pp. 29-54.

Brassell, S.C., Eglinton, G., Mo, F.J., 1986. Biological marker compounds as indicators of the depositions! history of the Maoming oil shale. Organic Geochemistry 10, 927-941.

Braun, R.L., Burnham, A.K., 1990. Mathematical model of oil generation, degradation, and expulsion. Energy & Fuels 4, 132-146.

Braun, R.L., Burnham, A.K., Reynolds, J.G., 1992. Oil and gas evolution kinetics for oil shale and petroleum source rocks determined from pyrolysis-TQMS data at two heating rates. Energy & Fuels 6, 468-474.

Brincat, M.P., Lisk, M., Kennard, J.M., Bailey, W.R., Eadington, P.J., 2004. Evaluating the oil potential of the Caswell Sub-basin: Insights from fluid inclusion studies, in: Ellis, G.K., Baillie, P.W., Munson, T.J. (Eds.), Proceedings of the Timor Sea Symposium, Northern Territory Geological Survey. Special Publication 1, Darwin, Northern Territory, pp. 437-455.

Brooks, J.D., 1970. The use of coals as indicators of the occurrence of oil and gas. Australian Petroleum Exploration Association Journal 10, 35-40.

Brooks, J.D., Smith, J.W., 1969. The diagenesis of plant lipids during the formation of coal, petroleum and natural gas—II. Coalification and the formation of oil and gas in the Gippsland Basin. Geochimica et Cosmochimica Acta 33, 1183-1194.

Bruns, B., di Primio, R., Berner, U., Littke, R., 2013. Petroleum system evolution in the inverted Lower Saxony Basin, northwest Germany: a 3D basin modeling study. Geofluids 13, 246-271.

Burnham, A.K., Braun, R.L., Samoun, A.M., 1988. Further comparison of methods for measuring kerogen pyrolysis rates and fitting kinetic parameters. Organic Geochemistry 13, 839-845.

Burnham, A.K., Schmidt, B.J., Braun, R.L., 1995. A test of the parallel reaction model using kinetic measurements on hydrous pyrolysis residues. Organic Geochemistry 23, 931-939.

Burns, B.J., Bostwick, T.R., Emmett, J.K., 1987. Gippsland terrestrial oils—recognition of compositional variations due to maturity and biodegradation effects. Australian Petroleum Exploration Association Journal 27, 73-84.

Cadman, S.J., Temple, P.R., 2004. 2004. Bonaparte Basin, NT, WA, AC & JPDA, Australian Petroleum Accumulations Report, in: 2nd Edition, G.A., Canberra. (Ed.), Report 5.

Carr, A.D., Petersen, H.I., 2004. Modelling of the hydrocarbon generation history and volumetric considerations of the coal-sourced Lulita Field, Danish North Sea. Petroleum Geoscience 10, 107-119.

Castillo, D.A., Bishop, D.J., Donaldson, I., Kuek, D., De Ruig, M., Trupp, M., Shuster, M.W., 2000. Trap integrity in the Laminaria high–Nancar trough region, Timor Sea: Prediction of fault seal failure sing well-constrained stress tensors and fault surfaces interpreted from 3D seismic. Australian Petroleum Production and Exploration Association Journal 40, 151-173.

Chen, G., Hill, K.C., Hoffman, N., O'Brien, G.W., 2002. Geodynamic evolution of the Vulcan Sub-basin, Timor Sea, northwest Australia: a pre-compression New Guinea analogue? Australian Journal of Earth Sciences 49, 719-736.

Chiupka, J., 1996. Hydrocarbon play fairways of the onshore Gippsland Basin, Victoria. *Department of Natural Resources and Environment Victorian Initiative for Minerals and Petroleum*, Report 30.

Clayton, J.L., 1988. Role of Amount and Type of Organic Matter in Recognition of Petroleum Source Rocks, in: Magoon, L.B. (Ed.), Petroleum systems of the United States: US Geological Survey Bulletin, pp. 16-19.

Cooles, G.P., Mackenzie, A.S., Quigley, T.M., 1986. Calculation of petroleum masses generated and expelled from source rocks. Organic Geochemistry 10, 235-245.

Cowley, R., O'Brien, G.W., 2000. Identification and interpretation of leaking hydrocarbons using seismic data: a comparative montage of examples from the major fields in Australia's north west shelf and Gippsland Basin. Australian Petroleum Production Exploration Association Journal 40, 121-150.

Creaney, S., Passey, Q.R., 1993. Recurring patterns of total organic carbon and source rock quality within a sequence stratigraphic framework. American Association of Petroleum Geologists Bulletin 77, 386-401.

Curry, D.J., Emmett, J.K., Hunt, J.W., 1994. Geochemistry of aliphatic-rich coals in the Cooper Basin, Australia and Taranaki Basin, New Zealand: implications for the occurrence of potentially oil-generative coals. Geological Society, London, Special Publications 77, 149-181.

de Ruig, M.J., Trupp, M., Bishop, D.J., Kuek, D., Castillo, D.A., 2000. Fault architecture and the mechanics of fault reactivation in the Nancar Trough/Laminaria area of the Timor Sea, northern Australia. Australian Petroleum Production and Exploration Association Journal 40(1), 174-193.

Demaison, G.J., Moore, G.T., 1980. Anoxic environments and oil source bed genesis. Organic Geochemistry 2, 9-31.

di Primio, R., Skeie, J.E., 2004. Development of a compositional kinetic model for hydrocarbon generation and phase equilibria modelling: a case study from Snorre Field, Norwegian North Sea. Geological Society, London, Special Publications 237, 157-174.

di Primio, R., Horsfield, B., 2006. From petroleum-type organofacies to hydrocarbon phase prediction. American Association of Petroleum Geologists Bulletin 90, 1031-1058.

di Primio, R., Dieckmann, V., Mills, N., 1998. PVT and phase behaviour analysis in petroleum exploration. Organic Geochemistry 29, 207-222.

Dickinson, J.A., Wallace, M.W., Holdgate, G.R., Gallagher, S.J., Thomas, L., 2002. Origin and timing of the Miocene-Pliocene unconformity in southeast Australia. Journal of Sedimentary Research 72, 288-303.

Didyk, B.M., Simoneit, B.R.T., Brassell, S.C., Eglinton, G., 1978. Organic geochemical indicators of palaeoenvironmental conditions of sedimentation. Nature 272, 216-222.

Dott, R.H., Reynolds, M.J., 1969. Sourcebook for Petroleum Geology. American Association of Petroleum Geologists Bulletin 5, p. 471.

Douglas, A.G., Grantham, P.J., 1974. Fingerprint gas chromatography in the analysis of some native bitumens, asphalts and related substances, in: Tissot, B., Bienner, F. (Eds.), In Advances in Organic Geochemistry. Editions Technip, pp. 261-276.

Dow, W.G., 1977. Kerogen studies and geological interpretations. Journal of Geochemical Exploration 7, 79-99.

Dow, W.G., 1978. Petroleum source beds on continental slopes and rises. American Association of Petroleum Geologists Bulletin 62, 1584-1606.

Duddy, I.R., Green, P.F., 1992. Tectonic development of the Gippsland Basin and environs: identification of key episodes using Apatite Fission Track Analysis (AFTA), Gippsland Basin Symposium. Australasian Institute of Mining and Metallurgy, Melbourne, pp. 111-121.

Durand, B., 1980. Sedimentary organic matter and kerogen. Definition and quantitative importance of kerogen, in: Durand, B. (Ed.), Kerogen: Insoluble Organic Matter From Sedimentary Rocks. Editions Technip, Paris, pp. 13-35.

Durand, B., Espitalié, J., 1976. Geochemical studies on the organic matter from the Douala Basin (Cameroon)—II. Evolution of kerogen. Geochimica et Cosmochimica Acta 40, 801-808.

Durand, B., Monin, J.C., 1980. Elemental analysis of kerogens (C, H, O, N, S, Fe), in: Durand, B. (Ed.), Kerogen – Insoluble Organic Matter from Sedimentary Rocks. Technip, Paris, pp. 113-142.

Durand, B., Paratte, M., 1983. Oil potential of coals: a geochemical approach. Geological Society, London, Special Publications 12, 255-265.

Dyt, C.P., Langhi, L., Bailey, W.P., 2012. Automating conceptual models to easily assess trap integrity and oil preservation risks associated with fault reactivation. Marine and Petroleum Geology 30, 81-97.

Eadington, P.J., Hamilton, P.J., Bai, G.P., 1991. Fluid history analysis-a new concept for prospect evaluation. The Australian Petroleum Exploration Association Journal 31, 282-294.

Edwards, D.S., Zumberge, J.E., 2005. The Oils of Western Australia II. Regional Petroleum Geochemistry and Correlation of Crude Oils and Condensates from Western Australia and Papua New Guinea. Geoscience Australia and GeoMark Research Ltd unpublished report, Canberra and Houston. GEOCAT 37512.

Edwards, D.S., Preston, J.C., Kennard, J.M., Boreham, C.J., van Aarssen, B.G.K., Summons, R.E., Zumberge, J.E., 2004. Geochemical characteristics of hydrocarbons from the Vulcan Sub-basin, western Bonaparte Basin, Australia, in: Ellis, G.K., Baillie, P.W., Munson, T.J. (Eds.), Timor Sea Petroleum Geoscience: Proceedings of the Timor Sea Symposium, Darwin, Northern Territory, pp. 169-201.

Eglinton, G., Murphy, M.T.J., 1969. Organic Geochemistry: Methods and Results. Longman, Springer Verlag, Berlin, Heidelberg, New York, 828 p.

England, W.A., Mackenzie, A.S., Mann, D.M., Quigley, T.M., 1987. The movement and entrapment of petroleum fluids in the subsurface. Journal of the Geological Society 144, 327-347.

Erdmann, M., Horsfield, B., 2006. Enhanced late gas generation potential of petroleum source rocks via recombination reactions: Evidence from the Norwegian North Sea. Geochimica et Cosmochimica Acta 70, 3943-3956.

Espitalié, J., Bordenave, M.L., 1993. Rock-eval pyrolysis, in: Bordenave, M.L. (Ed.), Applied petroleum geochemistry. Editions Technip, Paris, pp. 237-261.

Espitalié, J., Madec, M., Tissot, B., Mennig, J., Leplat, P., 1977a. Source rock characterization method for petroleum exploration, Offshore Technology Conference.

Espitalié, J., Laporte, J.L., Madec, M., Marquis, F., Leplat, P., Paulet, J., Boutefeu, A., 1977b. Méthode rapide de caractérisation des roches mères, de leur potentiel pétrolier et de leur degré d'évolution. Revue Institut Francais du Petrole 32, pp. 23-42.

Espitalié, J., Ungerer, P., Irwin, I., Marquis, F., 1988. Primary cracking of kerogens. Experimenting and modeling $C1$, $C2-C5$, $C6-C14$ and $C15+$ classes of hydrocarbons formed. Organic Geochemistry 13, 893-899.

Feinstein, S., Brooks, P.W., Fowler, M.G., Snowdon, L.R., Williams, G.K., 1988. Families of oils and source rocks in the central Mackenzie corridor: a geochemical oil-oil and oil-source rock correlation, in: James, D.P., Leckie, D.A. (Eds.), Sequences, Stratigraphy, Sedimentology: Surface and Subsurface. Canadian Society of Petroleum Geologists Memoir, vol. 15, pp. 543–552.

Flint, S., Aitken, J., Hampson, G., 1995. Application of sequence stratigraphy to coal-bearing coastal plain successions: implications for the UK Coal Measures. Geological Society, London, Special Publications 82, 1-16.

Forbes, P.L., Ungerer, P.M., Kuhfus, A.B., Rils, F., Eggen, S., 1991. Compositional modelling of petroleum generation and expulsion. Application to a three dimensional balance in the Smorbukk Beta field. American Association of Petroleum Geologists Bulletin 75, 873-893.

Forsman, J.P., Hunt, J.M., 1958. Insoluble organic matter (kerogen) in sedimentary rocks. Geochimica et Cosmochimica Acta 15, 170-182.

Frimmel, A., Oschmann, W., Schwark, L., 2004. Chemostratigraphy of the Posidonia Black Shale, SW Germany: I. Influence of sea-level variation on organic facies evolution. Chemical Geology 206, 199-230.

Gartrell, A., Zhang, Y., Lisk, M., Dewhurst, D., 2002. Numerical modelling of fault intersections: comparison with hydrocarbon leakage history of the Skua Field, Timor Sea. In: Hydrocarbon Sealing Potential of Faults and Cap Rocks, APCRC Technical Workshop Proceedings, Barossa Valley, South Australia, p. 3.

Gartrell, A., Bailey, W.R., Brincat, M., 2006. A new model for assessing trap integrity and oil preservation risks associated with postrift fault reactivation in the Timor Sea. American Association of Petroleum Geologists Bulletin 90, 1921-1944.

George, S.C., Lisk, M., Eadington, P., Quezada, R., Krieger, F.W., Greenwood, P.F., Wilson, M.A., 1996. Comparison of palaeo-oil charges with currently reservoired hydrocarbons using the geochemistry of oil-bearing fluid inclusions, SPE paper 36980, Society of Petroleum Engineers, Asia Pacific Oil and Gas Conference, Adelaide, Australia, pp. 159-171.

George, S.C., Greenwood, P.F., Logan, G.A., Quezada, R.A., Pang, L.S.K., Lisk, M., Krieger, F.W., Eadington, P., 1997. Comparison of palaeo oil charges with currently reservoired hydrocarbons using molecular and isotopic analyses of oil-bearing fluid inclusions: Jabiru oil field, Timor Sea. Australian Petroleum Production and Exploration Association Journal 37(1), 490-504.

George, S.C., Lisk, M., Eadington, P., Quezada, R., 1998a. Geochemistry of a palaeo-oil column: Octavius 2, Vulcan Sub-basin, in: Purcell, P.G., Purcell, R.R. (Eds.), The Sedimentary Basins of Western Australia 2: Proceedings of the West Australian Basins Symposium, Perth, Western Australia, pp. 195-210.

George, S.C., Eadington, P.J., Lisk, M., Quezada, R.A., 1998b. Geochemical comparison of oil trapped in fluid inclusions and reservoired oil in Blackback oilfield, Gippsland Basin, Australia. Petroleum Exploration Society of Australia Journal 26, 64-81.

George, S.C., Ruble, T.E., Dutkiewicz, A., Eadington, P., 2001. Assessing the maturity of oil trapped in fluid inclusions using molecular geochemistry data and visually-determined fluorescence colours. Applied Geochemistry 16, 451-473.

George, S.C., Volk, H., Ruble, T.E., Brincat, M.P., 2002. Evidence for a new oil family in the Nancar Trough area, Timor Sea. Australian Petroleum Production and Exploration Association Journal 42(1), 387–404.

George, S.C., Lisk, M., Eadington, P., 2004a. Fluid inclusion evidence for an early, marine-sourced oil charge prior to gas-condensate migration, Bayu-1, Timor Sea, Australia. Marine and Petroleum Geology 21, 1107-1128.

George, S.C., Ruble, T.E., Volk, H., Lisk, M., Brincat, M.P., Dutkiewicz, A., Ahmed, M., 2004b. Comparing the geochemical composition of fluid inclusion and crude oils from wells on the Laminaria High, Timor Sea, in: Ellis, G.K., Baillie, P.W., Munson, T.J. (Eds.), Timor Sea Petroleum Geoscience: Proceedings of the Timor Sea Symposium, Darwin, Northern Territory Geological Survey, Special Publication 1, pp. 203–230.

Given, P.H., 1984. An essay on the organic geochemistry of coal. Coal science 3, 63-252.

Golonka, J., 2007. Late Triassic and Early Jurassic palaeogeography of the world. Palaeogeography, Palaeoclimatology, Palaeoecology 244, 297-307.

Gradstein, F.M., Ogg, J.G., Smith, A.G., 2004. A geologic Time Scale 2004. Cambridge University Press, 589 p.

Gradstein, F.M., Ogg, J.G., Schmitz, M., 2012. The Geologic Time Scale 2012; Volumes 1 and 2. Elsevier BV, 1144 p.

Gratzer, R., Bechtel, A., Sachsenhofer, R.F., Linzer, H.G., Reischenbacher, D., Schulz, H.M., 2011. Oil–oil and oil-source rock correlations in the Alpine Foreland Basin of Austria: Insights from biomarker and stable carbon isotope studies. Marine and Petroleum Geology 28, 1171-1186.

Hagemann, H.W., Pickel, W., 1991. Characteristics of upper cretaceous coals from Enugu (Nigeria) related to bitumen generation and mobilization. Organic Geochemistry 17, 839-847.

Hamilton, D.S., Tadros, N.Z., 1994. Utility of coal seams as genetic stratigraphic sequence boundaries in nonmarine basins: an example from the Gunnedah Basin, Australia. American Association of Petroleum Geologists Bulletin 78, 267-286.

Hantschel, T., Kauerauf, A.I., 2009. Fundamentals of basin and petroleum systems modeling. Springer-Verlag, Heidelberg, 425 p.

Harris, A.G., 1979. Conodont color alteration, an organo-mineral metamorphic index, and its application to Appalachian Basin geology, in: Scholle, P.A., Schluger, P.R. (Eds.), Aspects of Diagenesis. Society of Economic Paleontologists and Mineralogists. Special Publication, 26, p. 31.

He, S., Middleton, M., 2002. Heat flow and thermal maturity modelling in the Northern Carnarvon Basin, North West Shelf, Australia. Marine and Petroleum Geology 19, 1073-1088.

Hedberg, H.D., 1968. Significance of high-wax oils with respect to genesis of petroleum. American Association of Petroleum Geologists Bulletin 52, 736-750.

Hermanrud, C., 1993. Basin modelling techniques-an overview. Basin modelling: advances and applications. Norwegian Petroleum Society. Special Publication 3, 1-34.

Heydari, E., Wade, W., Anderson, L.C., 1997. Depositional environments, organic carbon accumulation, and solar-forcing cyclicity in Smackover Formation lime mudstones, northern Gulf Coast. American Association of Petroleum Geologists Bulletin 81, 760-774.

Hitchon, B., 1974. Application of geochemistry to the search for crude oil and natural gas, in: Levinson, A.A. (Ed.), In Introduction to Exploration Geochemistry. Applied Publishing Ltd., Calgary, pp. 509-545.

Hoffmann, K.L., Totterdell, J.M., Dixon, O., Simpson, G.A., Brakel, A.T., Wells, A.T., McKellar, J.L., 2009. Sequence stratigraphy of Jurassic strata in the lower Surat Basin succession, Queensland. Australian Journal of Earth Sciences 56, 461-476.

Holmes, A.J., Griffith, C.E., Scotchman, I.C., 1999. The Jurassic petroleum system of the west of Britain Atlantic margin: an integration of tectonics, geochemistry and basin modelling, in: Fleet, A.J., Boldy, S.A.R. (Eds.), Petroleum Geology of Northwest Europe: Proceedings of the 5th Conference. Geological Society, London, pp. 1351-1365.

Horsfield, B., 1984. Pyrolysis studies and petroleum exploration. Advances in petroleum geochemistry 1, 247-298.

Horsfield, B., 1989. Practical criteria for classifying kerogens: some observations from pyrolysis-gas chromatography. Geochimica et Cosmochimica Acta 53, 891-901.

Horsfield, B., 1990. Evaluating kerogen type according to source quality, compositional heterogeneity and thermal lability. Review of Palaeobotany and Palynology 65, 357-365.

Horsfield, B., Douglas, A.G., 1980. The influence of minerals on the pyrolysis of kerogens. Geochimica et Cosmochimica Acta 44, 1119-1131.

Horsfield, B., McLimans, R.K., 1984. Geothermometry and geochemistry of aqueous and oil-bearing fluid inclusions from Fateh Field, Dubai. Organic Geochemistry 6, 733-740.

Horsfield, B., Dueppenbecker, S.J., 1991. The decomposition of Posidonia Shale and Green River Shale kerogens using microscale sealed vessel (MSSV) pyrolysis. Journal of Analytical and Applied Pyrolysis 20, 107-123.

Horsfield, B., Yordy, K.L., Crelling, J.C., 1988. Determining the petroleum-generating potential of coal using organic geochemistry and organic petrology. Organic Geochemistry 13, 121-129.

Horsfield, B., Disko, U., Leistner, F., 1989. The micro-scale simulation of maturation: outline of a new technique and its potential applications. Geologische Rundschau 78, 361-374.

Huc, A.Y., 1980. Origin and formation of organic matter in recent sediments and its relation to kerogen, in: Durand, B. (Ed.), Matière organique insoluble des roches sédimentaires. Technip, Paris, pp. 445-474.

Huc, A.Y., Durand, B., Roucachet, J., Vandenbroucke, M., Pittion, J.L., 1986. Comparison of three series of organic matter of continental origin. Organic Geochemistry 10, 65-72.

Hunt, J.M., 1991. Generation of gas and oil from coal and other terrestrial organic matter. Organic Geochemistry 17, 673-680.

Hunt, J.M., Philp, R.P., Kvenvolden, K.A., 2002. Early developments in petroleum geochemistry. Organic Geochemistry 33, 1025-1052.

Isaksen, G.H., Curry, D.J., Yeakel, J.D., Jenssen, A.I., 1998. Controls on the oil and gas potential of humic coals. Organic Geochemistry 29, 23-44.

James, K.H., 1990. The Venezuelan hydrocarbon habitat. Geological Society, London, Special Publications 50, 9-35.

Jarvie, D.M., 2001. Williston Basin petroleum systems: inferences from oil geochemistry and geology. The Mountain Geologist 38, 19-41.

Jones, R.W., 1984. Comparison of carbonate and shale source rocks. In Petroleum Geochemistry and Source Rock Potential of Carbonate Rocks, in: Palacas, J.G. (Ed.), American Association of Petroleum Geologists Bulletin. Studies in Geology, 18, pp. 163-180.

Jones, R.W., 1987. Organic facies, in: Brooks, J., Welte, D.H. (Eds.), In Advances in Petroleum Geochemistry. Academic Press, New York, pp. 1-90.

Kennard, J.M., Deighton, I., Edwards, D.S., Colwell, J.B., O'Brien, G.W., Boreham, C.J., 1999. Thermal history modelling and transient heat pulses: new insights into hydrocarbon expulsion and 'hot flushes' in the Vulcan Sub-basin, Timor Sea. Australian Petroleum Production and Exploration Association Journal 39(1), 177-207.

Khavari Khorasani, G., 1987. Oil-prone coals of the Walloon coal measures, Surat Basin, Australia. Geological Society, London, Special Publications 32, 303-310.

Killops, S.D., Woolhouse, A.D., Weston, R.J., Cook, R.A., 1994. A geochemical appraisal of oil generation in the Taranaki Basin, New Zealand. American Association of Petroleum Geologists Bulletin 78, 1560-1585.

Killops, S.D., Funnell, R.H., Suggate, R.P., Sykes, R., Peters, K.E., Walters, C., Woolhouse, A.D., Weston, R.J., Boudou, J.P., 1998. Predicting generation and expulsion of paraffinic oil from vitrinite-rich coals. Organic Geochemistry 29, 1-21.

Kopsen, E., 2002. Historical perspective of hydrocarbon volumes in the Westralian Superbasin: Where are the next billion barrels?, in: Keep, M., Moss, S.J. (Eds.), The sedimentary basins of Western Australia 3:

Proceedings of the Petroleum Exploration Society of Australia Symposium, Perth, Western Australia, pp. 577-598.

Kramer, L., Arouri, K.R., McKirdy, D.M., 2001. Petroleum expulsion from Permian coal seams in the Patchawarra Formation, Cooper Basin, South Australia, Eastern Australasian Basins Symposium. 25 – 28 November, 2001. Australian Institute of Mining and Metallurgy, Carlton, Victoria, pp. 329-340.

Labutis, V.R., Ruddock, A.D., Calcraft, A.P., 1998. Stratigraphy of the southern Sahul Platform. Australian Petroleum Production and Exploration Association Journal 38(1), 115-136.

Langhi, L., Borel, G.D., 2008. Reverse structures in accommodation zone and early compartmentalization of extensional system, Laminaria High (NW shelf, Australia). Marine and Petroleum Geology 25, 791-803.

Largeau, C., Derenne, S., Casadevall, E., Kadouri, A., Sellier, N., 1986. Pyrolysis of immature Torbanite and of the resistant biopolymer (PRB A) isolated from extant alga Botryococcus braunii. Mechanism of formation and structure of torbanite. Organic Geochemistry 10, 1023-1032.

Larter, S.R., 1984. Application of analytical pyrolysis techniques to kerogen characterization and fossil fuel exploration/exploitation, in: Voorhees, K.J. (Ed.), Analytical Pyrolysis: Methods and application, Butterworth, London, pp. 212-275.

Larter, S.R., Douglas, A.G., 1982. Pyrolysis methods in organic geochemistry: an overview. Journal of Analytical and Applied Pyrolysis 4, 1-19.

Larter, S.R., Senftle, J.T., 1985. Improved kerogen typing for petroleum source rock analysis. Nature 318, 277-280.

Larter, S.R., Horsfield, B., 1993. Determination of structural components of kerogens by the use of analytical pyrolysis methods, Organic Geochemistry. Springer, pp. 271-287.

Leenheer, M.J., Zumberge, J.E., 1987. Correlation and thermal maturity of Williston Basin crude oils and Bakken source rocks using terpane biomarkers, in: Longman, M.W. (Ed.), Williston Basin: Anatomy of a Cratonic Oil Province. Rocky Mountain Association of Geologists, Denver, pp. 287-298.

Lewan, M.D., Winters, J.C., McDonald, J.H., 1979. Generation of Oil-Like Pyrolyzates from Organic-Rich Shales. Science 203, 897-899.

Lewan, M.D., Spiro, B., Illich, H., Raiswell, R., Mackenzie, A.S., Durand, B., Manning, D.A.C., Comet, P.A., Berner, R.A., De Leeuw, J.W., 1985. Evaluation of petroleum generation by hydrous pyrolysis experimentation. Philosophical Transactions of the Royal Society of London. Series A 315, 123-134.

Lisk, M., 2012. Fluid migration and hydrocarbon charge history of the Vulcan Sub-basin. PhD thesis, Department of Applied Geology. Curtin University. Doctor of Philosophy, 734 p.

Lisk, M., Brincat, M.P., Eadington, P.J., O'Brien, G.W., 1998. Hydrocarbon charge in the Vulcan Sub-basin, in: Purcell, P.G., Purcell, R.R. (Eds.), The Sedimentary Basins of Western Australia 2: Proceedings of the West Australian Basins Symposium, Perth, Western Australia, pp. 287-305.

Lisk, M., O'Brien., G.W., Eadington, P.J., 2002. Quantitative evaluation of the oil-leg potential in the Oliver gas field, Timor Sea, Australia. American Association of Petroleum Geologists Bulletin 86, 1531-1542.

Littke, R., Leythaeuser, D., Rullkötter, J., Baker, D.R., 1991. Keys to the depositional history of the Posidonia Shale (Toarcian) in the Hils Syncline, northern Germany. Geological Society, London, Special Publications 58, 311-333.

Littke, R., Büker, C., Lückge, A., Sachsenhofer, R.F., Welte, D.H., 1994. A new evaluation of palaeo-heat flows and eroded thicknesses for the Carboniferous Ruhr basin, western Germany. International journal of coal geology 26, 155-183.

Longley, I.M., Buessenschuett, C., Clydsdale, L., Cubitt, C.J., Davis, R.C., Johnson, M.K., Marshall, N.M., Murray, A.P., Somerville, R., Spry, T.B., Thompson, N., 2002. The North West Shelf of Australia: a Woodside perspective, in: Keep, M., Moss, S. (Eds.), The Sedimentary Basins of Western Australia 3: Proceedings of Petroleum Exploration Society of Australia Symposium, Perth, Western Australia, pp. 27-88.

MacDaniel, R.P., 1988. The geological evolution and hydrocarbon potential of the western Timor Sea region. Petroleum in Australia: The First Century. Australian Petroleum Exploration Association Journal 28, 270-284.

Macgregor, D.S., 1994. Coal-bearing strata as source rocks—a global overview. Geological Society, London, Special Publications 77, 107-116.

Mackenzie, A.S., Patience, R.L., Maxwell, J.R., Vandenbroucke, M., Durand, B., 1980. Molecular parameters of maturation in the Toarcian shales, Paris Basin, France—I. Changes in the configurations of acyclic isoprenoid alkanes, steranes and triterpanes. Geochimica et Cosmochimica Acta 44, 1709-1721.

Magoon, L.B., 1988. The petroleum system: a classification scheme for research, exploration, and resource assessment, in: Magoon, L.B. (Ed.), Petroleum systems of the United States: US Geological Survey Bulletin, pp. 2-15.

Magoon, L.B., Dow, W.G., 1994. The petroleum system: From Source to Trap, in: Magoon, L.B., Dow, W.G. (Eds.), American Association of Petroleum Geologists Bulletin, pp. 3-24.

McCabe, P.J., 1984. Depositional environments of coal and coal-bearing strata, in: Rahmani, R.A., Flores, R.M. (Eds.), Sedimentology of coal and coal-bearing sequences. International Association of Sedimentologists, Special publication, pp. 13-42.

Megallaa, M., 1993. Tectonic evolution of the Gippsland Basin and hydrocarbon potential of its lower continental shelf. Australian Petroleum Exploration Association Journal 33, 45-61.

Moldowan, J.M., Seifert, W.K., Gallegos, E.J., 1985. Relationship between petroleum composition and depositional environment of petroleum source rocks. American Association of Petroleum Geologists Bulletin 69, 1255-1268.

Montilla, L.A., Martínez, M., Márquez, G., Escobar, M., Sierra, C., Gallego, J.R., Esteves, I., Gutiérrez, J.V., 2013. Geochemistry and chemostratigraphy of the Colón-Mito Juan units (Campanian-Maastrichtian), Venezuela: Implications for provenance, depositional conditions, and stratigraphic subdivision. Geochemical Journal 47, 537-546.

Moore, P.S., Burns, B.J., Emmett, J.K., Guthrie, D.A., 1992. Integrated source, maturation and migration analysis, Gippsland Basin, Australia. Australian Petroleum Exploration Association Journal 32 (1), 313-324.

Mory, A.J., 1991. Geology of the offshore Bonaparte Basin, Northwestern Australia. Geological Survey of Western Australia Report 29, 47 p.

Murray, A.P., Edwards, D.S., Hope, J.M., Boreham, C.J., Booth, W.E., Alexander, R.A., Summons, R.E., 1998. Carbon isotope biogeochemistry of plant resins and derived hydrocarbons. Organic Geochemistry 29, 1199-1214.

Naeth, J., di Primio, R., Horsfield, B., Schaefer, R.G., Shannon, P.M., Bailey, W.R., Henriet, J.P., 2005. Hydrocarbon seepage and carbonate mound Formation: A basin modelling study from the Porcupine Basin (Offshore Ireland). Journal of Petroleum Geology 28, 147-166.

Nedkvitne, T., Karlsen, D.A., Bjørlykke, K., Larter, S.R., 1993. Relationship between reservoir diagenetic evolution and petroleum emplacement in the Ula Field, North Sea. Marine and Petroleum Geology 10, 255-270.

Newell, N.A., 1999. Bonaparte and Browse basins-Water washing in the Northern Bonaparte Basin. Australian Petroleum Production and Exploration Association Journal 39(1), 227-247.

Nicoll, R.S., Kennard, J.M., Laurie, J.R., Kelman, A.P., Mantle, D.J., Edwards, D.S., 2009. Bonaparte Basin, Biozonation and Stratigraphy, 2009, Chart 33. Geoscience Australia.

Norvick, M.S., Smith, M.A., 2001. Mapping the plate tectonic reconstruction of southern and southeastern Australia and implications for petroleum systems. Australian Petroleum Production and Exploration Association Journal 41, 15-35.

O'Brien, G.W., 1993. Some ideas on the rifting history of the Timor Sea from the integration of deep crustal seismic and other data. Petroleum Exploration Society of Australia Journal 21, 95-113.

O'Brien, G.W., Woods, E.P., 1995. Hydrocarbon-related diagenetic zones (HRDZs) in the Vulcan Sub-basin, Timor Sea: recognition and exploration implications. Australian Petroleum Production and Exploration Association Journal 35, 220-220.

O'Brien, G.W., Lisk, M., Duddy, I.R., Hamilton, J., Woods, P., Cowley, R., 1999. Plate convergence, foreland development and fault reactivation: primary controls on brine migration, thermal histories and trap breach in the Timor Sea, Australia. Marine and Petroleum Geology 16, 533-560.

O'Brien, G.W., Tingate, P.R., Divko, L.M., Harrison, M.L., Boreham, C.J., Liu, K., Arian, N., Skladzien, P., 2008. First order sealing and hydrocarbon migration processes, Gippsland Basin, Australia: implications for CO2 geosequestration, in: Blevin, J.E., Bradshaw, B.E., Uruski, C. (Eds.), Eastern Australasian Basins Symposium III: Energy security for the 21th century. Petroleum Exploration Society of Australia, Special Publication, pp. 1-28.

Ogg, J.G., Ogg, G., Gradstein, F.M., 2008. The Concise Geologic Time Scale. Cambridge University Press, 178 p.

Osadetz, K.G., Brooks, P.W., Snowdon, L.R., 1992. Oil families and their sources in Canadian Williston Basin,(southeastern Saskatchewan and southwestern Manitoba). Bulletin of Canadian Petroleum Geology 40, 254-273.

Palacas, J.G., 1988. Characteristics of carbonate source rocks of petroleum, in: Magoon, L.B. (Ed.), Petroleum systems of the United States: US Geological Survey Bulletin, pp. 20-25.

Pang, L.S.K., George, S.C., Quezada, R.A., 1998. A study of the gross compositions of oil-bearing fluid inclusions using high performance liquid chromatography. Organic Geochemistry 29, 1149-1161.

Paton, D.A., di Primio, R., Kuhlmann, G., Van Der Spuy, D., Horsfield, B., 2007. Insights into the petroleum system evolution of the southern Orange Basin, South Africa. South African Journal of Geology 110, 261-274.

Pattillo, J., Nicholls, P.J., 1990. A tectonostratigraphic framework for the Vulcan Graben, Timor Sea region. Australian Petroleum Exploration Association Journal 30(1), 27-51.

Pedersen, T.F., Calvert, S.E., 1990. Anoxia vs. Productivity: What Controls the Formation of Organic-Carbon-Rich Sediments and Sedimentary Rocks?(1). American Association of Petroleum Geologists Bulletin 74, 454-466.

Peters, K.E., 1986. Guidelines for evaluating petroleum source rock using programmed pyrolysis. American Association of Petroleum Geologists Bulletin 70(3), 318-329.

Peters, K.E., Cassa, M.R., 1994. Applied source-rock geochemistry. In: Magoon, L.B., Dow, W.G. (Eds.), The Petroleum System—From Source to Trap. American Association of Petroleum Geologists Bulletin 60, 93-120.

Peters, K.E., Snedden, J.W., Sulaeman, A., Sarg, J.F., Enrico, R.J., 2000. A new geochemical-sequence stratigraphic model for the Mahakam Delta and Makassar Slope, Kalimantan, Indonesia. American Association of Petroleum Geologists Bulletin 84, 12-44.

Peters, K.E., Walters, C.C., Moldowan, J.M., 2005. The biomarker guide (2nd ed.). Part I, biomarkers and isotopes in the environmental and human history, and part II, biomarkers and isotopes in petroleum exploration and earth history. Cambridge University Press.

Petersen, H.I., Andsbjerg, J., 1996. Organic facies development within Middle Jurassic coal seams, Danish Central Graben, and evidence for relative sea-level control on peat accumulation in a coastal plain environment. Sedimentary Geology 106, 259-277.

Philp, R.P., Calvin, M., 1976. Possible origin for insoluble organic (kerogen) debris in sediments from insoluble cell-wall materials of algae and bacteria. Nature 262, 134-136.

Picha, F.J., Peters, K.E., 1998. Biomarker oil-to-source rock correlation in the Western Carpathians and their foreland, Czech Republic. Petroleum Geoscience 4, 289-302.

Poelchau, H.S., Baker, D.R., Hantschel, T., Horsfield, B., Wygrala, B., 1997. Basin simulation and the design of the conceptual basin model, in: Welte, D.H., Horsfield, B., Baker, D.R. (Eds.), Petroleum and basin evolution. Springer Berlin Heidelberg, pp. 3-70.

Powell, T.G., 1986. Petroleum geochemistry and depositional setting of lacustrine source rocks. Marine and Petroleum Geology 3, 200-219.

Powell, T.G., Boreham, C.J., Smyth, M., Russell, N., Cook, A.C., 1991. Petroleum source rock assessment in non-marine sequences: pyrolysis and petrographic analysis of Australian coals and carbonaceous shales. Organic Geochemistry 17, 375-394.

Power, M., Hill, K., Hoffman, N., Bernecker, T., Norvick, M., 2001. The structural and tectonic evolution of the Gippsland Basin: results from 2D section balancing and 3D structural modelling, in: Hill, K.C., Bernecker, T. (Eds.), Eastern Australasian Basins Symposium, A Refocused Energy. Perspective for the Future, Petroleum Exploration Society of Australia, pp. 373-384.

Preston, J.C., Edwards, D.S., 2000. The petroleum geochemistry of oils and source-rocks from the northern Bonaparte Basin, offshore northern Australia. Australian Petroleum Production and Exploration Association Journal 40(1), 257-282.

Price, L.C., Clayton, J.L., 1992. Extraction of whole versus ground source rocks: Fundamental petroleum geochemical implications including oil-source rock correlation. Geochimica et Cosmochimica Acta 56, 1213-1222.

Radke, M., Schaefer, R.G., Leythaeuser, D., Teichmüller, M., 1980. Composition of soluble organic matter in coals: relation to rank and liptinite fluorescence. Geochimica et Cosmochimica Acta 44, 1787-1800.

Rahmanian, V.D., Moore, P.S., Mudge, W.J., Spring, D.E., 1990. Sequence stratigraphy and the habitat of hydrocarbons, Gippsland Basin, Australia, in: Brooks, J.D. (Ed.), Classic petroleum provinces. Geological Society, London, Special Publication, pp. 525-541.

Rodriguez, J.F.R., Littke, R., 2001. Petroleum generation and accumulation in the Golfo San Jorge Basin, Argentina: a basin modeling study. Marine and Petroleum Geology 18, 995-1028.

Röhl, H.J., Schmid-Röhl, A., Oschmann, W., Frimmel, A., Schwark, L., 2001. The Posidonia Shale (Lower Toarcian) of SW-Germany: an oxygen-depleted ecosystem controlled by sea level and palaeoclimate. Palaeogeography, Palaeoclimatology, Palaeoecology 165, 27-52.

Rullkötter, J., Michaelis, W., 1990. The structure of kerogen and related materials. A review of recent progress and future trends. Organic Geochemistry 16, 829-852.

Sachsenhofer, R.F., 1994. Petroleum generation and migration in the Styrian Basin (Pannonian Basin system, Austria): an integrated geochemical and numerical modelling study. Marine and Petroleum Geology 11, 684-701.

Salehy, M.R., 1986. Determination of rank and petrographic composition of Jurassic coals from eastern Surat Basin, Australia. International journal of coal geology 6, 149-162.

Santamaría, O.D., Horsfield, B., 2003. Gas generation potential of Upper Jurassic (Tithonian) source rocks in the Sonda de Campeche, Mexico. The circum-Gulf of Mexico and the Caribbean; hydrocarbon habitats, basin formation, and plate tectonics. American Association of Petroleum Geologists Bulletin 79, 349-363.

Sassen, R., 1990. Geochemistry of carbonate source rocks and crude oils in Jurassic salt basins of the Gulf Coast. Geological Society, London, Special Publications 50, 265-277.

Sauer, P.E., Eglinton, T.I., Hayes, J.M., Schimmelmann, A., Sessions, A.L., 2001. Compound-specific D/H ratios of lipid biomarkers from sediments as a proxy for environmental and climatic conditions. Geochimica et Cosmochimica Acta 65, 213-222.

Schaefer, R.G., Schenk, H.J., Hardelauf, H., Harms, R., 1990. Determination of gross kinetic parameters for petroleum formation from Jurassic source rocks of different maturity levels by means of laboratory experiments. Organic Geochemistry 16, 115-120.

Schenk, H.J., Horsfield, B., 1993. Kinetics of petroleum generation by programmed-temperature closed-versus open-system pyrolysis. Geochimica et Cosmochimica Acta 57, 623-630.

Schenk, H.J., Horsfield, B., 1998. Using natural maturation series to evaluate the utility of parallel reaction kinetics models: an investigation of Toarcian shales and Carboniferous coals, Germany. Organic Geochemistry 29, 137-154.

Schenk, H.J., Dieckmann, V., 2004. Prediction of petroleum formation: the influence of laboratory heating rates on kinetic parameters and geological extrapolations. Marine and Petroleum Geology 21, 79-95.

Schoell, M., 1984. Recent advances in petroleum isotope geochemistry. Organic Geochemistry 6, 645-663.

Seifert, W.K., Moldowan, J.M., 1981. Paleoreconstruction by biological markers. Geochimica et Cosmochimica Acta 45, 783-794.

Seifert, W.K., Moldowan, J.M., 1986. Use of biological markers in petroleum exploration. Methods in geochemistry and geophysics 24, 261-290.

Shanmugam, G., 1985. Significance of coniferous rain forests and related organic matter in generating commercial quantities of oil, Gippsland Basin, Australia. American Association of Petroleum Geologists Bulletin 69, 1241-1254.

Shibaoka, M., Saxby, J.D., Taylor, G.H., 1978. Hydrocarbon Generation in Gippsland Basin, Australia--Comparison with Cooper Basin, Australia. American Association of Petroleum Geologists Bulletin 62, 1151-1158.

Shuster, M.W., Eaton, S., Wakefield, L.L., Kloosterman, H.J., 1998. Neogene tectonics, greater Timor Sea, offshore Australia: implications for trap risk. Australian Petroleum Production and Exploration Association Journal 38(1), 351-379.

Silverman, S.R., Epstein, S., 1958. Carbon isotopic compositions of petroleums and other sedimentary organic materials. American Association of Petroleum Geologists Bulletin 42, 998-1012.

Sloan, M., Moore, P., McCutcheon, A., 1992. Kipper-a unique oil and gas discovery, Gippsland Basin, Australia. Australian Petroleum Exploration Association Journal 32, 1-8.

Smith, G.C., 1988. Oil and gas. In: Douglas, J.G., Ferguson, J.A. (Eds.), Geology of Victoria. Victorian Division, Geological Society of Australia. pp. 514–546.

Smith, G.C., Cook, A.C., 1984. Petroleum occurrence in the Gippsland Basin and its relationship to rank and organic matter type. Australian Petroleum Exploration Association Journal 24, 196-216.

Smith, G.C., Tilbury, L.A., Chatfield, A., Senycia, P., Thompson, N., 1996. Laminaria: a new Timor Sea discovery. Australian Petroleum Production and Exploration Association Journal 36(1), 12-29.

Sofer, Z., 1984. Stable carbon isotope compositions of crude oils: application to source depositional environments and petroleum alteration. American Association of Petroleum Geologists Bulletin 68, 31-49.

Stach, E., Mackowsky, M.T., TeichmUller, M., Taylor, G.H., Chandra, D., Teichmuller, R., 1975. Stach's Textbook of Coal Petrology. Gebruder Borntraeger, Berlin, Stuttgart, 428 p.

Stahl, W.J., 1977. Carbon and nitrogen isotopes in hydrocarbon research and exploration. Chemical Geology 20, 121-149.

Stainforth, J.G., 1984. Gippsland hydrocarbons-perspective from the basin edge. Australian Petroleum Exploration Association Journal 24, 91-100.

Staplin, F.L., 1969. Sedimentary organic matter, organic metamorphism, and oil and gas occurrence. Bulletin of Canadian Petroleum Geology 17, 47-66.

Summons, R.E., Franzmann, P.D., Nichols, P.D., 1998. Carbon isotopic fractionation associated with methylotrophic methanogenesis. Organic Geochemistry 28, 465-475.

Summons, R.E., Zumberge, J.E., Boreham, C.J., Bradshaw, M.T., Brown, S.W., Edwards, D.S., Hope, J.M., Johns, N., 2002. The Oils of Eastern Australia Petroleum Geochemistry and Correlation. Open file report, Geoscience Australia and Geomark Research, 162 p.

Sun, Y., Sheng, G., Peng, P., Fu, J., 2000. Compound-specific stable carbon isotope analysis as a tool for correlating coal-sourced oils and interbedded shale-sourced oils in coal measures: an example from Turpan basin, north-western China. Organic Geochemistry 31, 1349-1362.

Sykes, R., 2001. Depositional and rank controls on the petroleum potential of coaly source rocks. In: Hill, K.C., Bernecker, T. (Eds.), Eastern Australasian basins symposium, a Refocused Energy Perspective for the Future. Petroleum Exploration Society of Australia, Special Publication, pp. 591-601.

Sykes, R., Snowdon, L.R., 2002. Guidelines for assessing the petroleum potential of coaly source rocks using Rock-Eval pyrolysis. Organic Geochemistry 33, 1441-1455.

Talukdar, S., Gallango, O., Chin-A-Lien, M., 1986. Generation and migration of hydrocarbons in the Maracaibo basin, Venezuela: An integrated basin study. Organic Geochemistry 10, 261-279.

Teerman, S.C., Hwang, R.J., 1991. Evaluation of the liquid hydrocarbon potential of coal by artificial maturation techniques. Organic Geochemistry 17, 749-764.

Tegelaar, E.W., Noble, R.A., 1994. Kinetics of hydrocarbon generation as a function of the molecular structure of kerogen as revealed by pyrolysis-gas chromatography. Organic Geochemistry 22, 543-574.

Tegelaar, E.W., De Leeuw, J.W., Derenne, S., Largeau, C., 1989. A reappraisal of kerogen formation. Geochimica et Cosmochimica Acta 53, 3103-3106.

Thomas, B.M., 1982. Land-plant source rocks for oil and their significance in Australian basins. Australian Petroleum Exploration Association Journal 22, 164-178.

Thomas, J.H., Bernecker, T., Driscoll, J., 2003. Hydrocarbon Prospectivity of Areas V03-3 and V03-4, Offshore Gippsland Basin, Victoria, Australia: 2003 Acreage Release, Victorian Initiative for Minerals and Petroleum Report 80, Depatment of Primary Industries.

Thompson, S., Cooper, B.S., Morley, R.J., Barnard, P.C., 1985. Oil-generating coals, in: Thomas, B.M.e.a. (Ed.), Petroleum geochemistry in exploration of the Norwegian Shelf. Graham & Trotman, London, pp. 59-73.

Thompson, S., Cooper, B.S., Barnard, P.C., 1994. Some examples and possible explanations for oil generation from coals and coaly sequences. Geological Society, London, Special Publications 77, 119-137.

Tissot, B.P., 1984. Recent advances in petroleum geochemistry applied to hydrocarbon exploration. American Association of Petroleum Geologists Bulletin 68, 545-563.

Tissot, B.P., Welte, D.H., 1984. Petroleum Formation and Occurrence. Springer Verlag, Berlin, 699 p.

Tissot, B.P., Durand, B., Espitalié, J., Combaz, A., 1974. Influence of nature and diagenesis of organic matter in formation of petroleum. American Association of Petroleum Geologists Bulletin 58, 499-506.

Ungerer, P., Pelet, R., 1987. Extrapolation of the kinetics of oil and gas formation from laboratory experiments to sedimentary basins. Nature 327, 52-54.

Ungerer, P., Burrus, J., Doligez, B., Chenet, P., Bessis, F., 1990. Basin Evaluation by Integrated Two-Dimensional Modeling of Heat Transfer, Fluid Flow, Hydrocarbon Generation, and Migration (1). American Association of Petroleum Geologists Bulletin 74, 309-335.

USGS, 2012. Assessment of Undiscovered Conventional Oil and Gas Resources of Bonaparte Basin, Browse Basin, Northwest Shelf, and Gippsland Basin Provinces, Australia, 2011. U.S. Department of the Interior, U.S. Geological Survey, p. 2.

van Aarssen, B.G.K., Hessels, J.K.C., Abbink, O.A., de Leeuw, J.W., 1992. The occurrence of polycyclic sesqui-, tri-, and oligoterpenoids derived from a resinous polymeric cadinene in crude oils from southeast Asia. Geochimica et Cosmochimica Acta 56, 1231-1246.

Vandenbroucke, M., Largeau, C., 2007. Kerogen origin, evolution and structure. Organic Geochemistry 38, 719-833.

Volk, H., George, S.C., Dutkiewicz, A., Ridley, J., 2005. Characterisation of fluid inclusion oil in a Mid-Proterozoic sandstone and dolerite (Roper Superbasin, Australia). Chemical Geology 223, 109-135.

Webster, R.L., 1984. Petroleum source rocks and stratigraphy of the Bakken Formation in North Dakota, in: Woodward, J., Meissner, F.F., Clayton, J.L. (Eds.), Hydrocarbon Source Rocks of the Greater Rocky Mountain Region. Rocky Mountain Association of Geologists, Denver, Colorado, pp. 57-81.

Welte, D.H., 1974. Recent advances m orgamc geochemistry of humlc substances and kerogen: A review, in: Tissot, B., Bienner, F. (Eds.), Advances in Organic Geochemistry. Editions Technip, Paris, pp. 3-313.

Welte, D.H., Yalçin, M.N., 1988. Basin modelling—A new comprehensive method in petroleum geology. Organic Geochemistry 13, 141-151.

Welte, D.H., Hantschel, T., Wygrala, B.P., Weissenburger, K.S., Carruthers, D., 2000. Aspects of petroleum migration modelling. Journal of Geochemical Exploration 69–70, 711-714.

Weston, R.J., Philp, R.P., Sheppard, C.M., Woolhouse, A.D., 1989. Sesquiterpanes, diterpanes and other higher terpanes in oils from the Taranaki basin of New Zealand. Organic Geochemistry 14, 405-421.

Whittam, D.B., Norvick, M.S., Mclntyre, C.L., 1996. Mesozoic and Cainozoic tectonostratigraphy of western ZOCA and adjacent areas. Australian Petroleum Production and Exploration Association Journal 36(1), 209-232.

Wiggins, W.D., Harris, P.M., 1985. Burial diagenetic sequence in deep-water allochtonous dolomites, Permian Bone Spring Formation, southeast New Mexico, in: Crevello, P.D., Harris, P.M. (Eds.), Deep-Water Carbonates: Build Turbidites, Debris Flows and Chalks, Society of Economic Paleontologists and Mineralogists, Core Workshop No. 6, pp. 140-173.

Wilkins, R.W.T., George, S.C., 2002. Coal as a source rock for oil: a review. International journal of coal geology 50, 317-361.

Wilkinson, M., Haszeldine, R.S., Fallick, A.E., 2006. Hydrocarbon filling and leakage history of a deep geopressured sandstone, Fulmar Formation, United Kingdom North Sea. American Association of Petroleum Geologists Bulletin 90, 1945-1961.

Willcox, J., Sayers, J., Stagg, H., Van de Beuque, S., 2001. Geological framework of the Lord Howe Rise and adjacent ocean basins, Eastern Australasian Basins Symposium, A Refocused Energy Perspective for the Future. Petroleum Exploration Society of Australia, Special Publication, pp. 211-227.

Winters, J.C., J.A., W., M.D., L., 1983. A laboratory study of petroleum generation by hydrous pyrolysis, in: Bjoroy, M., et al. (Ed.), In Advances in Organic Geochemistry. Wiley, Chichester, pp. 524-533.

Woods, E.P., 1994. A salt-related detachment model for the development of the Vulcan Sub-basin. The sedimentary basins of Western Australia 2, 259-274.

Zhang, S.C., Hanson, A.D., Moldowan, J.M., Graham, S.A., Liang, D.G., Chang, E., Fago, F., 2000. Paleozoic oil–source rock correlations in the Tarim basin, NW China. Organic Geochemistry 31, 273-286.

# Chapter 2. Methods and approaches

## 2.1. Geochemical characterisation

### 2.1.1. Sample preparation and solvent extraction

A total of 167 cuttings and core samples from 33 wells (**Appendices, 1, 2** and **3)** were selected for this study; they are distributed as follows:

- 61 cuttings samples and 3 core samples from the Vulcan Sub-basin,
- 22 cuttings samples from the Laminaria High,
- 67 cuttings samples and 13 core samples from the Gippsland Basin.

Before carrying out the solvent extraction, all the investigated samples from the Bonaparte Basin were washed with water and dried according to the level of drilling mud and lithology. In some cases, samples were hand-picked to separate the coal and shale and to remove obvious contamination. Samples from the Vulcan Sub-basin and the Laminaria High were then ground into fine powder using a mortar and pestle. Samples collected from the Gippsland Basin were powdered using a vibratory ring mill available at Geoscience Australia. The average weight of samples investigated in this study varied between 20 and 100 mg depending on the available material. Finally, samples were separated into two aliquots; one for solvent extraction and further analyses, and the second to be analysed by Rock-Eval pyrolysis.

For extraction, an ASE 300 accelerated solvent extraction system (Dionex) was used in order to remove the free organic matter including any possible contamination. A glass fibre filter was inserted on one side of each extraction cell to avoid fine particles eluting into the collection bottles. Then, 10 to 20g of sample was weighed and loaded into the cell; the empty volume was filled with clean sand at the inlet end of the cell. Additional glass-fibre filters were also placed between the sample and the sand to prevent mixing. ASE cells were set up enabling six samples to be extracted simultaneously.

The extraction was conducted under the following conditions:

- 2 min pre heat,
- 5 min heat up time,
- 2 min static time,
- 120% flush,

- 300 sec purge with nitrogen,
- A temperature of 100 $^0$C,
- A pressure of 1000 psi,
- The solvent mixture was 90% DCM and 10% MeOH.

At the end of the solvent extraction process, the cells were rinsed and flushed into the collection bottle before being purged with nitrogen for 5 min before the next run. For the coal samples and some contaminated samples, extraction was repeated multiple times, sometimes more than four times, to minimise the contamination effect (the extraction was repeated until the extracted solvent in the round-bottom flask became colourless). The solvent with the extracted organic matter (EOM) was then placed under a fume hood into a rotary evaporator system that allowed evaporation of the solvent and retaining but never taking to dryness the EOM. Finally, for each sample the EOM was dried and weighed and placed into vials for storage until further analyses, while the extracted sediments were placed into glass vials to be investigated in this study.

### 2.1.2. Rock-Eval pyrolysis

All the collected samples were analysed for total organic content (TOC) and by Rock-Eval pyrolysis using a Rock-Eval 6 instrument manufactured by Vinci Technology® at the organic geochemistry laboratory in Geoscience Australia. These screening analyses were performed on approximately 50-100 mg of ground rock, and were used to assess the petroleum-generative potential and thermal maturity of the sediments. More details on this method can be found in Lafargue et al. (1998) and Behar et al. (2001). For the Laminaria High and the Vulcan Sub-basin samples, both whole rock (un-extracted) and extracted samples were analysed for TOC content and by Rock-Eval pyrolysis because the majority of wells in these two areas were drilled with an oil-based drilling mud. The results derived from these measurements are listed in **Appendices 4, 5** and **6**.

The Rock-Eval was performed under the following analytical conditions:
- Inert atmosphere (helium flow) to enable a rapid transport of pyrolysis products to the detectors and minimise effects of secondary cracking processes.
- 300°C isothermal for 3 minutes. During this heating interval, the volatile or free compounds (the $S_1$ peak), which are proportional to the concentration of the EOM, were released.
- 25°C/min heating rate to 650°C, held at 650°C for 1 minute. During this programmed pyrolysis interval, the hydrocarbons generated by thermal cracking (the $S_2$ peak)

were released and quantified by flame-ionisation detector (FID). An additional important parameter derived from this experiment was the temperature at which the maximum of the non-volatile $S_2$ fraction was decomposed (the $T_{max}$ measured at the top of the $S_2$ peak), which was also measured by FID.

- Between 300 and 390°C, the compounds containing $CO_2$ (the $S_3$ peak) were measured; oxidation was completed at 580°C for 12 minutes, when compounds having CO were released. These oxygen-bearing compounds were monitored using an online infrared detector (IRD).

The two peaks $S_1$ and $S_2$ that were quantified by FID were used to calculate several parameters such as the petroleum potential ($S_1+S_2$), the production index ($S_1/[S_1+S_2]$) and the hydrogen index ($S_2*100/TOC$). The $S_3$ parameter was used to calculate the oxygen index ($S_3*100/TOC$).

### 2.1.3. Open-system pyrolysis-gas chromatography (Py-GC)

Both $T_{max}$ values and the amount of $S_2$ were used to identify the most favourable samples for artificial maturation analyses and for compositional kinetic measurements. Values above a $T_{max}$ threshold of 440°C and anomalous $T_{max}$ values were discarded. Sixty extracted samples were subjected to open-system pyrolysis-gas chromatography (Horsfield, 1989; Horsfield and Dueppenbecker, 1991) in the organic geochemistry laboratory at the GFZ Institute (Germany) in order to determine the type of kerogen and the type of organo-facies. Quartz wool was inserted at one end of a thin glass tube (diameter of 1 mm) before loading of between 5 to 20 mg of each sample, depending on the organic richness. The tube containing the sample was plugged at the other end by quartz wool. An Agilent 6890A GC instrument equipped by a programmable pyrolysis unit, a HP-Ultra 50m x 0.32mm capillary column (0.52 μm film thickness and dimethyl polysiloxane-phase) and an FID were used. The oven was initially set at 300°C for 4 minutes to allow venting (through a secondary valve) of the volatile fraction before pyrolysis. A programmed heating rate of 50°C/min to a temperature of 600°C under a constant flow of nitrogen (regulated at 30 ml/min) was then applied to release the pyrolysis products. During the pyrolysis process, the generated compounds were first retained in a cooled cryogenic trap, from which they were liberated by heating to 300°C for 10 minutes. The separation of the pyrolysis products was performed on the GC oven temperature was programmed from 30 to 320°C at 5°C /min (held for 35 min). Data was finally acquired and processed using Agilent Chemstation software. The processing consisted of the identification of the prominent peaks, which was conducted using retention time correlations with a standard sample. In addition, the quantification of the different

identified products was calculated with reference to *n*-butane which was used as an external standard. Because of the lower response factor of methane compared to the heavier gases the methane content was multiplied with 1.1. The proportion of the components and boiling ranges in the pyrolysates are reported in **Appendices 7, 8, 9, 10, 11** and **12.**

### 2.1.4. Pyrolysis-Flame Ionisation Detector (Py-FID)

Bulk kinetic parameters for 31 selected samples (solvent-extracted) were measured using a Source Rock Analyzer (SRA-TPH/IR), supplied by Humble Instruments. The derived parameters describe the conversion of kerogen to petroleum known as the primary cracking processes (Schaefer et al., 1990; Mahlstedt et al., 2008). The samples were subjected to pyrolysis under open-system-programmed-temperature at four different heating rates (0.7, 2, 5 and 15 °C/min). 10 to 40 mg of extracted sample was loaded in a small glass vessel which was then placed into the pyrolysis oven under a constant helium flow (50ml/min). After an isothermal interval of 15 minutes at 200°C, temperatures were then increased to 640°C at a constant rate of 15°C/min. Temperatures were measured by a thermocouple located immediately above the sample. A FID was used for a continuous measurement of the bulk rates at which the pyrolysis products were released. For numerical determination of the kinetic parameters, Kinetics 2000 and KMOD$^{TM}$ software developed by the Lawrence Livermore National Laboratory (Burnham et al., 1987; 1988) were used. The bulk petroleum formation rate curves (Schaefer et al., 1990) were predicted using a single frequency factor and a discrete activation energy model assuming a set of parallel, independent first-order reactions **(Appendices 13, 14** and **15)** . Finally, the established kinetic models were used to extrapolate bulk hydrocarbon generation under geological heating rates (Schaefer et al., 1990; Ungerer, 1990; Schenk et al., 1997). In this study, the 15°C /min laboratory heating rate was discarded and a hypothetical geological heating rate of 3.3°C/million years (my) was assumed. This assumption is reported to be in the average range of heating conditions (3-5°C/my) typical of sedimentary basins (Dieckmann, 2005). Moreover and based on the slowest laboratory heating rate of 0.7°C, temperatures corresponding to transformation ratios of 10, 30, 50, 70 and 90% were determined **(Appendices 16, 17** and **18)** and used to carry out analyses under closed-system pyrolysis-gas chromatography.

### 2.1.5. Micro-Scale Sealed Vessel pyrolysis-gas chromatography (MSSV-GC)

Pyrolysis under closed-system-programmed-temperature was performed on 11 solvent-extracted samples by the use of the micro-scale sealed vessel (MSSV) technique developed

by Horsfield et al. (1989) in order to simulate the maturation of organic matter **(Figure 2.1)**. The combination of data from open and closed-system pyrolysis allowed the development of a compositional kinetics model and thus the prediction of the petroleum phase behaviour under subsurface conditions. This approach, termed "Phase Kinetics", consisted of three steps, these (1) being the pyrolysis under programmed heating conditions (0.7°C/min starting at 200°C), (2) the determination of the generated pyrolysis products (GC-FID), and (3) the processing of the data. First, duplicate aliquots of 5 to 15 mg of each source rock sample were weighed into one-sided closed glass capillary tubes, which were then $H_2$-flame-sealed. Each of these closed tubes was heated in an oven at specific temperatures measured with a thermocouple placed in the brass block that served as the sample holder in the furnace.
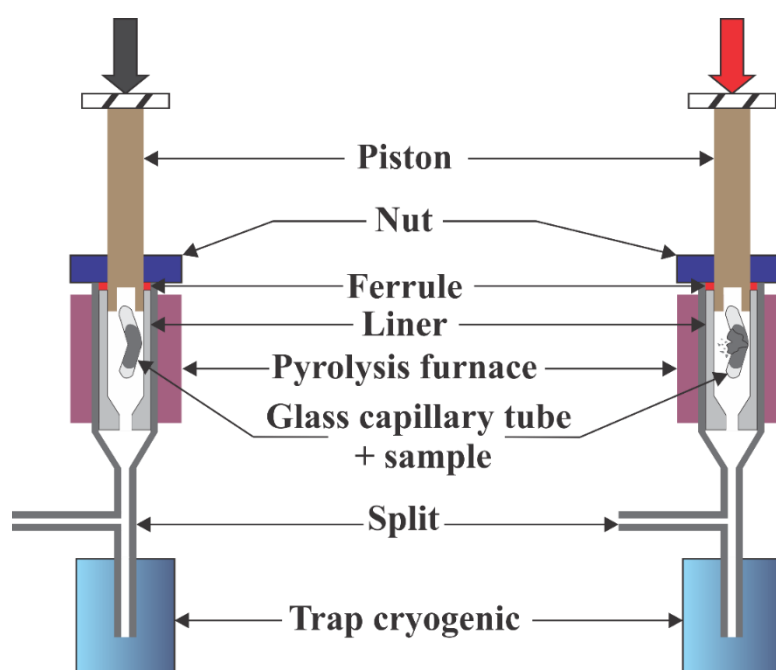


**Figure 2.1. Experimental configuration of the closed-system pyrolysis using a micro-scale sealed vessel in the pyrolysis furnace (after Horsfield and Dueppenbecker, 1991).**

The second step was to determine the composition of oil and gas formed in each tube at each temperature using the same analytical technique previously described for the open-system pyrolysis experiments (Horsfield et al., 1989; 1992). Cumulative yields of the different identifiable pyrolysis products and boiling ranges are given in **Appendices 16, 17, 18, 19, 20** and **21** with reference to an external *n*-butane standard. In addition, data derived from the MSSV-GC was used as input for phase kinetic modelling as described by di Primio and Horsfield (2006). The behaviour of the generated fluids at different pressure and temperature conditions were predicted using PVT simulation software (PVT Sim, Calsep, Denmark). The

molar composition of hydrocarbons generated by MSSV pyrolysis and PVT simulations on the pyrolysis data from the studied source rock pyrolysates at different transformation ratios (10, 30, 50, 70 and 90%) are given in **Appendices 22, 23** and **24**. The final kinetic models, developed for each of the investigated source rocks, consisted of two (oil and gas), four ($C_1$, $C_2$-$C_5$, $C_6$-$C_{14}$ and $C_{15+}$) and 14 component schemes **(Appendices 25, 26 and 27)**. In the 3D petroleum system model built for the Laminaria High-Nancar Trough area, hydrocarbon generation was simulated using models with 14 components which covered the gas to heavy liquid range ($C_1$, $C_2$, $C_3$, $i$-$C_4$, $n$-$C_4$, i-$C_5$, $n$-$C_5$, $C_6$, $C_7$-$C_{15}$, $C_{16}$-$C_{25}$, $C_{26}$-$C_{35}$, $C_{36}$-$C_{45}$, $C_{46}$–$C_{55}$ and $C_{55+}$). The heavier components ($C_7$-$C_{55+}$) were set-up to be subject to secondary cracking, with the assumption that the only generated product was methane (Dieckmann et al., 2000). The phase behaviour of a given fluid is generally described using specific physical properties (Danesh, 1998; Pedersen et al., 2012), such as saturation pressure ($P_{sat}$), formation volume factor ($B_O$) and gas to oil ratio (GOR). The $P_{sat}$ is by definition the bubblepoint pressure for an oil and the dewpoint pressure for a given gas. In other words, the $P_{sat}$ of a fluid is strongly governed by the proportion and composition of gas, where a methane-poor gas commonly results in a lower $P_{sat}$ than a comparably drier gas composition. $B_O$ is the ratio of reservoir liquid volume to surface liquid volume (in $m^3$), which is a function of fluid composition and pressure/temperature difference between the downhole and surface conditions. The predicted GORs, $B_O$ and $P_{sat}$ as a function of increasing transformation ratio (TR) are presented in **Appendices 28, 29** and **30**.

### 2.1.6. Gas chromatography-combustion-isotope ratio mass spectrometry (GC-IRMS)

Stable carbon isotopic compositions of individual light hydrocarbons (methane, ethane, propane and *n*-butane) were measured for eight solvent-extracted samples from both the Laminaria High and the Vulcan Sub-basin. No measurements of carbon isotope ratios were carried out on samples from the Gippsland Basin. For this experiment, closed-system conditions using the MSSV tubes with a heating rate of 0.7°C/min and covering the temperatures corresponding to 10, 30, 50, 70 and 90% transformation ratios were employed. The heating rates and end temperatures at which the analysed samples were heated up are given in **Appendix 28, 29** and **30**. A combined gas chromatography-isotope ratio mass spectrometry (GC-IRMS) MAT 253 instrument was used. This system consisted of a GC unit (6890N, Agilent Technology, USA) that was connected to a GCC/TC III combustion device via an open split to a MAT 253 mass spectrometer (Thermo Fisher Scientific, Germany). The GC was fitted with a Varian Poraplot Q column (50 m, i.d. 0.32 mm, film

thickness 10 μm), with helium as the carrier gas (1ml/min). The organic components of the GC effluent stream were oxidised to $CO_2$ in the combustion furnace on a CuO/Ni/Pt catalyst. The furnace was held at 940°C. The generated $CO_2$ was introduced on-line to the mass spectrometer. The gases were then injected onto the programmable temperature vaporisation inlet (PTV, Agilent Technology, USA) with a septumless head, working in split/splitless mode. The temperature of the injector was fixed to 230°C with a 1:3 split configuration. The temperature program of the GC oven was set at an initial temperature of 30°C, held isothermal for 10 minutes, then progressively heated from 30 to 150°C at 3°C/min, followed by another heating increase to 200°C at 4°C/min, and a final isothermal hold time for 15.8 min at 200°C. For each sample, the isotopic composition of $C_1$, $C_2$, $C_3$ and $n$-$C_4$ were determined on triplicate MSSV tubes to reproduce an average composition. The isotopic composition was reported in delta-notation ($\delta^{13}C$) relative to the Vienna Peedee Belemnite (VPDB) standard as defined by: $\delta^{13}C$ [‰] = [(($^{13}C$/$^{12}C$) $_{sample}$ / ($^{13}C$/$^{12}C$) $_{standard}$) -1] * 1000. The standard deviation of three similar samples was below ≤0.5 ‰ for all gas compounds.

Rock-Eval pyrolysis, open-system pyrolysis-gas chromatography, open-system pyrolysis and microscale-sealed-vessel pyrolysis-gas chromatography were used in this study and have now become standard methods employed to characterise source rocks and to develop kinetic schemes for petroleum generation. Accordingly, this thesis focuses more on the interpretation of the data, than the development of new methods. However, one should keep in mind that these aforementioned techniques do have limitations and the application of the experimentally-derived data to "geological systems" should be considered with great caution. These limitations have been extensively discussed in the literature (e.g., Burnham and Braun, 1990; Schaefer et al., 1990; Pepper and Corvi, 1995; Schenk and Horsfield, 1998; Stainforth, 2009). It is also important to mention that many of these limitations have largely been overcome by substantial improvements in the sensitivity of the analytical instruments and by continuous refinements in the concepts based on which these methods have been developed. Although beyond the scope of this study, the following section illustrates some limitations of the pyrolysis analytical methods and the validity of extrapolating laboratory-derived kinetics to geological conditions, which is one of the main objectives of this study.

The degradation of kerogen, in response to thermal stress, and its conversion into petroleum is governed by quasi-irreversible parallel and consecutive reactions (Burnham et al., 1988; Ungerer, 1990; Schenk and Dieckmann, 2004; Dieckmann, 2005). This process of kerogen cracking involves a tremendous number of chemical bonds and compounds. When cracked, these bonds are theoretically characterised by individual pairs of frequency factors and

activation energies. In contrast, and when simulated artificially under time-temperature at different heating rates, gross kinetic concepts are significantly simplified for practical computational reasons. As a result, the parallel reaction model with a single frequency factor and a distribution of activation energy is commonly employed, rendering the kinetic models too simplified for accurate timing predictions, especially in the case of heterogeneous organic matter (Dieckmann, 2005). A more reliable alternative, using pairs of frequency factors and activation energies has been proposed by Dieckmann (2005) to highlight the significant differences in kinetics sets between his model and the conventional models.

This bulk kinetic approach also has limitations in describing secondary cracking processes and products (in-source or in-reservoir oil to gas conversion) because it only gives a prediction of product generation from primary cracking caused by the thermal breakdown of kerogen into petroleum (Lewan et al., 1985; Tissot et al., 1987; Nielsen and Dahl, 1991; Pepper and Corvi, 1995; di Primio and Horsfield, 2006). Beside this, the chemical-kinetic models are not regarded as good tools in correctly describing natural product generation for source rocks which generate mainly gas and condensate (Schenk and Horsfield, 1998; Larter and di Primio, 2005).

Aside from these limitations, laboratory-derived kinetics can be sensitive to sample material. For instance, conventional core samples, which are much less common than the ubiquitous cuttings samples collected during drilling, may be more suitable for practical modelling of petroleum maturation and formation as well as for a better prediction of petroleum physical properties derived from compositional models. Likewise, differences can arise when comparing kinetic parameters obtained for kerogen concentrates (e.g. used to minimize mineral matrix effects) to those derived from whole rock samples (Horsfield and Douglas, 1980; Reynolds and Burnham, 1995).

One more limitation of the kinetic models is the uncertainty on how representative of their source rocks are the analysed samples. This is because under geological conditions, petroleum generation from an individual source rock, and even different vertical and lateral facies within a given source rock, are governed by distinct sets of kinetic parameters. Therefore, an accurate simulation and a reasonable representation of such variations remains relatively difficult to attain.

## 2.2. 3D seismic interpretation

The three-dimensional (3D) seismic method has been used for oil and gas exploration, development and production for over 30 years. The interpretation of 3D seismic data allows

the identification of potential structures where hydrocarbons can be trapped. In other terms, it helps defining the location where a well could be drilled if there is evidence of potential hydrocarbon charge. Several commercial software packages, mostly used by oil companies, were implemented to help interpreting and visualising the 3D seismic data. For instance, the Petrel software developed by Schlumberger has proven to be a powerful tool in integrating seismic and well data in 2D and 3D geological-based interpretations. The fundamentals of seismic interpretation are based on interpreting changes in the amplitude signal of seismic traces. Because large impedance contrasts at geological boundaries will generally have higher amplitudes in a seismic trace, changes in seismic amplitudes coincide with changes in geology. Amplitude variations are influenced by velocity density contrasts at bedding interfaces.

To build the 3D geological model for the Laminaria High-Nancar Trough, the following data sets were gathered and used: 3D seismic reflection data in the time domain, well data such as well coordinates (easting and northing), well headers (total depth, water depth, Kelly bushing, deviation), checkshot data, well completion reports and geological reports. Well tops and biostratigraphic data were also available in the Geoscience Australia database. Well control was provided by 35 production and exploration wells, located in the study area. The seismic dataset used in this study is part of a large (17,912 $Km^2$), merged, 3D pre-stack depth migrated seismic survey (the Vulcan Sub-basin mega survey), acquired in the late 1990s by PGS. The used data set covers the Laminaria High, the Nancar Trough and the Mallee Terrace which form some of the structural elements of the northern Bonaparte Basin, with a line spacing of 12.5 m. The extent of both the Vulcan mega survey and the seismic data used in this study are shown in **Figure 2.2**.
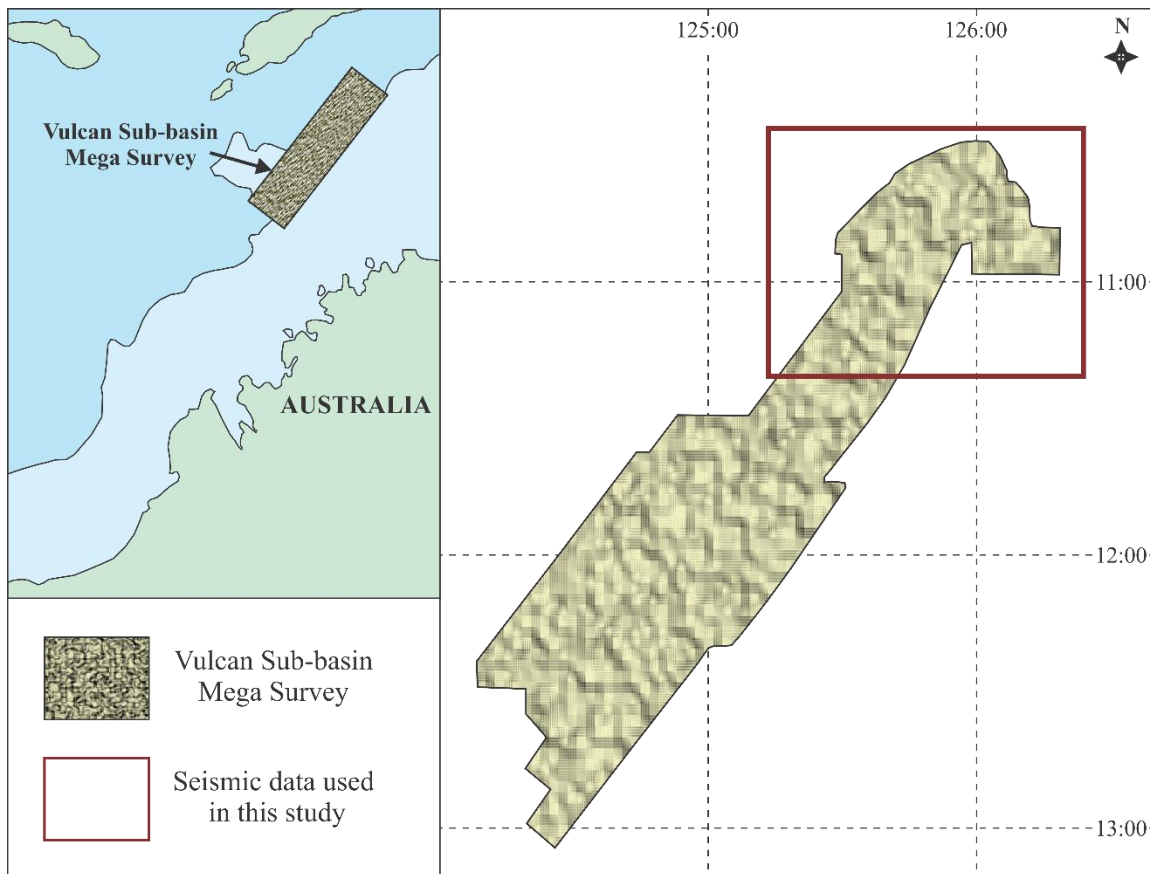
**Figure 2.2. The geographical extent of the 3D seismic survey interpreted and used to build the 3D geological model for the Laminaria High-Nancar Trough region.**

### 2.2.1. Data loading

The interpretation of the 3D seismic data used to model study area was performed using Petrel software and involved numerous steps, which are summarized in **Figure 2.3**. As a starting point, the 3D seismic data in SEG-Y format was loaded into Petrel and placed in a folder for the seismic data in the input pane. Well data such as well path trajectories and well tops or markers were listed in files which were prepared in a supported format. Similarly, these files were imported into Petrel in specific folders in the input pane.
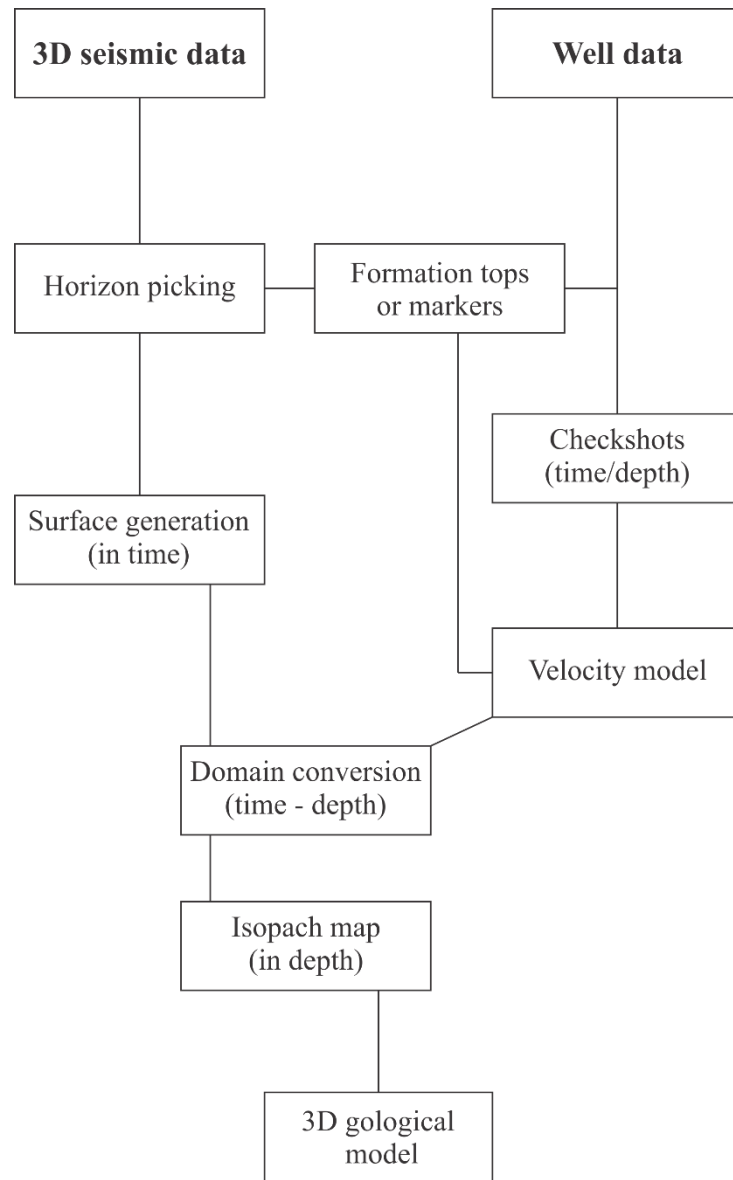
**Figure 2.3. Workflow of the 3D seismic interpretation.**

### 2.2.2. Dataset interpretation

The second stage involves horizon interpretation which was performed on inline and crossline using different tools available in seismic interpretation in the process pane. By definition, horizons delineate rocks with different densities or porosity properties. The quality of the seismic data was variable. Seismic horizons are clearly imaged from the seabed to the intra-Valanginian horizon. Below this level, it becomes more challenging to interpret the horizons (**Figure 2.4**). Thus, the manual interpretation method, which consists of picking points manually on the given horizon was preferentially used. Eight horizons were identified and mapped persistently (with a grid size of 30 x 30 lines m) throughout the study area (**Figure 2.4**). These horizons represent major geological time periods, comprising from the stratigraphically youngest to the oldest: the sea bed (SB), base Pliocene (BPLI), base

Miocene (TM3), base Cenozoic (T), top Cenomanian (KC), intra-Valanginian (KV), top Oxfordian (JO) and top Permian (Per).
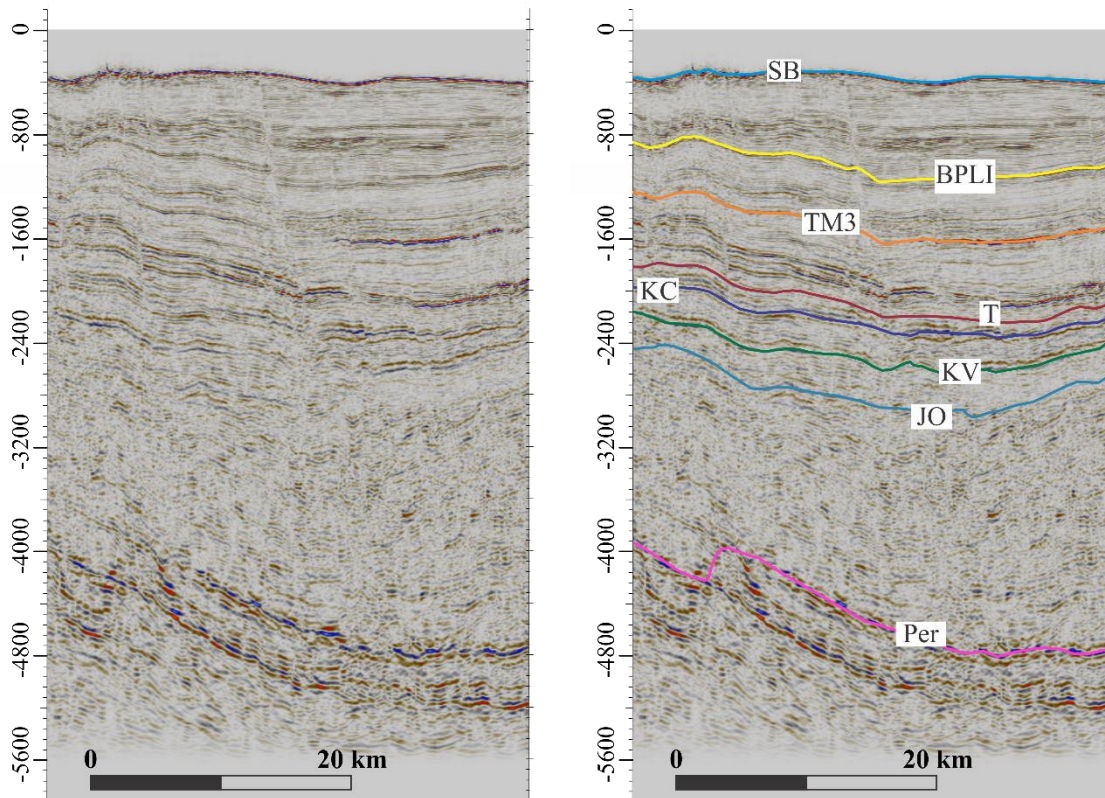


**Figure 2.4. Seismic cross section showing the eight horizons interpreted in this study.**

The definitions of these different horizons are listed in **Table 2.1**. These key horizons were traced out to honour well data. In areas, where there is a lack of well data, some segments of the horizon might have several continuation options. In this case, the horizon is traced out based on a number of hypotheses and the relation between the different reflectors. Based on the drilling results, the Laminaria reservoir is one of the main reservoir hosting hydrocarbons in the northern Bonaparte Basin; thus a special focus was given to accurately interpreting the top reservoir (JO). Possible inaccuracy in the seismic interpretation could be related to the poor seismic quality below the Valanginian marker. Following the horizon interpretations, different seismic operations, such as smoothing and interpolation methods were applied to make and edit surfaces (represented by contour lines). These stratigraphic surfaces are cut by fault surfaces, which result in a discontinuity in the trace coherence. In addition to horizon interpretations, faults are the most common structural features to consider in interpreting seismic data, as they may act as traps for hydrocarbons or as paths for fluid migration. Fault interpretations in this survey were provided by CSIRO.

**Table 2.1. Definitions and ages of the interpreted horizons on Figure 2.4**

| Horizon | Abbreviation | Definition |
|---|---|---|
| **Sea bed** | SB | Sea bed |
| **Base Pliocene** | BPLI | Base Barracouta Formation or Top Oliver Formation |
| **Base Miocene** | TM3 | Base Oliver Formation or Top Cartier Formation |
| **Base Cenozoic** | T | Base Johnson Formation or Top Turnstone Formation |
| **Cenomanian** | KC | Base Wollaston Formation or Top Jamieson Formation |
| **Intra-Valanginian** | KV | Base Echuca Shoals Formation or Top Flamingo Formation |
| **Oxfordian** | JO | Base Frigate Formation or Top Laminaria Formation |
| **Permian** | Per | Late Permian |

### 2.2.3. Domain conversion

Typically, the seismic data is displayed in time, which has to be converted to depth to allow for correlation with well data. The most difficult task is to create the most realistic velocity model by which these time maps are converted into depth maps. The workflow of this domain conversion involves two processes or steps. The first process is to make a velocity model which defines how the velocity varies in space. For defined zones comprising of a pair of surfaces (in two-way time), a velocity model was assigned. In Petrel, there is a range of methods available to define the velocity input. For example, in the constant model, a constant value ($V=V_{int}$) is assigned through the zone. In contrast, the Linvel method is based on the Linvel formula ($V=V_0 + kZ$), where Z represents the distance of the point from the datum, and where the velocity changes in the vertical direction by a factor of $K.V_0$ (velocity at the datum). The datum is by definition a constant depth, time or surface, used as a reference in measuring elevation. In the same model, a combination of these or more methods can also be used. However, the choice of the method and the accuracy of a given velocity model depend highly on the type and quality of the available data. Checkshots are time/depth pairs for a well obtained by determining the time required for seismic pulses generated by a surface energy source to reach known depths in the drilled well. These data can be used to establish time-depth conversion.The checkshot data give the most accurate measurement of vertical velocity to the bottom of the well. The second process consists of depth conversion, which used the established velocity model to generate the data conversion such as surfaces and fault interpretations.

For the purpose of depth conversion, available checkshot data were used to establish a velocity model for the Laminaria High-Nancar Trough area. Well tops were used for depth error correction. Before importing the checkshot data in Petrel (ASCII format), it was

important to make sure that the well tops were connected to individual wells. Because both checkshots and well tops are fundamental inputs into establishing a velocity model, a quality control is required to either filter or edit these data. This step was performed for each well by cross-plotting the interval velocity versus the depth (Z) and checking the outliers. This task was also conducted for the well tops. In some cases for a few wells, where there was a mismatch between a given well top with respect to its position to the time surface, these wells were not considered in the depth conversion process. Finally, the base of each interval was defined by a surface, using well tops as correction input. The velocity modelling was simulated using combined functions as previously described. The final velocity model was generated with lateral grid dimensions of 200 m x 200 m, after ensuring that the velocity model optimally ties the available well data such as the well tops. The generated products were depth maps that served as input for the 3D petroleum system modelling. This approach will be discussed in more detail in the following section.

## 2.3.    3D basin modelling approach

3D basin and petroleum system modelling is now used by petroleum companies for exploration purposes. The concept is based on numerically simulating in 3D the evolution of sedimentary basins (Welte and Yalcin, 1988; Poelchau et al., 1997) by integrating relevant geological, physical and chemical processes over geological time periods (Hantschel and Kauerauf, 2009). This integrated approach has been developed to provide insights to the burial and thermal history of a given basin and hence a better understanding of hydrocarbon generation, migration and reservoir filling. The potential of 3D basin models is to offer a range of strategies for petroleum activity in unexplored areas, and to optimise and predict risks in basins with ongoing petroleum exploration. However, uncertainties remain in terms of an accurate prediction of a petroleum accumulation's size and quality, even when the petroleum system is well known. These limitations and restrictions have widely described by numerous authors such as Ungerer (1990), Nielsen (1996) and Yalcin et al. (1997). The processes and inputs required to build the 3D model are illustrated in **Figure 2.5**; each process, including modelling principles and analytical equations used in the simulation, has been described in detail by Hantschel and Kauerauf (2009).

**INPUTS**

| **Present day geometry**<br>- Depth maps<br>- Lithologies<br>- Ages<br>- Faults, etc. | **Palaeo-geometry**<br>- Palaeo water depth<br>- Erosion, hiatus, etc. | **Boundary conditions**<br>- Sediment-water<br>interface temperature<br>- Heat flow, etc. |

**Burial history**
(Burial rates)

**Thermal history**
(Model calibration)

**Maturity data**
(Formation Temperatures
VR, Tmax, FAAM, etc)

**INPUTS**

**SIMULATION
+
OUTPUTS**

**Hydrocarbon generation**
(Transformation ratios,
temperature distribution)

**Source rock properties**
(TOC, HI, kinetics)

**Hydrocarbon migration**
(Accumulation locations,
oil and gas volumes)

**Fluid analysis**
(Fluid composition: GOR)

**Sensitivity analysis**

**Figure 2.5. Chart illustrating the workflow and the inputs used in the 3D petroleum system modelling.**

### 2.3.1. Input data and model conception

For the Laminaria High-Nancar Trough, basin modelling was carried out using the 3D basin modelling software PetroMod® (version 2012), developed by IES-Schlumberger in Aachen, Germany. The acquisition of data from regional geological studies, from wells and from seismic interpretation is the first step of basin modelling. In this study, data were gathered mainly from well completion reports, high resolution seismic interpretations and geochemical analyses, which were all mostly available from the open-file database at Geoscience Australia (http://dbforms.ga.gov.au/www/npm.well.search). Additional information was gained from published literature and unpublished reports.

55

An accurate reconstruction of the present day basin's geometry and the identification of the major events during the basin's evolution is the most delicate step in the basin modelling. The structural framework of the Laminaria High-Nancar Trough region was set-up based on the eight depth-converted seismic surfaces (see previous section). In addition to these primary surfaces, further subdivision into discrete chronological events was made, with a spatial resolution of 200 x 200 m, to reproduce the known stratigraphy. The final 3D basin model was represented by 19 events including the basement layer. For each event, numerous parameters were assigned (**Figure 2.6**). Relative ages of the respective units were defined using the lithostratigraphic chart of the northern Bonaparte basin. The chronostratigraphy was defined in accordance with the International Geological Time Scale (Cohen et al., 2012). Lithologies were assembled based on well logs, rock sample descriptions and geological knowledge, which show only minor vertical and lateral variations in the facies. Thus, no lateral facies variations were taken into account and only homogeneous lithologies were assigned for each stratigraphic unit. Lithologies were created by mixing two or three default lithologies using the lithology editor tool in PetroMod®. Thermal properties and compaction behaviour were automatically adopted from the default values available in PetroMod® internal databases. Based on the seismic and well data, there was no significant erosional event to influence the thermal maturity modelling. Therefore, no erosion was considered in the model. Although some unconformities were present, these were assumed to have had no significant effect on the heat flow history. Given the regional scale of the study area, other simplifications were made; these simplifications were discussed in detail by Abbassi et al. (2014c). Other input definitions included the faults (e.g. open versus closed), which were considered in the simulation of hydrocarbon migration and accumulation. In order to avoid an excessive number of gridpoints, only major and deep faults were incorporated in the model. These faults were generally associated with the Jurassic rifting phase and then reactivated during Cenozoic times. Key input data for the modelling also comprised palaeo-water depths and the sediment-water interface temperature (SWIT). Palaeo-bathymetry is essential in depicting the palaeo-surface topography and thus the structural pattern which controls the thermal maturity of the source rock units and migration pathways. The absolute palaeo-water depths employed in the model were interpolated based on micropalaeontological data available in the Geoscience Australia database (http://dbforms.ga.gov.au/www/npm.well.search).
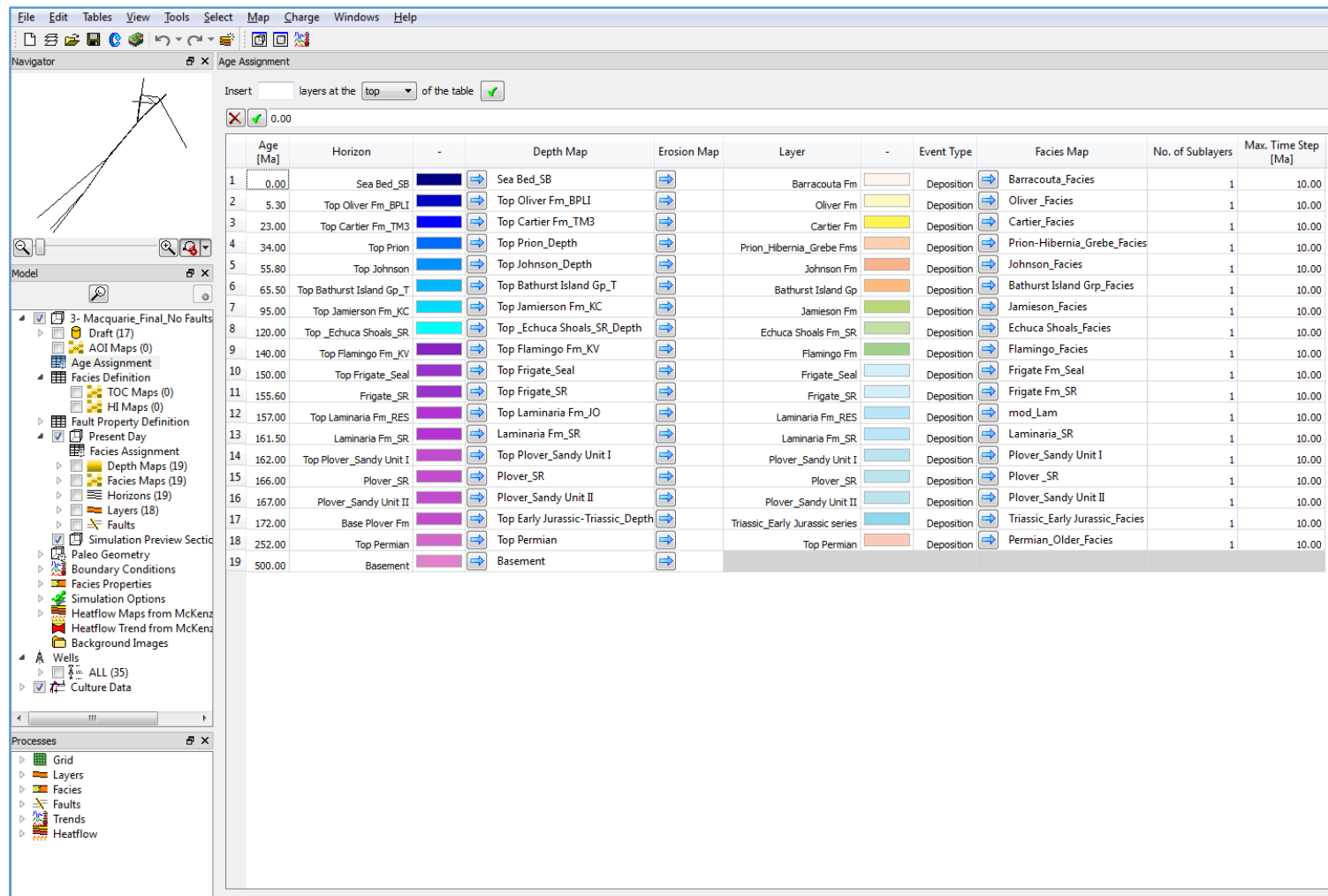
**Figure 2.6. Stratigraphic units and their depositional duration applied in the model.**

The temperatures at the sediment-water interface were assigned based on the time-latitude diagram proposed by Wygrala (1989), which is an implemented feature of the Petromod software (**Figure 2.7**). These temperatures are influenced by the water depth, the paleogeographic position, and oceanic currents.
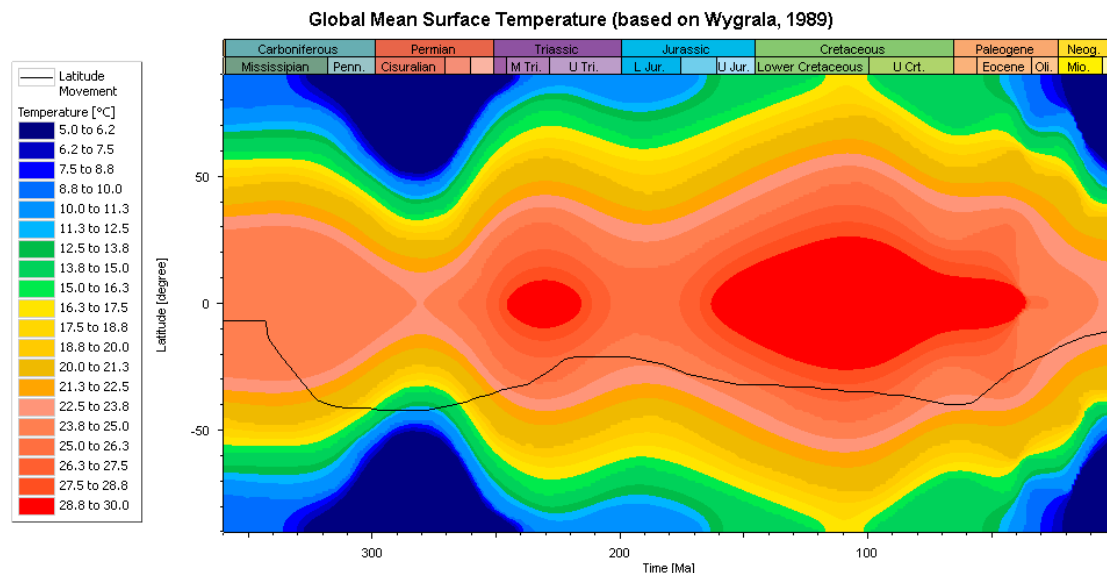


**Figure 2.7. Plot of surface ocean temperatures versus latitude versus geological time (Wygrala, 1989).**

For the petroleum system elements, two main sandstone units within the Plover and the Laminaria formations were considered with reservoir properties. The seal was provided by the shales of the Upper Jurassic Frigate and Flamingo formations and the Lower Cretaceous Jamieson Formation. The traps considered in the model were of the structural type. Four units within the Jurassic (the Plover, Laminaria and Frigate formations), and the Lower Cretaceous Echuca Shoals Formation were defined as potential source rocks. The thicknesses of most of these elements were approximately estimated based on stratigraphic data from well completion reports. For example, only a few of the drilled wells have reached the Plover Formation source rock unit. For this reason, the information about the composition of this unit and those below the upper sandy unit of the Plover Formation, is scarce. **Figure 2.8** shows the thickness maps of the four source rocks included in the model.

For each source rock layer, input values of total organic carbon (TOC) and hydrogen index (HI) were assigned based on average values reported in previous studies (e.g. Preston and Edwards, 2000) and/or calculated from the Geoscience database (**Figure 2.9**). The entire estimated thickness of individual source rock layers was considered as a generating interval with constant TOC and HI values.
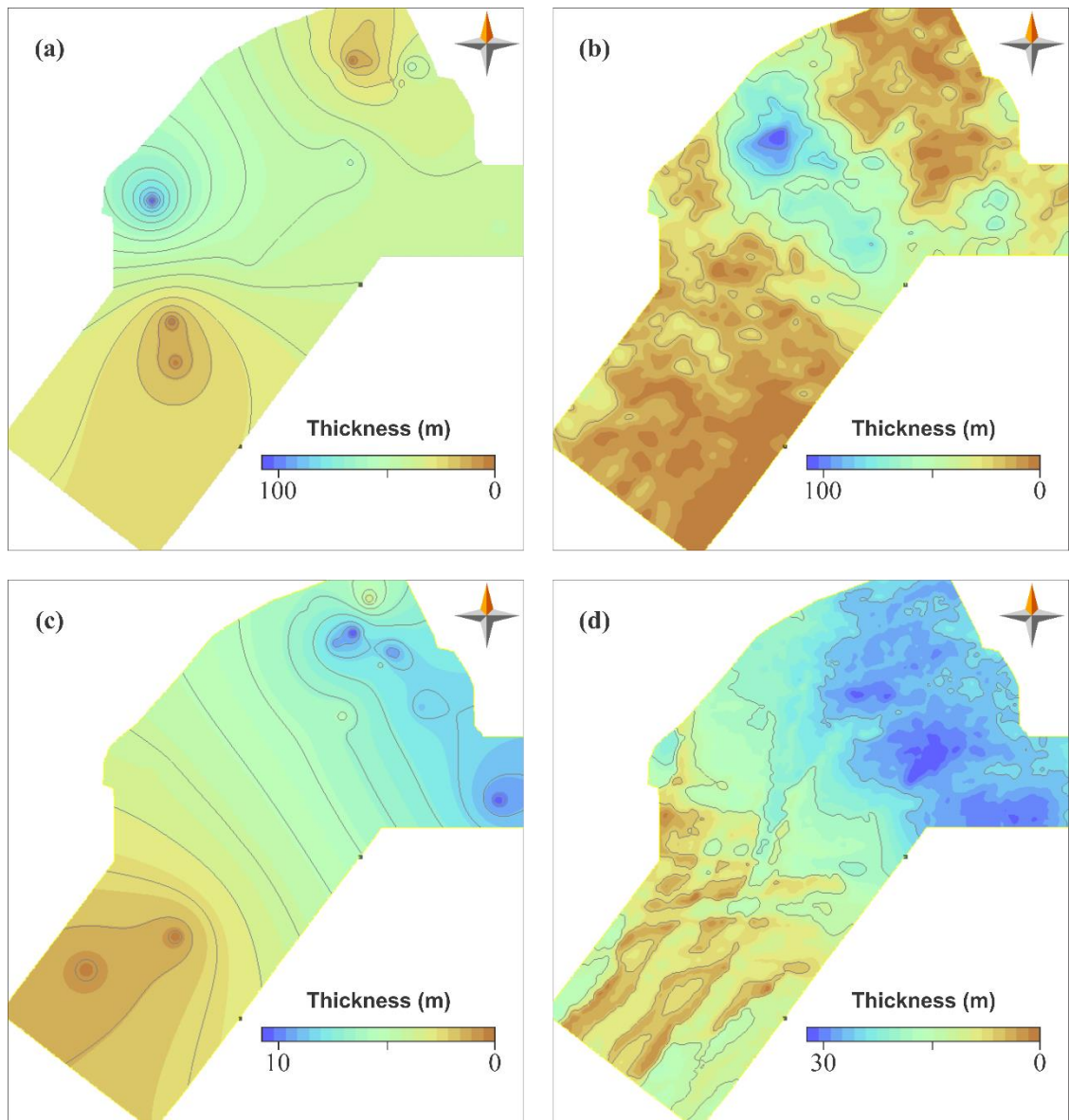
**Figure 2.8. Thickness maps of the source rocks units considered in the model. (a) Echuca Shoals Formation, (b) Frigate Formation, (c) Laminaria Formation and (D) Plover Formation.**

### 2.3.2. Model calibration

The second and the most challenging phase of the 3D basin modelling was to reconstruct the thermal history of the study area. Thermal maturity data such as formation temperatures (from drill stem test (DST) and bottom-hole temperatures (BHTs)), vitrinite reflectance (%$R_0$) and $T_{max}$ from Rock-Eval pyrolysis from 31 exploration and production wells drilled within the study area were used to calibrate the 3D model. These data were collected from well completion reports and the Geoscience Australia database.
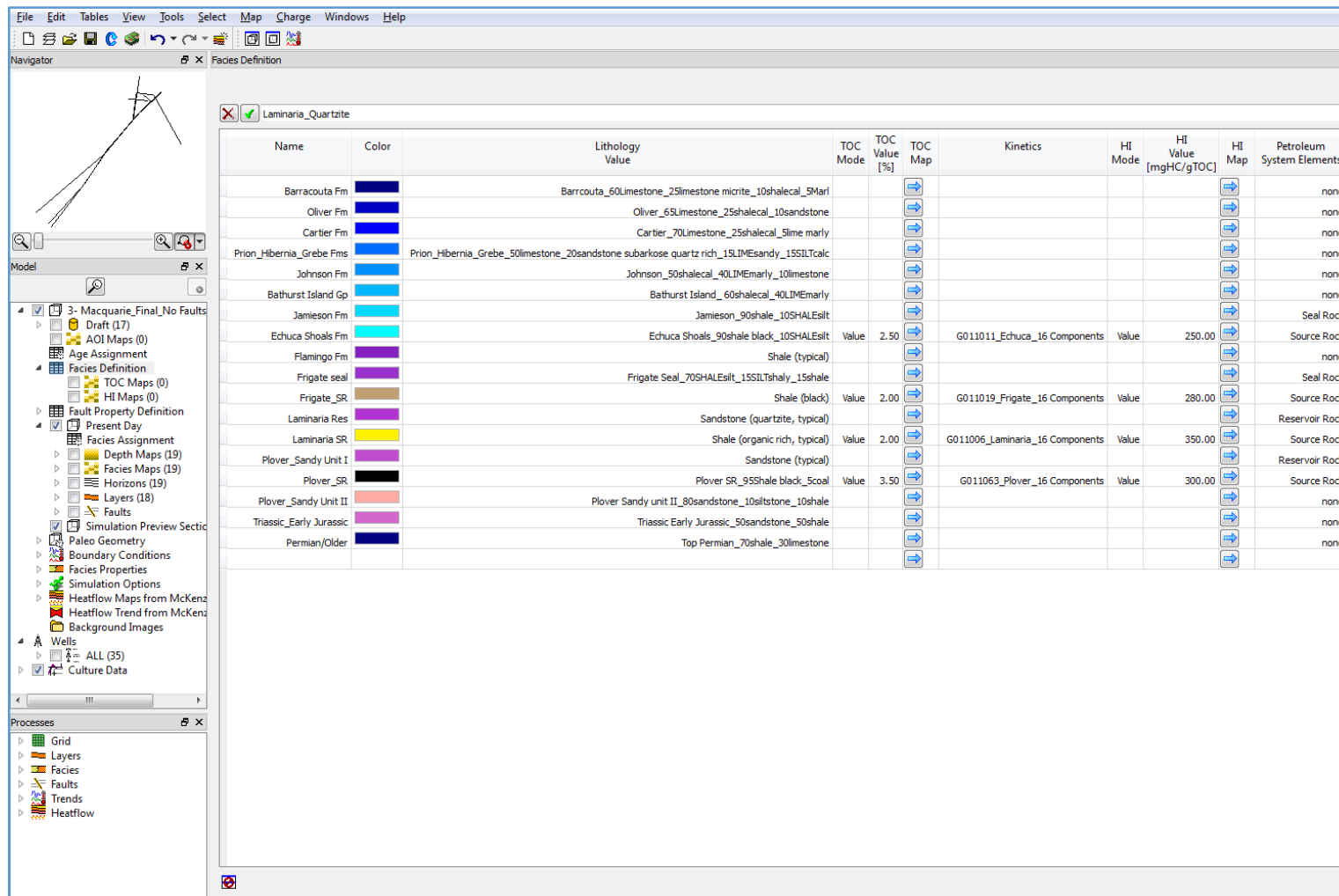
Figure 2.9. The stratigraphic units and their assigned lithologies including the petroleum system elements and their properties.

The present day heat flow was assessed based on the formation temperatures. The scenario that allowed the best calibration to these data, suggested values varying from 67 to 75 mW/m$^2$ across the study area. Variable heat flow history was defined using four heat flow maps with a similar pattern distribution, which were generated and used to constrain the evolution of the study area's thermal history. The Laminaria High-Nancar Trough region has been mainly influenced by the Jurassic phase of lithospheric stretching, during which time the heat flow might have been higher than the present-day value. A stretching factor of approximately 1.5 was estimated based on a published modelling study in the Vulcan Sub-basin (Kennard et al., 1999), following the approach of McKenzie (1978). Therefore, the general heat flow trend consisted of assigning the present day heat flow as the background value. Then, average values of 80 to 100 mW/m$^2$ during the rift phase were allocated and followed by an exponential post-rift thermal decay to the present day values. A good calibration of the model was achieved by a reasonable match and adjustment between the measured vitrinite reflectance and the calculated curve (EASY %R$_0$), which used the chemical kinetic model of vitrinite reflectance as defined by Sweeney and Burnham (1990).

### 2.3.3. Outputs and sensitivity analyses

After a successful model calibration to the maturity data, the simulation of petroleum generation and migration was performed. In addition to the TOC and HI values implemented for each of the source rock layers, kinetics models for petroleum generation and cracking were required as inputs in the model. The compositional kinetic models applied in all of the numerical models were those measured for immature samples representing the four source rocks considered in the model. The Plover Formation is mainly made of organic-rich shales and sandstones intercalated with thin coal beds. The contribution of the coals of the Plover Formation could not be confirmed and therefore only the shales were considered in the 3D model. The developed models were acquired using open- and closed-system pyrolysis techniques and were based on a 14 component scheme following the methodology of di Primio and Horsfield (2006). Hydrocarbon migration was simulated using the hybrid method implemented in PetroMod®. The hybrid method allows rapid simulation (computing time). It combines a Darcy flow model which takes into account the most important driving forces such as pressure and temperature in areas of low permeabilities and the flow path model which is applied in areas of higher permeabilities (Hantschel and Kauerauf, 2009). Accordingly, the physical properties of the generated fluids such as gas:oil ratios were predicted and compared to those measured on natural fields in the Laminaria High-Nancar Trough region. Similarly, accumulation predictions were calibrated against known fields in

the area. As a final phase of the 3D basin model built for the Laminaria High-Nancar Trough area, several sensitivity analyses were carried out to check individual or combined impacts of certain input parameters that might affect fluid accumulation and property predictions. These parameters included variation in the heat flow history and source rock properties. A special emphasis was given to sensitivity analyses with respect to different scenarios in which fault properties were varied.

## 2.4.    References

Abbassi, S., George, S.C., Edwards, D.S., di Primio, R., Horsfield, B., Volk, H., 2014c. Generation characteristics of Mesozoic syn- and post-rift source rocks, Bonaparte Basin, Australia: New insights from compositional kinetic modelling. Marine and Petroleum Geology 50, 148-165.

Behar, F., Beaumont, V., Penteado, H.D.B., 2001. Rock-Eval 6 technology: performances and developments. Oil & Gas Science and Technology 56, 111-134.

Burnham, A.K., Braun, R.L., 1990. Development of a detailed model of petroleum formation, destruction, and expulsion from lacustrine and marine source rocks. Organic Geochemistry 16, 27-39.

Burnham, A.K., Braun, R.L., Samoun, A.M., 1988. Further comparison of methods for measuring kerogen pyrolysis rates and fitting kinetic parameters. Organic Geochemistry 13, 839-845.

Burnham, A.K., Braun, R.L., Gregg, H.R., Samoun, A.M., 1987. Comparison of methods for measuring kerogen pyrolysis rates and fitting kinetic parameters. Energy & Fuels 1, 452-458.

Cohen, K., Finney, S., Gibbard, P., 2012. International Chronostratigraphic Chart: International Commission on Stratigraphy: 34th International Geological Congress, Brisbane, Australia.

Danesh, A., 1998. PVT and phase behaviour of petroleum reservoir fluids. Developments in petroleum science. Elsevier, 47, 388 p.

di Primio, R., Horsfield, B., 2006. From petroleum-type organofacies to hydrocarbon phase prediction. American Association of Petroleum Geologists Bulletin 90, 1031-1058.

Dieckmann, V., 2005. Modelling petroleum formation from heterogeneous source rocks: the influence of frequency factors on activation energy distribution and geological prediction. Marine and Petroleum Geology 22, 375-390.

Dieckmann, V., Horsfield, B., Schenk, H., 2000. Heating rate dependency of petroleum-forming reactions: implications for compositional kinetic predictions. Organic Geochemistry 31, 1333-1348.

Hantschel, T., Kauerauf, A.I., 2009. Fundamentals of basin and petroleum systems modeling. Springer-verlag, Berlin, Heidelberg, p. 492.

Horsfield, B., 1989. Practical criteria for classifying kerogens: some observations from pyrolysis-gas chromatography. Geochimica et Cosmochimica Acta 53, 891-901.

Horsfield, B., Douglas, A.G., 1980. The influence of minerals on the pyrolysis of kerogens. Geochimica et Cosmochimica Acta 44, 1119-1131.

Horsfield, B., Dueppenbecker, S.J., 1991. The decomposition of Posidonia Shale and Green River Shale kerogens using microscale sealed vessel (MSSV) pyrolysis. Journal of Analytical and Applied Pyrolysis 20, 107-123.

Horsfield, B., Disko, U., Leistner, F., 1989. The micro-scale simulation of maturation: outline of a new technique and its potential applications. Geologische Rundschau 78, 361-374.

Horsfield, B., Schenk, H., Mills, N., Welte, D., 1992. An investigation of the in-reservoir conversion of oil to gas: compositional and kinetic findings from closed-system programmed-temperature pyrolysis. Organic Geochemistry 19, 191-204.

Kennard, J.M., Deighton, I., Edwards, D.S., Colwell, J.B., O'Brien, G.W., Boreham, C.J., 1999. Thermal history modelling and transient heat pulses: new insights into hydrocarbon expulsion and 'hot flushes' in the Vulcan Sub-basin, Timor Sea. Australian Petroleum Production and Exploration Association Journal 39(1), 177-207.

Lafargue, E., Marquis, F., Pillot, D., 1998. Rock-Eval 6 applications in hydrocarbon exploration, production, and soil contamination studies. Oil & Gas Science and Technology 53, 421-437.

Larter, S.R., di Primio, R., 2005. Effects of biodegradation on oil and gas field PVT properties and the origin of oil rimmed gas accumulations. Organic Geochemistry 36, 299-310.

Lewan, M.D., Spiro, B., Illich, H., Raiswell, R., Mackenzie, A.S., Durand, B., Manning, D.A.C., Comet, P.A., Berner, R.A., De Leeuw, J.W., 1985. Evaluation of petroleum generation by hydrous pyrolysis experimentation. Philosophical Transactions of the Royal Society of London. Series A 315, 123-134.

Mahlstedt, N., Horsfield, B., Dieckmann, V., 2008. Second order reactions as a prelude to gas generation at high maturity. Organic Geochemistry 39, 1125-1129.

McKenzie, D., 1978. Some remarks on the development of sedimentary basins. Earth and Planetary Science Letters 40, 25-32.

Nielsen, S.B., 1996. Sensitivity analysis in thermal and maturity modelling. Marine and Petroleum Geology 13, 415-425.

Nielsen, S.B., Dahl, B., 1991. Confidence limits on kinetic models of primary cracking and implications for the modelling of hydrocarbon generation. Marine and Petroleum Geology 8, 483-492.

Pedersen, K.S., Christensen, P.L., Shaikh, J.A., 2012. Phase behavior of petroleum reservoir fluids. CRC Press, Taylor & Francis Group, Raton, FL.

Pepper, A.S., Corvi, P.J., 1995. Simple kinetic models of petroleum formation. Part I: oil and gas generation from kerogen. Marine and Petroleum Geology 12, 291-319.

Poelchau, H., Baker, D., Hantschel, T., Horsfield, B., Wygrala, B., 1997. Basin simulation and the design of the conceptual basin model, Petroleum and basin evolution. Springer, pp. 3-70.

Preston, J.C., Edwards, D.S., 2000. The petroleum geochemistry of oils and source-rocks from the northern Bonaparte Basin, offshore northern Australia. Australian Petroleum Production and Exploration Association Journal 40(1), 257-282.

Reynolds, J.G., Burnham, A.K., 1995. Comparison of kinetic analysis of source rocks and kerogen concentrates. Organic Geochemistry 23, 11-19.

Schaefer, R.G., Schenk, H.J., Hardelauf, H., Harms, R., 1990. Determination of gross kinetic parameters for petroleum formation from Jurassic source rocks of different maturity levels by means of laboratory experiments. Organic Geochemistry 16, 115-120.

Schenk, H.J., Horsfield, B., 1998. Using natural maturation series to evaluate the utility of parallel reaction kinetics models: an investigation of Toarcian shales and Carboniferous coals, Germany. Organic Geochemistry 29, 137-154.

Schenk, H.J., Dieckmann, V., 2004. Prediction of petroleum formation: the influence of laboratory heating rates on kinetic parameters and geological extrapolations. Marine and Petroleum Geology 21, 79-95.

Schenk, H.J., Horsfield, B., Krooss, B., Schaefer, R.G., Schwochau, K., 1997. Kinetics of petroleum formation and cracking. In: Welte, D.H., Horsfield, B., Baker, D.R. (Eds.), Petroleum and Basin Evolution. Springer, Verlag, Berlin, Heidelberg, pp. 231-269.

Stainforth, J.G., 2009. Practical kinetic modeling of petroleum generation and expulsion. Marine and Petroleum Geology 26, 552-572.

Sweeney, J.J., Burnham, A.K., 1990. Evaluation of a Simple Model of Vitrinite Reflectance Based on Chemical Kinetics. American Association of Petroleum Geologists Bulletin 74, 1559-1570.

Tissot, B., Pelet, R., Ungerer, P., 1987. Thermal history of sedimentary basins, maturation indices, and kinetics of oil and gas generation. American Association of Petroleum Geologists Bulletin 71, 1445–1466.

Ungerer, P., 1990. State of the art of research in kinetic modelling of oil formation and expulsion. Organic Geochemistry 16, 1-25.

Welte, D., Yalcin, M., 1988. Basin modelling—a new comprehensive method in petroleum geology. Organic Geochemistry 13, 141-151.

Wygrala, B., 1989. Integrated Study of an Oil Field in the Southern Po Basin. Berichte der Forschungszentrum Jülich 2313, 1-217.

Yalcin, M., Littke, R., Sachsenhofer, R., 1997. Thermal history of sedimentary basins, Petroleum and basin evolution. Springer, pp. 71-167.

# Chapter 3.

## Petroleum potential and kinetic models for hydrocarbon generation from the Upper Cretaceous to Paleogene Latrobe Group coals and shales in the Gippsland Basin, Australia

Soumaya Abbassi[1], Dianne S. Edwards[2], Simon C. George[1], Herbert Volk[3, a], Rolando di Primio[4], Brian Horsfield[4]

1. Department of Earth and Planetary Sciences, Macquarie University, Sydney, NSW 2109, Australia

2. Geoscience Australia, GPO Box 378, Canberra, ACT 2601, Australia

3. CSIRO, PO Box 136, North Ryde, NSW 1670, Australia

a. Present Address: BP Exploration Company, Sunbury-on-Thames, UK

4. Helmholtz Centre Potsdam, GFZ - German Research Centre for Geosciences, Germany

### *Statement of authors' contribution*

This Chapter is a final version of a manuscript that is expected to be submitted to *Organic Geochemistry* in October 2014. This paper has been formatted to conform to the font and referencing style adopted in the thesis. Figures and tables included within the text are prefixed with the chapter number.

I am the primary author. I examined data and prepared the samples used in this study, including sample selection, sampling and grinding (except for four samples that were collected and processed by Dianne Edwards). I performed open-system pyrolysis-gas chromatography measurements. Rock-Eval pyrolysis data acquired for samples used in this study was performed by Geoscience Australia and Geotechnical Services Pty Ltd, excluding sample preparation. Bulk and compositional kinetic experiments (excluding sample preparation) were performed by Ferdinand Perssen (GFZ, Potsdam). I processed and interpreted all the data derived from all the conducted measurements which are related to the paper. I wrote and designed the paper's structure. Simon George, Rolando di Primio, Dianne Edwards and Herbert Volk carefully reviewed and provided feedbacks and various refinements on the manuscript. Neither this manuscript nor one with similar content under our authorship has been published or is being considered for publication elsewhere, except as described and expected above.

# Abstract

The Upper Cretaceous to Paleogene sediments of the Latrobe Group in the Gippsland Basin contain different types of kerogen including Type III, Type II/III, Type II and Type I/II. Interbedded shales, shaly coals and coals, deposited within delta plain facies throughout the Santonian to Paleocene Golden Beach and Halibut subgroups, contain land-plant-dominated organic matter with variable potential for both gas and liquid hydrocarbon generation. Exceptions are oil-prone, hydrogen-rich shales and shaly coals deposited in lacustrine and lagoonal environments, as sampled from the Paleocene *L. balmei,* Maastrichtian *F. longus* and late Campanian *T. lilliei* palynological zones, which also contain variable proportions of algal remains in addition to the typical land-plant input. A lacustrine algal-rich shale was also sampled from the Turonian (Emperor Subgroup) *P. mawsonii* palynological biozone.

Based on this sample set, the open-system pyrolysis-gas chromatography results indicate that the late Campanian to Paleocene palynofacies are heterogeneous, being capable of generating both low and high wax paraffinic−naphthenic−aromatic (P-N-A) oils, and paraffinic oils with a high wax content. On the basin margins, a few wells penetrate organically-lean marginal marine shales of the older Santonian−early Campanian *T. apoxyexinus* and *N. senectus* biozones, which are demonstrated to produce gas and condensate. The distribution of activation energies determined for the Latrobe Group samples also shows that none of these biozones have a uniform kinetic composition. Assuming a constant geological heating rate of 3.3°C/Ma, kinetic modelling predicts that the main phase of petroleum formation from the Latrobe Group occurs between 150°C and 179°C, indicating different orders of kinetic stability as a result of the different types of organic matter and their state of preservation. Compositional kinetics and phase behaviour indicate that these sediments generate black oils at the early stages of kerogen cracking, and either light oils or gases and condensates at higher levels of thermal stress. These findings indicate that upon thermal maturation, the interbedded shales and shaly coals of the Latrobe Group can form the source of both oil and gas in the Gippsland Basin. Where sampled, coals from the *F. longus* and *L. balmei* biozones have lower HI values than are required for efficient oil expulsion. This finding, coupled with their relatively low proportion with respect to shales, suggests that the coals may not have contributed significant volumes of hydrocarbons to the oil and gas accumulations.

**Keywords:** Gippsland Basin, Latrobe Group, coals, shales, gas:oil ratio, kinetic model, petroleum formation

## 3.1. Introduction

The potential of coal-bearing sequences to generate and expel liquid hydrocarbons has been the topic of several studies and reviews (e.g. Saxby and Shibaoka, 1986; Littke et al., 1989; Hunt, 1991; Collinson et al., 1994; Killops et al., 1994; Pepper and Corvi, 1995; Boreham et al., 1999; Wilkins and George, 2002; Ahmed et al., 2009; Sykes et al., 2014). Many of these studies have demonstrated that the broad chemical and physical heterogeneity of coals accounts for variable potential for oil generation. These heterogeneities are reported to be controlled by the maceral content and thus the depositional environment under which coals were deposited (Durand and Paratte, 1983; Diessel, 1992; George et al., 1994; Petersen and Rosenberg, 1998; Sykes, 2001). Although numerous oil accumulations have been discovered in sedimentary basins in Australia (e.g. Cooper and Gippsland basins), Indonesia (e.g. Ardjuna and Kutai basins) and New Zealand (Buller Coalfield and Taranaki Basin) that are filled with non-marine sediments, some authors have, however, resisted the idea that coals have the ability to charge oil fields (e.g. Teerman and Hwang, 1991). One argument against coals being effective oil source rocks is the fact that oil with a land- plant geochemical signature may be derived from terrigenous organic matter in shales rather than from genuine coals (Sun et al., 2000). Hunt (1991) states that whilst significant amounts of oil can be generated from hydrogen-rich coals, the adsorptive capacity and pore size distribution of coals is a limiting factors for efficient expulsion.

The Gippsland Basin is a mature hydrocarbon province in southeastern Australia, which hosts oil (e.g. Flounder, Halibut, Fortescue, Cobia, and Kingfish) and gas (e.g. Barracouta, Snapper, Marlin and Tuna) accumulations (**Figure 3.1** and **Figure 3.2**). Fluvial coals of the Turonian−early Oligocene Latrobe Group have typically been proposed as the sources of the oil and gas fields (Smith and Cook, 1984; Shanmugam, 1985). Several authors (Alexander et al., 1987; Moore et al., 1992; Murray et al., 1998) have suggested that fluvial and lacustrine shales and coaly shales also contributed to the petroleum accumulations in the basin, or may indeed be the main source rocks. The interbedded nature of organic-rich shales, coaly shales and coals makes it difficult to determine which of these lithologies acted as oil source rocks. This study aims to decipher the potential source rock facies variability and provide insights into the hydrocarbon generation characteristics of the Emperor, Golden Beach and Halibut subgroups of the Latrobe Group in order to better understand the active petroleum systems in the Gippsland Basin.

## 3.2. Geological background and petroleum geology

### 3.2.1. Tectonic setting

The Gippsland Basin is an east–west trending failed rift basin located on Australia's south-eastern margin. The basin covers an approximate area of $56\,000\,\text{km}^2$ (Smith, 1982), of which only one third is onshore. The basin initially developed during the rifting of Australia from Antarctica, as a response to the Early Cretaceous Gondwana break-up (Rahmanian et al., 1990; Willcox et al., 1992; Norvick and Smith, 2001). This initial rifting event led to the formation of a series of major fault systems that subdivide the basin into several structural features. The Central Deep is the primary depocentre and is bounded to the north and south by relatively stable platforms, the Northern and Southern platforms and terraces (Bernecker and Partridge, 2001; Power et al., 2001). The onshore part of the Gippsland Basin comprises the Seaspray and Lake Wellington depressions to the south, which represent the onshore extensions of the Central Deep and Northern Terrace, respectively (Figure 3.1). These areas are delimited by a number of faults such as the Darriman and Foster faults on the southern basin margin, and the Rosedale and Lake Wellington faults on the northern margin (Figure 3.1).

The continuing rifting and separation of Australia from Antarctica was punctuated during the mid-Cretaceous by significant uplift and erosion events (Dumitru et al., 1991; Duddy and Green, 1992). Following these events, the depocentre shifted to the east. The second rift phase, principally related to the Tasman Sea spreading, occurred from the Late Cretaceous to the early Eocene and was responsible for the reactivation of the underlying Early Cretaceous and basement structures. Compression was initiated in the late Eocene and continued through to the middle Miocene, during which time a series of NE-SW trending anticlines formed. This inversional tectonism was due to intra-plate stress effects resulting in widespread erosion across the basin. By the end of the Eocene, the spreading of the Tasman Sea ceased, but faster spreading between Australia and Antarctica began (Veevers et al., 1991; Hill et al., 1995). Localised uplift took place during the late Miocene–Pliocene as recognised by an angular unconformity in the onshore part of the basin (Dickinson et al., 2002). The Pleistocene to the present-day is a period of reactivation and tectonic activity close to major fault systems (Holdgate et al., 2003).

**Figure 3.1. Regional map showing the location of the Gippsland Basin, the main structural elements and the hydrocarbon discoveries. Wells from which samples were taken for this study are shown in blue text. Modified from O'Brien et al. (2013).**

### 3.2.2. Stratigraphic setting

The multiple extensional and basin inversion phases have influenced both the sedimentation type and rate in the Gippsland Basin (Brown, 1986; Gibson-Poole et al., 2008). The stratigraphic succession **(Figure 3.2)** in the basin commenced in the Early Cretaceous with the deposition of thick non-marine arkoses and fluvial volcaniclastic-rich sediments of the Strzelecki Group (Holdgate and McNicol, 1992; Willcox et al., 1992). This group, deposited during the syn-rift phase, comprises interbedded sandstones, mudstones and several coal-rich units. The Upper Strzelecki Group includes volcanic sediment input following a period of igneous activity during the Barremian (Norvick, 2005). The top of the Strzelecki Group is marked by the Otway unconformity (Cenomanian) corresponding to uplift and erosion along the basin margins (Hill et al., 1995). The second major sedimentary sequence is the Latrobe Group, which was deposited during the second phase of rifting to the early post-rift. Four subgroups have been defined within this group; Emperor, Golden Beach, Halibut and Cobia, each of which is bounded by basin-wide unconformities. The Turonian−Coniacian Emperor Subgroup consists of marginal coarse-grained alluvial fan/plain (the Kersop Arkose) as well as lacustrine facies forming the Kipper Shale (Lowry and Longley, 1991). This shaly formation is interfingered by the Curlip Formation, which is made up of sandstones and conglomerates that are interbedded with thin shales and minor coals. The basin-wide Longtom Unconformity terminates deposition of the Emperor Subgroup (Partridge, 1999).

The Santonian−Campanian Golden Beach Subgroup, essentially confined to the Central Deep, is represented by two formations, the marine Anemone Formation and the fluvial Chimaera Formation (Bernecker and Partridge, 2001). The Anemone Formation is restricted to the eastern part of the basin and consists predominantly of mudstones and shales. The Chimaera Formation is missing on the Northern Platform and Northern Terrace, but elsewhere it consists of coarse-grained alluvial/fluvial sediments, as well as fine-grained floodplain deposits including some coals. Volcanic units are recognised within and toward the top of the Golden Beach Subgroup (Bernecker and Partridge, 2001). The Seahorse Unconformity corresponds to a depositional hiatus and separates the Golden Beach Subgroup from the overlying the Halibut Subgroup.

Renewed crustal extension during the Turonian to early Campanian resulted in rapid subsidence that developed across the basin (Veevers et al., 1991).
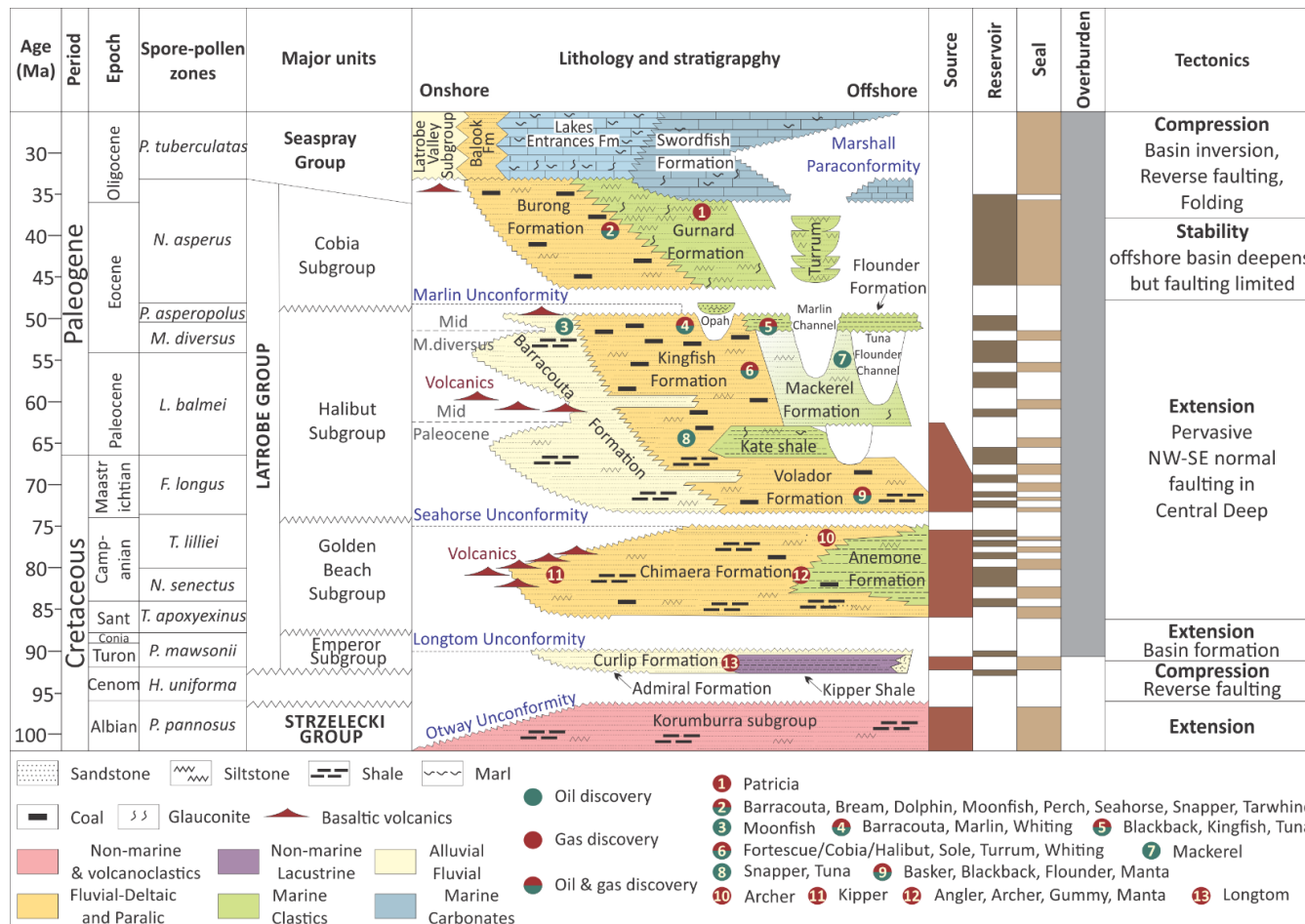
**Figure 3.2. Stratigraphy of the Gippsland Basin, showing lithologies, depositional environments, and main gas and oil discoveries. Also shown are the potential petroleum system elements and the main tectonic events. Modified after Bernecker and Partridge (2001). Cenom = Cenomanian, Turon = Turonian, Conia = Coniacian, Sant = Santonian.**

During the Late Cretaceous to Paleogene, a post-rift marginal sag basin developed and sediments of the upper Latrobe Group (Halibut and Cobia subgroups) were deposited under the influence of the widening of the Tasman Sea (Rahmanian et al., 1990). In an onshore–offshore direction, the Halibut Subgroup deposits consist of interbedded sandstones, shales and coals that were formed in environments ranging from upper coastal plain (Barracouta Formation) and lower coastal plain (the Volador and Kingfish formations) to a near-shore marine setting (Mackerel Formation). A marine unit, the Kate Shale, separates the Volador and Kingfish formations, being deposited at the Cretaceous−Paleogene boundary (Rahmanian et al., 1990; Thomas et al., 2003).

As a response to sea-level fall and associated erosion during the early Eocene, major submarine channels (e.g. Marlin and Tuna-Flounder channels) were developed and then filled with marine sediments (e.g. Flounder Formation) following subsequent transgression (Johnstone et al., 2001). This major erosional event is recorded in the Gippsland Basin by the Marlin Unconformity that terminated the deposition of the Halibut Subgroup (Marshall and Partridge, 1988). The overlying middle Eocene to early Oligocene Cobia Subgroup reflects changes in facies from the onshore to offshore parts of the basin (Holdgate, 2005). Onshore, the lower coastal plain facies of the Burong Formation was deposited which contains several coals. Offshore, as the siliciclastic sediment supply reduced, deep, condensed, glauconitic sediments (the Gurnard Formation) and marine channel-fill sediments (Turrum Formation) were deposited (Rahmanian et al., 1990).

The thick marine carbonate-dominated Seaspray Group, marked at its base by the regional Latrobe angular unconformity (Rahmanian et al., 1990), was deposited during the post-rift sag phase and under the influence of progressive opening of the Southern Ocean (Veevers et al., 1991; Hill et al., 1995). The Seaspray Group has a thickness in excess of 2.5 km in the offshore Gippsland Basin (Bernecker and Partridge, 1997; Partridge, 1999; Holdgate et al., 2000) and up to 700 m in the onshore part of the basin (Holdgate and Gallagher, 1997). The basal unit of this group is represented by the regional Oligocene Lakes Entrance Formation, which is made up predominantly of marls with some minor shales (O'Brien et al., 2008). In contrast, continental sedimentation continued in the onshore part. During the mid-Miocene, the transition from the marl and shale deposits of the Lakes Entrance Formation to the thick Gippsland Limestone is marked by extensive marine canyons (Gallagher et al., 2001).

### 3.2.3. Hydrocarbon source and charge in the Gippsland Basin: a review

Molecular, isotopic and oil−source rock correlation studies have shown considerable evidence that both oil and gas accumulations in the Gippsland Basin are predominantly derived from non-marine source rock facies, deposited in coastal-plain swamps, lakes and lagoons (Brooks and Smith, 1969; Stainforth, 1984; Alexander et al., 1987; Burns et al., 1987). Most of these studies have concluded that these petroleum accumulations were sourced from coaly shale and coal-bearing sequences within the Latrobe Group (Smith and Cook, 1984; Shanmugam, 1985; Moore et al., 1992; Murray et al., 1998). Organic-rich sediments within the lower coastal plain facies of the early Maastrichtian−early Eocene Halibut Subgroup have been described as containing significant oil-prone rocks, sourcing accumulations at the top of the Latrobe Group in the central part of the offshore basin (Bernecker and Partridge, 2001). This period was dominated by gymnosperms, which explains the high amount of diterpane biomarkers present in the oils (Thomas, 1982; Smith and Cook, 1984; Alexander et al., 1987; Killops et al., 1994). Gippsland Basin oils have high wax contents, high pristane/phytane ratios, and their biomarker signatures are dominated by gymnosperm (particularly resins) and angiosperm-derived compounds such as diterpanes and oleanane, etc (Brooks, 1970; Shanmugam, 1985; Moore et al., 1992; George et al., 1998). Thomas (1982) related the variations in wax content of the oils to either variations in source input or to thermal maturity differences. The isotopic compositions of the gases suggest their generation from similar organic facies of different ages, or multiple facies with similar isotopic signatures (Boreham et al., 2001). Additional dry gas accumulations located onshore and along the northern margin of the Gippsland Basin are interpreted to have been provided by over-mature source rocks within the Lower Cretaceous Strzelecki Group (O'Brien et al., 2008).

Apart from having a terrigenous origin, biomarker and fluid inclusion studies have indicated that some oils in the Gippsland Basin were generated from marine-influenced source rocks (Cook and Struckmeyer, 1986; Philp and Gilbert, 1986). George et al. (1998) showed that oil inclusions in the Blackback oil field originated from a marine source rock, deposited in a less anoxic environment compared to the terrigenous-sourced reservoired oil. The occurrence of such a marine facies was explained by the palaeogeographical proximity of the Blackback oil field to the palaeo-shoreline during the Late Cretaceous (Moore et al., 1992). A marine origin was also proposed by Gorter (2001) for gas and light oil recovered from the Anemone and Archer accumulations, respectively (**Figure 3.1**), which has been substantiated by their correlation to shales within the *T. lilliei* biozone of the Golden Beach Subgroup (Ahmed et al., 2013).

In the Gippsland Basin, the major oil fields are located offshore within the Central Deep, with the giant gas fields being mainly distributed along the northern part of the basin (Smith and Cook, 1984). Such a distribution was interpreted to be due to the complex migration pathways and thermal maturation variations within the basin, rather than changes in source rock type. For instance, Rahmanian et al. (1990) suggested that the overall distribution of oil and gas in the basin is controlled by differences in the thermal maturity of source rocks, and/or by the occurrence in the southern part of the basin of deep source rock units with the potential to generate more oil than gas. Fluid inclusion analyses have shown that the oil fields (e.g., Halibut, Kingfish, and Blackback) have not had a palaeo-gas cap (O'Brien et al., 2008). The accumulation and preservation of an initial oil charge, rather than leakage of gas, was proposed as an explanation for the predominance of oil fields in the southeastern Gippsland Basin (Cowley and O'Brien, 2000). Analyses of fluid inclusions indicated that the initial hydrocarbon charge into most of the present-day gas fields (e.g., Barracouta and Marlin fields) was oil that was subsequently displaced by a later gas charge (O'Brien et al., 2008). The early oil is thought to have been generated during the Paleocene to early Eocene from Upper Cretaceous depocentres (Moore et al., 1992) as a result of elevated heat flows (Summons et al., 2002). The later gas charge was preserved in the major gas fields (Barracouta, Bream, Marlin and Snapper) and was generated during the Miocene due to increased thermal maturities resulting from the rapid loading of the Gippsland Limestone carbonates (O'Brien et al., 2013). It has been also reported that maximum temperatures have been reached at the present day and that hydrocarbon generation is ongoing (Duddy and Green, 1992). O'Brien et al. (2008) modelled the petroleum systems in the Gippsland Basin and provided new insights into the hydrocarbon migration patterns. These authors identified two fill-spill hydrocarbon pathways; one gas-dominated in the north, and one oil-dominated in the south. More recently, Hoffman and Preston (2014) compiled and analysed pre-existing geochemical data in an attempt to identify possible mechanisms controlling the distribution and compositions of accumulations in the offshore part of the Gippsland Basin. These authors explained compositional variations observed within the reservoired fluids in the Gippsland Basin by the combined effects of both in-source primary processes (e.g. organic matter quality, type and maturity) and in-reservoir secondary processes (e.g. water-washing, biodegradation, evaporative fractionation). For instance, gases at both the Golden Beach and Patricia-Baleen fields are dry, suggesting the occurrence of biogenic methane in these relatively shallow structures. In contrast, the Barracouta, Snapper, Marlin and Bream fields host wet gases that are the result of the balance of water-washing and an unaltered charge provided by highly mature source rock within the Latrobe Group. In their study, Hoffman

and Preston (2014) concluded that most of the oils in the Central Deep (e.g. Fortescue, Mackerel and Kingfish) have typical black-oil API gravities (45–47°), high wax contents (10–27%), and low GORs (42–250 scf/stb). These oils are interpreted to have been generated at low level of thermal maturity from terrigenous-dominated source rock (Moore et al., 1992; Grant, 2004). However, lower wax contents (< 5-10%) and higher GORs (28,000 to 60,000 scf/stb) were measured for wet gas fields in the northern and towards the western part of the basin (e.g. Marlin, Snapper and Barracouta).

### 3.2.4. Upper Cretaceous−Paleocene Coal and Shale Distribution

In the Gippsland Basin, intraformational carbonaceous shales and variable amounts of coal occur at different stratigraphic levels within the Latrobe Group **(Figure 3.2)**. Data from wells drilled in the offshore Gippsland Basin indicate that thick coals and several carbonaceous shales are present within the Golden Beach and Halibut subgroups. Both vertical and lateral distributions of the Chimaera and Anemone formations of the Golden Beach Subgroup are uncertain because few petroleum wells penetrate them. The Chimaera and Anemone formations contain, from oldest to youngest, the *Tricolporites apoxyexinus* (Santonian), *Nothofagidites senectus* (early Campanian) and *Tricolporites lilliei* (mid-Campanian) spore−pollen biozones. Interbedded coals and carbonaceous shales attributed to these three palynological biozones represent predominantly fluvio-deltaic deposits (Sloan et al., 1992). In the Central Deep, the *T. lilliei* shales of the Anemone Formation were deposited in a marine environment (Rahmanian et al., 1990; Moore et al., 1992). To the east–southeast of the basin, non-marine facies equivalents of these sediments (Chimaera Formation) accumulated in a low energy, lagoonal setting (Gorter, 2001).

As the post-rift sag basin developed from the latest Cretaceous to the Paleocene, interbedded sandstones, shales and coals were deposited in alluvial and coastal plain depositional environments (Rahmanian et al., 1990; Thomas et al., 2003). The Halibut Subgroup is represented by the Volador and Kingfish formations, which contain coal and carbonaceous shales. The Volador Formation, dated by the *Forcipites longus* palynological biozone (late Campanian−Maastrichtian), consists of interbedded sandstones, carbonaceous shales and coals, deposited mainly in a lower coastal plain environment (Moore et al., 1992). In contrast, the Paleocene coal deposits (*Lygistepollenites balmei*) of the Kingfish Formation are interpreted to have been deposited in an upper coastal plain environment (Moore et al., 1992).

### 3.3. Sample details

A total of 91 ditch-cutting and core samples were chosen on the basis of their ages and pre-existing geochemical data, extracted from well completion reports and the Geoscience Australia database (http://dbforms.ga.gov.au/www/npm.well.search). The sample selection was made to ensure that shales, coaly shales and coals were investigated, and that the least thermally mature samples were preferentially used. The sample set was designed to include petroleum wells throughout the Central Deep. The source rock sample set used in this study represents different units of the Latrobe Group (Emperor, Golden Beach and Halibut subgroups). For simplicity and to avoid nomenclature confusion, the age designation for the investigated samples is given according to their palynological biozones: the *L. balmei* (26 samples), the *F. longus* (35 samples), and the *T. lilliei* (27 samples). In addition, three samples representing each of the *N. senectus*, *T. apoxyexinus* and *P. mawsonii* biozones were included to assess the deepest section of the Latrobe Group. The sample depths selected from each petroleum well and biozone and their bulk characteristics, such as Rock-Eval pyrolysis parameters and Total Organic Carbon (TOC) content, are listed in **Table 3.1**. The location of the Central Deep and wells from which the samples were taken are shown in **Figure 3.1**.

### 3.4. Experimental procedures

Prior to analysis, each source rock sample was crushed to a fine powder and subdivided into two aliquots. The first aliquot was subjected to Rock-Eval pyrolysis (Espitalié et al., 1977; Lafargue et al., 1998) using a Rock-Eval 6 instrument, allowing the measurement of TOC content, free hydrocarbons ($S_1$), hydrocarbon generative potential ($S_2$), carbon dioxide ($CO_2$) content produced during thermal cracking ($S_3$), and temperature ($T_{max}$) at the maximum of the $S_2$ peak. Other parameters, such as Hydrogen Index (HI), Oxygen Index (OI), total Petroleum Potential (PP), and Production Index (PI) were calculated (**Table 3.1**).

**Table 3.1. Sample identity, TOC and Rock-Eval pyrolysis data for 91 samples from the Gippsland Basin. Horizontal bold lines divide the samples from different palynological biozones.**

| Sample ID | Well name | Sample type | Depth (m) | Palynological zone | TOC | $S_1$ | $S_2$ | $S_3$ | PI | $T_{max}$ | HI | OI |
|---|---|---|---|---|---|---|---|---|---|---|---|---|
| 20110090 | Bream 2 | Cuttings | 2725−2740 | *L. balmei* | 10.84 | 1.20 | 24.17 | 2.47 | 0.05 | 424 | 223 | 23 |
| 20110091 | Bream 2 | Cuttings | 2743−2752 | *L. balmei* | 10.65 | 1.04 | 21.20 | 3.53 | 0.05 | 424 | 199 | 33 |
| 20110092 | Bream 2 | Core | 2754 | *L. balmei* | 4.38 | 0.53 | 16.71 | 1.02 | 0.03 | 438 | 382 | 23 |
| 20110093 | Bream 2 | Cuttings | 2752−2758 | *L. balmei* | 9.83 | 1.73 | 34.86 | 1.64 | 0.05 | 422 | 355 | 17 |
| 20110113 | Marlin A6 | Cuttings | 2387−2390 | *L. balmei* | 52.65 | 4.67 | 84.66 | 31.52 | 0.05 | 417 | 161 | 60 |
| 20110114 | Marlin A6 | Cuttings | 2438−2441 | *L. balmei* | 18.69 | 2.72 | 26.37 | 18.70 | 0.09 | 422 | 141 | 100 |
| 20110115 | Marlin A6 | Cuttings | 2499−2505 | *L. balmei* | 44.41 | 15.39 | 77.86 | 25.72 | 0.17 | 411 | 175 | 58 |
| 20110116 | Marlin A6 | Core | 2512 | *L. balmei* | 1.88 | 0.13 | 1.09 | 0.57 | 0.11 | 421 | 58 | 30 |
| 20110117 | Marlin A6 | Core | 2519 | *L. balmei* | 1.51 | 0.10 | 0.68 | 0.57 | 0.13 | 421 | 45 | 38 |
| 20110118 | Marlin A6 | Core | 2527 | *L. balmei* | 3.28 | 0.17 | 1.97 | 1.08 | 0.08 | 420 | 60 | 33 |
| 20110119 | Marlin A6 | Cuttings | 2563−2569 | *L. balmei* | 73.27 | 30.99 | 105.01 | 47.97 | 0.23 | 414 | 143 | 65 |
| 20110120 | Marlin A6 | Cuttings | 2615−2618 | *L. balmei* | 58.39 | 29.56 | 113.62 | 27.84 | 0.21 | 412 | 195 | 48 |
| 20110121 | Marlin A6 | Cuttings | 2624−2630 | *L. balmei* | 72.41 | 16.99 | 115.54 | 36.81 | 0.13 | 422 | 160 | 51 |
| 20110122 | Marlin A6 | Cuttings | 2691−2694 | *L. balmei* | 59.21 | 25.24 | 110.43 | 58.32 | 0.19 | 416 | 186 | 98 |
| 20110123 | Marlin A6 | Cuttings | 2804−2810 | *L. balmei* | 44.76 | 9.44 | 68.76 | 35.60 | 0.12 | 426 | 154 | 80 |
| 20110124 | Marlin A6 | Cuttings | 2987−2993 | *L. balmei* | 60.55 | 7.77 | 103.80 | 22.90 | 0.07 | 430 | 171 | 38 |
| 20110125 | Sawbelly 1 | Cuttings | 2980−2985 | *L. balmei* | 16.45 | 1.69 | 32.13 | 13.89 | 0.05 | 429 | 195 | 84 |
| 20110126 | Sawbelly 1 | Cuttings | 3015 | *L. balmei* | 13.84 | 2.23 | 29.24 | 9.69 | 0.07 | 431 | 211 | 70 |
| 20110250 | Turrum 3 | Cuttings | 1780−1790 | *L. balmei* | 27.82 | 4.65 | 51.98 | 10.74 | 0.08 | 420 | 187 | 39 |
| 20110138 | Turrum 3 | Cuttings | 1795−1805 | *L. balmei* | 8.82 | 1.08 | 6.83 | 10.63 | 0.14 | 421 | 77 | 120 |
| 20110139 | Turrum 3 | Cuttings | 2385−2400 | *L. balmei* | 3.79 | 0.17 | 5.02 | 3.04 | 0.03 | 426 | 133 | 80 |
| 20110140 | Turrum 3 | Cuttings | 2565−2580 | *L. balmei* | 23.18 | 2.57 | 41.17 | 9.20 | 0.06 | 425 | 178 | 40 |
| 20110141 | Veilfin 1 | Cuttings | 2640−2650 | *L. balmei* | 6.86 | 0.09 | 5.62 | 6.29 | 0.02 | 427 | 82 | 92 |
| 20110142 | Veilfin 1 | Cuttings | 2660−2670 | *L. balmei* | 7.19 | 0.08 | 7.99 | 4.94 | 0.01 | 426 | 111 | 69 |
| 20110152 | Whiting 2 | Cuttings | 2145−2155 | *L. balmei* | 2.70 | 0.08 | 2.76 | 1.88 | 0.03 | 433 | 102 | 70 |
| 20110153 | Whiting 2 | Cuttings | 2325−2335 | *L. balmei* | 3.78 | 0.38 | 9.76 | 1.31 | 0.04 | 433 | 259 | 35 |
| 20110024 | Anemone 1 | Cuttings | 3065−3075 | *F. longus* | 9.40 | 0.24 | 13.64 | 11.13 | 0.02 | 416 | 145 | 118 |

**Table 3.1. (Continued) Sample identity, TOC and Rock-Eval pyrolysis data for 91 samples from the Gippsland Basin. Horizontal bold lines divide the samples from different palynological biozones.**

| Sample ID | Well name | Sample type | Depth (m) | Palynological zone | TOC | $S_1$ | $S_2$ | $S_3$ | PI | $T_{max}$ | HI | OI |
|-----------|-----------|-------------|-----------|--------------------|-----|-------|-------|-------|-----|-----------|-----|-----|
| 20110026 | Angler 1 | Cuttings | 3120−3130 | *F. longus* | 8.77 | 0.24 | 16.66 | 9.32 | 0.01 | 419 | 190 | 106 |
| 20110030 | Basker 1 | Cuttings | 2982−2985 | *F. longus* | 8.38 | 0.19 | 14.41 | 5.94 | 0.01 | 425 | 172 | 71 |
| 20110031 | Basker 1 | Cuttings | 3009−3024 | *F. longus* | 21.97 | 1.05 | 44.93 | 8.37 | 0.02 | 421 | 205 | 38 |
| 20110032 | Basker 1 | Cuttings | 3066−3072 | *F. longus* | 16.74 | 0.80 | 37.34 | 6.91 | 0.02 | 427 | 223 | 41 |
| 20110033 | Basker 1 | Cuttings | 3099−3105 | *F. longus* | 9.02 | 0.95 | 22.16 | 3.69 | 0.04 | 428 | 246 | 41 |
| 20110034 | Basker 1 | Core | 3109 | *F. longus* | 4.02 | 0.68 | 12.72 | 1.29 | 0.05 | 430 | 316 | 32 |
| 20110036 | Bignose 1 | Cuttings | 3319−3322 | *F. longus* | 13.20 | 0.26 | 20.39 | 8.31 | 0.01 | 425 | 154 | 63 |
| 20110037 | Bignose 1 | Cuttings | 3331−3334 | *F. longus* | 6.10 | 0.17 | 10.01 | 4.20 | 0.02 | 428 | 164 | 69 |
| 20110038 | Bignose 1 | Cuttings | 3358−3364 | *F. longus* | 4.68 | 0.15 | 8.63 | 3.01 | 0.02 | 428 | 184 | 64 |
| 20110100 | Hermes 1 | Cuttings | 3175−3180 | *F. longus* | 3.36 | 0.21 | 6.57 | 1.75 | 0.03 | 427 | 195 | 52 |
| 20110101 | Hermes 1 | Cuttings | 3210−3215 | *F. longus* | 3.13 | 0.16 | 6.96 | 1.30 | 0.02 | 426 | 223 | 42 |
| 20110102 | Hermes 1 | Cuttings | 3230−3245 | *F. longus* | 7.82 | 0.28 | 13.37 | 5.18 | 0.02 | 425 | 171 | 66 |
| 20110103 | Hermes 1 | Cuttings | 3255−3255 | *F. longus* | 24.84 | 3.24 | 87.64 | 4.90 | 0.04 | 418 | 353 | 20 |
| 20110104 | Hermes 1 | Cuttings | 3295−3305 | *F. longus* | 12.17 | 4.55 | 19.90 | 4.65 | 0.19 | 422 | 163 | 38 |
| 20110105 | Hermes 1 | Cuttings | 3485−3500 | *F. longus* | 11.41 | 0.62 | 19.47 | 3.98 | 0.03 | 427 | 171 | 35 |
| 20110106 | Hermes 1 | Cuttings | 3520−3525 | *F. longus* | 9.68 | 0.72 | 19.45 | 3.02 | 0.04 | 426 | 201 | 31 |
| 20110107 | Hermes 1 | Cuttings | 3540−3550 | *F. longus* | 17.75 | 0.96 | 33.45 | 4.70 | 0.03 | 426 | 188 | 26 |
| 20110129 | Shark 1 | Cuttings | 2061−2064 | *F. longus* | 5.45 | 0.29 | 14.53 | 1.75 | 0.02 | 425 | 267 | 32 |
| 20110130 | Tarra 1 | Cuttings | 2502−2505 | *F. longus* | 3.32 | 0.26 | 8.78 | 1.18 | 0.03 | 427 | 265 | 36 |
| 20110131 | Tarra 1 | Cuttings | 2517−2520 | *F. longus* | 1.17 | 0.15 | 2.79 | 0.78 | 0.05 | 431 | 239 | 67 |
| 20110143 | Veilfin 1 | Cuttings | 3205−3215 | *F. longus* | 2.16 | 0.04 | 1.06 | 1.57 | 0.04 | 443 | 49 | 73 |
| 20110144 | Veilfin 1 | Cuttings | 3355−3365 | *F. longus* | 19.21 | 1.53 | 29.08 | 2.91 | 0.05 | 439 | 151 | 15 |
| 20110145 | Veilfin 1 | Cuttings | 3405−3410 | *F. longus* | 14.98 | 1.41 | 21.83 | 4.60 | 0.06 | 440 | 146 | 31 |
| 20110146 | Veilfin 1 | Cuttings | 3430−3435 | *F. longus* | 9.56 | 0.30 | 9.50 | 5.02 | 0.03 | 440 | 99 | 52 |
| 20110251 | Veilfin 1 | Core | 3460 | *F. longus* | 1.54 | 0.32 | 3.50 | 0.08 | 0.08 | 448 | 228 | 5 |
| 20110147 | Veilfin 1 | Cuttings | 3460−3470 | *F. longus* | 2.62 | 0.30 | 21.93 | 5.57 | 0.01 | 445 | 838 | 213 |
| 20110148 | Volador 1 | Cuttings | 3552 | *F. longus* | 19.83 | 1.07 | 36.16 | 4.88 | 0.03 | 419 | 182 | 25 |

**Table 3.1. (Continued) Sample identity, TOC and Rock-Eval pyrolysis data for 91 samples from the Gippsland Basin. Horizontal bold lines divide the samples from different palynological biozones.**

| Sample ID | Well name | Sample type | Depth (m) | Palynological zone | TOC | $S_1$ | $S_2$ | $S_3$ | PI | $T_{max}$ | HI | OI |
|---|---|---|---|---|---|---|---|---|---|---|---|---|
| 20110149 | Volador 1 | Cuttings | 3573 | *F. longus* | 17.46 | 0.75 | 31.86 | 7.66 | 0.02 | 424 | 182 | 44 |
| 20110252 | Volador 1 | Cuttings | 3675 | *F. longus* | 11.02 | 0.60 | 22.79 | 2.56 | 0.03 | 432 | 207 | 23 |
| 20110150 | Volador 1 | Cuttings | 3687 | *F. longus* | 3.25 | 0.14 | 4.43 | 1.17 | 0.03 | 433 | 136 | 36 |
| 20110151 | Volador 1 | Cuttings | 3693−3696 | *F. longus* | 6.34 | 0.79 | 12.69 | 3.72 | 0.06 | 427 | 200 | 59 |
| 20110279C | Volador 1 | Cuttings | 3849−3852 | *F. longus* | 68.53 | 7.69 | 169.55 | 7.70 | 0.04 | 432 | 247 | 11 |
| 20110253 | Whiting 2 | Cuttings | 3015−3025 | *F. longus* | 2.26 | 0.36 | 4.33 | 0.79 | 0.08 | 443 | 192 | 35 |
| 20110154 | Whiting 2 | Cuttings | 3168−3180 | *F. longus* | 1.82 | 0.24 | 2.68 | 0.59 | 0.08 | 443 | 147 | 32 |
| 20110025 | Anemone 1 | Cuttings | 3335−3345 | *T. lilliei* | 13.43 | 0.62 | 25.48 | 12.59 | 0.02 | 420 | 190 | 94 |
| 20110027 | Angler 1 | Cuttings | 3790−3795 | *T. lilliei* | 1.36 | 0.07 | 1.52 | 1.12 | 0.04 | 424 | 112 | 83 |
| 20110028 | Angler 1 | Cuttings | 3810−3820 | *T. lilliei* | 2.36 | 0.11 | 3.42 | 1.38 | 0.03 | 424 | 145 | 59 |
| 20110029 | Angler 1 | Cuttings | 3905−3915 | *T. lilliei* | 1.66 | 0.10 | 2.21 | 2.04 | 0.04 | 430 | 133 | 123 |
| 20110267 | Angler 1 | Cuttings | 4030−4035 | *T. lilliei* | 1.94 | 0.14 | 3.22 | 2.05 | 0.04 | 431 | 166 | 106 |
| 20110035 | Basker 1 | Cuttings | 3615−3621 | *T. lilliei* | 28.25 | 0.69 | 28.53 | 32.20 | 0.02 | 423 | 101 | 114 |
| 20110039 | Bignose 1 | Cuttings | 3469−3472 | *T. lilliei* | 8.57 | 0.38 | 14.94 | 4.64 | 0.02 | 425 | 174 | 54 |
| 20110040 | Bignose 1 | Cuttings | 3544−3547 | *T. lilliei* | 47.55 | 0.68 | 28.37 | 6.88 | 0.02 | 427 | 60 | 14 |
| 20110086 | Bignose 1 | Cuttings | 3709−3712 | *T. lilliei* | 8.15 | 0.59 | 18.17 | 3.43 | 0.03 | 430 | 223 | 42 |
| 20110087 | Bignose 1 | Cuttings | 3730−3733 | *T. lilliei* | 15.99 | 0.76 | 31.11 | 4.23 | 0.02 | 427 | 195 | 26 |
| 20110088 | Bignose 1 | Cuttings | 3775−3778 | *T. lilliei* | 6.40 | 0.74 | 14.21 | 2.58 | 0.05 | 430 | 222 | 40 |
| 20110089 | Bignose 1 | Cuttings | 3811 | *T. lilliei* | 6.39 | 0.87 | 14.28 | 2.42 | 0.06 | 429 | 224 | 38 |
| 20110094 | Bream 2 | Cuttings | 3097−3106 | *T. lilliei* | 28.51 | 4.67 | 57.35 | 9.55 | 0.08 | 419 | 201 | 33 |
| 20110095 | Bream 2 | Cuttings | 3146−3152 | *T. lilliei* | 24.66 | 2.53 | 45.99 | 13.75 | 0.05 | 419 | 187 | 56 |
| 20110096 | Bream 2 | Cuttings | 3167−3182 | *T. lilliei* | 37.57 | 2.38 | 70.49 | 16.98 | 0.03 | 419 | 188 | 45 |
| 20110097 | Bream 2 | Core | 3242 | *T. lilliei* | 15.42 | 2.45 | 27.52 | 1.82 | 0.08 | 442 | 179 | 12 |
| 20110098 | Helios 1 | Cuttings | 3380 | *T. lilliei* | 21.13 | 0.76 | 45.96 | 16.71 | 0.02 | 419 | 218 | 79 |
| 20110099 | Helios 1 | Cuttings | 3390 | *T. lilliei* | 10.45 | 0.10 | 13.30 | 10.49 | 0.01 | 421 | 127 | 100 |
| 20110108 | Hermes 1 | Cuttings | 3595−3600 | *T. lilliei* | 17.20 | 1.43 | 33.96 | 5.33 | 0.04 | 427 | 197 | 31 |
| 20110109 | Hermes 1 | Cuttings | 3775−3785 | *T. lilliei* | 16.35 | 1.05 | 28.06 | 5.13 | 0.04 | 430 | 172 | 31 |

**Table 3.1. (Continued) Sample identity, TOC and Rock-Eval pyrolysis data for 91 samples from the Gippsland Basin. Horizontal bold lines divide the samples from different palynological biozones.**

| Sample ID | Well name | Sample type | Depth (m) | Palynological zone | TOC | S₁ | S₂ | S₃ | PI | Tmax | HI | OI |
|---|---|---|---|---|---|---|---|---|---|---|---|---|
| 20110110 | Hermes 1 | Cuttings | 3845−3860 | *T. lilliei* | 15.39 | 1.59 | 28.99 | 4.10 | 0.05 | 433 | 188 | 27 |
| 20110111 | Hermes 1 | Cuttings | 4075−4080 | *T. lilliei* | 16.31 | 2.85 | 28.62 | 7.83 | 0.09 | 435 | 175 | 48 |
| 20110112 | Hermes 1 | Cuttings | 4275−4285 | *T. lilliei* | 19.82 | 4.59 | 33.92 | 5.48 | 0.12 | 441 | 171 | 28 |
| 20110127 | Selene 1 | Core | 3143 | *T. lilliei* | 2.14 | 0.10 | 3.48 | 0.37 | 0.03 | 423 | 163 | 17 |
| 20110128 | Selene 1 | Core | 3149 | *T. lilliei* | 9.35 | 0.58 | 29.89 | 9.35 | 0.02 | 418 | 498 | 156 |
| 20110287 | Volador 1 | Cuttings | 4335−4338 | *T. lilliei* | 17.57 | 5.44 | 43.43 | 1.46 | 0.11 | 442 | 247 | 8 |
| 20110292 | Volador 1 | Cuttings | 4527−4530 | *T. lilliei* | 14.57 | 4.22 | 28.59 | 1.92 | 0.13 | 443 | 196 | 13 |
| 20110296 | Archer 1 | Cuttings | 3915−3925 | *N. senectus* | 1.95 | 0.27 | 2.22 | 2.25 | 0.11 | 433 | 114 | 115 |
| 20110262 | Anemone 1 | Cuttings | 4390−4400 | *T. apoxyexinus* | 1.65 | 0.22 | 1.30 | 1.22 | 0.14 | 429 | 79 | 74 |
| 20110275 | Omeo ST1 | Cuttings | 3363−3369 | *P. mawsonii* | 12.13 | 2.22 | 73.16 | 0.99 | 0.03 | 430 | 603 | 8 |

$S_1$: Amount of free hydrocarbons in the sample in mg HC/g rock
$S_2$: Amount of hydrocarbons generated during pyrolysis in mg HC/g rock
$S_3$: Amount of oxygen containing compounds generated during pyrolysis in mg $CO_2$/g rock
**PI**: Production Index [$(S_1/S_1+S_2)*100$]
$T_{max}$: Temperature of maximum hydrocarbon generation in °C
**HI**: Hydrogen Index ($S_2*100$/TOC) in mg HC/g TOC
**OI**: Oxygen Index ($S_3*100$/TOC) in mg $CO_2$/g TOC
**TOC**: Total Organic Carbon in %

The second aliquot was solvent-extracted with a mixture of dichloromethane and methanol to minimise the influence of the bitumen fraction on subsequent geochemical measurements. Based on the measured Rock-Eval pyrolysis parameters, selected immature samples were analysed by open-system pyrolysis-gas chromatography (Py-GC) as described by Horsfield (1989) and Horsfield and Dueppenbecker (1991) to provide further details on kerogen and petroleum type. The pyrolysis products were released onto an HP-Ultra 1 dimethyl polysiloxane capillary column (50 m length, inner diameter of 0.32 mm, film thickness of 0.52 μm) and measured on-line with an Agilent 6890A gas chromatograph equipped with a pyrolysis unit and Flame-Ionisation-Detector (FID). Pyrolysate compositions were identified based on reference chromatograms using Agilent Chemstation software and quantified using *n*-butane as an internal standard. Response factors for all compounds were assumed to be the same, except for methane whose response factor was 1.1 (di Primio et al., 1998). Calculated percentages of boiling ranges ($C_1$−$C_5$, $C_6$−$C_{14}$ and $C_{15+}$) and selected components (*m+p* xylene, *n*-octene and phenol) are reported in **Table 3.2**.

Following Py-GC analysis, non-isothermal open-system pyrolysis was performed using a Source Rock Analyser$^{TM}$ instrument (SRA-TPH/IR) on selected solvent-extracted samples to calculate kinetic parameters of primary kerogen to petroleum conversion. Each sample was pyrolysed at four laboratory heating rates of 0.7°C/min, 2°C/min, 5°C/min and 15°C/min, using a furnace set-up described by Schaefer et al. (1990). To obtain reasonable geological predictions (Schenk and Dieckmann, 2004), bulk petroleum formation rates were measured based on the lowest heating rates (0.7°C/min, 2°C/min, 5°C/min). The optimisation performed within the Kinetics 2000 and KMOD$^{TM}$ programs (Lawrence Livermore National Laboratory) on each kinetic dataset consisted of establishment of a discrete activation energy (EA) distribution with a single frequency factor (A). See Burnham et al. (1987) for a detailed description of the discrete model.

Non-isothermal closed-system pyrolysis-GC experiments were carried out on four selected samples, using micro-scale-sealed-vessel (MSSV) following the approach and method described by Horsfield et al. (1989) and Dieckmann et al. (1998). The samples were heated at 0.7°C/min from 200°C up to the temperature estimated from bulk kinetic data at which 10, 30, 50, 70 and 90% transformation ratios were measured to be achieved. The composition of hydrocarbons in each tube was determined by a single-step, on-line gas-chromatography as for the Py-GC analysis. The major components (resolved and total) in the gas ($C_1$−$C_5$) and oil ($C_{6+}$) range were quantified with respect to the internal standard, *n*-butane. Combining bulk kinetic parameters describing the primary cracking, and the hydrocarbon

composition measured at the five aforementioned heating transformation ratios, enabled compositional kinetic models to be developed with two components (oil and gas) and four components ($C_1$, $C_2$–$C_5$, $C_6$–$C_{14}$ and $C_{15+}$). However, in this study more emphasis was given to models with 14 components ($C_1$, $C_2$, $C_3$, $i$-$C_4$, $n$-$C_4$, $i$-$C_5$, $n$-$C_5$, pseudo-$C_6$, $C_7$–$C_{15}$, $C_{16}$–$C_{25}$, $C_{26}$–$C_{35}$, $C_{36}$–$C_{45}$, $C_{46}$–$C_{55}$, $C_{56}$–$C_{80}$), which were developed following the PhaseKinetics approach established by di Primio and Horsfield (2006). These models and physical properties, such as the gas:oil ratio (GOR), the formation volume factor ($B_O$) and the saturation pressure ($P_{sat}$) were determined using PVT simulation software (PVT Sim, Calsep, Denmark).

## 3.5. Results

### 3.5.1. Source rock quality and petroleum potential

The studied source rock samples have variable organic richness, with TOC contents ranging from 1.2 to 73.2%. On the basis of the Peters and Cassa (1994) guidelines, these samples are considered as good to excellent source rocks (**Figure 3.3**). The highest TOC (>50%) values were measured for six samples from the *L. balmei* biozone and one sample from the *F. longus* biozone, classifying these sediments as coals. TOC values ranging from 20 to 50%, were measured for samples from the *L. balmei* (4 samples), *F. longus* (2 samples) and *T. lilliei* (6 samples) biozones, categorising these sediments as shaly coals. The remaining samples, with TOC <20%, are considered as shales in this study.

The sample set used herein has $S_2$ values ranging from 0.7 to 169.5 mg HC/g rock, with averages of 42.3, 23.0 and 26.1 mg HC/g rock for the *L. balmei*, *F. longus* and *T. lilliei* biozones, respectively. According to Peter and Cassa (1994), samples with $S_2$ values ranging between 1 and 2 mg HC/g rock are classified as having good petroleum potential, whereas those with $S_2$ values greater than 4 mg HC/g rock are considered to have excellent petroleum potential. On this basis, all of the rock samples used in this study, except one sample from *L. balmei* (20110117), have at least good petroleum potential. The highest $S_2$ values were measured for the coals of the *L. balmei* biozone (84.7–115.5 mg HC/g rock) and one coal sample from the *F. longus* biozone (169.5 mg HC/g rock). In term of their total petroleum potential, values spread from 0.8 to 177.2 mg HC/g rock. Generally, the coals and shaly coals have the highest PP values, whilst lower values were calculated for the shales (**Figure 3.3**).

**Table 3.2. Selected components from open-system pyrolysis-gas chromatography, used to determine petroleum-type organofacies and phenolic content in solvent-extracted samples from the Gippsland Basin.**

| Sample ID | Well name | Depth (m) | Palynological zone | $C_1$–$C_5$ (%) | $C_6$–$C_{14}$ (%) | $C_{15+}$ (%) | $m$+$p$ Xylene (%) | $n$-Octene (%) | Phenol (%) |
|---|---|---|---|---|---|---|---|---|---|
| 20110092 | Bream 2 | 2754 | *L. balmei* | 52 | 25 | 23 | 35 | 51 | 13 |
| 20110113 | Marlin A6 | 2387−2390 | *L. balmei* | 72 | 14 | 14 | 40 | 10 | 50 |
| 20110121 | Marlin A6 | 2624−2630 | *L. balmei* | 74 | 12 | 13 | 35 | 9 | 56 |
| 20110126 | Sawbelly 1 | 3015 | *L. balmei* | 75 | 14 | 10 | 47 | 20 | 33 |
| 20110140 | Turrum 3 | 2565−2580 | *L. balmei* | 77 | 13 | 10 | 43 | 14 | 42 |
| 20110153 | Whiting 2 | 2325−2335 | *L. balmei* | 60 | 20 | 20 | 34 | 23 | 42 |
| 20110034 | Basker 1 | 3109 | *F. longus* | 55 | 22 | 23 | 39 | 31 | 29 |
| 20110103 | Hermes 1 | 3255−3255 | *F. longus* | 69 | 14 | 16 | 37 | 16 | 47 |
| 20110130 | Tarra 1 | 2502−2505 | *F. longus* | 70 | 17 | 13 | 34 | 15 | 51 |
| 20110251 | Veilfin 1 | 3460 | *F. longus* | 70 | 20 | 11 | 47 | 28 | 26 |
| 20110149 | Volador 1 | 3573 | *F. longus* | 65 | 18 | 17 | 34 | 21 | 45 |
| 20110252 | Volador 1 | 3675 | *F. longus* | 71 | 16 | 14 | 33 | 14 | 53 |
| 20110025 | Anemone 1 | 3335−3345 | *T. lilliei* | 63 | 18 | 19 | 29 | 17 | 54 |
| 20110267 | Angler 1 | 4030−4035 | *T. lilliei* | 73 | 17 | 10 | 38 | 22 | 40 |
| 20110086 | Bignose 1 | 3709−3712 | *T. lilliei* | 68 | 17 | 15 | 40 | 21 | 39 |
| 20110098 | Helios 1 | 3380 | *T. lilliei* | 71 | 14 | 15 | 32 | 13 | 55 |
| 20110128 | Selene 1 | 3149 | *T. lilliei* | 47 | 21 | 32 | 27 | 32 | 41 |
| 20110287 | Volador 1 | 4335−4338 | *T. lilliei* | 69 | 17 | 14 | 41 | 27 | 31 |
| 20110292 | Volador 1 | 4527−4530 | *T. lilliei* | 73 | 16 | 11 | 46 | 28 | 26 |
| 20110296 | Archer 1 | 3915−3925 | *N. senectus* | 80 | 16 | 3 | 36 | 19 | 45 |
| 20110262 | Anemone 1 | 4390−4400 | *T. apoxyexinus* | 87 | 12 | 1 | 73 | 15 | 12 |
| 20110275 | Omeo ST1 | 3363−3369 | *P. mawsonii* | 58 | 26 | 16 | 44 | 41 | 15 |
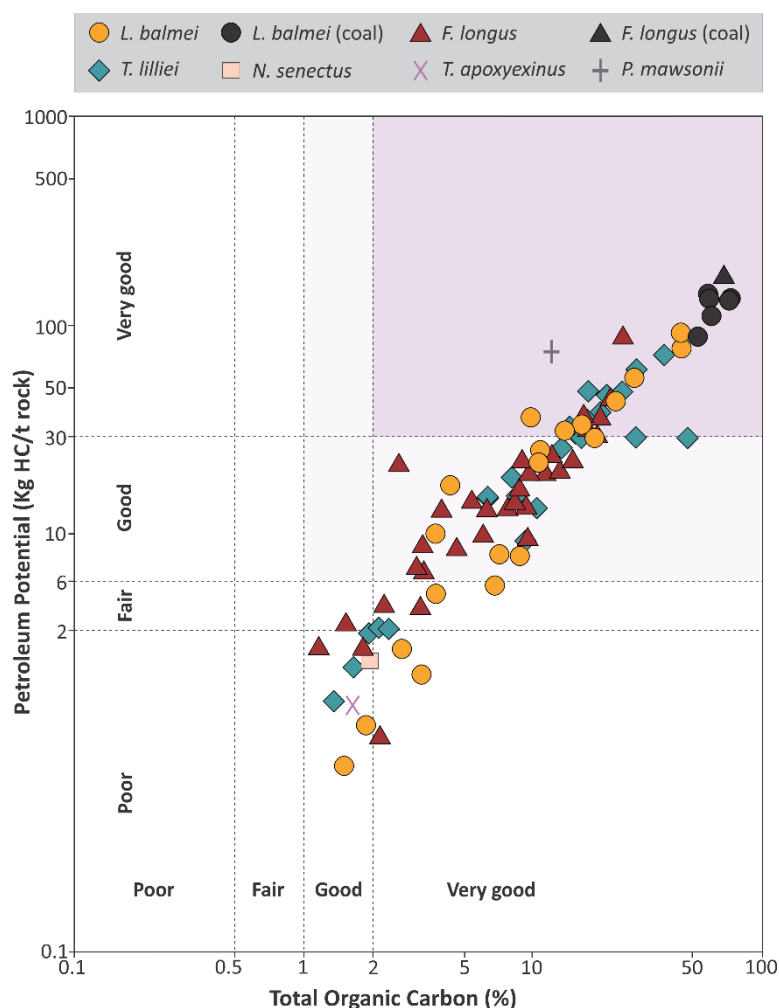
**Figure 3.3. Cross-plot of total petroleum potential (PP; $S_1 + S_2$) versus Total Organic Carbon for the 91 source rock samples from the Gippsland Basin. Classification of organic content is based on (Peters and Cassa, 1994).**

### 3.5.2. Thermal maturity

The Rock-Eval pyrolysis $T_{max}$ values were used to assess the thermal maturity attained by the studied samples. Overall, $T_{max}$ values vary between 411 and 448°C, indicating variable levels of thermal maturity, as shown on the $T_{max}$ versus HI diagram (**Figure 3.4**). For 85% of the Latrobe Group samples, the $T_{max}$ values are below 435°C and the $S_1$ (< 0.5 to 31.0 mg HC/g rock) and PI (<0.15) values are typically low, suggesting that they are thermally immature to early mature (**Figures 3.4** and **3.5**). Apart from one sample from Bream 2 (20110092) that has a $T_{max}$ value of 438°C, all of the samples from the *L. balmei* biozone are thermally immature to marginally mature with respect to the oil generation window. Similarly, all of the samples from the *F. longus* and *T. lilliei* biozones are immature, except for the deepest samples from Veilfin 1, Whiting 2, Bream 2, Volador 1 and Hermes 1 that have $T_{max}$ values in the range of 439–448°C, signifying that these samples are within the early to main stages of the oil generation window. The three stratigraphically older samples

from the *N. senectus*, *T. apoxyexinus* and *P. mawsonii* biozones (20110296, 20110262 and 20110275, respectively) are thermally immature.
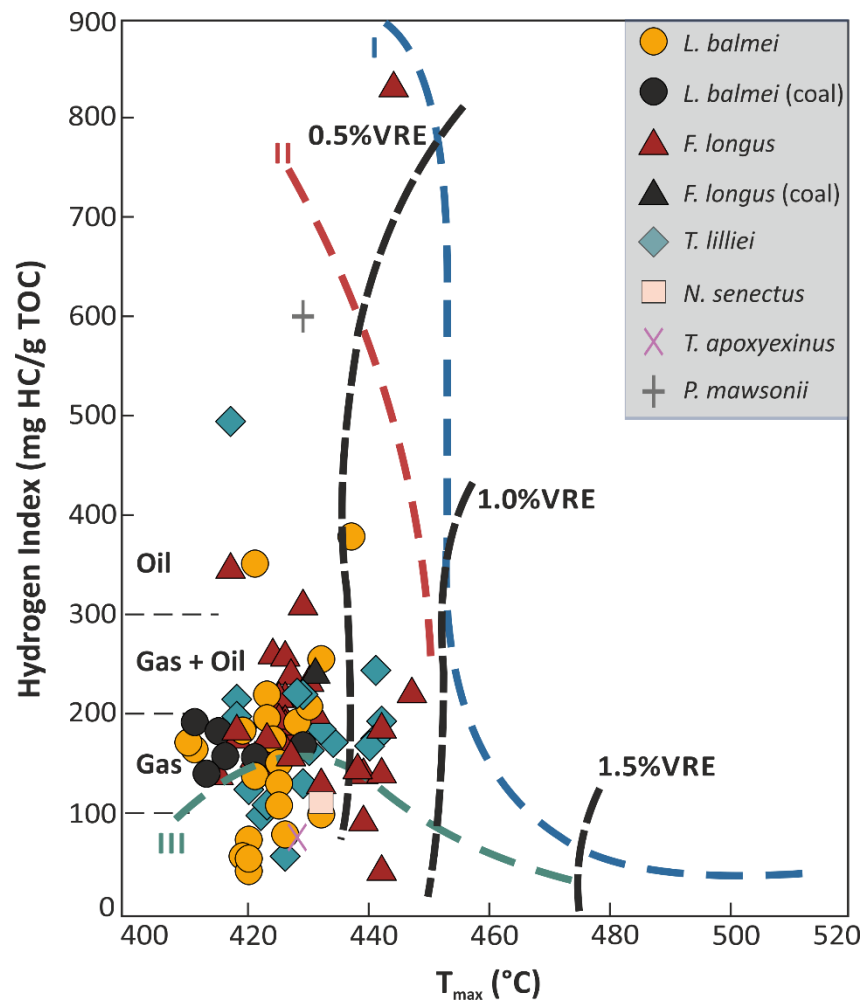


**Figure 3.4. Cross-plot of Hydrogen Index versus $T_{max}$, showing the thermal maturity of the 91 source rock samples from the Gippsland Basin. VRE = vitrinite reflectance equivalent.**

Despite their low maturity, the *L. balmei* coals and a few of the shaly coals have high $S_1$ and PI values, indicating either their contamination by drilling fluids or their impregnation by migrated hydrocarbons from interbedded or deeper source rock units **(Figure 3.5)**. Moriarty (2010) also evaluated the source rock potential of the Latrobe Group in 15 petroleum wells in the Central Deep. Using the Rock-Eval parameters $S_1$, $S_2$, PI and $T_{max}$, this study showed that oil contamination and impregnation is common in such source rock samples, particularly in those from the *T. lilliei* biozone, and suggested that this was evidence of oil expulsion and migration. However, vitrinite reflectance data measured for *L. balmei* coals and gathered from the Geoscience Australia database (http://dbforms.ga.gov.au/www/npm.well.search) range from 0.72% to 0.78%, indicating an early to main stage of oil window. The high

bitumen fraction in these coals, as well as in the *F. longus* coal, may have been generated by thermal cracking and thus may represent the first phase of generation from these coals.
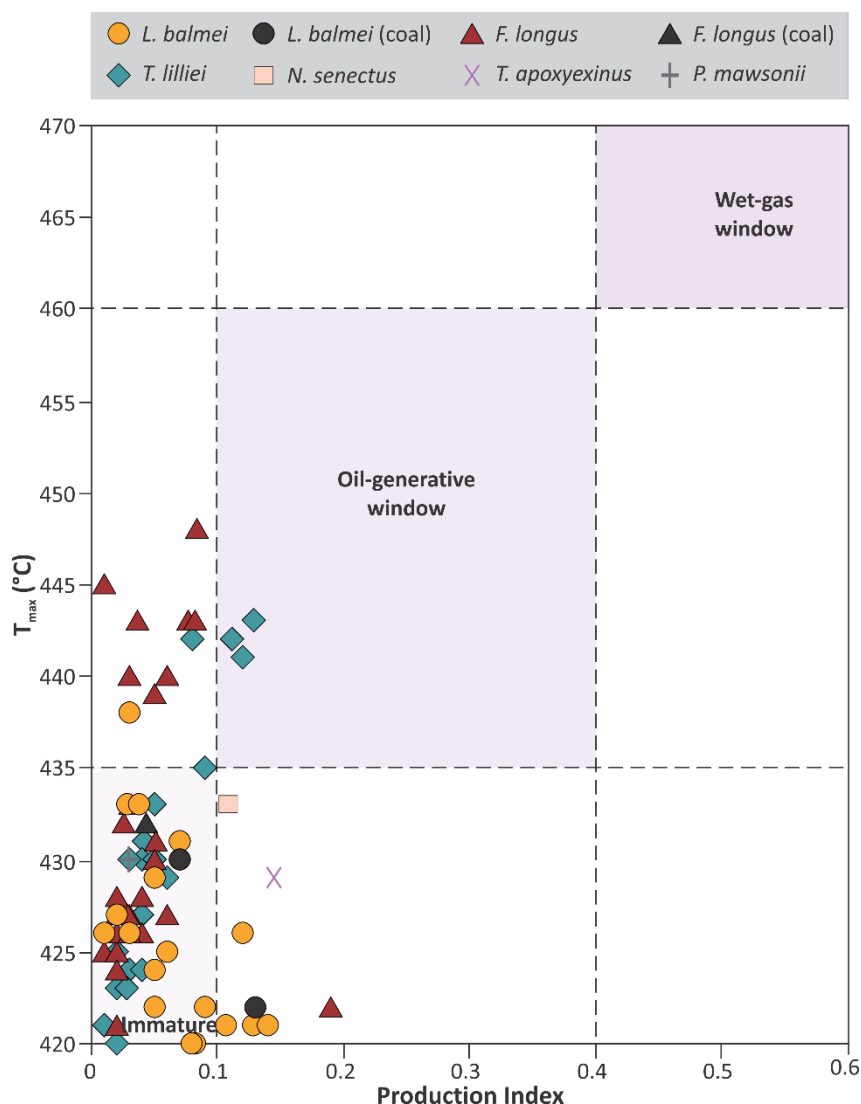


Figure 3.5. Cross-plot of $T_{max}$ versus Production Index (PI; $S_1/[S_1 + S_2]$) and the rank thresholds for oil and gas generation, illustrating the overall low thermal maturity of the sample set.

### 3.5.3. Kerogen type

The kerogen type within samples from the Latrobe Group was assessed based on the modified van Krevelen HI versus OI diagram (**Figure 3.6**). Samples from the investigated palynological biozones mainly plot in the Type II/III to III kerogen field and their OI varies from 5 to 213 mg $CO_2$/g TOC, with an average value of 54 mg $CO_2$/g TOC. Although the *L. balmei* biozone coal samples come from a single well (Marlin A6), their OI values are variable and range from 38 to 98 mg $CO_2$/g TOC. The coal sample from the *F. longus* biozone has an OI of 11 mg $CO_2$/g TOC, which is lower than generally reported for Type III kerogen (e.g. Peters and Cassa, 1994). Nonetheless, similarly low OI values were

documented by Boreham et al. (1999) for the German Greek, Rangal, Wolfang and Blair Athol Coal Measures, and a series of Permian coals in the Bowen Basin. Such wide fluctuations in OI values suggest either depositional environment redox changes, or structural variations in the organic matter within the source rock units of the Latrobe Group. For example, the low OI values (<20 mg $CO_2$/g TOC) and high HI values in some samples (e.g. 20110275) indicate that their deposition was under less oxygenated conditions.
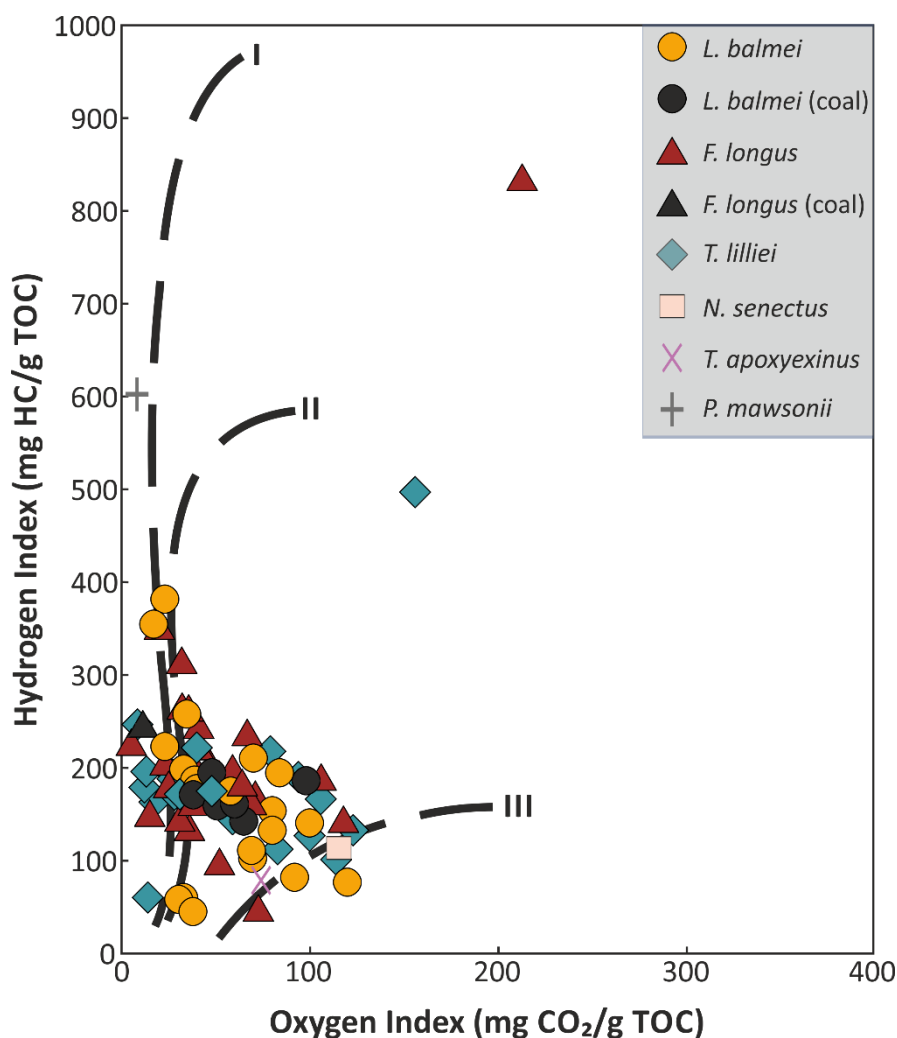


**Figure 3.6. Cross-plot of Oxygen Index versus Hydrogen Index illustrating the kerogen type for the 91 source rock samples from the Gippsland Basin.**

For the sample set, the HI varies from 45 to 603 mg HC/g TOC, indicating the occurrence of numerous kerogen types. Most of the samples have an affinity to Type II-III kerogen, although some shale samples contain Type III kerogen. The *L. balmei* coals have HI values between 143 to 195 mg HC/g TOC, with an average of 169 mg HC/g TOC, indicating Type III kerogen. These HI values are lower than those (HI= 200 mg HC/g TOC) typically reported for oil-generating coals (Hunt, 1991; Pepper and Corvi, 1995). Only one coal sample was available from the *F. longus* biozone, which has a HI of 247 mg HC/g TOC,

indicative of a moderately oil-prone Type II/III kerogen capable of generating liquid hydrocarbons. The two organically-lean samples (20110143 and 20110117) contain Type IV kerogen (HI = 45–49 mg HC/g TOC), with no potential for hydrocarbon generation.

Exceptions to these ranges are as follows: One sample from the *F. longus* biozone has a HI of 838 mg HC/g TOC and a very high OI of 213 mg $CO_2$/g TOC, suggesting it contains highly oil-prone Type I. Similar high HI values were reported for samples within the underlying *T. lilliei* biozone within Bignose 1 by Moriarty (2010), and in this study a shale from Selene 1 (HI = 498 mg HC/g TOC) has Type II kerogen. The *P. mawsonii* biozone shale has a HI of 603 mg HC/g TOC, typical for Type I or Type I/II kerogen.

### 3.5.4. Molecular composition

Py-GC was used to obtain the molecular composition of kerogen pyrolysates in order to provide further insights into the type of petroleum they could generate. **Figure 3.7** shows the pyrolysate composition of selected source rock samples, with major peak identifications. In addition to these representative chromatograms, the relative abundance of total resolved aliphatic, mono-aromatic, phenolic and naphthalene moieties in all of the analysed pyrolysates are illustrated in **Figure 3.8**.

The Py-GC traces of the analysed samples are generally dominated by *n*-alkane/*n*-alkene doublets ranging up to *n*-$C_{30}$ for most of the sample set. These pyrolysis products are generally present in significant amounts compared to the other major compound classes. Three distinct distribution patterns of *n*-alkane/*n*-alkene doublets can be distinguished (**Figure 3.7**). The first distinct pattern is identified in the *P. mawsonii* biozone shale, being characterised by a series of *n*-alkane/*n*-alkene doublets that extend to *n*-$C_{30}$ and show a linear decrease towards higher molecular weight homologues. Such a unimodal distribution is characteristic of marine algal Type II kerogen (Larter and Douglas, 1980). The second pattern, comprising the two samples from the *N. senectus* and *T. apoxyexinus* biozones, has *n*-alkane/*n*-alkene doublets in the low molecular weight range (up to *n*-$C_{17}$), while homologues at higher carbon numbers are either absent or are discernible in very low amounts, suggesting Type III kerogen. Similarly, the *n*-alkyl distribution of these two pyrolysates is unimodal with a predominance of short-chain compounds in the $C_1$−$C_7$ range.
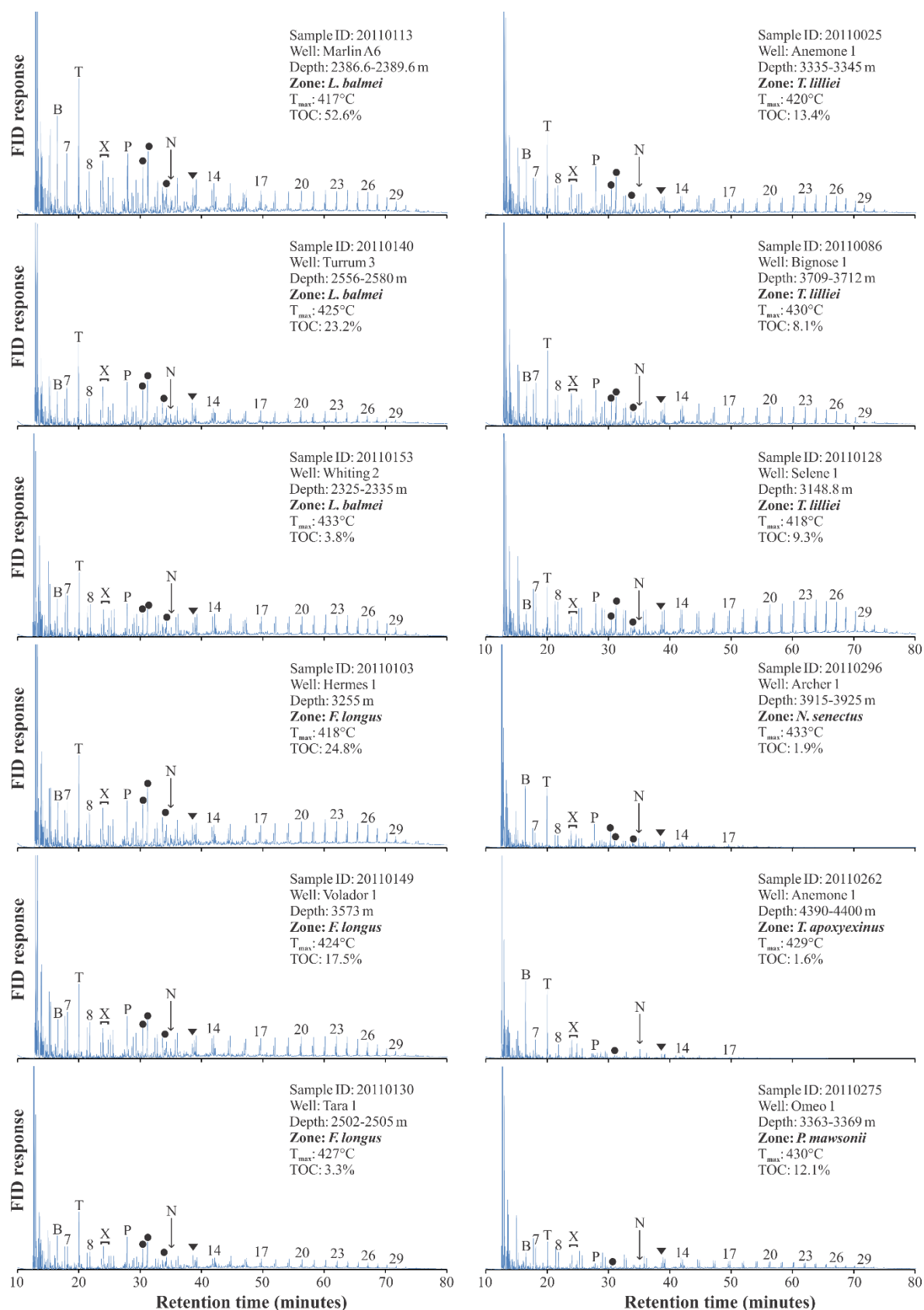
**Figure 3.7. Open-system pyrolysis-gas chromatography traces for 12 selected solvent-extracted source rock samples. Numbered peaks denote the number of carbon atoms in the *n*-alkane/*n*-alkene homologues; B = benzene; T = toluene; X = C₂ alkylbenzenes (ethylbenzene, *meta* + *para*-xylene, styrene, *ortho*-xylene, respectively); P = phenol; N = naphthalene. Black circles indicate C₃ alkylbenzenes and black triangles indicate alkylnaphthalenes.**

The third and most common pattern is recognised in the *F. longus*, *L. balmei* and *T. lilliei* samples, and has *n*-alkane/*n*-alkene doublets extending up to *n*-$C_{32}$ and displays a bimodal distribution, with a low molecular weight maxima, and a second maxima in the *n*-$C_{20+}$ range. Most pyrolysates with this third pattern have nearly identical Py-GC fingerprints. However, a characteristic feature of the hydrogen-rich shale from the *T. lilliei* biozone in Anemone 1 (sample 20110025) is the slight even-over-odd carbon number predominance in the *n*-$C_{20+}$ range that is suggestive of an aquatic plant input (Eglinton and Hamilton, 1963; Brooks, 1970), and is in keeping with the marine depositional environment inferred for the Anemone Formation.
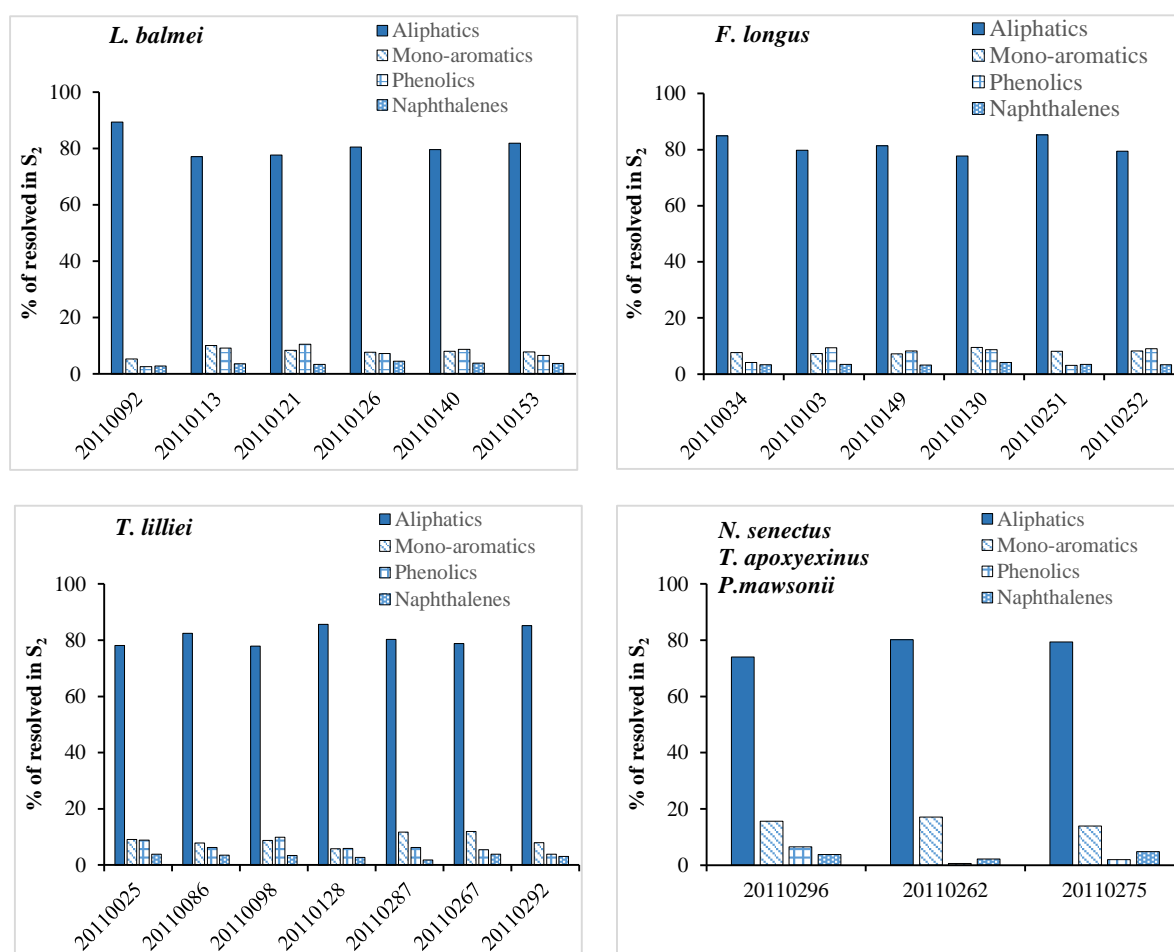


**Figure 3.8. Calculated percentages of the major resolved compound classes in 22 selected extracted kerogen pyrolysates from the Gippsland Basin. Aliphatics = Σ *n*-Alkanes + *n*-Alkenes; mono-aromatics = Σ Benzene + Styrene + $C_1$-$C_3$ Alkylbenzenes; phenolics = Σ Phenol + Methylphenols; naphthalenes = Σ Naphthalene + $C_1$-$C_2$ Alkylnaphthalenes.**

Apart from the enrichment in *n*-alkane/*n*-alkene doublets, the analysed pyrolysates contain variable amounts of mono-aromatic hydrocarbons, phenolic compounds and naphthalenes. The most dominant aromatic hydrocarbons in all of the chromatograms are toluene, followed by *m*- plus *p*-xylene and then benzene. Short chain alkylbenzenes and trimethylbenzenes are

also present in moderate amounts. For most of the studied samples, the mono-aromatic moieties are discernible in comparable amounts to those measured for the phenolic moieties **(Figure 3.8)**. Exceptions are shales from *T. lilliei* (20110287, 20110267 and 20110292) the *N. senectus*, *T. apoxyexinus* and *P. mawsonii* biozones, where mono-aromatic hydrocarbons form the second major pyrolysis class following the aliphatics. Phenol and alkylphenols are present in all of the chromatograms and their distributions do not differ greatly, indicating a higher land plant input into the organic matter (Larter and Senftle, 1985). The presence of these phenolic compounds together with the high concentration of long-chain *n*-alkane/*n*-alkenes suggest their derivation from a ligno-cellulosic precursor (Horsfield, 1997). Exceptions are the *T. apoxyexinus* and *P. mawsonii* samples that are more depleted in phenol, and in which alkylphenols are almost absent, suggesting only a minor land-plant contribution to the organic matter within the stratigraphically oldest sediments of the Latrobe Group. In most of the pyrolysates, naphthalene represents only a minor proportion of the identified components.

### 3.5.5. Predicted petroleum types

**Table 3.2** lists components used to determine the petroleum type that can be generated from the source rocks and the phenolic content of selected samples analysed by Py-GC. The *n*-alkyl chain length distributions were used by Horsfield (1989) to define the petroleum type that can be generated from a given source rock during its thermal maturation **(Figure 3.9)**. Source rock samples from the Gippsland Basin cluster in four different fields, resembling gas-condensates and oils with both low and high wax content. Out of the 22 samples analysed by Py-GC, only the two samples from the *N. senectus* and *T. apoxyexinus* biozones plot in the gas-condensate field, with the former plotting on the boundary with the paraffinic-naphthenic-aromatic (P-N-A) field. This affinity to generate gas rather than oil is in agreement with their low HI values (79 and 114 mg HC/g TOC, respectively) and their high light hydrocarbon abundance **(Figure 3.7)**, which indicate the presence of mainly gas-prone organic matter.
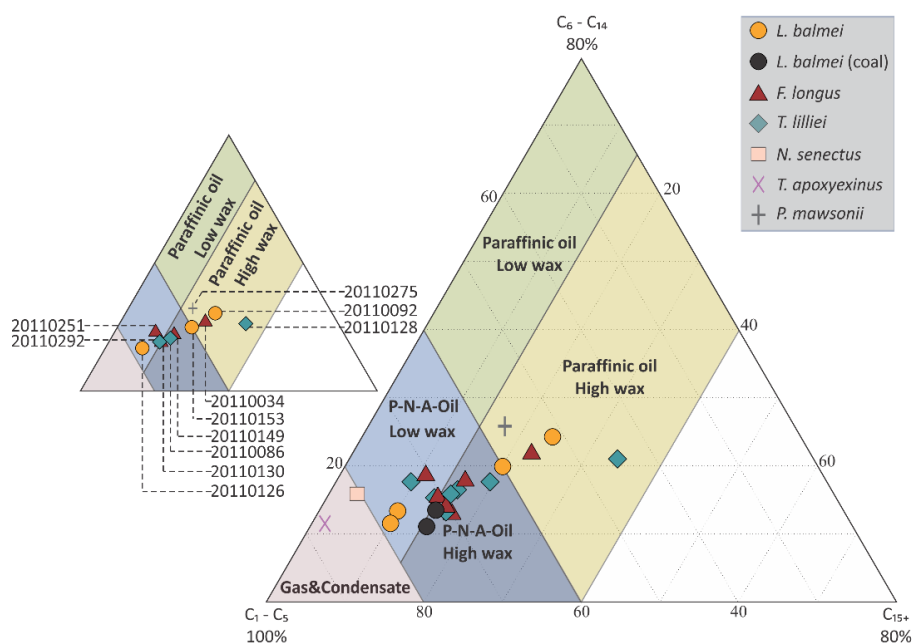
**Figure 3.9.** Ternary diagram of total C$_1$−C$_5$ hydrocarbons, C$_6$−C$_14$ *n*-alkenes plus *n*-alkanes, and C$_{15+}$ *n*-alkenes plus *n*-alkanes (Horsfield, 1989), showing the composition of the extracted kerogen pyrolysates for the studied source rocks. P-N-A = paraffinic-naphthenic-aromatic. Samples numbered on the small subset diagram are the samples chosen for bulk kinetic analyses.

Four samples, including the two *L. balmei* biozone coal samples, plot at the boundary of the low wax and high wax P-N-A petroleum generating facies. Similarly, four samples from the *L. balmei*, *F. longus* and *T. lilliei* biozones show the potential to produce low wax P-N-A oils. Generally kerogens plotting in this field are thought to be derived from marine shales with autochthonous organic matter (Horsfield, 1989). Hydrocarbons generated from the *P. mawsonii* biozone shale sample, and three samples each from the *L. balmei*, *F. longus* and *T. lilliei* biozones, correspond to high wax-paraffinic oils. The three samples from these latter biozones are defined as shales (based on their TOC content) and have HI > 300 mg HC/g TOC. Similar gross pyrolysate compositions were documented to be generated from lacustrine sediments (Horsfield, 1989). The remaining samples fall in the high wax P-N-A oils and grade into either high wax paraffinic oils or the low wax P-N-A oils. In the second diagram **(Figure 3.10)**, defined by Larter (1984) on the basis of the relative percentages of three chromatographically resolved components (*n*-octene, *m*- plus *p*-xylene and phenol), the source rock samples are less scattered and fall in the Type II/III kerogen field. Three exceptions are samples from the *L. balmei* (20110092) and *P. mawsonii* biozones (20110275) that show more affinity towards Type I-II kerogen, and the *T. apoxyexinus* biozone sample, which has affinity towards Type IV kerogen. As expected, coals show higher amounts of phenols compared to shales and shaly coals. The lowest phenolic contents

were measured for samples that are thermally mature to late mature ($T_{max}$ = 438–448°C), and thus any interpretation may be misleading.
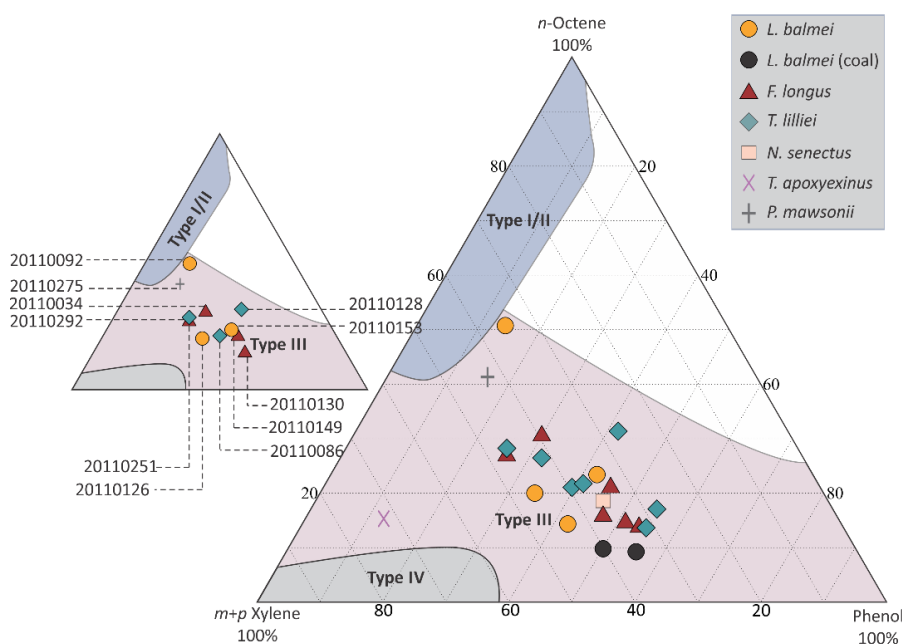


**Figure 3.10. Ternary diagram of phenol, *m*- and *p*-xylene and *n*-octene (Larter, 1984), showing the type of the extracted kerogen pyrolysates for the studied source rocks. Samples numbered on the small subset diagram are the samples chosen for bulk kinetic analyses.**

### 3.5.6. Bulk kinetic results

#### 3.5.6.1. Activation energy distribution

Kinetics for bulk petroleum generation, in terms of activation energy and frequency factor distribution, were measured by open-system pyrolysis for selected samples **(Figure 3.11)**. None of the samples used in this study have a narrow activation energy distribution consisting of one single peak, as is typical for homogenous marine and lacustrine organic matter. Instead, the overall activation energy distributions are broad, reflecting heterogeneous compositions, which are typical for terrigenous organic matter (Schenk et al., 1997; Petersen and Rosenberg, 2000). The activation energies measured for the sample set cover a range from 51 to 59 kcal/mol, with associated frequency factors between $2.13E^{+13}$/sec and $1.06E^{+15}$/sec, indicating a predominance of waxy organofacies D/E (Type III kerogen), according to the Pepper and Corvi (1995) classification. One exception is the shale sample from the *P. mawsonii* biozone, which has a relatively narrow activation energy distribution, with principal peaks at 51, 52 and 53 kcal/mol accounting for 25%, 33%, and 18% for the total generation potential, respectively. The sample 20110092 from the *L. balmei* biozone also has a relatively narrow activation energy distribution. Such a narrow activation energy distribution and the low frequency factor ($2.13E^{+13}$/sec) are indicative of a more

homogeneous organic precursor. Despite the HI of 603 mg HC/g TOC, the dominant activation energies defined for this shale are different from those previously reported (55–56 kcal/mol) for Type I kerogen deposited in a typical lacustrine environment (Petersen et al., 2010). In contrast, when comparing these dominant activation energies with those defined by Pepper and Corvi (1995), the *P. mawsonii* biozone shale can be regarded as an intermediate between organofacies B (Type II kerogen) and organofacies C (Type I kerogen). The thermally immature *T. lilliei* shales (20110128 and 20110086) have some similarities to the *P. mawsonii* biozone shale, having a tighter activation energy distribution than most samples with a mean activation energy in the range of 54–57 kcal/mol, suggesting similar precursors. In contrast, the more thermally mature sample 20110292 from the *T. lilliei* biozone shows a shift to a higher activation energy range (56–60 kcal/mol). Such an increase in the activation energy can be explained by a thermal maturity effect, which is also apparent from the slightly higher frequency factor ($5.80E^{+14}$/sec). The thermally immature and organic-rich (HI > 250) *F. longus* (20110034 and 20110130) and *L. balmei* (201101253) biozone shales show narrower activation energy distributions than most samples, with maxima at 52–56 kcal/mol and fewer peaks at both lower and higher activation energy values. The only coal sample within the *F. longus* biozone (20110279C) that was subjected to kinetic analysis reveals the broadest activation energy pattern, suggesting a complex organic composition. For this sample, activation energies extend from about 49 to 70 kcal/mol, with mean activation energies in the range of 55–60 kcal/mol defining approximately 70% of the petroleum potential.

### 3.5.6.2. Petroleum formation timing predictions

**Figure 3.12** shows temperatures of bulk petroleum generation and the corresponding transformation ratios (TR), determined assuming a constant geological heating rate of 3.3°C/Ma. This geological heating rate is reported to be in the average range of heating conditions (3–5°C/Ma) typical of sedimentary basins (Dieckmann, 2005). The sample variability in terms of activation energy distributions and frequency factors as shown in **Figure 3.11** is clearly reflected in the temperatures at which kerogen conversion occurs. The onset of petroleum generation (10% TR) from the least to the most stable organic matter ranges from 125°C to approximately 150°C, respectively. In contrast, the peak of petroleum generation (70% TR) occurs over a broader temperature range of 150 to 182°C, likely indicating the involvement of different cracking reactions with increasing thermal maturation.
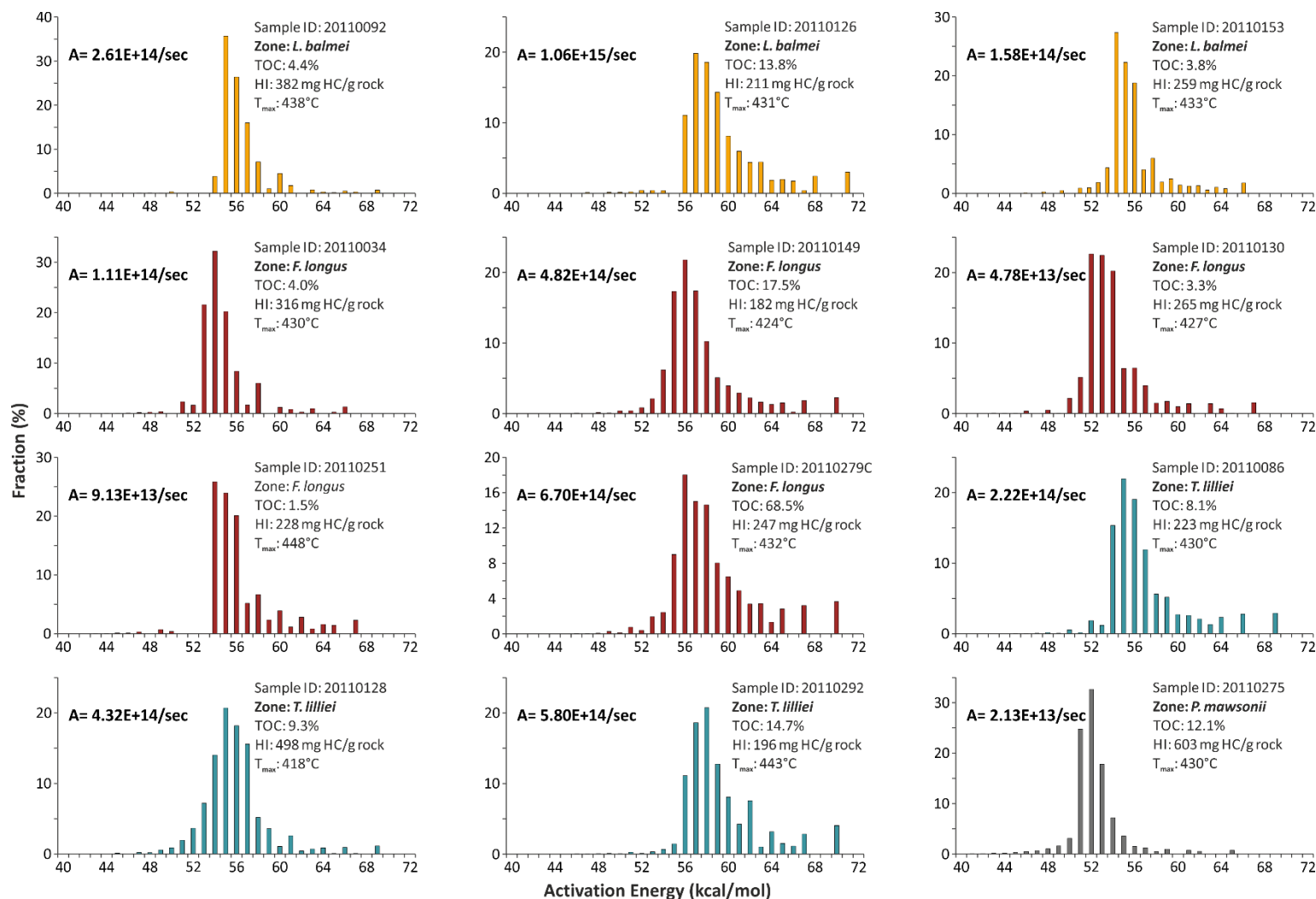
**Figure 3.11. Bulk kinetic parameters in terms of activation energy distribution (Ea) and frequency factors (A) of 12 selected solvent-extracted source rock samples. Data were determined from open-system pyrolysis at three heating rates (0.1, 0.7 and 5°C/min).**

A closer examination of the petroleum formation evolution shows that each of the investigated biozones displays a wide range of thermal stability and different petroleum generation characteristics. The main phase of petroleum formation takes place at 163 to 179°C for the *L. balmei* biozone source rocks, at 158 to 178°C for the *F. longus* biozone source rocks, and at 160 to 182°C for the *T. lilliei* biozone source rocks. Such high and variable generation temperatures are compatible with heterogeneous Type II/III kerogen within the Upper Cretaceous to Paleocene source rocks. Hydrocarbon generation from the *F. Longus* biozone coal sample is predicted to start at 140°C, with the peak oil window being at 178°C. Interestingly, two shale samples, one from the *L. balmei* biozone (20110126) and the other from the *T. lilliei* biozone (20110292), exhibit higher temperatures for the onset of petroleum formation (~147–150°C) than the coal sample. For the former, these high temperatures can be explained by the sample containing complex but stable organic matter, as revealed by its high-skewed activation energy distribution and its high frequency factor. For the later, the high stability is related to its high level of thermal stress ($T_{max}$ = 443°C), which results in the loss of the less stable bonds within the kerogen during increased thermal degradation (Schenk and Horsfield, 1998). Compared to all the other samples, the onset of bulk petroleum formation (10%TR) from the *P. mawsonii* biozone sample containing Type I to I/II kerogen, is predicted to occur at the lowest temperature of 125°C, with peak petroleum formation at 150°C.
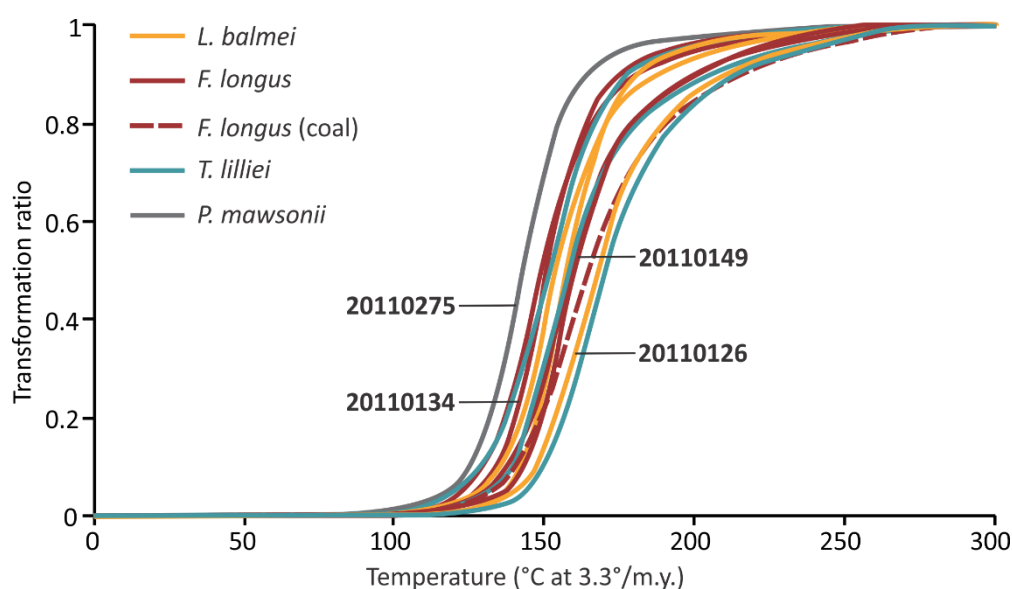


**Figure 3.12.Transformation ratio evolution of 12 selected solvent-extracted source rock samples at a geological heating rate of 3.3°C/Ma. The numbered samples correspond to samples selected for compositional kinetic experiments.**

### 3.5.7. Compositional kinetics and phase behaviour

Compositional kinetic models describing the primary cracking of kerogen into petroleum were measured for four selected source rock samples using a closed-pyrolysis system. These four samples are thermally immature shales and were chosen based on two criteria: (1), to be representative of each of the main defined petroleum types (high wax paraffinic, low wax P-N-A and high wax P-N-A); and (2), to cover the variations observed in the bulk kinetic behaviour, from the kinetically least to most stable. The petroleum products and their physical properties (GORs, $B_O$ and $P_{sat}$) were predicted at five transformation ratios (10%, 30%, 50%, 70% and 90% TR), as summarised in **Table 3.3**. Three sets of models were developed based on two components ($C_1$−$C_5$ and $C_{6+}$; **Table 3.4**), four components ($C_1$, $C_2$−$C_5$, $C_6$−$C_{14}$ and $C_{15+}$; **Table 3.4**) and 14 components.

**Table 3.3. Predicted gas:oil ratios (GOR), formation volume factor ($B_O$) and saturation pressure ($P_{sat}$) as a function of increasing Transformation Ratio (TR) for four source rock samples from the Gippsland Basin.**

| End temperature (°C) | TR (%) | GOR ($Sm^3/Sm^3$) | $B_O$ ($m^3/m^3$) | $P_{sat}$ (bar) |
|---|---|---|---|---|
| Sample ID: 20110126 | | | | |
| Palynological zone: *L. balmei* | | | | |
| 385 | 10 | 213 | 1.75 | 197 |
| 409 | 30 | 214 | 1.73 | 213 |
| 425 | 50 | 234 | 1.78 | 227 |
| 445 | 70 | 360 | 2.22 | 254 |
| 493 | 90 | 1443 | – | 410 |
| Sample ID: 20110034 | | | | |
| Palynological zone: *F. longus* | | | | |
| 374 | 10 | 119 | 1.44 | 145 |
| 397 | 30 | 118 | 1.42 | 155 |
| 411 | 50 | 133 | 1.47 | 163 |
| 425 | 70 | 147 | 1.51 | 173 |
| 453 | 90 | 291 | 2.02 | 218 |
| Sample ID: 20110149 | | | | |
| Palynological zone: *F. longus* | | | | |
| 375 | 10 | 145 | 1.49 | 195 |
| 399 | 30 | 165 | 1.56 | 196 |
| 415 | 50 | 172 | 1.57 | 210 |
| 433 | 70 | 222 | 1.75 | 218 |
| 481 | 90 | 827 | – | 458 |
| Sample ID: 20110275 | | | | |
| Palynological zone: *P. mawsonii* | | | | |
| 370 | 10 | 120 | 1.42 | 168 |
| 395 | 30 | 108 | 1.37 | 174 |
| 409 | 50 | 113 | 1.37 | 189 |
| 424 | 70 | 124 | 1.41 | 197 |
| 447 | 90 | 175 | 1.59 | 205 |

**Table 3.4. Compositional kinetics used for models with two components (oil and gas) and four components generated during the primary cracking of kerogens by closed-system MSSV pyrolysis of four source rock samples from the Gippsland Basin.**

| Sample ID | Well name | Depth (m) | Palynological zone | Kerogen type (Py-GC) | Oil (%) | Gas (%) | $C_1$ (%) | $C_2$–$C_5$ (%) | $C_6$–$C_{14}$ (%) | $C_{15+}$ (%) |
|---|---|---|---|---|---|---|---|---|---|---|
| 20110126 | Sawbelly 1 | 3015 | *L. balmei* | P-N-A low wax | 68 | 32 | 16 | 16 | 31 | 37 |
| 20110034 | Basker 1 | 3109 | *F. longus* | Paraffinic high wax | 81 | 19 | 7 | 12 | 35 | 46 |
| 20110149 | Volador 1 | 3573 | *F. longus* | P-N-A high wax | 74 | 26 | 12 | 14 | 30 | 44 |
| 20110275 | Omeo ST1 | 3363–3369 | *P. mawsonii* | Paraffinic high wax | 83 | 17 | 6 | 11 | 28 | 55 |

The latter set of models, displayed in **Figure 3.13**, was established based on $C_1$, $C_2$, $C_3$, *i*-$C_4$, *n*-$C_4$, *i*-$C_5$, *n*-$C_5$, *n*-$C_6$, $C_7$−$C_{15}$, $C_{16}$−$C_{25}$, $C_{26}$−$C_{35}$, $C_{36}$−$C_{45}$, $C_{46}$−$C_{55}$, and $C_{56}$−$C_{80}$ components. Together, $C_7$−$C_{15}$ and $C_{16}$−$C_{25}$ represent the dominant fractions in hydrocarbons generated by the four shales, accounting for the predominantly liquid petroleum potential of the Latrobe Group.

In terms of physical properties, a special emphasis was given to the evolution of GORs with increasing kerogen conversion to liquid and gaseous hydrocarbons **(Figure 3.14)**. During the earliest stages of kerogen cracking (between 10 and 50% TR), all four of the investigated samples show the potential to generate relatively similar GORs ranging from 107.9 to 234.3 $Sm^3/Sm^3$. In contrast, broader variations are observed during the main oil window (70% TR) and at advanced stages of thermal maturation (90% TR). Overall, the highest GORs were produced from the low-wax P-N-A generating sample (20110126). This sample displays a distinct evolution with increasing transformation ratio, generating black oil (GOR < 350 $Sm^3/Sm^3$) at 10−50% TR, light oil (350 <GOR <600 $Sm^3$) at 70% TR, and gas-condensate (GOR > 600 $Sm^3$) at 90% TR. Gas-condensate was also produced by the high wax P-N-A-generating sample (20110149) at 90% TR. This pronounced increase in GORs at higher conversion rates is attributed to the initiation of secondary cracking reactions. The *F. longus* and *P. mawsonii* high-wax paraffinic samples (20110034 and 20110275) exhibit similar compositional evolution, with only black oils being generated at all levels of transformation. However, sample 20110034 produced a slightly higher GOR at 90% TR (291 $Sm^3/Sm^3$) compared to sample 20110275 (175 $Sm^3/Sm^3$). This observation indicates that source rocks with the potential to generate the same petroleum type would also produce fluids with comparably similar GORs, but not necessarily over the same temperature range.

In the Gippsland Basin, reservoired fluids have variable GORs that range from very low (8 $Sm^3/Sm^3$) to high (9708 $Sm^3/Sm^3$) values **(Figure 3.15)**. Overall, these measured GORs (e.g. Blackback, Flounder and Grunter) are in good agreement with those predicted under laboratory conditions for shales of the Latrobe Group. However, the discrepancy between the predicted GORs and the low GORs measured in the oil fields could be either due to maturity effects (Fortescue, Halibut and Mackerel) or to secondary alteration processes, such as biodegradation (e.g. Perch and Whiptail) or water-washing (e.g. Seahorse and Tarwhine), as can be seen on the interpretative **Figure 3.15** of Hoffman and Preston (2014).
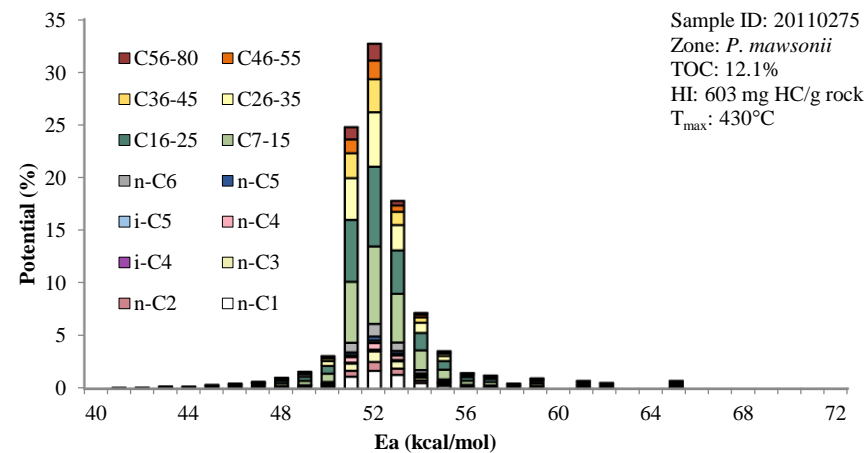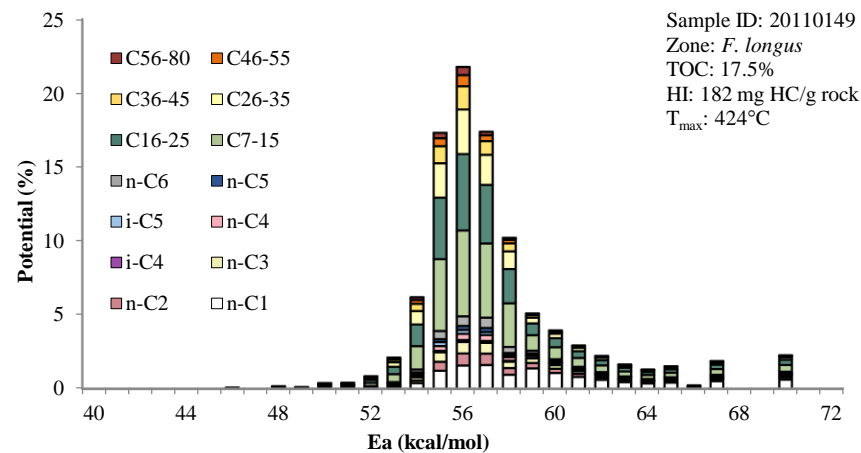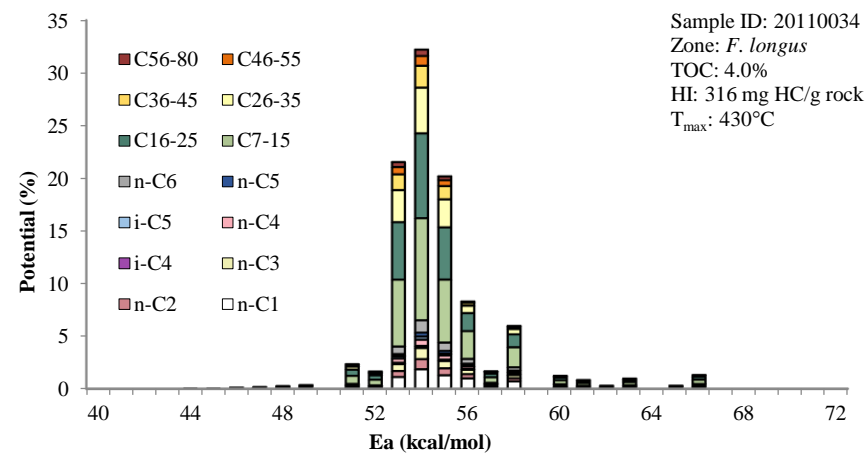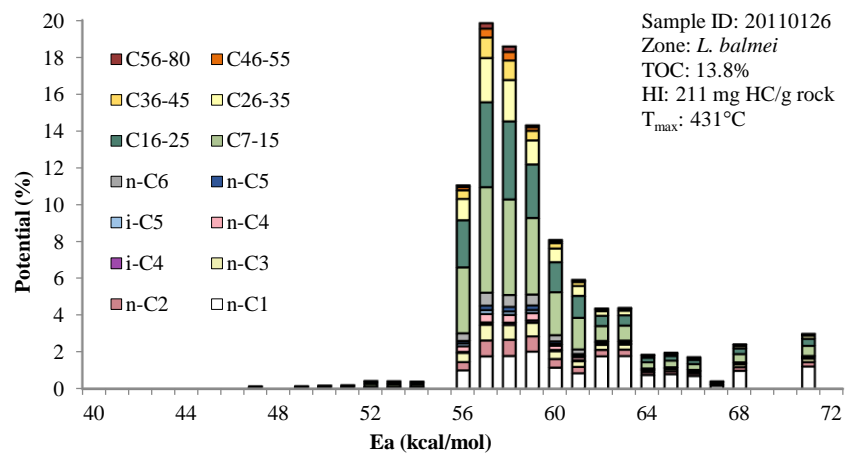
**Figure 3.13. Compositional kinetic models with fourteen components for four source rock samples from the Gippsland Basin.**
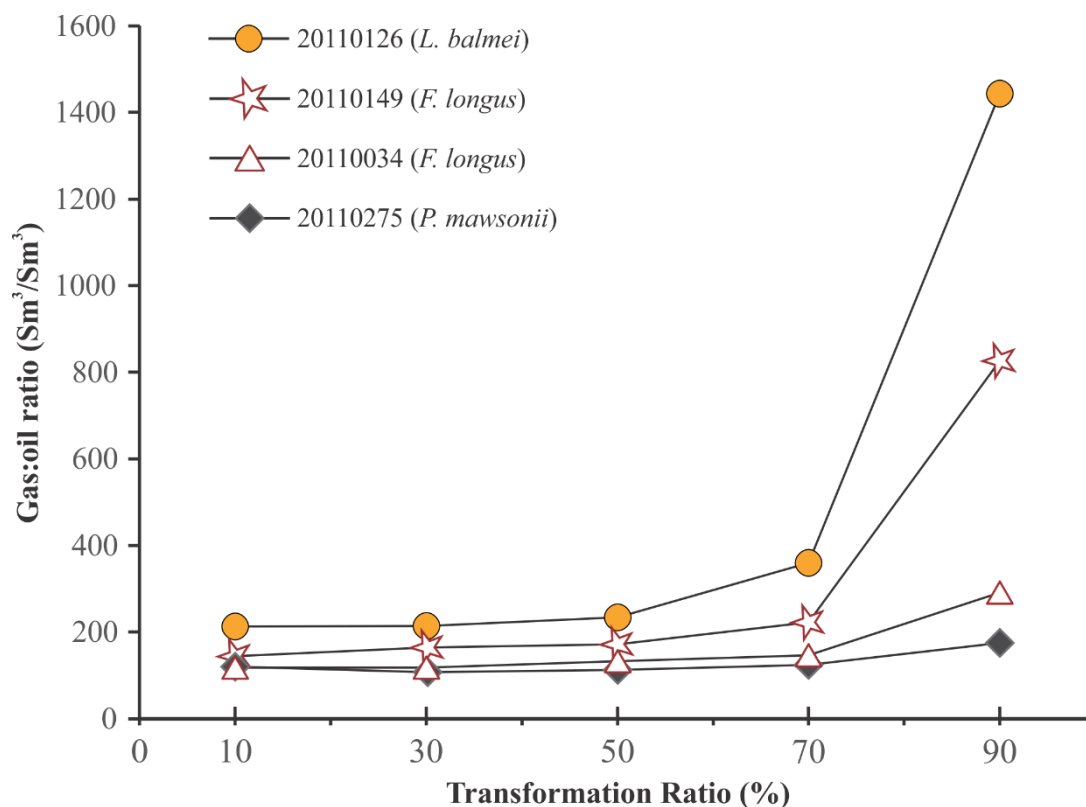
**Figure 3.14. Gas:oil ratio evolution as a function of increasing transformation ratio generated from pyrolysis experiments in a closed-system MSSV of four selected source rock samples from the Gippsland Basin.**

### 3.5.8. Maceral assemblages

To determine the influence of the bulk maceral groups (liptinite, vitrinite and inertinite) on the type of petroleum than can be generated, the *n*-alkane chain length for samples, where both data types were available, was used **(Figure 3.16)**. The petrographic data, illustrated in the pie diagrams, were gathered from the Geoscience Australia database compiled from well completion reports and destructive analysis reports. There are considerable variations in the reported maceral group content of the source rock units in the Latrobe Group. These variations are observed at different ages and within the same stratigraphic unit. In the majority of samples from the *L. balmei, F. longus* and *T. lilliei* biozones, either vitrinite or inertinite comprise the major maceral groups **(Figure 3.16)**. The dominance of liptinite was reported only for the *P. mawsonii* biozone shale sample.

Samples plotting in the high wax-paraffinic oil zone of **Figure 3.16** are the hydrogen-rich shales from the *P. mawsonii* (HI = 603 mg HC/g TOC) and *T. lilliei* (HI = 498 mg HC/g TOC) biozones. The former has a high liptinite (90%) and low inertinite (10%) content, whereas the latter has a more heterogeneous maceral composition, with comparable proportions of inertinite and vitrinite (47 and 41%, respectively) and 12% liptinite. Although

not clearly noticeable in the case of the *T. lilliei* biozone shale, the high amount of liptinite in the *P. mawsonii* shale is in accordance with its paraffinic oil-generating potential.
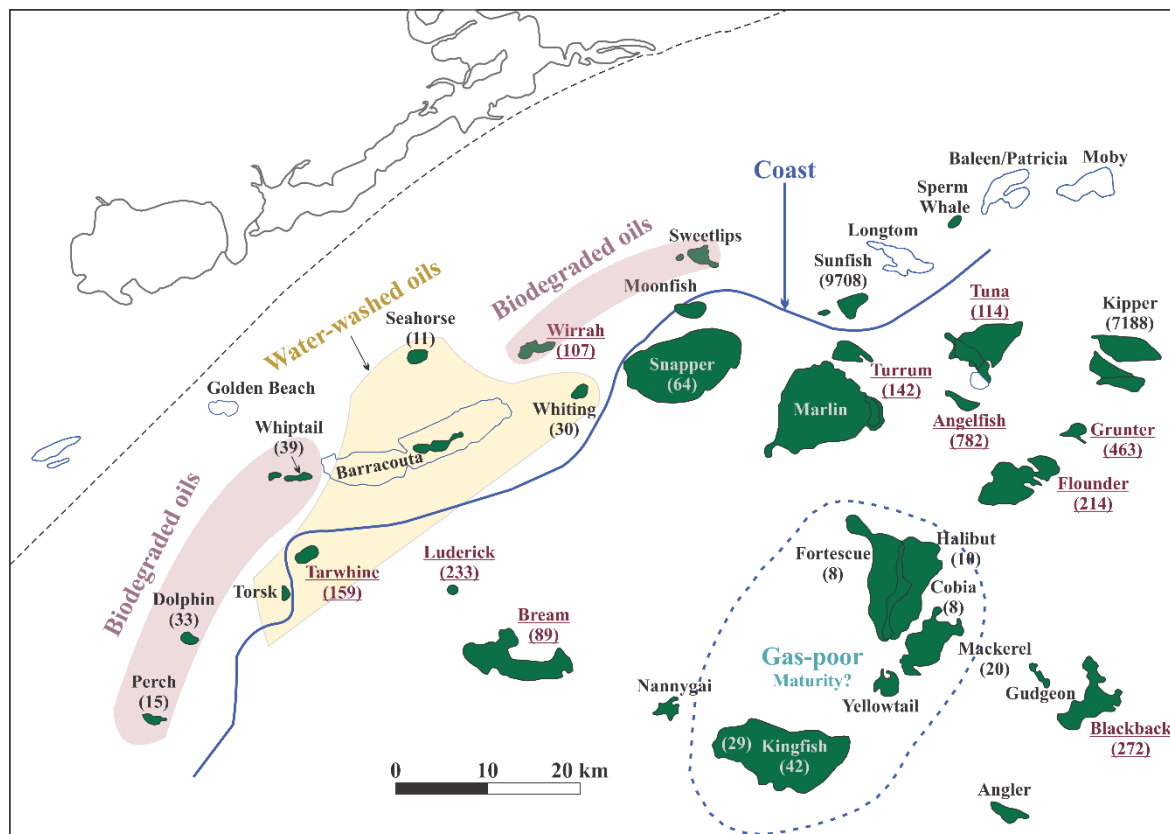


**Figure 3.15. Liquid hydrocarbon distribution in the Gippsland Basin. Numbers represent the measured gas:oil ratios (GORs) expressed in Sm$^3$/Sm$^3$. Underlined in red are measured GORs that show good correlation with model predictions under laboratory conditions. Interpretations are after (Hoffman and Preston, 2014).**

Samples falling in the high wax P-N-A field correspond generally to those with high vitrinite content (62 to 90%) and variable amounts of inertinite (1 to 22%) and liptinite (9 to 21%). Similarly, the low wax P-N-A−generating sample (20110086) is enriched in vitrinite (64%) with slightly higher liptinite (21%) compared to inertinite (12%) content. The *L. balmei* biozone coal (20110121) and the *T. lilliei* biozone shale (20110086) plot on the border between the high and low-wax P-N-A fields, but have different bulk maceral contents, with the former being dominated by vitrinite (82%) and the latter by inertinite (75%). Shales from the *N. senectus* and *T. apoxyexinus* biozones display similar maceral proportions, with up to 90% inertinite and equal proportions of vitrinite and liptinite. The low HI values measured for the *N. senectus* and *T. apoxyexinus* biozone samples and their inertinite-dominated composition is consistent with their position in the gas-condensate field.
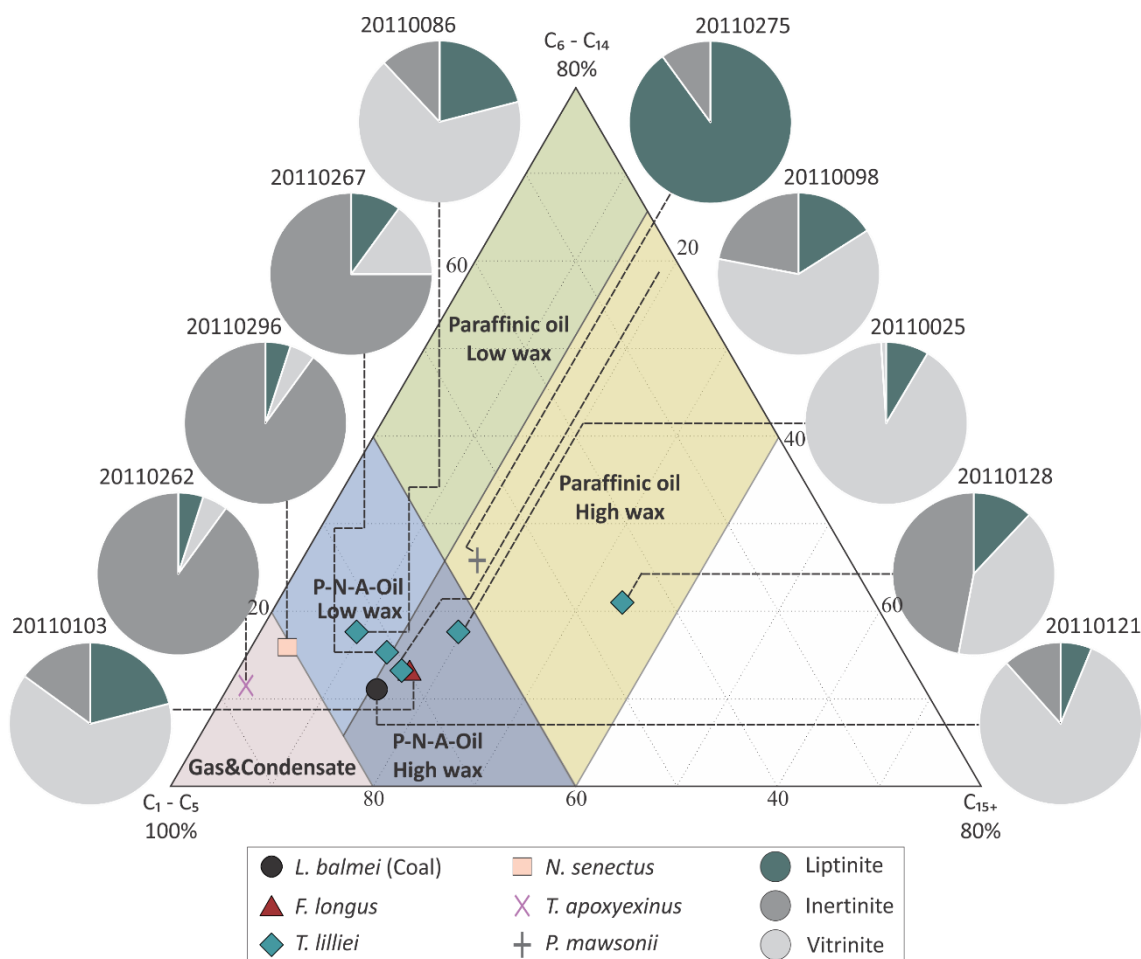
**Figure 3.16. Ternary diagram of the chain length distribution of ten source rock pyrolysates, with superimposed pie charts showing maceral group composition, illustrating the relationship between petroleum-type organofacies and bulk maceral group composition in the Gippsland Basin.**

Hence, differences in petroleum type cannot be fully elucidated by the bulk maceral group content, and other factors such as changes in sea-level, and redox and preservation conditions. Most of the samples with the potential for liquid hydrocarbon generation show a predominance of vitrinite in their composition and variable amounts of liptinite, which are typical for mixed Type II/III kerogens. By combining molecular, bulk and compositional properties, it is, however, possible to gain some insights into the depositional conditions of the source rocks in the Latrobe Group. Similar generation characteristics were observed over a wide range of thermal maturation for the hydrogen-enriched and paraffinic oil-generating *P. mawsonii* and *T. lilliei* biozone shales. The absence of inertinite, low OI values, abundance of aliphatic components and the high liptinite content of the *P. mawsonii* biozone shale can be related to the abundance of algae preserved in anoxic lacustrine shales. The high OI values and the high inertinite and vitrinite contents in the *T. lilliei* biozone shale (20110128) suggest initial deposition under more oxic lacustrine conditions. Apart from these two shales, no

algal signature was detected in the overlying land-plant-influenced *L. balmei* and *F. longus* biozones, as indicated by their overall low liptinite content.

A marine influence can be discerned in some samples as indicated by their potential to generate P-N-A oil with a low wax content. The organic matter within the *N. senectus* and *T. apoxyexinus* shales of the Golden Beach Subgroup originates from a mixture of land-plant material with a minor input of algal remains, and can produce either gas-condensate or low wax P-N-A oils. Solvent extracts from the shale samples of the *N. senectus* and *T. apoxyexinus* biozones, together with the shale extract of the *P. mawsonii* biozone have been analysed and examined for their biomarker distribution by (Ahmed et al., 2013). These authors group together these source rock extracts, which have a marine signature and which have a genetic relationship to oil reservoired in Anemone 1A. The marine affinity in these hydrocarbons was attributed based on the presence of low to moderate amounts of tricyclic terpanes (($C_{19}+C_{20}$)/$C_{23}$ = 0.33–3.2), $C_{29}$ regular steranes (42–54%), and the very low concentration of oleanane. The relative abundance of inertinite within both the *N. senectus* ad *T. apoxyexinus* biozones may imply that oxidation altered the structure of the originally marine preserved organic material.

The characteristics of the remaining shaly coals and coals of the *T. lilliei*, *F. longus* and *L. balmei* biozones, with the potential to generate P-N-A oils, are likely compatible with their deposition in lower to upper delta plain settings, where land-plant material generally dominates. Evidence for terrigenous precursors in these sediments was documented by Moore et al. (1992) and Ahmed et al. (2013), based on the high amounts of a number of biomarker compounds (e.g. tricyclic terpanes, oleanane, and $C_{29}$ steranes). Within these biozones, sediments with relatively high HI values could also have been deposited in marginal marine conditions.

## 3.6.  Discussion

Based on the Rock-Eval pyrolysis HI values alone, the majority of samples analysed from the Latrobe Group are regarded as having the potential for gas generation with no or little oil generative capacity. These results are not in agreement with those derived from the Py-GC analyses, which indicate that the coals, shaly coals and shales within the *L. Balmei*, *F. longus* and *T. lilliei* biozones, have the capacity to produce P-N-A oils. This discrepancy reveals that the HI values are inaccurate indicators of the oil-generating potential of the land-plant-dominated kerogens. Such an outcome has been addressed by Horsfield et al. (1988) for Indonesian coals within the Talang Akar Formation, Ardjuna Basin. Conventionally,

coals are considered to be effective sources of oil and gas in the Gippsland Basin (Burns et al., 1984; 1987; Cook and Struckmeyer, 1986; Moore et al., 1992). In spite of their relatively low HI values, the six coals from the *L. balmei* biozone and one coal from the *F. longus* biozone are also herein interpreted to be capable of generating liquid hydrocarbons. This result is consistent with that reported by Powell et al. (1991), who concluded that Cenozoic Australian coals can be enriched in aliphatic structures and thus contain oil-prone organic matter. The Cretaceous *F. longus* biozone coal has slightly higher liquid petroleum potential compared to the Cenozoic *L. balmei* biozone coals, possibly as a result of different preservation conditions. In addition, Partridge (2012) conducted a palynological and kerogen study of seven wells in both the onshore and offshore parts of the Gippsland Basin, in which an overall decrease in percentages of gymnosperms from the Lower Cretaceous sediments (+94%, Omeo 1) to the Upper Cretaceous (55%, Volador 1) was demonstrated. Although less discernible, there is an increase in percentages of angiosperms towards the stratigraphically younger sediments, so therefore plant input may also influence the petroleum generative potential of coals and associated shales. Examined core and well log data show that coal beds are typically thin and represent only a minor proportion of the whole sedimentary package. Hence, the 7 coals, out of the 91 samples examined in this study, are believed to be representative of the Halibut Subgroup. These coal samples, except the one from *F. longus* biozone, have low HI values (< 200 mg HC/g TOC), but they show the potential to generate P-N-A oils with intermediate wax content (they plot at the boundary between the low and high wax P-N-A field). The *F. longus* coal sample that was analysed for bulk kinetics has a broad activation energy distribution, typical for Type III kerogen, and the highest kinetic stability compared to the thermally immature shales and coaly shales analysed. The ability of the investigated coals to expel liquid hydrocarbons is not addressed in this study. However, the significant proportion of free hydrocarbons within these facies and their probable restricted thickness, indicate that expulsion could occur. These results suggest that it is unlikely that the coals have contributed significantly to the oil accumulations in the basin. This can be supported to some extent by the Ahmed et al. (2013) biomarker study, in which no genetic relationship was established between the coal extract from the *F. longus* biozone (the same sample as used in this study) and oils recovered from the Gippsland Basin.

Shales and shaly coals have higher HI values than those measured for coals, and thus a higher oil-generating potential, leading Brooks (1970) to conclude that shales and shaly coals, rather than coals, are the major source of hydrocarbons in the Gippsland Basin. Apart from their potential to produce P-N-A oils, some shales in this study can also generate paraffinic

oils. On a bulk scale, the shales and shaly coals show variable kinetic stabilities and wide heterogeneities in their petroleum generation characteristics. These heterogeneities are also noticeable on the compositional scale, where black oils, light oils and gas-condensates are generated at different stages of thermal maturation. These overall properties explain to a large extent the variable compositions of the unaltered oils in the basin, which range from paraffinic to naphthenic with variable wax content (e.g. Hedberg, 1968; Brooks and Smith, 1969). Overall, most of the oils in the basin are interpreted to have been generated over a narrow thermal maturity range. Burns et al. (1987) proposed that the wide compositional variations of the Gippsland Basin oils are the result of different levels of thermal maturity, interpreted to be at equivalent vitrinite reflectances of between 0.9% and 1.16%. More recently, Moore et al. (1992), in his evaluation of the thermal maturity of the Gippsland Basin, suggested that higher vitrinite reflectance ranges of 1.15–1.3% and 1.25–2.0% are required for oil and gas generation, respectively. The kinetic model predictions for bulk oil formation are consistent with both the ranges reported by Burns et al. (1987) and Moore et al. (1992), which using the Easy %$R_O$ calibration of vitrinite reflectance, correspond to temperatures of 125–145°C and 145–160°C, respectively. Over these temperature intervals, compositional kinetic models developed for representative shales of the Latrobe Group show the potential to generate light and black oils. In contrast, at the very low vitrinite reflectance range of 0.4 to 0.8% suggested by Smith and Cook (1984) and that would be equivalent to a temperature range of ~ 65 to 120°C, the kinetic models developed in this study predict that none of the source rock units of the Latrobe Group would be capable of generating hydrocarbons (~7% TR).

The *P. mawsonii* biozone shale of the basal Emperor Subgroup is interpreted as having a significant potential for oil generation. However, both thickness and distribution of this shale are unknown, so its contribution to petroleum in the Gippsland Basin cannot yet be constrained.

Gas-condensate is predicted to have been produced by the *T. apoxyexinus* and *N. senectus* biozone shales of the Golden Beach Subgroup. In addition, shales and coaly shales of the *L. balmei* and *F. longus* biozones, and possibly those of the *T. lilliei* biozone, show potential to generate gas and condensate towards the end of the oil generation window. Further oil and gas charge from deeper and stratigraphically older and organic-rich sediments could also contribute to hydrocarbon accumulations in the Gippsland Basin. For instance, O'Brien et al. (2008) anticipated a further gas charge in both onshore and offshore fields to be provided by mature sediments of the Strzelecki Group. Taking into account the low present-day thermal

maturities ($R_0$ = 0.4 to 0.6%) measured at reservoir levels (Rahmanian et al., 1990), it is unlikely that secondary cracking of oil into gas could have occurred. Similar land-plant-dominated shales and shaly coals are proposed to be the main sources for both gas and oil in the basin. Previous studies have shown that several mechanisms, such the timing of oil and gas generation and expulsion and the filling and spilling of the traps, seal quality and secondary alteration processes (e.g. water-washing and evaporative fractionation) explain the overall oil and gas field distribution in the basin (Burns et al., 1987; Rahmanian et al., 1990; Moore et al., 1992; O'Brien et al., 2013; Hoffman and Preston, 2014). Elevated levels of thermal maturity, induced by the deposition of thick carbonates and thus deep burial of the Latrobe Group, are thought to have favoured gas over oil generation in the northwestern part of the basin (Rahmanian et al., 1990; O'Brien et al., 2013). Moore et al. (1992) attributed the high maturity and gas generation in the eastern part to anomalously high heat flows during the opening of the Tasman Sea. Results derived from this study cannot sustain any of the aforementioned mechanisms, but suggest that thermal maturity differences and facies variations, combined with the effects of secondary alteration processes, are the main controls on the gross compositions of gases and oils in the Gippsland Basin.

## 3.7. Conclusions

The Upper Cretaceous to Paleogene Latrobe Group organic-rich sediments sampled from petroleum wells within the Gippsland Basin comprise Type II/III kerogens with variable petroleum potential. The coals (>50% TOC) within the *L. balmei* and *F. longus* biozones of the Halibut Subgroup contain Type III kerogens which have relatively low HI values, typically < 200 mg HC/g TOC. Most of the shales and shaly coals within the *L. balmei, F. longus* and *T. lilliei* biozones have potential for both oil and gas generation and expulsion. In contrast, shales of the *N. senectus* and *T. apoxyexinus* biozones (Golden Beach Subgroup) contain Type III Kerogen and can generate mainly gas.

The *P. mawsonii* biozone (Emperor Subgroup) shale and some hydrogen-enriched shales within the *T. lilliei* biozone (Golden Beach Subgroup) show an affinity to Type I-II kerogen, indicating a high capacity for liquid petroleum generation. Open-system pyrolysis-gas chromatography traces reveal the presence of three *n*-alkyl distribution patterns, which are suggestive of at least three organic precursors, with no obvious association with their maceral group composition. Upon thermal maturation, the shales and shaly coals from the *L. balmei*, *F. longus* and *T. lilliei* biozones can produce three petroleum types– low P-N-A oils, high wax P-N-A oils and high wax paraffinic oils. Marine shales of the *N. senectus* and *T. apoxyexinus* biozones have the potential to generate gas and condensate. The abundance

of the inertinite maceral group in these shales may indicate unfavourable conditions of preservation and thus alteration of their marine organic matter. The high amount of liptinite and the low concentration of phenolic compounds in the lacustrine shale from within the *P. mawsonii* biozone explains to a large extent their capacity to generate paraffinic oils.

The distribution of activation energies determined for shales, shaly coals and coals from *L. balmei*, *F. longus* and *T. lilliei* biozones are broad, indicating inhomogeneous organic matter dominated by land-plant material. The main phase of bulk petroleum formation, determined by open-system pyrolysis and extrapolated to geological conditions, are predicted to occur over the temperature range of 158 to 178°C. The lacustrine shale from the *P. mawsonii* biozone has a narrow distribution of activation energy and temperatures as low as 150°C are required to release petroleum from this shale at 70% of kerogen conversion, suggesting lower levels of kinetic stability compared to the overlying palynofacies.

In response to increased thermal stress under closed-system pyrolysis, representative shale samples from the Latrobe Group have the potential to produce variable petroleum compositions. During the early and main stages of petroleum generation, black oils with variable GORs (107–222 $Sm^3/Sm^3$) are generated from these shales. In contrast, either black oils with higher GORs, light oils, or gas-condensates are produced at higher levels of thermal maturation (at 70 to 90% transformation ratios). The implications of the molecular data, the bulk properties and these compositional schemes are that oil fields in the Gippsland Basin received waxy and paraffinic oils with variable GORs (depending on their thermal maturity) from the Upper Cretaceous to Paleogene shales and shaly coals. Gas fields may have received charge either from more mature equivalents of the *L. balmei*, *F. longus* and *T. lilliei* biozones of the Halibut and Golden Beach subgroups or from the stratigraphically older *N. senectus* and *T. apoxyexinus* biozone shales of the Golden Beach Subgroup. Coals previously interpreted to be the primary source of both oil and gas have the potential to generate P-N-A oils, but further work is required to check whether these coals have the capacity to expel liquid hydrocarbons.

## 3.8. Acknowledgments

## 3.9.    References

Ahmed, M., Volk, H., George, S.C., Faiz, M., Stalker, L., 2009. Generation and expulsion of oils from Permian coals of the Sydney Basin, Australia. Organic Geochemistry 40, 810-831.

Ahmed, M., Edwards, D.S., Volk, H., Gong, S., Tingate, P.R., Boreham, C.J., 2013. Using biomarkers and multivariate statistics to unravel the genesis of petroleum in the Gippsland Basin, Australia (Oral presentation). International Meeting on Organic Geochemistry, Tenerife-Spain, 15-20 September.

Alexander, R., Noble, R., Kagi, R., 1987. Fossil resin biomarkers and their application in oil to source-rock correlation, Gippsland Basin, Australia. Australian Petroleum Exploration Association Journal 27, 63-72.

Bernecker, T., Partridge, A.D., 1997. Mid-Late Tertiary deep-water temperate carbonate deposition, offshore Gippsland Basin, southeastern Australia, in: James, N.J., Clarke, J. (Eds.), Cool and Temperate Water Carbonates. Special Publication 56, Society of Economic Palaeontologists and Mineralogists, Tulsa, pp. 22-23.

Bernecker, T., Partridge, A.D., 2001. Emperor and Golden Beach subgroups: the onset of Late Cretaceous sedimentation in the Gippsland Basin, SE Australia, in: Hill, K.C., Bernecker, T. (Eds.), Eastern Australasian Basins Symposium, A Refocused Energy. Perspective for the Future, Petroleum Exploration Society of Australia, pp. 391-402.

Boreham, C.J., Horsfield, B., Schenk, H.J., 1999. Predicting the quantities of oil and gas generated fromAustralian Permian coals, Bowen Basin using pyrolyticmethods. Marine and Petroleum Geology 16, 165-188.

Boreham, C.J., Hope, J.M., Hartung-Kagi, B., 2001. Understanding source, distribution and preservation of Australian natural gas: a geochemical perspective. Australian Petroleum Production and Exploration Association Journal 41, 523-547.

Brooks, J.D., 1970. The use of coals as indicators of the occurrence of oil and gas. Australian Petroleum Exploration Association Journal 10, 35-40.

Brooks, J.D., Smith, J.W., 1969. The diagenesis of plant lipids during the formation of coal, petroleum and natural gas—II. Coalification and the formation of oil and gas in the Gippsland Basin. Geochimica et Cosmochimica Acta 33, 1183-1194.

Brown, B., 1986. Offshore Gippsland silver jubilee, in: Glenie, R.C. (Ed.), Second South-Eastern Australia Oil Exploration Symposium. Petroleum Exploratin Society of Australia, pp. 29-56.

Burnham, A.K., Braun, R.L., Gregg, H.R., Samoun, A.M., 1987. Comparison of methods for measuring kerogen pyrolysis rates and fitting kinetic parameters. Energy & Fuels 1, 452-458.

Burns, B., James, A., Emmett, J., 1984. The use of gas isotopes in determining the source of some Gippsland Basin oils. Australian Petroleum Exploration Association Journal 24, 217-221.

Burns, B.J., Bostwick, T.R., Emmett, J.K., 1987. Gippsland terrestrial oils—recognition of compositional variations due to maturity and biodegradation effects. Australian Petroleum Exploration Association Journal 27, 73-84.

Collinson, M.E., Van Bergen, P.F., Scott, A.C., De Leeuw, J.W., 1994. The oil-generating potential of plants from coal and coal-bearing strata through time: a review with new evidence from Carboniferous plants. Geological Society, London, Special Publications 77, 31-70.

Cook, A., Struckmeyer, H., 1986. The role of coal as a source rock for oil, in: Glenie, R.C. (Ed.), Second South-Eastern Australia Oil Exploration Symposium. Petroleum Exploration Society of Australia, pp. 419-432.

Cowley, R., O'Brien, G.W., 2000. Identification and interpretation of leaking hydrocarbons using seismic data: a comparative montage of examples from the major fields in Australia's north west shelf and Gippsland Basin. Australian Petroleum Production Exploration Association Journal 40, 121-150.

di Primio, R., Horsfield, B., 2006. From petroleum-type organofacies to hydrocarbon phase prediction. American Association of Petroleum Geologists Bulletin 90, 1031-1058.

di Primio, R., Dieckmann, V., Mills, N., 1998. PVT and phase behaviour analysis in petroleum exploration. Organic Geochemistry 29, 207-222.

Dickinson, J.A., Wallace, M.W., Holdgate, G.R., Gallagher, S.J., Thomas, L., 2002. Origin and timing of the Miocene-Pliocene unconformity in southeast Australia. Journal of Sedimentary Research 72, 288-303.

Dieckmann, V., 2005. Modelling petroleum formation from heterogeneous source rocks: the influence of frequency factors on activation energy distribution and geological prediction. Marine and Petroleum Geology 22, 375-390.

Dieckmann, V., Schenk, H.J., Horsfield, B., Welte, D.H., 1998. Kinetics of petroleum generation and cracking by programmed-temperature closed-system pyrolysis of Toarcian Shales. Fuel 77, 23-31.

Diessel, C.F.K., 1992. Coal-Bearing Depositional Systems. Springer-Verlag, Berlin, 721 p.

Duddy, I.R., Green, P.F., 1992. Tectonic development of the Gippsland Basin and environs: identification of key episodes using Apatite Fission Track Analysis (AFTA), Gippsland Basin Symposium. Australasian Institute of Mining and Metallurgy, Melbourne, pp. 111-121.

Dumitru, T., Hill, K., Coyle, D., Duddy, I., Foster, D., Gleadow, A., Green, P., Kohn, B., Laslett, G., O'sullivan, A., 1991. Fission track thermochronology: application to continental rifting of south-eastern Australia. Australian Petroleum Exploration Association Journal 31, 131-142.

Durand, B., Paratte, M., 1983. Oil potential of coals: a geochemical approach. Geological Society, London, Special Publications 12, 255-265.

Eglinton, G., Hamilton, R.J., 1963. The distribution of alkanes. Chemical plant taxonomy, pp. 187-217.

Espitalié, J., Laporte, J.L., Madec, M., Marquis, F., Leplat, P., Paulet, J., Boutefeu, A., 1977. Méthode rapide de caractérisation des roches mères, de leur potentiel pétrolier et de leur degré d'évolution. Revue Institut Francais du Petrole 32, pp. 23-42.

Gallagher, S.J., Smith, A.J., Jonasson, K., Wallace, M.W., Holdgate, G.R., Daniels, J., Taylor, D., 2001. The Miocene palaeoenvironmental and palaeoceanographic evolution of the Gippsland Basin, Southeast Australia: a record of Southern Ocean change. Palaeogeography, Palaeoclimatology, Palaeoecology 172, 53-80.

George, S., Smith, J., Jardine, D., 1994. Vitrinite reflectance suppression in coal due to a marine transgression: a case study of the organic geochemistry of the Greta Seam, Sydney Basin. Australian Petroleum Exploration Association Journal 34, 241-255.

George, S.C., Eadington, P., Lisk, M., Quezada, R., 1998. Geochemical comparison of oil trapped in fluid inclusions and reservoired oil in Blackback oilfield, Gippsland Basin, Australia. Petroleum Exploration Society of Australia Journal 26, 64-81.

Gibson-Poole, C.M., Svendsen, L., Underschultz, J., Watson, M.N., Ennis-King, J., Ruth, P.J., Nelson, E.J., Daniel, R.F., Cinar, Y., 2008. Site characterisation of a basin-scale CO2 geological storage system: Gippsland Basin, southeast Australia. Environmental Geology 54, 1583-1606.

Gorter, J., 2001. A marine source rock in the Gippsland Basin, Eastern Australasian Basins Symposium, A Refocused Energy Perspective for the Future, Petroleum Exploration Society of Australia, Special Publication, pp. 385-390.

Grant, C.W., 2004. Geochemical Analysis of Oils and Condensates from the Gippsland Basin: Implications for Future Prospectivity. B.Sc. Honours Thesis, University of Adelaide School of Petroleum. Open File report PE911520 held by Victoria Department of Environment and Primary Industry (DEPI). http://er-info.dpi.vic.gov.au/energy/assets/pe91152.htm#pe911520.

Hedberg, H.D., 1968. Significance of high-wax oils with respect to genesis of petroleum. American Association of Petroleum Geologists Bulletin 52, 736-750.

Hill, P.J., Exon, N.F., Royer, J.Y., 1995. Swath-mapping the Australian continental margin: results from offshore Tasmania. Exploration Geophysics 26, 403-411.

Hoffman, N., Preston, J.C., 2014. Geochemical interpretation of partially-filled hydrocarbon traps in the Nearshore Gippsland Basin. Australian Petroleum Production and Exploration Association Journal.

Holdgate, G.R., 2005. Geological processes that control lateral and vertical variability in coal seam moisture contents—Latrobe Valley (Gippsland Basin) Australia. International journal of coal geology 63, 130-155.

Holdgate, G.R., McNicol, M.D., 1992. New Directions-Old Ideas Hydrocarbon Prospects of the Strzelecki Group Onshore Gippsland Basin, in: Foster, J., Kepton, N. (Eds.), Energy, Economics and Environment — Gippsland Basin Symposium, Australian Institute of Mining and metallurgy, pp. 121-131.

Holdgate, G.R., Gallagher, S., 1997. Microfossil paleoenvironments and sequence stratigraphy of Tertiary cool-water carbonates, onshore Gippsland Basin, southeastern Australia, in: James, N.J., Clarke, J. (Eds.), Cool and Temperate Water Carbonates. Special Publication, 56, Society of Economic Palaeontologists and Mineralogists, Tulsa, pp. 205-220.

Holdgate, G.R., Wallace, M.W., Daniels, J., Gallagher, S.J., Keene, J.B., Smith, A.J., 2000. Controls on Seaspray Group sonic velocities in the Gippsland Basin—a multidisciplinary approach to the canyon 'seismic velocity problem'. Australian Petroleum Production and Exploration Association Journal 40, 295-313.

Holdgate, G.R., Wallace, M.W., Gallagher, S.J., Smith, A.J., Keene, J.B., Moore, D., Shafik, S., 2003. Plio-Pleistocene tectonics and eustasy in the Gippsland Basin, southeast Australia: evidence from magnetic imagery and marine geological data. Australian Journal of Earth Sciences 50, 403-426.

Horsfield, B., 1989. Practical criteria for classifying kerogens: some observations from pyrolysis-gas chromatography. Geochimica et Cosmochimica Acta 53, 891-901.

Horsfield, B., 1997. The bulk composition of first-formed petroleum in source rocks, in: Welte, D., Horsfield, B., Baker, D. (Eds.), Petroleum and basin evolution. Springer Verlag, Berlin, Heidelberg, pp. 335-402.

Horsfield, B., Dueppenbecker, S.J., 1991. The decomposition of Posidonia Shale and Green River Shale kerogens using microscale sealed vessel (MSSV) pyrolysis. Journal of Analytical and Applied Pyrolysis 20, 107-123.

Horsfield, B., Yordy, K.L., Crelling, J.C., 1988. Determining the petroleum-generating potential of coal using organic geochemistry and organic petrology. Organic Geochemistry 13, 121-129.

Horsfield, B., Disko, U., Leistner, F., 1989. The micro-scale simulation of maturation: outline of a new technique and its potential applications. Geologische Rundschau 78, 361-374.

Hunt, J.M., 1991. Generation of gas and oil from coal and other terrestrial organic matter. Organic Geochemistry 17, 673-680.

Johnstone, E.M., Jenkins, C.C., Moore, M.A., 2001. An integrated structural and palaeogeographic investigation of Eocene erosional events and related hydrocarbon potential in the Gippsland Basin, in: Hill, K.C., Bernecker, T. (Eds.), Eastern Australasian Basins Symposium, A Refocused Energy Perspective for the Future, Petroleum Exploration Society of Australia, Special Publication, pp. 403-412.

Killops, S.D., Woolhouse, A.D., Weston, R.J., Cook, R.A., 1994. A geochemical appraisal of oil generation in the Taranaki Basin, New Zealand. American Association of Petroleum Geologists Bulletin 78, 1560-1585.

Lafargue, E., Marquis, F., Pillot, D., 1998. Rock-Eval 6 applications in hydrocarbon exploration, production, and soil contamination studies. Oil & Gas Science and Technology 53, 421-437.

Larter, S.R., 1984. Application of analytical pyrolysis techniques to kerogen characterization and fossil fuel exploration/exploitation, in: Voorhees, K.J. (Ed.), Analytical Pyrolysis: Methods and application, Butterworth, London, pp. 212-275.

Larter, S.R., Douglas, A.G., 1980. A pyrolysis-gas chromatographic method for kerogen typing. Physics and Chemistry of the Earth 12, 579-583.

Larter, S.R., Senftle, J.T., 1985. Improved kerogen typing for petroleum source rock analysis. Nature 318, 277-280.

Littke, R., Horsfield, B., Leythaeuser, D., 1989. Hydrocarbon distribution in coals and in dispersed organic matter of different maceral compositions and maturities. Geologische Rundschau 78, 391-410.

Lowry, D., Longley, I., 1991. A new model for the Mid-Cretaceous structural history of the northern Gippsland Basin. Australian Petroleum Exploration Association Journal 31, 143-153.

Marshall, N.G., Partridge, A.D., 1988. The Eocene acritarch Tritonites gen. nov. and the age of the Marlin Channel, Gippsland Basin, southeastern Australia. Memoirs of the Association of Australasian Palaeontologists 5, 239-257.

Moore, P.S., Burns, B.J., Emmett, J.K., Guthrie, D.A., 1992. Integrated source, maturation and migration analysis, Gippsland Basin, Australia. Australian Petroleum Exploration Association Journal 32 (1), 313-324.

Moriarty, S.G., 2010. Source rock characterisation in the Gippsland Basin: An analysis of Rock-Eval pyrolysis data from 15 wells in the Central Deep. Honours thesis, Australian School of Petroleum. The University of Adelaide, 73 p.

Murray, A.P., Edwards, D.S., Hope, J.M., Boreham, C.J., Booth, W.E., Alexander, R.A., Summons, R.E., 1998. Carbon isotope biogeochemistry of plant resins and derived hydrocarbons. Organic Geochemistry 29, 1199-1214.

Norvick, M.S., 2005. Plate tectonic reconstructions of Australia's southern margin. Geoscience Australia Record 2005/07.

Norvick, M.S., Smith, M.A., 2001. Mapping the plate tectonic reconstruction of southern and southeastern Australia and implications for petroleum systems. Australian Petroleum Production and Exploration Association Journal 41, 15-35.

O'Brien, G., Tingate, P., Goldie Divko, L., Miranda, J., Campi, M., Liu, K., 2013. Basin-scale fluid flow in the Gippsland Basin: implications for geological carbon storage. Australian Journal of Earth Sciences 60, 59-70.

O'Brien, G.W., Tingate, P.R., Divko, L.M., Harrison, M.L., Boreham, C.J., Liu, K., Arian, N., Skladzien, P., 2008. First order sealing and hydrocarbon migration processes, Gippsland Basin, Australia: implications for CO2 geosequestration, in: Blevin, J.E., Bradshaw, B.E., Uruski, C. (Eds.), Eastern Australasian Basins Symposium III: Energy security for the 21th century. Petroleum Exploration Society of Australia, Special Publication, pp. 1-28.

Partridge, A.D., 1999. Late Cretaceous to Tertiary geological evolution of the Gippsland Basin, Victoria. La Trobe University, PhD thesis (unpubl.).

Partridge, A.D., 2012. Palynology and Kerogen analyses from seven wells in Gippsland Basin: Anemone-1 & 1A, Carrs Creek-1, Hermes-1, Omeo-1, Perch-1, Sunday Island-1 and Volador-1. Biostrata Report 2012/03, 51 p.

Pepper, A.S., Corvi, P.J., 1995. Simple kinetic models of petroleum formation. Part I: oil and gas generation from kerogen. Marine and Petroleum Geology 12, 291-319.

Peters, K.E., Cassa, M.R., 1994. Applied source-rock geochemistry. In: Magoon, L.B., Dow, W.G. (Eds.), The Petroleum System—From Source to Trap. American Association of Petroleum Geologists Bulletin 60, 93-120.

Petersen, H., Rosenberg, P., 1998. Reflectane retardation (suppression) and source rock properties related to hydrogen-enriched vitrinite in Middle Jurassic coals, Danish North Sea. Journal of Petroleum Geology 21, 247-263.

Petersen, H., Rosenberg, P., 2000. The relationship between the composition and rank of humic coals and their activation energy distributions for the generation of bulk petroleum. Petroleum Geoscience 6, 137-149.

Petersen, H., Nytoft, H., Vosgerau, H., Andersen, C., Bojesen-Koefoed, J., Mathiesen, A., 2010. Source rock quality and maturity and oil types in the NW Danish Central Graben: implications for petroleum prospectivity evaluation in an Upper Jurassic sandstone play area, Geological Society, London, Petroleum Geology Conference series. Geological Society of London, pp. 95-111.

Philp, R.P., Gilbert, T.D., 1986. Biomarker distributions in Australian oils predominantly derived from terrigenous source material. Organic Geochemistry 10, 73-84.

Powell, T.G., Boreham, C.J., Smyth, M., Russell, N., Cook, A.C., 1991. Petroleum source rock assessment in non-marine sequences: pyrolysis and petrographic analysis of Australian coals and carbonaceous shales. Organic Geochemistry 17, 375-394.

Power, M., Hill, K., Hoffman, N., Bernecker, T., Norvick, M., 2001. The structural and tectonic evolution of the Gippsland Basin: results from 2D section balancing and 3D structural modelling, in: Hill, K.C., Bernecker, T. (Eds.), Eastern Australasian Basins Symposium, A Refocused Energy. Perspective for the Future, Petroleum Exploration Society of Australia, pp. 373-384.

Rahmanian, V.D., Moore, P.S., Mudge, W.J., Spring, D.E., 1990. Sequence stratigraphy and the habitat of hydrocarbons, Gippsland Basin, Australia, in: Brooks, J.D. (Ed.), Classic petroleum provinces. Geological Society, London, Special Publication, pp. 525-541.

Saxby, J.D., Shibaoka, M., 1986. Coal and coal macerals as source rocks for oil and gas. Applied Geochemistry 1, 25-36.

Schaefer, R.G., Schenk, H.J., Hardelauf, H., Harms, R., 1990. Determination of gross kinetic parameters for petroleum formation from Jurassic source rocks of different maturity levels by means of laboratory experiments. Organic Geochemistry 16, 115-120.

Schenk, H.J., Horsfield, B., 1998. Using natural maturation series to evaluate the utility of parallel reaction kinetics models: an investigation of Toarcian shales and Carboniferous coals, Germany. Organic Geochemistry 29, 137-154.

Schenk, H.J., Dieckmann, V., 2004. Prediction of petroleum formation: the influence of laboratory heating rates on kinetic parameters and geological extrapolations. Marine and Petroleum Geology 21, 79-95.

Schenk, H.J., Horsfield, B., Krooss, B., Schaefer, R.G., Schwochau, K., 1997. Kinetics of petroleum formation and cracking. In: Welte, D.H., Horsfield, B., Baker, D.R. (Eds.), Petroleum and Basin Evolution. Springer, Verlag, Berlin, Heidelberg, pp. 231-269.

Shanmugam, G., 1985. Significance of coniferous rain forests and related organic matter in generating commercial quantities of oil, Gippsland Basin, Australia. American Association of Petroleum Geologists Bulletin 69, 1241-1254.

Sloan, M., Moore, P., McCutcheon, A., 1992. Kipper-a unique oil and gas discovery, Gippsland Basin, Australia. Australian Petroleum Exploration Association Journal 32, 1-8.

Smith, G., 1982. A review of the Tertiary-Cretaceous tectonic history of the Gippsland Basin and its control on coal measure sedimentation. Australian Coal Geology 4, 1-38.

Smith, G.C., Cook, A.C., 1984. Petroleum occurrence in the Gippsland Basin and its relationship to rank and organic matter type. Australian Petroleum Exploration Association Journal 24, 196-216.

Stainforth, J.G., 1984. Gippsland hydrocarbons-perspective from the basin edge. Australian Petroleum Exploration Association Journal 24, 91-100.

Summons, R.E., Zumberge, J.E., Boreham, C.J., Bradshaw, M.T., Brown, S.W., Edwards, D.S., Hope, J.M., Johns, N., 2002. The Oils of Eastern Australia Petroleum Geochemistry and Correlation. Open file report, Geoscience Australia and Geomark Research, 162 p.

Sun, Y., Sheng, G., Peng, P., Fu, J., 2000. Compound-specific stable carbon isotope analysis as a tool for correlating coal-sourced oils and interbedded shale-sourced oils in coal measures: an example from Turpan basin, north-western China. Organic Geochemistry 31, 1349-1362.

Sykes, R., 2001. Depositional and rank controls on the petroleum potential of coaly source rocks. In: Hill, K.C., Bernecker, T. (Eds.), Eastern Australasian basins symposium, a Refocused Energy Perspective for the Future. Petroleum Exploration Society of Australia, Special Publication, pp. 591-601.

Sykes, R., Volk, H., George, S.C., Ahmed, M., Higgs, K.E., Johansen, P.E., Snowdon, L.R., 2014. Marine influence helps preserve the oil potential of coaly source rocks: Eocene Mangahewa Formation, Taranaki Basin, New Zealand. Organic Geochemistry 66, 140-163.

Teerman, S.C., Hwang, R.J., 1991. Evaluation of the liquid hydrocarbon potential of coal by artificial maturation techniques. Organic Geochemistry 17, 749-764.

Thomas, B.M., 1982. Land-plant source rocks for oil and their significance in Australian basins. Australian Petroleum Exploration Association Journal 22, 164-178.

Thomas, J.H., Bernecker, T., Driscoll, J., 2003. Hydrocarbon Prospectivity of Areas V03-3 and V03-4, Offshore Gippsland Basin, Victoria, Australia: 2003 Acreage Release, Victorian Initiative for Minerals and Petroleum Report 80, Depatment of Primary Industries.

Veevers, J.J., Powell, C.M., Roots, S.R., 1991. Review of seafloor spreading around Australia. I. synthesis of the patterns of spreading. Australian Journal of Earth Sciences 38, 373-389.

Wilkins, R.W.T., George, S.C., 2002. Coal as a source rock for oil: a review. International journal of coal geology 50, 317-361.

Willcox, J.B., Colwell, J.B., Constantine, A.E., 1992. New ideas on Gippsland Basin regional tectonics, Gippsland Basin Symposium. Australian Institute of Mining and Metallurgy, pp. 93-110.

## Chapter 4.

**Predicted bulk chemical and isotopic signatures of petroleum generated from Jurassic and Cretaceous source rocks in the Vulcan Sub-basin, Bonaparte Basin, North West Shelf of Australia**

Soumaya Abbassi[1], Brian Horsfield[2], Simon C. George[1], Dianne S. Edwards[3], Herbert Volk[4, a], Rolando di Primio[2]

1. Department of Earth and Planetary Sciences, Macquarie University, Sydney, NSW 2109, Australia

2. Helmholtz Centre Potsdam, GFZ - German Research Centre for Geosciences, Germany

3. Geoscience Australia, GPO Box 378, Canberra, ACT 2601, Australia

4. CSIRO, PO Box 136, North Ryde, NSW 1670, Australia

a. Present Address: BP Exploration Company, Sunbury-on-Thames, UK

*Corresponding author:* [soumaya.abbassi@gmail.com, soumaya.abbassi@students.mq.edu.au](mailto:soumaya.abbassi@gmail.com)

### *Statement of authors' contribution*

This Chapter is a final version of a manuscript that is currently a published paper in *Organic Geochemistry*. This paper has been formatted to conform to the font and referencing style adopted in this thesis. Figures and tables included within the text are prefixed with the chapter number.

I am the primary author. I examined data and prepared the samples used in this study, including sample selection, sampling, grinding and most of the solvent extraction. I performed the open-system pyrolysis-gas chromatography and compositional kinetic measurements. Rock-Eval pyrolysis data acquired for all samples was performed by Geoscience Australia, excluding sample preparation. Rock-Eval pyrolysis data acquired for solvent-extracted samples (excluding sample preparation) was performed by Applied Petroleum Technology AS (Norway). Bulk kinetic and carbon isotope measurements (excluding solvent extraction) were performed by Ferdinand Perssen and Michael Gabriel (GFZ, Potsdam), respectively. I processed and interpreted all the data derived from all the conducted measurements which are related to the paper. I wrote and designed the paper's structure. All co-authors carefully reviewed and provided feedbacks and various refinements on the final version of the manuscript, and approved it for submission. Neither this manuscript nor one with similar content under our authorship has been published or is being considered for publication elsewhere, except as described above.

**Abstract**

The molecular, kinetic and isotopic characteristics of selected Mesozoic source rocks in the offshore Vulcan Sub-basin of the Bonaparte Basin, Australia, reveal that they contain Type II, Type II/III and Type III kerogen, with maceral assemblage variation being controlled by changes in the depositional environment. The marine Lower Cretaceous Echuca Shoals Formation and Upper Jurassic–Lower Cretaceous upper Vulcan Formation have fair to moderate quality organic matter, whereas the marine Middle–Upper Jurassic lower Vulcan and fluvio-deltaic Lower–Middle Jurassic Plover formations contain good to very good quality organic matter. Both the lower Vulcan and Plover formations are mature for hydrocarbon generation in this sub-basin and contain predominantly heterogeneous mixed Type II/III organic matter. Oils showing a terrestrial geochemical signature can be generated from both the lower delta plain Plover Formation and the more marginal marine source rocks of the lower Vulcan Formation, as sampled from wells on the Montara Terrace, while oils with a marine signature can be sourced from the deep-water, anoxic mudstones of the lower Vulcan Formation deposited in the Swan and Paqualin graben. Where sampled in the Vulcan Sub-basin, the upper Vulcan and Echuca Shoals formations are thermally marginally mature, but where burial is sufficient to attain higher maturity, as for example, in the Nancar Trough – to the north of the Vulcan Sub-basin, they have the potential to provide additional sources for marine oils. Assuming a constant geological heating rate of 3.3°C/Ma, the onset of bulk hydrocarbon generation, at a transformation ratio (TR) of 10%, from the Echuca Shoals and upper Vulcan formations occurs at a lower burial temperature of 120°C as compared to 120–160°C for the lower Vulcan and Plover formations. Generally, low gas:oil ratios (GORs), comparable with those measured in the naturally occurring accumulations, were reproduced at low transformation ratios (<50%TR) for both coals and shales of the lower Vulcan and Plover formations. Shales of the Echuca Shoals, Vulcan and Plover formations generate Paraffinic-Naphthenic-Aromatic (PNA) oils. Plover Formation coals exhibit a high phenolic content, with the potential to generate both PNA-oils with high wax content, and gas and condensate.

## 4.1. Introduction

Comprehensive geochemical studies have been conducted in the Vulcan Sub-basin (**Figure 4.1**) in order to characterise source rock potential and the properties of crude oils, condensates and gases (e.g., Scott and Hartung-Kagi, 1998; Edwards et al., 2004; Dawson et al., 2007). While gas-source rock correlations have not been established, the heterogeneous isotopic and molecular composition of the gases indicates generation from multiple Jurassic coals and marine shales over a broad range of thermal maturities (Edwards et al., 2004). In addition, an input of late dry gas to some accumulations, such as those at Skua, Montara and Padthaway in the southern Vulcan Sub-basin, and at Crux in the Heywood Graben of the of the Browse Basin, was recognized. Trap reactivation and alteration processes make gas-source correlations difficult. However, both the Plover and lower Vulcan formations are inferred to be the primary sources of these gases (**Figure 4.2**; Edwards et al., 2004).

Two distinct end-member groups (A and B) of oils and condensates in the Vulcan Sub-basin were delineated by Edwards et al. (2004) based on their molecular and isotopic compositions. The main characteristics of Group A oils (e.g. Challis, Jabiru and Skua) are a high proportion of lower molecular-weight compounds, a strongly negative bulk carbon isotopic composition ($\delta^{13}C$ = -28.0 to -27.2‰) and the high abundance of $C_{23}$ tricyclic terpane with respect to the $C_{19}$ tricyclic terpane. In contrast, Group B oils and condensates (e.g. Montara, Padthaway and Maret) contain high amounts of waxy *n*-alkanes, a significant proportion of mono-aromatic hydrocarbons, and have significantly less negative $\delta^{13}C$ values (-26.1 to -25.1‰) than those of the Group A oils and condensates. These characteristics suggest that the Group A oils have marine organic precursors, while Group B oils were sourced from more terrestrially influenced organofacies. Group A oils are stated to be sourced from marine mudstones of the lower Vulcan Formation. Group B oils are thought to be sourced from the fluvio-deltaic mudstones and coals of the Plover Formation (Edwards et al., 2004). Oils with mixed A–B composition have been described at the Puffin and Oliver accumulations (**Figure 4.1**) and are interpreted to be sourced from the Jurassic Plover Formation (and/or older source rocks) and the lower Vulcan Formation. In addition to the source type and thermal maturity control on the defined oil and condensate groups, post-generation processes, such as evaporative fractionation and water washing, have modified the composition of the present-day accumulations reservoired in the Vulcan Sub-basin (Edwards and Zumberge, 2005). Evaporative fractionation is characteristic of Group B oils and condensates, resulting in a deficiency in their low-molecular-weight straight-chain hydrocarbons, and an enrichment in branched/cyclic alkanes and mono-aromatic

hydrocarbons (Edwards et al., 2004). In contrast, Group A oils and condensates were subjected to varying degrees of water washing, leading to preferential removal of benzene and toluene. Both of these secondary alteration processes are associated with fault leakage and gas flushing (e.g., Lisk and Eadington, 1994; O'Brien et al., 1999; George et al., 2004b; Gartrell and Lisk, 2005). In an attempt to reconstruct the hydrocarbon charge at Jabiru 1A well, Bourdet et al. (2012) mapped oil inclusion assemblages. These maps, used in conjunction with spectroscopic and PVT analysis show that an extensive palaeo-oil column was reduced to its current height during the late Miocene by imbibition of water and gas displacement.

George et al. (1997) examined an early oil trapped in fluid inclusions (FI) in the same well, and showed that it displayed an unaltered geochemical composition, believed to be representative of the inferred Middle–Upper Jurassic mudstone source rock signature (MacDaniel, 1988a), but generated at a slightly lower thermal maturity as compared to the present-day oil accumulation. Similar analyses by George et al. (2004a) on two oil-bearing FI samples from Champagny 1 and Delamere 1 wells **(Figure 4.1)** showed that they were generated at early- to mid-oil window thermal maturities. These FI oils show affinities to two different source rocks; the Champagny 1 FI oil correlates with a dominantly marine source and displays similarities with the Group A oils, whereas the Delamere 1 FI oil suggests a greater terrigenous input mixed with a severely biodegraded palaeo-oil residue. The lower Vulcan Formation was proposed as the source of the Champagny 1 FI oil, whereas the Delamere 1 FI oil was inferred to be derived from the Plover Formation and/or an older source rock (George et al., 2004b). In addition, previous basin models and studies on palaeo-oil columns (Baxter et al., 1997; Lisk et al., 1998; Kennard et al., 1999; Fujii et al., 2004; Neumann et al., 2009) have revealed the occurrence of multiple episodes of hydrocarbon charge in the Vulcan Sub-basin. Some authors suggested the occurrence of an early gas charge during the Late Jurassic–Early Cretaceous (Baxter et al., 1997; Lisk et al., 1998) followed by a second and main phase of oil charge in the middle to late Eocene and a third late gas and oil charge from the Miocene onwards (Kennard et al., 1999).

Despite efforts to correlate petroleum accumulations with potential source rocks and to reconstruct the fill history of the Vulcan Sub-basin, no significant attention has been paid to the kinetic behaviour controlling the cracking of organic matter preserved in this sub-basin (Kennard et al., 1999; Neumann et al., 2009). Thus, the aim of this paper is to provide compositional kinetic parameters for the most significant source rocks of the Vulcan Sub-basin, i.e. those proven within the Plover and Vulcan formations, and potential source rocks within the Echuca Shoals Formation. Kinetic models for hydrocarbon generation are used to

determine whether variability in the previously defined groups of oils, condensates and gases can be linked to different sources or is the result of heterogeneity within these inferred source rocks.
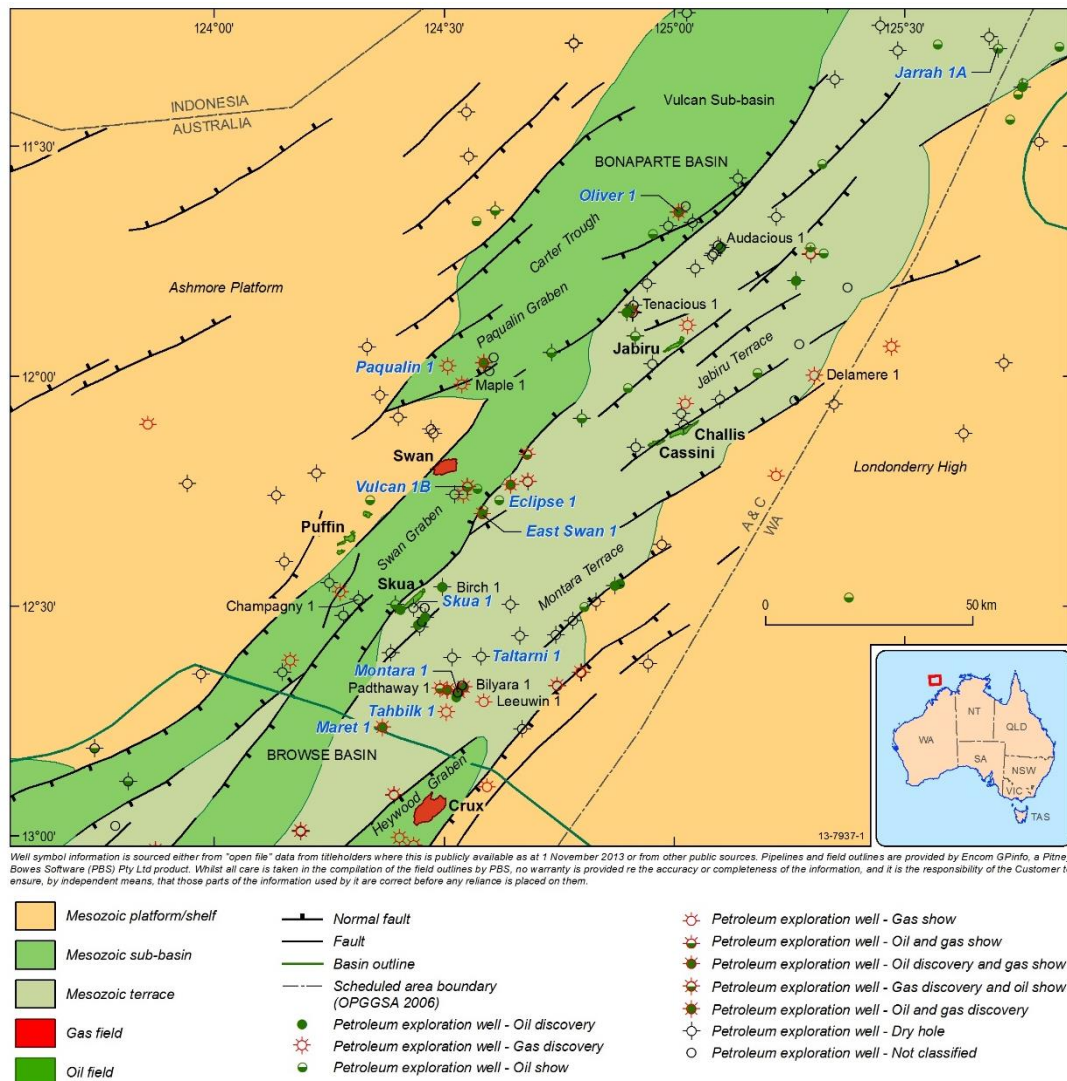


**Figure 4.1. Regional map showing the location and structure of the Vulcan Sub-basin within the Bonaparte Basin (NW margin, Australia) and petroleum wells (after Edwards et al., 2004). Wells, from which samples were studied are shown in blue.**

## 4.2. Study area and chronostratigraphy

The Vulcan Sub-basin is a major structural feature, about 250 km long, in the Bonaparte Basin on the North West Shelf of Australia (Purcell and Purcell, 1988). The sub-basin is bounded by Permo–Triassic platforms, with the Londonderry High to the southeast and the Ashmore Platform to the northwest **(Figure 4.1)**. Tectonically, this sub-basin is a northeast-southwest-trending Jurassic extensional depocentre (MacDaniel, 1988b; Osborne, 1990), which consists of a series of horsts, elongated graben and terraces. These include the Jurassic Swan and Paqualin graben, of which the latter dies out to the northeast beneath the Neogene

Carter Trough (Kennard et al., 1999). The eastern margin of the Paqualin Graben and Carter Trough is bordered by the Jabiru Terrace, while the Montara Terrace flanks the Swan Graben. The northeast-trending proto-Vulcan Sub-basin was structurally developed as a response to initial northwest-trending Upper Devonian–Lower Carboniferous and east-northeast-trending Upper Carboniferous–Permian rift systems (O'Brien, 1993). Following these late Paleozoic extensional phases, north–south compression in the Late Triassic formed horst and graben structures (e.g. the Skua Trough) and was associated with phases of uplift and erosion (O'Brien, 1993; O'Brien et al., 1996; Shuster et al., 1998). The Lower to Middle Jurassic Plover Formation was characterised by widespread fluvio-deltaic deposition **(Figure 4.2)** and includes interbedded sandstones with organic-rich coals and shales (Labutis et al., 1998). During the Middle Jurassic–Early Cretaceous, a major phase of northwest–southeast upper crustal extension resulted in the formation of the current Vulcan Sub-basin architecture (Chen et al., 2002), coincident with the onset of sea-floor spreading in the Argo Abyssal plain (Mihut and Müller, 1998).

The Swan and Paqualin graben formed during the mid-Oxfordian to early Kimmeridgian (Baxter et al., 1998), and were progressively filled by transgressive sandstones of the Montara Formation and organic-rich, anoxic restricted marine claystones of the lower Vulcan Formation **(Figure 4.2)**. The Tithonian–lower Valanginian marine mudstones and proximal fan sandstones of the upper Vulcan Formation, cover a broader area, being deposited across the previously eroded Jabiru Horst (Pattillo and Nicholls, 1990). This major rifting episode was terminated in the Valanginian and is marked by a regional flooding event and the commencement of a post-rift phase and the outbuilding of a passive margin driven by thermal subsidence (e.g., Baxter et al., 1999). The early post-rift sequences are represented by the Valanginian–Aptian transgressive marine claystones of the Echuca Shoals Formation **(Figure 4.2)**, which filled intra-Valanginian palaeotopographic depressions within the graben. As post-rift thermal subsidence continued and clastic sedimentation declined, the Aptian–Albian shales and marls of the Jamieson Formation were deposited. The prevalence of deep-water conditions and restricted sediment supply triggered the accumulation of fine grained carbonates and clastics of the Cenomanian–Campanian Woolaston, Gibson and Fenelon formations. During the Maastrichtian, the pelagic ramp succession was punctuated by a sea-level fall, leading to deposition of the Puffin Formation fan sandstones (Mory, 1988; Benson et al., 2004).

During the Cenozoic, a thick carbonate-dominated shelf represented by the Woodbine Group blanketed the region in response to a sub-tropical climatic shift triggered by oceanographic factors and a drop in global sea-level (Haq et al., 1987). This promoted the deposition of the

prograding submarine fans of the lower Eocene Hibernia and Oligocene–Miocene Oliver formations. Miocene–Pliocene plate convergence, resulting in the collision of the Australian plate with the Asian microplates in the Timor Sea, reactivated extensional faults leading to the breaching of hydrocarbon traps within the sub-basin (O'Brien and Woods, 1995; Lisk et al., 1998, 2002; O'Brien et al., 1999).

## 4.3.    Petroleum systems and exploration history

In the Vulcan Sub-basin, the primary traps are complex tilted fault blocks and horsts within clastic reservoirs **(Figure 4.2)** ranging in age from the Late Triassic (pre-rift) to Late Cretaceous (post-rift). Typically, these reservoirs have good to excellent porosity and permeability properties over structural highs. For example, the Upper Triassic fluvio-deltaic Challis Formation forms the reservoir in the Challis-Cassini and Talbot accumulation. The Skua and Jabiru petroleum accumulations are reservoired within sandstones of the Lower−Middle Jurassic Plover Formation (MacDaniel, 1988b; Osborne, 1990). In spite of their limited extent, the Upper Cretaceous sandstones of the Puffin Formation provide reservoirs within the Swan gas accumulation and the Puffin oil field (Mory, 1988; De Boer, 2004). This reservoir is interpreted to be a 'thief zone' hosting migrated mixed oils from pre- and syn-rift traps (Edwards et al., 2004). In addition to these primary reservoirs, secondary targets include sandstones of the Upper Triassic Nome Formation (e.g. Challis field), the fan-delta sandstones of the Upper Jurassic Montara Formation (the Montara, Bilyara and Tahbilk oil and gas accumulations) and the submarine fan sandstones of the upper Vulcan Formation (e.g. Tenacious and Allaru discoveries). The pre- and syn-rift reservoirs are sealed regionally by shales of the Lower Cretaceous Echuca Shoals Formation and by carbonates of the Paleocene Johnson Formation. Claystones of the Vulcan Formation provide localised seals (Kivior et al., 2002). The Cenozoic succession provides the overburden but also includes potential reservoir units such as the Eocene Hibernia and the Oligocene–Miocene Cartier and Oliver formations, which lack proven seals (Lisk, 2012).

Numerous oil and gas discoveries have made the Vulcan Sub-basin one of the most prospective areas on the North West Shelf. Approximately 357 million barrels of oil reserves were estimated by Longley et al. (2002). Although petroleum exploration activity in this sub-basin started in the 1960s leading to the discovery of oil in the Puffin 1 and Puffin 2 wells (in 1972 and 1974, respectively), the first significant accumulation was found at Jabiru 1A in 1983, which encountered a 57 m oil column in Jurassic sandstones (Lindner, 1984; MacDaniel, 1988a). This initial commercial success was followed from 1984 to 1988 by the discoveries of three smaller economic oil accumulations at Challis, Skua and Cassini. Since

then, this area has experienced intense phases of drilling activity, reaching its peak in 1990 when many exploration wells were drilled and thousands of kilometres of 2D and 3D seismic data were acquired. This phase of exploration resulted in the discoveries of small-sized oil and gas accumulations, such as Bilyara, Montara, Oliver, Keeling, and Maple. These disappointing results led to a decline in drilling activity, with only minor oil and gas discoveries (e.g. Padthaway 1 and Audacious 1) being made from 1997−2001. The last decade was highlighted by periods of episodic or no drilling activity, mostly due to structural complexity and difficulty in imaging prospective targets on seismic (e.g., Pattillo and Nicholls, 1990; Woods, 1992, 2004; O'Brien, 1993). Current activity is focussed on the commercialisation of existing accumulations; first oil from the Montara accumulation was produced in June 2013 (PTTEP-Australasia, 2013), and the Cash/Maple gas discoveries are currently under development. Post-drill appraisals of wells coupled with 2D and 3D seismic interpretation have indicated that numerous hydrocarbon-bearing traps have been breached during phases of fault reactivation (Whibley and Jacobson, 1990; Lisk and Eadington, 1994; George et al., 1997; 1998; O'Brien et al., 1998; Brincat et al., 2001; Gartrell et al., 2003). Hence, to facilitate future exploration, there is a requirement to better understand the charge history of the basin and predict where undiscovered resources may exist.

## 4.4. Materials and analytical methods

### 4.4.1. Sample set and Rock-Eval pyrolysis

A total of 61 core and cutting samples representing four different source rocks from eleven petroleum wells drilled in the Vulcan Sub-basin (**Figure 4.1** and **Figure 4.2)** were chosen for geochemical analyses. In some cases, coal and shale from the same depth were handpicked and analysed separately. Before conducting the analyses, all samples were crushed and subdivided into two subsets. The first subset was used to determine the Total Organic Carbon (TOC) content and Rock-Eval pyrolysis parameters, such as the free hydrocarbon fraction ($S_1$), the fraction released by thermal cracking ($S_2$), and the temperature ($T_{max}$) measured at the top of the $S_2$ peak, as described by Espitalié et al. (1977). The TOC content was determined by summing the pyrolysed and residual carbon fractions; other parameters, such as the genetic potential ($S_1+S_2$), the Hydrogen Index (HI) and the Oxygen Index (OI), were calculated (**Table 4.1**). These analyses are routinely used to assess the hydrocarbon generative potential, the thermal maturity and kerogen type. The second set of ground samples were solvent-extracted using an Accelerated Solvent Extractor (ASE 200) with a mixture (by volume) of 90% dichloromethane and 10% methanol to remove the extractable organic matter and any compounds arising from drilling fluid contamination. The

second subset of samples was then subjected to open-system pyrolysis-gas chromatography, bulk and compositional kinetic measurements.
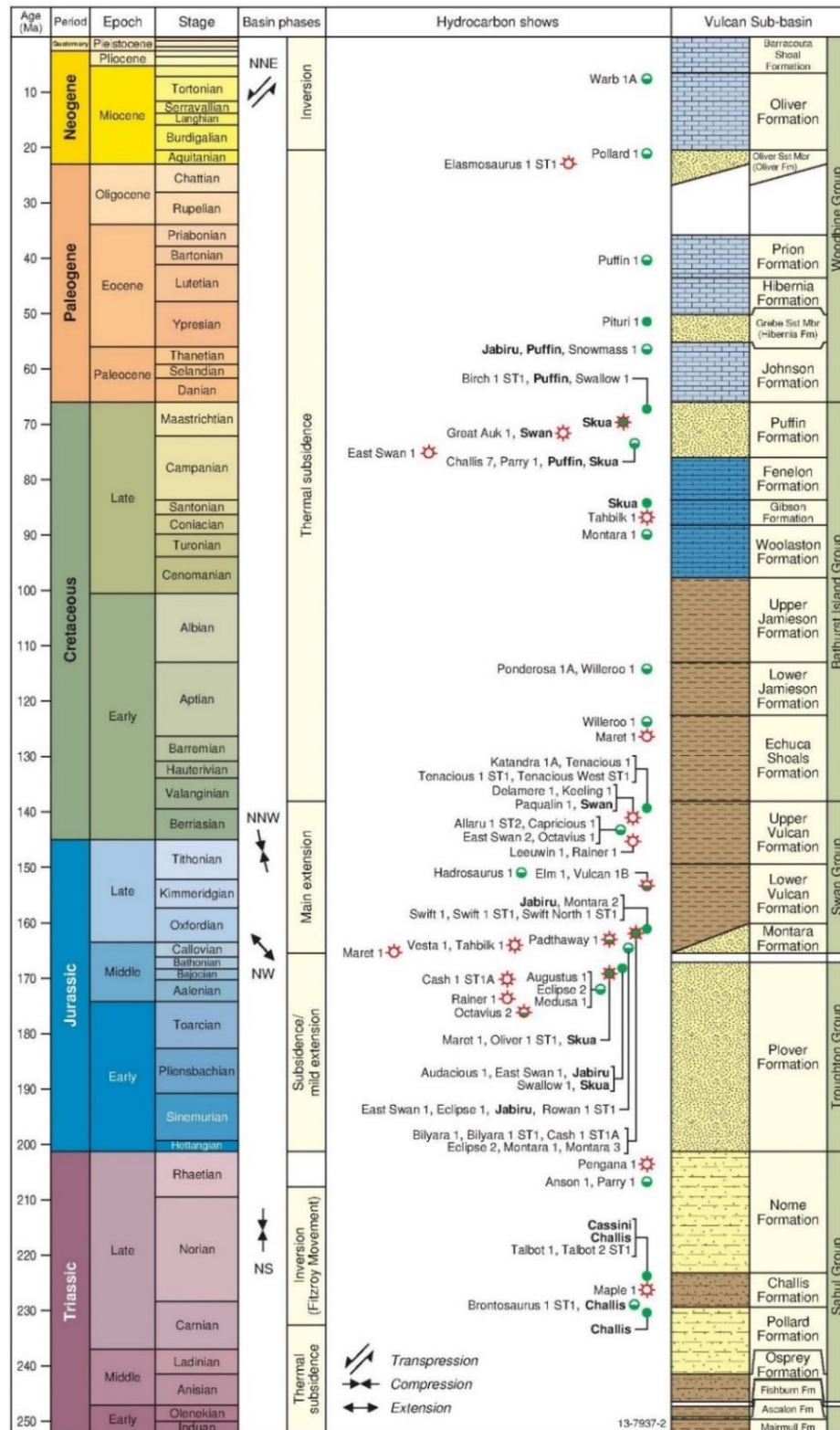


**Figure 4.2. Stratigraphy of the Vulcan Sub-basin, based on the Bonaparte Basin Biozonation and Stratigraphy Chart 33 (Kelman et al., 2014). Geological time scale after Gradstein et al. (2012), also showing oil and gas accumulations and discoveries.**

### 4.4.2. Open-system pyrolysis-gas chromatography

Open-system pyrolysis-gas chromatography (Py-GC) was performed on 24 solvent-extracted samples following the technique described by Horsfield (1989) and Horsfield and Dueppenbecker (1991) to determine the type of petroleum products generated during thermal maturation in terms of their petroleum type organofacies. After five minutes of purge at 300°C, the glass tube holding 2-15 mg of sample was heated from 300-600°C under a constant flow of helium (30 ml/min) at a rate of 50°C/min. The generated hydrocarbon fractions were first trapped in a liquid nitrogen-cooled trap and then released by ballistic heating of the trap to 300°C after the end of the pyrolysis step. The pyrolysis products were then analysed using an Agilent 6890A GC instrument, equipped with a programmable pyrolysis unit, a HP-Ultra 50 m x 0.32 mm i.d. capillary column (0.52 µm film thickness and dimethyl polysiloxane-phase) and a flame ionisation detector (FID). Peak areas were measured for compound quantitation with respect to the internal standard, *n*-butane.

### 4.4.3. Bulk kinetic experiments

Of the 24 samples analysed by Py-GC, 12 samples were selected for bulk kinetic measurements. A Source Rock Analyser[TM] instrument (SRA-TPH/IR) was used to conduct non-isothermal open-system pyrolysis of 10–20 mg aliquots of extracted samples at four different laboratory heating rates: 0.7°C/min, 2°C/min, 5°C/min and 15°C/min. After an isothermal hold at 200°C for 15 minutes, the temperature was increased to 640°C at the selected heating rates using a furnace set-up previously described by Schaefer et al. (1990). The pyrolysis products were transported to a FID using a constant helium flow (50 mL/min) for a continuous registration of bulk formation rates. Parameters derived from this analysis using the three lower heating rates (0.7°C/min, 2°C/min, 5°C/min), served to determine the activation energy (Ea) distribution and single frequency factor (A) for each sample. The derived data was processed using Kinetics 2000 and KMOD[TM] software developed by the Lawrence Livermore National Laboratory (Burnham et al., 1987; 1988).

### 4.4.4. Compositional kinetic experiments

Of the 12 samples chosen for bulk kinetic measurements, four samples representative of the studied source rocks were subjected to closed-system pyrolysis–gas chromatography in a Micro-Scaled Sealed Vessel (MSSV) to determine the evolving petroleum compositions as a function of kerogen conversion following the PhaseKinetic approach of di Primio and Horsfield (2006). The low heating rate of 0.7°C/min, used for bulk kinetic experiments, served to calculate the temperatures corresponding to the transformation ratios of 10%, 30%,

50%, 70% and 90% and to allow reasonable geological predictions (Schenk and Dieckmann, 2004). Five aliquots from each solvent-extracted sample (5-40 mg), for the five transformation ratios were sandwiched between quartz-powder in one-sided closed glass tubes, which were then sealed by a hydrogen flame before being placed into a furnace to be heated from 200°C to the final defined temperatures at 0.7°C/min. The composition and weight of the generated pyrolysates (resolved and total) in each tube were determined online by a single GC-FID run as described above for Py-GC.

### 4.4.5. Kinetic Modelling

Data obtained from closed-system pyrolysis analyses were corrected, by adjusting gas compositions using a GOR - gas dryness correlation based on PVT data of natural petroleum fluids, and incorporated into a compositional kinetic model using PVT simulation software (PVT Sim, Calsep, Denmark). This approach, described in detail by di Primio and Horsfield (2006), allows the determination of the gas ($C_1$, $C_2$, $C_3$, $i$-$C_4$, $n$-$C_4$, $i$-$C_5$, $n$-$C_5$) and liquid (pseudo-$C_6$, $C_7$–$C_{15}$, $C_{16}$–$C_{25}$, $C_{26}$–$C_{35}$, $C_{36}$–$C_{45}$, $C_{46}$–$C_{55}$, $C_{56}$–$C_{80}$) components, as well as the prediction of the evolving fluids physical properties, such as gas:oil ratio, saturation pressure ($P_{sat}$), and formation volume factor ($B_O$).

### 4.4.6. Gas Chromatography-Isotope Ratio Mass Spectrometry (GC-IRMS) analysis

Measurement of stable carbon isotope ratios of individual light hydrocarbons (methane, ethane, propane and $n$-butane) were carried out on four solvent-extracted samples (the same as used for the compositional kinetic determination) using GC-IRMS analysis. The GC unit was connected to a GCC/TC III combustion device via an open split to a MAT 253 mass spectrometer. For this experiment, closed-system conditions using MSSV tubes with a heating rate of 0.7°C/min, and covering temperatures corresponding to 10%, 30%, 50%, 70% and 90% Transformation Ratios (TR) were employed. The GC analysis was performed using an Agilent 6890N GC fitted with a Varian Poraplot Q column (50 m x 0.32 mm i.d. capillary column, film thickness 10 μm). The temperature of the injector was maintained at 230°C with a 1:3 split configuration and helium was used as the carrier gas. The following temperature program was set for the GC oven: 30°C held for 10 min, then increased to 150°C and 200°C at 3°C/min and 4°C/min, respectively with a final isothermal hold time of 15.8 min at 200°C. The reported isotopic data are average values of at least three runs given in the delta notation ($\delta^{13}C$) normalised to the Vienna Peedee Belemnite (VPDB) standard (Craig, 1957). For all components, the standard deviation is $\leq 0.5$‰.

## 4.5. Results and Discussion

### 4.5.1. Organic richness and hydrocarbon generation potential

Bulk geochemistry and TOC measurements were undertaken on 61 samples (3 cores, 58 cuttings) that were selected from the Lower-Middle Jurassic Plover Formation (21), Upper Jurassic lower Vulcan Formation (31), the Upper Jurassic−Lower Cretaceous upper Vulcan Formation (5) and the Lower Cretaceous Echuca Shoals Formation (4, **Table 4.1**). Interpretations of Rock-Eval pyrolysis parameters used to assess source rock quality, petroleum potential and thermal maturity were carried out according to the standard guidelines proposed by Peters and Cassa (1994). Coals, defined in this study as having TOC values >20%, were hand-picked from cuttings comprising predominantly medium to dark shales and coals. Overall, the highest TOC contents and generative potentials were measured for the Plover and lower Vulcan formation source rocks **(Figure 4.3)**.
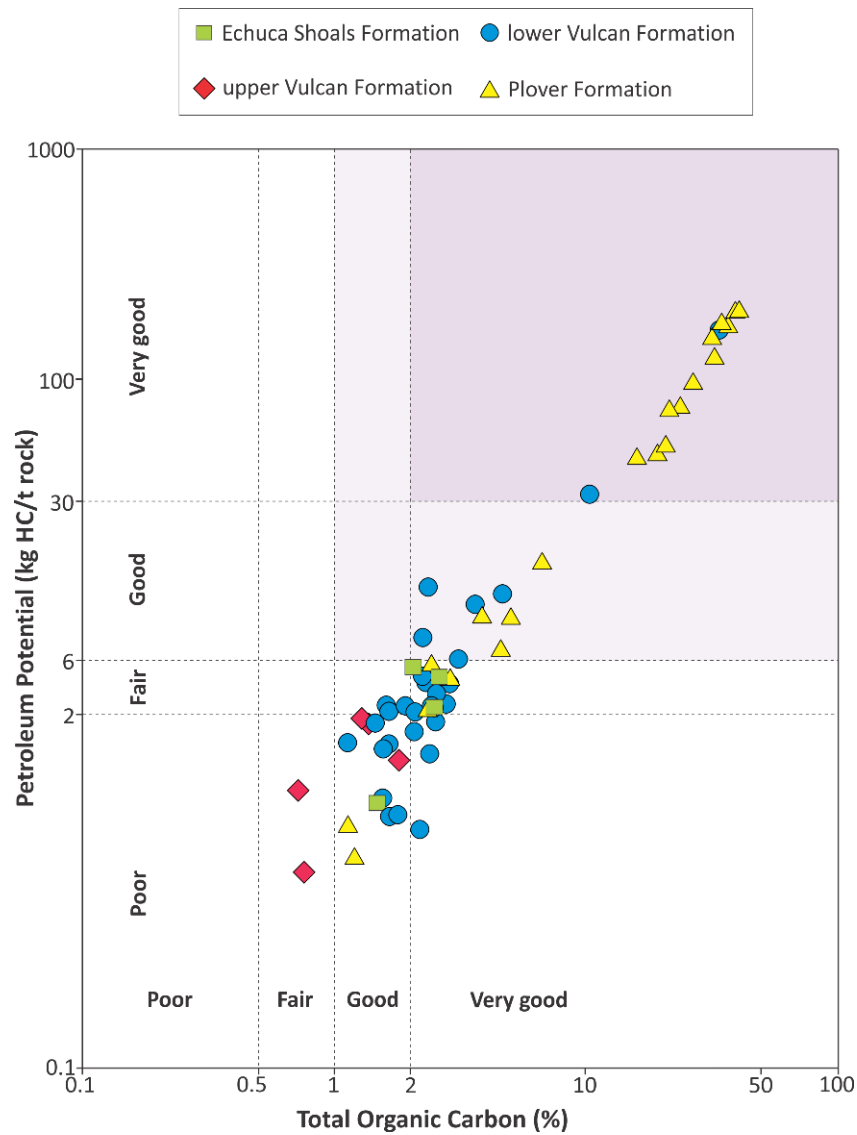
**Figure 4.3. Cross-plot of petroleum potential (PP; $S_1 + S_2$) versus Total Organic Carbon showing the variable petroleum potential of 61 source rock samples from the Vulcan Sub-basin.**

The Plover Formation contains variable TOC and $S_2$ values ranging from 1.1-39.9% (average of 17.4%) and from <1-185 mg HC/g rock (average of 64.4 mg HC/g rock), respectively. These values indicate that the Plover Formation is a good to very good source rock with an excellent hydrocarbon generative potential. Similarly, the lower Vulcan Formation has a TOC content varying from 1.1-33.1%, with more than 93% of the analysed samples having a TOC between 1% and 5%. The mean $S_2$ value of samples from the lower Vulcan Formation is 9.1 mg HC/g rock, indicating the good quality of this source rock. The lowest TOC values were measured for the upper Vulcan Formation with an average value of <2%. The Lower Cretaceous Echuca Shoals Formation has low to moderate TOC and $S_2$ values, in the range of 1.5-2.6% and 1.0-5.2 mg HC/g rock, respectively.

**Table 4.1. Sample identity, Rock-Eval pyrolysis and TOC data for Vulcan Sub-basin source rock samples.**

| Sample ID | Location | Well | Sample Type | Depth (mKB) | Formation | $S_1$ | $S_2$ | $S_3$ | PI | $T_{max}$ | HI | OI | TOC |
|---|---|---|---|---|---|---|---|---|---|---|---|---|---|
| 20110049 | Jabiru Terrace | Jarrah 1A | Cuttings | 1854 - 1860 | Echuca Shoals | 0.44 | 3.28 | 3.3 | 0.12 | 427 | 133 | 134 | 2.47 |
| 20110051 | Montara Terrace | Maret 1 | Cuttings | 3158 - 3164 | Echuca Shoals | 0.31 | 5.23 | 2.41 | 0.06 | 438 | 257 | 119 | 2.03 |
| 20110065 | Paqualin Graben | Paqualin 1 | Cuttings | 2517 - 2523 | Echuca Shoals | 0.46 | 4.57 | 4.15 | 0.09 | 430 | 177 | 161 | 2.58 |
| 20110074 | Montara Terrace | Skua 1 | Cuttings | 2411 - 2417 | Echuca Shoals | 0.39 | 1.04 | 1.92 | 0.27 | 431 | 71 | 132 | 1.46 |
| 20110061 | Carter Trough | Oliver 1 | Cuttings | 2867 - 2873 | upper Vulcan | 0.2 | 2 | 4.73 | 0.09 | 435 | 113 | 266 | 1.78 |
| 20110066 | Paqualin Graben | Paqualin 1 | Cuttings | 2709 - 2715 | upper Vulcan | 0.3 | 2.86 | 2.5 | 0.09 | 433 | 212 | 185 | 1.35 |
| 20110067 | Paqualin Graben | Paqualin 1 | Cuttings | 2778 - 2787 | upper Vulcan | 0.44 | 2.9 | 5.03 | 0.13 | 433 | 228 | 396 | 1.27 |
| 3848 | Swan Graben | Vulcan 1B | Cuttings | 2438 - 2457 | upper Vulcan | 0.12 | 0.6 | nd | 0.17 | 425 | 80 | nd | 0.75 |
| 3849 | Swan Graben | Vulcan 1B | Cuttings | 2579 - 2597 | upper Vulcan | 0.39 | 1.24 | nd | 0.24 | 433 | 175 | nd | 0.71 |
| 20110041 | Swan Graben | East Swan 1 | Cuttings | 2405 - 2414 | lower Vulcan | 0.15 | 3.59 | 1.98 | 0.04 | 435 | 191 | 106 | 1.88 |
| 20110042 | Swan Graben | East Swan 1 | Cuttings | 2441 - 2448 | lower Vulcan | 1.3 | 10.17 | 9.98 | 0.11 | 430 | 223 | 218 | 4.57 |
| 20110043 | Swan Graben | East Swan 1 | Cuttings | 2478 - 2484 | lower Vulcan | 0.11 | 4.64 | 1.46 | 0.02 | 434 | 205 | 64 | 2.27 |
| 20110044 | Swan Graben | East Swan 1 | Cuttings | 2588 - 2594 | lower Vulcan | 1.18 | 29.8 | 3.62 | 0.04 | 434 | 294 | 36 | 10.13 |
| 20110044C | Swan Graben | East Swan 1 | Cuttings | 2588 - 2594 | lower Vulcan | 13.33 | 146.7 | 1.72 | 0.08 | 444 | 444 | 5 | 33.07 |
| 20110047 | Montara Terrace | Eclipse 1 | Cuttings | 2418 - 2421 | lower Vulcan | 0.37 | 4.32 | 3.08 | 0.08 | 431 | 153 | 109 | 2.82 |
| 20110052 | Montara Terrace | Maret 1 | Cuttings | 3338 - 3344 | lower Vulcan | 0.44 | 4.6 | 3.49 | 0.09 | 434 | 209 | 159 | 2.2 |
| 20110062 | Carter Trough | Oliver 1 | Cuttings | 2918 - 2927 | lower Vulcan | 0.16 | 2.4 | 2.41 | 0.06 | 434 | 149 | 149 | 1.62 |
| 20110068 | Paqualin Graben | Paqualin 1 | Cuttings | 3399 - 3405 | lower Vulcan | 0.67 | 3.09 | 3.89 | 0.18 | 445 | 129 | 163 | 2.39 |
| 20110069 | Paqualin Graben | Paqualin 1 | Cuttings | 3444 - 3447 | lower Vulcan | 0.7 | 3.55 | 3.68 | 0.16 | 447 | 142 | 147 | 2.5 |
| 20110070 | Paqualin Graben | Paqualin 1 | Cuttings | 3501 - 3507 | lower Vulcan | 0.83 | 3.2 | 2.49 | 0.21 | 446 | 129 | 101 | 2.48 |
| 20110071 | Paqualin Graben | Paqualin 1 | Cuttings | 3654 - 3657 | lower Vulcan | 0.92 | 2.28 | 2.83 | 0.29 | 447 | 92 | 114 | 2.48 |
| 20110072 | Paqualin Graben | Paqualin 1 | Cuttings | 3861 - 3867 | lower Vulcan | 0.75 | 1.57 | 3.62 | 0.32 | 462 | 67 | 154 | 2.35 |
| 20110073 | Paqualin Graben | Paqualin 1 | Cuttings | 4056 - 4062 | lower Vulcan | 0.38 | 0.71 | 2.17 | 0.35 | 469 | 33 | 101 | 2.15 |

130

**Table 4.1. (Continued) Sample identity, Rock-Eval pyrolysis and TOC data for Vulcan Sub-basin source rock samples.**

| Sample ID | Location | Well | Sample Type | Depth (mKB) | Formation | $S_1$ | $S_2$ | $S_3$ | PI | $T_{max}$ | HI | OI | TOC |
|---|---|---|---|---|---|---|---|---|---|---|---|---|---|
| 20110078 | Montara Terrace | Tahbilk 1 | Cuttings | 2907 - 2916 | lower Vulcan | 0.75 | 5.23 | 5.29 | 0.13 | 431 | 171 | 172 | 3.06 |
| 20110079 | Montara Terrace | Taltarni 1 | Cuttings | 2931 - 2934 | lower Vulcan | 0.43 | 3.39 | 2.16 | 0.11 | 432 | 124 | 79 | 2.74 |
| 20110080 | Montara Terrace | Taltarni 1 | Cuttings | 2934 - 2937 | lower Vulcan | 0.44 | 3.41 | 2.41 | 0.11 | 433 | 130 | 92 | 2.62 |
| 20110081 | Montara Terrace | Taltarni 1 | Cuttings | 2937 - 2940 | lower Vulcan | 0.42 | 3.27 | 2.6 | 0.11 | 432 | 133 | 106 | 2.45 |
| 20110083 | Swan Graben | Vulcan 1B | Cuttings | 2819 - 2825 | lower Vulcan | 0.15 | 3.39 | 3.01 | 0.04 | 437 | 210 | 186 | 1.62 |
| 20110084 | Swan Graben | Vulcan 1B | Cuttings | 2944 - 2950 | lower Vulcan | 0.34 | 7.06 | 3.7 | 0.05 | 439 | 319 | 167 | 2.21 |
| 20110085 | Swan Graben | Vulcan 1B | Cuttings | 3594 - 3597 | lower Vulcan | 0.55 | 2.35 | 3.72 | 0.19 | 447 | 115 | 182 | 2.04 |
| 3850 | Swan Graben | Vulcan 1B | Cuttings | 2691 - 2707 | lower Vulcan | 0.43 | 2.17 | nd | 0.17 | 435 | 196 | nd | 1.11 |
| 3851 | Swan Graben | Vulcan 1B | Cuttings | 2926 - 2932 | lower Vulcan | 0.65 | 11.66 | nd | 0.05 | 431 | 503 | nd | 2.32 |
| 3852 | Swan Graben | Vulcan 1B | Cuttings | 3109 - 3115 | lower Vulcan | 0.51 | 2.65 | nd | 0.16 | 438 | 185 | nd | 1.43 |
| 3853 | Swan Graben | Vulcan 1B | Cuttings | 3246 - 3252 | lower Vulcan | 0.83 | 2.95 | nd | 0.22 | 443 | 187 | nd | 1.58 |
| 3854 | Swan Graben | Vulcan 1B | Cuttings | 3380 - 3386 | lower Vulcan | 1.14 | 2.38 | nd | 0.32 | 446 | 116 | nd | 2.06 |
| 3855 | Swan Graben | Vulcan 1B | Cuttings | 3545 - 3551 | lower Vulcan | 2.17 | 8.15 | nd | 0.21 | 434 | 229 | nd | 3.56 |
| 3856 | Swan Graben | Vulcan 1B | Cuttings | 3594 - 3603 | lower Vulcan | 0.86 | 1.58 | nd | 0.35 | 447 | 103 | nd | 1.54 |
| 3857 | Swan Graben | Vulcan 1B | Core | 3690 - 3690 | lower Vulcan | 0.6 | 0.89 | nd | 0.4 | 481 | 58 | nd | 1.53 |
| 3858 | Swan Graben | Vulcan 1B | Core | 3691 | lower Vulcan | 0.58 | 0.66 | nd | 0.47 | 465 | 40 | nd | 1.63 |
| 3859 | Swan Graben | Vulcan 1B | Core | 3692 | lower Vulcan | 0.49 | 0.77 | nd | 0.39 | 473 | 44 | nd | 1.76 |
| 20110045 | Swan Graben | East Swan 1 | Cuttings | 2752 - 2755 | Plover | 0.35 | 5.45 | 2.19 | 0.06 | 433 | 227 | 91 | 2.4 |
| 20110046 | Swan Graben | East Swan 1 | Cuttings | 2896 - 2899 | Plover | 0.12 | 3.57 | 3.56 | 0.03 | 431 | 154 | 154 | 2.32 |
| 20110050 | Jabiru Terrace | Jarrah 1A | Cuttings | 1920 - 1923 | Plover | 14.41 | 184.6 | 9.24 | 0.07 | 428 | 462 | 23 | 39.94 |
| 20110053 | Montara Terrace | Maret 1 | Cuttings | 3527 - 3533 | Plover | 0.6 | 15.47 | 1.51 | 0.04 | 431 | 235 | 23 | 6.59 |
| 20110053C | Montara Terrace | Maret 1 | Cuttings | 3527 - 3533 | Plover | 7.27 | 89.46 | 1.46 | 0.08 | 433 | 341 | 6 | 26.2 |
| 20110054 | Montara Terrace | Maret 1 | Cuttings | 3554 - 3560 | Plover | 3.49 | 70.15 | 1.87 | 0.05 | 435 | 332 | 9 | 21.1 |

**Table 4.1. (Continued) Sample identity, Rock-Eval pyrolysis and TOC data for Vulcan Sub-basin source rock samples.**

| Sample ID | Location | Well | Sample Type | Depth (mKB) | Formation | $S_1$ | $S_2$ | $S_3$ | PI | $T_{max}$ | HI | OI | TOC |
|-----------|----------|------|-------------|-------------|-----------|-------|-------|-------|-----|-----------|-----|-----|-----|
| 20110054C | Montara Terrace | Maret 1 | Cuttings | 3554 - 3560 | Plover | 15.91 | 159.6 | 2.08 | 0.09 | 437 | 470 | 6 | 33.98 |
| 20110055 | Montara Terrace | Montara 1 | Cuttings | 3177 - 3186 | Plover | 2.31 | 43.36 | 3.81 | 0.05 | 431 | 277 | 24 | 15.66 |
| 20110055C | Montara Terrace | Montara 1 | Cuttings | 3177 - 3186 | Plover | 9.72 | 115.2 | 6.24 | 0.08 | 428 | 362 | 20 | 31.85 |
| 20110056 | Montara Terrace | Montara 1 | Cuttings | 3201 - 3204 | Plover | 0.67 | 6.05 | 1.95 | 0.1 | 428 | 134 | 43 | 4.52 |
| 20110057 | Montara Terrace | Montara 1 | Cuttings | 3306 - 3312 | Plover | 0.2 | 4.85 | 2.36 | 0.04 | 440 | 170 | 83 | 2.85 |
| 20110058 | Montara Terrace | Montara 1 | Cuttings | 3315 - 3318 | Plover | 2.22 | 49.43 | 4.14 | 0.04 | 429 | 242 | 20 | 20.4 |
| 20110060 | Montara Terrace | Montara 1 | Cuttings | 3417 - 3426 | Plover | 0.3 | 9.06 | 1.06 | 0.03 | 425 | 238 | 28 | 3.81 |
| 20110060C | Montara Terrace | Montara 1 | Cuttings | 3417 - 3426 | Plover | 9.56 | 141.8 | 4.93 | 0.06 | 427 | 455 | 16 | 31.17 |
| 20110063 | Carter Trough | Oliver 1 | Cuttings | 2979 - 2982 | Plover | 0.07 | 1.09 | 2.59 | 0.06 | 434 | 97 | 231 | 1.12 |
| 20110064 | Carter Trough | Oliver 1 | Cuttings | 3123 - 3129 | Plover | 0.09 | 0.75 | 2.7 | 0.11 | 436 | 63 | 226 | 1.19 |
| 20110075 | Montara Terrace | Skua 1 | Cuttings | 2560 - 2563 | Plover | 4.14 | 72.14 | 5.78 | 0.05 | 426 | 310 | 25 | 23.28 |
| 20110076 | Montara Terrace | Skua 1 | Cuttings | 2585 - 2588 | Plover | 2.78 | 44.54 | 4.8 | 0.06 | 422 | 235 | 25 | 18.93 |
| 20110076C | Montara Terrace | Skua 1 | Cuttings | 2585 - 2588 | Plover | 21.28 | 176.2 | 14.1 | 0.11 | 411 | 457 | 37 | 38.55 |
| 20110077C | Montara Terrace | Skua 1 | Cuttings | 2630 - 2633 | Plover | 19.95 | 150.9 | 15.05 | 0.12 | 412 | 419 | 42 | 36.04 |
| 20110082 | Montara Terrace | Taltarni 1 | Cuttings | 3294 - 3297 | Plover | 0.62 | 8.64 | 1.67 | 0.07 | 436 | 174 | 34 | 4.96 |

**C**: Hand-picked coals
$S_1$: Amount of free hydrocarbons in the sample in mg HC/g rock
$S_2$: Amount of hydrocarbons generated during pyrolysis in mg HC/g rock
$S_3$: Amount of oxygen containing compounds generated during pyrolysis in mg $CO_2$/g rock
**PI**: Production Index [($S_1$/S1+$S_2$)*100]
$T_{max}$: Temperature of maximum hydrocarbon generation in °C
**HI**: Hydrogen Index ($S_2$*100/TOC) in mg HC/g TOC
**OI**: Oxygen Index ($S_3$*100/TOC) in mg $CO_2$/g TOC
**TOC**: Total Organic Carbon in %

### 4.5.2. Thermal maturity

Rock-Eval pyrolysis $T_{max}$ and Production Index (PI) values were used to assess the degree of thermal maturity reached by the investigated source rocks in the Vulcan Sub-basin **(Figure 4.4)**. Where sampled, low $T_{max}$ values were measured in the upper Vulcan (425-435°C) and Echuca Shoals (427-438°C) formations. High $T_{max}$ values were recorded for the lower Vulcan Formation (430-481°C), indicating that samples from this formation have reached either the early stage of the oil window or the wet gas window. $T_{max}$ values measured for the Plover Formation range from 411°C to 440°C, indicating that these samples range from immature to mature (on the Montara Terrace) with respect to the oil window.
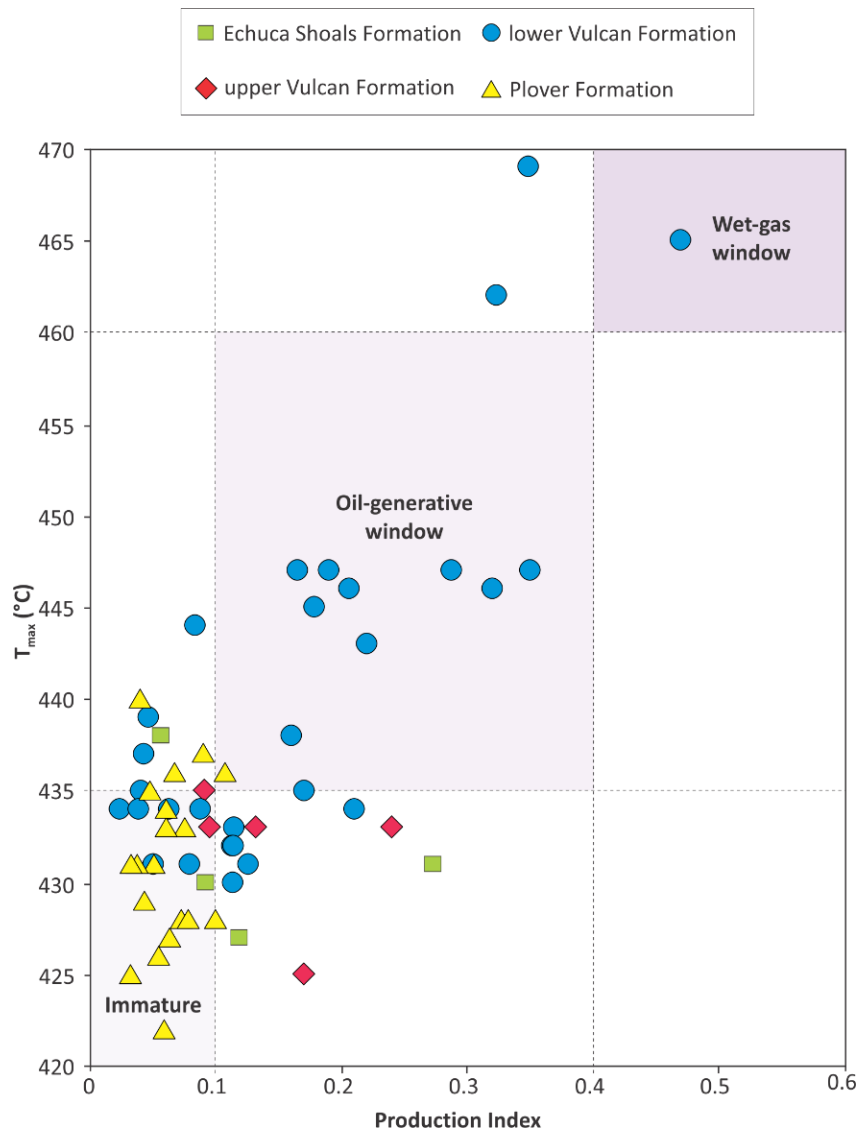


**Figure 4.4. Cross-plot of $T_{max}$ versus Production Index (PI) and the rank thresholds for oil and gas generation for the 61 samples from the Vulcan Sub-basin.**

The coal sample (20110076C) selected from the Plover Formation in Skua 1 has $S_1$ values up to 21.3 mg HC/g rock, with an anomalously low $T_{max}$ value (411°C) and may represent

either an indigenous fraction or migrated hydrocarbons. In addition, most of the PI values are in a good agreement with the $T_{max}$ values, and indicate varying levels of maturity in the source rocks of the Vulcan Sub-basin. The PI values up to 0.5 in the lower Vulcan Formation, suggest relatively advanced maturity and indicate that active petroleum generation is likely to have occurred. The PI values measured for the Plover, upper Vulcan and Echuca Shoals formations are comparatively lower (0.03-0.27), rarely exceeding 0.1, suggesting that these sediments are either immature or have just entered the oil window.

Many of the marine source rock units occurring in the North West Shelf of Australia, including those in the Vulcan Sub-basin, contain perhydrous vitrinite, on which reflectance measurements generally lead to an underestimation of thermal maturity (Wilkins et al., 1992; Kaiko and Tingate, 1996). Likewise, Rock-Eval pyrolysis $T_{max}$ data may be affected by the presence of migrated bitumen or unexpelled hydrocarbons (Tarafa et al., 1983; Espitalié, 1986). Thus, the $T_{max}$ data reported in this study was used as an indication of the minimum level of thermal maturity attained. The Fluorescence Alteration of Multiple Macerals (FAMM) technique, developed by Wilkins et al. (1992), was used as a tool to investigate vitrinite reflectance anomalies in the Vulcan Sub-basin, where vitrinite suppression ranges from 0.1 to 0.4% absolute (Faiz et al., 2000). FAMM-derived equivalent vitrinite reflectance (EqVR) data listed in **Table 4.2** were gathered from CSIRO Petroleum reports and were used to further assess thermal maturity in the Vulcan Sub-basin. Overall, there is a reasonable agreement between the measured $T_{max}$ and reported EqVR values. However, in some samples (e.g. Maret 1, Montara 1 and Vulcan 1B), cavings and additives caused the $T_{max}$ values to indicate lower thermal maturity than that given by EqVR data **(Table 4.1 and 4.2)** EqVR data measured for samples from the Echuca Shoals Formation vary from less than 0.70% in the Paqualin Graben to 0.77% on the flank of Swan Graben, indicating an early to main stage of oil window. In contrast, in the southern part of the sub-basin (e.g. Maret 1), samples from this formation fall within the late stage of oil generation (EqVR = 0.95%). Similarly, the samples selected from the upper Vulcan Formation are marginally mature to mature for oil generation (EqVR = 0.68-0.87%) in the Paqualin Graben (e.g. Maple 1), Carter Trough (e.g. Oliver 1) and Swan Graben (e.g. Vulcan 1B). On the Montara Terrace (e.g. Montara 1) and on the eastern flanks of the Carter Trough (Octavius 1) and Swan Graben (e.g. Eclipse 1, 2 and East Swan 1), the Plover Formation sediments are within the main generation window (EqVR = 0.72-0.96%).

**Table 4.2. FAMM-derived equivalent vitrinite reflectance data for samples from the Vulcan Sub-basin. Sample depths in mKB shown in brackets. See location map of the wells in Figure 4.1.**

| | EqVR (%) | | | |
| --- | --- | --- | --- | --- |
| Formation | Echuca Shoals Fm | upper Vulcan Fm | lower Vulcan Fm | Plover Fm |
| **East Swan 2** | 0.73 (2298-2301) | | 0.72 (2364-2367) | 0.81 (2668-2694) |
| | | | 0.77 (2484-2487) | 0.82 (2733-2736) |
| | | | 0.75 (2553-2558) | 0.78 (2796-2799) |
| | | | 1.00 (2633.4) | |
| **Eclipse 1** | 0.73 (2310) | | 0.68 (2376) | 0.68 (2661) |
| | | | 0.73 (2388) | 0.72 (2910) |
| | | | 0.70 (2406) | |
| | | | 0.65 (2421) | |
| | | | 0.73 (2439) | |
| | | | 0.69 (2488) | |
| | | | 0.73 (2457) | |
| | | | 0.72 (2559) | |
| **Eclipse 2** | 0.77 (2400-2403) | | 0.75 (2452) | 0.91 (2784-2787) |
| | | | 0.76 (2555) | 0.86 (2788) |
| | | | 0.80 (2610) | 0.80 (2850-2853) |
| | | | 0.75 (2649-2652) | 0.82 (2928-2931) |
| | | | 0.75 (2700-2703) | |
| | | | 0.86 (2757) | |
| **Maple 1** | < 0.70 (2835) | 0.70 (2900) | 0.80 (3101) | |
| | | 0.68 (2938) | 0.92 (3210) | |
| | | 0.72 (3018) | 0.95 (3298.5) | |
| | | | 0.85 (3427) | |
| | | | 1.09 (3519) | |
| | | | 1.15 (3614) | |
| **Maret 1** | 0.95 (3145-3150) | | 0.92 (3300-3305) | 0.90 (3420-3425) |
| | | | 0.97 (3325-3330) | |
| **Montara 1** | | | 0.64 (2526-2529) | 0.75 (3180-3183) |
| | | | 0.72 (2577-2580) | 0.73 (3318-3321) |
| | | | 0.64 (2596-2601) | |
| | | | 0.62 (2601-2604) | |
| | | | 0.64 (2652-2655) | |
| | | | 0.70 (3132-3135) | |
| | | | 0.72 (3147-3150) | |

**Table 4.2. (Continued) FAMM-derived equivalent vitrinite reflectance data for samples from the Vulcan Sub-basin. Sample depths in mKB shown in brackets. See location map of the wells in Figure 4.1.**

| | EqVR (%) | | |
|---|---|---|---|
| **Octavius 1** | 0.82 (2735-2740) | 0.92 (2905-2910) | 0.95 (3185-3190) |
| | 0.87 (2800-2805) | 0.88 (2925-2930) | 0.95 (3200-3205) |
| | 0.82 (2895-2900) | 0.97 (3095-3100) | 0.95 (3270-3275) |
| | | 0.98 (3155-3160) | 0.96 (3290) |
| **Oliver 1/ST1** | 0.70 (2885-2888) | 0.88 (2924-2927) | |
| | | 0.78 (2940-2943) | |
| **Swan 2** | | 1.13 (3453) | |
| | | 1.17 (3516) | |
| | | 1.20 (3630) | |
| | | 1.15 (3744) | |
| | | > 1.20 (3825) | |
| **Vulcan 1B** | 0.73 (2386.6) | 0.93 (3066.3) | |
| | 0.77 (2718.8) | 1.20 (3377.2) | |
| | 0.77 (2883.4) | > 1.20 (3657.6) | |

The largest variation in the thermal maturity of the selected samples is observed within the lower Vulcan Formation, which shows a wide range of maturity (EqVR = 0.62 to ≥ 1.20%), depending on the location. The highest EqVR values are measured for the lower Vulcan Formation in the Paqualin Graben (e.g. Maple 1) and in the western Swan Graben (e.g. Swan 2 and Vulcan 1B).

### 4.5.3. Kerogen type

The variations observed in the organic richness and petroleum potential of source rock units within the Vulcan Sub-basin are also reflected in the kerogen type (**Figure 4.5**). The Hydrogen Indices (HI) measured for samples from the Plover Formation are up to 462 mg HC/g TOC (20110050). Samples from the lower Vulcan Formation have HI values ranging from 33-503 mg HC/g TOC, with an average value of 172 mg HC/g TOC. Most samples from this formation that have a HI below 200 mg HC/g TOC are thermally mature to overmature (**Figure 4.5a**). Based on the modified van Krevelen diagram of HI versus OI (**Figure 4.5b**), the majority of HI values measured for the Plover and lower Vulcan formations suggest mixed Type II and III kerogen, indicating moderate to good potential for liquid and gas generation. The limited set of samples from the upper Vulcan and Echuca Shoals formations typically display lower HI values, ranging from 80-228 mg HC/g TOC (average of 162 mg HC/g TOC) and from 71-257 mg HC/g TOC (average of

160 mg HC/g TOC), respectively. As indicated by their position close to the Type III kerogen evolution curve **(Figure 4.5b)**, both the upper Vulcan and Echuca Shoals formations show fair to moderate potential for liquid hydrocarbon generation.
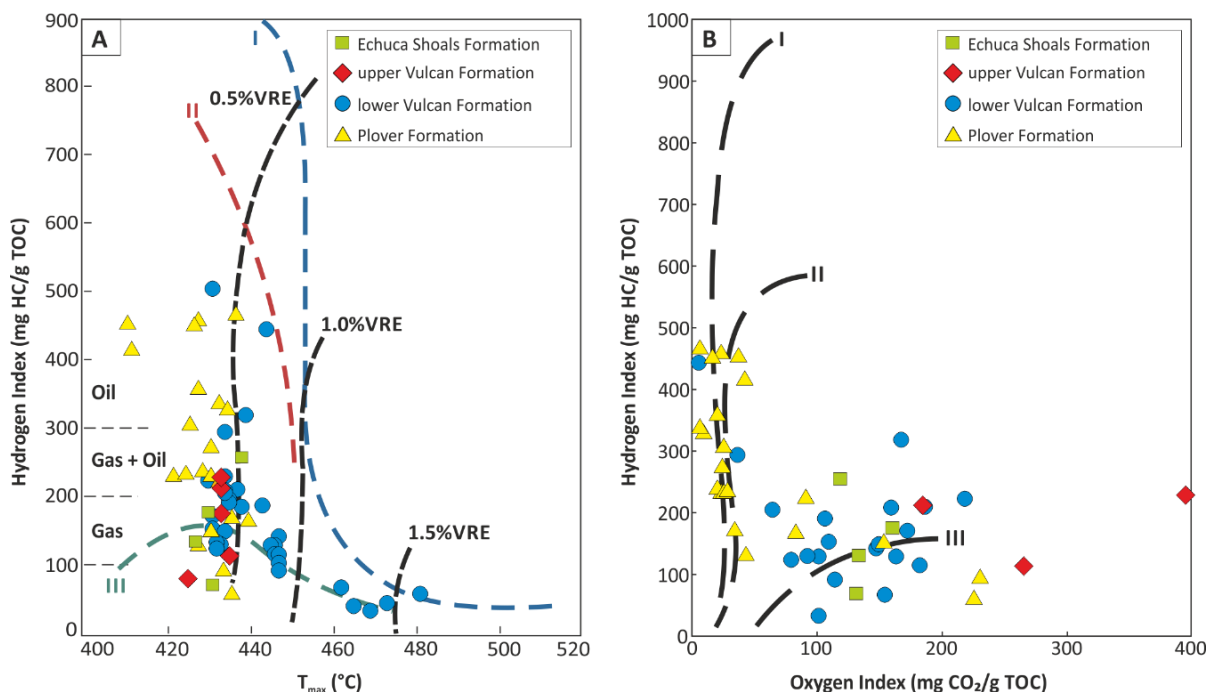


Figure 4.5. Rock-Eval data for 61 samples from the Vulcan Sub-basin. (a) Hydrogen Index versus $T_{max}$, showing the variable thermal maturity of the sample set. (b) Oxygen Index (OI) versus Hydrogen Index, illustrating the kerogen type. VRE = vitrinite reflectance equivalent.

The type of kerogen can be further investigated by the use of the $S_2$ versus TOC diagram **(Figure 4.6).** Most of the analysed samples (56%) fall below the HI=200 line and only 11% of samples have HI values exceeding 400 mg HC/g TOC. These HI values suggest that samples collected from the Vulcan Sub-basin contain a mixture of oil-prone Type II and gas-prone Type III organic matter**.** The presence of Type II/III oil- and gas-prone organic matter is also supported by the $S_2/S_3$ ratios, where two out of 21 samples from the lower Vulcan Formation and 15 out of 21 samples from the Plover Formation display a $S_2/S_3$ ratio of more than 5. The predominance of Type III kerogen indicates a significant contribution of terrestrial organic matter. In addition, it can be concluded that coals from the Plover and lower Vulcan formations with HI values above 400 mg HC/g TOC are potentially oil-prone source rocks. Assessing the potential of these coals to efficiently expel liquid hydrocarbons is, however, beyond the scope of this paper.
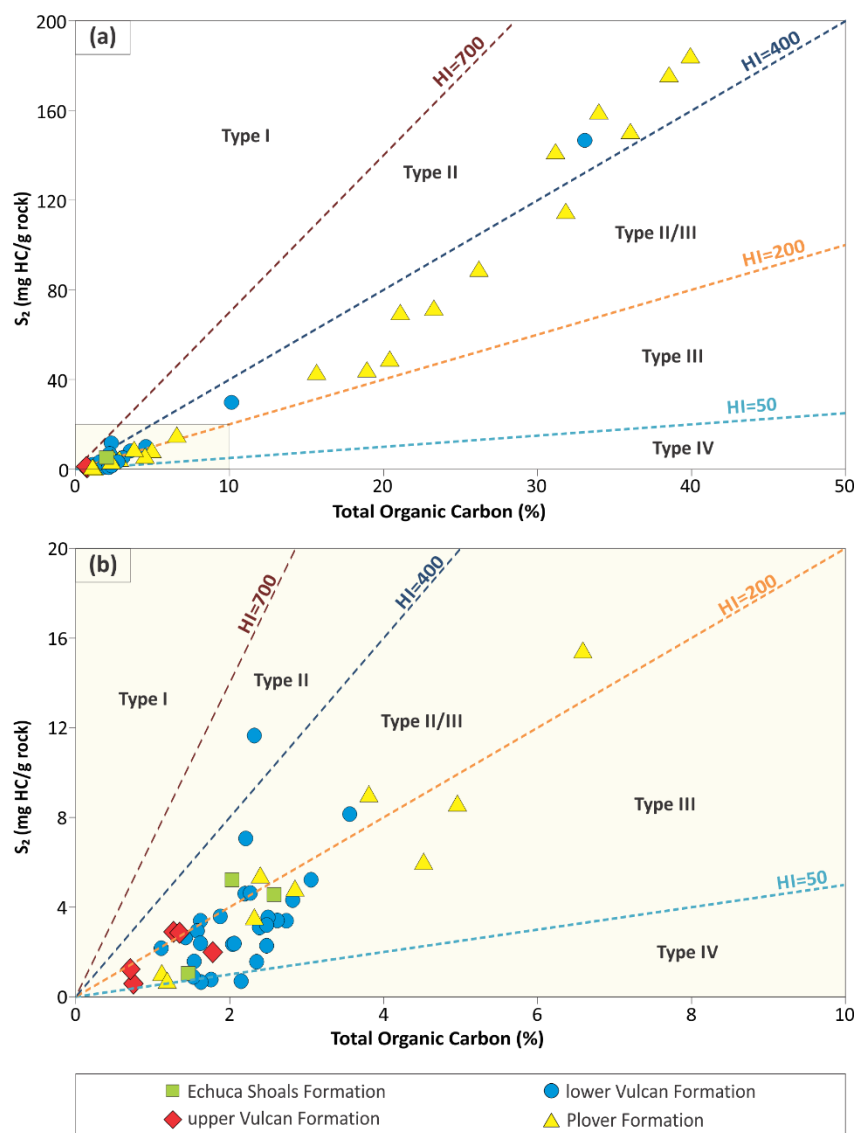
**Figure 4.6. (a) Residual petroleum potential ($S_2$) versus Total Organic Carbon diagrams by formation, indicating that the majority of the studied samples have HI > 50 mg HC/g TOC, except three samples from the Middle−Upper Jurassic lower Vulcan Formation. (b) Expansion of sample distribution in $S_2$ ≤ 20 mg HC/g rock and TOC ≤ 10% range. The Hydrogen Index lines delimit kerogen type fields. Fields defined by Langford and Blanc-Valleron (1990).**

### 4.5.4. Molecular composition and organic facies

Selected open Py-GC chromatograms of the investigated source rocks are illustrated in **Figure 4.7**. In all of the marine shale samples, the main components comprise *n*-alkane/alkene doublets (**Table 4.3**). In contrast, the coal samples from the Plover Formation (e.g. 20110076C) and the lower Vulcan Formation (20110044C) show an enrichment in alkylphenols and aromatic hydrocarbons (benzene, toluene and xylene) relative to the *n*-alkanes/alkenes. These characteristics suggest the occurrence of a lignocellulosic organic matter content (van de Meent et al., 1980; Larter and Senftle, 1985).
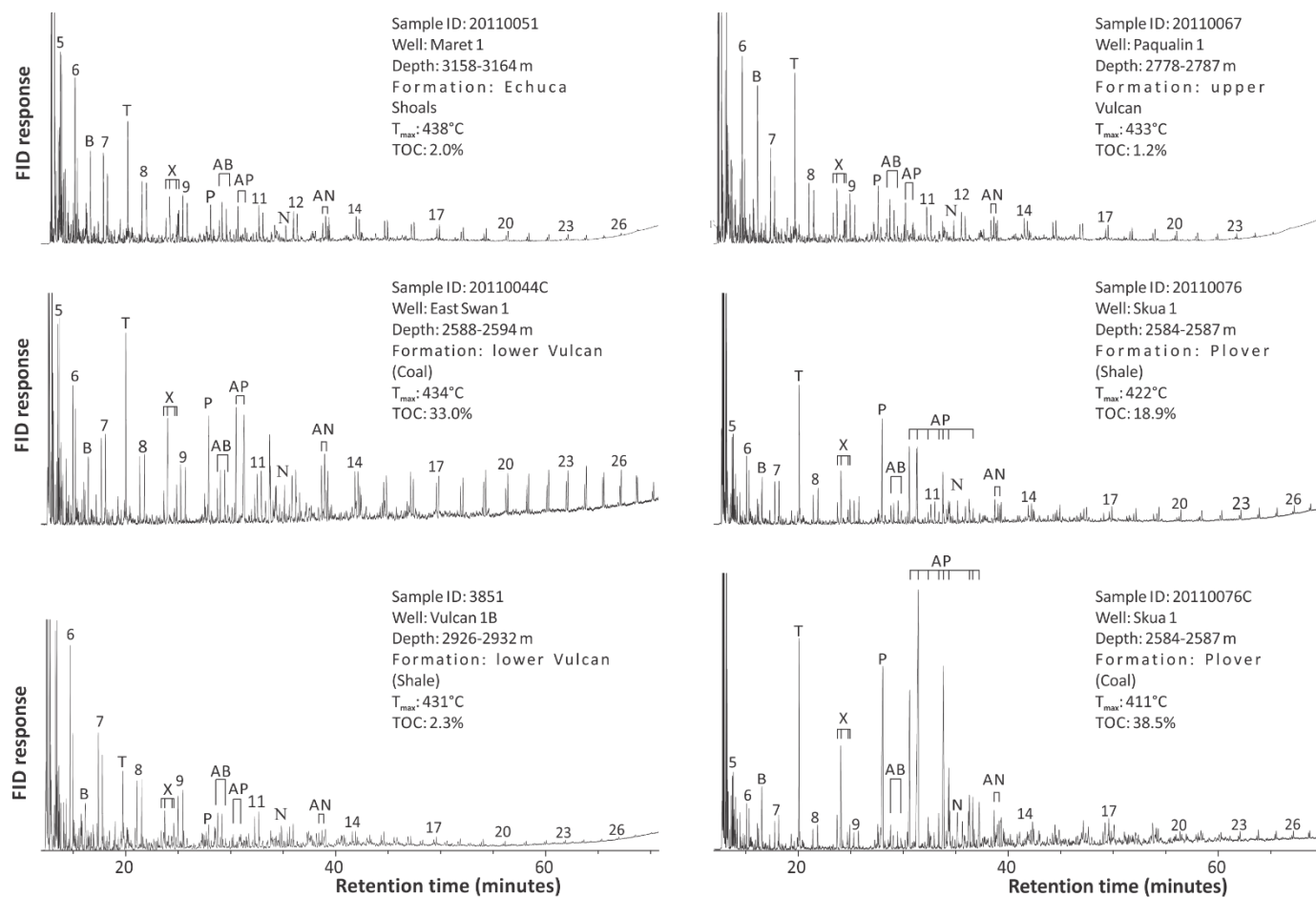
**Figure 4.7. Open-system pyrolysis-gas chromatograms for six representative solvent-extracted rock samples. Numbers indicate the number of carbon atoms in the *n*-alkane/*n*-alkene doublets; B: benzene; T: toluene; X: C₂ alkylbenzenes (ethylbenzene, *meta* + *para*-xylene, styrene, *ortho*-xylene, respectively); P: phenol; AB: C₃ alkylbenzenes; AP: alkylphenols; N: naphthalene; AN: alkylnaphthalenes.**

**Table 4.3. Calculated percentages of the main resolved classes and selected components used to determine petroleum type, source rock organic facies and phenolic content from open-system pyrolysis-gas chromatography of 24 solvent-extracted rock samples from the Vulcan Sub-basin.**

| Sample ID | Well | Depth range (m) | Formation | % of resolved components in $S_2$ | | | | (%) | | | (%) | | |
|---|---|---|---|---|---|---|---|---|---|---|---|---|---|
| | | | | Aliphatics | Mono-aromatics | Phenolics | Naphthalenes | $C_1$-$C_5$ | $C_6$-$C_{14}$ | $C_{15+}$ | *m*+*p* Xylene | *n*-Octene | Phenol |
| 20110051 | Maret 1 | 3158 - 3164 | Echuca Shoals | 83.2 | 10.9 | 2.5 | 3.3 | 71 | 22 | 7 | 40 | 34 | 26 |
| 20110065 | Paqualin 1 | 2517 - 2523 | Echuca Shoals | 79.8 | 14.3 | 2.3 | 3.5 | 75 | 20 | 5 | 47 | 28 | 25 |
| 20110067 | Paqualin 1 | 2778 - 2787 | upper Vulcan | 79.2 | 13.8 | 3.3 | 3.7 | 74 | 19 | 7 | 37 | 29 | 33 |
| 3849 | Vulcan 1B | 2579 - 2597 | upper Vulcan | 76.1 | 17.6 | 3 | 3.3 | 75 | 23 | 2 | 35 | 28 | 37 |
| 20110042 | East Swan 1 | 2441 - 2448 | lower Vulcan | 81.7 | 11.2 | 3.3 | 3.8 | 73 | 20 | 7 | 43 | 25 | 32 |
| 20110044 | East Swan 1 | 2588 - 2594 | lower Vulcan | 82.9 | 7.1 | 5.9 | 4.1 | 65 | 18 | 17 | 40 | 20 | 40 |
| 20110044C | East Swan 1 | 2588 - 2594 | lower Vulcan | 83 | 7 | 6 | 4.1 | 68 | 15 | 17 | 42 | 17 | 41 |
| 20110047 | Eclipse 1 | 2418 - 2421 | lower Vulcan | 79.6 | 12.3 | 3.2 | 4.8 | 70 | 23 | 8 | 39 | 29 | 32 |
| 20110052 | Maret 1 | 3338 - 3344 | lower Vulcan | 78.5 | 12.2 | 3.9 | 5.3 | 69 | 23 | 9 | 35 | 29 | 36 |
| 20110062 | Oliver 1 | 2918 - 2927 | lower Vulcan | 81.4 | 12.2 | 2.1 | 4.2 | 73 | 22 | 5 | 44 | 31 | 25 |
| 20110078 | Tahbilk 1 | 2907 - 2916 | lower Vulcan | 81.4 | 11 | 4.2 | 3.4 | 70 | 21 | 9 | 35 | 25 | 40 |
| 20110081 | Taltarni | 2937 - 2940 | lower Vulcan | 78.1 | 13.3 | 3.4 | 5.2 | 70 | 23 | 7 | 38 | 28 | 34 |
| 20110084 | Vulcan 1B | 2944 - 2950 | lower Vulcan | 82.8 | 10.6 | 1.9 | 4.7 | 71 | 24 | 5 | 45 | 34 | 21 |
| 3851 | Vulcan 1B | 2926 - 2932 | lower Vulcan | 84.3 | 9 | 2.2 | 4.6 | 68 | 27 | 5 | 37 | 40 | 23 |
| 3853 | Vulcan 1B | 3246 - 3252 | lower Vulcan | 75.4 | 12.7 | 7.2 | 4.8 | 69 | 23 | 8 | 27 | 20 | 53 |
| 20110045 | East Swan 1 | 2752 - 2755 | Plover | 81.6 | 10.5 | 3 | 4.9 | 71 | 21 | 8 | 43 | 27 | 30 |
| 20110050 | Jarrah 1A | 1920 - 1923 | Plover | 80.8 | 8 | 5 | 6.1 | 64 | 17 | 19 | 34 | 20 | 46 |
| 20110054 | Maret 1 | 3554 - 3560 | Plover | 81.1 | 7.1 | 5.4 | 6.5 | 65 | 18 | 17 | 41 | 20 | 39 |
| 20110054C | Maret 1 | 3554 - 3560 | Plover | 81.7 | 6.4 | 5.3 | 6.6 | 64 | 17 | 18 | 40 | 23 | 37 |
| 20110055 | Montara 1 | 3177 - 3186 | Plover | 81.5 | 7 | 5.4 | 6.1 | 63 | 19 | 19 | 33 | 22 | 46 |
| 20110058 | Montara 1 | 3315 - 3318 | Plover | 45.9 | 9.9 | 41.5 | 2.7 | 86 | 7 | 6 | 20 | 1 | 79 |
| 20110076 | Skua 1 | 2585 - 2588 | Plover | 76.4 | 10 | 9.1 | 4.5 | 74 | 15 | 10 | 32 | 12 | 56 |
| 20110076C | Skua 1 | 2585 - 2588 | Plover | 61.3 | 9.5 | 25 | 4.1 | 80 | 10 | 10 | 24 | 3 | 73 |
| 20110077C | Skua 1 | 2630 - 2633 | Plover | 46.8 | 8.2 | 43.3 | 1.7 | 87 | 6 | 7 | 19 | 0 | 81 |

The majority of the marine shale samples from the lower Vulcan Formation (e.g. sample 3851) are relatively depleted in long-chained $n$-alkanes/alkenes, suggesting a less prominent terrestrial signature. The Py-GC traces for both the upper Vulcan and Echuca Shoals formations show a series of homologous $n$-alkanes/alkenes ranging from $n$-$C_1$ to $n$-$C_{26}$. For these latter two formations, the relative abundance of the $n$-alkane/alkene doublets, which decrease with increasing carbon number, and the low to moderate concentration of phenolic compounds indicate the presence of organic matter derived from marine organisms (van de Meent et al., 1980). The most abundant resolved aromatic hydrocarbon in all of the pyrolysates is toluene. Although identified in all pyrolysates, alkylnaphthalenes, typical for coals in general, are present in the highest concentration within the coal sample from the lower Vulcan Formation.

To further assess the hydrocarbon products that can be generated from these source rocks, pyrolysate fractions calculated from the open Py-GC data **(Table 4.3)** were plotted on two ternary diagrams (**Figure 4.8**; Larter, 1984; Horsfield, 1989). A significant variation of petroleum type organofacies is observed, ranging from PNA oils to gas and condensate **(Figure 4.8a)**. The samples plotting in the gas/condensate field represent coal samples from the Plover Formation. However, some coal samples from the Plover Formation and one coal and one shale sample from the lower Vulcan Formation are enriched in long chain alkane/alkene homologues and show the potential to generate PNA oils with high wax content. These geochemical characteristics are usually attributed to lower delta plain and inner shelf depositional environments (Tissot and Welte, 1984; Horsfield, 1997) and are consistent with the environments interpreted for the Plover Formation (Labutis et al., 1998). The majority of the lower Vulcan Formation marine shale samples, and all of the marine shales from the upper Vulcan and Echuca Shoals formations, plot in the low wax PNA oil field, inferring the presence of allochthonous organic matter. Two of the Plover Formation samples (samples 20110076 and 20110076C) plotting in this field grade into the gas/condensate field and likewise indicate mixed terrestrial plant and marine algal organic matter. From the second diagram **(Figure 4.8b)**, it is clear that predominantly Type II/III kerogen is preserved in the studied rocks. A few samples from the lower Vulcan Formation display more affinity to Type II kerogen (e.g. sample 3851). In contrast, shale samples from the Plover Formation and the coal (sample 20110044C) from the lower Vulcan Formation show high amounts of phenols, implying Type III kerogen with a significant proportion of terrestrial organic matter. The Plover Formation coals show a higher relative abundance of alkylphenols than in the shales, with alkylbenzenes being present in low concentrations in both lithologies.
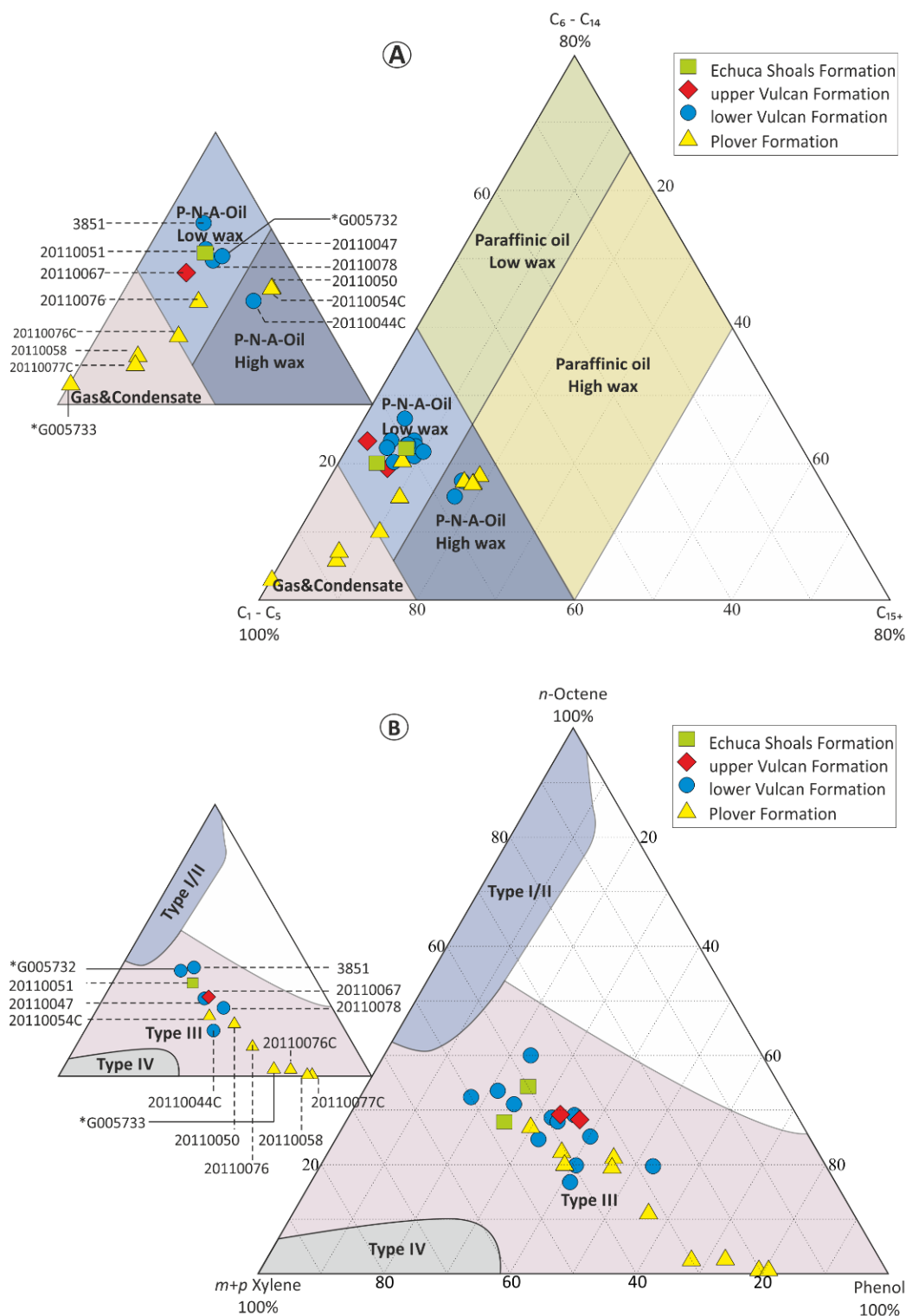
**Figure 4.8. Ternary diagrams showing: (A) The composition of the pyrolysates from the studied source rocks, on the basis of the balance of total C₁−C₅ hydrocarbons, C₆−C₁₄ *n*-alkenes plus *n*-alkanes, and C₁₅₊ *n*-alkenes plus *n*-alkanes. (B) The type of the extracted kerogen pyrolysates from the studied source rocks, on the basis of the balance of phenol, *m*- and *p*-xylene and *n*-octene (Larter, 1984). P-N-A = paraffinic-naphthenic-aromatic. Samples numbered on the small subset ternary diagrams are the samples selected for bulk kinetic experiments. * denotes samples from Geoscience Australia (GA).**

### 4.5.5. Controls on the heterogeneity of organic matter

Information on maceral assemblages for Mesozoic sediments of the Vulcan Sub-basin was gathered from well completion reports and from the Geoscience Australia database (http://dbforms.ga.gov.au/www/npm.well.search) to gain further insights into the type and origin of the organic matter preserved **(Figure 4.9)**. As can be seen, some samples have >50% liptinites, but whether these are genuine data or a problem with the quality of the Geoscience Australia database is uncertain. Support for these data comes from **Figure 4.10**, which also shows high liptinite contents in many samples from the Vulcan Sub-basin. The variability in organic richness, petroleum potential and organic facies type can be explained by the maceral composition of these source rocks, although a definite correlation cannot be made. Petrographically, there is an overall trend of increasing organic matter heterogeneity from the youngest to the oldest source rock units in the Vulcan Sub-basin. However, due to the limited number of samples from the Echuca Shoals and upper Vulcan formations, a broader variability in maceral content cannot be excluded.
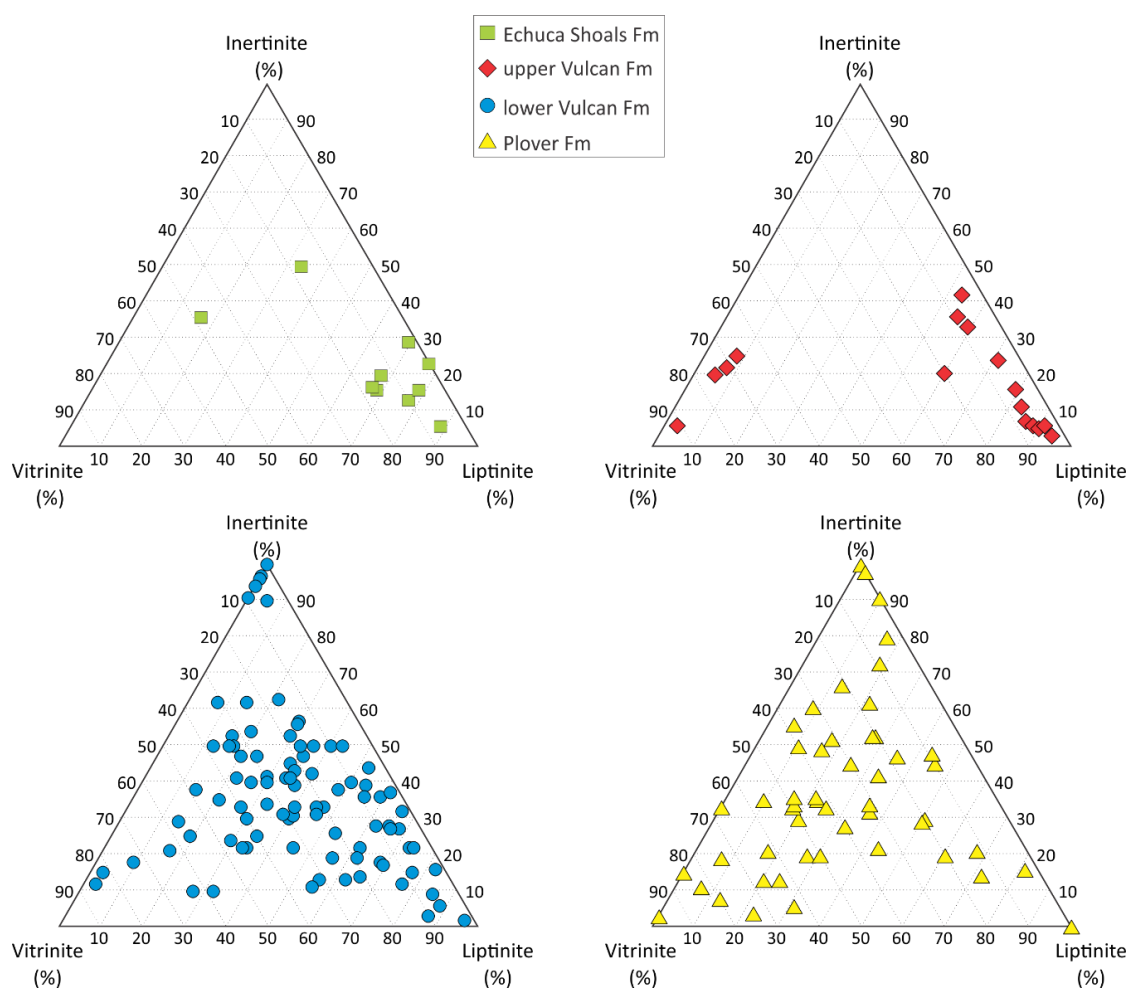


**Figure 4.9. Maceral content for Middle Jurassic to Lower Cretaceous source rocks in the Vulcan Sub-basin. Data compiled from (http://dbforms.ga.gov.au/www/npm.well.search).**

More detailed petrographic analyses of selected samples from the Vulcan Sub-basin were conducted by CSIRO Petroleum. Maceral data on mineral matter-free bases and palaeoenvironment interpretations are summarised in **Figure 4.10**. Although the Echuca Shoals Formation is interpreted to have been deposited in an open marine environment, the reported petrographic composition does not support an increase in marine-derived macerals, such as liptinite and bituminite. This observation indicates that apart from variability in organic matter input, heterogeneities in source rock properties in the Vulcan Sub-basin are the result of redox conditions. Changes in redox conditions from sub-oxic during the deposition of the lower Vulcan Formation to oxic during the deposition of the Echuca Shoals formations, can be supported by the abundance of inertinite macerals and low proportions of liptinite. Open marine conditions during the deposition of the upper Vulcan Formation are also supported by the presence of dinoflagellate/acritarch cysts (e.g. *Veryhachium*, Tappan, 1980). Similar cysts are found in the uppermost section of the lower Vulcan Formation, indicating brackish-water depositional conditions. The organic matter in samples from the lower Vulcan Formation is rich in liptodetrinite and lamalginite (0.5 to 2% by volume). In addition, low amounts of telalginite and particularly tasmanitid-derived telalginite are present in numerous samples (e.g. Eclipse 2 and Maple 1). According to Batten (1982) and Dodsworth (2004), these algal-derived macerals can be used as indicators of deposition under confined marine environments. A clear transition between the lower Vulcan Formation and the underlying Plover Formation is signalled by decreasing amounts of liptinite. Samples from the Plover Formation are characterised by low amounts (<0.5% by volume) of liptodetrinite and lamalginite, with lesser contents (<0.1% by volume) of suberinite. In one sample from the Plover Formation (Eclipse), possible *Botryococcus*-related telalginite was identified and could account for its high Hydrogen Index. The high amount of vitrinite and inertinite in the Plover Formation suggests are in accordance with its deposition in deltaic to marginal marine environments. Higher plant-derived liptinite macerals, such as sporinite and cutinite are present in low amounts (<0.5% by volume) in the selected samples, indicating limited terrestrial input. Resinite is also found in trace amounts (<0.1% by volume) in some samples from the upper Vulcan and Plover formations, suggesting the absence of resin/gum producing plants.
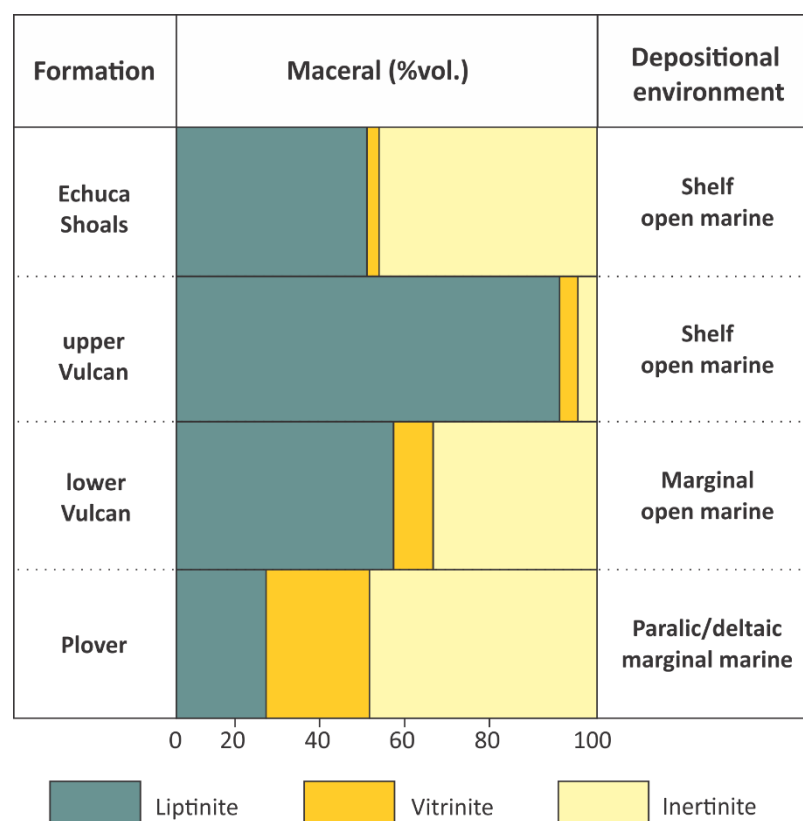
**Figure 4.10. Palaeoenvironment interpretations and average maceral compositions (on mineral matter-free basis) for Middle Jurassic to Lower Cretaceous source rocks in the Vulcan Sub-basin. (Data from CSIRO, Petroleum).**

### 4.5.6. Bulk kinetics

Petroleum generation from a given kerogen is governed by the cracking of chemical bonds as a function of time and temperature (e.g., Tissot and Welte, 1984; Schenk et al., 1997). This cracking can be described by chemical kinetics, which comprise a discrete activation energy distribution and a single frequency factor. The bulk kinetics, determined by pyrolysis experiments under laboratory conditions and extrapolated to geological conditions (Behar et al., 1991; Tang et al., 1996), are related to kerogen structure and the heterogeneity of the covalent bonds. The activation energy distributions and the corresponding pre-exponential factors for selected samples from the Vulcan Sub-basin are shown in **Figure 4.11** and listed in **Table 4.4**. The mean activation energies calculated for samples from the Plover Formation show a broad distribution ranging from 53-66 kcal/mol, with variable frequency factors from 1.56E+14/sec to 9.07E+16/sec. This broad distribution of activation energies is typical of heterogeneous Type II/III or Type III organic matter (Tegelaar and Noble, 1994; Reynolds and Burnham, 1995; Schenk et al., 1997). The lower Vulcan Formation kerogen is less

heterogeneous, with the mean activation energies varying from 50 to 57 kcal/mol, with frequency factors of 1.65E+13/sec to 2.63E+16/sec. One lower Vulcan Formation marine shale sample from Vulcan 1B (3851) shows a very narrow activation energy distribution pattern (61-64 kcal/mol). This sample has a high HI (503 mg HC/g TOC), and is predicted to generate up to 80% of its petroleum potential at an activation energy of 61 kcal/mol and a frequency factor of 1.72E+16/sec. This very narrow activation energy distribution indicates a homogeneous kerogen structure dominated by a limited number of bonds. Usually, such features are characteristic of lacustrine environments, but the pyrolysate composition of this sample shown in **Figure 4.7** indicates a marine depositional environment. Thus, this sample is interpreted as containing Type II rather than Type I kerogen. Compared to the samples from the Plover and lower Vulcan formations, those from the upper Vulcan and Echuca Shoals formations are characterised by narrower activation energy ranges (51-54 kcal/mol), indicating more homogeneous Type II kerogen The maximum petroleum yields from both the upper Vulcan and Echuca Shoals formations are reached at the relatively low activation energies of 51-52 kcal/mol, with frequency factors of 1.38E+13/sec to 3.36E+13/sec, respectively.

Based on this bulk kinetic data set, transformation ratios and the corresponding temperatures of hydrocarbon generation were predicted for a constant heating rate of 3.3°C/Ma **(Figure 4.12)** which is reported as an average value for sedimentary basins (Schenk et al., 1997). For 70% TR, which is stated here as the ratio at which the main phase of petroleum generation occurs, there is a broad range of generation temperatures which vary with source rock age. At 70% TR, the most stable kerogens are typically those from the Plover Formation, which show a temperature range of 160-192°C. The highest temperatures (180-192°C) were measured for the coals and one shale (20110058) from the Plover Formation. The main phase of hydrocarbon generation from the lower Vulcan Formation occurs over a wide range, and is predicted to be 147-180°C. This is consistent with the temperature range published for Type II kerogen (Burnham et al., 1987). In contrast, the most labile kerogens are those from the upper Vulcan and Echuca Shoals formations, for which 70% TR temperatures were estimated to be 145-146°C for both formations. Since the samples that were subjected to bulk kinetic measurements are immature with respect to the oil window, these differences in the bulk kinetics are related to the different organic matter type and degree of preservation in these sediments.
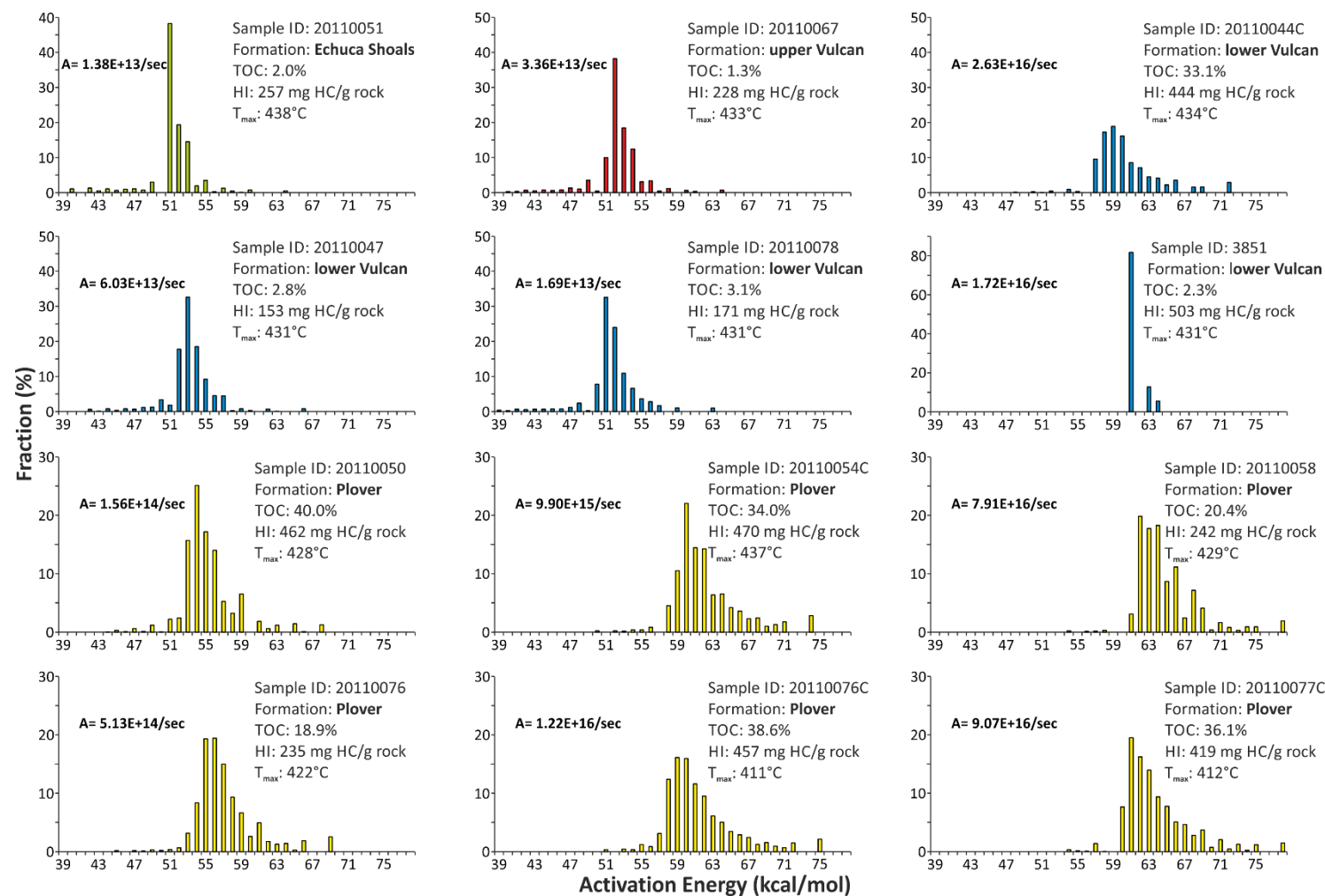
**Figure 4.11. Activation energy (Ea) distributions and frequency factors (A) of 12 selected samples calculated from open-system pyrolysis at heating rates of 0.1°C/min, 0.7°C/min and 5°C/min.**

**Table 4.4. Kinetic parameters Activation energy (Ea), distribution and frequency factors (A) for 14 source rock samples from the Vulcan Sub-basin. * denotes samples from Geoscience Australia (GA).**

| Sample ID | 20110051 | 20110067 | 20110044 C | 20110047 | 20110078 | 3851 | *G005732 |
|---|---|---|---|---|---|---|---|
| Formation | Echuca Shoals | upper Vulcan | lower Vulcan | lower Vulcan | lower Vulcan | lower Vulcan | lower Vulcan |
| Pre-exponential Factor A (S⁻¹) | 1.38E+13 | 3.36E+13 | 3.56E+15 | 6.03E+13 | 1.69E+13 | 1.72E+16 | 1.65E+13 |
| **Activation Energy (kcal/mol)** | | | | | | | |
| 39 | 0 | 0 | 0 | 0 | 0.36 | 0 | 0 |
| 40 | 1.02 | 0.34 | 0 | 0 | 0.21 | 0 | 0 |
| 41 | 0 | 0.38 | 0 | 0 | 0.63 | 0 | 0 |
| 42 | 1.23 | 0.67 | 0 | 0.55 | 0.56 | 0 | 0 |
| 43 | 0.43 | 0.52 | 0 | 0.04 | 0.61 | 0 | 0 |
| 44 | 1.02 | 0.78 | 0 | 0.72 | 0.62 | 0 | 0.1 |
| 45 | 0.54 | 0.59 | 0 | 0.29 | 0.75 | 0 | 0.1 |
| 46 | 0.93 | 0.81 | 0 | 0.75 | 0.74 | 0 | 0.7 |
| 47 | 0.99 | 1.33 | 0 | 0.58 | 1.14 | 0 | 0.1 |
| 48 | 0.66 | 1.05 | 0.14 | 1.12 | 2.38 | 0 | 0 |
| 49 | 2.94 | 3.58 | 0 | 1.18 | 0.2 | 0 | 0 |
| 50 | 0 | 0.46 | 0.2 | 3.34 | 7.76 | 0 | 23.7 |
| 51 | 48.19 | 10.05 | 0.04 | 1.76 | 32.53 | 0 | 28.5 |
| 52 | 19.31 | 38.44 | 0.46 | 17.79 | 23.96 | 0 | 19.3 |
| 53 | 14.46 | 18.6 | 0 | 32.7 | 10.93 | 0 | 13.9 |
| 54 | 1.86 | 12.54 | 0.9 | 18.51 | 6.6 | 0 | 5.1 |
| 55 | 3.41 | 3.1 | 0.34 | 9.16 | 3.61 | 0 | 3.2 |
| 56 | 0.21 | 3.39 | 0 | 4.49 | 2.77 | 0 | 2 |
| 57 | 1.21 | 0.44 | 9.57 | 4.42 | 1.65 | 0 | 1.5 |
| 58 | 0.39 | 1.19 | 17.22 | 0.17 | 0 | 0 | 0 |
| 59 | 0.06 | 0 | 18.9 | 0.74 | 1.02 | 0 | 0.6 |
| 60 | 0.7 | 0.65 | 16.15 | 0.26 | 0 | 0 | 1.1 |
| 61 | 0 | 0.36 | 8.53 | 0 | 0 | 81.7 | 0 |
| 62 | 0 | 0 | 7.09 | 0.68 | 0 | 0 | 0.2 |
| 63 | 0 | 0 | 4.5 | 0.01 | 0.97 | 12.8 | 0 |
| 64 | 0.44 | 0.72 | 4.1 | 0 | 0 | 5.5 | 0 |
| 65 | 0 | 0 | 2.2 | 0 | 0 | 0 | 0 |
| 66 | 0 | 0 | 3.56 | 0.74 | 0 | 0 | 0 |
| 67 | 0 | 0 | 0 | 0 | 0 | 0 | 0 |
| 68 | 0 | 0 | 1.58 | 0 | 0 | 0 | 0 |
| 69 | 0 | 0 | 1.61 | 0 | 0 | 0 | 0 |
| 70 | 0 | 0 | 0 | 0 | 0 | 0 | 0 |
| 71 | 0 | 0 | 0 | 0 | 0 | 0 | 0 |
| 72 | 0 | 0 | 2.91 | 0 | 0 | 0 | 0 |

**Table 4.4. (Continued) Kinetic parameters Activation energy (Ea), distribution and frequency factors (A) for 14 source rock samples from the Vulcan Sub-basin. \* denotes samples from Geoscience Australia (GA).**

| Sample ID | 20110050 | 20110054C | 20110058 | 20110076 | 20110076C | 20110077C | *G005733 |
|---|---|---|---|---|---|---|---|
| Formation | Plover | Plover | Plover | Plover | Plover | Plover | Plover |
| Pre-exponential Factor A (S⁻¹) | 1.56E+14 | 9.90E+15 | 7.91E+16 | 5.13E+14 | 1.22E+16 | 9.07E+16 | 1.53E+15 |
| **Activation Energy (kcal/mol)** | | | | | | | |
| 44 | 0.02 | 0 | 0 | 0 | 0 | 0 | 0 |
| 45 | 0.28 | 0 | 0 | 0.18 | 0 | 0 | 0 |
| 46 | 0.07 | 0 | 0 | 0 | 0 | 0 | 0 |
| 47 | 0.58 | 0 | 0 | 0.2 | 0 | 0 | 0 |
| 48 | 0.11 | 0 | 0 | 0.11 | 0 | 0 | 0 |
| 49 | 1.16 | 0 | 0 | 0.31 | 0 | 0 | 0.2 |
| 50 | 0.03 | 0.22 | 0 | 0.22 | 0 | 0 | 0 |
| 51 | 2.18 | 0 | 0 | 0.36 | 0.32 | 0 | 0.4 |
| 52 | 2.39 | 0.21 | 0 | 0.66 | 0 | 0 | 0.2 |
| 53 | 15.69 | 0.16 | 0 | 3.17 | 0.44 | 0 | 0 |
| 54 | 25.09 | 0.35 | 0.21 | 8.35 | 0.36 | 0.32 | 0 |
| 55 | 17.16 | 0.36 | 0 | 19.32 | 1.24 | 0.15 | 16.4 |
| 56 | 13.98 | 0.8 | 0.13 | 19.43 | 0.87 | 0.06 | 15.2 |
| 57 | 5.25 | 0 | 0.2 | 15.02 | 3.12 | 1.39 | 16 |
| 58 | 3.21 | 4.5 | 0.29 | 9.33 | 12.39 | 0.04 | 10.8 |
| 59 | 6.52 | 10.52 | 0 | 6.65 | 16.11 | 0 | 9.5 |
| 60 | 0 | 22.04 | 0 | 2.61 | 15.97 | 7.64 | 6.2 |
| 61 | 1.82 | 14.45 | 3.1 | 4.95 | 11.6 | 19.51 | 5.7 |
| 62 | 0.58 | 14.24 | 19.83 | 1.75 | 9.51 | 16.23 | 3.6 |
| 63 | 1.16 | 6.37 | 17.74 | 1.27 | 6.12 | 13.96 | 3.4 |
| 64 | 0 | 6.52 | 18.25 | 1.42 | 5.05 | 9.37 | 2.1 |
| 65 | 1.41 | 4.19 | 8.67 | 0.29 | 3.47 | 7.75 | 2 |
| 66 | 0.07 | 3.58 | 11.13 | 1.86 | 2.89 | 5.08 | 0.8 |
| 67 | 0 | 2.28 | 2.43 | 0 | 2.44 | 4.66 | 2.2 |
| 68 | 1.24 | 2.41 | 7.14 | 0 | 1.26 | 2.8 | 0 |
| 69 | 0 | 0.98 | 4.11 | 2.54 | 1.57 | 3.7 | 1.9 |
| 70 | 0 | 1.29 | 0.35 | 0 | 0.95 | 0.73 | 0.7 |
| 71 | 0 | 1.73 | 1.63 | 0 | 0.68 | 2.04 | 0.2 |
| 72 | 0 | 0 | 0.79 | 0 | 1.5 | 0.45 | 0 |
| 73 | 0 | 0 | 0.3 | 0 | 0 | 1.25 | 2.6 |
| 74 | 0 | 2.8 | 0.89 | 0 | 0 | 0.22 | 0 |
| 75 | 0 | 0 | 0.9 | 0 | 2.14 | 1.18 | 0 |
| 76 | 0 | 0 | 0 | 0 | 0 | 0 | 0 |
| 77 | 0 | 0 | 0 | 0 | 0 | 0 | 0 |
| 78 | 0 | 0 | 1.91 | 0 | 0 | 1.47 | 0 |
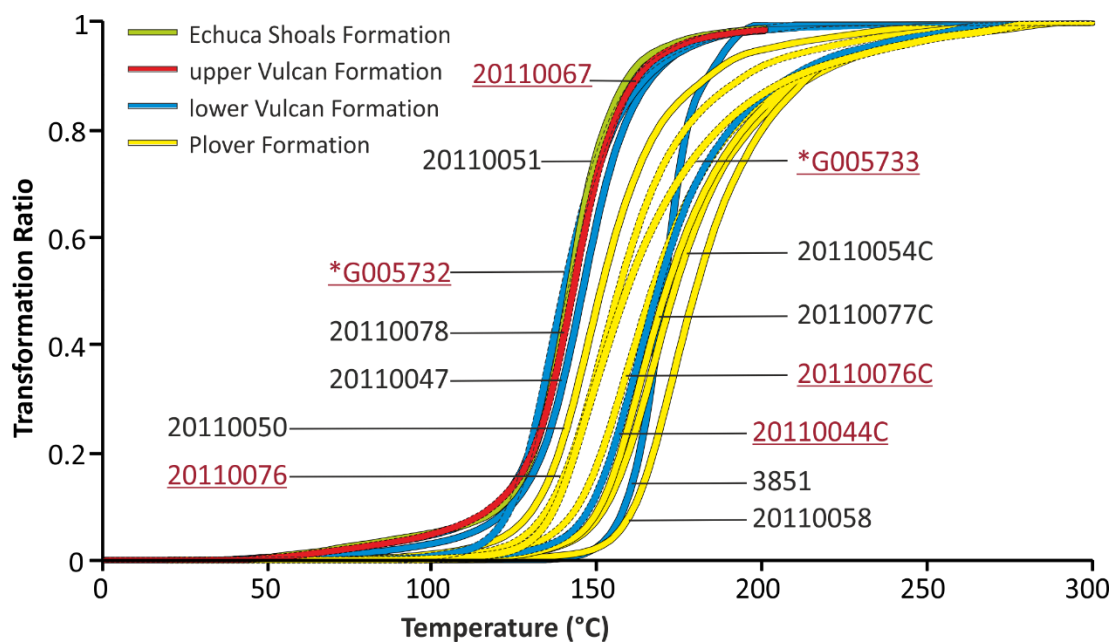
**Figure 4.12. Transformation Ratio evolution of 14 samples calculated for a heating rate of 3.3°C/Ma. The underlined sample codes correspond to the six samples selected for compositional kinetic analysis. * denotes samples from Geoscience Australia (GA).**

### 4.5.7. Compositional kinetics and phase behaviour

The upper Vulcan and Echuca Shoals formations show similar pyrolysate compositions and kinetic parameters, with a difference of about 1°C in the temperature at which both the onset and main phase of petroleum generation is predicted to occur. Therefore, the upper Vulcan Formation sample (20110067) was used to represent both of these formations for compositional kinetic measurements. The five additional samples for compositional kinetic measurements are from the Plover Formation (one coal: 20110076C, and two shales: 20110076 and G005733), and the lower Vulcan Formation (one coal: 20110044C and one shale: G005732). The compositional evolution and physical properties of the petroleum products generated from these source rocks were predicted using a combination of open and closed-system pyrolysis, as a function of increasing transformation ratios (10%, 30%, 50%, 70% and 90% TR). The models generated for these six samples have fourteen components ($C_1$, $C_2$, $C_3$, $i$-$C_4$, $n$-$C_4$, $i$-$C_5$, $n$-$C_5$, $n$-$C_6$, $C_7$–$C_{15}$, $C_{16}$–$C_{25}$, $C_{26}$–$C_{35}$, $C_{36}$–$C_{45}$, $C_{46}$–$C_{55}$, and $C_{56}$–$C_{80}$) derived from the primary cracking of kerogen and are illustrated in **Figure 4.13**. The composition of hydrocarbons that can be expelled from these source rocks is dominated by the $C_7$–$C_{15}$ and $C_{16}$–$C_{25}$ fractions. For the Plover Formation, similar compositional kinetics were observed between the coal (20110076C) and the shale (20110076) lithologies, despite the differences in their bulk kinetic parameters **(Figure 4.12)**. In addition, compositional schemes with four components including black oil ($C_{15+}$), light oil ($C_6$–$C_{14}$), wet gas ($C_2$–$C_5$) and dry gas ($C_1$) were defined **(Table 4.5)**. For the six investigated samples,

physical properties such as the GOR, formation volume factor ($B_O$) and saturation pressure ($P_{sat}$) show a steady increase with increasing TR **(Table 4.6)**.

**Table 4.5. Compositional kinetic data, showing the proportions of the main compounds generated during the primary cracking of kerogens by closed-system MSSV pyrolysis of six source rock samples from the Vulcan Sub-basin. * denotes samples from Geoscience Australia (GA).**

| Sample ID<br>Formation<br>Kerogen type<br>(Py-GC) | 20110067<br>upper Vulcan<br>PNA<br>Low Wax | 20110044C<br>lower Vulcan<br>PNA<br>High Wax | *G005732<br>lower Vulcan<br>PNA<br>Low Wax | 20110076<br>Plover (Shale)<br>PNA<br>Low Wax | 20110076C<br>Plover (Coal)<br>Gas and<br>Condensate | *G005733<br>Plover<br>Gas and<br>Condensate |
|---|---|---|---|---|---|---|
| **Oil (%)** | 71.9 | 75.2 | 82.93 | 76.1 | 80.5 | 81.22 |
| **Gas (%)** | 28.1 | 24.8 | 17.07 | 23.9 | 19.5 | 18.79 |
| **$C_1$ (%)** | 11.4 | 10.8 | 6.09 | 10.2 | 8 | 7.96 |
| **$C_2$-$C_5$ (%)** | 16.8 | 14 | 10.98 | 13.7 | 11.5 | 10.83 |
| **$C_6$-$C_{14}$ (%)** | 44.7 | 28.1 | 35.57 | 33.9 | 31.9 | 33.71 |
| **$C_{15+}$ (%)** | 27.2 | 47.1 | 47.36 | 42.3 | 48.5 | 47.51 |
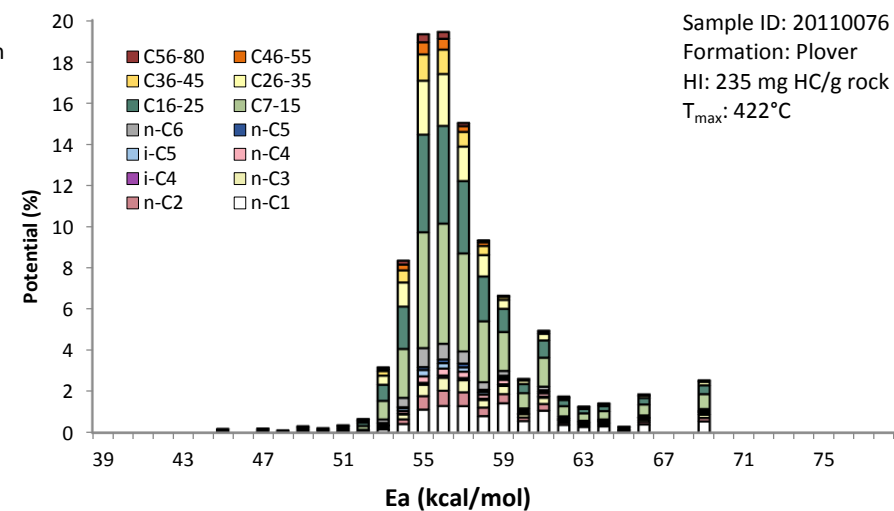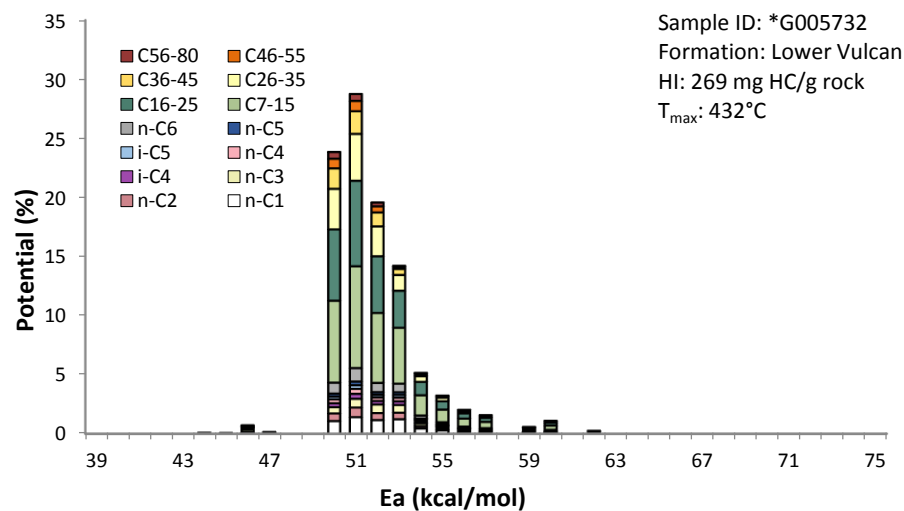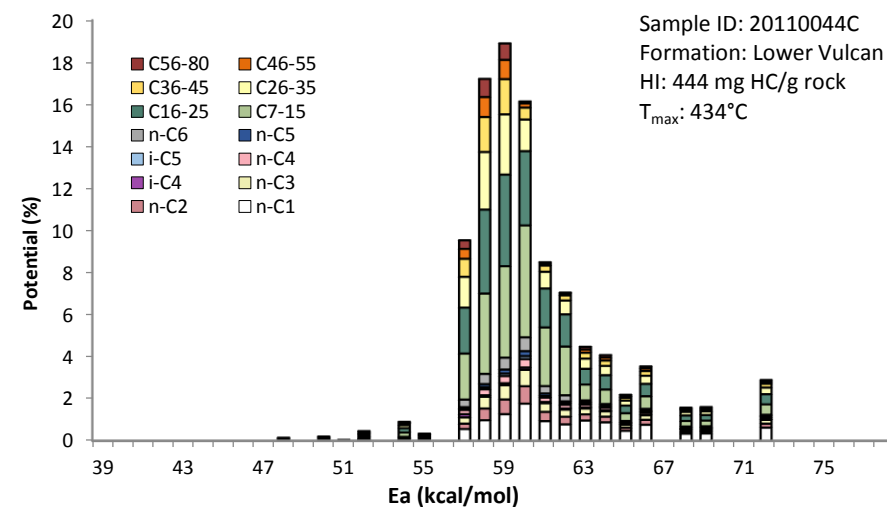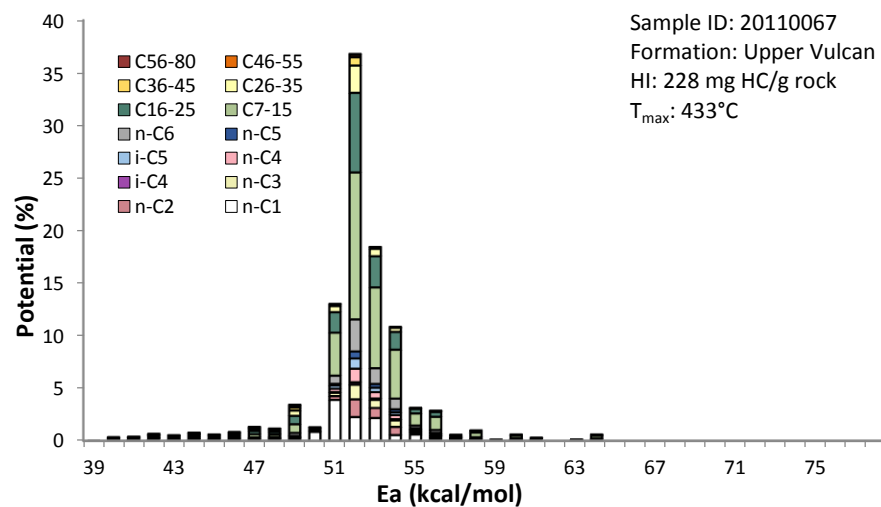
*Note: Figure caption is on the next page.*
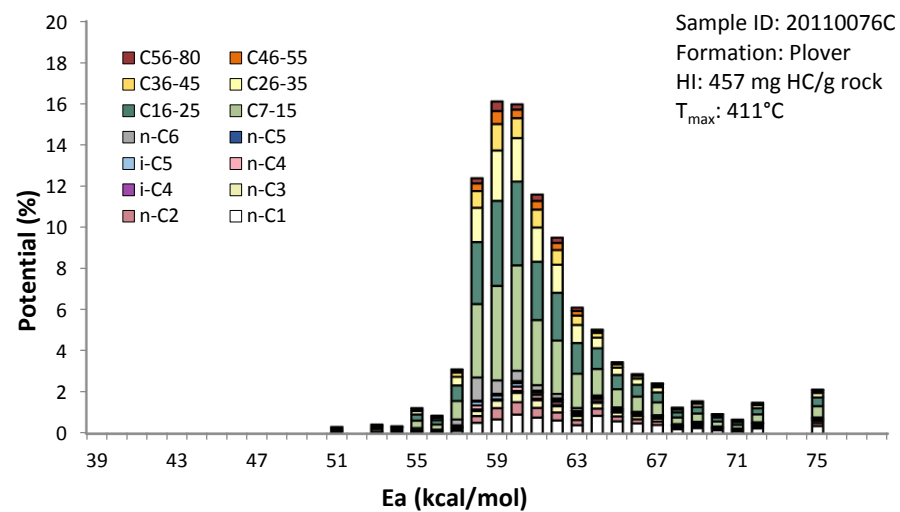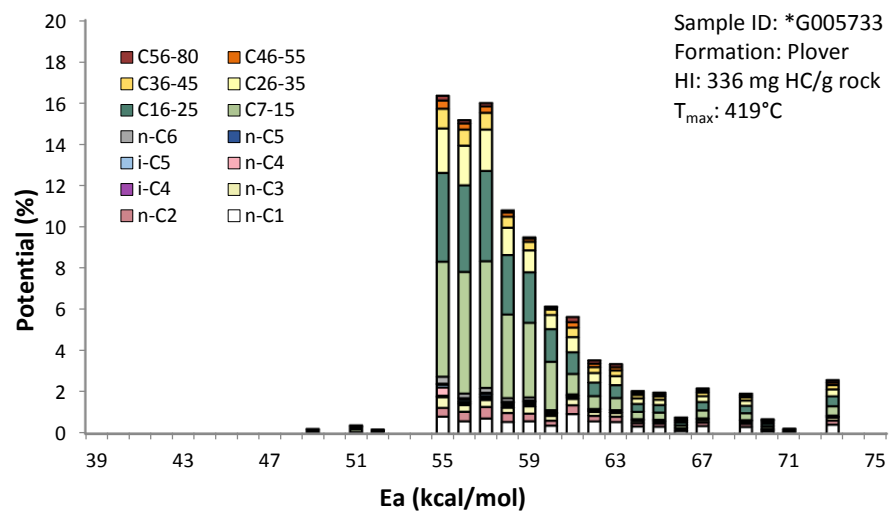
**Figure 4.13. Compositional kinetic models for six source rock samples from the Vulcan Sub-basin. * denotes samples from Geoscience Australia (GA).**

**Table 4.6. Predicted gas:oil ratios (GOR), formation volume factors (B$_O$) and saturation pressures (P$_{sat}$) as a function of increasing Transformation Ratio (TR) for six source rock samples from the Vulcan Sub-basin. * denotes samples from Geoscience Australia (GA).**

| End temperature (°C) | TR (%) | GOR (Sm$^3$/Sm$^3$) | B$_o$ (m$^3$/Sm$^3$) | P$_{sat}$ (bar) |
|---|---|---|---|---|
| **Sample ID: 20110067** | | | | |
| **Formation: upper Vulcan** | | | | |
| 357 | 10 | 88 | 1.34 | 128 |
| 389 | 30 | 188 | 1.74 | 148 |
| 406 | 50 | 238 | 1.9 | 175 |
| 420 | 70 | 292 | 2.13 | 178 |
| 442 | 90 | 451 | 2.71 | 215 |
| **Sample ID: 20110044C** | | | | |
| **Formation: lower Vulcan** | | | | |
| 382 | 10 | 142 | 1.47 | 205 |
| 405 | 30 | 140 | 1.44 | 222 |
| 421 | 50 | 165 | 1.53 | 236 |
| 440 | 70 | 267 | 1.93 | 216 |
| 484 | 90 | 630 | - | 580 |
| **Sample ID: *G005732** | | | | |
| **Formation: lower Vulcan** | | | | |
| 369 | 10 | 104 | 1.37 | 147 |
| 392 | 30 | 102 | 1.36 | 145 |
| 407 | 50 | 111 | 1.4 | 148 |
| 422 | 70 | 138 | 1.48 | 165 |
| 448 | 90 | 207 | 1.74 | 182 |
| **Sample ID: 20110076** | | | | |
| **Formation: Plover (shale)** | | | | |
| 373 | 10 | 114 | 1.41 | 150 |
| 396 | 30 | 134 | 1.47 | 167 |
| 412 | 50 | 155 | 1.54 | 181 |
| 430 | 70 | 203 | 1.7 | 198 |
| 471 | 90 | 596 | 2.97 | 304 |
| **Sample ID: 20110076C** | | | | |
| **Formation: Plover (coal)** | | | | |
| 368 | 10 | 95 | 1.36 | 124 |
| 393 | 30 | 99 | 1.35 | 150 |
| 410 | 50 | 133 | 1.47 | 164 |
| 432 | 70 | 161 | 1.53 | 209 |
| 479 | 90 | 455 | 2.39 | 348 |
| **Sample ID: *G005733** | | | | |
| **Formation: Plover** | | | | |
| 371 | 10 | 114 | 1.41 | 143 |
| 393 | 30 | 86 | 1.32 | 117 |
| 411 | 50 | 118 | 1.42 | 145 |
| 435 | 70 | 144 | 1.51 | 158 |
| 489 | 90 | 464 | - | 596 |

The highest GORs were measured for the lower Vulcan Formation coal sample. The GORs of the upper Vulcan Formation vary from 88 Sm$^3$/Sm$^3$ at a TR of 10% to 451 Sm$^3$/Sm$^3$ at a TR of 90% **(Figure 4.14)**. Interestingly, at 30%, 50% and 70% TR, petroleums produced from the upper Vulcan Formation show higher GORs than those from the Plover and lower Vulcan formations. GORs from both the lower Vulcan and Plover shales are similar ranging from 10-70% TR. At 90% TR, the highest GORs were measured for the PNA high wax-producing coal from the lower Vulcan Formation (630 Sm$^3$/Sm$^3$), and the PNA low wax-generating shale (20110076) from the Plover Formation (596 Sm$^3$/Sm$^3$), indicating that mainly gas is generated at higher transformation ratios. The lowest GORs are generated from the more labile marine shale of the lower Vulcan Formation (207 Sm$^3$/Sm$^3$). Based on these

predicted GORs, the fluids generated from the source rocks in the Vulcan Sub-basin, at relatively low TR (10-70%), can be classified as black oils (>350 $Sm^3/Sm^3$; $m^3/m^3$ at standard surface conditions, equivalent to 2000 scf/bbl), where the contribution of heavy compounds present in evolved gases in reservoir to the total liquid recovery is not significant. A divergence in GOR is clearly observed at the highest maturity level when marine shales from the lower Vulcan Formation continue to produce black oils, whereas light oil to gas/condensate are generated from the upper Vulcan and Plover formations, and lower Vulcan Formation coal. These generation kinetic parameters can be incorporated into 3D basin models for the Vulcan Sub-basin.

Measured GORs in the Vulcan Sub-basin are in the range 40-380 $Sm^3/Sm^3$ (**Table 4.7**) and generally match those predicted by the kinetic models. It should be noted that the lowest measured GORs are likely related to secondary alteration effects described above, such as water washing, or evaporative fractionation (see also di Primio, 2002). Evidence for the operation of these secondary alteration processes in the reservoirs of the Vulcan Sub-basin include either the selective removal of water-soluble benzene and toluene, or on the contrary the abundance of mono-aromatic hydrocarbons in the oils and condensates (Edwards et al., 2004).
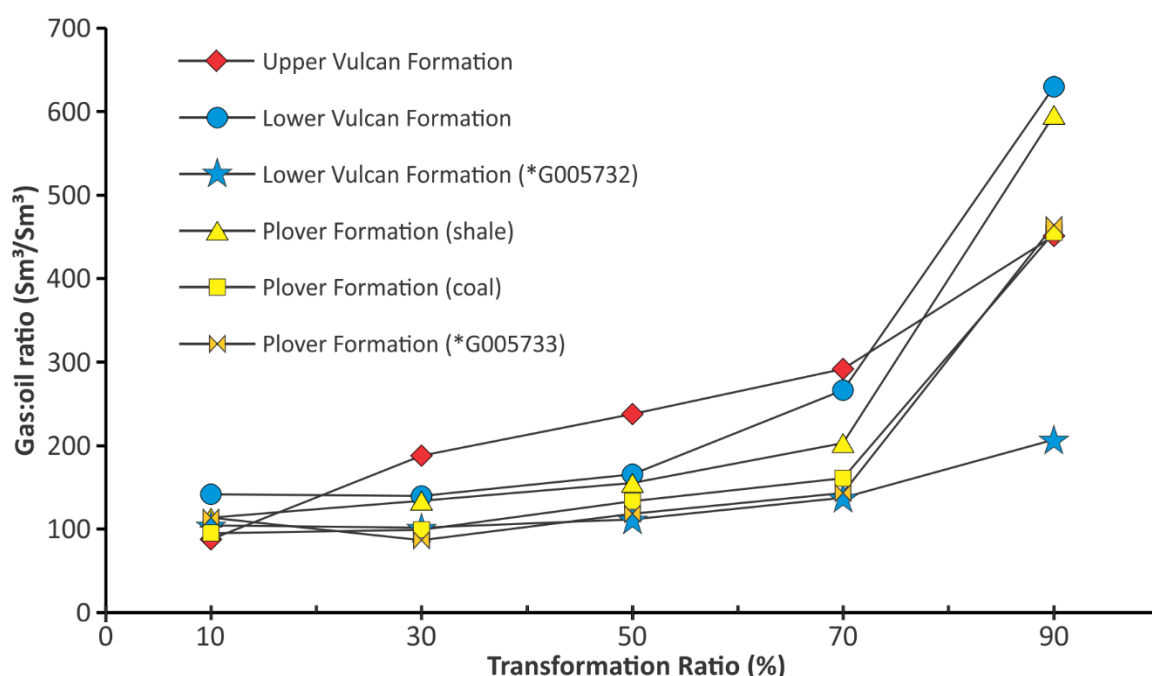


**Figure 4.14. Gas:oil ratio evolution as a function of increasing Transformation Ratio during MSSV pyrolysis of six source rock samples. * denotes samples from Geoscience Australia (GA).**

**Table 4.7. Gas:oil ratios (GORs) (Edwards et al., 2004) for natural gases in the Vulcan Sub-basin.**

| Well name | GOR (Sm³/Sm³) |
|---|---|
| Bilyara 1ST1 | 173.9 |
| Birch 1 | 39.5 |
| Cassini 1 | 41 |
| Challis 1 | 58.1 |
| Jabiru 1A | 62 |
| Montara 2 | 113.3 |
| Oliver 1 | 112 |
| Skua 2 | 129.9 |
| Skua 3 | 378.7 |
| Talbot 1 | 132 |
| Tenacious 1 | 92 |

### 4.5.8. Stable carbon isotopic composition of light hydrocarbons

The carbon isotopic composition of methane, ethane, propane and *n*-butane, measured using the MSSV pyrolysis system are shown in **Figure 4.15**. All four analysed source rock samples show similar trends with heavier isotopic compositions for these compounds with increasing pyrolysis temperature **(Table 4.8)**. This increase in the $\delta^{13}C$ enrichment of these individual light hydrocarbons in the order: *n*-butane > propane > ethane > methane, is likely due to a gradual loss of the isotopically lighter components and the cracking of two or more isotopically distinct precursors (e.g., James, 1983; Lorant et al., 1998; Tang et al., 2000). This trend of isotopically lighter compositions produced at low maturity, has been reported by several authors (e.g., Clayton, 1991; Bjorøy et al., 1992; Lorant et al., 1998; Galimov, 2006) to be the result of primary reactions involving the cracking of thermally unstable bonds (Cramer, 2004). There is a prominent difference between the $\delta^{13}C$ values measured for each of these four studied source rocks. For the whole gas range, the lightest isotopic composition was measured for gases generated from the upper Vulcan Formation samples, while the heaviest composition was determined for the coal sample from the Plover Formation. This difference is particularly noticeable for the isotopic composition of both ethane and propane measured for the upper Vulcan Formation, where the $\delta^{13}C$ values for ethane are at least 7-9‰ lighter than those of the Plover and lower Vulcan formations. The stable $\delta^{13}C$ isotope composition of methane produced from the four samples is in the range of −34‰ to −40‰, similar to values typically measured in thermogenic gases (Schoell, 1980; Whiticar, 1999). The isotopic value of methane measured for the Plover Formation coal sample (~ -34‰, 20110076C) is consistent with terrestrially-influenced organic matter, generally enriched in $^{13}C$ (Degens, 1989). The lightest values were determined for the upper Vulcan Formation (-39‰), which is probably consistent with more marine-influenced

organic matter, and is isotopically distinguishable from that preserved in the Plover and lower Vulcan formations. With increasing temperature, the lower Vulcan Formation and Plover Formation coals are characterised by a relatively large methane carbon isotopic variability, in the range of -39.8‰ and -34‰ at 10% TR to -35.4‰ and 33.9‰ at 90% TR respectively. At similar transformation ratios, the Plover Formation shale shows consistently less negative $\delta^{13}$C values of light hydrocarbons than those from the coal. As these two Plover Formation samples were hand-picked from the same depth in Skua 1, and consequently have the same maturity, the slight differences can be accounted for by different structures and intermolecular effects.
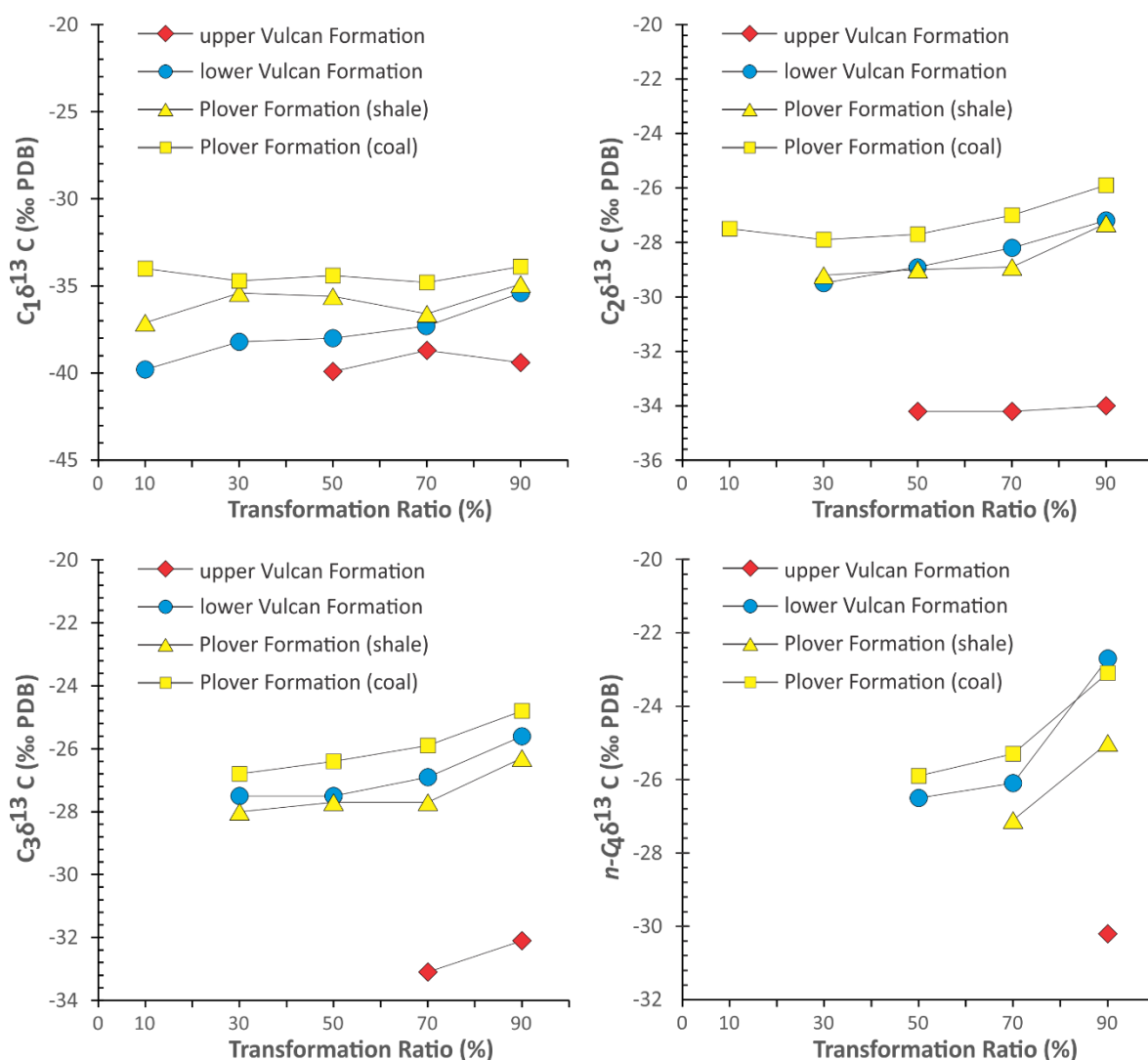


**Figure 4.15. Stable carbon isotopic distributions of methane, ethane, propane and *n*-butane generated from pyrolysis experiments in a closed system as function of increasing Transformation Ratio.**

**Table 4.8. Carbon isotopic composition of C₁−C₄ hydrocarbons generated by the closed system MSSV pyrolysis of four solvent-extracted rock samples as a function of increasing Transformation Ratio.**

| End temp. (°C) | TR (%) | $C_1\ \delta^{13}C$ (‰ PDB) | $C_2\ \delta^{13}C$ (‰ PDB) | $C_3\ \delta^{13}C$ (‰ PDB) | $n\text{-}C_4\ \delta^{13}C$ (‰ PDB) |
|---|---|---|---|---|---|
| **20110067** | | | | | |
| **upper Vulcan Fm** | | | | | |
| 357 | 10 | - | - | - | - |
| 389 | 30 | - | - | - | - |
| 406 | 50 | -39.9 | -34.2 | - | - |
| 420 | 70 | -38.7 | -34.2 | -33.1 | - |
| 442 | 90 | -39.4 | -34 | -32.1 | -30.2 |
| **20110044C** | | | | | |
| **lower Vulcan Fm** | | | | | |
| 382 | 10 | -39.8 | - | - | - |
| 405 | 30 | -38.2 | -29.5 | -27.5 | - |
| 421 | 50 | -38 | -28.9 | -27.5 | -26.5 |
| 440 | 70 | -37.3 | -28.2 | -26.9 | -26.1 |
| 484 | 90 | -35.4 | -27.2 | -25.6 | -22.7 |
| **20110076** | | | | | |
| **Plover Fm (Shale)** | | | | | |
| 373 | 10 | -37.1 | - | - | - |
| 396 | 30 | -35.4 | -29.2 | -28 | - |
| 412 | 50 | -35.6 | -29 | -27.7 | - |
| 430 | 70 | -36.6 | -28.9 | -27.7 | -27.1 |
| 471 | 90 | -34.9 | -27.3 | -26.3 | -25 |
| **20110076C** | | | | | |
| **Plover Fm (Coal)** | | | | | |
| 368 | 10 | -34 | -27.5 | - | - |
| 393 | 30 | -34.7 | -27.9 | -26.8 | - |
| 410 | 50 | -34.4 | -27.7 | -26.4 | -25.9 |
| 432 | 70 | -34.8 | -27 | -25.9 | -25.3 |
| 479 | 90 | -33.9 | -25.9 | -24.8 | -23.1 |

The stable carbon isotopic signatures of individual light hydrocarbons, generated from kerogen cracking by artificial maturation, were validated against those measured in natural oil and gas fields in the Vulcan Sub-basin (**Table 4.9**). As expected, none of the artificially pyrolysed source rock samples alone can account for the variable and light isotopic compositions measured in the Vulcan Sub-basin, but the range of isotopic variability is comparable among experimental and natural data (6‰). As suggested by Tian et al. (2010), the position of data on a diagram plotting the difference of $\delta^{13}C$ between ethane and propane versus $\delta^{13}C$ of methane can be used to determine the origin of gases by differentiating between gases derived from kerogen cracking and those from oil cracking (**Figure 4.16**). Data from the Vulcan Sub-basin fall well within the kerogen cracking gas field. In this respect, the natural gases are more likely to be the result of the mixing of gases generated at different levels of thermal stresses. This possibly includes older and deeper source rocks that have not been considered in this paper (Edwards et al., 1997; Summons et al., 1998; Boreham et al., 2001).

**Table 4.9. Carbon isotopic composition of C₁−C₄ hydrocarbons (Edwards et al., 2004) in natural gases in the Vulcan Sub-basin. GA: Geoscience Australia database; CSIRO: CSIRO Petroleum database; WCR: Well Completion Report.**

| GA Sample No./Source | Well | C₁ δ¹³C (‰ PDB) | C₂ δ¹³C (‰ PDB) | C₃ δ¹³C (‰ PDB) | n-C₄ δ¹³C (‰ PDB) |
|---|---|---|---|---|---|
| 1365123 | Leeuwin 1 | -43.1 | -32.2 | -30.1 | -29.5 |
| 1365203 | Maple 1 | -41.5 | -28 | -25.3 | -24.6 |
| 1365205 | Montara 1 | -38.7 | -29.9 | -28.5 | -27.2 |
| 1365204 | Oliver 1 ST1 | -40.9 | -27.1 | -25.6 | -24.8 |
| 1376184 | Tahbilk 1 (2305 m) | -42.9 | -30.7 | -29 | -28 |
| 1376183 | Tahbilk 1 (2690.2 m) | -44.1 | -32.5 | -30 | -29.5 |
| CSIRO | Skua 4 | -40.3 | -29.7 | -28 | -27.7 |
| CSIRO | Skua 5 | -40.9 | -27.7 | -28.1 | -27.9 |
| CSIRO | Cassini 1 | -43.2 | -29.9 | -28.2 | -27.5 |
| CSIRO | Swan 3 | -43.5 | -30.4 | -29.8 | -29.6 |
| CSIRO | Pengana 1 | -43.6 | -28.6 | -26.5 | -25.5 |
| WCR | Pengana 1 | -42.2 | -28.7 | -25 | -27 |
| 1991720 | Padthaway 1 | -38.2 | -30.6 | -28.5 | -27.4 |
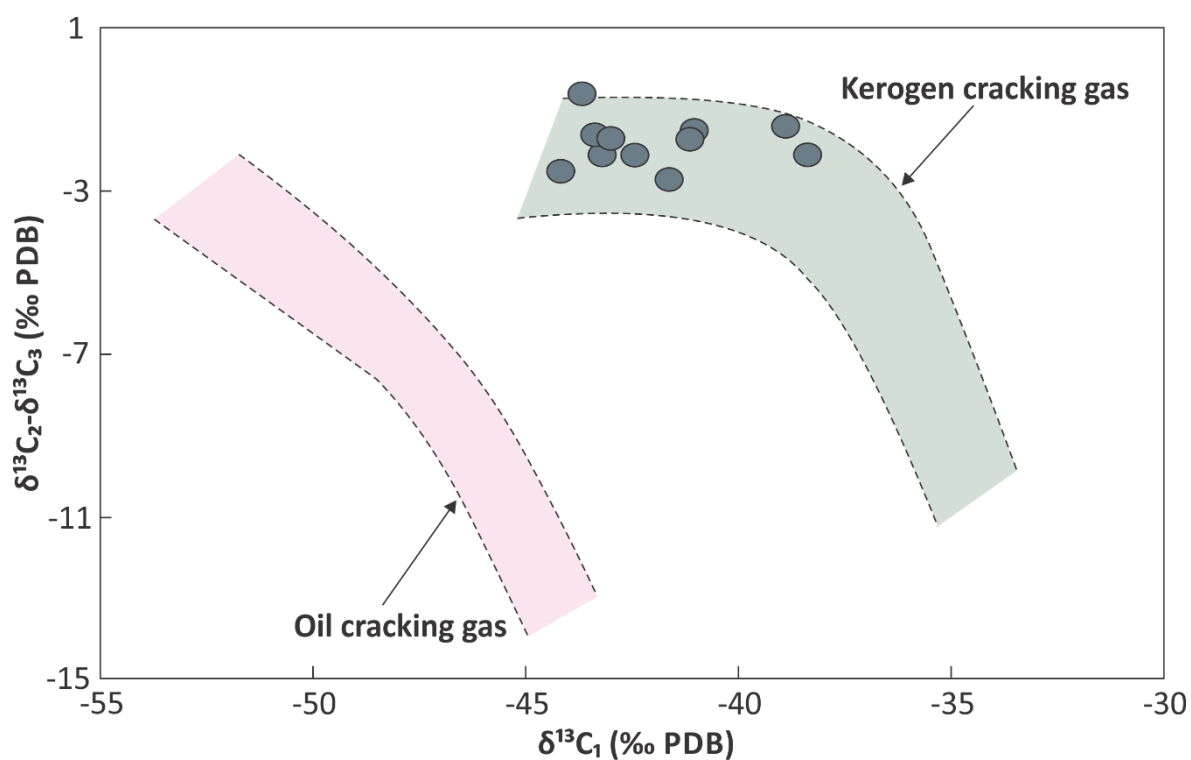


**Figure 4.16. Cross plot of (δ¹³C₁) versus (δ¹³C₂ − δ¹³C₃) for natural gases from the Vulcan Sub-basin. See Table 9 for sample details. Domain limits are defined by Tian et al. (2010).**

## 4.6.    Synthesis

Total organic carbon content and Rock-Eval pyrolysis data show that the source rock samples analysed in this study of the Vulcan Sub-basin fall into two groups; (1) a comparatively organic-lean group with marginal potential for black oil generation, including the late syn- to post-rift upper Vulcan and the Echuca Shoals formations; and (2) a highly organic-rich group with good to excellent generative potential comprising the pre- to syn-rift Plover and lower Vulcan formations. Based on $T_{max}$ values and FAMM-EqVR data, most of the samples studied are marginally mature to late mature with respect to the oil generation window. Of the four source rocks investigated in the Vulcan Sub-basin, the highest activation energies and frequency factors were measured for coals and shales containing Type II-III kerogen from the Plover and lower Vulcan formations, resulting in a calculated broad temperature range for the onset of petroleum generation (120–160°C). These heterogeneous kerogens have the potential to generate low to high wax, PNA oil from shales, and gas and condensate from coals of only the Plover Formation.

The onset of bulk petroleum generation in the lower Vulcan Formation is highly variable, being between 120–157°C for the marine shale samples and 148°C for the coal sample. Shales from the Plover Formation commence generating petroleum at relatively comparable temperatures (130–136°C), while petroleum generation from the coal samples occur over a temperature range of 143–160°C. Compared to the shale samples, coals from the Plover Formation are kinetically more stable and their high HI values (over 400 mg HC/g TOC), suggest the potential for oil generation, in addition to gas and condensates. Although both the upper Vulcan and Echuca Shoals formations contain Type III kerogen, they show a narrower distribution of activation energies, more typical of Type I kerogen. The onset of hydrocarbon generation from these formations occurs at the low and similar temperatures of 120 to 123°C. The similarity in kinetic parameters, as well as in the petroleum type generated (low wax PNA oil) from the upper Vulcan and Echuca Shoals formations, indicates similar precursors.

Variability in the kerogen type preserved in the Middle Jurassic to Early Cretaceous source rocks can be attributed to fluctuations in the amount of marine versus terrestrial organic matter being deposited, the redox conditions at the time of deposition and burial and the change in the depositional environment from fluvio-deltaic conditions, to restricted and open marine conditions. The depositional settings of the Plover and lower Vulcan formations although varied are suitable for the accumulation and preservation of organic matter. Perhydrous vitrinite-rich samples are preserved within the Plover Formation source rocks

160

and suggest less oxygenated bottom waters during deposition. Anoxic conditions are also indicated by the observed high pyrite content within the samples from the Plover and lower Vulcan formations. In contrast, the organic matter within the upper Vulcan and Echuca Shoals formations, although deposited in marine settings where planktonic material preferentially accumulates, has less organic matter preserved. The moderate organic richness and high inertinite content of the Echuca Shoals Formation can be explained to a large extent by oxidation processes affecting the organic matter prior to or after deposition. These less favourable conditions for the preservation of organic matter were also reported for the Upper Jurassic to Lower Cretaceous source rocks in the Laminaria High region of the northern Bonaparte Basin (Abbassi et al., 2014a).

The compositional kinetic models generated for the Plover, lower Vulcan and upper Vulcan formations reveal the potential to generate GORs ranging from 86 $Sm^3/Sm^3$-630 $Sm^3/Sm^3$. These model predictions show that low GORs or black oils (GOR $\leq$ 350 $Sm^3/Sm^3$) in the Vulcan Sub-basin can be generated from the three source rock sequences at 10-70% TR, while higher GORs characteristic for light oils (350 < GOR < 600 $Sm^3/Sm^3$) can be generated from the Plover and upper Vulcan formations at 90% TR and above. However, it is unlikely that the upper Vulcan Formation has attained a late oil window thermal maturity in the Vulcan Sub-basin to generate oils with such high GORs. The effect of alteration processes, such as preferential leakage and/or water washing were not taken into consideration during the kinetic modelling of this study, so it is difficult to definitively determine the source of the reservoired fluids in the Vulcan Sub-basin. Isotopically, gases generated by artificial maturation are generally heavy and cannot individually reproduce the isotopic compositions measured in the natural oil and gas fields in the Vulcan Sub-basin, which likely resemble mixtures of hydrocarbons produced from multiple source rocks at different maturity levels. This interpretation is in agreement with previous findings reported by Edwards et al. (2004) who stated that the gases/condensates in the Vulcan Sub-basin were generated over a range of thermal maturities.

In summary, the data reported herein are in agreement with previous studies suggesting that the Plover and lower Vulcan formations are the primary source rocks for hydrocarbons generated in the Vulcan Sub-basin. Although, the contribution of each of these source rocks to the oil and gas accumulations in the Vulcan Sub-basin cannot be assessed, facies variation in the Plover and lower Vulcan formations may explain the geochemical heterogeneity of the oils. Oils with a marine source signature were probably generated from the shales of the lower Vulcan Formation. An additional contribution of oil from both the upper Vulcan and

Echuca Shoals formations is precluded by their lack of maturity in the Swan and Paqualin graben, but could generate where more deeply buried elsewhere in the northern Bonaparte Basin. Oils with terrestrial source signatures were probably generated from coals and shales of the Plover Formation and the lower Vulcan Formation, whereas gas and condensate are mainly derived from the coals of the Plover Formation.

## 4.7.    Conclusions

There is considerable variation in the organic richness and petroleum potential of the studied Mesozoic source rocks in the Vulcan Sub-basin. The petroleum potential is greatest in the terrestrially influenced fluvio-deltaic source rocks of the Lower–Middle Jurassic Plover Formation and the restricted marine source rocks of the Upper Jurassic lower Vulcan Formation. The source rocks within the Upper Jurassic−Lower Cretaceous upper Vulcan and Lower Cretaceous Echuca Shoals formations have less potential due to oxidation of the organic matter in the open marine conditions. The lower Vulcan and Plover formations are organic-rich and have moderate to very good petroleum potential containing a predominance of Type II/III kerogen, capable of generating both oil and gas. Where sampled, these formations show a range in thermal maturity, from marginally mature on the Montara Terrace to within the middle to late oil window in the Swan and Paqualin graben. High wax PNA oils were generated under laboratory conditions from coals within the Plover and lower Vulcan formations, which were deposited in lower delta plain and inner shelf environments. Low wax PNA oils were generated from marine shales of the lower Vulcan formation. In contrast, the source rocks sampled from the upper Vulcan and Lower Cretaceous Echuca Shoals formations are immature to marginally mature with respect to the oil window in the Swan and Paqualin graben. When pyrolysed, they produced low wax PNA oils, and could be a source of oil elsewhere in the Bonaparte Basin.

Based on bulk kinetic parameters, samples from the Plover Formation show a marked variability in their response to thermal stress compared to those from the lower and upper Vulcan and Echuca Shoals formations. The source rocks of the Plover Formation have a pronounced terrestrial influence and the resultant coals and shales have a high abundance of aromatic hydrocarbons and exhibit a broad range in their activation energies. The lower Vulcan coal sample has similar kinetics to those of the Plover Formation samples, suggesting also terrestrial influence. Typically, the lower Vulcan Formation shales contain mixed terrestrial and marine Type II/III kerogen with a range in their activation energies. However, one sample from the lower Vulcan Formation displayed a narrow activation energy distribution and contains homogeneous Type II kerogen. This sample had an increased algal

input, and was deposited under more reducing conditions. Heterogeneity in the samples from the Plover and lower Vulcan formations is also observed in the bulk hydrocarbon generation onset temperatures. The generation of hydrocarbons from the Plover and lower Vulcan formations is predicted to commence between 120°C and 162°C. In contrast, the organic matter in the Echuca Shoals and upper Vulcan formations is more homogeneous with the onset of hydrocarbon generation taking place from 120 to 123°C.

The results from this study are consistent with previous findings in that the primary source rocks in the Vulcan Sub-basin are the Plover and lower Vulcan formations. The upper Vulcan and Echuca Shoals formations are thermally marginally mature in the Vulcan Sub-basin, but where burial is sufficient to attain higher maturity, as for example, in the Nancar Trough – they have the potential to provide additional sources for marine oils. The $\delta^{13}$C of individual light hydrocarbons and their derived GORs indicate that the natural gases and oils in the Vulcan Sub-basin cannot be derived from a single source. Ignoring the effects of alteration processes, the oils reservoired in the Vulcan Sub-basin were generated at variable stages of thermal maturity with respect to the oil window. Results from the current study suggest that the lower Vulcan Formation coal sample has the potential to generate high wax PNA oils, whereas the Plover Formation coals have the potential to generate either gas/condensates or PNA oils with high wax content and low GORs.

## 4.8. Acknowledgments

## 4.9. References

Abbassi, S., George, S.C., Edwards, D.S., di Primio, R., Horsfield, B., Volk, H., 2014a. Generation characteristics of Mesozoic syn- and post-rift source rocks, Bonaparte Basin, Australia: New insights from compositional kinetic modelling. Marine and Petroleum Geology 50, 148-165.

Batten, D., 1982. Palynofacies, palaeoenvironments and petroleum. Journal of Micropalaeontology 1, 107-114.

Baxter, K., Hill, K., Cooper, G., 1998. Quantitative modelling of the Jurassic-Holocene subsidence history of the Vulcan Sub-basin, North West Shelf: Constraints on lithosphere evolution during continental breakup. Australian Journal of Earth Sciences 45, 143-154.

Baxter, K., Cooper, G., Hill, K., O'Brien, G., 1999. Late Jurassic subsidence and passive margin evolution in the Vulcan Sub-basin, north-west Australia: constraints from basin modelling. Basin Research 11, 97-111.

Baxter, K., Cooper, G.T., O'Brien, G.W., Hill, K.C., Sturrock, S., 1997. Flexural isostatic modelling as a constraint on basin evolution, the development of sediment systems and palaeo-heat flow: application to the Vulcan Sub-basin, Timor Sea. Australian Petroleum Production and Exploration Association Journal 37, 136-153.

Behar, F., Ungerer, P., Kressmann, S., Rudkiewicz, J., L., 1991. Evolution thermique des huiles dans les bassins sédimentaires : simulation expérimentale par pyrolyse en milieu confiné et modélisation cinétique. Oil & Gas Science and Technology - Rev. IFP 46, 151-181.

Benson, J., Brealey, S., Luxton, C., Walshe, P., Tupper, N., 2004. Late Cretaceous ponded turbidite systems: A new stratigraphic play fairway in the Browse Basin. Australian Petroleum Production and Exploration Association Journal 44, 269-285.

Bjorøy, M., Hall, P.B., Hustad, E., Williams, J.A., 1992. Variation in stable carbon isotope ratios of individual hydrocarbons as a function of artificial maturity. Organic Geochemistry 19, 89-105.

Boreham, C.J., Hope, J.M., Hartung-Kagi, B., 2001. Understanding source, distribution and preservation of Australian natural gas: a geochemical perspective. Australian Petroleum Production and Exploration Association Journal 41, 523-547.

Bourdet, J., Eadington, P., Volk, H., George, S.C., Pironon, J., Kempton, R., 2012. Chemical changes of fluid inclusion oil trapped during the evolution of an oil reservoir: Jabiru-1A case study (Timor Sea, Australia). Marine and Petroleum Geology 36, 118-139.

Brincat, M., O'Brien, G., Lisk, M., De Ruig, M., George, S., 2001. Hydrocarbon charge history of the northern Londonderry: Implications for trap integrity and future prospectivity. Australian Petroleum Production and Exploration Association Journal 41(1), 483-496.

Burnham, A.K., Braun, R.L., Gregg, H.R., Samoun, A.M., 1987. Comparison of methods for measuring kerogen pyrolysis rates and fitting kinetic parameters. Energy & Fuels 1, 452-458.

Burnham, A.K., Braun, R.L., Samoun, A.M., 1988. Further comparison of methods for measuring kerogen pyrolysis rates and fitting kinetic parameters. Organic Geochemistry 13, 839-845.

Chen, G., Hill, K.C., Hoffman, N., O'Brien, G.W., 2002. Geodynamic evolution of the Vulcan Sub-basin, Timor Sea, northwest Australia: a pre-compression New Guinea analogue? Australian Journal of Earth Sciences 49, 719-736.

Clayton, C., 1991. Carbon isotope fractionation during natural gas generation from kerogen. Marine and Petroleum Geology 8, 232-240.

Craig, H., 1957. Isotopic standards for carbon and oxygen and correction factors for mass-spectrometric analysis of carbon dioxide. Geochimica et Cosmochimica Acta 12, 133-149.

Cramer, B., 2004. Methane generation from coal during open system pyrolysis investigated by isotope specific, Gaussian distributed reaction kinetics. Organic Geochemistry 35, 379-392.

Dawson, D., Grice, K., Alexander, R., Edwards, D., 2007. The effect of source and maturity on the stable isotopic compositions of individual hydrocarbons in sediments and crude oils from the Vulcan Sub-basin, Timor Sea, Northern Australia. Organic Geochemistry 38, 1015-1038.

De Boer, R., 2004. The Puffin Sandstone, Timor Sea, Australia: anatomy of a sub-marine fan, in: Ellis, G.K., Baillie, P.W., Munson, T.J. (Eds.), Timor Sea Petroleum Geoscience: Proceedings of the Timor Sea Symposium, Darwin, Northern Territory, pp. 373-390.

Degens, E.T., 1989. Perspectives on Biogeochemistry. Springer-Verlag GmbH & Co. KG, D-100 Berlin 33.

di Primio, R., 2002. Unraveling secondary migration effects through the regional evaluation of PVT data: a case study from Quadrant 25, NOCS. Organic Geochemistry 33, 643-653.

di Primio, R., Horsfield, B., 2006. From petroleum-type organofacies to hydrocarbon phase prediction. American Association of Petroleum Geologists Bulletin 90, 1031-1058.

Dodsworth, P., 2004. The palynology of the Cenomanian-Turonian (Cretaceous) boundary succession at Aksudere in Crimea, Ukraine. Palynology 28, 129-141.

Edwards, D.S., Zumberge, J.E., 2005. The Oils of Western Australia II. Regional Petroleum Geochemistry and Correlation of Crude Oils and Condensates from Western Australia and Papua New Guinea. Geoscience Australia and GeoMark Research Ltd unpublished report, Canberra and Houston. GEOCAT 37512.

Edwards, D.S., Summons, R.E., Kennard, J., Nicoll, R., Bradshaw, J., Bradshaw, M., Foster, C., O'Brien, G., Zumberge, J., 1997. Geochemical characterisation of Palaeozoic petroleum systems in north-western Australia. Australian Petroleum Production and Exploration Association Journal 37(1), 351-379.

Edwards, D.S., Preston, J.C., Kennard, J.M., Boreham, C.J., van Aarssen, B.G.K., Summons, R.E., Zumberge, J.E., 2004. Geochemical characteristics of hydrocarbons from the Vulcan Sub-basin, western Bonaparte Basin, Australia, in: Ellis, G.K., Baillie, P.W., Munson, T.J. (Eds.), Timor Sea Petroleum Geoscience: Proceedings of the Timor Sea Symposium, Darwin, Northern Territory, pp. 169-201.

Espitalié, J., 1986. Use of Tmax as a maturation index for different types of organic matter. Comparison with vitrinite reflectance. Thermal modeling in sedimentary basins: Paris, Editions Technip, pp. 475-496.

Espitalié, J., Laporte, J.L., Madec, M., Marquis, F., Leplat, P., Paulet, J., Boutefeu, A., 1977. Méthode rapide de caractérisation des roches mères, de leur potentiel pétrolier et de leur degré d'évolution. Revue Institut Francais du Petrole 32, pp. 23-42.

Faiz, M., Sherwood, N., Wilkins, R., Russell, N., Buckingham, C., 2000. Applications of microprobe techniques for improved source rock evaluation, Timor Sea region, Australia, Abstracts and Program: 17th Annual Meeting of the Society for Organic Petrology, Bloomington, Indiana, pp. 103-105.

Fujii, T., O'Brien, G., Tingate, P., Chen, G., 2004. Using 2D and 3D basin modelling to investigate controls on hydrocarbon migration and accumulation in the Vulcan Sub-basin, Timor Sea, Northwestern Australia. Australian Petroleum Production and Exploration Association Journal 44(1), 93-122.

Galimov, E., 2006. Isotope organic geochemistry. Organic Geochemistry 37, 1200-1262.

Gartrell, A., Lisk, M., 2005. Potential new method for paleostress estimation by combining by combining 3D fault restoration and fault slip inversion techniques: First test on the Skua field, Timor Sea, in: Boult, P., Kaldi, J.K. (Eds.), Evaluating fault and cap rock seals. AAPG Hedberg Series, no. 2, pp. 23-36.

Gartrell, A., Zhang, Y., Lisk, M., Dewhurst, D., 2003. Enhanced hydrocarbon leakage at fault intersections: an example from the Timor Sea, Northwest Shelf, Australia. Journal of Geochemical Exploration 78–79, 361-365.

George, S.C., Greenwood, P.F., Logan, G.A., Quezada, R.A., Pang, L.S.K., Lisk, M., Krieger, F.W., Eadington, P., 1997. Comparison of palaeo oil charges with currently reservoired hydrocarbons using molecular and isotopic analyses of oil-bearing fluid inclusions: Jabiru oil field, Timor Sea. Australian Petroleum Production and Exploration Association Journal 37(1), 490-504.

George, S.C., Lisk, M., Eadington, P., Quezada, R., 1998. Geochemistry of a palaeo-oil column: Octavius 2, Vulcan Sub-basin, in: Purcell, P.G., Purcell, R.R. (Eds.), The Sedimentary Basins of Western Australia 2: Proceedings of the West Australian Basins Symposium, Perth, Western Australia, pp. 195-210.

George, S.C., Ahmed, M., Liu, K., Volk, H., 2004a. The analysis of oil trapped during secondary migration. Organic Geochemistry 35, 1489-1511.

George, S.C., Ruble, T.E., Volk, H., Lisk, M., Brincat, M.P., Dutkiewicz, A., Ahmed, M., 2004b. Comparing the geochemical composition of fluid inclusion and crude oils from wells on the Laminaria High, Timor Sea, in: Ellis, G.K., Baillie, P.W., Munson, T.J. (Eds.), Timor Sea Petroleum Geoscience: Proceedings of the Timor Sea Symposium, Darwin, Northern Territory Geological Survey, Special Publication 1, pp. 203–230.

Gradstein, F.M., Ogg, J.G., Schmitz, M., 2012. The Geologic Time Scale 2012; Volumes 1 and 2. Elsevier BV, 1144 p.

Haq, B.U., Hardenbol, J., Vail, P.R., 1987. Chronology of fluctuating sea levels since the Triassic. Science 235, 1156-1167.

Horsfield, B., 1989. Practical criteria for classifying kerogens: some observations from pyrolysis-gas chromatography. Geochimica et Cosmochimica Acta 53, 891-901.

Horsfield, B., 1997. The bulk composition of first-formed petroleum in source rocks, in: Welte, D., Horsfield, B., Baker, D. (Eds.), Petroleum and basin evolution. Springer Verlag, Berlin, Heidelberg, pp. 335-402.

Horsfield, B., Dueppenbecker, S.J., 1991. The decomposition of Posidonia Shale and Green River Shale kerogens using microscale sealed vessel (MSSV) pyrolysis. Journal of Analytical and Applied Pyrolysis 20, 107-123.

James, A.T., 1983. Correlation of natural gas by use of carbon isotopic distribution between hydrocarbon components. American Association of Petroleum Geologists Bulletin 67, 1176-1191.

Kaiko, A., Tingate, P., 1996. Suppressed vitrinite reflectance and its effect on thermal history modelling in the Barrow and Dampier Sub-Basins. Australian Petroleum Production and Exploration Association Journal 36(1), 428-444.

Kelman, A.P., Edwards, D.S., Kennard, J.M., Laurie, J.R., Lepoidevin, S., Lewis, B., Mantle, D.J., Nicoll, R.S., 2014. Bonaparte Basin Biozonation and Stratigraphy, Chart 34, Geoscience Australia. GEOCAT 76687.

Kennard, J.M., Deighton, I., Edwards, D.S., Colwell, J.B., O'Brien, G.W., Boreham, C.J., 1999. Thermal history modelling and transient heat pulses: new insights into hydrocarbon expulsion and 'hot flushes' in the Vulcan Sub-basin, Timor Sea. Australian Petroleum Production and Exploration Association Journal 39(1), 177-207.

Kivior, T., Kaldi, J.G., Lang, S.C., 2002. Seal potential in Cretaceous and Late Jurassic rocks of the Vulcan Sub-basin, North West Shelf Australia. Australian Petroleum Production and Exploration Association Journal 42(1), 203-224.

Labutis, V.R., Ruddock, A.D., Calcraft, A.P., 1998. Stratigraphy of the southern Sahul Platform. Australian Petroleum Production and Exploration Association Journal 38(1), 115-136.

Langford, F., Blanc-Valleron, M.-M., 1990. Interpreting Rock-Eval Pyrolysis Data Using Graphs of Pyrolizable Hydrocarbons vs. Total Organic Carbon. American Association of Petroleum Geologists Bulletin 74, 799-804.

Larter, S.R., 1984. Application of analytical pyrolysis techniques to kerogen characterization and fossil fuel exploration/exploitation, in: Voorhees, K.J. (Ed.), Analytical Pyrolysis: Methods and application, Butterworth, London, pp. 212-275.

Larter, S.R., Senftle, J.T., 1985. Improved kerogen typing for petroleum source rock analysis. Nature 318, 277-280.

Lindner, A., 1984. Oil and gas developments in Australia in 1983. American Association of Petroleum Geologists Bulletin 68, 1600-1616.

Lisk, M., 2012. Fluid migration and hydrocarbon charge history of the Vulcan Sub-basin. PhD thesis, Department of Applied Geology. Curtin University. Doctor of Philosophy, 734 p.

Lisk, M., Eadington, P., 1994. Oil migration in the Cartier Trough, Vulcan Sub-basin, in: Purcell, P.G., Purcell, R.R. (Eds.), The Sedimentary Basins of Western Australia: Proceedings of the Petroleum Exploration Society of Australia, Perth, Western Australia, pp. 301-312.

Lisk, M., Brincat, M.P., Eadington, P.J., O'Brien, G.W., 1998. Hydrocarbon charge in the Vulcan Sub-basin, in: Purcell, P.G., Purcell, R.R. (Eds.), The Sedimentary Basins of Western Australia 2: Proceedings of the West Australian Basins Symposium, Perth, Western Australia, pp. 287-305.

Lisk, M., O'Brien., G.W., Eadington, P.J., 2002. Quantitative evaluation of the oil-leg potential in the Oliver gas field, Timor Sea, Australia. American Association of Petroleum Geologists Bulletin 86, 1531-1542.

Longley, I.M., Buessenschuett, C., Clydsdale, L., Cubitt, C.J., Davis, R.C., Johnson, M.K., Marshall, N.M., Murray, A.P., Somerville, R., Spry, T.B., Thompson, N., 2002. The North West Shelf of Australia: a Woodside perspective, in: Keep, M., Moss, S. (Eds.), The Sedimentary Basins of Western Australia 3: Proceedings of Petroleum Exploration Society of Australia Symposium, Perth, Western Australia, pp. 27-88.

Lorant, F., Prinzhofer, A., Behar, F., Huc, A.-Y., 1998. Carbon isotopic and molecular constraints on the formation and the expulsion of thermogenic hydrocarbon gases. Chemical Geology 147, 249-264.

MacDaniel, R., 1988a. Jabiru oilfield, in: Purcell, P.G., Purcell, R.R. (Eds.), The North West Shelf, Australia: Proceedings of the Petroleum Exploration Society of Australia Symposium, Perth, Western Australia, pp. 439-440.

MacDaniel, R.P., 1988b. The geological evolution and hydrocarbon potential of the western Timor Sea region. Petroleum in Australia: The First Century. Australian Petroleum Exploration Association Journal 28, 270-284.

Mihut, D., Müller, R., 1998. Revised sea-floor spreading history of the Argo Abyssal Plain, in: Purcell, P.G., Purcell, R.R. (Eds.), The Sedimentary Basins of Western Australia 2: Proceedings of the West Australian Basins Symposium, Perth, Western Australia, pp. 73-80.

Mory, A.J., 1988. Regional geology of the offshore Bonaparte Basin, The North West Shelf, Australia: Proceedings of the Petroleum Exploration Society of Australia Symposium, Perth, Western Australia, pp. 287-309.

Neumann, V., di Primio, R., Horsfield, B., 2009. Source rock distributions and petroleum fluid bulk compositional predictions on the Vulcan Sub-basin, offshore Western Australia: Report for Geoscience Australia 67, 64 p.

O'Brien, G.W., 1993. Some ideas on the rifting history of the Timor Sea from the integration of deep crustal seismic and other data. Petroleum Exploration Society of Australia Journal 21, 95-113.

O'Brien, G.W., Woods, E.P., 1995. Hydrocarbon-related diagenetic zones (HRDZs) in the Vulcan Sub-basin, Timor Sea: recognition and exploration implications. Australian Petroleum Production and Exploration Association Journal 35, 220-220.

O'Brien, G.W., Lisk, M., Duddy, I., Eadington, P., Cadman, S., Fellows, M., 1996. Late Tertiary fluid migration in the Timor Sea: a key control on thermal and diagenetic histories. Australian Petroleum Production and Exploration Association Journal 36(1), 399-427.

O'Brien, G.W., Quaife, P., Cowley, R., Morse, M., Wilson, D., Fellows, M., Lisk, M., 1998. Evaluating trap integrity in the Vulcan sub-basin, Timor Sea, Australia, using integrated remote-sensing geochemical technologies, in: Purcell, P.G., Purcell, R.R. (Eds.), The Sedimentary Basins of Western Australia 2: Proceedings of Petroleum Exploration Society of Australia Symposium, Perth, Western Australia, pp. 237-254.

O'Brien, G.W., Lisk, M., Duddy, I.R., Hamilton, J., Woods, P., Cowley, R., 1999. Plate convergence, foreland development and fault reactivation: primary controls on brine migration, thermal histories and trap breach in the Timor Sea, Australia. Marine and Petroleum Geology 16, 533-560.

Osborne, M., 1990. The exploration and appraisal history of the Skua field AC/P2-Timor Sea. Australian Petroleum Exploration Association Journal 30, 197-201.

Pattillo, J., Nicholls, P.J., 1990. A tectonostratigraphic framework for the Vulcan Graben, Timor Sea region. Australian Petroleum Exploration Association Journal 30(1), 27-51.

Peters, K.E., Cassa, M.R., 1994. Applied source-rock geochemistry. In: Magoon, L.B., Dow, W.G. (Eds.), The Petroleum System—From Source to Trap. American Association of Petroleum Geologists Bulletin 60, 93-120.

PTTEP-Australasia, 2013. [Web page] PTTEP News. http://www.au.pttep.com/news/2013/june/oil-production-begins-from-pttep-aa's-montara-field.

Purcell, P.G., Purcell, R.R., 1988. The North West Shelf, Australia - An introduction, in: Purcell, P.G., Purcell, R.R. (Eds.), The North West Shelf, Australia: Proceedings of the Petroleum Exploration Society of Australia Symposium, Perth, Western Australia, pp. 3-15.

Reynolds, J.G., Burnham, A.K., 1995. Comparison of kinetic analysis of source rocks and kerogen concentrates. Organic Geochemistry 23, 11-19.

Schaefer, R.G., Schenk, H.J., Hardelauf, H., Harms, R., 1990. Determination of gross kinetic parameters for petroleum formation from Jurassic source rocks of different maturity levels by means of laboratory experiments. Organic Geochemistry 16, 115-120.

Schenk, H.J., Dieckmann, V., 2004. Prediction of petroleum formation: the influence of laboratory heating rates on kinetic parameters and geological extrapolations. Marine and Petroleum Geology 21, 79-95.

Schenk, H.J., Horsfield, B., Krooss, B., Schaefer, R.G., Schwochau, K., 1997. Kinetics of petroleum formation and cracking. In: Welte, D.H., Horsfield, B., Baker, D.R. (Eds.), Petroleum and Basin Evolution. Springer, Verlag, Berlin, Heidelberg, pp. 231-269.

Schoell, M., 1980. The hydrogen and carbon isotopic composition of methane from natural gases of various origins. Geochimica et Cosmochimica Acta 44, 649-661.

Scott, J., Hartung-Kagi, B., 1998. Oil families and effective source rocks of Western Australia. Petroleum Exploration Society of Australia Journal 26, 22-36.

Shuster, M.W., Eaton, S., Wakefield, L.L., Kloosterman, H.J., 1998. Neogene tectonics, greater Timor Sea, offshore Australia: implications for trap risk. Australian Petroleum Production and Exploration Association Journal 38(1), 351-379.

Summons, R.E., Bradshaw, M., Crowley, J., Edwards, D.S., George, S.C., Zumberge, J.E., 1998. Vagrant oils: geochemical signposts to unrecognised petroleum systems, in: Purcell, P.G., Purcell, R.R. (Eds.), The Sedimentary Basins of Western Australia 2: Proceedings of the West Australian Basins Symposium, Perth, Western Australia, pp. 169-184.

Tang, Y., Jenden, P., Nigrini, A., Teerman, S., 1996. Modeling early methane generation in coal. Energy & Fuels 10, 659-671.

Tang, Y., Perry, J., Jenden, P., Schoell, M., 2000. Mathematical modeling of stable carbon isotope ratios in natural gases. Geochimica et Cosmochimica Acta 64, 2673-2687.

Tappan, H.N., 1980. The paleobiology of plant protists. W.H. Freeman San Francisco.

Tarafa, M.E., Hunt, J.M., Ericsson, I., 1983. Effect of hydrocarbon volatility and adsorption on source-rock pyrolysis. Journal of Geochemical Exploration 18, 75-85.

Tegelaar, E.W., Noble, R.A., 1994. Kinetics of hydrocarbon generation as a function of the molecular structure of kerogen as revealed by pyrolysis-gas chromatography. Organic Geochemistry 22, 543-574.

Tian, H., Xiao, X., Wilkins, R.W., Gan, H., Guo, L., Yang, L., 2010. Genetic origins of marine gases in the Tazhong area of the Tarim basin, NW China: Implications from the pyrolysis of marine kerogens and crude oil. International journal of coal geology 82, 17-26.

Tissot, B.P., Welte, D.H., 1984. Petroleum Formation and Occurrence. Springer Verlag, Berlin, 699 p.

van de Meent, D., Brown, S.C., Philp, R.P., Simoneit, B.R.T., 1980. Pyrolysis-high resolution gas chromatography and pyrolysis gas chromatography-mass spectrometry of kerogens and kerogen precursors. Geochimica et Cosmochimica Acta 44, 999-1013.

Whibley, M., Jacobson, T., 1990. Exploration in the northern Bonaparte Basin. Timor Sea-WA-199-P. Australian Petroleum Exploration Association Journal 30(1), 7-25.

Whiticar, M.J., 1999. Carbon and hydrogen isotope systematics of bacterial formation and oxidation of methane. Chemical Geology 161, 291-314.

Wilkins, R.W.T., Wilmshurst, J.R., Russell, N.J., Hladky, G., Ellacott, M.V., Buckingham, C., 1992. Fluorescence alteration and the suppression of vitrinite reflectance. Organic Geochemistry 18, 629-640.

Woods, E., 1992. Vulcan Sub-basin fault styles-implications for hydrocarbon migration and entrapment. Australian Petroleum Exploration Association Journal 32(1), 138-138.

Woods, E., 2004. Twenty years of Vulcan Sub-basin exploration since Jabiru-what lessons have been learnt?, in: Ellis, G.K., Baillie, P.W., Munson, T.J. (Eds.), Timor Sea Petroleum Geoscience: Proceedings of the Timor Sea Symposium, Darwin, Northern Territory, pp. 83-97.

# Chapter 5.

**Generation characteristics of Mesozoic syn- and post-rift source rocks, Bonaparte Basin, Australia: new insights from compositional kinetic modelling**

Soumaya Abbassi[1], Brian Horsfield[2], Simon C. George[1], Dianne S. Edwards[3], Herbert Volk[4], Rolando di Primio[2]

1. Department of Earth and Planetary Sciences, Macquarie University, Sydney, NSW 2109, Australia

2. Geoscience Australia, GPO Box 378, Canberra, ACT 2601, Australia

3. Helmholtz Centre Potsdam, GFZ - German Research Centre for Geosciences, Germany

4. CSIRO, Australia. Present Address: BP Exploration Company, Sunbury-on-Thames, UK

*Corresponding author:* _soumaya.abbassi@gmail.com, soumaya.abbassi@students.mq.edu.au_

## *Statement of authors' contribution*

This Chapter is a published article in *Marine and Petroleum Geology*. This paper has been formatted to conform to the font and referencing style adopted in this thesis. Figures and tables included within the text are prefixed with the chapter number.

I am the primary author. I examined data and prepared the samples used in this study, including sample selection, sampling, grinding and solvent extraction. I performed open-system pyrolysis-gas chromatography and compositional kinetic measurements. Rock-Eval pyrolysis data acquired for all samples was performed by Geoscience Australia, excluding sample preparation. Rock-Eval pyrolysis data acquired for solvent-extracted samples (excluding solvent extraction) was performed by Applied Petroleum Technology AS (Norway). Bulk kinetic and carbon isotope measurements (excluding sample preparation) were performed by Ferdinand Perssen and Michael Gabriel (GFZ, Potsdam), respectively. I processed and interpreted all the data derived from all the conducted measurements which are related to the paper. I wrote and designed the paper's structure. All co-authors carefully reviewed and provided feedbacks and various refinements on the final version of the manuscript, and approved it for submission and publication. Neither this manuscript nor one with similar content under our authorship has been published or is being considered for publication elsewhere, except as described above.

**Abstract**

Potential source rocks on the Laminaria High, a region of the northern Bonaparte Basin on the North West Shelf of Australia, occur within the Middle Jurassic to Lower Cretaceous early to post-rift sequences. Twenty-two representative immature source rock samples from the Jurassic to Lower Cretaceous (Plover, Laminaria, Frigate, Flamingo and Echuca Shoals) sequences were analysed to define the hydrocarbon products that analogous mature source rocks could have generated during thermal maturation and filled the petroleum reservoirs in the Laminaria High region. Rock-Eval pyrolysis data indicate that all the source rocks contain Type II–III organic matter and vary in organic richness and quality. Open-system pyrolysis-gas chromatography on extracted rock samples show a dominance of aliphatic components in the pyrolysates. The Plover source rocks are the exception which exhibit high phenolic contents due to their predominant land-plant contribution. Most of the kerogens have the potential to generate Paraffinic−Naphthenic−Aromatic oils with low wax contents. Bulk kinetic analyses reveal a relatively broad distribution of activation energies that are directly related to the heterogeneity in the kerogens. These kinetic parameters suggest different degrees of thermal stability, with the predicted commencement of petroleum generation under geological heating conditions covering a relatively broad temperature range from 95-135°C for the Upper Jurassic−Lower Cretaceous source rocks. Both shales and coals of the Middle Jurassic Plover Formation have the potential to generate oil at relatively higher temperatures (140-145 $^{0}$C) than those measured for crude oils in previous studies. Hence, the Frigate and Flamingo formations are the main potential sources of oils reservoired in the Laminaria and Corallina fields. Apart from being a reservoir, the Laminaria Formation also contains organic-rich shales with the potential to generate oil. For the majority of samples analysed, the compositional kinetic model predictions indicate that 80% of the hydrocarbons were generated as oil and 20% as gas. The exception is the Lower Cretaceous Echuca Shoals Formation which shows the potential to generate a greater proportion (40%) of gas despite its marine source affinity, due to inertinite dominating the maceral assemblage.

172

## 5.1.    Introduction

The Laminaria High is a Mesozoic to Cenozoic east–west-trending platform in the northern Bonaparte Basin (Smith et al., 1996) which comprises the northernmost basin of the North West Shelf of Australia **(Figure 5.1)**. This high is bordered by the Flamingo Syncline to the northeast and the Nancar Trough and Sahul Syncline to the south. The Laminaria High hosts the Laminaria and Corallina oil accumulations, the most significant oil fields in the Bonaparte Basin, from which production commenced in 1999 via a Floating Production, Storage and Offloading (FPSO) facility. Also located within the northern Bonaparte Basin is the Bayu-Undan gas field, which is piped to LNG facilities in Darwin, as well as many smaller oil and gas accumulations. Mature Jurassic to Lower Cretaceous organic-rich rocks within the Nancar Trough and Sahul and Flamingo synclines are considered to be the source of these accumulations (Edwards et al., 1997, 2004; George et al., 1997, 2004b; Preston and Edwards, 2000). To explain the absence of gas within the Laminaria and Corallina oil fields, some authors (e.g. Castillo et al., 1998; Cooper et al., 1998; Hillis, 1998; Shuster et al., 1998; de Ruig et al., 2000; George et al., 2004b) suspect that the gas may have preferentially escaped from the traps, although there is no indication that wet gas was ever present in the Laminaria High. The Laminaria High has been subjected to an extensive drilling history, yet oil-source rock correlations are not well understood. This is because well penetrations are biased towards reservoir characterisation, its structural history is complex, and multiple source rocks occur in several nearby depocentres, such as the Nancar Trough and the Sahul and Flamingo synclines, located to the south and southeast of the Laminaria High, respectively. Hence, there is uncertainty regarding the proportion of oil and gas generated by the source rocks, the timing of expulsion, and the migration pathways taken from the source kitchen(s) to the accumulations.

Previous studies have concentrated on the characterisation of the oils from the Laminaria and Flamingo highs and their differentiation into groups according to their isotopic and biomarker compositions. Edwards et al. (2004) determined that oils produced from both the northern Bonaparte Basin and the Vulcan Sub-basin are similar, being, sourced by Jurassic marine mudstones that contain variable amounts of terrigenous organic matter. George et al. (2002; 2004b) conducted a series of studies on fluid inclusions collected from reservoirs within the northern Bonaparte Basin and showed that they had similar geochemical properties to the oils on the Laminaria High. One exception is the Ludmilla-1 fluid inclusion oil which has an unusually high abundance of mid-chain substituted monomethylalkanes and believed to have been generated from a highly mature source rock found within the Nancar

Trough which is located to the south of the Laminaria High (George et al., 2002). Another group of oils (e.g. Elang West-1, Kakatua North-1) reservoired in the Lower Cretaceous Darwin Formation have been shown to correlate with sediment extracts from the Lower Cretaceous Echuca Shoals Formation (Preston and Edwards, 2000). In addition, gas at Firebird-1, located on the flank of the Bayu-Undan gas field, is reported to originate from organic-rich marine sediments in the Lower Cretaceous Echuca Shoals Formation in the Sahul Syncline (ConocoPhillips, 2008). At the nearby Bayu-Undan gas condensate field, oil-bearing fluid inclusions trapped prior to gas charge provide further evidence for an-oil-prone marine rock which is most likely sourced from the Upper Jurassic–Lower Cretaceous Flamingo Formation (George et al., 2004a).

This study aims at improving our understanding of the geochemical characteristics of potential source rocks to better define hydrocarbon types that might be generated and expelled in the northern Bonaparte Basin. This study documents the bulk, carbon isotopic and compositional analyses on cuttings samples from five wells on the Laminaria High and additional samples from the Vulcan Sub-basin. Implications for petroleum systems active in the region, and their contribution to the filling of structures within the Laminaria High are discussed.

## 5.2. Geological background

### 5.2.1. Tectonic setting

The geological history of the Laminaria High provides tectonic context for understanding petroleum systems in the region. The Laminaria High was initially subjected to extension in the Middle Jurassic (late Callovian), when Gondwana rifted from the Australian Plate and the opening of the Argo Abyssal Plain commenced (AGSO, 1994; Baillie et al., 1994; Müller et al., 1998; Borel and Stampfli, 2002). This extensional episode was typified by the NE−SW structural trend that is reflected in the present day geometry of the North West Shelf (Longley et al., 2002).

The syn-rift phase (ending with the break-up of Gondwana) was associated with the development of accommodation space and uplift in the Callovian, as a response to flexure driven by sea-floor spreading (Chen et al., 2002; Harrowfield and Keep, 2005). Following this uplift, an erosive phase took place which led to an unconformity at the base of the Valanginian, marking the limit between the syn-rift and post-rift sequences. On the Laminaria High, this rifting was accompanied by the generation of an E−W-trending horst and graben system (de Ruig et al., 2000) due to the pre-existing structures related to

Paleozoic rifting episodes (O'Brien, 1993; Baillie et al., 1994; Langhi and Borel, 2005). The extensional regime lasted into the Early Cretaceous. During the mid-Cretaceous, the area experienced a period of tectonic waning and underwent post-rift thermal subsidence (de Ruig et al., 2000). This subsidence continued into the Cenozoic, leading to the deposition of a thick prograding carbonate shelf (Whittam et al., 1996; McIntyre and Stickland, 1998).
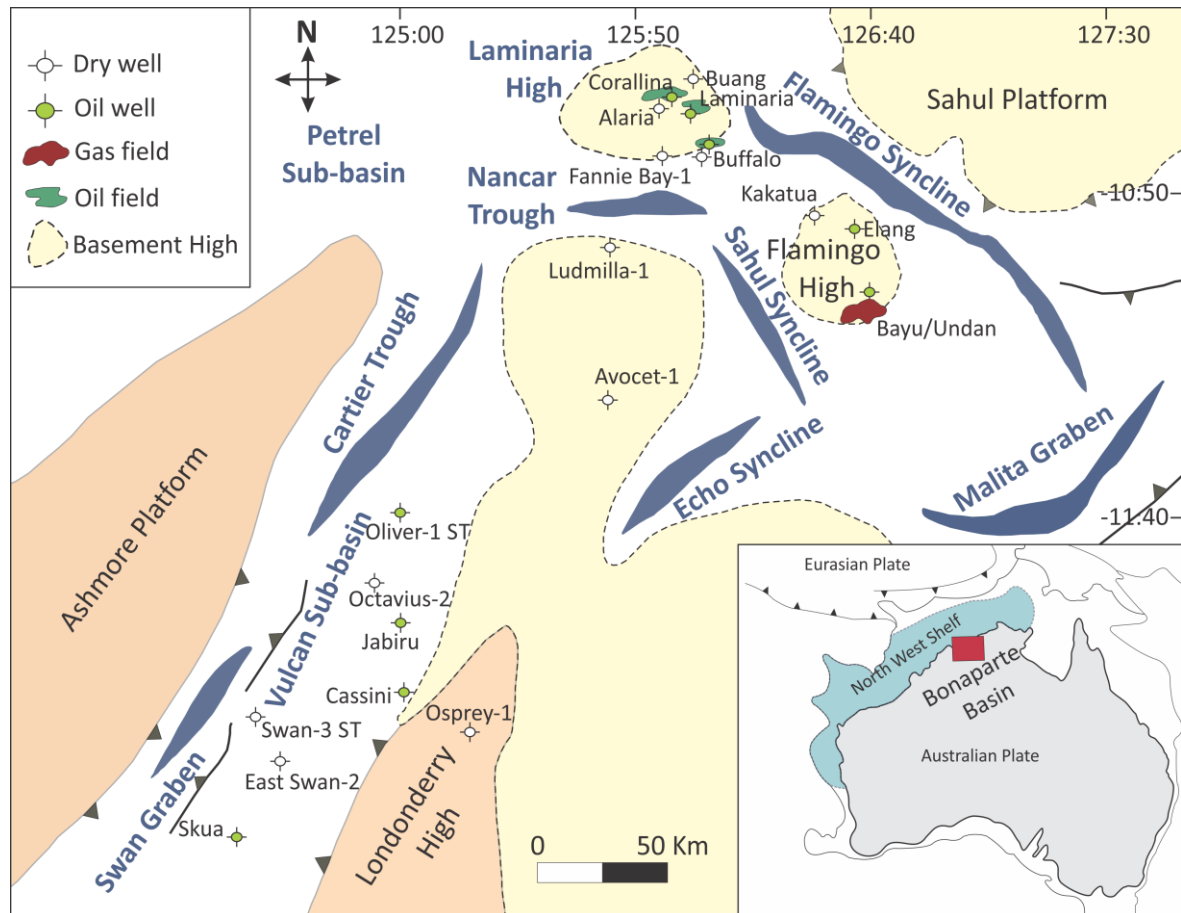


**Figure 5.1. Regional map showing the location of the Laminaria High and wells in the northern Bonaparte Basin.**

During the latest Cenozoic, the geological evolution of the Laminaria High was strongly controlled by the oblique collision of the Australian continental plate and the Southeast Asian micro plates (O'Brien, 1993). This tectonic event initiated in the late Miocene (Woods, 1994; Shuster et al., 1998) with a north−north−west extensional regime (Gartrell and Lisk, 2005; Gartrell et al., 2006). As a response to this extension, the inherited configuration prevailing during Mesozoic times was reactivated. The maximum of fault growth was recorded during the late Pliocene (Langhi et al., 2011), when a series of new shallow Miocene−Pliocene transtensional faults (O'Brien et al., 1999) was produced. Later, from the late Pleistocene to the present-day, fault activity decreased. Details of the mechanisms leading to the reactivation of the Mesozoic faults and formation of the Neogene fault system

can be found elsewhere (O'Brien et al., 1998; Shuster et al., 1998; O'Brien et al., 1999; de Ruig et al., 2000; Londoño and Lorenzo, 2004; Harrowfield and Keep, 2005; Keep et al., 2007; Langhi et al., 2011).

### 5.2.2. Stratigraphy and depositional setting

The Laminaria High formed as part of the Bonaparte Basin rift system in the Late Jurassic (de Ruig et al., 2000) across an uplifted and eroded Paleozoic−Triassic sequence which constitutes the basement (Smith et al., 1996). The subsequent Mesozoic sequence has been affected in part by the palaeo-topography of this basement.

The pre-rift to early syn-rift phase is represented by the Sinemurian−Bathonian Plover Formation, which consists mainly of sandstones, with minor claystones and interbedded shales and coals. These siliciclastic sediments were deposited in a fluvial-deltaic to marginal marine environment (Labutis et al., 1998). The top part of this sequence has been partly removed by uplift and erosion at the Callovian unconformity (JC marker: **Figure 5.2**). Subsequent shoreface to shallow marine sandstones of the Laminaria Formation (early Callovian−Oxfordian) were deposited in a deltaic setting with low average rates of subsidence and sedimentation. The top of this formation is a regional unconformity (JO) reflecting the onset of the syn-rift phase. Following this extensional phase which continued until the early Valanginian, sandstone sedimentation ceased and the Laminaria Formation was overlain by thick marine claystones of the Oxfordian−Kimmeridgian Frigate Formation (Gorter and Kirk, 1995). The lower Tithonian sediments, which have been described in more proximal areas, such as the Vulcan Sub-basin, are not present in the Laminaria High. These sediments record the onset of substantial extension and growth faulting (Woods, 1992; Baxter et al., 1999). This hiatus is mapped as the JT unconformity (Pattillo and Nicholls, 1990; Gorter and Kirk, 1995) which occurs at the base of the marine shales of the Tithonian−Berriasian Flamingo Formation.

The shales of the Flamingo Formation grade vertically into those of the Echuca Shoals Formation. The Echuca Shoals Formation comprises a condensed sequence of glauconitic claystones, representing deep-water shelf sedimentation which was starved of coarse-grained clastic sediments from the mid-Valanginian to the end of the Barremian. The influence of the rifting ceased during the Valanginian upon break-up of the northwest margin of Australia, and commencement of a passive margin setting. This transition is recorded as a short time hiatus termed the Intra-Valanginian horizon (KV) (Longley et al., 2002).
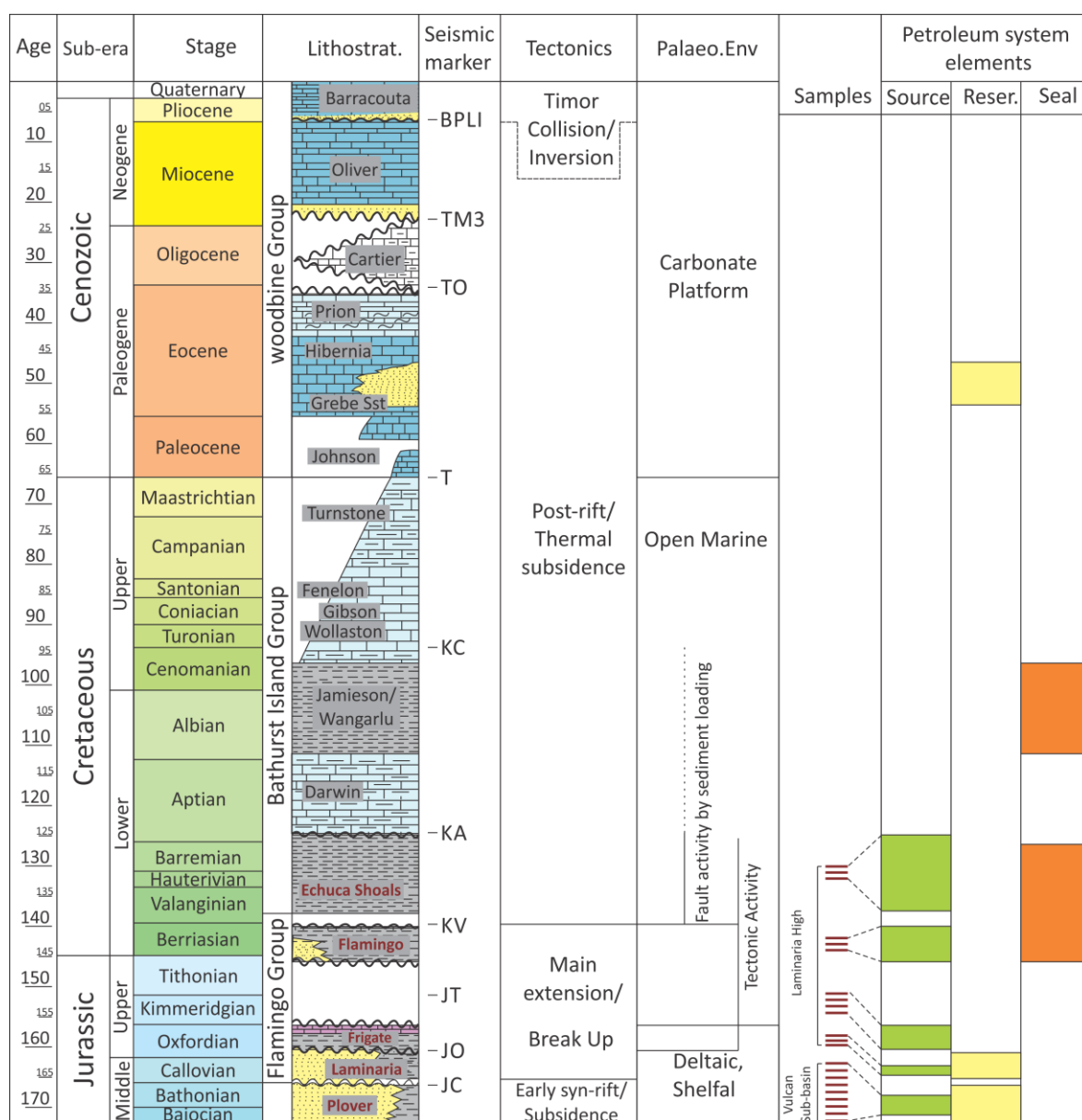
**Figure 5.2. Lithostratigraphic chart of the Laminaria High, showing the main tectonic events and the potential source rock units (after de Ruig et al. (2000). Formations that were analysed are written in red.**

KA is a major Aptian unconformity, occurring in the early post-rift phase at the commencement of the Upper Cretaceous to Cenozoic thermal subsidence dominated passive margin phase. This phase was followed by a significant seal level rise and cessation of thermal subsidence. Longley et al. (2002) suggested that the KA event marks the change from restricted to open marine conditions associated with the rifting of India from Antarctica. The Echuca Shoals Formation passes upwards into the Darwin Formation (Aptian) which comprises condensed, dark grey, radiolarian-rich claystones that records the maximum flooding surface. The Aptian−Maastrichtian succession (Darwin, Jamieson,

Woolaston, Gibson, Fenelon and Turnstone formations) comprises stacked progradational wedges of silty claystones, calcareous shale and marls (Whittam et al., 1996).

The Paleocene Johnson Formation, made up of argillaceous limestones and marls, marks the change from clastic- to carbonate-dominated deposition (Bradshaw et al., 1988; Shuster et al., 1998). During the late Paleocene−Eocene, a rapid sea level fall was responsible for the coarse clastic sedimentation, known as the Grebe Sandstone Member. The overlying upper part of the passive margin sequence, the Hibernia (early Eocene) and Prion (late Eocene) formations, reflect a return to carbonate deposition which was interrupted by regional unconformities resulting from fluctuating sea levels and climate change (Kennard et al., 1999). The TM3 unconformity recorded at the base of the Miocene marks the initiation of the collisional event and fault reactivation (O'Brien et al., 1999; Keep et al., 2000; 2002; Longley et al., 2002). The overlying Cartier Formation is defined as a limestone unit that consists of bioclastic carbonates deposited in inner neritic water depths. Further carbonate shelf progradation continued during the Miocene (Oliver Formation) and into the Pliocene Barracouta Formation (**Figure 5.2**).

This prograding carbonate system, reflecting the mature phase of the passive margin, resulted in additional loading that enhanced the maturation of the Cretaceous and Jurassic source rock units. The resulting rapid heating of the source rocks has been a major contributing factor in the generation, expulsion and entrapment of oil and gas (Smith et al., 1996). The renewed extension during the late Miocene−early Pliocene (commencement of the active margin phase) resulted in the reactivation of most of the Mesozoic fault-bounded structures, with the consequent loss of oil and gas and resultant residual oil columns (Lisk et al., 1998; O'Brien et al., 1999; Lisk et al., 2000).

## 5.3. Petroleum systems

Variations in the subsidence history, together with the different tectonic events, have a direct impact on the timing of oil and gas generation in the northern Bonaparte Basin. Initial phases of oil and gas expulsion (Lisk and Eadington, 1994; O'Brien et al., 1996; Lisk et al., 1998; Kennard et al., 1999; Brincat et al., 2001) are thought to have occurred in the Late Jurassic−Early Cretaceous, largely in response to elevated heat flows during rifting (Lisk et al., 1998). This phase was followed by the main phase of oil expulsion and migration, probably in the middle to late Eocene. Late stage gas and oil charges are also suggested to have occurred during renewed subsidence from the Miocene onward (Kennard et al., 1999; Kennard et al., 2002).

### 5.3.1. Source rocks

In the depocentres surrounding the Laminaria High, source rocks were deposited during the Lower Jurassic to Lower Cretaceous syn-rift and post-rift phases. Lower delta plain coals and shales within the Lower to Middle Jurassic Plover Formation are considered to be a significant source for gas and lesser amounts of oil in the northern Bonaparte Basin and Vulcan Sub-basin (Botten and Wulff, 1990; Whibley and Jacobson, 1990; Preston and Edwards, 2000; George et al., 2004b). The Laminaria Formation also includes potential source rocks, as shown by the samples analysed in this study. The Upper Jurassic Frigate Formation and Upper Jurassic–Lower Cretaceous Flamingo Formation are composed mainly of restricted marine shales and are regarded as a prime source of oil as well as gas. In the later rifting phase, the claystones of the Lower Cretaceous Echuca Shoals Formation were deposited under marine conditions. These sediments can also be considered part of the petroleum system where sufficient burial and thermal maturation has occurred.

### 5.3.2. Reservoirs

The majority of oil and gas discoveries on the Laminaria High and adjacent Flamingo High have been made within the Callovian−Oxfordian shallow marine sandstones of the Laminaria Formation and within the distributary channel sandstones of the Plover Formation (Whittam et al., 1996; Labutis et al., 1998). The early Eocene Grebe Sandstone Member forms a secondary exploration objective in the area (Cadman and Temple, 2003).

### 5.3.3. Seals

The Lower Cretaceous (Valanginian−Aptian) Echuca Shoals Formation is the regional seal for the Plover and Laminaria reservoirs in the northern Bonaparte Basin (Kivior et al., 2002). The Upper Jurassic (Kimmeridgian) Frigate Formation and Upper Jurassic–Lower Cretaceous (Tithonian−Valanginian) Flamingo clastic claystones and shales deposited during the late stages of the rifting phase form additional top seals (de Ruig et al., 2000; Dyt et al., 2012). These seals are known to have a moderate efficiency for oil and low sealing capacity for gas (O'Brien et al., 1999).

### 5.3.4. Traps

The development of tilted faulted blocks and anticlines during the rifting stages created numerous potential targets in the northern Bonaparte Basin, with Jurassic structures being the most dominant trap types (Pattillo and Nicholls, 1990; Whittam et al., 1996; Gartrell et al., 2006). Many of these structures were found either to be dry or have a residual oil leg

(e.g., George et al., 2004b). As discussed by many authors (e.g., O'Brien et al., 1996; 1999) these traps have been breached and leaked oil and gas due to the reactivation of the bounding faulting system during the Cenozoic. Gartrell et al. (2006) suggested that even though fault reactivation occurred, oil and gas columns can be preserved where the crest of the trap has closure bounded by a fault, or fault segment, with relatively low post-rift displacements (typically < 60 m). Langhi et al. (2010) demonstrated that during fault reactivation, the size, length, height and distribution of the fault system play a critical role in defining either breached or preserved structures.

## 5.4.    Samples and experimental techniques

Potential source rocks sampled from the Laminaria High were identified from data available from the Geoscience Australia database (http://dbforms.ga.gov.au/www/npm.well.search). Based on total organic carbon (TOC) and Rock-Eval pyrolysis data, five potential source rock formations; the Plover, Laminaria, Frigate, Flamingo and Echuca Shoals, were sampled. Fourteen cutting samples representing these five formations were selected from five wells drilled on the Laminaria High (Buang-1, Corallina-1, Laminaria-1, Laminaria-3, and Laminaria East-1) (**Table 5.1**). In some cases, where the amount of available sample was limited, cuttings from several bags (5–15 m) were combined for the same source rock unit. On the Laminaria High, few wells penetrate the Plover Formation and potential source rock samples were difficult to obtain. To fill this gap, nine additional samples from the Plover Formation (**Table 5.1**) were collected from five wells (East Swan-1, Jarrah-1A, Maret-1, Montara-1 and Skua-1) drilled within the Vulcan Sub-basin, located to the southwest of the Laminaria High. These samples were used to characterise the Plover Formation that is believed to be one of the major source rocks. In some cases, samples from the Plover Formation were hand-picked to separate the coal and shale lithologies. However, it is important to keep in mind that the Plover Formation kerogens preserved within the Vulcan Sub-basin can be different (facies change) and thus their characteristics may not be representative of those in the Laminaria High. The samples were crushed to powder using a mortar and pestle. The powdered samples were solvent-extracted to remove the extractable organic matter (EOM) using a mixture of dichloromethane:methanol (9:1 v/v) in an accelerator solvent extractor (ASE300).

**Table 5.1. Sample identity, Rock-Eval pyrolysis and TOC data for the 23 solvent-extracted rock samples.**

| Sample ID | Well | Depth (m) | Formation | $S_1$ | $S_2$ | $S_3$ | $T_{max}$ | HI | OI | TOC |
|---|---|---|---|---|---|---|---|---|---|---|
| G011000 | Buang 1 | 3120 | Echuca Shoals Fm | 1.05 | 9.77 | 1.08 | 434 | 366 | 40 | 2.67 |
| G011008 | Corallina 1 | 2930 - 2945 | Echuca Shoals Fm | 0.1 | 2.77 | 1.2 | 437 | 158 | 69 | 1.75 |
| G011011 | Laminaria 1 | 2940 - 2950 | Echuca Shoals Fm | 0.08 | 3.72 | 0.63 | 436 | 197 | 33 | 1.89 |
| G011002 | Buang 1 | 3170 | Flamingo Fm | 0.24 | 7.62 | 1.42 | 435 | 428 | 80 | 1.78 |
| G011009 | Corallina 1 | 2950 - 2955 | Flamingo Fm | 0.11 | 5.89 | 1.17 | 435 | 209 | 41 | 2.82 |
| G011016 | Laminaria 3 | 3110 - 3120 | Flamingo Fm | 0.05 | 1.06 | 1.88 | 440 | 107 | 189 | 1 |
| G011005 | Buang 1 | 3580 | Frigate Fm | 0.14 | 5.51 | 0.86 | 439 | 220 | 34 | 2.51 |
| G011013 | Laminaria 1 | 3195 - 3200 | Frigate Fm | 0.12 | 1.22 | 0.98 | 425 | 79 | 64 | 1.54 |
| G011017 | Laminaria 3 | 3230 - 3240 | Frigate Fm | 0.15 | 1.53 | 2.48 | 435 | 107 | 173 | 1.43 |
| G011019 | Laminaria East 1 | 3250 - 3255 | Frigate Fm | 0.3 | 4.06 | 4.27 | 432 | 196 | 206 | 2.07 |
| G011006 | Buang 1 | 3615 | Laminaria Fm | 0.14 | 4.46 | 1.37 | 433 | 286 | 88 | 1.56 |
| G011015 | Laminaria 1 | 3285 - 3290 | Laminaria Fm | 0.1 | 1.08 | 0.76 | 431 | 114 | 80 | 0.95 |
| G011020 | Laminaria East 1 | 3310 - 3320 | Laminaria Fm | 0.07 | 1.4 | 1.45 | 439 | 123 | 127 | 1.14 |
| G011021* | Laminaria East 1 | 3390 - 3400 | Plover Fm | 0.06 | 0.51 | 1.11 | 427 | 82 | 178 | 0.62 |
| G011027 | East Swan 1 | 2752 - 2755 | Plover Fm | 0.07 | 3.79 | 1.2 | 436 | 187 | 59 | 2.03 |
| G011032 | Jarrah 1A | 1920 - 1923 | Plover Fm | 0.26 | 13.27 | 2.4 | 430 | 191 | 35 | 6.95 |
| G011037 (Shale) | Maret 1 | 3554 - 3560 | Plover Fm | 0.34 | 51.81 | 2.25 | 433 | 262 | 11 | 19.8 |
| G011038 (Coal) | Maret 1 | 3554 - 3560 | Plover Fm | 0.75 | 125.09 | 2.73 | 434 | 300 | 7 | 41.7 |
| G011039 | Montara 1 | 3177 - 3186 | Plover Fm | 0.51 | 31.68 | 2.61 | 432 | 226 | 19 | 14 |
| G011043 | Montara 1 | 3315 - 3318 | Plover Fm | 0.92 | 38.34 | 2.68 | 430 | 219 | 15 | 17.5 |
| G011063 (Shale) | Skua 1 | 2584 - 2587 | Plover Fm | 0.51 | 22.22 | 2.28 | 427 | 204 | 21 | 10.9 |
| G011064 (Coal) | Skua 1 | 2584 - 2587 | Plover Fm | 1.83 | 80.25 | 7.06 | 416 | 252 | 22 | 31.9 |
| G011066 | Skua 1 | 2630 - 2633 | Plover Fm | 3.57 | 196.81 | 9.87 | 412 | 383 | 19 | 51.4 |

**\***: Not used for further analyses

$S_1$: Amount of free hydrocarbons in the sample in mg HC/g rock

$S_2$: Amount of hydrocarbons generated during pyrolysis in mg HC/g rock

$S_3$: Amount of oxygen containing compounds generated during pyrolysis in mg $CO_2$/g rock

$T_{max}$: Temperature of maximum hydrocarbon generation in °C

**HI**: Hydrogen Index ($S_2$*100/TOC) in mg HC/g TOC

**OI**: Oxygen Index ($S_3$*100/TOC) in mg $CO_2$/g TOC

**TOC**: Total Organic Carbon in %

To assess the petroleum generative potential and thermal maturity, aliquots of the solvent-extracted rock (80 mg) were pyrolysed using a Rock-Eval 6 instrument with a TOC module (Lafargue et al., 1998). **Table 5.1** shows Rock-Eval pyrolysis and TOC data for the 23 cuttings samples analysed. Based on their TOC content and $T_{max}$ values, 22 thermally immature, solvent-extracted, samples were analysed by pyrolysis-gas chromatography (Py-GC) (Horsfield, 1989; Horsfield and Dueppenbecker, 1991) in order to predict the type of petroleum products generated during thermal maturation (Larter and Senftle, 1985; Horsfield, 1989). An Agilent 6890A GC instrument equipped by a programmable pyrolysis unit, a HP-Ultra 50 m x 0.32 mm i.d. capillary column (0.52 μm film thickness and dimethyl polysiloxane-phase) and a flame ionisation detector (FID) were used. Powdered and extracted rock samples were weighed (2−25 mg) and placed into the central part of a glass tube; the remaining volume was filled by purified quartz wool. The samples were introduced into the sample holder of a pyrolysis unit on top of the Agilent GC. The tubes were purged for 5 min at 300°C and then pyrolysed. The hydrocarbon fractions released by pyrolysis at programmed temperatures from 300 to 600°C under a constant flow of helium (30 ml/min) were trapped in a liquid nitrogen-cooled trap. The trapped hydrocarbons were released by ballistic heating of the trap to 300°C and subsequently analysed using gas chromatography. Peak heights of the identified pyrolysates, calibrated with an *n*-butane external standard, were used for calculating their concentrations **(Table 5.2)**.

The Source Rock Analyser[TM] instrument (SRA-TPH/IR) was used for the determination of activation energy distributions and single frequency factors (A), and thus, the bulk kinetics of 13 selected solvent-extracted samples **(Table 5.5)**. This experiment consisted of heating 10 to 40 mg of extracted samples (loaded into a small vessel) using a furnace set-up previously described (Schaefer et al., 1990; Mahlstedt et al., 2008) at different rates under non-isothermal open-system pyrolysis conditions. Initially, the isothermal temperature of 200°C was maintained for 15 minutes, after which the temperature was increased to 640 °C at different heating rates. In this study, four heating rates were chosen (0.7°C/min, 2°C/min, 5°C/min and 15°C/min) and were controlled by a thermocouple placed just above the sample. For a continuous registration of bulk formation rates, a constant helium flow (50 mL/min) was maintained to allow the transport of the pyrolysis products to the FID. The generated bulk petroleum formation curves were used to calculate kinetic parameters using Kinetics 2000 and KMOD[TM] software developed by the Lawrence Livermore National Laboratory (Burnham et al., 1987; 1988).

**Table 5.2. Calculated percentages of the main resolved classes from open-system pyrolysis of 22 solvent-extracted rock samples.**

| Sample ID | Area | Well | Depth (m) | Formation | % of resolved components in $S_2$ | | | |
|---|---|---|---|---|---|---|---|---|
| | | | | | Aliphatics | Mono-aromatics | Phenolics | Naphthalenes |
| G011000 | | Buang 1 | 3120 | Echuca Shoals | 85.2 | 9.6 | 2.4 | 2.8 |
| G011008 | | Corallina 1 | 2930 - 2945 | Echuca Shoals | 83.9 | 11.6 | 1.2 | 3.4 |
| G011011 | | Laminaria 1 | 2940 - 2950 | Echuca Shoals | 83.4 | 11.7 | 1.4 | 3.5 |
| G011002 | | Buang 1 | 3170 | Flamingo | 84 | 10.3 | 2.1 | 3.6 |
| G011009 | | Corallina 1 | 2950 - 2955 | Flamingo | 84.6 | 10.6 | 1.5 | 3.3 |
| G011016 | | Laminaria 3 | 3110 - 3120 | Flamingo | 76.4 | 17.5 | 2.2 | 3.9 |
| G011005 | **Laminaria High** | Buang 1 | 3580 | Frigate | 84.3 | 11.1 | 0.5 | 4 |
| G011013 | | Laminaria 1 | 3195 - 3200 | Frigate | 77.3 | 18.9 | 0.7 | 3.1 |
| G011017 | | Laminaria 3 | 3230 - 3240 | Frigate | 79.1 | 17.9 | 0.5 | 2.5 |
| G011019 | | Laminaria East 1 | 3250 - 3255 | Frigate | 79 | 14.8 | 2.5 | 3.6 |
| G011006 | | Buang 1 | 3615 | Laminaria | 82.6 | 12.6 | 1.5 | 3.3 |
| G011015 | | Laminaria 1 | 3285 - 3290 | Laminaria | 81.6 | 16.8 | 0.2 | 1.4 |
| G011020 | | Laminaria East 1 | 3310 - 3320 | Laminaria | 82.2 | 14.4 | 1.2 | 2.2 |
| G011027 | | East Swan 1 | 2752 - 2755 | Plover | 81.6 | 10.5 | 3 | 4.9 |
| G011032 | | Jarrah 1A | 1920 - 1923 | Plover | 80.8 | 8 | 5 | 6.1 |
| G011037 | | Maret 1 | 3554 - 3560 | Plover | 81.1 | 7.1 | 5.4 | 6.5 |
| G011038 | | Maret 1 | 3554 - 3560 | Plover | 81.7 | 6.4 | 5.3 | 6.6 |
| G011039 | **Vulcan Sub-basin** | Montara 1 | 3177 - 3186 | Plover | 81.5 | 7 | 5.4 | 6.1 |
| G011043 | | Montara 1 | 3315 - 3318 | Plover | 45.9 | 9.9 | 41.5 | 2.7 |
| G011063 | | Skua 1 | 2584 - 2587 | Plover | 76.4 | 10 | 9.1 | 4.4 |
| G011064 | | Skua 1 | 2584 - 2587 | Plover | 61.3 | 9.5 | 25 | 4.1 |
| G011066 | | Skua 1 | 2630 - 2633 | Plover | 46.7 | 8.2 | 43.3 | 1.8 |

From the samples selected for bulk kinetics, five solvent-extracted samples were also subjected to compositional kinetic analysis **(Table 5.6)**. This method is designed to simulate the maturation of organic matter in a closed pyrolysis system using the microscale-sealed-vessel (MSSV) technique (Horsfield et al., 1989; Dieckmann et al., 1998). For a heating rate of 0.7°C/min, the temperatures corresponding to the transformation ratios of 10, 30, 50, 70 and 90% were determined and used to carry out the MSSV pyrolysis. A few milligrams (5 to 15 mg) of solvent-extracted samples (5 aliquots from each sample, for the 5 transformation ratios) were weighed into one-sided closed glass capillary tubes. These tubes were sealed by a hydrogen flame and then placed into a furnace to be heated from 200°C to the final defined temperatures (at 0.7°C/min). The composition of the generated products was measured online in a single GC-FID run. The detected products, both resolved and total, were then quantified with reference to relative retention times, and their weights were determined using an external *n*-butane standard. In addition, data derived from the MSSV-gas chromatography was employed as input for phase kinetic modelling as described by di Primio and Horsfield (2006) using PVT simulation software (PVT Sim, Calsep, Denmark).

The carbon isotopic compositions of methane, ethane, propane and butane were measured on six solvent-extracted samples using combined gas chromatography-isotope ratio mass spectrometry (GC-IR MS) MAT 253 equipment. Closed-system conditions using the MSSV tubes were used, with a heating rate of 0.7°C/min and covering the temperatures corresponding to 10, 30, 50, 70 and 90% transformation ratio. GC analysis of the gases was performed using an Agilent 6890N GC equipped with a Varian Poraplot Q column (50 m, i.d. 0.32 mm, film thickness 10 μm), with helium as the carrier gas. The temperature of the injector was fixed to 230°C with a 1:3 split configuration. The temperature program of the GC oven started at an initial temperature of 30°C, held isothermal for 10 minutes, then progressively heated from 30 to 150°C at 3°C/min, followed by another heating increase to 200°C at 4°C/min, and a final isothermal period for 15.8 min at 200°C. All isotopic values are presented in delta-notation ($\delta^{13}$C) relative to the Vienna Peedee Belemnite (VPDB: **Table 5.7**).

## 5.5.    Results and discussion

### 5.5.1.  Rock-Eval pyrolysis data and bulk chemical properties

Rock-Eval pyrolysis was performed on 14 solvent-extracted samples from the Laminaria High so as to avoid any possible effect of contamination, since the majority of the wells in this area were drilled with synthetic oil-based mud. The Bathonian−mid Callovian Plover Formation sediments are rarely penetrated by wells drilled on the Laminaria High. In this

study, only one Plover Formation sample, from Laminaria East-1, was collected. This sample has a TOC content of 0.6% and an $S_2$ value of 0.5 mg HC/g rock; values below those defined for a source rock (Peters and Cassa, 1994). To compensate for this, nine representative Plover Formation samples were collected from the Vulcan Sub-basin, located in the south-western part of the basin (**Figure 5.1**: **Table 5.1**). TOC values of these samples, which were also solvent-extracted, range from 2 to 51%. The mid-Callovian−Oxfordian Laminaria Formation contains thin potential source rocks with average TOC values of 1.5%. The Kimmeridgian Frigate and Tithonian–Valanginian Flamingo formations and the Valanginian–Aptian Echuca Shoals Formation source rocks have TOC contents varying from 1.5 to 3%. The genetic potential ($S_1 + S_2$) of the studied samples cannot be interpreted as the free hydrocarbon fraction has been partly removed by solvent extraction. The hydrogen index (HI) values vary from less than 100 to 400 mg HC/g TOC. When plotted against the oxygen index (OI) on a modified van Krevelen diagram (Tissot and Welte, 1984), these values suggest the predominance of Type II/III organic matter (**Figure 5.3a)** for all the studied samples.
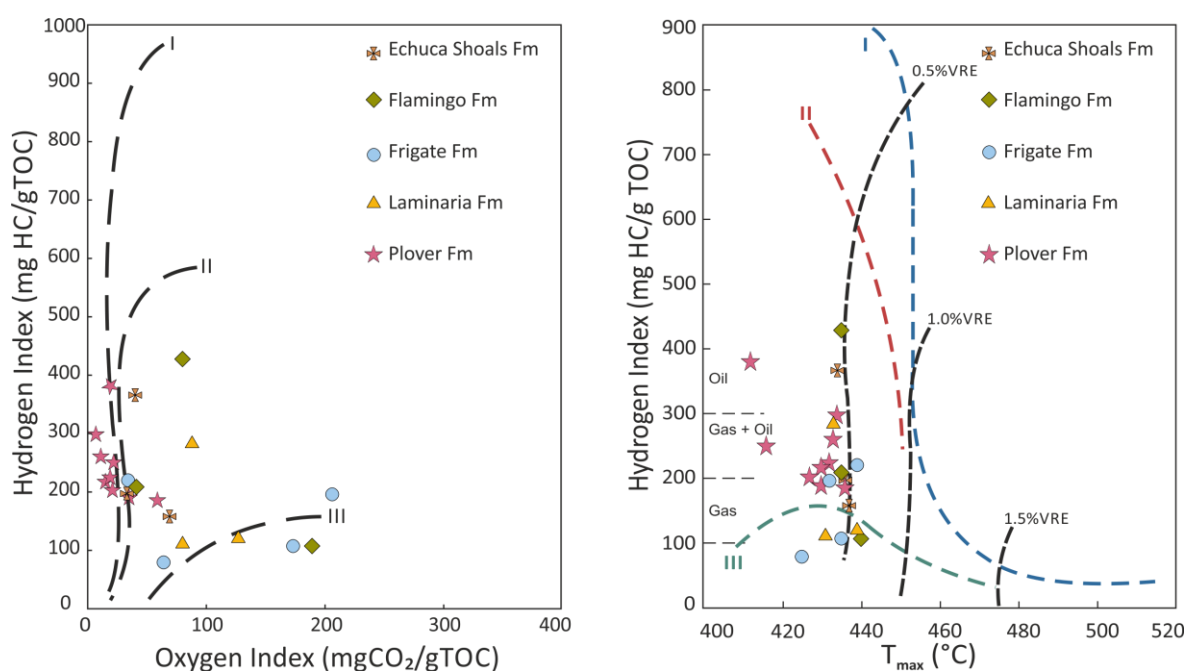


**Figure 5.3. Rock Eval data for 23 samples from the Laminaria High, and nine samples from the Vulcan Sub-basin. (a) Oxygen index versus hydrogen index** (Espitalié et al., 1977) **illustrating the kerogen type. (b) Hydrogen index versus T$_{max}$** (Cornford et al., 1998) **showing the low thermal maturity of the sample set. VRE = vitrinite reflectance equivalent.**

The production index ($PI = S_1/S_1 + S_2$) cannot be used as a tool for thermal maturity assessment, due to the prior solvent extraction. Therefore, only the Rock-Eval $T_{max}$ values were used. These values range from 412 to 440°C indicating that all the source rocks investigated in this study are immature to very early mature (e.g., Espitalié, 1986; Peters and Cassa, 1994), with respect to the oil window **(Figure 5.3b)**.

## 5.5.2. Open-system pyrolysis-Gas Chromatography (Py-GC) data and molecular composition

### 5.5.2.1. Distribution of normal alkanes and alkenes

All the studied samples are composed of sulphur-lean organic matter, as indicated by the absence of thiophenic compounds in the pyrolysates (Sinninghe Damsté et al., 1988; Saiz-Jimenez, 1995; Sinninghe Damsté et al., 1998). This observation supports the assumption that these source rocks were deposited under fluvial to marine environments (Arditto, 1996; Whittam et al., 1996), where redox conditions were likely to be unfavourable for the preservation of organic sulfur compounds. The pyrograms show *n*-alkene/*n*-alkane homologous series ranging from $C_1$ up to $C_{27}$ **(Figure 5.4)**. Straight chain hydrocarbons are less prominent in the kerogens collected from the Frigate Formation. The samples from the Plover Formation are more enriched in straight chain hydrocarbons with a higher carbon-number range, whilst samples from other formations have detectable, but lower abundances of these. Compared to the *n*-alkanes, the *n*-alkenes are minor components in the $C_{15+}$ range.

### 5.5.2.2. Aromatic hydrocarbon distributions

In the pyrograms of the Laminaria High kerogens, pyrolysis products such as alkylbenzenes, naphthalene, and alkylnaphthalenes are present **(Figure 5.4)**, but quantitatively are only of moderate importance relative to the *n*-alkene/*n*-alkane doublets **(Table 5.2)**. Toluene is the most abundant alkylbenzene in all the pyrolysates. Other alkylbenzenes such as trimethylbenzenes and tetramethylbenzenes are present in low amounts. Although aromatic compounds form the second most abundant class, their relative concentrations are low in the pyrolysates from the Laminaria High (6 to 19% of resolved components of the pyrolysate).

### 5.5.2.3. Phenolic component distributions

The main phenolic compounds (phenol and methylphenols) are present in trace amounts in the pyrolysates from the Laminaria High **(Figure 5.4)**. One exception is found within the pyrolysates from the Plover Formation that exhibits higher phenolic content. The concentration of these compounds is more pronounced in the coaly samples **(Table 5.2)**.
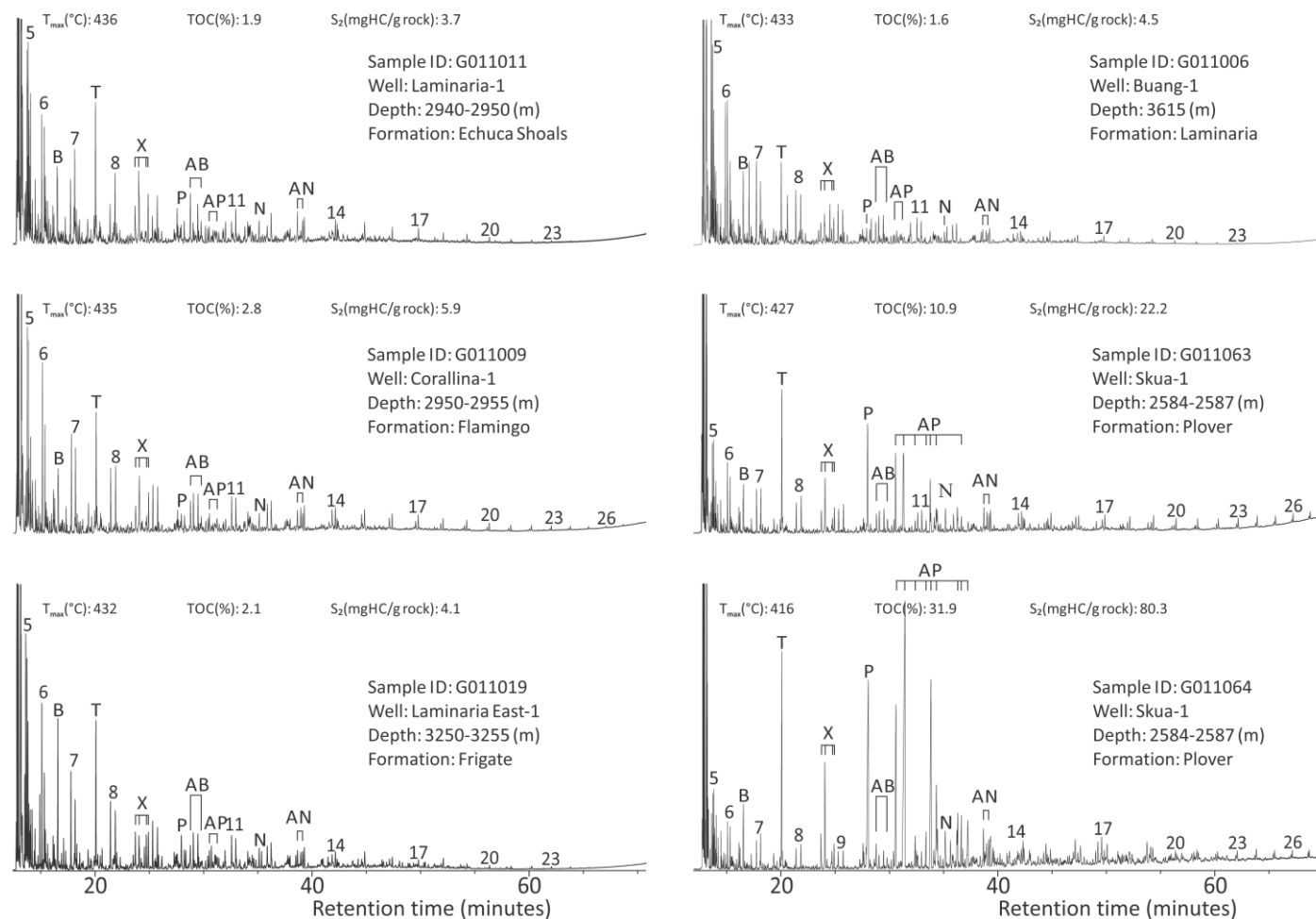
**Figure 5.4. Open-system pyrolysis-gas chromatograms for six representative solvent-extracted rock samples included in this study. Numbers indicate the number of carbon atoms in the *n*-alkane/*n*-alkene doublets; B: benzene; T: toluene; X: C₃ alkylbenzenes (ethylbenzene, *meta* + *para*-xylene, styrene, *ortho*-xylene, respectively); P: phenol; AB: C₃ alkylbenzenes; AP: alkylphenols; N: naphthalene; AN: alkylnaphthalenes.**

### 5.5.2.4. Kerogen composition and type

Two ternary diagrams, usually used to define hydrocarbon composition and type, are shown in **Figure 5.5**. The first diagram was defined by Horsfield (1989) to assess the composition of the generated hydrocarbons, and uses the total resolved $C_1$ to $C_5$ hydrocarbons, the sum of the *n*-alkenes/*n*-alkanes in the $C_6$ to $C_{14}$ range, and the sum of the *n*-alkenes/*n*-alkanes in the $C_{15+}$ range **(Table 5.3)**. The second diagram, originally defined by Larter (1984) to assess kerogen type and phenolic content, uses the relative percentages of three components (*n*-octene, phenol and *m*- plus *p*-xylene). Kerogens from the Frigate and Flamingo formations on the Laminaria High plot in the paraffinic-naphthenic-aromatic oil field (low wax), whereas some kerogens from the Echuca Shoals and Laminaria formations plot in the condensate and gas field. When placed in Larter's diagram, all but one sample from the Frigate Formation plot in the Type III kerogen field and have relatively low phenolic content. One Frigate sample, in which phenol is present in low abundance, plots in the mixed Type I/II kerogen field, a result that is not in accordance with the low hydrogen index (79 mg HC/g TOC) and the low thermal maturity ($T_{max} = 425^0C$) of this sample. Samples from the Plover Formation have higher phenol amounts **(Figure 5.5b)**.

Overall, there is a good correlation between the Py-GC and Rock Eval pyrolysis results, and both are in accordance with the oil- and gas-prone nature of the Laminaria High area. The variability between the studied kerogens, particularly the Plover kerogens, is interpreted to be a direct result of the varied depositional environments under which these facies were deposited (Whittam et al., 1996). While the majority of the studied samples show signatures of terrigenous organic matter, different organic facies can be distinguished. The Plover Formation samples plotting in the gas and condensate petroleum type organofacies of **Figure 5.5a** are representative of the fluvial to deltaic environments, and the samples plotting in the P-N-A field (low and high wax content) reflect the transition to inner shelf environments (Arditto, 1996; Whittam et al., 1996). In addition, the relatively high abundance of phenolic components indicates that the terrigenous input (van de Meent et al., 1980; Bordenave, 1993) is higher for the Plover Formation than for the overlying source rocks **(Figure 5.5b)**. Two samples from the Laminaria Formation plot in the gas and condensate field, while only one sample is found within the low wax P-N-A oil. This differentiation can be explained by relatively deeper water of these depositional environments. Samples from both the Flamingo and Frigate formations plot mainly in the low wax P-N-A oil field which indicates the transition from a deltaic to open marine environment in response to fault activity and regional subsidence during the Late Jurassic to Early Cretaceous (Whittam et al., 1996).

However, one sample from the Frigate Formation plots in the gas and condensate field, most likely because of renewed siliciclastic input after the Tithonian uplift (Whittam et al., 1996).
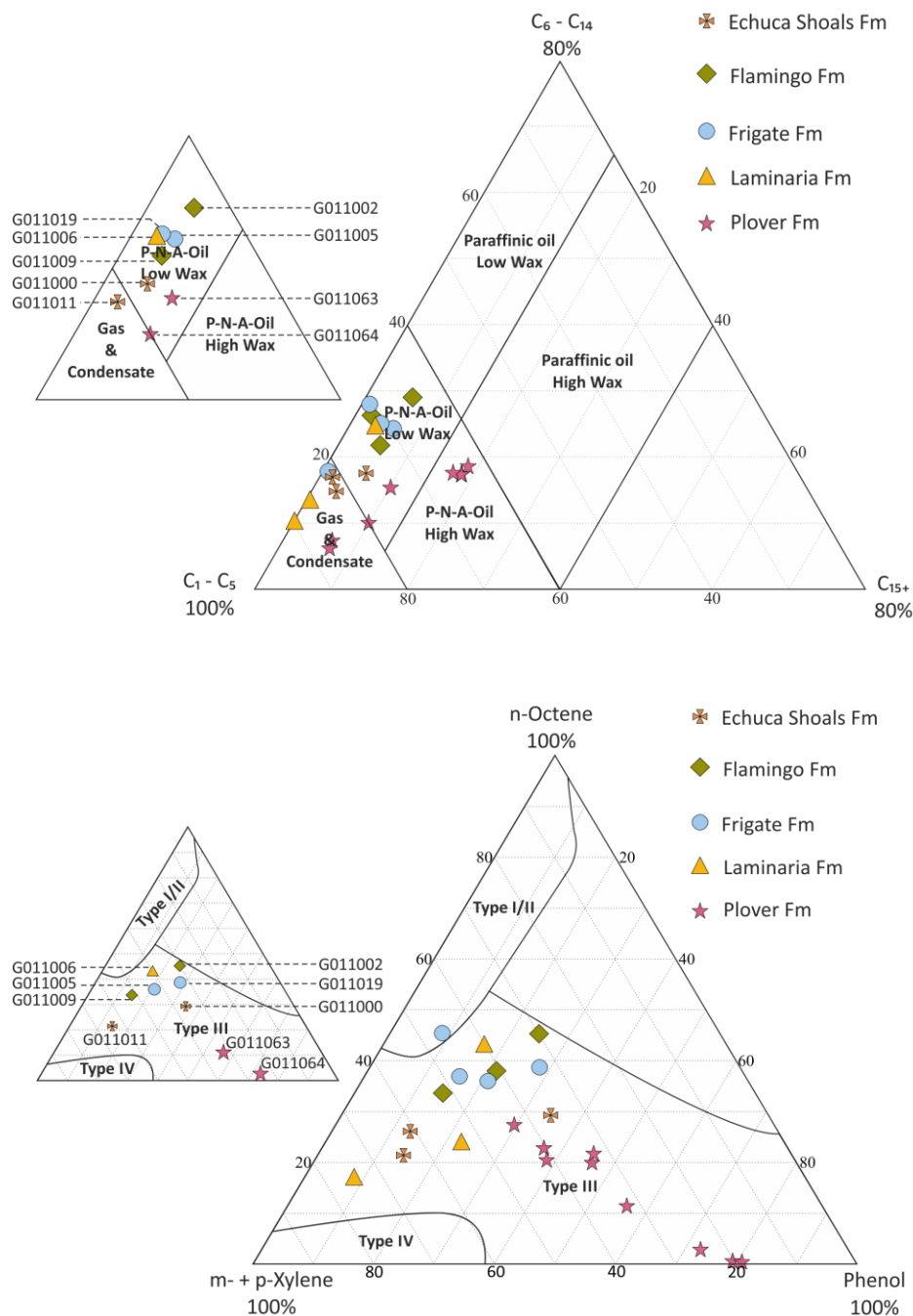


**Figure 5.5. Ternary diagrams showing: (a) The composition of the extracted kerogen pyrolysates from the studied source rocks, on the basis of the balance of total $C_1−C_5$ hydrocarbons, $C_6−C_{14}$ *n*-alkenes plus *n*-alkanes, and $C_{15+}$ *n*-alkenes plus *n*-alkanes (Horsfield, 1989). (b) The type of the extracted kerogen pyrolysates from the studied source rocks, on the basis of the balance of phenol, *m*- and *p*-xylene and *n*-octene (Larter, 1984). P-N-A = paraffinic-naphthenic-aromatic. Samples numbered on the small subset ternary diagrams are the samples selected for further analyses.**

**Table 5.3. Selected components from open-system pyrolysis−gas chromatography, used to determine petroleum type, source rock organic facies and phenolic content.**

| Formation | Sample | $C_1$-$C_5$ (%) | $C_6$-$C_{14}$ (%) | $C_{15+}$ (%) | $m$+$p$ xylene (%) | $n$-octene (%) | Phenol (%) |
|---|---|---|---|---|---|---|---|
| Echuca Shoals | G011000 | 77 | 18 | 6 | 36 | 29 | 35 |
| | G011008 | 81 | 17 | 2 | 61 | 26 | 13 |
| | G011011 | 82 | 15 | 3 | 64 | 21 | 14 |
| Flamingo | G011002 | 65 | 29 | 6 | 30 | 45 | 25 |
| | G011009 | 73 | 22 | 6 | 52 | 34 | 15 |
| | G011016 | 72 | 26 | 2 | 41 | 38 | 21 |
| Frigate | G011005 | 70 | 24 | 6 | 43 | 36 | 21 |
| | G011013 | 71 | 28 | 1 | 46 | 45 | 9 |
| | G011017 | 82 | 18 | 1 | 47 | 37 | 16 |
| | G011019 | 71 | 25 | 4 | 33 | 39 | 28 |
| Laminaria | G011006 | 72 | 25 | 3 | 40 | 43 | 17 |
| | G011015 | 90 | 10 | 0 | 75 | 17 | 8 |
| | G011020 | 86 | 14 | 0 | 53 | 24 | 22 |
| Plover | G011027 | 71 | 21 | 8 | 43 | 27 | 30 |
| | G011032 | 64 | 17 | 19 | 34 | 20 | 46 |
| | G011037 | 65 | 18 | 17 | 41 | 20 | 39 |
| | G011038 | 64 | 17 | 18 | 40 | 23 | 37 |
| | G011039 | 63 | 19 | 19 | 33 | 22 | 46 |
| | G011043 | 86 | 7 | 6 | 20 | 1 | 79 |
| | G011063 | 74 | 15 | 10 | 32 | 12 | 56 |
| | G011064 | 80 | 10 | 10 | 24 | 3 | 73 |
| | G011066 | 87 | 6 | 7 | 19 | 0 | 81 |

Biomarker data reported by Preston and Edwards (2000) on extracts from this formation showed that there is a significant abundance of land plant-derived components. As the relative sea level continued rising, the sediments of the Echuca Shoals Formation were deposited in open marine conditions. Surprisingly, two samples from this latter formation plot in the gas and condensate field, and one displays a relatively higher abundance of phenolic compounds (sample G011000) compared to the underlying Laminaria, Frigate and Flamingo sediments. Although sedimentological data (Whittam et al., 1996) and biomarker data (Preston and Edwards, 2000) show that the Echuca Shoals Formation has a more pronounced marine signature, oxidation of the organic matter during deposition is likely. This observation can be clarified by reference to the organic petrology that has been described for these samples (http://dbforms.ga.gov.au/www/npm.well.search). Petrographically, the Middle Jurassic to Lower Cretaceous sediments display significant variation **(Figure 5.6**: **Table 5.4)** which is in agreement with the depositional environments under which these sediments were deposited. As expected, the vitrinite maceral group is

more abundant in the Plover and Laminaria source rock samples, while alginite is more abundant in the Flamingo and Echuca Shoals formation samples, and to a lesser extent in the Frigate Formation samples. In addition, liptinite is the most common maceral group in the Plover Formation source rocks, thus explaining the position of the Plover Formation samples in the high wax P-N-A oil field. The main liptinite macerals in the sediments of the Plover Formation are lamalginite derived from dinoflagellate/acritarch cysts and liptodetrinite (Faiz et al., 1998). Rare cutinite, sporinite and possible Botryococcus-related telalginite also occur in this formation. The organic matter preserved within the Echuca Shoals Formation contains abundant inertinite macerals (especially in the uppermost section), and is up to 100% of the macerals in some wells such as Alaria-1 **(Table 5.4)**. The abundance of this maceral group can explain why the Echuca Shoals source rock would generate gas and condensate if buried sufficiently, and correlates with the relatively high phenolic content for the sample (G011000) measured by open-system pyrolysis-GC **(Figure 5.5b)**.
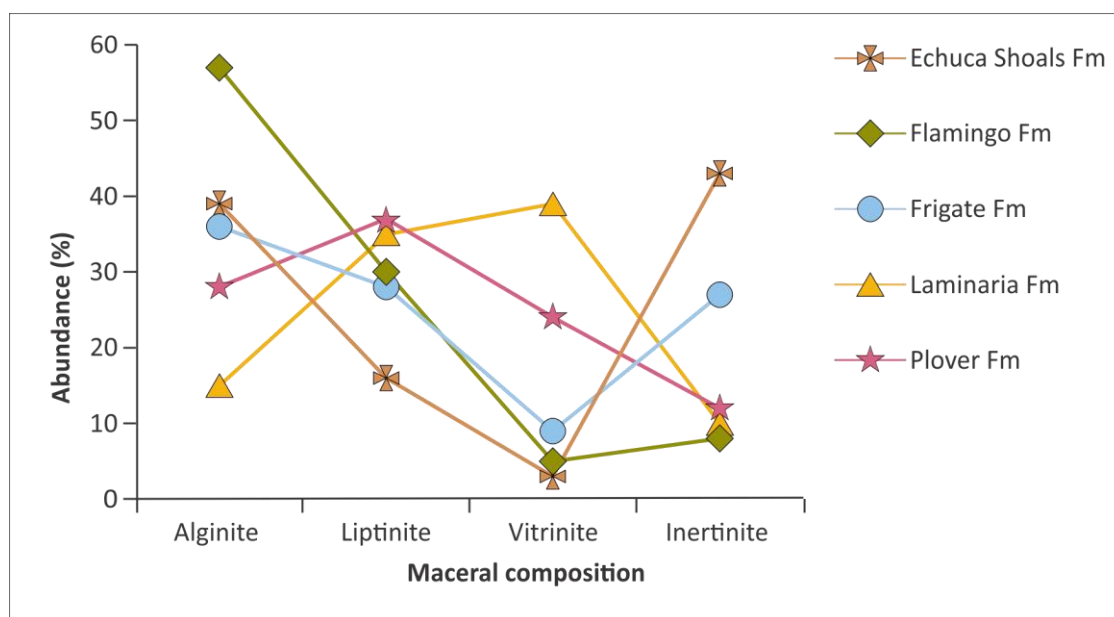


**Figure 5.6. Average maceral composition for the Middle Jurassic to Lower Cretaceous source rocks in the northern Bonaparte Basin (http://dbforms.ga.gov.au/www/npm.well.search). See Table 5.4 for maceral group definitions.**

**Table 5.4. Maceral composition of the Middle Jurassic to Lower Cretaceous source rocks from wells in the northern Bonaparte Basin (http://dbforms.ga.gov.au/www/npm.well.search). Bracketed numbers represent average values.**

| Source rock | Well Name | Sample number | Alginite (%) | Liptinite (%) | Vitrinite (%) | Inertinite (%) |
|---|---|---|---|---|---|---|
| **Echuca Shoals** | Alaria 1 | 4 | | | | |
| | Buller 1 | 1 | 0 – 67 | 0 – 29 | 0 – 11 | 8 -100 |
| | Bluff 1 | 3 | (39) | (16) | (3) | (43) |
| | Tanjil 1ST1 | 4 | | | | |
| **Flamingo** | Alaria 1 | 2 | | | | |
| | Buller 1 | 4 | | | | |
| | Bogong 1 (BHP) | 3 | 18 – 80 | 14 – 59 | 0 – 45 | 0 – 25 |
| | Bluff 1 | 3 | (57) | (30) | (5) | (8) |
| | Tanjil 1 | 2 | | | | |
| **Frigate** | Laminaria 3 | 4 | | | | |
| | Buller 1 | 1 | 0 – 74 | 0 – 69 | 0 – 25 | 4 – 100 |
| | Bogong 1 (BHP) | 3 | (36) | (28) | (9) | (37) |
| | Tanjil 1ST1 | 4 | | | | |
| **Laminaria** | Alaria 1 | 1 | 0 – 100 | 0 – 79 | 0 – 100 | 0 – 33 |
| | Vidalia 1 | 9 | (15) | (35) | (39) | (10) |
| | Buller 1 | 3 | | | | |
| | Bogong 1 (BHP) | 1 | | | | |
| | Bluff 1 | 6 | | | | |
| **Plover** | Laminaria 3 | 4 | | | | |
| | Alaria 1 | 22 | 0 – 100 | 0 – 76 | 0 – 100 | 0 – 48 |
| | Vidalia 1 | 1 | (28) | (37) | (24) | (12) |
| | Buller 1 | 1 | | | | |
| | Bogong 1 (BHP) | 1 | | | | |

### 5.5.3. Source rock analyser and MSSV data

#### 5.5.3.1. Activation energy distributions

Kinetics for bulk petroleum generation were measured for thirteen samples **(Table 5.5)** representative of the studied source rocks. For optimisation reasons, each kinetic model is simplified by fixing a single frequency factor (representing the average of all frequency factors involved in the transformation reactions) for all individual hydrocarbon fraction (Ungerer, 1990; Vandenbroucke et al., 1999). Since only one range of heating rates (0.7, 2, 5 and $15^0$C/min) was used, the distribution of these frequency factors will depend mainly on the type of organic matter (Dieckmann, 2005). Almost all of the studied samples display a relatively broad distribution of activation energies, reflecting heterogeneity of the organic matter in these samples **(Figure 5.7)**.

The main activation energies range from 54 to 64 kcal/mol for the Plover Formation and from 52 to 55 kcal/mol for the Upper Jurassic to Lower Cretaceous source rocks, with pre-exponential factors varying from 2.83E+13/sec to 1.65E+14/sec and from 5.13E+14/sec to

1.22E+16/sec, respectively. The broadest and highest activation energy distribution is observed within the Plover samples but mainly the coaly sample (G011064), where the activation energies are spread over a range of 58 up to70 kcal/mol. In contrast, the primary cracking of two samples coming from the Echuca Shoals (G011011) and the Flamingo (G011009) kerogens are described by a relatively low and narrow range of activation energies mainly between 52 and 55 kcal/mol. The characteristics of these two samples indicate more homogeneous precursor materials likely in more marine source rocks.

**Table 5.5. Kinetic parameters (Activation energy (Ea) distribution and frequency factors) of 13 solvent-extracted rock samples.**

| Formation | Echuca Shoals | Echuca Shoals | Flamingo | Flamingo | Frigate | Frigate | Laminaria |
|---|---|---|---|---|---|---|---|
| Sample | G011000 | G011011 | G011002 | G011009 | G011005 | G011019 | G011006 |
| Pre-exponential Factor A (S$^{-1}$) | 9.82E + 13 | 7.75E + 13 | 4.19E +13 | 4.86E + 13 | 2.83E + 13 | 1.65E + 14 | 8.10E + 13 |
| Activation Energy (kcal/mol) | | | | | | | |
| 40 | 0 | 0 | 0.59 | 0 | 0.66 | 0 | 0 |
| 41 | 0.28 | 0 | 0.45 | 0 | 0.22 | 0 | 0.9 |
| 42 | 0.12 | 0.32 | 0.99 | 0.27 | 1 | 0.92 | 0.1 |
| 43 | 0.54 | 0 | 0.97 | 0 | 0.74 | 0.31 | 1.15 |
| 44 | 0.42 | 0.22 | 1.43 | 0.16 | 1.24 | 1.46 | 0.86 |
| 45 | 0.91 | 0.29 | 1.45 | 0.28 | 1.61 | 1.06 | 1.47 |
| 46 | 0.67 | 0 | 2.45 | 0.06 | 1.77 | 2.03 | 1.78 |
| 47 | 1.91 | 0.49 | 2.63 | 0.67 | 2.66 | 2.75 | 2.07 |
| 48 | 1.45 | 0.58 | 3.63 | 0 | 2.66 | 3.27 | 3.26 |
| 49 | 3.67 | 0 | 4.5 | 0 | 4.7 | 4.64 | 2.35 |
| 50 | 2.32 | 0 | 5.27 | 0 | 0 | 4.05 | 5.39 |
| 51 | 5.26 | 0 | 8.31 | 0 | 6.16 | 6.55 | 3.1 |
| 52 | 8.36 | 0 | 17.58 | 23.26 | 32.17 | 4.67 | 8.28 |
| 53 | 18.8 | 34.54 | 22.08 | 37.14 | 21.97 | 10.07 | 23.43 |
| 54 | 19.56 | 27.32 | 13.05 | 19.16 | 9.85 | 18.31 | 19.89 |
| 55 | 18.25 | 18.84 | 7.01 | 6.76 | 7.47 | 17.03 | 8.35 |
| 56 | 5.24 | 5.18 | 6.12 | 9.13 | 3.84 | 10.08 | 12.55 |
| 57 | 10.58 | 8.26 | 0 | 0 | 0 | 5.81 | 0.39 |
| 58 | 0 | 0 | 0.34 | 1.34 | 0.26 | 3.92 | 2.17 |
| 59 | 0.18 | 2.19 | 0.51 | 0.48 | 0.45 | 0.89 | 0.7 |
| 60 | 0.8 | 0.17 | 0 | 0 | 0.13 | 0.62 | 0 |
| 61 | 0 | 0.7 | 0.25 | 0.47 | 0 | 0.38 | 0.92 |
| 62 | 0.25 | 0.34 | 0.04 | 0 | 0 | 0.13 | 0 |
| 63 | 0 | 0 | 0 | 0 | 0 | 0.48 | 0 |
| 64 | 0 | 0.48 | 0.35 | 0 | 0.43 | 0 | 0 |
| 65 | 0.43 | 0 | 0 | 0 | 0 | 0 | 0.87 |
| 66 | 0 | 0.08 | 0 | 0.82 | 0 | 0.57 | 0 |

**Table 5.5. (Continued) Kinetic parameters (Activation energy (Ea) distribution and frequency factors) of 13 solvent-extracted rock samples.**

| Formation | Plover | Plover | Plover | Plover | Plover | Plover |
|---|---|---|---|---|---|---|
| Sample | G011032 | G011038 | G011043 | G011063 | G011064 | G011066 |
| Pre-exponential Factor A (S$^{-1}$) | 1.56E + 14 | 9.90E + 15 | 7.91E + 16 | 5.13E + 14 | 1.22E + 16 | 9.07E + 16 |
| Activation Energy (kcal/mol) | | | | | | |
| 44 | 0.02 | 0 | 0 | 0 | 0 | 0 |
| 45 | 0.28 | 0 | 0 | 0.18 | 0 | 0 |
| 46 | 0.07 | 0 | 0 | 0 | 0 | 0 |
| 47 | 0.58 | 0 | 0 | 0.2 | 0 | 0 |
| 48 | 0.11 | 0 | 0 | 0.11 | 0 | 0 |
| 49 | 1.16 | 0 | 0 | 0.31 | 0 | 0 |
| 50 | 0.03 | 0.22 | 0 | 0.22 | 0 | 0 |
| 51 | 2.18 | 0 | 0 | 0.36 | 0.32 | 0 |
| 52 | 2.39 | 0.21 | 0 | 0.66 | 0 | 0 |
| 53 | 15.69 | 0.16 | 0 | 3.17 | 0.44 | 0 |
| 54 | 25.09 | 0.35 | 0.21 | 8.35 | 0.36 | 0.32 |
| 55 | 17.16 | 0.36 | 0 | 19.32 | 1.24 | 0.15 |
| 56 | 13.98 | 0.8 | 0.13 | 19.43 | 0.87 | 0.06 |
| 57 | 5.25 | 0 | 0.2 | 15.02 | 3.12 | 1.39 |
| 58 | 3.21 | 4.5 | 0.29 | 9.33 | 12.39 | 0.04 |
| 59 | 6.52 | 10.52 | 0 | 6.65 | 16.11 | 0 |
| 60 | 0 | 22.04 | 0 | 2.61 | 15.97 | 7.64 |
| 61 | 1.82 | 14.45 | 3.1 | 4.95 | 11.6 | 19.51 |
| 62 | 0.58 | 14.24 | 19.83 | 1.75 | 9.51 | 16.23 |
| 63 | 1.16 | 6.37 | 17.74 | 1.27 | 6.12 | 13.96 |
| 64 | 0 | 6.52 | 18.25 | 1.42 | 5.05 | 9.37 |
| 65 | 1.41 | 4.19 | 8.67 | 0.29 | 3.47 | 7.75 |
| 66 | 0.07 | 3.58 | 11.13 | 1.86 | 2.89 | 5.08 |
| 67 | 0 | 2.28 | 2.43 | 0 | 2.44 | 4.66 |
| 68 | 1.24 | 2.41 | 7.14 | 0 | 1.26 | 2.8 |
| 69 | 0 | 0.98 | 4.11 | 2.54 | 1.57 | 3.7 |
| 70 | 0 | 1.29 | 0.35 | 0 | 0.95 | 0.73 |
| 71 | 0 | 1.73 | 1.63 | 0 | 0.68 | 2.04 |
| 72 | 0 | 0 | 0.79 | 0 | 1.5 | 0.45 |
| 73 | 0 | 0 | 0.3 | 0 | 0 | 1.25 |
| 74 | 0 | 2.8 | 0.89 | 0 | 0 | 0.22 |
| 75 | 0 | 0 | 0.9 | 0 | 2.14 | 1.18 |
| 76 | 0 | 0 | 0 | 0 | 0 | 0 |
| 77 | 0 | 0 | 0 | 0 | 0 | 0 |
| 78 | 0 | 0 | 1.91 | 0 | 0 | 1.47 |
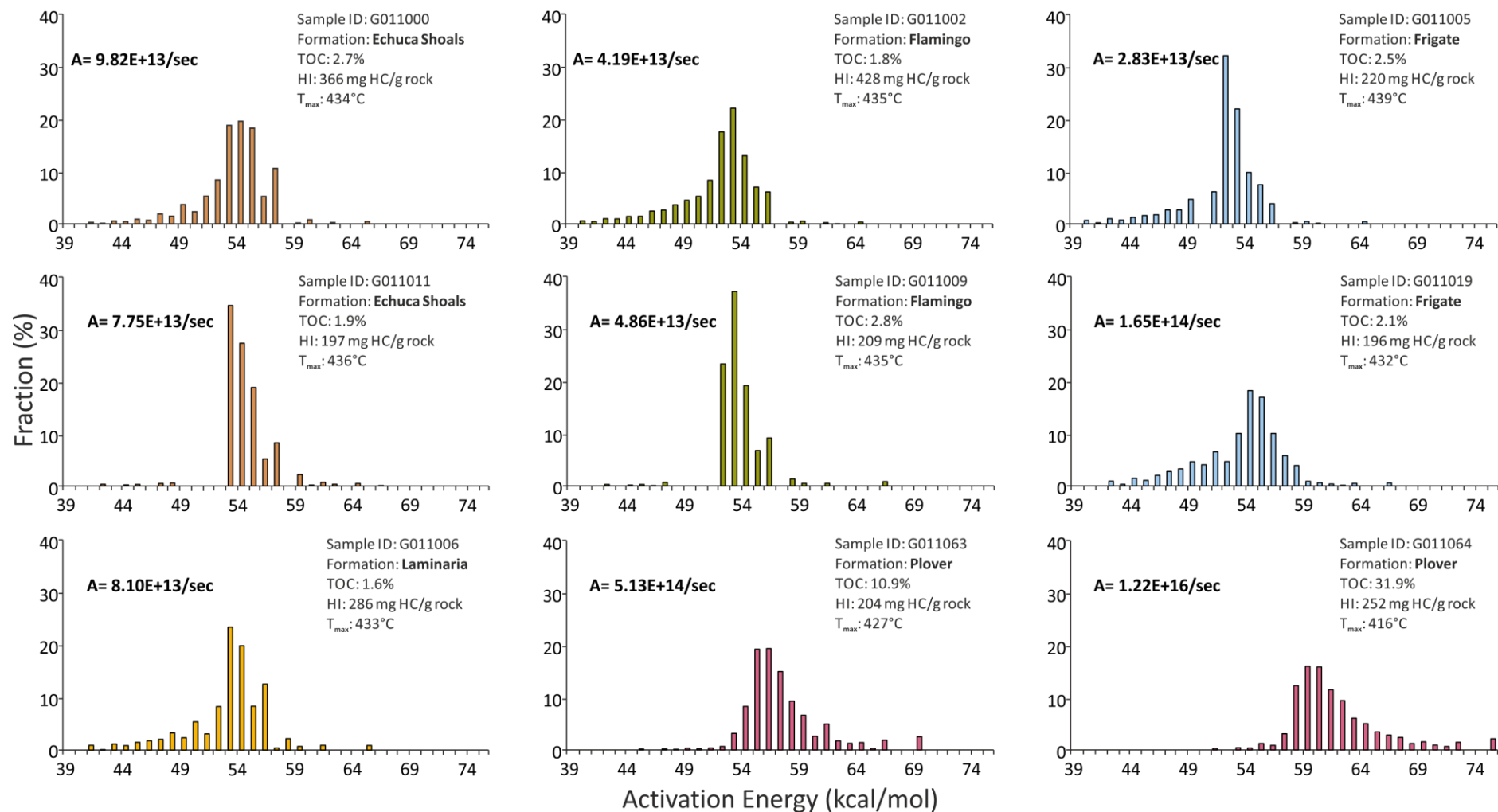
**Figure 5.7. Activation energy distributions and frequency factors of selected samples calculated from open-system pyrolysis at three different heating rates (0.1, 0.7 and 5°C/min).**

*5.5.3.2. Predictions of geological heating conditions*

The derived kinetic parameters enable estimation of the temperatures of hydrocarbon generation extrapolated to geological heating rates. With the assumption of a constant heating rate of 3.3°C/M.a. (**Figure 5.8**), the Laminaria and Frigate formation source rocks are thermally more labile than the other kerogens. The Echuca Shoals Formation enters into the oil generation window (defined as 10% transformation) at variable temperatures ranging from lower (~115°C) for sample G011000 to relatively higher temperatures (~135°C) for sample G011011. Although there are significant differences in the distribution of activation energies and the composition of pyrolysates between the Echuca Shoals (G011011) and the Plover (G011063) kerogens, the onset of bulk petroleum generation from these two samples is predicted to occur at a similar temperature (~135°C), suggesting the more stable character of these kerogens. The high abundance of inertinite in the Echuca Shoals source rocks indicates that oxidation processes may influence the structure of the originally preserved organic material and thus its kinetic properties. Different orders of thermal stability are present, not only between different formations but also within the same organofacies. For example, the Plover Formation coaly kerogen (sample G011064) is the most stable, while Plover Formation shaly kerogen (sample G011063) coming from the same sample (hand-picked) reaches a transformation ratio of 50% at slightly lower temperatures (~10°C). The higher temperatures for the start of the oil window, calculated for the Plover Formation, are typical of Type III kerogens (Quigley et al., 1987). The results presented herein confirm that defined bulk kinetics are directly controlled by the molecular structure of the different kerogens. Using specific compound-derived temperatures such as $C_7$ light hydrocarbon and aromatic hydrocarbon ratios, temperatures at which the oils on the Laminaria High were expelled from the Plover and Laminaria formation source rocks were estimated to cover a range of 127 to 137°C (Preston and Edwards, 2000). When plotting these values against the transformation ratios measured from the bulk kinetic analysis, it appears that all the potential source rocks, except the Plover Formation, could have generated relatively immature oils and contributed to these accumulations. The Laminaria and Corallina oils could not be derived from the Plover Formation at these estimated thermal levels, because over this temperature range the kerogen has not reached any significant transformation (less than 15% transformation). In addition, these authors suspected an additional source input from the Frigate Formation into these oil accumulations. Based on the kinetic parameters measured in this study, and on the thermal maturity of the oils, the coal and the coaly shale of the Plover Formation are unlikely to be major sources of oil. It is concluded that the Upper

Jurassic to Lower Cretaceous formations contain the source rocks most capable of generating the oils reservoired on the Laminaria High.
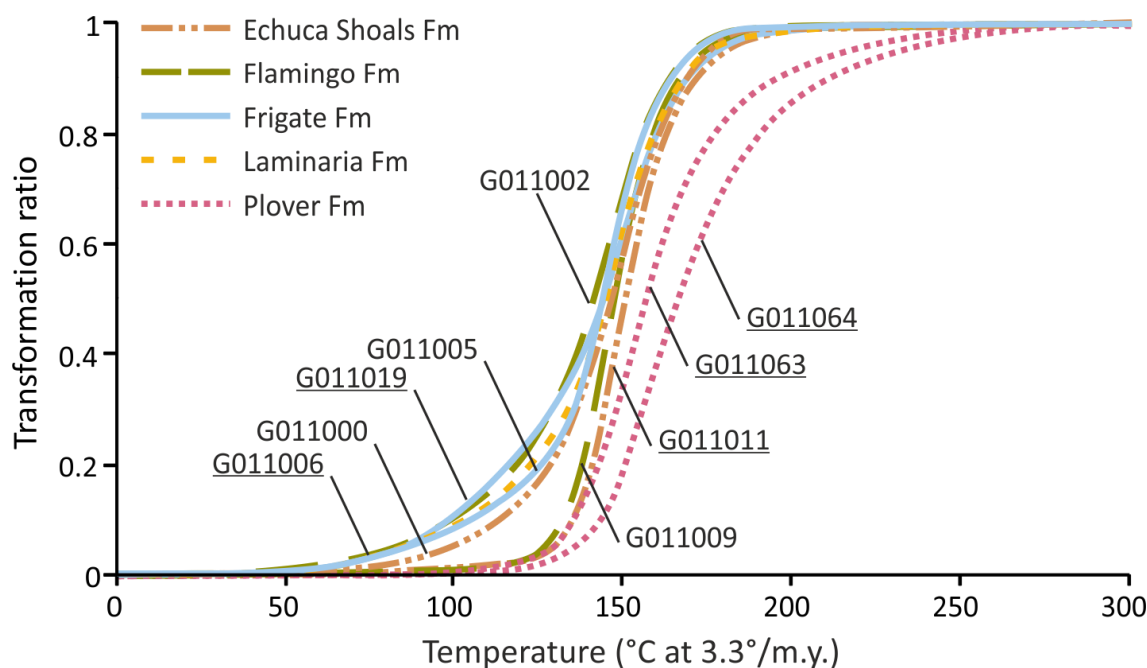


**Figure 5.8. Transformation ratio evolution of the nine selected samples calculated for a geological heating rate of 3.3°C/M.a. The underlined sample codes correspond to those selected for compositional kinetic analysis.**

### 5.5.4. Compositional Kinetics

Artificial maturation using closed-system pyrolysis at a heating rate of 0.7°C/min was performed on the kerogens representative of the different potential source rocks on the Laminaria High. These experiments were established following the methodology of di Primio and Horsfield (2006), with two ($C_1$–$C_5$) and ($C_{6+}$) and four components ($C_1$, $C_2$–$C_5$, $C_6$–$C_{14}$ and $C_{15+}$: **Table 5.6**). The compositional kinetic models with 14 components are shown in **Figure 5.9**. The pyrolysate compositions of the Plover, Laminaria and Frigate formations are relatively similar; the major difference is found within the Echuca Shoals Formation. **Figure 5.10** shows the evolution of gas:oil ratios (GORs) with increasing transformation of kerogen to primary liquid and gaseous hydrocarbons generated from the source rocks on the Laminaria High. GORs predicted for the main oil window, stated to occur at 70% transformation, vary between 160 to 200 $Sm^3/Sm^3$, except for the Echuca Shoals Formation where a ratio of 550 $Sm^3/Sm^3$ was determined. The GORs of petroleum generated from both Plover source rock samples (coaly and shaly) show a progressive increase with increasing transformation ratios and thus with increasing maturity during MSSV pyrolysis. At lower conversion ratios (between 10 and 30% transformation), the

Laminaria, Frigate and Echuca Shoals formation source rocks are characterised by a decrease in GOR. This decrease is more pronounced in the case of the Echuca Shoals Formation and is likely due to the composition of the organic matter in these source rocks.

**Table 5.6. Compositional kinetic data, showing the proportions of the main compounds generated during the primary cracking of selected kerogens by closed-system MSSV pyrolysis of five solvent-extracted rock samples.**

| Formation | Echuca Shoals | Frigate | Laminaria | Plover | Plover |
|---|---|---|---|---|---|
| **Sample ID** | G011011 | G011019 | G011006 | G011063 | G011064 |
| **Kerogen type (from Py-GC)** | Condensate & Gas | PNA_Low Wax | PNA_Low Wax | PNA_High Wax | PNA_High Wax |
| **Oil (%)** | 57.5 | 78.6 | 76.8 | 76.1 | 80.5 |
| **Gas (%)** | 42.6 | 21.4 | 23.3 | 23.9 | 19.5 |
| **$C_1$ (%)** | 23 | 7.4 | 8.4 | 10.2 | 8 |
| **$C_2$-$C_5$ (%)** | 19.6 | 14 | 14.9 | 13.7 | 11.5 |
| **$C_6$-$C_{14}$ (%)** | 42.6 | 50.2 | 35.4 | 33.9 | 31.9 |
| **$C_{15+}$ (%)** | 14.9 | 28.4 | 41.4 | 42.3 | 48.6 |

Interestingly, the Echuca Shoals formation, interpreted to be deposited under an open marine environment, shows significantly higher GOR values when compared with the other source rock samples. At higher conversion rates, the Echuca Shoals and Plover formation source rock samples are characterised by a larger increase in GOR compared to the Laminaria and Frigate samples which only show a slight increase. Overall, this increase in GORs at 90% transformation can be explained by the onset of secondary gas generation reactions in the experimental closed-system pyrolysis (Dieckmann et al., 1998). On the Laminaria High, the Jurassic reservoirs within the Laminaria and Corallina fields contain light oils with low GOR ratios (<45 $Sm^3$/$Sm^3$). Disregarding alteration and leakage processes that might affect the GORs of natural fluids, the low GORs predicted for the Frigate source rock sample under laboratory conditions show a good correlation with those measured on natural fluids. At all transformation ratios, this source rock sample generates fluids with the lowest GOR (65 $Sm^3$/Sm3 at 30% transformation) compared to the other source rocks. However, Newell (1999) explained the occurrence of oils with low GORs in the northern Bonaparte Basin as a result of water washing due to the passage of hot, short-lived and deep-sourced fluids (approximately $90-120^0C$), triggered by the late Miocene to early Pliocene fault reactivation event (O'Brien et al., 1996; Lisk et al., 1998). Thus, it is relatively difficult to correlate the GORs predicted as a function of maturity in this study (considered to be the signature of the initial charge), with those measured on the reservoired crude oils.
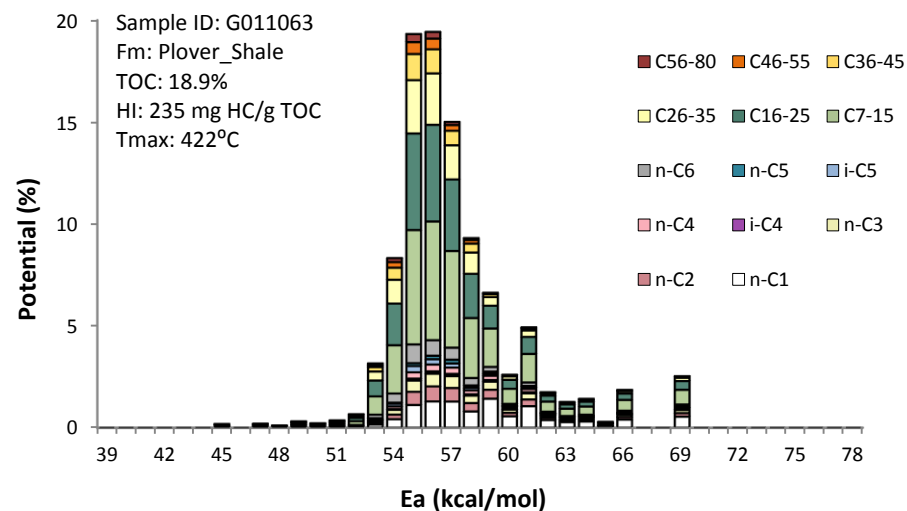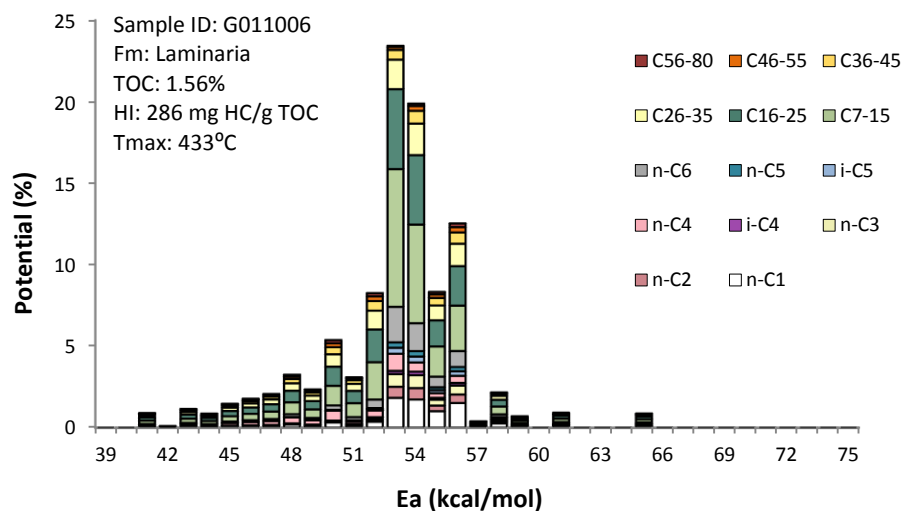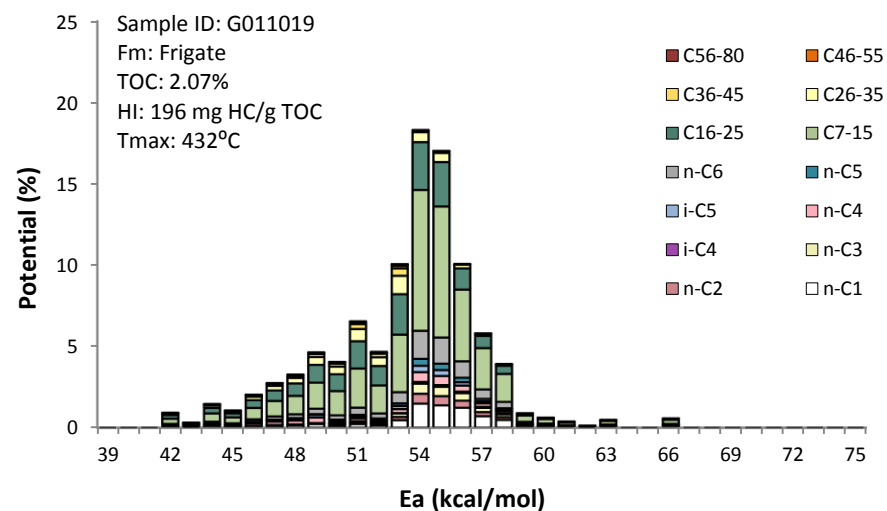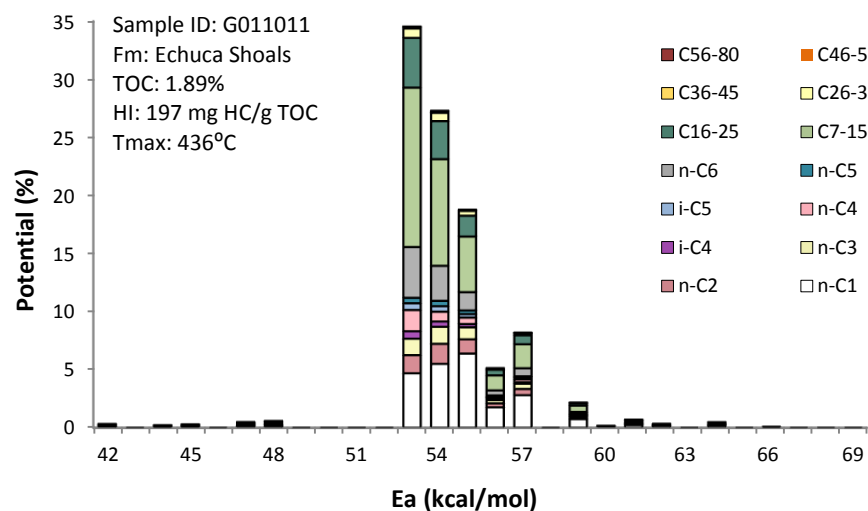
**Figure 5.9. Compositional kinetic models (14 components) for the five selected samples used in this study.**
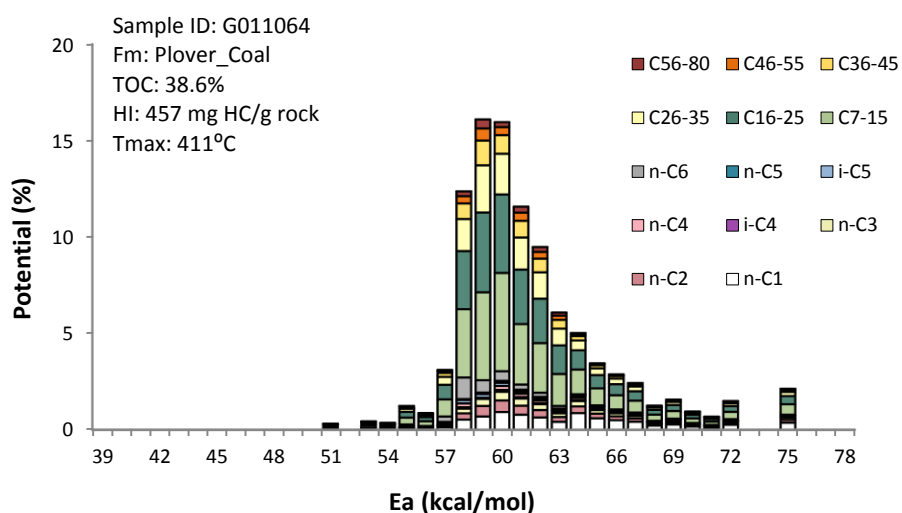
**Figure 5.9. (Continued) Compositional kinetic models (14 components) for the five selected samples used in this study.**

However, it is more likely that the primary products were mainly heavy oils (with low thermal maturity) and light oils, as is supported by fluid inclusion oil geochemistry (2004a; George et al., 2004b), rather than wet gas being trapped first. A later water washing event may then have led to the measured present-day low GORs. Apart from the possible effects of this hydrothermodynamic regime, other processes such as vertical fault seal and top seal leakage (e.g., O'Brien et al., 1999; Jones and Hillis, 2003; Gartrell and Lisk, 2005; Langhi and Borel, 2005) may have led to a total or partial loss of these oils and the under-filled structures on the Laminaria High (George et al., 2004b; Gartrell et al., 2006).

In addition, the model predictions indicate that nearly 80% of the hydrocarbons were generated as oil and 20% as gas, except for the Echuca Shoals Formation which shows the potential to generate a greater proportion of gas (40% gas). The compositional kinetics established for the different source rocks are in generally good agreement with the results obtained from a more detailed study conducted by Preston and Edwards (2000) on the geochemistry of both oils and source rock extracts. These authors concluded that the potential source rocks in the northern Bonaparte Basin are able to generate both liquid and gaseous hydrocarbons. According to these authors, the Echuca Shoals Formation shows a dominance of algal-derived $C_{27}$ steranes, whereas the Frigate, Laminaria and Plover formations reflect stronger land-plant source affinity. The Echuca Shoals Formation is believed to be the most marine-influenced unit that sourced the oils recovered from the Lower Cretaceous Darwin Formation reservoirs (Preston and Edwards, 2000).
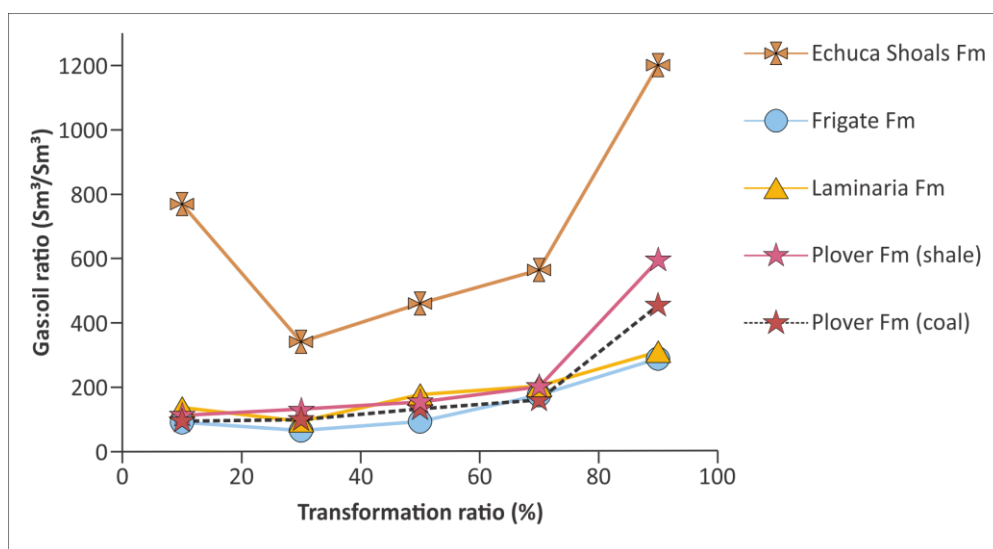
**Figure 5.10. Gas-oil ratios evolution as a function of increasing transformation ratio during MSSV pyrolysis.**

Counterintuitively, however, our results indicate that the marine Echuca Shoals sediments are considered to have greater ability to form gas than the other source rocks. The $C_{15+}$ $n$-alkane fraction **(Table 5.3)** can be used to show the gradual decrease of the influence of terrigenous input from the older to the younger source rocks, reflecting the change in the depositional environments. This fraction is up to 48% for the Plover Formation (coaly sample), yet only 14% for the Echuca Shoals Formation. In addition, despite the differences in their bulk kinetics, shale and coal samples from the Plover Formation show no obvious variation in their compositional kinetics.

### 5.5.5. Carbon isotopic composition of the light hydrocarbons

Under closed-system pyrolysis, the carbon isotopic compositions of generated light hydrocarbons ($C_1$, $C_2$, $C_3$ and $C_4$) are controlled by the degree of transformation of the kerogen **(Table 5.7)**. They generally become more enriched in $^{13}C$ with increasing transformation ratio and hence temperature (Dieckmann et al., 2006). For all the samples, methane is most depleted in $^{13}C$ and with increasing cracking **(Figure 5.11)**, the $^{13}C$ concentrations increase by about 10‰ for the Echuca Shoals **(**sample G011033: **Table 5.7)** to 1‰ for the Plover Formation (sample G011064: **Table 5.7)**.

**Table 5.7. Carbon isotopic composition of $C_1$-$C_4$ hydrocarbons generated by the closed-system MSSV pyrolysis of six solvent-extracted rock samples, measured at different temperatures to represent five transformation ratios (TR).**

| End temp. ($^0C$) | TR (%) | $C_1$ $\delta^{13}C$ (‰ PDB) | $C_2$ $\delta^{13}C$ (‰ PDB) | $C_3$ $\delta^{13}C$ (‰ PDB) | $C_4$ $\delta^{13}C$ (‰ PDB) |
|---|---|---|---|---|---|
| **Echuca Shoals Fm** | | | | | |
| **G011011** | | | | | |
| 379 | 10 | - | - | - | - |
| 401 | 30 | - | - | - | - |
| 414 | 50 | -55.3 | -39.5 | -36.4 | -33.6 |
| 427 | 70 | -50.6 | -37.3 | -35.2 | -32.6 |
| 450 | 90 | -45.6 | -35.6 | -33.7 | -31.4 |
| **Flamingo Fm** | | | | | |
| **G011009** | | | | | |
| 376 | 10 | -47.5 | - | - | - |
| 399 | 30 | -44.0 | -35.4 | -33.4 | - |
| 412 | 50 | -48.7 | -35.9 | -33.8 | -31.4 |
| 425 | 70 | -47.1 | -35.1 | -33.5 | -31.7 |
| 446 | 90 | -39.7 | -33.7 | -32.5 | -30.8 |
| **Frigate Fm** | | | | | |
| **G011019** | | | | | |
| 321 | 10 | - | - | - | - |
| 370 | 30 | - | - | - | - |
| 396 | 50 | -42.2 | -32.6 | -31.7 | -30.3 |
| 415 | 70 | -40.1 | -32.8 | -31.8 | -30.1 |
| 441 | 90 | -38.4 | -32.7 | -31.7 | -30.3 |
| **Laminaria Fm** | | | | | |
| **G011006** | | | | | |
| 331 | 10 | - | - | - | - |
| 380 | 30 | -44.2 | - | - | - |
| 402 | 50 | -40.4 | -33.4 | -32.6 | -32.2 |
| 420 | 70 | -38.7 | -33.4 | -32.1 | -30.7 |
| 448 | 90 | -38.3 | -33.2 | -32.2 | -30.6 |
| **Plover Fm (Shale)** | | | | | |
| **G011063** | | | | | |
| 373 | 10 | -37.1 | - | - | - |
| 396 | 30 | -35.4 | -29.2 | -28.0 | - |
| 412 | 50 | -35.6 | -29.0 | -27.7 | - |
| 430 | 70 | -36.6 | -28.9 | -27.7 | -27.1 |
| 471 | 90 | -34.9 | -27.3 | -26.3 | -25.0 |
| **Plover Fm (Coal)** | | | | | |
| **G011064** | | | | | |
| 368 | 10 | -34.0 | -27.5 | - | - |
| 393 | 30 | -34.7 | -27.9 | -26.8 | - |
| 410 | 50 | -34.4 | -27.7 | -26.4 | -25.9 |
| 432 | 70 | -34.8 | -27.0 | -25.9 | -25.3 |
| 479 | 90 | -33.9 | -25.9 | -24.8 | -23.1 |

The carbon isotopic ratio determined for methane generally shows a gradual increase at a transformation ratio of 50% which corresponds to a starting temperature (during closed-system pyrolysis) of about 400°C. This observation is valid for all the investigated samples, except for the two samples from the Plover Formation where this increase is found at higher transformation ratios (70%). For the Plover coaly sample, the isotopic ratio of methane shows a slight decrease at low transformation ratios from -34.0‰ at 10% and -34.7‰ at 30%. Similarly, the $\delta^{13}C$ values of ethane, propane and butane becomes heavier at higher transformation ratios. Data obtained from this study conforms to previous published work (e.g., Arneth and Matzigkeit, 1986; Andresen et al., 1993; Lorant et al., 1998) in that under closed system conditions and at higher ratios of kerogen conversion into hydrocarbons, isotopically heavier gaseous compounds such as methane, ethane, propane and butane are generated. Since all of the studied samples are thermally immature, the differences observed

between the five samples can be related to the variability in the organic matter type, as influenced by the depositional environments of the source rocks. Oils in Darwin Formation reservoirs show source affinities to the Echuca Shoals Formation and are characterised by strongly depleted $\delta^{13}C$ values (Preston and Edwards, 2000). The results demonstrate that with increasing thermal maturity of the Echuca Shoals kerogen, there is a corresponding increase in the carbon isotope ratios of all the produced light hydrocarbons, indicating an isotopic homogeneity of the precursors from which these compounds are derived. Furthermore, the isotopic ratios of the $C_1-C_4$ hydrocarbons generated from the Plover Formation samples are heavier compared to the other source rocks from the Frigate, Flamingo and Echuca Shoals formations, often by > 5‰ at the same transformation ratio. The isotopic ratio of ethane has been used to distinguish between coal-derived and oil-associated gases (Dai et al., 2009). The $\delta^{13}C$ measured for the ethane (> −28‰) in the Plover Formation coal are typical for coal-derived gas.
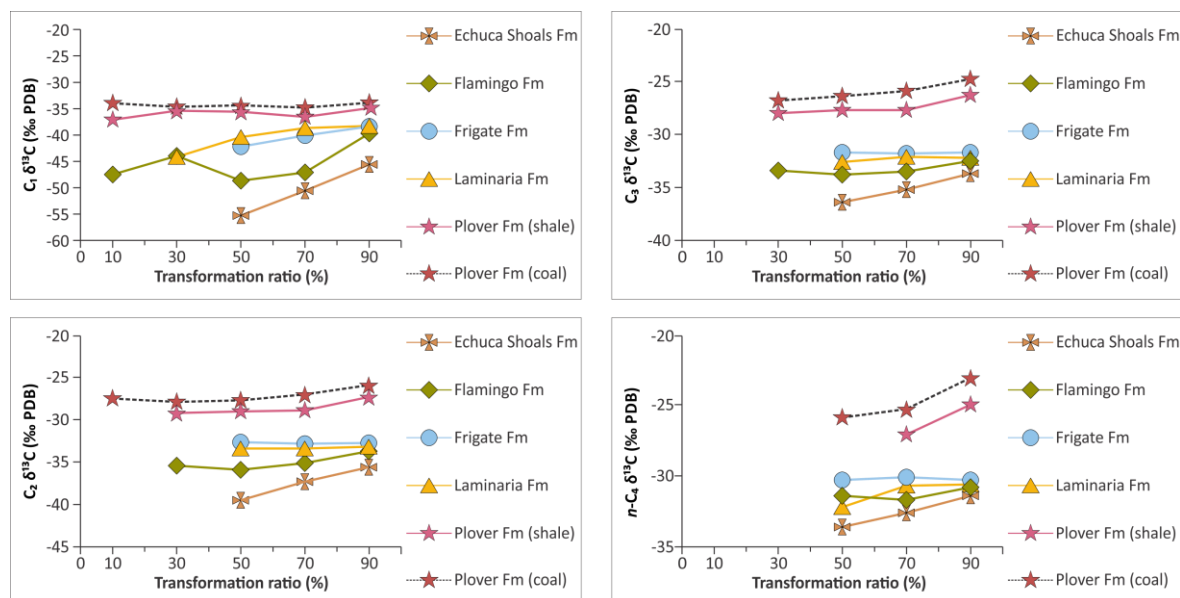


**Figure 5.11. Stable carbon isotopic distributions of methane, ethane, propane and *n*-butane generated from pyrolysis experiments in a closed-system as function of increasing transformation ratio.**

The isotopic ratios from artificial maturation of the organic matter preserved in the source rocks were compared to the ratios of the natural gases from the Laminaria High (**Table 5.8**). The Laminaria and Corallina natural gases are isotopically relatively similar to one another, but have values that are significantly different to those generated from the closed-system pyrolysis of most of the formations. Since the natural gases could be generated at different stages of thermal maturity from multiple source rocks, it seems to be relatively difficult to compare our calculations of carbon isotope ratios with those measured in these accumulations. For instance, methane in the natural reservoirs is unlikely to be derived from

only one source rock. However, the isotopic ratios measured for the ethane, propane and butane could be correlated best with the shale sample from the Plover source rock. When the effects of maturation, migration, and alteration processes are taken into consideration, this suggests that the light oils on the Laminaria High may be derived from all the studied source rocks, while gas is mainly generated from the shale units within the Plover Formation, where they are sufficiently mature. Moreover, the Plover Formation is thought to have generated a significant gas charge and lesser amounts of oil throughout the northern Bonaparte Basin (Edwards et al., 2004).

**Table 5.8. Carbon isotopic composition of $C_1$-$C_4$ hydrocarbons in natural gases from fields in the Laminaria High, taken from the Geoscience Australia database.**

| Well | $C_1$ $\delta^{13}C$ (‰ PDB) | $C_2$ $\delta^{13}C$ (‰ PDB) | $C_3$ $\delta^{13}C$ (‰ PDB) | $C_4$ $\delta^{13}C$ (‰ PDB) |
|------|------|------|------|------|
| Corallina 1 | -44.5 | -29.2 | -28.5 | -28 |
| Laminaria 1 | -44.9 | -30 | -28.1 | -27.8 |
| Laminaria 2 | -45.4 | -30.3 | -28.1 | -27.8 |
| Laminaria 4 | -44.8 | -30.3 | -28.5 | -28.4 |
| Laminaria 5 | -45 | -30 | -28.2 | -28.2 |
| Laminaria 6 | -45.3 | -30.4 | -28.1 | -27.9 |

## 5.6.    Conclusions

The investigation of Mesozoic source rocks from the Bonaparte Basin has enabled a better understanding of the origin of the oil accumulations on, and adjacent to, the Laminaria High. TOC and Rock−Eval pyrolysis data show that the studied source rocks have fair to excellent potential for petroleum generation. The highest genetic potential and TOC values occur in the Middle Jurassic coals and shales of the Plover Formation. For all the investigated source rocks, including those from the Plover, Laminaria, Frigate, Flamingo and Echuca Shoals formations, their typically moderate hydrogen indices (less than 400 mg HC/g TOC) suggest that they comprise Type II to Type III kerogen with variable potential for oil and gas generation.

Open-system pyrolysis-gas chromatography data indicate that all of the Upper Jurassic to Lower Cretaceous samples can generate both low wax P-N-A oils and wet gases, except for the Flamingo Formation which generates mainly P-N-A oils with low wax content. In addition to producing low wax P-N-A oils, other organic facies within the Plover Formation can also produce high wax P-N-A oils and wet gas.

Artificial maturation by open-system pyrolysis demonstrates that the majority of the samples generate petroleum products within broad temperature ranges and activation energies. Exceptions are found within the Flamingo and the Echuca Shoals formations which both exhibit more homogeneous kerogen. The coals and shales of the Plover Formation show

high levels of kinetic stability compared to the Upper Jurassic to Lower Cretaceous source rocks. Temperatures as high as 150°C are required to release petroleum from these facies at 70% of kerogen transformation. The oil maturity measured by Preston and Edwards (2000) can be correlated with that measured for the Flamingo, Frigate and Laminaria kerogens in this study. Thus, the Plover Formation is unlikely to be the source of oils in the Laminaria and Corallina fields. However, the definite exclusion of an additional contribution from this source rock cannot be made given the wide variability in organic facies.

Based on the compositional kinetics, mainly heavy oils can be generated from the source rocks on the Laminaria High. At higher rates of kerogen transformation, light oils are formed from the shale and coals of the Plover Formation. The most marine Echuca Shoals Formation source rock shows the potential to generate either light oils or wet gases. The predicted gas to oil ratios, are relatively higher than those measured in the petroleum accumulations. This is because they are not solely dependent on source rock properties, but are also controlled by other processes such as alteration (water washing) and vertical leakage.

The carbon isotope ratios of the artificially generated light hydrocarbons indicate that the gases are most likely the result of the mixing of gases generated from multiple source rocks at different levels of thermal maturity. Further processes such as phase fractionation, secondary cracking of oils, and the possible limitations imposed by the heating rates and type of system used for the artificial maturation need to be considered when interpreting these data.

This paper serves as an example of the different steps that lead to the input parameters required for 3D petroleum systems modelling, and thus enables an evaluation of the absolute timing of oil and gas generation and pre-drill prediction of petroleum quality.

## 5.7. Acknowledgments

# 5.8. References

AGSO, 1994. Deep reflections on the North West Shelf: changing perceptions of basin formation, in: Purcell, P.G., Purcell, R.R. (Eds.), The Sedimentary Basins of Western Australia: Proceedings of the Petroleum Exploration Society of Australia Symposium, Perth, Western Australia, pp. 63-76.

Andresen, B., Barth, T., Irwin, H., 1993. Yields and carbon isotopic composition of pyrolysis products from artificial maturation processes. Chemical Geology 106, 103-119.

Arditto, P., 1996. A sequence stratigraphic study of the Callovian fluvio-deltaic to marine succession within the ZOCA region. Australian Petroleum Production and Exploration Association Journal 36(1), 269-283.

Arneth, J.D., Matzigkeit, U., 1986. Variations in the carbon isotope composition and production yield of various pyrolysis products under open and closed system conditions. Organic Geochemistry 10, 1067-1071.

Baillie, P., Powell, C.M.A., Li, Z., Ryall, A., 1994. The tectonic framework of Western Australia's Neoproterozoic to Recent sedimentary basins, in: Purcell, P.G., Purcell, R.R. (Eds.), The Sedimentary Basins of Western Australia: Proceedings of the Petroleum Exploration Society of Australia Symposium, Perth, Western Australia, pp. 45-62.

Baxter, K., Cooper, G., Hill, K., O'Brien, G., 1999. Late Jurassic subsidence and passive margin evolution in the Vulcan Sub-basin, north-west Australia: constraints from basin modelling. Basin Research 11, 97-111.

Bordenave, M.L., 1993. Applied petroleum geochemistry. Editions Technip, Paris, 524 p.

Borel, G., Stampfli, G., 2002. Geohistory of the North West Shelf: a tool to assess the Palaeozoic and Mesozoic motion of the Australian Plate, in: Keep, M., Moss, S.J. (Eds.), The Sedimentary Basins of Western Australia 3: Proceedings of Petroleum Exploration Society of Australia Symposium, Perth, Western Australia, pp. 119-128.

Botten, P., Wulff, K., 1990. Exploration potential of the Timor Gap Zone of Cooperation. Australian Petroleum Exploration Association Journal 30(1), 53-68.

Bradshaw, M., Yeates, A., Beynon, R., Brakel, A., Langford, R., Totterdell, J., Yeung, M., 1988. Palaeogeographic evolution of the North West Shelf region, in: Purcell, P.G., Purcell, R.R. (Eds.), The North West Shelf, Australia: Proceedings of the Petroleum Exploration Society of Australia Symposium, Perth, Western Australia, pp. 29-54.

Brincat, M., O'Brien, G., Lisk, M., De Ruig, M., George, S., 2001. Hydrocarbon charge history of the northern Londonderry: Implications for trap integrity and future prospectivity. Australian Petroleum Production and Exploration Association Journal 41(1), 483-496.

Burnham, A.K., Braun, R.L., Gregg, H.R., Samoun, A.M., 1987. Comparison of methods for measuring kerogen pyrolysis rates and fitting kinetic parameters. Energy & Fuels 1, 452-458.

Burnham, A.K., Braun, R.L., Samoun, A.M., 1988. Further comparison of methods for measuring kerogen pyrolysis rates and fitting kinetic parameters. Organic Geochemistry 13, 839-845.

Cadman, S.J., Temple, P.R., 2003. Bonaparte Basin, NT, WA, AC & JPDA, Australian Petroleum Accumulations Report 5, 2nd Edition, Geoscience Australia, Canberra, 335 p.

Castillo, D., Hillis, R., Asquith, K., Fischer, M., 1998. State of stress in the Timor Sea area, based on deep wellbore observations and frictional failure criteria: Application to fault-trap integrity, in: Purcell, P.G.,

Purcell, R.R. (Eds.), The Sedimentary Basins of Western Australia 2: Proceedings of Petroleum Exploration Society of Australia Symposium, Perth, Western Australia, pp. 325-341.

Chen, G., Hill, K.C., Hoffman, N., O'Brien, G.W., 2002. Geodynamic evolution of the Vulcan Sub-basin, Timor Sea, northwest Australia: a pre-compression New Guinea analogue? Australian Journal of Earth Sciences 49, 719-736.

ConocoPhillips, 2008. Firebird-1 Well Completion Report Volume 2: Interpretive Data. Conocopillips (03-12) Pty Ltd, Document No: Fire-1/013. (unpublished).

Cooper, G.T., Barnes, C.R., Bourne, J.D., Channon, G.J., 1998. Hydrocarbon leakage on the North West Shelf: New information from the integration of airborne laser fluorosensor (ALF) and structural data, in: Purcell, P.G., Purcell, R.R. (Eds.), The Sedimentary Basins of Western Australia 2: Proceedings of the Petroleum Exploration Society of Australia Symposium, Perth, Western Australia, pp. 255-271.

Cornford, C., Gardner, P., Burgess, C., 1998. Geochemical truths in large data sets. I: Geochemical screening data. Organic Geochemistry 29, 519-530.

Dai, J., Ni, Y., Zou, C., Tao, S., Hu, G., Hu, A., Yang, C., Tao, X., 2009. Stable carbon isotopes of alkane gases from the Xujiahe coal measures and implication for gas-source correlation in the Sichuan Basin, SW China. Organic Geochemistry 40, 638-646.

de Ruig, M.J., Trupp, M., Bishop, D.J., Kuek, D., Castillo, D.A., 2000. Fault architecture and the mechanics of fault reactivation in the Nancar Trough/Laminaria area of the Timor Sea, northern Australia. Australian Petroleum Production and Exploration Association Journal 40(1), 174-193.

di Primio, R., Horsfield, B., 2006. From petroleum-type organofacies to hydrocarbon phase prediction. American Association of Petroleum Geologists Bulletin 90, 1031-1058.

Dieckmann, V., 2005. Modelling petroleum formation from heterogeneous source rocks: the influence of frequency factors on activation energy distribution and geological prediction. Marine and Petroleum Geology 22, 375-390.

Dieckmann, V., Schenk, H.J., Horsfield, B., Welte, D.H., 1998. Kinetics of petroleum generation and cracking by programmed-temperature closed-system pyrolysis of Toarcian Shales. Fuel 77, 23-31.

Dieckmann, V., Ondrak, R., Cramer, B., Horsfield, B., 2006. Deep basin gas: New insights from kinetic modelling and isotopic fractionation in deep-formed gas precursors. Marine and Petroleum Geology 23, 183-199.

Dyt, C.P., Langhi, L., Bailey, W.P., 2012. Automating conceptual models to easily assess trap integrity and oil preservation risks associated with fault reactivation. Marine and Petroleum Geology 30, 81-97.

Edwards, D.S., Summons, R.E., Kennard, J., Nicoll, R., Bradshaw, J., Bradshaw, M., Foster, C., O'Brien, G., Zumberge, J., 1997. Geochemical characterisation of Palaeozoic petroleum systems in north-western Australia. Australian Petroleum Production and Exploration Association Journal 37(1), 351-379.

Edwards, D.S., Preston, J.C., Kennard, J.M., Boreham, C.J., van Aarssen, B.G.K., Summons, R.E., Zumberge, J.E., 2004. Geochemical characteristics of hydrocarbons from the Vulcan Sub-basin, western Bonaparte Basin, Australia, in: Ellis, G.K., Baillie, P.W., Munson, T.J. (Eds.), Timor Sea Petroleum Geoscience: Proceedings of the Timor Sea Symposium, Darwin, Northern Territory, pp. 169-201.

Espitalié, J., 1986. Use of Tmax as a maturation index for different types of organic matter. Comparison with vitrinite reflectance. Thermal modeling in sedimentary basins: Paris, Editions Technip, pp. 475-496.

Espitalié, J., Laporte, J.L., Madec, M., Marquis, F., Leplat, P., Paulet, J., Boutefeu, A., 1977. Méthode rapide de caractérisation des roches mères, de leur potentiel pétrolier et de leur degré d'évolution. Revue Institut Francais du Petrole 32, pp. 23-42.

Faiz, M., Wilkins, R., Sherwood, N., Buckingham, C., Russell, N., Kinealy, K., 1998. Perhydrous vitrinite in the source rocks of the Western Timor Sea region. APCRC Confidential Report No.320, 223 p.

Gartrell, A., Lisk, M., 2005. Potential new method for paleostress estimation by combining by combining 3D fault restoration and fault slip inversion techniques: First test on the Skua field, Timor Sea, in: Boult, P., Kaldi, J.K. (Eds.), Evaluating fault and cap rock seals. AAPG Hedberg Series, no. 2, pp. 23-36.

Gartrell, A., Bailey, W.R., Brincat, M., 2006. A new model for assessing trap integrity and oil preservation risks associated with postrift fault reactivation in the Timor Sea. American Association of Petroleum Geologists Bulletin 90, 1921-1944.

George, S.C., Greenwood, P.F., Logan, G.A., Quezada, R.A., Pang, L.S.K., Lisk, M., Krieger, F.W., Eadington, P., 1997. Comparison of palaeo oil charges with currently reservoired hydrocarbons using molecular and isotopic analyses of oil-bearing fluid inclusions: Jabiru oil field, Timor Sea. Australian Petroleum Production and Exploration Association Journal 37(1), 490-504.

George, S.C., Volk, H., Ruble, T.E., Brincat, M.P., 2002. Evidence for a new oil family in the Nancar Trough area, Timor Sea. Australian Petroleum Production and Exploration Association Journal 42(1), 387–404.

George, S.C., Lisk, M., Eadington, P., 2004a. Fluid inclusion evidence for an early, marine-sourced oil charge prior to gas-condensate migration, Bayu-1, Timor Sea, Australia. Marine and Petroleum Geology 21, 1107-1128.

George, S.C., Ruble, T.E., Volk, H., Lisk, M., Brincat, M.P., Dutkiewicz, A., Ahmed, M., 2004b. Comparing the geochemical composition of fluid inclusion and crude oils from wells on the Laminaria High, Timor Sea, in: Ellis, G.K., Baillie, P.W., Munson, T.J. (Eds.), Timor Sea Petroleum Geoscience: Proceedings of the Timor Sea Symposium, Darwin, Northern Territory Geological Survey, Special Publication 1, pp. 203–230.

Gorter, J., Kirk, A., 1995. The Kimmeridgian marl in the Timor Sea: relevance to regional and geological evolution and possible hydrocarbon plays. Australian Petroleum Production and Exploration Association Journal 35(1), 152-168.

Harrowfield, M., Keep, M., 2005. Tectonic modification of the Australian North-West Shelf: episodic rejuvenation of long-lived basin divisions. Basin Research 17, 225-239.

Hillis, R., 1998. Mechanisms of dynamic seal failure in the Timor Sea and central North Sea, in: Purcell, P.G., Purcell, R.R. (Eds.), The Sedimentary Basins of Western Australia 2: Proceedings of the Petroleum Exploration Society of Australia Symposium Perth, Western Australia, pp. 313-324.

Horsfield, B., 1989. Practical criteria for classifying kerogens: some observations from pyrolysis-gas chromatography. Geochimica et Cosmochimica Acta 53, 891-901.

Horsfield, B., Dueppenbecker, S.J., 1991. The decomposition of Posidonia Shale and Green River Shale kerogens using microscale sealed vessel (MSSV) pyrolysis. Journal of Analytical and Applied Pyrolysis 20, 107-123.

Horsfield, B., Disko, U., Leistner, F., 1989. The micro-scale simulation of maturation: outline of a new technique and its potential applications. Geologische Rundschau 78, 361-374.

Jones, R.M., Hillis, R.R., 2003. An integrated, quantitative approach to assessing fault-seal risk. American Association of Petroleum Geologists Bulletin 87, 507-524.

Keep, M., Bishop, A., Longley, I., 2000. Neogene wrench reactivation of the Barcoo Sub-basin, northwest Australia: implications for Neogene tectonics of the northern Australian margin. Petroleum Geoscience 6, 211-220.

Keep, M., Clough, M., Langhi, L., 2002. Neogene tectonic and structural evolution of the Timor Sea region, NW Australia, in: Keep, M., Moss, S. (Eds.), The Sedimentary Basins of Western Australia 3: Proceedings of the Petroleum Exploration Society of Australia Symposium, Perth, Western Australia, pp. 341-353.

Keep, M., Harrowfield, M., Crowe, W., 2007. The Neogene tectonic history of the North West Shelf, Australia. Exploration Geophysics 38, 151-174.

Kennard, J., Deighton, I., Edwards, D., Boreham, C., Barrett, A., 2002. Subsidence and thermal history modelling: new insights into hydrocarbon expulsion from multiple petroleum systems in the Petrel Sub-basin, Bonaparte Basin, in: Keep, M., Moss, S. (Eds.), The Sedimentary Basins of Western Australia 3: Proceedings of the Petroleum Exploration Society of Australia Symposium, Perth, Western Australia, pp. 409-437.

Kennard, J.M., Deighton, I., Edwards, D.S., Colwell, J.B., O'Brien, G.W., Boreham, C.J., 1999. Thermal history modelling and transient heat pulses: new insights into hydrocarbon expulsion and 'hot flushes' in the Vulcan Sub-basin, Timor Sea. Australian Petroleum Production and Exploration Association Journal 39(1), 177-207.

Kivior, T., Kaldi, J.G., Lang, S.C., 2002. Seal potential in Cretaceous and Late Jurassic rocks of the Vulcan Sub-basin, North West Shelf Australia. Australian Petroleum Production and Exploration Association Journal 42(1), 203-224.

Labutis, V.R., Ruddock, A.D., Calcraft, A.P., 1998. Stratigraphy of the southern Sahul Platform. Australian Petroleum Production and Exploration Association Journal 38(1), 115-136.

Lafargue, E., Marquis, F., Pillot, D., 1998. Rock-Eval 6 applications in hydrocarbon exploration, production, and soil contamination studies. Oil & Gas Science and Technology 53, 421-437.

Langhi, L., Borel, G.D., 2005. Influence of the Neotethys rifting on the development of the Dampier Sub-basin (North West Shelf of Australia), highlighted by subsidence modelling. Tectonophysics 397, 93-111.

Langhi, L., Zhang, Y., Gartrell, A., Underschultz, J., Dewhurst, D., 2010. Evaluating hydrocarbon trap integrity during fault reactivation using geomechanical three-dimensional modeling: An example from the Timor Sea, Australia. American Association of Petroleum Geologists Bulletin 94, 567-591.

Langhi, L., Ciftci, N.B., Borel, G.D., 2011. Impact of lithospheric flexure on the evolution of shallow faults in the Timor foreland system. Marine Geology 284, 40-54.

Larter, S.R., 1984. Application of analytical pyrolysis techniques to kerogen characterization and fossil fuel exploration/exploitation, in: Voorhees, K.J. (Ed.), Analytical Pyrolysis: Methods and application, Butterworth, London, pp. 212-275.

Larter, S.R., Senftle, J.T., 1985. Improved kerogen typing for petroleum source rock analysis. Nature 318, 277-280.

Lisk, M., Eadington, P., 1994. Oil migration in the Cartier Trough, Vulcan Sub-basin, in: Purcell, P.G., Purcell, R.R. (Eds.), The Sedimentary Basins of Western Australia: Proceedings of the Petroleum Exploration Society of Australia, Perth, Western Australia, pp. 301-312.

Lisk, M., Eadington, P.J., O'Brien, G.W., 1998. Unravelling complex filling histories by constraining the timing of events which modify oil fields after initial charge. Geological Society, London, Special Publications 144, 189-203.

Lisk, M., Faiz, M.M., Bekele, E.B., Ruble, T.E., 2000. Transient fluid flow in the Timor Sea, Australia: implications for prediction of fault seal integrity. Journal of Geochemical Exploration 69–70, 607-613.

Londoño, J., Lorenzo, J.M., 2004. Geodynamics of continental plate collision during late tertiary foreland basin evolution in the Timor Sea: constraints from foreland sequences, elastic flexure and normal faulting. Tectonophysics 392, 37-54.

Longley, I.M., Buessenschuett, C., Clydsdale, L., Cubitt, C.J., Davis, R.C., Johnson, M.K., Marshall, N.M., Murray, A.P., Somerville, R., Spry, T.B., Thompson, N., 2002. The North West Shelf of Australia: a Woodside perspective, in: Keep, M., Moss, S. (Eds.), The Sedimentary Basins of Western Australia 3: Proceedings of Petroleum Exploration Society of Australia Symposium, Perth, Western Australia, pp. 27-88.

Lorant, F., Prinzhofer, A., Behar, F., Huc, A.-Y., 1998. Carbon isotopic and molecular constraints on the formation and the expulsion of thermogenic hydrocarbon gases. Chemical Geology 147, 249-264.

Mahlstedt, N., Horsfield, B., Dieckmann, V., 2008. Second order reactions as a prelude to gas generation at high maturity. Organic Geochemistry 39, 1125-1129.

McIntyre, C., Stickland, P., 1998. Sequence stratigraphy and hydrocarbon prospectivity of the Campanian to Eocene succession, Northern Bonaparte Basin, Australia. Australian Petroleum Production and Exploration Association Journal 38(1), 313-338.

Müller, D., Mihut, D., Baldwin, S., 1998. A new kinematic model for the formation and evolution of the west and northwest Australian margin, in: Purcell, P.G., Purcell, R.R. (Eds.), The Sedimentary Basins of Western Australia 2: Proceedings of Petroleum Exploration Society of Australia Symposium, Perth, Western Australia, pp. 473-490.

Newell, N.A., 1999. Bonaparte and Browse basins-Water washing in the Northern Bonaparte Basin. Australian Petroleum Production and Exploration Association Journal 39(1), 227-247.

O'Brien, G.W., 1993. Some ideas on the rifting history of the Timor Sea from the integration of deep crustal seismic and other data. Petroleum Exploration Society of Australia Journal 21, 95-113.

O'Brien, G.W., Lisk, M., Duddy, I., Eadington, P., Cadman, S., Fellows, M., 1996. Late Tertiary fluid migration in the Timor Sea: a key control on thermal and diagenetic histories. Australian Petroleum Production and Exploration Association Journal 36(1), 399-427.

O'Brien, G.W., Quaife, P., Cowley, R., Morse, M., Wilson, D., Fellows, M., Lisk, M., 1998. Evaluating trap integrity in the Vulcan sub-basin, Timor Sea, Australia, using integrated remote-sensing geochemical technologies, in: Purcell, P.G., Purcell, R.R. (Eds.), The Sedimentary Basins of Western Australia 2: Proceedings of Petroleum Exploration Society of Australia Symposium, Perth, Western Australia, pp. 237-254.

O'Brien, G.W., Lisk, M., Duddy, I.R., Hamilton, J., Woods, P., Cowley, R., 1999. Plate convergence, foreland development and fault reactivation: primary controls on brine migration, thermal histories and trap breach in the Timor Sea, Australia. Marine and Petroleum Geology 16, 533-560.

Pattillo, J., Nicholls, P.J., 1990. A tectonostratigraphic framework for the Vulcan Graben, Timor Sea region. Australian Petroleum Exploration Association Journal 30(1), 27-51.

Peters, K.E., Cassa, M.R., 1994. Applied source-rock geochemistry. In: Magoon, L.B., Dow, W.G. (Eds.), The Petroleum System: From Source to Trap. American Association of Petroleum Geologists Bulletin 60, 93-120.

Preston, J.C., Edwards, D.S., 2000. The petroleum geochemistry of oils and source-rocks from the northern Bonaparte Basin, offshore northern Australia. Australian Petroleum Production and Exploration Association Journal 40(1), 257-282.

Quigley, T., Mackenzie, A., Gray, J., 1987. Kinetic theory of petroleum generation, in: Tissot, B. (Ed.), Migration of hydrocarbons in sedimentary basins, Paris, France. Editions Technip, Colloques et Seminaires 45, pp. 649-665.

Saiz-Jimenez, C., 1995. The origin of alkylbenzenes and thiophenes in pyrolysates of geochemical samples. Organic Geochemistry 23, 81-85.

Schaefer, R.G., Schenk, H.J., Hardelauf, H., Harms, R., 1990. Determination of gross kinetic parameters for petroleum formation from Jurassic source rocks of different maturity levels by means of laboratory experiments. Organic Geochemistry 16, 115-120.

Shuster, M.W., Eaton, S., Wakefield, L.L., Kloosterman, H.J., 1998. Neogene tectonics, greater Timor Sea, offshore Australia: implications for trap risk. Australian Petroleum Production and Exploration Association Journal 38(1), 351-379.

Sinninghe Damsté, J.S., Kock-Van Dalen, A.C., de Leeuw, J.W., Schenck, P.A., 1988. Identification of homologous series of alkylated thiophenes, thiolanes, thianes and benzothiophenes present in pyrolysates of sulphur-rich kerogens. Journal of Chromatography A 435, 435-452.

Sinninghe Damsté, J.S., Kohnen, M.E.L., Horsfield, B., 1998. Origin of low-molecular-weight alkylthiophenes in pyrolysates of sulphur-rich kerogens as revealed by micro-scale sealed vessel pyrolysis. Organic Geochemistry 29, 1891-1903.

Smith, G.C., Tilbury, L.A., Chatfield, A., Senycia, P., Thompson, N., 1996. Laminaria: a new Timor Sea discovery. Australian Petroleum Production and Exploration Association Journal 36(1), 12-29.

Tissot, B.P., Welte, D.H., 1984. Petroleum Formation and Occurrence. Springer Verlag, Berlin, 699 p.

Ungerer, P., 1990. State of the art of research in kinetic modelling of oil formation and expulsion. Organic Geochemistry 16, 1-25.

van de Meent, D., Brown, S.C., Philp, R.P., Simoneit, B.R.T., 1980. Pyrolysis-high resolution gas chromatography and pyrolysis gas chromatography-mass spectrometry of kerogens and kerogen precursors. Geochimica et Cosmochimica Acta 44, 999-1013.

Vandenbroucke, M., Behar, F., Rudkiewicz, J., 1999. Kinetic modelling of petroleum formation and cracking: implications from the high pressure/high temperature Elgin Field (UK, North Sea). Organic Geochemistry 30, 1105-1125.

Whibley, M., Jacobson, T., 1990. Exploration in the northern Bonaparte Basin. Timor Sea-WA-199-P. Australian Petroleum Exploration Association Journal 30(1), 7-25.

Whittam, D.B., Norvick, M.S., Mclntyre, C.L., 1996. Mesozoic and Cainozoic tectonostratigraphy of western ZOCA and adjacent areas. Australian Petroleum Production and Exploration Association Journal 36(1), 209-232.

Woods, E., 1992. Vulcan Sub-basin fault styles-implications for hydrocarbon migration and entrapment. Australian Petroleum Exploration Association Journal 32(1), 138-138.

Woods, E.P., 1994. A salt-related detachment model for the development of the Vulcan Sub-basin. The sedimentary basins of Western Australia 2, 259-274.

# Chapter 6.

## On the filling and leakage of petroleum from traps in the Laminaria High region of the northern Bonaparte Basin, Australia

Soumaya Abbassi[1], Rolando di Primio[2], Brian Horsfield[2], Herbert Volk[3, a], Dianne S. Edwards[4], Zahie Anka[2], Simon C. George[1]

1. Department of Earth and Planetary Sciences, Macquarie University, Sydney, NSW 2109, Australia

2. GeoForschungsZentrum Potsdam, German Research Centre for Geosciences, Germany

3. CSIRO, PO Box 136, North Ryde, NSW 1670, Australia.

a. Present Address: BP Exploration Company, Sunbury-on-Thames, UK

4. Geoscience Australia, GPO Box 378, Canberra, ACT 2601, Australia

*Corresponding author: soumaya.abbassi@gmail.com, soumaya.abbassi@students.mq.edu.au*

### *Statement of authors' contribution*

This Chapter is a final version of a manuscript that is currently a published paper in *Marine and Petroleum Geology*. This paper has been formatted to conform to the font and referencing style adopted in this thesis. Figures and tables included within the text are prefixed with the chapter number.

I am the primary author. I analysed, interpreted the 3D seismic data, and constrained the 3D geological model and 3D petroleum system models. I wrote and designed the paper's structure. All co-authors carefully reviewed and provided feedbacks and various refinements on the final version of the manuscript, and approved it for submission. Zahie Anka assisted in finalising the 3D geological model. Rolando di Primio gave valuable comments during the conception of the 3D petroleum system modelling. Neither this manuscript nor one with similar content under our authorship has been published or is being considered for publication elsewhere, except as described above.

**Abstract**

A 3D petroleum systems model of the Laminaria High and Nancar Trough area indicates that the potential Nancar Trough source kitchen is currently expelling hydrocarbons and that the reservoirs can be sourced by numerous Jurassic source rocks. Based on a range of kinetic models defined for such source rocks within the Plover, Laminaria and Frigate formations, two phases of hydrocarbon generation are predicted. Source rocks within the Lower Cretaceous Echuca Shoals Formation are deemed immature for hydrocarbon generation in this region. The onset of hydrocarbon generation in the Laminaria High commenced during the mid to late Cenozoic, and during the Early Cretaceous for the Nancar Trough, in response to elevated heat flow during the syn-rift phase. The second and main phase of hydrocarbon generation and expulsion started in the mid-Eocene and is still ongoing. This phase was controlled by deposition of the thick Cenozoic carbonate shelf, which resulted in deep burial of these Mesozoic source rocks. This second phase of expulsion coincided with the reactivation of fault-bounded traps, the consequence of which is that either some or all of the initially trapped hydrocarbons could have escaped out of charged structures. Thus, the most plausible explanation for the occurrence of under-filled or dry structures within the study area is that the faults bounding these traps remained permeable from the late Miocene to the present-day. An additional light oil and/or gas condensate charge from nearby kitchens and secondary alteration processes, such as water washing and/or phase fractionation, are necessary to explain the bulk composition of Laminaria High and neighbouring under-saturated oil accumulations. Our results also imply that most exploration failures in this region are not due to a lack of hydrocarbon charge, as has previously been interpreted, but that leakage associated with tectonic reactivation of faults is the main process leading to hydrocarbon losses.

## 6.1. Introduction

Under-filled structures are considered potential risks for hydrocarbon exploration in many basins in Australia and globally. Several mechanisms have been proposed to explain the absence of hydrocarbons in these traps. Vertical leakage due to fault reactivation is thought to play a major role in controlling hydrocarbon column heights (Sibson, 1996). The loss of initial hydrocarbon charge can also be affected by in-situ alteration (Newell, 1999; Aitken et al., 2004). Alternatively, the initial hydrocarbon charge may be insufficient to fill the traps (Brincat et al., 2004; Dyt et al., 2012).

In the northern Bonaparte Basin, which is located in the Timor Sea (**Figure 6.1**), hydrocarbon discoveries are found reservoired within Middle Jurassic sandstones in tilted, fault-bounded traps (Whittam et al., 1996; Longley et al., 2002). These structures are sealed by thick mudstones of the Upper Jurassic to Lower Cretaceous Flamingo Group and Echuca Shoals Formation (de Ruig et al., 2000). Middle Jurassic to Lower Cretaceous deltaic to marine source rocks within the Plover, Laminaria, Frigate, Flamingo and Echuca Shoals formations are believed to have generated the accumulations found within this region (Gorter and Kirk, 1995; Preston and Edwards, 2000; George et al., 2004b). Despite the exploration maturity of the Laminaria High and the neighbouring Nancar Trough and western Sahul Syncline, under-filled structures and structures without hydrocarbons continue to be drilled. The first commercial petroleum success in the Laminaria High region occurred in 1994, when Laminaria-1 discovered liquid petroleum and identified a new oil play. Within a few years, oil fields such as Laminaria, Corallina and Buffalo were developed. Bayu/Undan is the only known gas field in the region, and is located on the Flamingo High, to the east of the study area (**Figure 6.1**). After this first phase of exploration, the frequency and size of discoveries declined (Powell, 2004), with exploration drilling encountering either dry or under-filled structures (de Ruig et al., 2000; Brincat et al., 2004), despite Upper Jurassic to Lower Cretaceous seals being considered sufficient to retain hydrocarbon accumulations (de Ruig et al., 2000; Dyt et al., 2012). Several comprehensive studies (O'Brien and Woods, 1995; O'Brien et al., 1996; Smith et al., 1996; Cooper et al., 1998; de Ruig et al., 2000; Gartrell et al., 2006) on the fill-spill history of traps within the region have postulated mechanisms responsible for both the exploration failures and the partial or complete loss of hydrocarbons. Reconstructions of the composition and height of oil columns were performed based on fluid inclusion analyses (George et al., 2004b), which showed that the oil columns were more extensive in the past than they are today. Several authors (e.g., O'Brien et al., 1999; George et al., 2004b; Gartrell et al., 2006; Langhi et al., 2011) proposed that fault movement during the post-rift late Miocene collisional event resulted in trap breach and

hydrocarbon leakage, either partially or completely reducing the accumulated volumes, as recorded by the palaeo-oil columns. Several structural studies were performed in order to find a relationship between the reactivated faults and the distribution of palaeo- and current oil columns. During reactivation, long Jurassic faults terminating near the sea floor generally display higher amounts of post-rift displacement than smaller rift faults (Gartrell et al., 2006; Langhi et al., 2010). In addition, Gartrell and Lisk (2005) proposed that breached structures, previously receiving hydrocarbon charge, are found bounded by large reactivated faults accommodating displacement greater than 60 m. Based on this assumption, Dyt et al. (2012) focused on the leak point formed by the intersection between the top reservoir surface and a reactivated fault, and determined that hydrocarbons were preserved when the leak point was situated down dip of the trap crest. These authors used a structural model to predict trap integrity for the Laminaria High and Nancar Trough and, although their model did not take into consideration the lateral interaction between fault planes, they were able to validate the same displacement threshold value above which hydrocarbons are not preserved. According to some authors (e.g. Lisk et al., 1998), hydrocarbons may have escaped by the structural tilting of traps in response to differential loading during the post rift phase of the basin evolution. Furthermore, numerical modelling of the fault network in the Vulcan Sub-basin showed that fault intersection zones, rather than individual fault planes, are regarded as preferential sites for hydrocarbon leakage (Gartrell et al., 2004).

The aim of this paper is to identify and understand the mechanisms leading to exploration failure in the Laminaria High and surrounding area by addressing the following two questions using petroleum systems modelling. (1) Was there enough hydrocarbon charge to fill potential structures? (2) If there was sufficient hydrocarbon charge, then what are the most likely processes that resulted in the loss of hydrocarbons?

## 6.2. Geological setting

This study focuses on the northern part of the Londonderry High, Nancar Trough and Laminaria High in the northern Bonaparte Basin (**Figure 6.1**). The Londonderry High is a Permo–Triassic horst and graben complex, which acted as a source of sediments for adjacent depocentres during Jurassic rifting (Whibley and Jacobson, 1990). The Laminaria High is a Mesozoic to Cenozoic east–west trending platform (Smith et al., 1996), which is bordered by the Flamingo Syncline to the northeast and the Nancar Trough to the south.
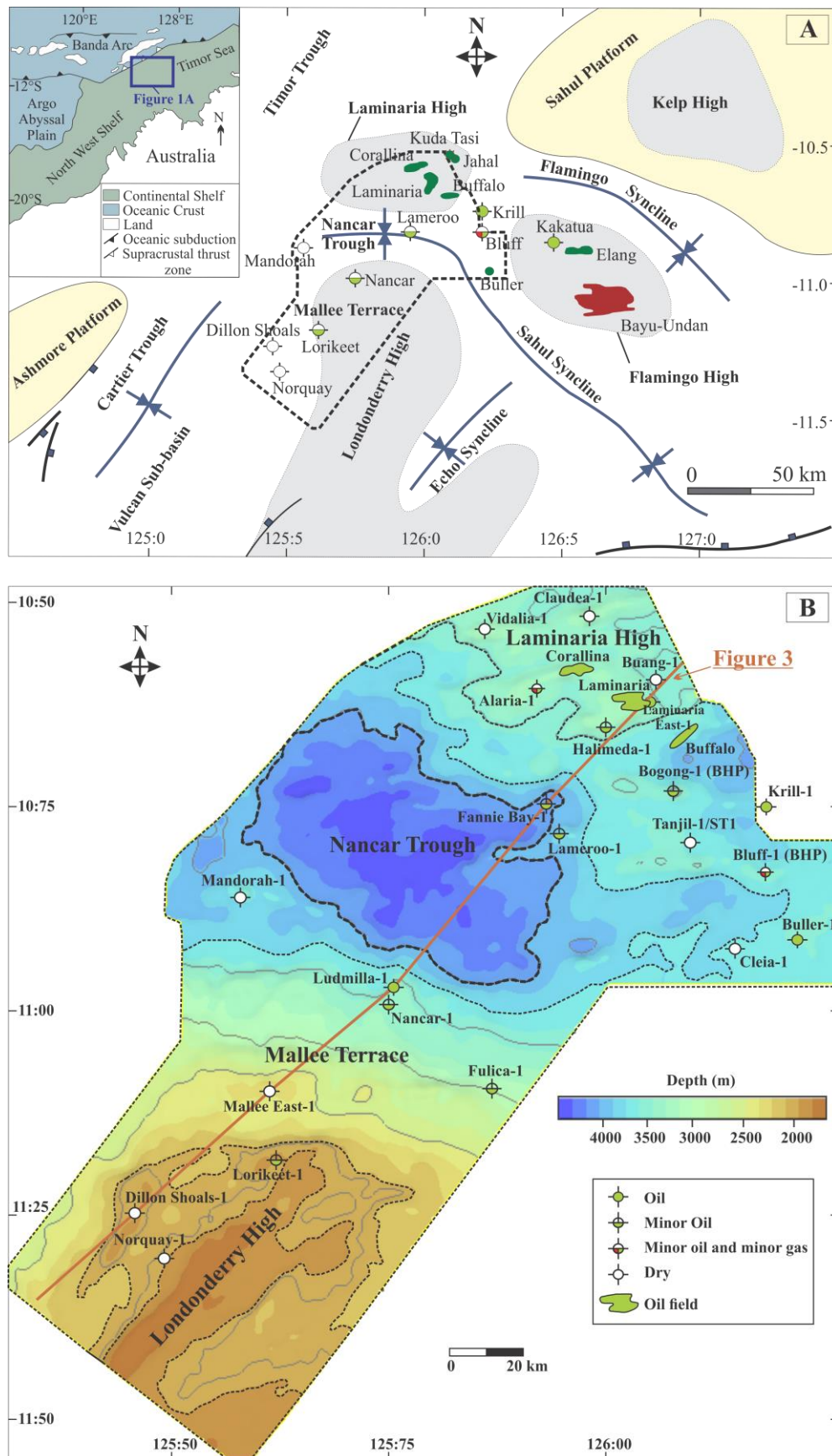
**Figure 6.1. (A) Location map of the study area on the North West Shelf of Australia, showing the main structural elements of the Bonaparte Basin, the hydrocarbon discoveries and location of wells used in this study, and the outline of the interpreted 3D seismic survey (dashed zone), modified from de Ruig et al. (2000). (B) Depth map interpreted at Top Reservoir (JO) level, showing the outline of the interpreted 3D seismic survey. The brown line represents the position of the Figure 6.3 seismic section.**

**217**

The Nancar Trough is a northwest-trending depocentre containing up to 8 km of Mesozoic−Cenozoic sediments (de Ruig et al., 2000). This depocentre represents the western extension of the Sahul Syncline and is flanked to the south by the Londonderry High.

Early development of the Bonaparte Basin was marked by rifting events from the late Carboniferous to the early Permian, which correspond with the initiation of the Neotethys rift system (Borel and Stampfli, 2002). This extensional deformation formed northwest-southeast trending basins and highs and controlled the thickness of the Mesozoic and Cenozoic succession. The main rifting phase occurred during the Middle–Late Jurassic to Early Cretaceous and is believed to be related to the breakup of Gondwana (Baillie et al., 1994; Longley et al., 2002). This later rifting event generated northeast-southwest trending structures (de Ruig et al., 2000), such as the Vulcan Sub-basin and Malita Graben. Locally this northeast-southwest regional trend varies to east-west as seen on the Laminaria High, Flamingo High and in the Nancar Trough areas (de Ruig et al., 2000; Langhi and Borel, 2008). Extension was accompanied by uplift in the Late Jurassic and was interpreted to be due to flexure driven by sea-floor spreading (Harrowfield and Keep, 2005). The end of the rifting event is marked by the Aptian unconformity (KA; **Figure 6.2**), which records the onset of the Upper Cretaceous to Cenozoic post-rift thermal subsidence dominated passive margin (Gartrell et al., 2006). Subsequently, a carbonate platform prevailed until the late Miocene–early Pliocene when the Australian plate obliquely collided with the Eurasian plate (Charlton et al., 1991; O'Brien and Woods, 1995; O'Brien et al., 1999). In addition to the development of a new phase of east-northeast−west-southwest trending faulting (O'Brien et al., 1999; Gartrell et al., 2006), this collisional event caused localised reactivation of the fault-bounded structures (Whittam et al., 1996; Langhi et al., 2011).

## 6.3. Lithostratigraphy and petroleum system elements

### 6.3.1. Paleozoic basement

The Paleozoic succession is usually regarded as economic basement in the northern Bonaparte Basin (de Ruig et al., 2000). Few wells penetrate the Permian succession, due to the thickness of the overlying Mesozoic and Cenozoic strata. However, by analogy to the Petrel Sub-basin, the Permian sediments predominantly comprise glacial or glacio-marine clastics at the base, which are overlain by shallow marine, deltaic sandstones, limestones and carbonates of the Hyland Bay Subgroup (Bhatia et al., 1984; Bradshaw et al., 1988).
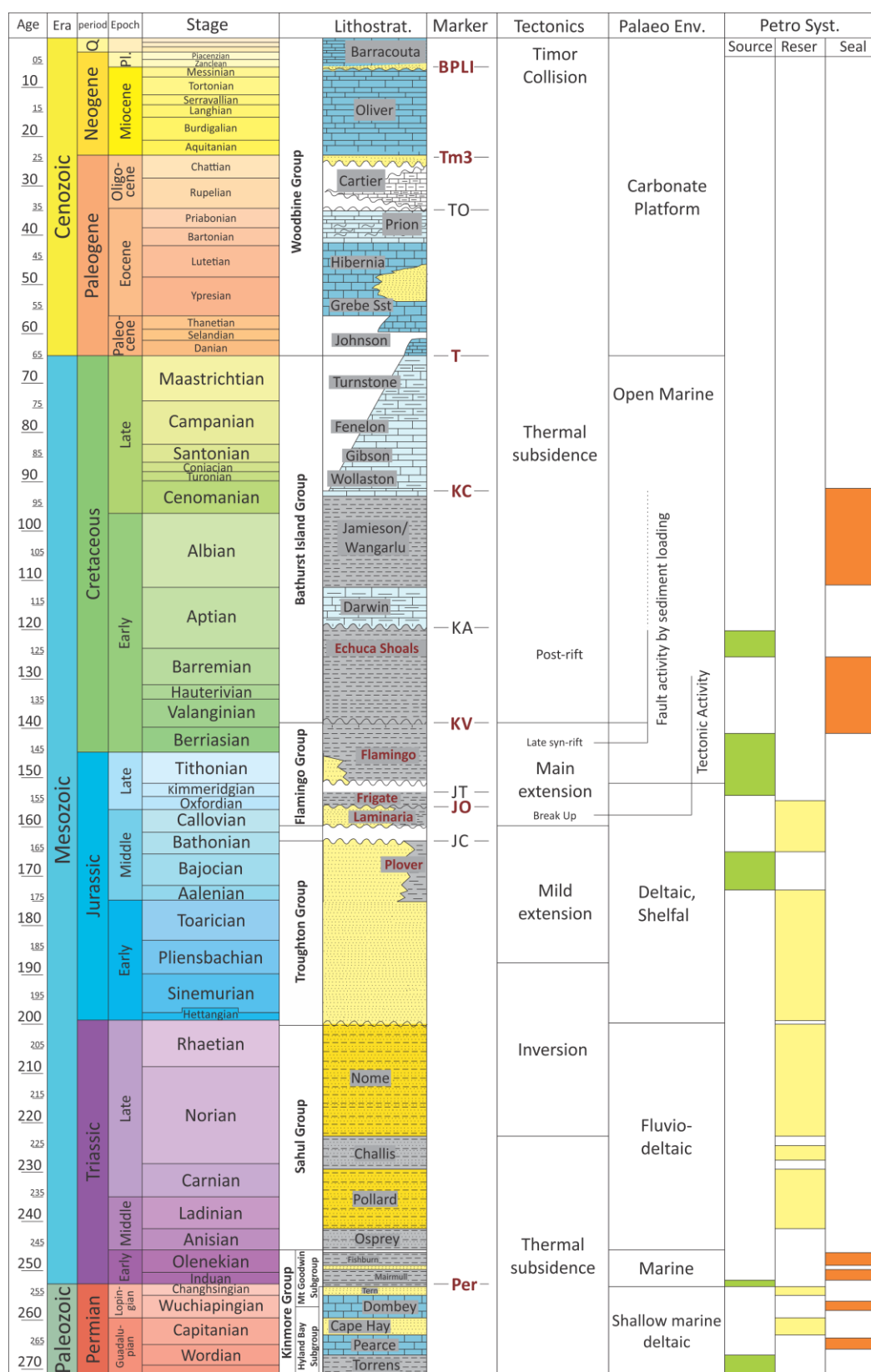
**Figure 6.2. Mesozoic stratigraphic column of the northern Bonaparte Basin, showing lithologies, interpreted seismic surfaces and the main tectonic events. Seismic surfaces marked in red are those mapped in this study. Also shown are the depositional environments and the potential petroleum system elements. Modified after (de Ruig et al., 2000). Env. = environment, Lithostrat. = lithostratigraphy, Petro. Syst. = petroleum system, Pl = Pleistocene, Q = Quaternary.**

### 6.3.2. The Triassic to Lower Jurassic pre-rift phase

Triassic sediments mark the end of the late Paleozoic tectonism and comprise basal marine shales of the Mount Goodwin Subgroup that is overlain by prograding fluvio-deltaic sediments of the Sahul Group (Helby et al., 1987). During the Early Triassic to Late Jurassic the depositional environment was characterised by fluvial and floodplain sediments of the Sahul, Troughton and Flamingo groups (Gorter et al., 1998). However, most of the Triassic to Lower Jurassic sediments are absent throughout most of the northern Bonaparte Basin due to either non-deposition or erosion during the Late Triassic (Bhatia et al., 1984). This surface forms a regional unconformity separating the Triassic from the overlying Lower Jurassic sediments **(Figure 6.2)**. Uplift and erosion of the structural highs during the Late Triassic, increased clastic sediment supply (Whibley and Jacobson, 1990; de Ruig et al., 2000) resulting in fluvio-deltaic sandstone-dominated complexes of the Sahul Group (Osprey, Pollard, Challis and Nome formations) and Plover Formation over much of the Bonaparte Basin.

### 6.3.3. Lower to Middle Jurassic early syn-rift phase

The Hettangian to Callovian sediments of the Plover Formation comprise sandstones interbedded with claystones and occasional coals (Labutis et al., 1998). The top of this formation (JC; **Figure 6.2**) is marked by the Callovian unconformity (Hocking et al., 1988) that reflects the onset of rifting and the resultant cessation of fluvio-deltaic sedimentation (Veevers and Conaghan, 1984). The early Callovian to early Oxfordian sediments of the Laminaria Formation comprise sand-dominated deltaic to marginal marine deposits (Smith et al., 1996). The early Oxfordian (JO) unconformity separates the early syn-rift and syn-rift sedimentary packages (Longley et al., 2002). The Plover Formation is considered to be a gas and oil-prone source rock, while the Laminaria Formation contains potential oil-prone source rock units in the northern Bonaparte Basin (Preston and Edwards, 2000).

### 6.3.4. The Upper Jurassic to Lower Cretaceous syn-rift phase

The Oxfordian to Kimmeridgian succession comprise marine claystones and shales of the Frigate Formation and is separated from the Tithonian to Berriasian Flamingo Formation marine shales by the JT unconformity **(Figure 6.2)** (Mory, 1991; Whittam et al., 1996). A major transgressive event occurred during the Valanginian, with the intra-Valanginian unconformity (KV) indicating the onset of thermal subsidence (Baxter et al., 1997) and post-rift deposition. Following the Valanginian transgression, the clastic supply was reduced in response to the flooding of the Londonderry High. Valanginian to Aptian glauconitic

claystones of the Echuca Shoals Formation indicate the first expression of deep marine conditions, which grade vertically into radiolarian-rich claystones of the Darwin Formation that record maximum water depths (Mory, 1991; Whittam et al., 1996). The Frigate and Flamingo formations are also considered to be potential source rocks (Edwards et al., 2000).

### 6.3.5. Upper Cretaceous to Tertiary passive margin phase

The Lower and Upper Cretaceous marine claystones and marls of the Jamieson Formation and Bathurst Island Group are separated by the Cenomanian (KC) unconformity (**Figure 6.2**). The unconformity (T), at the base of the Paleocene, marks the change from a siliciclastic-dominated basin to a progradational carbonate platform (Whittam et al., 1996). Carbonate and argillaceous carbonate sedimentation dominated during the Paleocene to Oligocene as seen in the Johnson, Hibernia, Prion and Cartier formations which terminate at the regional unconformity Tm3. As subsidence–induced accommodation increased in the late Oligocene to early Miocene (Seggie et al., 2000), a thick carbonate shelf extended over the Bonaparte Basin and deposited the Oliver and Barracouta formations. Locally, during low stand events in the Eocene and Miocene, reservoir quality sandstones such as those of the Grebe and Oliver members developed (Mory, 1991).

### 6.3.6. Petroleum system elements

The principal source rocks of the northern Bonaparte Basin (**Figure 6.2**) comprise shales of the Plover, Laminaria, Frigate and Flamingo formations (Botten and Wulff, 1990; Whibley and Jacobson, 1990; Gorter and Kirk, 1995; Preston and Edwards, 2000; George et al., 2004b). These formations contain type II/III kerogens with different levels of thermal maturity that tend to increase towards the Nancar Trough and the Sahul Syncline (Preston and Edwards, 2000; Abbassi et al., 2014a). Additional source rock units occur within the post-rift Lower Cretaceous Echuca Shoals Formation. In the study area, hydrocarbons are mainly reservoired in the Jurassic sandstones of the Plover and Laminaria formations (Longley et al., 2002). These primary exploration targets are believed to have wide distribution and good quality (Whittam et al., 1996). The main structural traps consist of horst blocks or east-west trending tilted normal fault blocks formed during Upper Jurassic rifting (Pattillo and Nicholls, 1990; Woods, 1992; Smith et al., 1996; Whittam et al., 1996). Langhi and Borel (2008) suggested that the secondary reverse structures associated with the main east−west fault system could act as secondary hydrocarbon traps and/or as migration barriers. The thick marine mudstones and claystones of the Flamingo and Echuca Shoals

formations deposited during the late stages of the rifting and early post-rift phase form proven regional seals (de Ruig et al., 2000; Dyt et al., 2012).

## 6.4. Input data set and model calibration

The petroleum system modelling was conducted using the Schlumberger PetroMod 3D (Versions 2011 and 2012) software packages. Input parameters included a 3D geological model derived from the interpretation of 3D seismic reflection data using Petrel interpretation software. Nineteen stratigraphic events were defined. All the assigned layers and their input data used in the model are presented in **Table 6.1**.

**Table 6.1. Geological layers, depositional durations and lithologies used as input parameters for the 3D basin model. Lithological data were compiled from well completion reports.**

| Layer | Duration (Ma) | Lithology |
|---|---|---|
| Barracouta | 5.3 – 0 | 60% limestone + 25% limestone (micrite) + 10% shale (calcareous) + 5% marl |
| Oliver | 23 – 5.3 | 65% limestone + 25% shale (calcareous) + 10% sandstone |
| Cartier | 34 – 23 | 70% limestone + 25% shale (calcareous) + 5% limestone (marly) |
| Prion/Hibernia/Grebe | 55.8 – 34 | 50% limestone + 20% sandstone (quartz rich) + 15% limestone (sandy) + 15% silt |
| Johnson | 65.5 – 55.8 | 50% shale (calcareous) + 40% limestone (marly) +10% limestone |
| Bathurst Island Group | 95 – 65.5 | 60% shale (calcareous) + 10% limestone (marly) |
| Jamieson | 120 – 95 | 90% shale + 10% shale (silt) |
| Echuca Shoals (source rock) | 140 - 120 | 90% shale (black) + 10% shale (silt) |
| Flamingo | 150 - 140 | Shale |
| Frigate seal | 155.6 - 150 | 70% shale (silt) + 15% silt (shaly) + 15% shale |
| Frigate (source rock) | 157 - 155.6 | Shale (black) |
| Laminaria (reservoir) | 161.5 - 157 | Sandstone |
| Laminaria (source rock) | 162 - 161.5 | Shale (organic-rich) |
| Plover sandy unit I (reservoir) | 166 - 162 | Sandstone |
| Plover (source rock) | 167 - 166 | 95% shale (black) + 5% coal |
| Plover sandy unit II (reservoir) | 172 - 167 | 80% sandstone + 10% siltstone + 10% shale |
| Triassic / Early Jurassic | 252 - 172 | 50% sandstone + 50% shale |

Specific parameters were assigned to each layer, such as relative age and lithology data from well completion reports, and lithostratigraphic nomenclature. For the majority of the layers, a mixing of two or more default lithologies was used, to which pre-defined petrophysical properties were automatically assigned. No lateral facies changes were considered in the model for the different layers. Biostratigraphic information from well cuttings and cores provided age constraints. The thicknesses of the reservoir, source rock and seal units were estimated from well data and correlation with depth-converted seismic surfaces. Palaeogeometry (palaeo-water depths) and boundary conditions (sediment water interface temperatures (SWIT) and heat flow history) were also used as input parameters. Palaeo-

water depths were estimated based on micropalaeontological data available in the Geoscience Australia database (http://dbforms.ga.gov.au/www/npm.well.search). Surface temperatures were estimated using the palaeo-latitudes tool implemented in the modelling software, as described by Wygrala (1989).

### 6.4.1. Present-day geometry

The present-day geometry was constrained by the information from well completion reports and interpretation of part of the Vulcan Sub-basin Mega-Survey 3D seismic reflection data (17 912 $Km^2$; Edwards et al., 2005) that was acquired in the late 1990s by PGS. The stratigraphic succession studied, and shown in the representative northeast-southwest seismic cross section **(Figure 6.3),** ranges from the Top Permian to the present-day sea floor. The migrated two way time 3D seismic data are generally good quality from the sea floor down to the Valanginian unconformity (KV), but signal deteriorates below this surface. Eight surfaces, mainly representing stratigraphic unconformities, were picked and correlated throughout the study area. The surface ages are: present-day sea bed, base Pliocene, base Miocene, base Cenozoic, Cenomanian unconformity, Intra-Valanginian unconformity, early Oxfordian unconformity and the top Permian **(Figure 6.2** and **Figure 6.3)**. The top of the Laminaria reservoir (the early Oxfordian unconformity) was not straightforward to recognise over the study area due to the poor seismic data quality and the frequency of faults. A high reflectivity package on the sea bed corresponds to modern-day carbonate shoals developed mainly around the Laminaria, Buffalo and Mandorah structures **(Figure 6.1)**. Depth conversion was performed using interval velocities derived from wells where check-shot data were available. Eight maps with 200 m x 200 m grid resolution were built. As can be seen in **Figure 6.3**, there is a thickening of the Mesozoic to Cenozoic succession from the Londonderry High northward into the Nancar Trough. The syn-rift sequence, which includes the effective source rocks, is significantly thinner as compared to the pre- and post-rift sequences. The internal geometry of the interpreted successions consists mainly of sub-parallel and laterally continuous seismic reflections that are strongly affected by extensional structures at different stratigraphic levels **(Figure 6.3)**. These structures correspond to normal faults, some of which die out just below the sea floor and others which end at the Lower Cretaceous Valanginian unconformity. Significant erosional features that could influence the thermal maturity history were not observed and therefore no erosional event was introduced in the model.

The depth maps derived from seismic interpretation were imported into the Petromod software, where higher resolution stratigraphic subdivision interpretation was carried out.

Subdivision of the sedimentary package between the late Permian and the Oxfordian surface was required to delineate two source rocks (Laminaria and Plover formation source rocks) and two reservoir units (Laminaria and Plover formation reservoirs). The sub-division was achieved using well completion report information and some assumptions, such as the thinning out or complete absence of these units over structural highs. The thicknesses assigned for the Plover Formation source rock and reservoir units represent an approximation as few wells intersected these sediments within the study area, and their seismic quality is relatively poor.

### 6.4.2. Source rock properties

Four source rock units were routinely included in the 3D petroleum system model: the Echuca Shoals (Aptian−Valanginian), Frigate (Berriasian−Tithonian), Laminaria (Oxfordian−Callovian) and Plover (Bathonian−Hettangian) formations. A fifth source rock unit, the Berriasian upper Flamingo Formation, exhibits similar source rock characteristics as the Frigate Formation and was only considered in some modelling scenarios that are not discussed in this paper. In other scenarios, the Flamingo Formation served as a sealing unit for the underlying source rocks. The source rock properties of hydrogen index (HI) and total organic carbon (TOC) content were assigned to each layer based on previous studies conducted by Preston and Edwards (2000). Activation energy distribution, interpreted kerogen type and kinetic data (with fourteen components) were obtained from the artificial maturation of immature samples (Abbassi et al., 2014a) and were used as inputs to the model. The characteristics assigned for each source rock layer are summarised in **Table 6.2**. The activation energy distribution for bulk petroleum generation is broad, indicating varying thermal stability and a heterogeneous type II/III kerogen structure within these Middle Jurassic to Lower Cretaceous formations (Abbassi et al., 2014a). Kinetic parameters for the primary cracking of kerogen indicate hydrocarbons in the Echuca Shoals, Frigate, Laminaria and Plover (shale) formations were generated at different temperatures covering a range of 15°C (at 50% transformation ratio) extrapolated using a geological heating rate of 3.3°C/Ma. The kinetic models developed for the Plover Formation by Abbassi et al. (2014a) used samples from the Vulcan Sub-basin **(Figure 6.1)**, because too few wells in the study area penetrated the source rock unit of this formation. The Plover Formation, inferred to be one of the major source rocks for petroleum in the Bonaparte and Browse basins (Botten and Wulff, 1990; Whibley and Jacobson, 1990; Preston and Edwards, 2000; George et al., 2004b) consists of coals and shales deposited in deltaic to marginal marine environments.
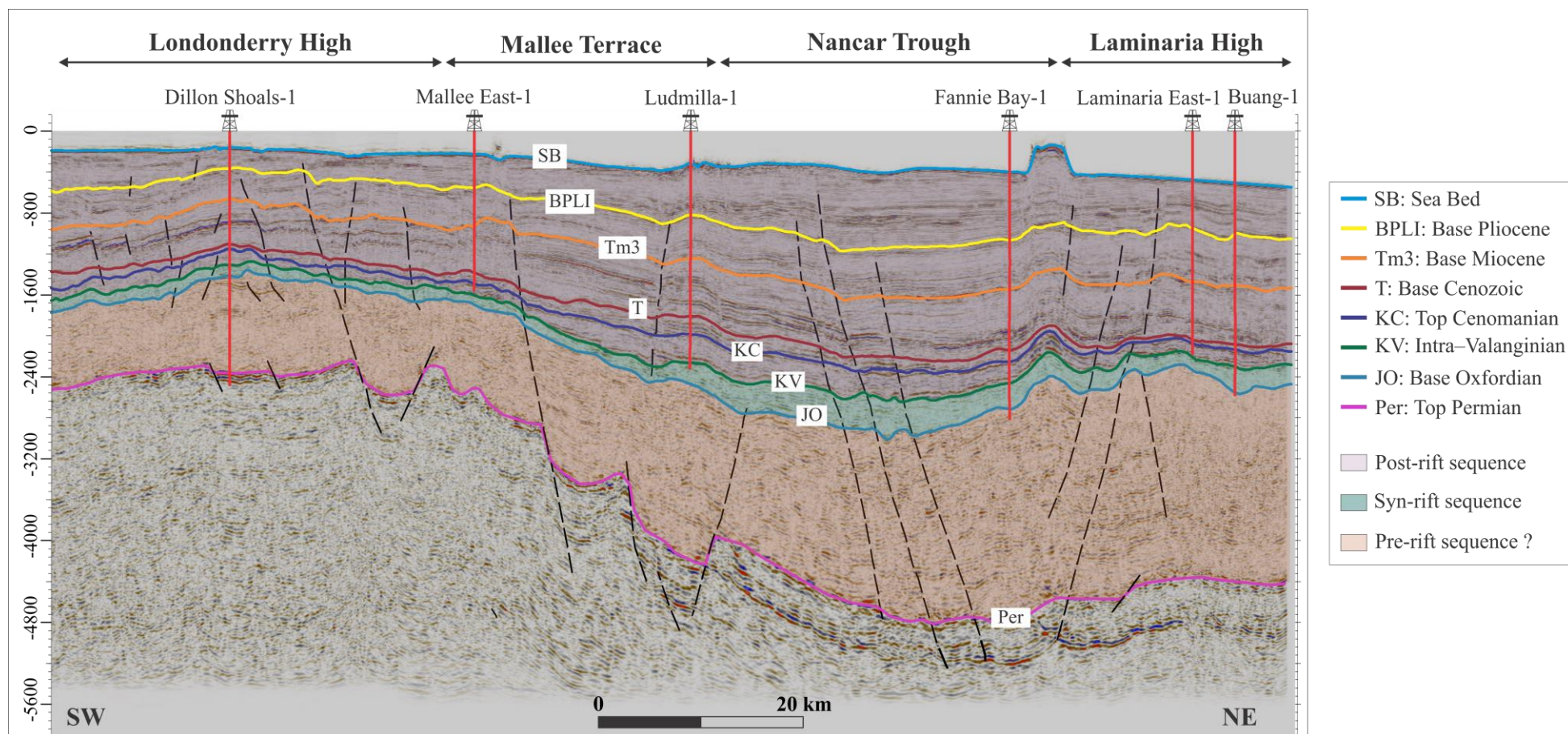
**Figure 6.3. Northeast-southwest two-way time regional seismic section across the modelled area, illustrating Permian to present-day sequences and the key surfaces mapped in this study. Note the poor quality of the seismic data below the (KV) surface and the relative thickness of the syn-rift sequence compared to the pre- and post-rift sequences. Fault systems are well developed at three stratigraphic levels: late Permian, Middle Jurassic−Lower Cretaceous, and Cenozoic.**

The lateral extent of the coals is uncertain and it is unknown whether coals are present in the Nancar Trough. Accordingly, only the shale units of the Plover Formation were considered in the model documented here.

**Table 6.2. Source rock properties and compositional kinetic components used as input parameters for the 3D basin model. Data are from Preston and Edwards (2000) and Abbassi et al. (2014a).**

| Formation | Echuca Shoals | Frigate | Laminaria | Plover |
|---|---|---|---|---|
| TOC (%) | 2.5 | 2 | 2 | 3.5 |
| HI (mg HC/g TOC) | 250 | 280 | 350 | 300 |
| Kerogen type | II/III | II/III | II/III | II/III |
| Frequency factor A ($S^{-1}$) | 7.75E+13 | 1.65E+14 | 8.10E+13 | 5.13E+14 |
| Main activation energy (kcal/mol) | 53 - 55 | 53 - 56 | 53 - 56 | 55 - 57 |
| $n$-$C_1$ (%) | 22.98 | 7.4 | 8.36 | 10.18 |
| $n$-$C_2$ (%) | 5.71 | 2.69 | 2.74 | 4.4 |
| $n$-$C_3$ (%) | 4.93 | 2.73 | 2.99 | 3.94 |
| $i$-$C_4$ (%) | 1.75 | 0.49 | 0.98 | 0.7 |
| $n$-$C_4$ (%) | 3.96 | 3.86 | 5.27 | 2.11 |
| $i$-$C_5$ (%) | 1.66 | 3.34 | 1.54 | 1.45 |
| $n$-$C_5$ (%) | 1.55 | 1.93 | 1.37 | 1.08 |
| $n$-$C_6$ (%) | 10.57 | 8.53 | 7.66 | 4.2 |
| $C_7$-$C_{15}$ (%) | 32 | 41.62 | 27.75 | 29.66 |
| $C_{16}$-$C_{15}$ (%) | 11.03 | 18.91 | 21.16 | 22.44 |
| $C_7$-$C_{25}$ (%) | 2.45 | 6.3 | 10.92 | 11.24 |
| $C_{26}$-$C_{35}$ (%) | 0.66 | 2.13 | 5.2 | 5.08 |
| $C_{36}$-$C_{45}$ (%) | 0.36 | 0.73 | 2.39 | 2.17 |
| $C_{46}$-$C_{80}$ (%) | 0.36 | 0.35 | 1.68 | 1.36 |

### 6.4.3. Thermal history: present and palaeo heat flows

#### 6.4.3.1. Present-day heat flow

There are no published heat flow data in the northern Bonaparte Basin. Hence, the present and palaeothermal history used in the model are based on thermal maturation parameters: vitrinite reflectance, vitrinite reflectance-equivalent values from the Fluorescence Alteration of Multiple Macerals (FAMM), $T_{max}$ from Rock-Eval pyrolysis, bottom-hole temperatures (BHTs), temperatures measured from drill-stem tests (DST) and modular dynamic tests (MDT). The average present-day heat flows, estimated from a range of measured and corrected formation temperatures (using the Horner plot correction method) vary from 67 mW/m$^2$ in the Nancar Trough, to 75 mW/m$^2$ in the Laminaria High. The average heat flow estimated for the Londonderry High is 70 mW/m$^2$. Twenty-six wells were calibrated to present-day temperatures. The results of the thermal calibration for four representative wells in the study area are shown in **Figure 6.4**.
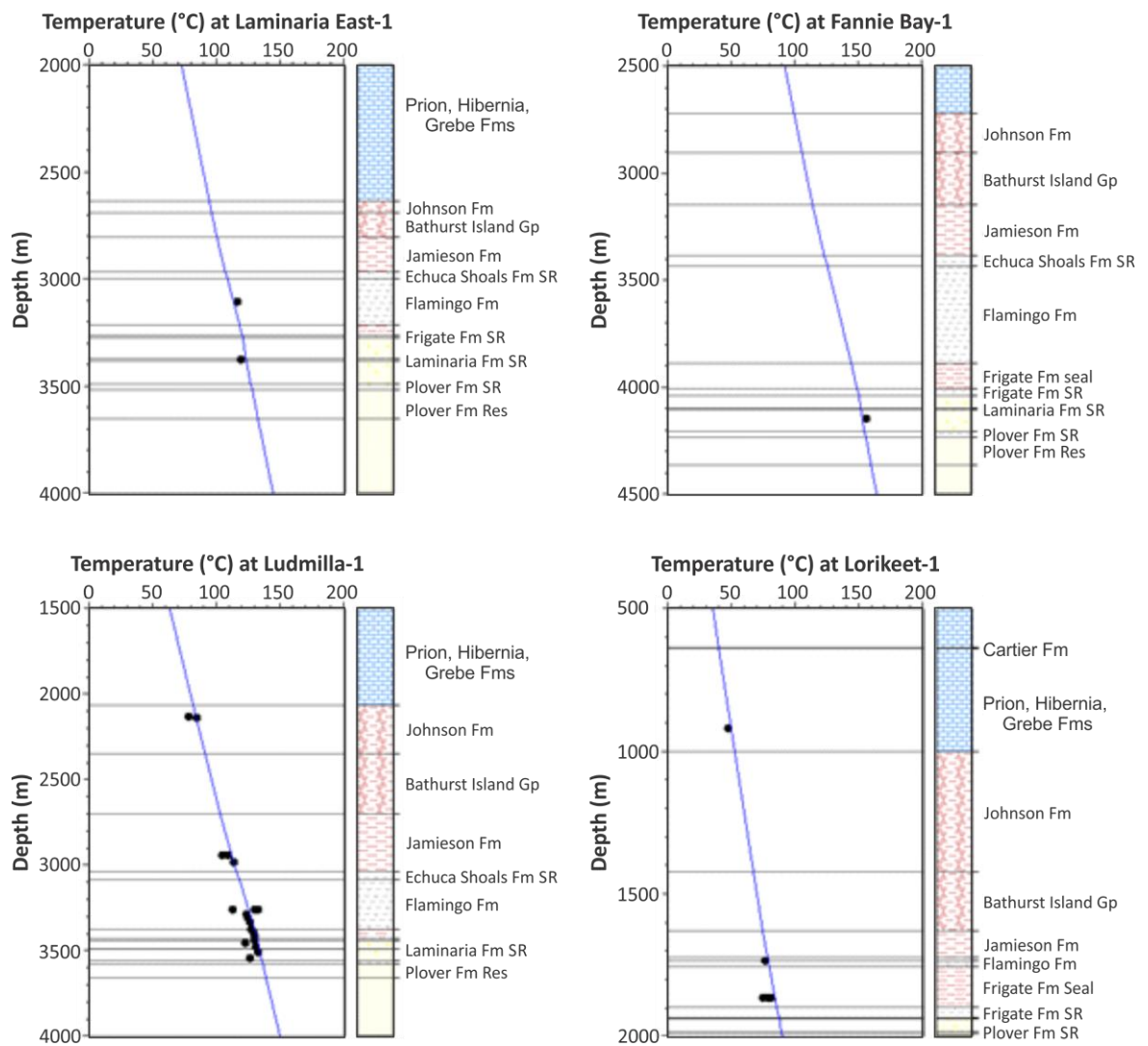
**Figure 6.4. Measured values and modelled trends of present-day temperature for four representative wells across the study area. See Figure 6.1 for the location of the wells. Black dots represent measured formation temperatures; the blue line represents the modelled temperature. Fm = Formation, Gp = Group, SR = source rock, Res = Reservoir.**

### 6.4.3.2. *Palaeo heat flow scenarios*

To model palaeo heat flow, three scenarios were tested (**Figure 6.5**). The tested scenarios 'a', 'b' and 'c' were implemented based on different thermal maturity data, such as measured vitrinite reflectance data (scenario 'b') and calculated vitrinite reflectance data from Rock-Eval pyrolysis $T_{max}$ and FAMM data (scenario 'c'). The first scenario 'a' assumes constant heat flow over time. This assumption, even though it does not honour the geological evolution of the study area, does provide a reasonable calibration with maturity data for some wells (e.g. Alaria-1, Buang-1 and Laminaria-East 1), indicating that the present−day temperature approaches the maximum reached in the area. For other wells (e.g. Bogong-1 (BHP) and Ludmilla-1), the assumption of a constant heat-flow does not allow calibration

with the measured reflectance vitrinite values. Scenario 'b' incorporated a variable heat flow history **(Figure 6.5)** with respect to the available measured vitrinite reflectance data.
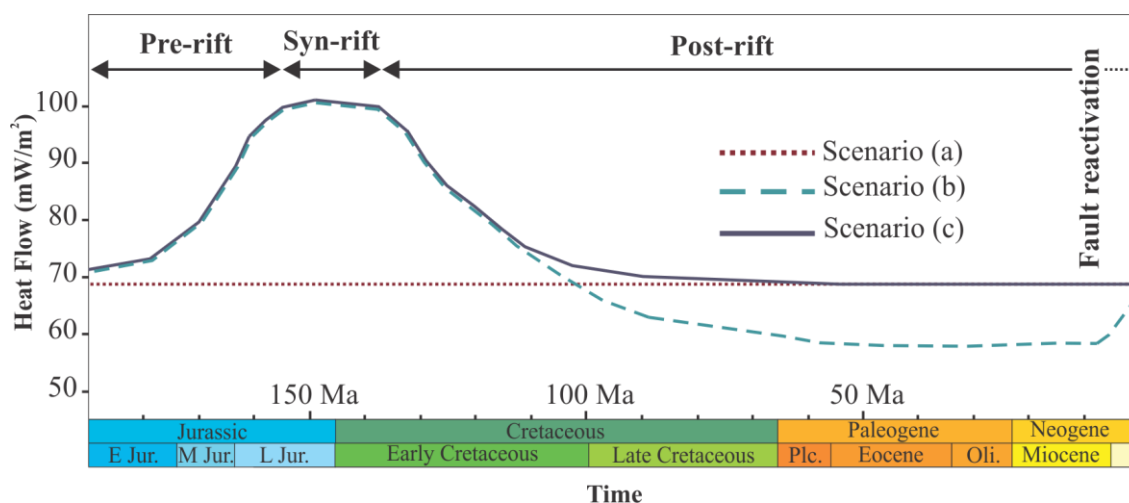


**Figure 6.5. Schematic heat flow scenarios tested in this study. Note that values indicate averages of heat flow and do not reflect the lateral distribution estimated for each of the modelled structural features. The overall trend assigned for the palaeo heat flows is based on the model by Kennard et al. (1999). Jur. = Jurassic, Plc. = Paleocene, Oli. = Oligocene.**

The variable heat flow history applied consists of an elevated heat flow pulse during the rifting phase followed by gradual decay during the post-rift period. Values 10 mW/m$^2$ lower than the present-day were needed to obtain a good accordance with the measured vitrinite reflectance in the post-rift period. The results of this scenario did not match the present-day thermal maturity profile. The assignment of an increased heat flow value (~55 mW/m$^2$) from the background post rift at 7 Ma to the present-day was necessary for scenario 'b' to better match the temperature and vitrinite reflectance data. The outcomes of scenario 'b' derived from the modelled calibration for Alaria-1 and Mandorah-1 are illustrated in **Figure 6.6**. The heat flow increase over the last 7 Ma that is required to obtain a good calibration with the available measured maturation data in scenario 'b' cannot be justified in a collisional setting, where established thermal models generally predict cooler temperatures than the thermal background (Huerta et al., 1998). Thus, the prediction of the heat flow history based on measured vitrinite reflectance values in isolation could lead to erroneous results, even when a good agreement is achieved with regard to the modelled trend.

On the North West Shelf of Australia, the measured vitrinite reflectance in source rock units can be anomalously low when considering overall depth trends (Wilkins et al., 1992; Kaiko and Tingate, 1996). The likely causes of such anomalous values, also called suppressed values (Price and Baker, 1985; Lewan, 1993) as discussed by Wilkins et al. (1992), are attributed either to perhydrous vitrinite commonly associated with marine environments (e.g.

Price and Baker, 1985; Gurba and Ward, 1998), or to the difficulty of identifying vitrinite dispersed within the marine to marginal marine Jurassic to Lower Cretaceous sediments. Rock-Eval pyrolysis $T_{max}$ values were therefore used as a supplementary thermal indicator to correlate with equivalent vitrinite reflectance data obtained by FAMM. $T_{max}$ values from samples with a TOC <1 wt.% and <2 mg HC/g TOC $S_2$ (the hydrocarbon fraction generated by thermal cracking) were discarded.
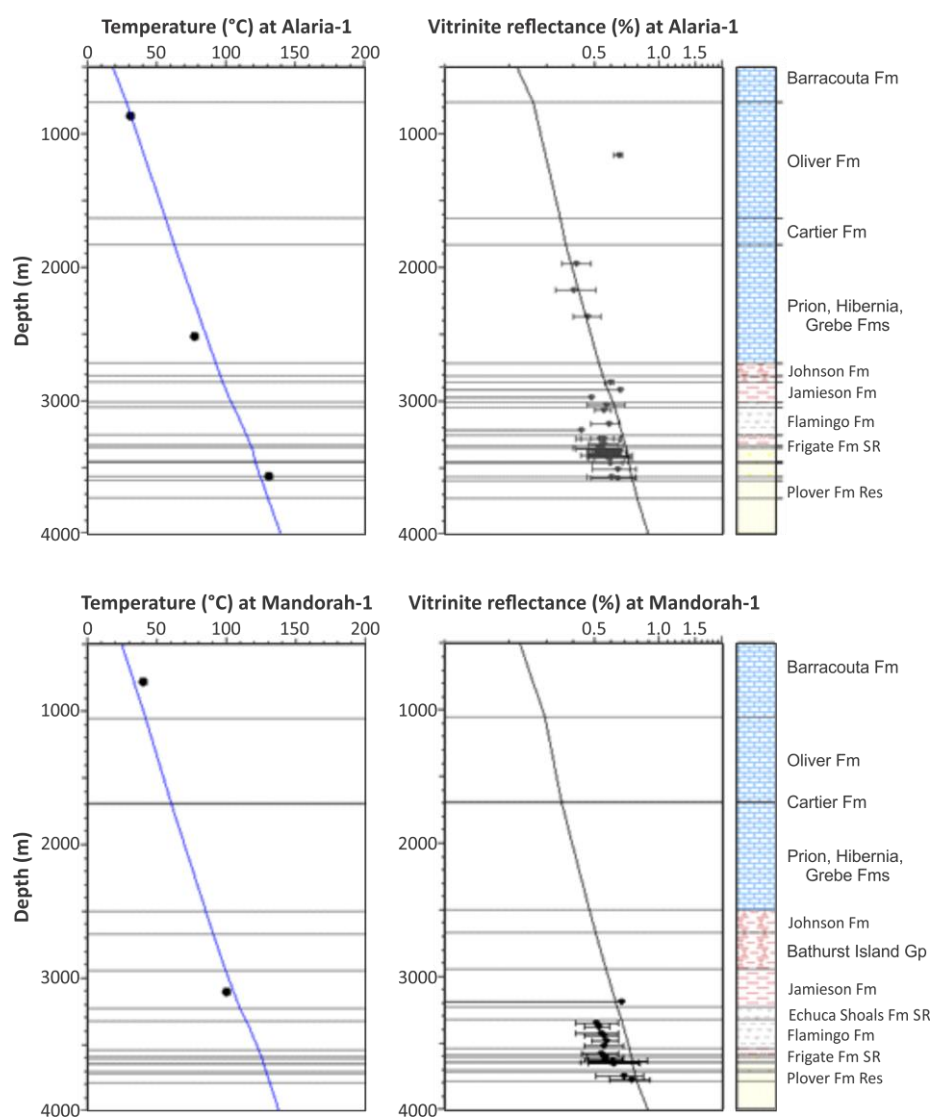


**Figure 6.6. Calibration of modelled vitrinite reflectance (black trend) against measured vitrinite reflectance (black dots) for Alaria-1 and Mandorah-1 using scenario 'b'. Model calibration by comparison with measured temperatures (black dots) and modelled temperatures (blue trend) is also shown. Well locations are shown in Figure 6.1. For abbreviations, see Figure 6.4.**

The FAMM technique was used to correct the suppression of vitrinite reflectance for samples in the Vulcan Sub-basin in order to improve evaluation of thermal maturity (Faiz et al., 1998; Kennard et al., 1999). Samples from the Vulcan Sub-basin have an average level of vitrinite

reflectance suppression of 0.27%, with 47% of the samples having vitrinite reflectance suppression amounts ranging from 0.2 to 0.4% **(Figure 6.7)**. Due to the lack of FAMM data in the study area, samples from the Vulcan Sub-basin were used to establish an empirical relationship between $T_{max}$ and equivalent vitrinite reflectance from FAMM **(Figure 6.8)**. In the study area, the only vitrinite reflectance data corrected for suppression using FAMM comes from Nancar-1. This well served as a reference to compare the measured equivalent vitrinite reflectance from FAMM to those obtained from the empirical relationship of $T_{max}$ versus FAMM. **Figure 6.9** shows a good match between the calculated vitrinite reflectance values and the equivalent vitrinite reflectance measured by FAMM, both of which imply greater thermal maturity than those obtained from the measured vitrinite reflectance values.
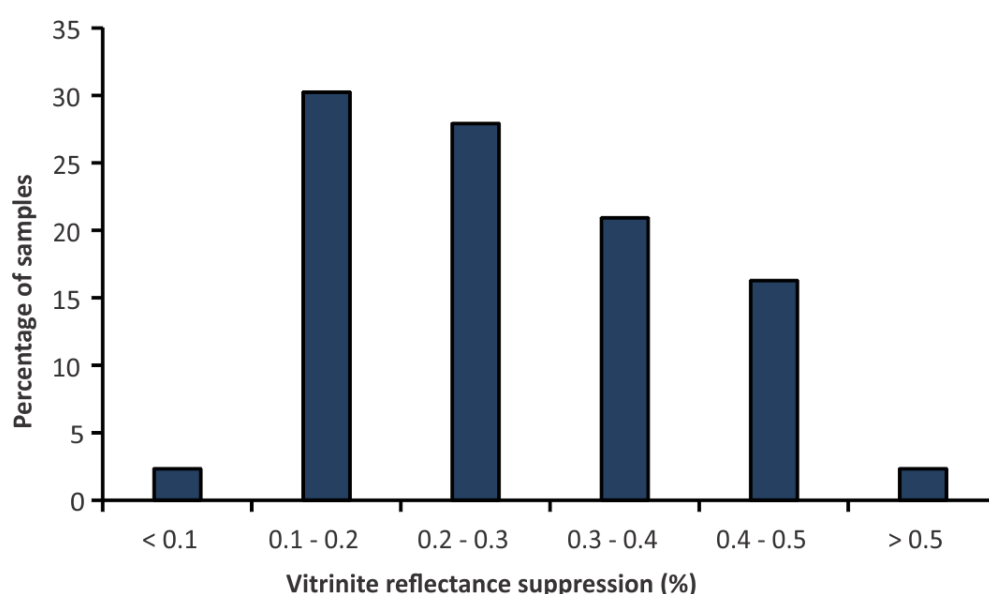


**Figure 6.7. Vitrinite reflectance suppression (%) distribution for Middle Jurassic to Lower Cretaceous source rock samples in the Vulcan Sub-basin. Vitrinite reflectance suppression is based on the difference between measured vitrinite reflectance data and equivalent vitrinite reflectance data derived from FAMM (CSIRO Petroleum reports).**

Taking into account the calculated vitrinite reflectance data, we tested scenario 'c' **(Figure 6.5)** in which an increased heat flow during the rift phase was considered, followed by a gradual decrease in the heat flow during the post-rift phase to present-day values (McKenzie, 1978; Allen and Allen, 1990).
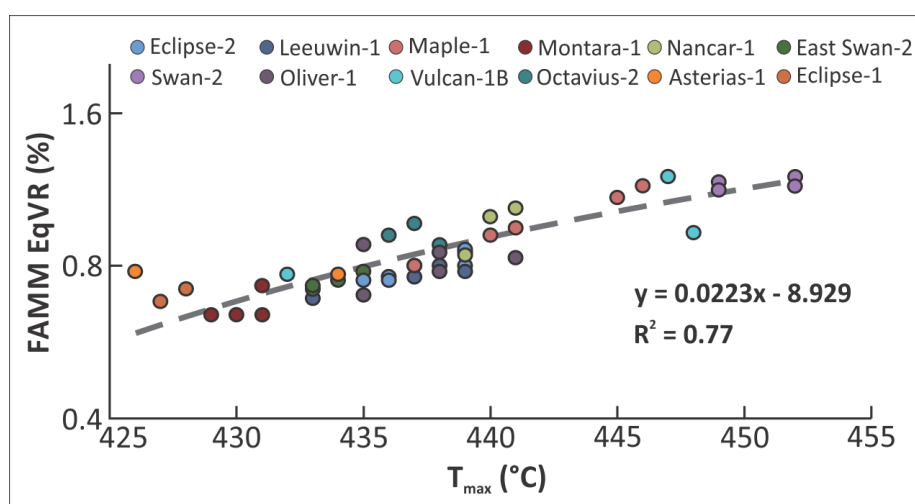
**Figure 6.8. Relationship between equivalent vitrinite reflectance from FAMM (%) and T_max (°C) values derived from Rock-Eval pyrolysis for Middle Jurassic to Lower Cretaceous source rock samples in the Vulcan Sub-basin. FAMM and Rock-Eval pyrolysis T_max data were compiled from CSIRO Petroleum reports and the Geoscience Australia database (http://dbforms.ga.gov.au/www/npm.well.search), respectively.**
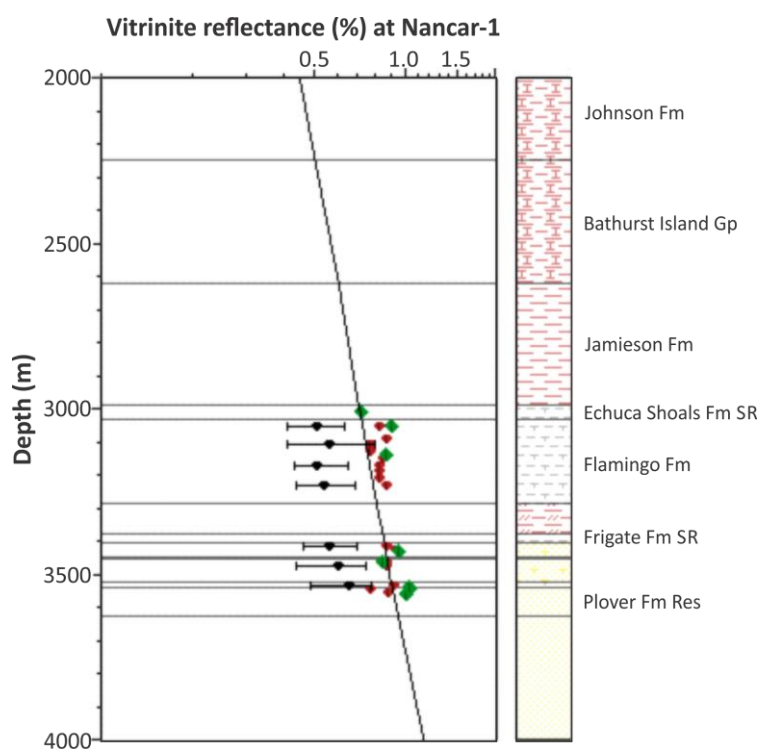


**Figure 6.9. Comparison of modelled vitrinite reflectance trend (black line) and three sets of vitrinite reflectance data in Nancar-1. Measured vitrinite reflectance (black dots), equivalent vitrinite reflectance calculated from T_max using the equation in Figure 6.8 (red dots) and equivalent vitrinite reflectance measured by FAMM (green dots) are shown. The range of vitrinite reflectance measurements in samples are shown by black range bars. The location of Nancar-1 is shown in Figure 6.1. For abbreviations, see Figure 6.4.**

Average heat flows used in scenario "b" and "c" were based on previous modelling studies conducted in neighbouring areas. For example, Kennard et al. (1999) investigated the thermal history of the Vulcan Sub-basin based on McKenzie's model (McKenzie, 1978) with a lithospheric stretching factor of approximately 1.5. The current model (scenario 'c') used an average heat flow value of 100 mW/m$^2$ during the rifting phase, followed by a gradual decrease and then a constant heat flow of 68 mW/m2 from the Eocene until the present-day **(Figure 6.5)**. The assignment of a heat flow pulse in this scenario was based on evidence of a Middle Jurassic−Lower Cretaceous extensional event in the study area (Baillie et al., 1994). In some wells, there is no direct evidence to constrain the rifting heat flow pulse, since the maximum temperatures recorded during the post-rift and Cenozoic burial obviously exceed those experienced in the rifting phase. Scenario 'c' is geologically more plausible than scenarios 'a' and 'b', and produces the best fit with the modelled trend shown in **Figure 6.10** for four representative wells.
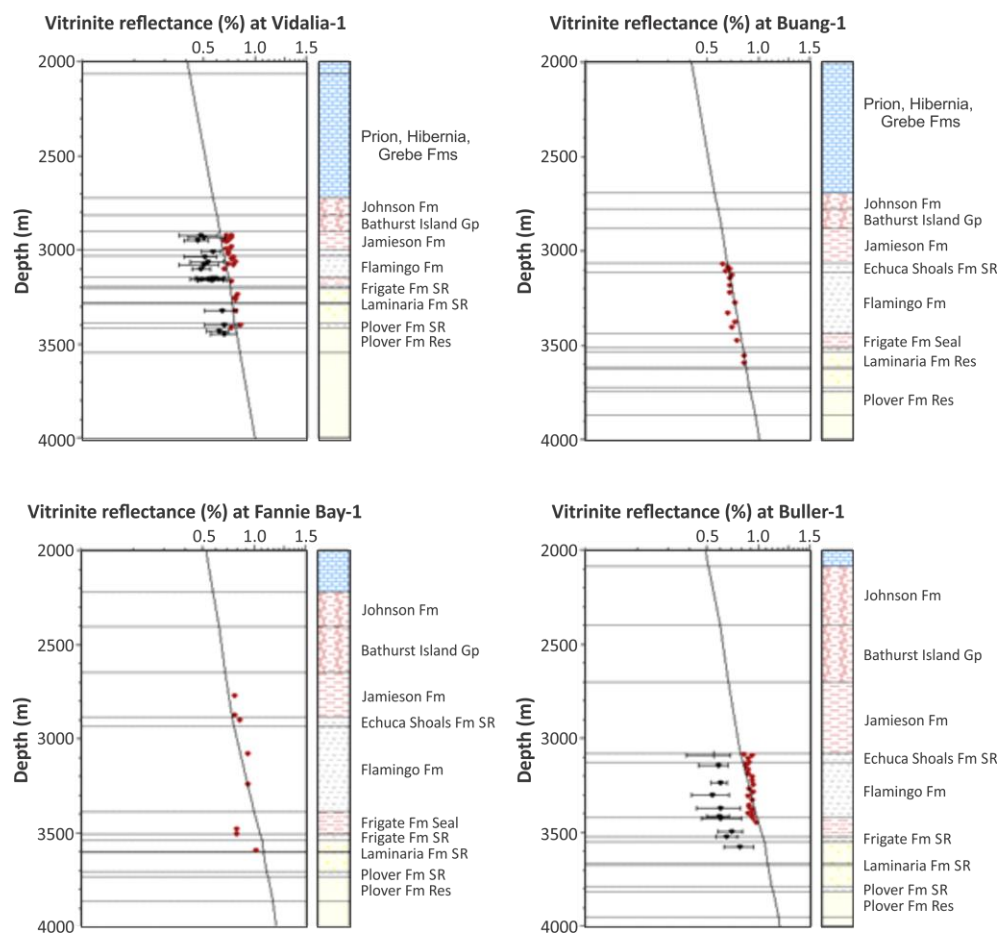


**Figure 6.10. Calibration of modelled vitrinite reflectance (black line) against calculated vitrinite reflectance (red dots) from T$_{max}$ values for four wells across the study area. T$_{max}$ values are based on the equation displayed in Figure 6.8. Black dots with range bars are measured vitrinite reflectance values (only known for Vidalia-1 and Buller-1). Well locations are shown in Figure 6.1. For abbreviations, see Figure 6.4.**

## 6.5. Burial history and source rock maturation

**Figure 6.11** shows the burial history of representative 1D extractions from the 3D model for four wells across the modelled area. Despite their different structural settings, these wells have relatively similar burial histories that reached maximum burial at the present-day. During the Middle Jurassic to Lower Cretaceous rifting phase the highest burial rates of 58 m/Ma were reconstructed around Fannie Bay-1, whereas lower rates of about 39 m/Ma and less than 20 m/Ma characterised the Laminaria-1 and Dillon Shoals-1 locations, respectively **(Figure 6.11)**. The Laminaria and Frigate formations and the uppermost part of the Plover Formation, deposited during this time period, thin considerably over the Londonderry High. Following this rifting event, these areas continued subsiding and a thick series of sediments were deposited until the present-day. Subsidence rates increased from the Miocene onwards in response to increased tectonic activity associated with Neogene collisional deformation (Woods, 1992; Harrowfield et al., 2003). The present-day burial depth reached by the Plover Formation ranges between 3500 m and 3600 m at Laminaria-1 and Ludmilla-1, and 4300 m at Fannie Bay-1. The increased rate of thermal subsidence led to rapid burial and hence increased thermal maturation. **Figure 6.12** shows the present-day temperatures reached by the four examined source rocks across the studied region. Temperatures for all source rocks range between 125 and 160°C in the Nancar Trough, and to < 90°C across parts of the Londonderry High. Due to its shallower burial, lower temperatures of 70-130°C were measured for the Echuca Shoals Formation.
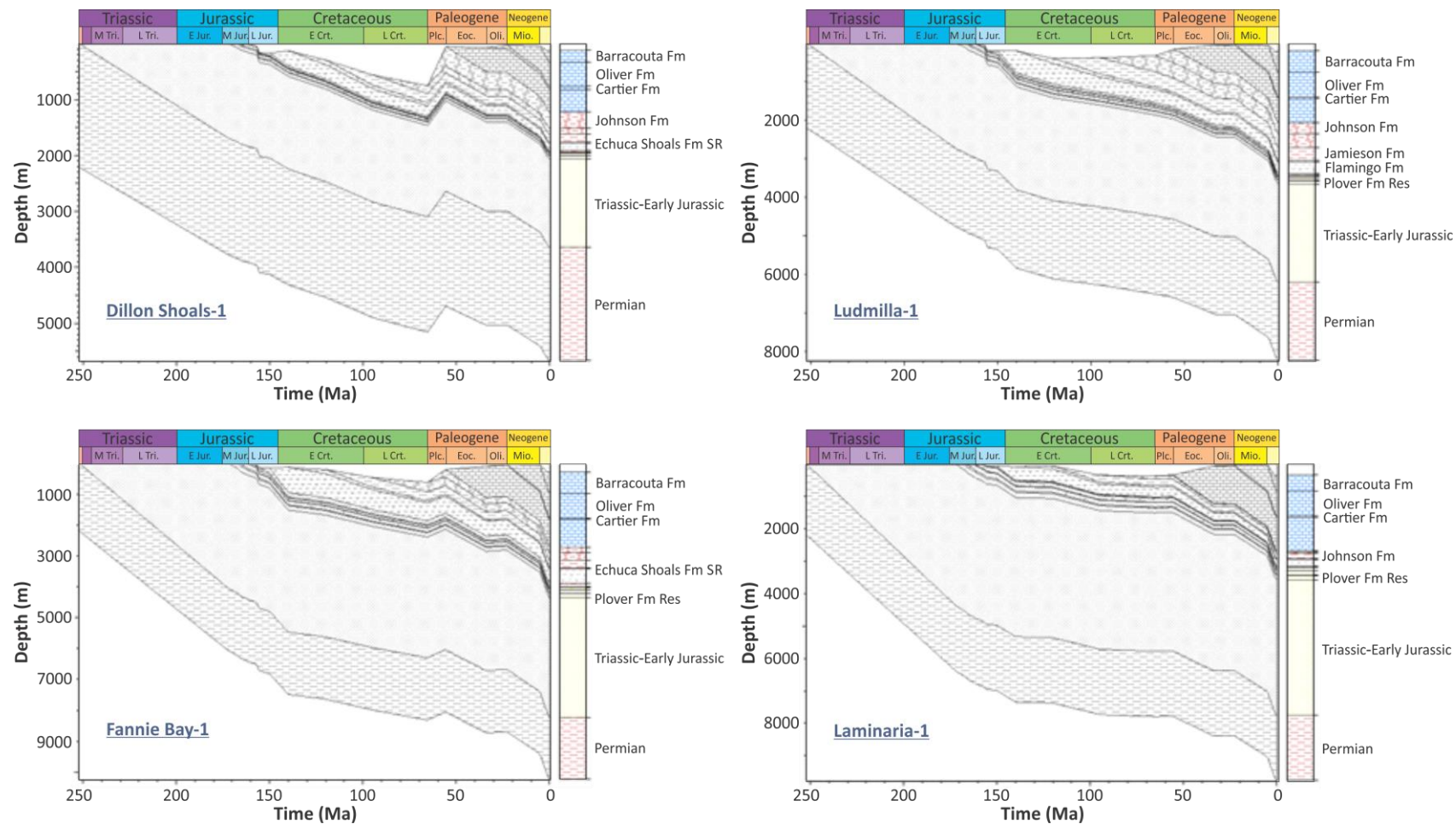
Figure 6.11. Modelled burial history of Dillon Shoals-1, Ludmilla-1, Fannie Bay-1 and Laminaria-1. Lithological well logs for each well are shown at the right of the burial history chart. Well locations are shown in Figure 6.1. For abbreviations, see Figures 6.4 and 5. Tri. = Triassic, Crt. = Cretaceous, Eoc. = Eocene, Mio. = Miocene.

234
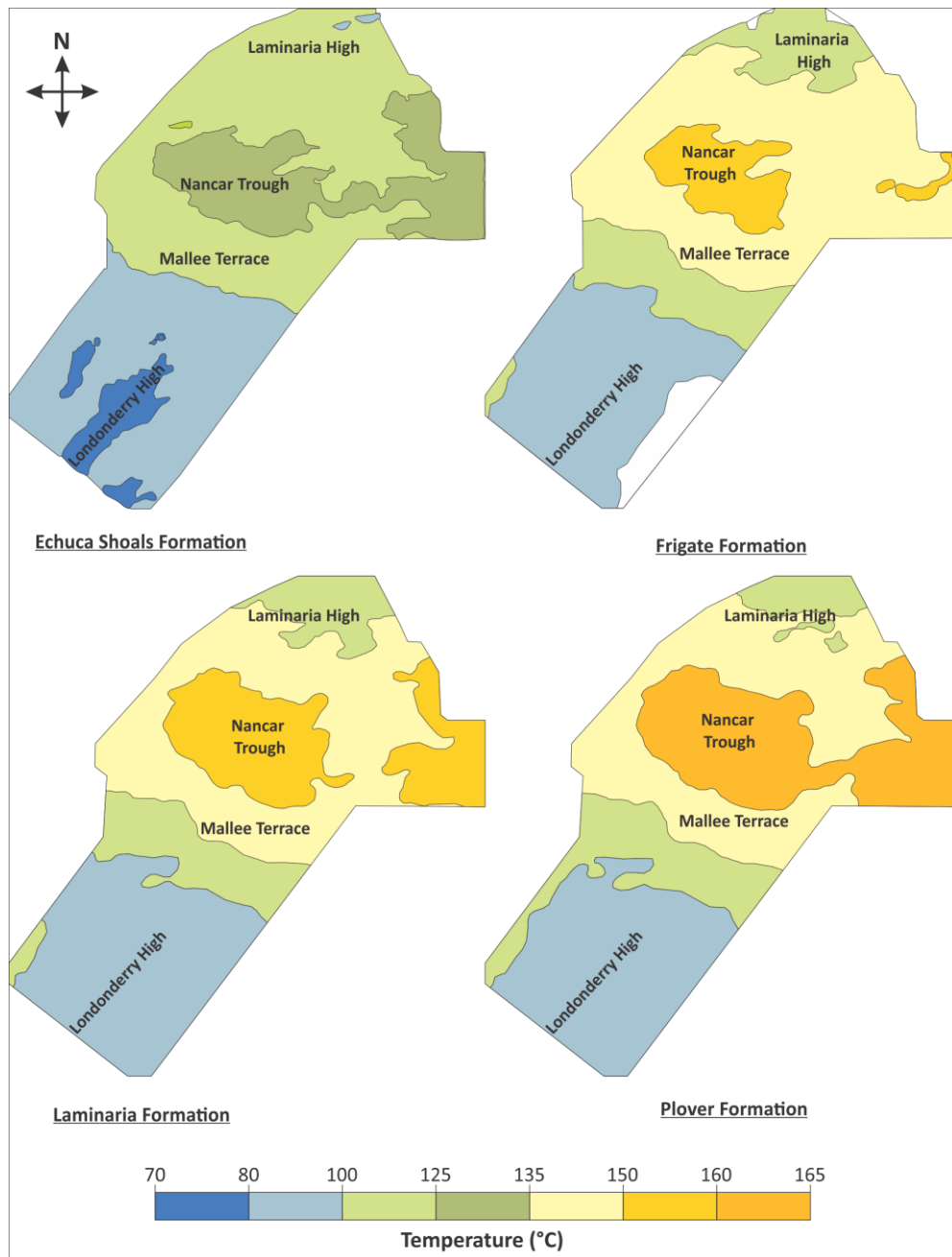
**Figure 6.12. Modelled present-day temperature maps for the Echuca Shoals, Frigate, Laminaria and Plover formations.**

## 6.6. Hydrocarbon generation and model sensitivity to maturation data

### 6.6.1. Hydrocarbon generation

Hydrocarbon generation was modelled using heat flow scenario 'c' for the wells Corallina-1, Fannie Bay-1 and Ludmilla-1, which were selected to be representative of the study area. The evolution of the transformation ratios (TR) through time and their modelled present-day values for the different source rocks (based on scenario 'b' and 'c') are shown in **Figure 6.13.** There is a remarkable variability in transformation ratios both through time, and over the structural elements of the study area. All of the investigated source rocks show

transformation ratios of less than 100%, which suggests that kerogen conversion is currently ongoing. The model indicates that the Lower Cretaceous Echuca Shoals Formation source rock is immature across the study area, as the present-day transformation ratio is less than 5%. The onset of hydrocarbon generation (10% TR) from both the Laminaria and the Frigate formation source rocks occurred in the Early Cretaceous within the Nancar Trough (Fannie Bay-1), in the Late Cretaceous for the Laminaria High (Corallina-1), and in the Eocene, for the Mallee Terrace (Ludmilla-1) **(Figure 6.13)**. These source rocks have present-day transformation ratios of 75-80% within the Nancar Trough, 30% on the Laminaria High, and 45% on the Mallee Terrace. Although buried deeper than the other source rock units, the Plover Formation displays present-day transformation ratios of 60% in the Nancar Trough, 23% on the Mallee Terrace, and only 12% on the Laminaria High. The onset of hydrocarbon generation from the Plover Formation occurred in the Late Eocene within the Nancar Trough, in the Pliocene on the Laminaria High, and in the Miocene on the Mallee Terrace. Based on the kinetic parameters measured in the laboratory and extrapolated to geological conditions, the shales of the Plover Formation exhibit more of an affinity to Type III organic matter than the other source rocks and, hence, require significantly higher temperatures to generate hydrocarbons (Abbassi et al., 2014a). This variability indicates that in addition to the present-day burial depth, the degree of kerogen conversion is controlled by organic matter type and molecular composition.

Based on these predictions, hydrocarbon generation occurred during at least two episodes **(Figure 6.13)**. The first phase and the onset of hydrocarbon generation was controlled by the influence of heating events related to rifting processes. The second and main phase of hydrocarbon generation and migration appears to have been triggered by the development of the thick Cenozoic carbonate platform that led to an increase in burial depth. During this time, fault-bounded structures were breached and subsequent loss of hydrocarbons occurred. This finding is in agreement with several previous basin models and studies on palaeo-oil columns which revealed the occurrence of multiple episodes of hydrocarbon charge in the Bonaparte Basin (Baxter et al., 1997; Lisk et al., 1998; Kennard et al., 1999; Fujii et al., 2004; Neumann et al., 2009).

### 6.6.2. Model sensitivity to maturation data

As previously mentioned, the data used to reconstruct the heat flow history of the study area is poorly constrained. Hence, for the two heat flow scenarios 'b' and 'c' the sensitivity of the timing of petroleum generation and the rate of kerogen conversion were investigated. Generation scenarios were tested and, apart from the thermal maturity data, no other changes

to the input parameters were applied. The major difference between the two scenarios is the predicted present-day transformation ratios **(Figure 6.13)**. The maximum temperature was attained in the Late Jurassic to Early Cretaceous for both scenarios, but in the case of scenario 'c', the higher post-rift heat flows resulted in higher present-day transformation ratios. The onset of petroleum generation is similar in both scenarios **(Figure 6.13)**, although scenario 'c' resulted in an earlier onset of petroleum generation.
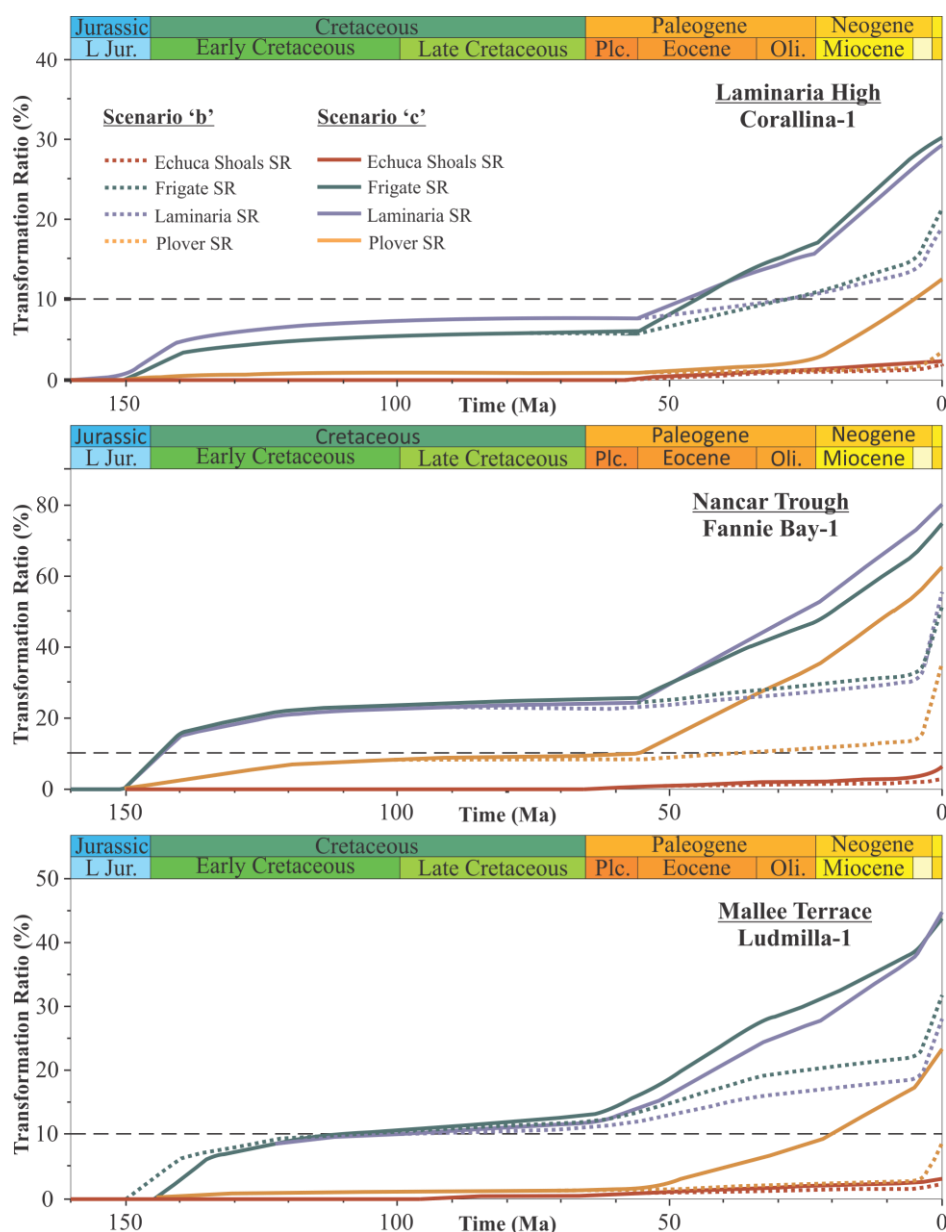


**Figure 6.13. Transformation ratio (TR) evolution for the Echuca Shoals, Frigate, Laminaria and Plover source rock (SR) samples from four representative wells across the study area, based on two palaeo heat flow scenarios ('b' and 'c', see text for discussion). Well locations are shown in Figure 6.1. For abbreviations, see Figure 6.5.**

The PetroReport module allows the calculation of the generation and expulsion balance and the amount of hydrocarbons accumulated in the reservoirs. As shown in **Figure 6.14**, the amount of generated and expelled hydrocarbons from all of the source rocks is much lower when scenario 'b' is used for the thermal calibration. As vitrinite reflectance suppression is a common feature in this region, a re-evaluation of the regional thermal maturity (e.g. using FAMM) is recommended, since the use of calculated vitrinite reflectance from Rock-Eval pyrolysis $T_{max}$ values has limitations, and the degree of suppression may not be the same as in the Vulcan Sub-basin.
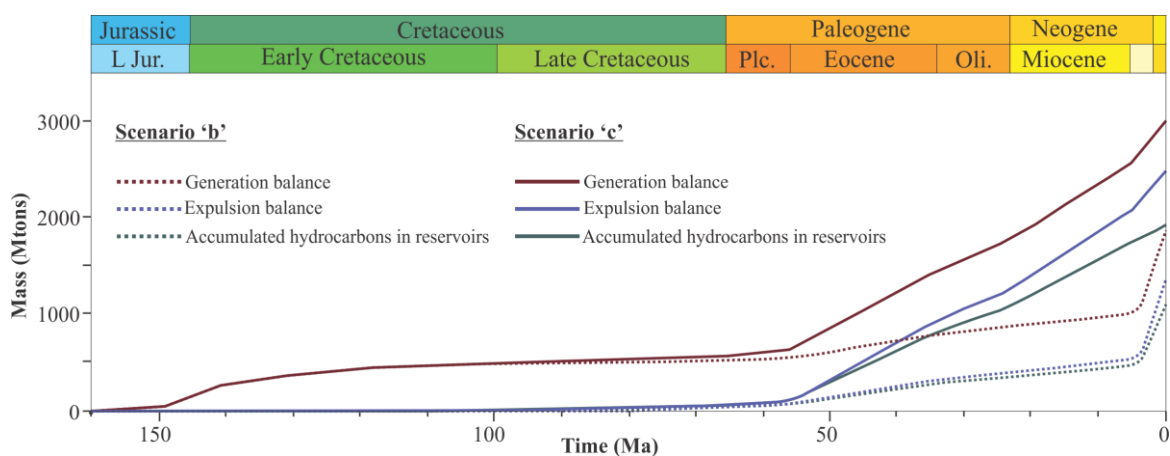


**Figure 6.14. Modelled hydrocarbon accumulations, hydrocarbon generation and expulsion balance based on two palaeo heat flow scenarios ('b' and 'c'). These outputs were generated in the PetroReport module implemented in the Petromod software. For abbreviations, see Figure 6.5.**

## 6.7. Hydrocarbon migration and model sensitivity to fault properties

Before presenting the migration results, it is important to highlight the geological simplifications and assumptions used in the model that may play a role in hydrocarbon accumulation predictions. The thickness and distribution of both reservoir and source rock units within the Plover Formation are poorly constrained due to sparse well data in this area, but also because stratigraphic units below the Oxfordian surface could not be mapped with confidence due to poor seismic resolution. The least geologically realistic assumption made in the model is the definition of homogeneous lithologies for the source rock and reservoir units. Variations of kinetic parameters of petroleum generation with facies were also not taken into account. Geochemically, the Plover Formation source rock contains heterogeneous type II/III organic matter (Abbassi et al., 2014a), and thus the use of one kinetic model may account for some of the discrepancies between the natural and modelled fluid properties. Another simplification of the model is that only Jurassic and Cretaceous

source rocks were incorporated. Potential older source rocks were not considered since these are below well penetrations. The 3D model developed for the Laminaria High and Nancar Trough region also has limitations. In this model, the available 3D seismic survey does not cover adjacent synclines, such as the Sahul Syncline and the Flamingo Syncline. It has been proposed that the northern Flamingo Syncline forms another potential mature kitchen that sourced the oil accumulations within the Laminaria High region (Preston and Edwards, 2000), and thus the omission of this source kitchen from the model will likely underestimate the amount of hydrocarbon charge available within the region.

Several migration scenarios were modelled so as to predict potential hydrocarbon accumulations and assess the ability of the model to reproduce naturally occurring fields in the study area. The different migration modelling scenarios used the hybrid flow module of Petromod, which combines both Darcy and Flowpath methods (Welte et al., 2000). This allows a better estimation of hydrocarbon distribution and accumulation. **Table 6.3** lists the different scenarios which were tested to identify the impact that faults may have on the modelled accumulations. Scenario I, in which no faults were included, was modelled as a control scenario. Scenarios II, III, IV, V and VI were used to conduct sensitivity analyses for a range of fault properties through time, and to identify whether these faults could have served as pathways for hydrocarbon migration. For the simulations based on the 3D seismic interpretation, 46 fault planes, some extending almost to the sea floor, show sub-vertical connectivity between the Mesozoic and Cenozoic fault systems. Thus, migration pathways across the Lower Cretaceous claystone top seal were important to model, and intersection planes were preferentially selected **(Figure 6.15)**. For the first scenarios with faults (II and III), fault properties were defined in individual sensitivity scenarios as open (scenario II, permeable) and closed (scenario III, impermeable) with respect to hydrocarbon migration **(Table 6.3)**. In scenario IV the main tectonic events were used to define the behaviour of the incorporated faults over time, and were based on the assumption that these faults remained open during active extensional events and closed during periods of tectonic quiescence (e.g. Hooper, 1991). The maximum post-rift displacement was mapped at the Late Miocene–Pliocene level (Charlton et al., 1991; O'Brien et al., 1999). This event is considered critical for hydrocarbon migration and scenarios V and VI were run to address this **(Table 6.3)**. In both scenarios V and VI, fault properties were defined as open during the syn-rift phase (163 to 137 Ma), closed during the post-rift phase (137 to 5.3 Ma) and either open from 5.3 Ma onwards (scenario V) or open from 5.3 to 1 Ma and then closed from 1 Ma onwards (scenario VI).

The outcomes from these different migration modelling scenarios were compared to the actual petroleum distribution including filled, under-filled, breached and dry structures throughout the study area **(Table 6.3)**. Results obtained from the scenario without faults (scenario I) show that the Laminaria, Corallina and Buller accumulations have been reproduced **(Table 6.3)**, whereas the fourth accumulation at Buffalo was not replicated. Oil accumulations were also predicted at structures where there is evidence of palaeo-oil columns or residual oil legs, such as at Ludmilla-1, Nancar-1 and Lameroo-1. In the study area, the direct contact between the reservoir and source rock units facilitates the movement of the hydrocarbons expelled from both the Plover and Laminaria source rocks into the carrier beds. Hydrocarbon migration is considered to be less efficient for the Frigate source rock which is overlain by the thick, relatively impermeable claystones of the Flamingo Group **(Figure 6.2)**.

In scenario II, smaller hydrocarbon accumulations or a complete loss of the previously trapped hydrocarbons which migrated into unsealed units **(Table 6.3)** were observed. Under filled structures, such as those at Corallina, Laminaria and Buller, show a residual oil charge. In the closed faults scenario (scenario III), faults seem to play a role in enhancing hydrocarbon trapping and slightly increasing the volume of oil accumulations **(Table 6.3)**. Scenario IV yields results similar to those of scenarios I and III, with the addition of scattered oil accumulations in the eastern part of the modelled area and towards the Londonderry High, and minor oil shows were modelled at Fannie Bay-1 and Lameroo-1 **(Figure 6.1)**. The Buffalo accumulation, unsuccessfully replicated by all the tested scenarios, was also partially reproduced by this scenario. The modelled under-filled structures could be due to either inadequacies in the seismic mapping due to the poor quality of the top reservoir reflector, or to the disregard in the model for the role played by these newly formed Cenozoic faults in the entrapment of hydrocarbons. However, the inability to reproduce charge in the Buffalo structure, where hydrocarbons are known to exist, could support a hydrocarbon charge mainly from the nearby, but un-modelled Flamingo Syncline. By the same reasoning, and as suggested by Preston and Edwards (2000), the source of the terrestrially-influenced oil in Jahal-1 ST1, located to the north of the Laminaria field, is inferred to be from a hydrocarbon charge from the northern Flamingo Syncline.
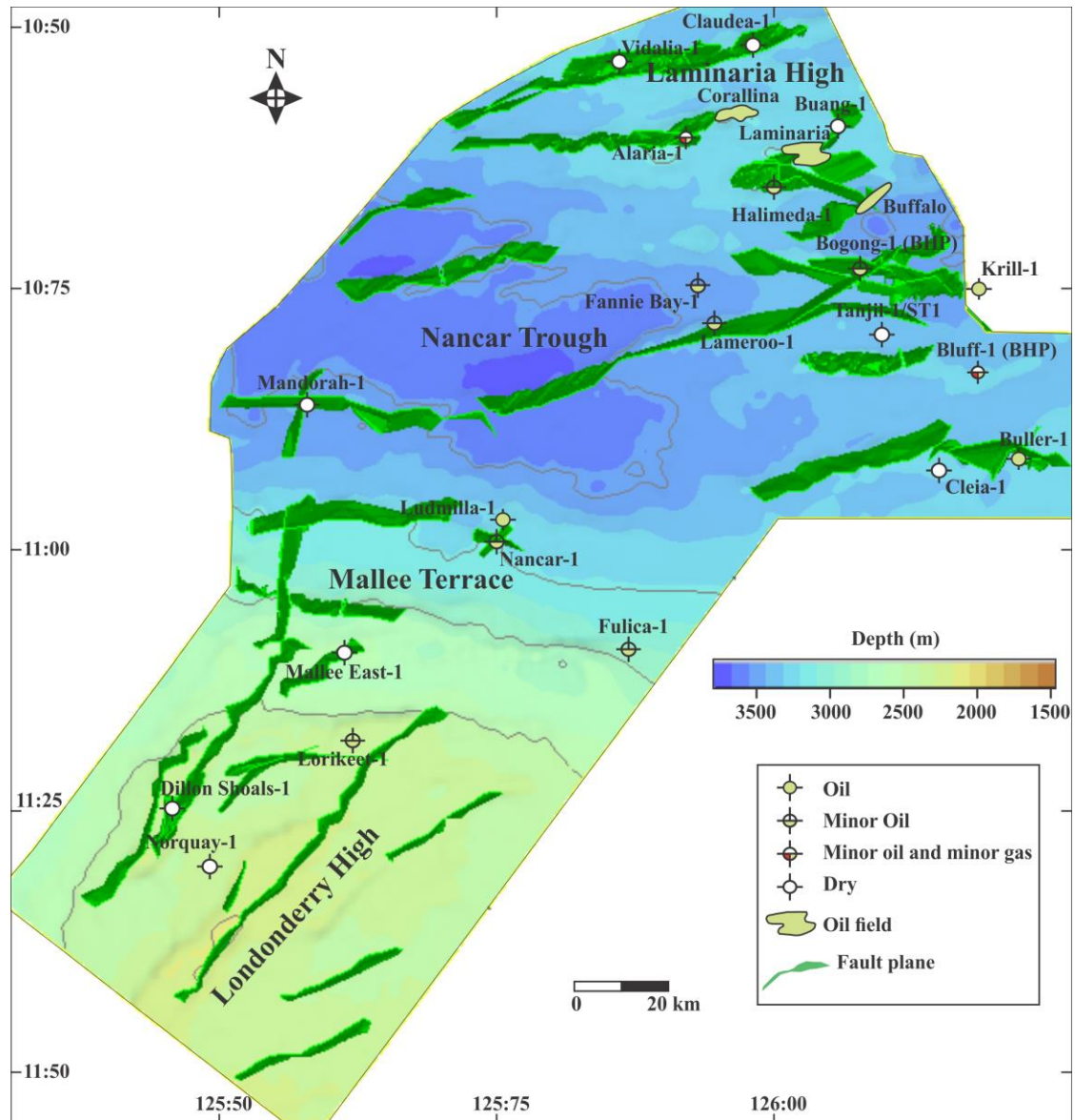
**Figure 6.15. Distribution of the fault planes interpreted at the top Echuca Shoals Formation (KA) surface, and incorporated into the migration scenarios II, III, IV, V and VI (see Table 6.3).**

Scenarios V and VI provide similar results to scenario II and indicate that most of the known accumulations previously filled and reproduced have been lost. This is explained by the fact that the assigned period for open fault conditions in these scenarios coincides with the main phase of hydrocarbon generation and expulsion **(Figure 6.13)**. Gas accumulations above the seal units were predicted based on the open faults scenarios **(Table 6.3)**; this is in agreement with gas shows observed in Alaria-1. The amount of accumulated hydrocarbons with respect to hydrocarbon losses estimated based on the control scenario (scenario I) and the most geologically plausible scenario was generated in the PetroReport module implemented in the

**241**

Petromod software (**Figure 6.16**). These estimations are qualitative rather than being volume predictive, and indicate that the modelling of open faults during the syn-rift and reactivation events affected not only the distribution of the predicted accumulations, but also the amount of hydrocarbon leakage out of the reservoirs into the overlying Upper Cretaceous and Cenozoic succession.

Overall, the tested migration scenarios presented show how faults can form either a structural trap, or act as hydrocarbon migration pathways. With respect to the present-day under-filled structures and structures with or without palaeo-oil columns, the model results point to leakage associated with fault reactivation rather than a lack of hydrocarbon charge. However, these simulations represent simplified scenarios for the complex fault systems that are developed within the Laminaria High and Nancar Trough regions. Further detailed modelling of the faults is required on a prospect scale, but this is beyond the scope of this regional study.
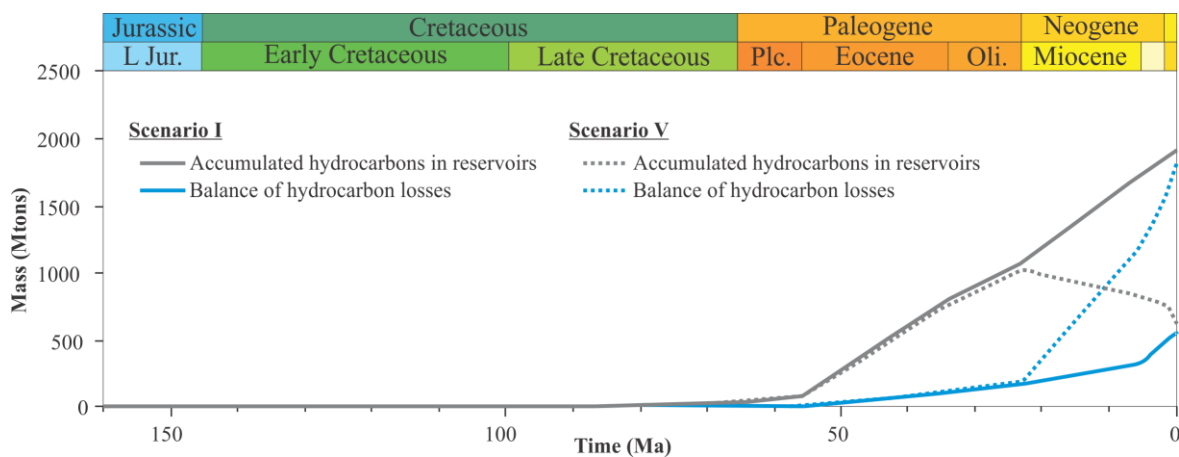


**Figure 6.16. Modelled volume of hydrocarbons accumulated in reservoirs and hydrocarbon losses, based on scenarios with faults (scenario V) and without faults (scenario I). In scenario V, faults were assigned as open from 163-137 Ma, closed from 137-5.3 Ma, and open again from 5.3-0 Ma. For abbreviations, see Figure 6.5.**

**Table 6.3. Fault properties used for the six modelled migration scenarios. The main observations and model predictions are also summarised.**

| Scenario | Fault inputs | | Model predictions |
|---|---|---|---|
| | **Syn-rift (163 – 137 Ma)** | **Post-rift (137 – 0 Ma)** | |
| I | No faults | No faults | - Present-day accumulations such as at the Laminaria, Corallina and Buller structures were reproduced. <br> - Accumulation were predicted at the Ludmilla-1 location, which currently has a residual oil leg (~4m). <br> - No accumulations were predicted around the Buffalo oil field and at the Fannie Bay-1 location. |
| II | Open | Open | - Total or complete loss of the previously reservoired hydrocarbons. <br> - Only small oil accumulations were predicted. <br> - Small gas accumulations and gas shows above the seal units. |
| III | Closed | Closed | - Similar results to those of scenario I. <br> - A slight increase in the volume of oil accumulations. |
| IV | Open | Closed | - Present day accumulations such as at the Laminaria, Corallina and Buller structures were reproduced. <br> - Small accumulations around the Buffalo Field. <br> - Scattered oil accumulations in the eastern and southern part of the modelled area. |
| V | Open | Closed: 137 – 5.3 Ma <br> Open: 5.3 – 0 Ma | - The distribution of the previously predicted accumulations was highly affected by loss of the known accumulations. <br> - A significant increase in the amount of hydrocarbon leakage. <br> - Small gas accumulations and gas shows above the seal units. |
| VI | Open | Closed: 137 – 5.3 Ma <br> Open: 5.3 – 1 Ma <br> Closed: 1 – 0 Ma | - Similar results to those of scenarios II and V. |

## 6.8.   Inferred accumulation history on the Laminaria High and Nancar Trough area

Oils retained in residual oil columns and oils trapped in fluid inclusions at Fannie Bay-1 and Ludmilla-1 in the Nancar Trough area have previously been reported to have been partially generated from a marine source rock facies, containing significant cyanobacterial input, as determined from the presence of monomethylalkanes (George et al., 2002). The depositional age and lateral extent of this cyanobacterial-rich source rock remains uncertain. However, it is emphasised that these accumulations could have received oils from both this source rock and from the more typical Jurassic source rocks. In contrast, the source rocks that generated the oil now trapped in the Laminaria, Corallina and Buffalo fields had a relatively strong land-plant component, and these oils are considered to have been sourced from the marginal marine to fluvio-deltaic package of the Plover and Laminaria formations in the northern Flamingo Syncline and Sahul−Nancar Trough region (Preston and Edwards, 2000). A possible mixing and co-sourcing from the cyanobacterial-rich source rock and the Middle to Upper Jurassic source rocks was suggested by George et al. (2004b) to explain the intermediate character of oils between the Laminaria and Flamingo highs.

Despite inferring a role for source kitchens beyond those modelled here, for the oils reservoired in the study area, the model predicts the distribution of the majority of present−day oil accumulations, including the Laminaria, Corallina and Buller oil fields. These predictions may be accounted for by an oil charge from the Nancar Trough kitchen. This theory is partially supported by the fluid inclusion study of George et al. (2004b), which suggested that liquid oil and not gas was originally retained in the traps within the Laminaria High and Nancar Trough region.

The transition from a liquid charge provided by the Nancar Trough kitchen to the unusual present-day light oils with low GORs seems to be have been driven by an additional light oil and/or gas condensate charge, most likely from coals of the Plover Formation within other mature kitchens, which postdates oil inclusion formation. Following late stage fault reactivation and trap breach, a complete or partial loss of hydrocarbons occurred. Likewise, the un-modelled Bayu/Undan gas field, located on the Flamingo High, could have received a liquid charge from the Nancar Trough kitchen (and possibly from the Flamingo Syncline), as well as a later significant gas and condensate charge from the Sahul Syncline (Edwards et al., 2004) that was preferentially retained. Oil inclusion abundance and geochemical data acquired on samples from Bayu-1 support this hypothesis (George et al., 2004a).

The secondary cracking of oil into gas under reservoir conditions, simulated by programmed-temperature closed-system pyrolysis, is predicted to begin at approximately 170°C (e.g. Horsfield et al., 1992; Schenk et al., 1997). In the deepest part of the Laminaria High and Nancar Trough area, the maximum present-day temperatures measured at reservoir levels range from 80°C to 160°C, indicating that in-reservoir oil-to-gas cracking is unlikely to have occurred. Equivalent vitrinite reflectance data deduced from aromatic hydrocarbon-based maturity parameters measured for oils reservoired in this area ranges from 0.72% to 0.98% (Preston and Edwards, 2000), less than that required to indicate the start of oil-to-gas cracking in the reservoir ($R_0 \sim 1.2\%$; Hill et al., 2003). In-source secondary cracking is implemented in the PhaseKinetics models that were used (di Primio and Horsfield, 2006), so any effect of residual oil secondary cracking in the source rocks could be calculated by the model. The model assumption is that secondary cracking of the six carbon chain groups ($C_7-C_{15}$, $C_{16}-C_{25}$, $C_{26}-C_{35}$, $C_{36}-C_{45}$, $C_{46}-C_{55}$ and $C_{55+}$) would lead to methane generation, as supported by data measured for naturally occurring fields (di Primio et al., 2011). In the Laminaria High and Nancar Trough region, modelled temperatures at source rock levels do not exceed 163°C (**Figure 6.12**) suggesting that major in-source secondary cracking of unexpelled oils can be excluded, although minor conversion could occur. Thus the displacement of oil from the Nancar source kitchen by a light oil and/or gas condensate charge implies the occurrence of one or more source rock kitchens that are sufficiently deeply buried for oil thermal degradation to occur (Dieckmann et al., 1998; Erdmann and Horsfield, 2006). More terrestrially-influenced source rocks, such as those within the Plover Formation, have the potential to have generated primary gas by kerogen cracking, and thus to have provided the gas charge to structures in the northern Bonaparte Basin.

Although the use of compositional kinetics in basin modelling allows prediction of the physical properties of accumulated fluids, the phase-state in natural fields within the modelled area is difficult to predict given some limitations. No GORs were measured on oils recovered from Ludmilla-1 and Fannie Bay-1, and hence verification of the modelled values is not possible. Fluids reservoired in the Laminaria and Corallina fields are reported to be unusually depleted in more water soluble low molecular weight hydrocarbons, such as toluene and benzene (Newell, 1999; Preston and Edwards, 2000; George et al., 2004b), and they have low GORs (**Table 6.4**). Not considering any additional potential kitchens in the modelling process renders any comparison between the predicted GORs and those measured in natural fields difficult. Moreover, the extrapolation of kinetic parameters assigned for the Plover Formation from the Vulcan Sub-basin into the Laminaria High and Nancar Trough region may affect the type of fluids generated, and also may result in the preferential

generation of one hydrocarbon phase over another. The complex filling history and variable fluid compositions in the region adds further complexity to any GOR comparison. It also remains challenging to accurately predict and explain the present-day GORs in this region, where both secondary alteration effects and the vertical leakage of hydrocarbons have occurred.

**Table 6.4. Measured gas-oil ratios (GORs) and API gravities from the northern Bonaparte Basin, as reported in well completion reports.**

| Well | GOR (scf/stb) | API ($^0$) |
|------|---------------|-----------|
| Buller-1 | 114 | 52 |
| Buffalo-1 | 126 | 53 |
| Laminaria-1 | 175 | 59 |
| Corallina-1 | 239 | 60 |

## 6.9.    Modelling outcomes and relevance to hydrocarbon prospectivity

The main outcomes of the 3D model and the previous interpretations of exploration drilling test for wells located in the Laminaria High and Nancar Trough region are summarised in **Table 6.5**. Out of the nine wells which penetrated dry structures (Dillon Shoals-1, Mallee East-1, Mandorah-1, Norquay-1, Tanjil-1), and structures with a restricted (e.g. Vidalia-1, Nancar-1 and Lameroo-1) or absent palaeo-oil column (e.g. Claudea-1), that were exploration failures previously attributed to a lack of hydrocarbon charge, five of these wells are predicted to have had access to hydrocarbon charge at least from the Nancar Trough kitchen, with only Dillon Shoals-1 being in a migration shadow. This charge was ostensibly lost through open faults as migration occurred in the mid-Eocene. Alternatively, lack of adequate hydrocarbon charge has been proposed to account for the dry structure drilled at Dillon Shoals-1. The model failed to reproduce structures where relatively significant palaeo-oil columns occurred, such as those encountered at Buang-1 and Buffalo-1. The absence of predicted accumulations in these structures may indicate hydrocarbon charge from adjacent kitchens such as the Flamingo syncline, instead of from the Nancar Trough, which has then been completely or partially lost. This result may also be due to the inaccurately mapped geometries for these structures as a result of poor seismic resolution. The latter rationale can also be applied for the structure at Fannie Bay-1, in which the model failed to reproduce a hydrocarbon accumulation.

**Table 6.5. Previous interpretations of structures drilled in the northern Bonaparte Basin compared with interpretations derived from this 3D model. The reservoir and primary targets, hydrocarbon shows, hydrocarbon indications, and previous interpretation data were compiled from Geoscience Australia interpretations, well completion reports and previous studies** (de Ruig et al., 2000; Brincat et al., 2001; Gartrell et al., 2002; Gartrell et al., 2005; 2006; Dyt et al., 2012).

| Well/Field name | Hydrocarbon show | Reservoir/Primary target | Result | Model interpretation | Previous interpretation |
|---|---|---|---|---|---|
| **Alaria-1** | Oil and gas show | Laminaria Formation | Evidence of a palaeo-oil column (15-26 m) and palaeo gas cap | Breached | Off-structure or breached |
| **Bluff-1 (BHP)** | Oil accumulation Gas show | Laminaria Formation Darwin Formation | ± 30 m oil column and a palaeo-oil column | Breached | Oil discovery, partially breached |
| **Bogong-1 (BHP)** | Oil show Oil show | Laminaria Formation Plover Formation | Evidence of a palaeo-oil column (~ 63m) | Breached | Inadequate seal or breached |
| **Buang-1** | No hydrocarbon shows | Laminaria Formation | Evidence of a palaeo-oil column (24-45 m) | Misinterpreted structure or other charge | Breached |
| **Buffalo** | Oil accumulation | Laminaria Formation | ± 50 m oil column and a palaeo-oil column (120-140 m) | Misinterpreted structure or other charge | Oil discovery, partially breached |
| **Buller-1** | Oil accumulation | Laminaria Formation | ± 27 m oil column and a palaeo-oil column | Partially breached | Oil discovery partially breached |
| **Claudea-1** | No hydrocarbon shows | Plover and Laminaria formations | No evidence for a palaeo-oil column | Breached | Lack of charge or breached? |
| **Cleia-1** | Oil show | Darwin Formation | Remigrated hydrocarbon shows | Breached | Off-structure or breached? |
| **Corallina** | Oil accumulation | Laminaria Formation | ± 77 m oil column and a palaeo-oil column (150 m) | Partially breached | Oil discovery, partially breached |
| **Dillon Shoals-1** | No hydrocarbon shows | Upper Triassic sandstones (Nome Formation) | No evidence for a palaeo-oil column | Lack of charge | Lack of charge? |
| **Fannie Bay-1** | Oil show | Laminaria Formation | Residual oil column | Misinterpreted structure | Poor reservoir quality or breached |
| **Fulica-1** | Oil show | Sandpiper Sandstone (Flamingo Formation) | No evidence for a palaeo-oil column | Lack of charge | Off-structure or breached |
| **Halimeda-1** | Oil show | Laminaria Formation | No evidence for a palaeo-oil column | Breached? | Off-structure or breached? |
| **Lameroo-1** | Oil show | Laminaria Formation | Residual oil column | Breached | Breached or lack of charge? |
| **Laminaria** | Oil accumulation | Laminaria Formation | 100 m oil column and a 10 m palaeo-oil column | Partially breached | Oil discovery, partially breached |
| **Lorikeet-1** | Oil show Oil show | Radiolarite Member (Jamieson Formation) Sandpiper Sandstone (Flamingo Formation) | No evidence for a palaeo-oil column | breached | Breached |
| **Ludmilla-1** | Oil accumulation | Sandpiper Sandstone (Flamingo Formation | 4 m oil column and a 50 m palaeo-oil column | Breached | Breached? |
| **Mallee East-1** | No hydrocarbon shows | Sandpiper Sandstone (Flamingo Formation) | No evidence for a palaeo-oil column | Breached | breached |
| **Mandorah-1** | No hydrocarbon shows | Plover and Laminaria formations | No evidence for a palaeo-oil column | Breached | Lack of charge or breached? |
| **Nancar-1** | No hydrocarbon shows | Plover and Sandpiper Sandstone (Flamingo Formation) | Palaeo-oil column (9 m)? | Breached | Lack of charge or breached |
| **Norquay-1** | No hydrocarbon shows | Sandstones of Prion and Grebe formations | No remigrated oil | Lack of charge | Breached (before trap formation)? |
| **Tanjil-1** | No hydrocarbon shows | Laminaria Formation | No evidence for a palaeo-oil column | Lack of charge | Breached? |
| **Vidalia-1** | No hydrocarbon shows | Plover and Laminaria formations | Evidence of a palaeo-oil column (~5m) | Breached | Lack of charge or breached? |

The model predicts a number of hydrocarbon accumulations, which are untested by exploration so far. For instance, to the southwest of Tanjil-1, a relatively large oil accumulation was reproduced by all tested scenarios. However, this newly predicted accumulation should not considered an exploration target before a detailed analysis of the structure is made since Tanjil-1 ST1 encountered only minor hydrocarbon shows with most sandstones being water-bearing. The mapping of present-day active leakage indicators, such as those determined from seismic attribute analysis and seepage surveys, would improve understanding of the fault system and its impact on hydrocarbon migration efficiency.

In summary, the application of this model has provided an explanation for traps within the Laminaria High and Nancar Trough region that are either dry or show evidence of a palaeo oil column. Most of the structures may have received charge from the mature hydrocarbon kitchen in the Nancar Trough. The scenario that best fits the geological evidence is scenario 'V', where the properties of faults were defined as leaking during the main phase of hydrocarbon generation and migration. These findings are in agreement with those reported by de Ruig et al. (2000), indicating that trap integrity is the principal risk in the Laminaria High and Nancar Trough region. Strong evidence for hydrocarbon leakage has been identified previously by hydrocarbon-related diagenetic zones on seismic (O'Brien and Woods, 1995; Cowley and O'Brien, 2000) and sea surface slicks detected by airborne laser fluorescence (Cooper et al., 1998).

Results from this study suggest fields in the Laminaria High and Nancar Trough region have received an oil charge from the mature Nancar Trough kitchen. Although it is beyond the aim of this paper to link hydrocarbon accumulations to their active source rock kitchens, it is possible that the oil compositions in these fields are a combination of a southerly Plover, Laminaria and Frigate-derived oil from the Nancar Trough kitchen and its extension into the Sahul Syncline, and a northerly Plover and Laminaria-derived low wax condensate-like hydrocarbon charge from the northern Flamingo Syncline. The gas has then been partially lost from traps and the retained oils have been subjected to further alteration by water washing (Newell, 1999) and/or evaporative fractionation (Edwards and Zumberge, 2005). Possible analogues for the oils observed in this region have been described by di Primio (2002) in Quadrant 25 in the North Sea, where an under-saturated oil was directly related to phases of severe fractionation. Hence, the residual light, high-API gravity oils currently reservoired in the Laminaria High and Nancar Trough region are the result of the co-sourcing of oils from multiple source rock units in several kitchens, as well as secondary alteration processes.

Further work which would enhance the findings from this study should include a 3D model which incorporates all potential source rock and reservoir units and their lateral and vertical variations in all three potential source kitchens (i.e. the Nancar Trough, and the Sahul and Flamingo synclines). This would provide more detailed insights into the fill history of accumulations in this region.

## 6.10. Conclusions

Three-dimensional petroleum system modelling indicate there is considerable variation in the thermal maturity reached by the Middle Jurassic to Lower Cretaceous source rocks throughout the Laminaria High and Nancar Trough region of the northern Bonaparte Basin. At the present-day, the Lower Cretaceous Echuca Shoals Formation is predicted to be immature for hydrocarbon generation across the entire study area. The Middle Jurassic Plover Formation source rock is mature for oil and gas generation within the Nancar Trough. The Jurassic Frigate and Laminaria formation source rocks are within the oil window within the study area, and if adequate structural traps remain intact, oil charge from these source rocks could have been preserved. The onset of hydrocarbon generation from these source rocks commenced during the Early Cretaceous. Modelling shows an increase in the degree of kerogen conversion between the Cenozoic and the present-day, indicating ongoing petroleum generation. Hence, there is minimal risk regarding the timing of hydrocarbon generation/expulsion in the area as it was after trap formation. This phase of hydrocarbon generation and migration provided significant oil charge in the Laminaria High and Nancar Trough areas. In spite of considering only the potential hydrocarbon charge from the Nancar Trough source kitchen, the model reproduced most of the present-day oil accumulations in the study area. Vertical leakage from faults that are open at the present-day was found to be the most likely explanation for structures that are completely or partially emptied of hydrocarbons. The present-day occurrence of light oils with low GOR may be explained by additional light oil and/or gas condensate dominated-charge from adjacent kitchens, such as the northern Flamingo Syncline. Oil-dominated fluids with relatively high GORs from the Nancar Trough kitchen were probably mixed to some degree with this northerly-sourced gas-rich charge. The reactivation of faults led to the migration and leakage of both the gas and the oil phase, which may partially explain the present-day under-filled structures and also the low GORs of the reservoir fluids.

## 6.11. Acknowledgments

## 6.12. References

Abbassi, S., George, S.C., Edwards, D.S., di Primio, R., Horsfield, B., Volk, H., 2014a. Generation characteristics of Mesozoic syn- and post-rift source rocks, Bonaparte Basin, Australia: New insights from compositional kinetic modelling. Marine and Petroleum Geology 50, 148-165.

Aitken, C.M., Jones, D., Larter, S., 2004. Anaerobic hydrocarbon biodegradation in deep subsurface oil reservoirs. Nature 431, 291-294.

Allen, P.A., Allen, J.R., 1990. Basin analysis: principles and applications. Blackwell Scientific Publications, Oxford, 451 p.

Baillie, P., Powell, C.M.A., Li, Z., Ryall, A., 1994. The tectonic framework of Western Australia's Neoproterozoic to Recent sedimentary basins, in: Purcell, P.G., Purcell, R.R. (Eds.), The Sedimentary Basins of Western Australia: Proceedings of the Petroleum Exploration Society of Australia Symposium, Perth, Western Australia, pp. 45-62.

Baxter, K., Cooper, G.T., O'Brien, G.W., Hill, K.C., Sturrock, S., 1997. Flexural isostatic modelling as a constraint on basin evolution, the development of sediment systems and palaeo-heat flow: application to the Vulcan Sub-basin, Timor Sea. Australian Petroleum Production and Exploration Association Journal 37, 136-153.

Bhatia, M., Thomas, M., Boirie, J., 1984. Depositional framework and diagenesis of the Late Permian gas reservoirs of the Bonaparte Basin. Australian Petroleum Exploration Association Journal 24, 299-313.

Borel, G., Stampfli, G., 2002. Geohistory of the North West Shelf: a tool to assess the Palaeozoic and Mesozoic motion of the Australian Plate, in: Keep, M., Moss, S.J. (Eds.), The Sedimentary Basins of Western Australia 3: Proceedings of Petroleum Exploration Society of Australia Symposium, Perth, Western Australia, pp. 119-128.

Botten, P., Wulff, K., 1990. Exploration potential of the Timor Gap Zone of Cooperation. Australian Petroleum Exploration Association Journal 30(1), 53-68.

Bradshaw, M., Yeates, A., Beynon, R., Brakel, A., Langford, R., Totterdell, J., Yeung, M., 1988. Palaeogeographic evolution of the North West Shelf region, in: Purcell, P.G., Purcell, R.R. (Eds.), The North West Shelf, Australia: Proceedings of the Petroleum Exploration Society of Australia Symposium, Perth, Western Australia, pp. 29-54.

Brincat, M., O'Brien, G., Lisk, M., De Ruig, M., George, S., 2001. Hydrocarbon charge history of the northern Londonderry: Implications for trap integrity and future prospectivity. Australian Petroleum Production and Exploration Association Journal 41(1), 483-496.

Brincat, M.P., Lisk, M., Kennard, J.M., Bailey, W.R., Eadington, P.J., 2004. Evaluating the oil potential of the Caswell Sub-basin: Insights from fluid inclusion studies, in: Ellis, G.K., Baillie, P.W., Munson, T.J. (Eds.), Proceedings of the Timor Sea Symposium, Northern Territory Geological Survey. Special Publication 1, Darwin, Northern Territory, pp. 437-455.

Charlton, T.R., Barber, A.J., Barkham, S.T., 1991. The structural evolution of the Timor collision complex, eastern Indonesia. Journal of Structural Geology 13, 489-500.

Cooper, G.T., Barnes, C.R., Bourne, J.D., Channon, G.J., 1998. Hydrocarbon leakage on the North West Shelf: New information from the integration of airborne laser fluorosensor (ALF) and structural data, in: Purcell, P.G., Purcell, R.R. (Eds.), The Sedimentary Basins of Western Australia 2: Proceedings of the Petroleum Exploration Society of Australia Symposium, Perth, Western Australia, pp. 255-271.

Cowley, R., O'Brien, G.W., 2000. Identification and interpretation of leaking hydrocarbons using seismic data: a comparative montage of examples from the major fields in Australia's north west shelf and Gippsland Basin. Australian Petroleum Production Exploration Association Journal 40, 121-150.

de Ruig, M.J., Trupp, M., Bishop, D.J., Kuek, D., Castillo, D.A., 2000. Fault architecture and the mechanics of fault reactivation in the Nancar Trough/Laminaria area of the Timor Sea, northern Australia. Australian Petroleum Production and Exploration Association Journal 40(1), 174-193.

di Primio, R., 2002. Unraveling secondary migration effects through the regional evaluation of PVT data: a case study from Quadrant 25, NOCS. Organic Geochemistry 33, 643-653.

di Primio, R., Horsfield, B., 2006. From petroleum-type organofacies to hydrocarbon phase prediction. American Association of Petroleum Geologists Bulletin 90, 1031-1058.

di Primio, R., Lehne, E., Kuhn, P., Baur, F., Horsfield, B., 2011. Petroleum Quality Prediction in Basin Modelling (Oral Presentation), International Meeting on Organic Geochemistry, Interlaken-Switzerland, 18–23 September.

Dieckmann, V., Schenk, H.J., Horsfield, B., Welte, D.H., 1998. Kinetics of petroleum generation and cracking by programmed-temperature closed-system pyrolysis of Toarcian Shales. Fuel 77, 23-31.

Dyt, C.P., Langhi, L., Bailey, W.P., 2012. Automating conceptual models to easily assess trap integrity and oil preservation risks associated with fault reactivation. Marine and Petroleum Geology 30, 81-97.

Edwards, D.S., Zumberge, J.E., 2005. The Oils of Western Australia II. Regional Petroleum Geochemistry and Correlation of Crude Oils and Condensates from Western Australia and Papua New Guinea. Geoscience Australia and GeoMark Research Ltd unpublished report, Canberra and Houston. GEOCAT 37512.

Edwards, D.S., Kennard, J.M., Preston, J.C., Summons, R.E., Boreham, C.J., Zumberge, J.E., 2000. Bonaparte Basin. Geochemical characteristics of hydrocarbon families and petroleum systems. Geoscience Australia Research Newsletter 33, 14-18.

Edwards, D.S., Preston, J.C., Kennard, J.M., Boreham, C.J., van Aarssen, B.G.K., Summons, R.E., Zumberge, J.E., 2004. Geochemical characteristics of hydrocarbons from the Vulcan Sub-basin, western Bonaparte Basin, Australia, in: Ellis, G.K., Baillie, P.W., Munson, T.J. (Eds.), Timor Sea Petroleum Geoscience: Proceedings of the Timor Sea Symposium, Darwin, Northern Territory, pp. 169-201.

Edwards, H., Crosby, J., David, N., Loader, C., Westlake, S., 2005. Australian Megasurveys—The key to new discoveries in maturing areas. Australian Petroleum Production and Exploration Association Journal 45, 407-420.

Erdmann, M., Horsfield, B., 2006. Enhanced late gas generation potential of petroleum source rocks via recombination reactions: Evidence from the Norwegian North Sea. Geochimica et Cosmochimica Acta 70, 3943-3956.

Faiz, M., Wilkins, R., Sherwood, N., Buckingham, C., Russell, N., Kinealy, K., 1998. Perhydrous vitrinite in the source rocks of the Western Timor Sea region. APCRC Confidential Report No.320, 223 p.

Fujii, T., O'Brien, G., Tingate, P., Chen, G., 2004. Using 2D and 3D basin modelling to investigate controls on hydrocarbon migration and accumulation in the Vulcan Sub-basin, Timor Sea, Northwestern Australia. Australian Petroleum Production and Exploration Association Journal 44(1), 93-122.

Gartrell, A., Lisk, M., 2005. Potential new method for paleostress estimation by combining by combining 3D fault restoration and fault slip inversion techniques: First test on the Skua field, Timor Sea, in: Boult, P., Kaldi, J.K. (Eds.), Evaluating fault and cap rock seals. AAPG Hedberg Series, no. 2, pp. 23-36.

Gartrell, A., Lisk, M., Underschultz, J., 2002. Controls on the trap integrity of the Skua oil field, Timor Sea, in: Keep, M., Moss, S.J. (Eds.), The sedimentary basins of Western Australia 3: Proceedings of the Petroleum Exploration Society of Australia Symposium, Perth, Western Australia, pp. 389-407.

Gartrell, A., Zhang, Y., Lisk, M., Dewhurst, D., 2004. Fault intersections as critical hydrocarbon leakage zones: integrated field study and numerical modelling of an example from the Timor Sea, Australia. Marine and Petroleum Geology 21, 1165-1179.

Gartrell, A., Bailey, W., Brincat, M., 2005. Strain localisation and trap geometry as key controls on hydrocarbon preservation in the Laminaria High area. Australian Petroleum Production and Exploration Association Journal 45, 477-492.

Gartrell, A., Bailey, W.R., Brincat, M., 2006. A new model for assessing trap integrity and oil preservation risks associated with postrift fault reactivation in the Timor Sea. American Association of Petroleum Geologists Bulletin 90, 1921-1944.

George, S.C., Volk, H., Ruble, T.E., Brincat, M.P., 2002. Evidence for a new oil family in the Nancar Trough area, Timor Sea. Australian Petroleum Production and Exploration Association Journal 42(1), 387–404.

George, S.C., Lisk, M., Eadington, P., 2004a. Fluid inclusion evidence for an early, marine-sourced oil charge prior to gas-condensate migration, Bayu-1, Timor Sea, Australia. Marine and Petroleum Geology 21, 1107-1128.

George, S.C., Ruble, T.E., Volk, H., Lisk, M., Brincat, M.P., Dutkiewicz, A., Ahmed, M., 2004b. Comparing the geochemical composition of fluid inclusion and crude oils from wells on the Laminaria High, Timor Sea, in: Ellis, G.K., Baillie, P.W., Munson, T.J. (Eds.), Timor Sea Petroleum Geoscience: Proceedings of the Timor Sea Symposium, Darwin, Northern Territory Geological Survey, Special Publication 1, pp. 203–230.

Gorter, J., Kirk, A., 1995. The Kimmeridgian marl in the Timor Sea: relevance to regional and geological evolution and possible hydrocarbon plays. Australian Petroleum Production and Exploration Association Journal 35(1), 152-168.

Gorter, J., Ziolkowski, V., Bayford, S., 1998. Evidence of Lower Triassic reservoirs with possible hydrocarbon charge in the southern Bonaparte Basin, in: Purcell, P.G., Purcell, R.R. (Eds.), The Sedimentary Basins

of Western Australia 2: Proceedings of the Petroleum Exploration Society of Australia Symposium, Perth, Western Australia, pp. 229-235.

Gurba, L.W., Ward, C.R., 1998. Vitrinite reflectance anomalies in the high-volatile bituminous coals of the Gunnedah Basin, New South Wales, Australia. International journal of coal geology 36, 111-140.

Harrowfield, M., Keep, M., 2005. Tectonic modification of the Australian North-West Shelf: episodic rejuvenation of long-lived basin divisions. Basin Research 17, 225-239.

Harrowfield, M., Cunneen, J., Keep, M., Crowe, W., 2003. Early-stage orogenesis in the Timor Sea region, NW Australia. Journal of the Geological Society 160, 991-1001.

Helby, R., Morgan, R., Partridge, A., 1987. A palynological zonation of the Australian Mesozoic. Memoir of the Association of Australasian Palaeontologists 4, 1-94.

Hill, R.J., Tang, Y., Kaplan, I.R., 2003. Insights into oil cracking based on laboratory experiments. Organic Geochemistry 34, 1651-1672.

Hocking, R.M., Moors, H.T., van de Graaf, W.J.E., 1988. Geology of the northern Carnarvon Basin. In The North West Shelf, Australia, in: Purcell, P.G., Purcell, R.R. (Eds.), Proceedings of the Petroleum Exploration Society of Australia Symposium, Perth, Western Australia, pp. 97-114.

Hooper, E., 1991. Fluid migration along growth faults in compacting sediments. Journal of Petroleum Geology 14, 161-180.

Horsfield, B., Schenk, H., Mills, N., Welte, D., 1992. An investigation of the in-reservoir conversion of oil to gas: compositional and kinetic findings from closed-system programmed-temperature pyrolysis. Organic Geochemistry 19, 191-204.

Huerta, A.D., Royden, L.H., Hodges, K.V., 1998. The thermal structure of collisional orogens as a response to accretion, erosion, and radiogenic heating. Journal of Geophysical Research 103, 287-215.

Kaiko, A., Tingate, P., 1996. Suppressed vitrinite reflectance and its effect on thermal history modelling in the Barrow and Dampier Sub-Basins. Australian Petroleum Production and Exploration Association Journal 36(1), 428-444.

Kennard, J.M., Deighton, I., Edwards, D.S., Colwell, J.B., O'Brien, G.W., Boreham, C.J., 1999. Thermal history modelling and transient heat pulses: new insights into hydrocarbon expulsion and 'hot flushes' in the Vulcan Sub-basin, Timor Sea. Australian Petroleum Production and Exploration Association Journal 39(1), 177-207.

Labutis, V.R., Ruddock, A.D., Calcraft, A.P., 1998. Stratigraphy of the southern Sahul Platform. Australian Petroleum Production and Exploration Association Journal 38(1), 115-136.

Langhi, L., Borel, G.D., 2008. Reverse structures in accommodation zone and early compartmentalization of extensional system, Laminaria High (NW shelf, Australia). Marine and Petroleum Geology 25, 791-803.

Langhi, L., Zhang, Y., Gartrell, A., Underschultz, J., Dewhurst, D., 2010. Evaluating hydrocarbon trap integrity during fault reactivation using geomechanical three-dimensional modeling: An example from the Timor Sea, Australia. American Association of Petroleum Geologists Bulletin 94, 567-591.

Langhi, L., Ciftci, N.B., Borel, G.D., 2011. Impact of lithospheric flexure on the evolution of shallow faults in the Timor foreland system. Marine Geology 284, 40-54.

Lewan, M.D., 1993. Identifying and understanding suppressed vitrinite reflectance through hydrous pyrolysis experiments, Tenth Annual Meeting of the Society for Organic Petrology, Abstracts and Program, V. 10, pp. 1-3.

Lisk, M., Brincat, M.P., Eadington, P.J., O'Brien, G.W., 1998. Hydrocarbon charge in the Vulcan Sub-basin, in: Purcell, P.G., Purcell, R.R. (Eds.), The Sedimentary Basins of Western Australia 2: Proceedings of the West Australian Basins Symposium, Perth, Western Australia, pp. 287-305.

Longley, I.M., Buessenschuett, C., Clydsdale, L., Cubitt, C.J., Davis, R.C., Johnson, M.K., Marshall, N.M., Murray, A.P., Somerville, R., Spry, T.B., Thompson, N., 2002. The North West Shelf of Australia: a Woodside perspective, in: Keep, M., Moss, S. (Eds.), The Sedimentary Basins of Western Australia 3: Proceedings of Petroleum Exploration Society of Australia Symposium, Perth, Western Australia, pp. 27-88.

McKenzie, D., 1978. Some remarks on the development of sedimentary basins. Earth and Planetary Science Letters 40, 25-32.

Mory, A.J., 1991. Geology of the offshore Bonaparte Basin, Northwestern Australia. Geological Survey of Western Australia Report 29, 47 p.

Neumann, V., di Primio, R., Horsfield, B., 2009. Source rock distributions and petroleum fluid bulk compositional predictions on the Vulcan Sub-basin, offshore Western Australia: Report for Geoscience Australia 67, 64 p.

Newell, N.A., 1999. Bonaparte and Browse basins-Water washing in the Northern Bonaparte Basin. Australian Petroleum Production and Exploration Association Journal 39(1), 227-247.

O'Brien, G.W., Woods, E.P., 1995. Hydrocarbon-related diagenetic zones (HRDZs) in the Vulcan Sub-basin, Timor Sea: recognition and exploration implications. Australian Petroleum Production and Exploration Association Journal 35, 220-220.

O'Brien, G.W., Lisk, M., Duddy, I., Eadington, P., Cadman, S., Fellows, M., 1996. Late Tertiary fluid migration in the Timor Sea: a key control on thermal and diagenetic histories. Australian Petroleum Production and Exploration Association Journal 36(1), 399-427.

O'Brien, G.W., Lisk, M., Duddy, I.R., Hamilton, J., Woods, P., Cowley, R., 1999. Plate convergence, foreland development and fault reactivation: primary controls on brine migration, thermal histories and trap breach in the Timor Sea, Australia. Marine and Petroleum Geology 16, 533-560.

Pattillo, J., Nicholls, P.J., 1990. A tectonostratigraphic framework for the Vulcan Graben, Timor Sea region. Australian Petroleum Exploration Association Journal 30(1), 27-51.

Powell, T., 2004. Australia's hydrocarbon provinces-Where will future production come from? Australian Petroleum Production and Exploration Association Journal 44, 729-740.

Preston, J.C., Edwards, D.S., 2000. The petroleum geochemistry of oils and source-rocks from the northern Bonaparte Basin, offshore northern Australia. Australian Petroleum Production and Exploration Association Journal 40(1), 257-282.

Price, L.C., Baker, C.E., 1985. Suppression of Vitrinite reflectance in amorphous rick kerogen-A major unrecognized problem. Journal of Petroleum Geology 8, 59-84.

Schenk, H., Di Primio, R., Horsfield, B., 1997. The conversion of oil into gas in petroleum reservoirs. Part 1: Comparative kinetic investigation of gas generation from crude oils of lacustrine, marine and fluviodeltaic origin by programmed-temperature closed-system pyrolysis. Organic Geochemistry 26, 467-481.

Seggie, R., Ainsworth, R., Johnson, D., Koninx, J., Spaagaren, B., Stephenson, P., 2000. Field management and reservoir characterisation-Awakening of a super giant, Sunrise-Troubadour Gas-Condensate Field. Australian Petroleum Production and Exploration Association Journal 40, 417-438.

Sibson, R.H., 1996. Structural permeability of fluid-driven fault-fracture meshes. Journal of Structural Geology 18, 1031-1042.

Smith, G.C., Tilbury, L.A., Chatfield, A., Senycia, P., Thompson, N., 1996. Laminaria: a new Timor Sea discovery. Australian Petroleum Production and Exploration Association Journal 36(1), 12-29.

Veevers, J.J., Conaghan, P.J., 1984. Phanerozoic earth history of Australia. Clarendon Press, Oxford, 418 p.

Welte, D.H., Hantschel, T., Wygrala, B.P., Weissenburger, K.S., Carruthers, D., 2000. Aspects of petroleum migration modelling. Journal of Geochemical Exploration 69–70, 711-714.

Whibley, M., Jacobson, T., 1990. Exploration in the northern Bonaparte Basin. Timor Sea-WA-199-P. Australian Petroleum Exploration Association Journal 30(1), 7-25.

Whittam, D.B., Norvick, M.S., Mclntyre, C.L., 1996. Mesozoic and Cainozoic tectonostratigraphy of western ZOCA and adjacent areas. Australian Petroleum Production and Exploration Association Journal 36(1), 209-232.

Wilkins, R.W.T., Wilmshurst, J.R., Russell, N.J., Hladky, G., Ellacott, M.V., Buckingham, C., 1992. Fluorescence alteration and the suppression of vitrinite reflectance. Organic Geochemistry 18, 629-640.

Woods, E., 1992. Vulcan Sub-basin fault styles-implications for hydrocarbon migration and entrapment. Australian Petroleum Exploration Association Journal 32(1), 138-138.

Wygrala, B., 1989. Integrated Study of an Oil Field in the Southern Po Basin. Berichte der Forschungszentrum Jülich 2313, 1-217.

## 7.1. Coal contribution to oil and gas accumulations in the Gippsland and Bonaparte basins

In the Gippsland Basin, coals deposited within the delta plain facies throughout the Maastrichtian−Paleocene Halibut Subgroup contain land-plant-dominated organic matter with variable potential for both gas and liquid hydrocarbon generation. Based on the sample set used in this study, the Py-GC results indicate that these coals are heterogeneous, being capable of generating high wax P-N-A oils (**Figure 7.1**). Assuming a constant geological heating rate of 3.3°C/Ma, kinetic modelling predicts that the main phase of petroleum formation (at 70% transformation ratio) for the coals of the Halibut Subgroup occurs at 178°C, indicating high kinetic stability (**Figure 7.1**). Where sampled, coals from this subgroup have lower HI values (< 200 mg HC/ g TOC) than are required for efficient oil generation/expulsion (e.g. Hunt, 1991; Sykes and Snowdon, 2002). This finding, coupled with the relatively low volume proportion of coals compared to shales, suggests that the coals of the Gippsland Basin may not have contributed significant volumes of hydrocarbons to the oil accumulations. However, gas can be generated and expelled from these coals by the cracking of retained and non-expelled hydrocarbons.

In the Bonaparte Basin, coals of the Middle Jurassic Plover Formation that were deposited in a fluvio-deltaic setting have excellent petroleum potential and HI values above 400 mg HC/g TOC, indicating that they have the potential to efficiently expel liquid hydrocarbons. These coals show an enrichment in alkylphenols and aromatic hydrocarbons (benzene, toluene and xylene) relative to the *n*-alkanes/alkenes in their pyrolysates. These characteristics, combined with a broad activation energy distribution (58 to 70 kcal/mol), suggest the occurrence of lignocellulosic organic matter content and thus a pronounced land-plant influence. The Py-GC results reveal that they have the potential to generate two petroleum organofacies: gas-condensates and P-N-A oils with a high wax content (**Figure 7.1**). With the assumption of a constant geological heating rate of 3.3°C/Ma, the main phase of petroleum formation occurs over a broad temperature range of 160–180°C, indicating that bulk kinetic predictions are directly controlled by the molecular structure of the kerogens within these coals (**Figure 7.1**). Artificial maturation using closed-system pyrolysis at a heating rate of 0.7°C/min indicates that within the main oil window, coals of the Plover Formation generate black oils with low GORs (160 $Sm^3/Sm^3$), whereas at advanced levels

of kerogen conversion (90%), light oils are produced. Oils on the Laminaria High, an area within the northern Bonaparte Basin, are interpreted to be expelled over a temperature range of 127−137°C. Thus, these oils could not be derived from coals of the Plover Formation, as at these estimated thermal maturities the kerogen within these coals has not reached any significant conversion (less than 15% transformation). In contrast, kinetic model predictions show that the high wax P-N-A generating facies could produce some oils with low GORs, as inferred to be the case in the southern Vulcan Sub-basin where waxy oils were recovered at Montara and Maret. However, gas and condensate are typically the most abundant products derived from the Plover Formation coals.

Results from this study also show that the liquid hydrocarbon generative potential of coals in the Gippsland Basin is not discerned using Rock-Eval pyrolysis HI values alone. The inability of this technique to evaluate the oil-generating potential of coals was addressed by Horsfield et al. (1988). HI values determined for coals within the Gippsland Basin are below 200 mg HC/g TOC, indicating gas-prone organic matter. Despite the low HI of the coals, data derived from Py-GC show that coal pyrolysates are characterised by extended series of *n*-alkane/*n*-alkene homologues, suggesting some oil potential for these coals. Based on this study, coals in both the Gippsland and Bonaparte basins show the potential to generate liquid hydrocarbons (P-N-A oils). However, the Jurassic Plover Formation coals have better oil potential than the Latrobe Group coals, and seem to have the capacity to produce more liquid hydrocarbons. This has a great significance in implying that oil-source potential characteristics of coals may vary over relatively small geographical distances. Depositional conditions may account for variations in the generation potential between coals of similar age or within specific coal measures. On a time scale, this finding is unexpected since several studies have shown a decrease in oil potential from the stratigraphically younger to older coals (e.g. Petersen and Nytoft, 2006). However, this in a good agreement with observations made by Macgregor (1994), in that stratigraphically oil-prone coals are mainly restricted to Jurassic and younger sequences, with one exception being the Permian Coals of the Australian Cooper Basin, where microbial biomass accounts for the good oil potential of these coals (Curry et al., 1994; Powell and Boreham, 1994). Mechanisms controlling oil generation/expulsion from coals have been a topic of debate for many years (e.g. Durand and Paratte, 1983; Murchison, 1987; Hunt, 1991; Wilkins and George, 2002). Numerous workers have attempted to constrain these mechanism by palaeobotanical investigations (e.g. Scott, 1987; Bertrand, 1991).

In the following two sections, the potential processes controlling the oil potential of coals as well as some interpretations regarding their contribution to oil and gas in both the Gippsland and Bonaparte basins are provided. To achieve these, it is important to understand floral evolution and the conditions of the preservation of higher plants through the Jurassic to early Neogene time interval.
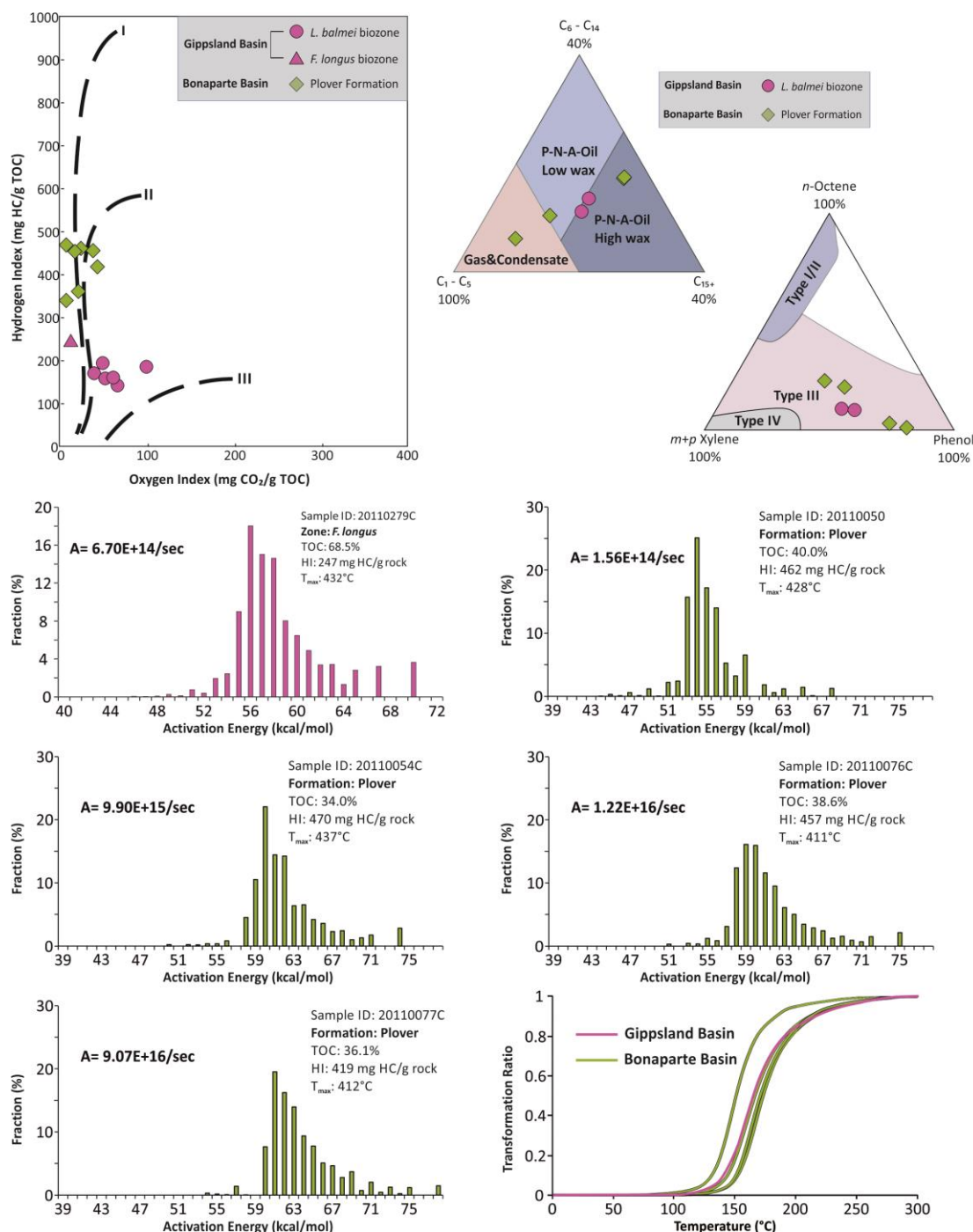


**Figure 7.1. Geochemical characteristics of coals in the Gippsland and Bonaparte basins.**

## 7.2.    Possible controls on coal characteristics in the Gippsland Basin

Overall, the Cretaceous and younger flora are predominantly composed of angiosperms. Swamp margin and aquatic herbaceous angiosperms are reported to have been dominant during the Late Cretaceous (Hedges and Parker, 1976; Retallack and Dilcher, 1981; Spicer and Parrish, 1986). The Upper Cretaceous to Cenozoic is referred to as a period of great variety of peat types similar to those of modern peat-forming environments, where diverse and large amounts of resins from gymnosperms, cones and seeds accumulated (Teichmuller and Teichmuller, 1968; Gould and Shibaoka, 1980). In eastern and southern Australia, the Cretaceous period is described as being a period of widespread development of conifer/angiosperm rainforests (Dettmann, 1981). Most coals deposited in these regions are vitrinite-rich, implying their derivation from the woody parts of terrigenous plants. In the Gippsland Basin, Thomas (1982) related the occurrence of oil-prone coals in Australian basins, including the Gippsland Basin, to the dominance of conifers that proliferated after the separation of Australia from Gondwana in the Late Jurassic, and to the evolution of angiosperms from the Late Cretaceous. However, there is only a limited amount of data that has been available in unpublished reports on the maceral composition of the coal-bearing fluvio-deltaic Latrobe Group. These data indicate that the Latrobe Group coals are composed predominantly of vitrinite. In addition, these coals contain variable amounts of liptinite and resinite (15-20%) that are generally considered to have the capacity to generate oil (Jones, 1987; Hunt, 1991). Based on hydrous pyrolysis data, Shanmugam (1985) concluded that the paraffinic oils in the Gippsland Basin correlate with waxy lipids in coals, whereas the naphthenic oils are largely derived from resins. In the current study, an attempt was made to link bulk maceral composition and petroleum organofacies for the shales and coals in the Gippsland Basin, but this revealed that there is no strong relationship. Such a lack of correlation has been largely attributed to varying chemical properties of vitrinite and liptinite maceral groups (e.g. Bertrand et al., 1986b). This raises the possibility that the occurrence and properties of hydrogen-rich vitrinite, and additional processes, such as environmental preservation conditions led to varying oil-generating potential and type in coals of the Latrobe Group.

Coals deposited in lower delta plains, such as is the case for the coals in the Gippsland Basin, are generally described as being laterally widespread but vertically thin (Horne et al., 1978; Fielding, 1985). Based on their relatively low HI values, coals of the Halibut Subgroup in the Gippsland Basin do not have a significant liquid hydrocarbon generating potential. However, coals of the Latrobe Group, as a whole, are traditionally regarded in the literature and by oil exploration companies as the main sources for oil and gas in the Gippsland Basin

(e.g. Smith and Cook, 1984; Shanmugam, 1985). Compared to other South-east Asian basins, where there are uncertainties over which of (1) lacustrine shales, (2) interbedded shales with coals, and (3) coals act as effective source rocks, the Gippsland Basin is typically viewed as the least disputed case of a coal-sourced oil province. Evidence emerging from analyses conducted in this study indicate that shales and coaly shales appear to have higher potential for liquid hydrocarbon generation compared to coals, at least for the coals from the Halibut Subgroup. Based on the low HI values measured for the coals, expulsion seems to be a critical factor controlling the oil potential of these coals (Pepper, 1991; Pepper and Corvi, 1995). Alternatively, gas rather oil could be produced from these coals by secondary cracking of (1) the retained bitumen fraction and (2) the generated hydrocarbons trapped within the coal structure, when sufficiently high temperatures (~ 150 - 220°C; Clayton, 1991) are reached for this process to occur.

The lines of evidence drawn to relate oils in the Gippsland Basin to coals within the Latrobe Group are mainly based on (1) the high wax content of the oils, (2) the high pristane/phytane ratio, and (3) the large similarity between oils and coal extracts with respect to their *n*-alkane distribution and pattern (Shanmugam, 1985). Apart from shales of the *P. mawsonii*, *T. apoxyexinus* and *N. senectus* biozones, Py-GC data reported in the current study reveal that, at a molecular and even at a bulk kinetic level, there are no systematic differences between shales, coaly shales and coals. All of these sediments display the potential to generate high-wax oils at relatively advanced levels of thermal maturity, indicating their mainly stable nature at lower temperatures. These geochemical similarities and the consistency of shale pyrolysates with waxy oil-generating potential would render it difficult to ascertain which of these coals and shales have contributed to oil and gas accumulations in the Gippsland Basin. The hydrocarbon and more specifically the biomarker content may also have originated from the same precursors, and thus differentiating oils generated by coals from those produced by associated or interbedded shales can be a delicate task to solve. With these constraints in mind, the fact that the coals investigated in this study are incapable of expelling oil and thus contributing to oil and gas accumulations in the Gippsland Basin should be taken with caution, as this could be due to sampling factors. Specifically, the coal samples investigated in this study are from the Halibut Subgroup (the *L. balmei* and *F. longus* biozones) and may not be representative of the Latrobe Group as a whole. Unsampled coals within potential source kitchen areas may have higher hydrogen index values and accordingly the possibility that oil has been generated and migrated out of the coal to charge reservoir structures in the Gippsland Basin cannot be discounted. Results from this study also favour significant potential oil contributions from oil-prone lacustrine (e.g. *P. mawsonii*

biozone) facies, which have previously been ignored and/or underestimated. Although regarded in this study as gas-prone, equivalents of the *N. senectus* and *T. apoxyexinus* biozones are potentially organic-rich sources for oils in the Gippsland Basin (unpublished work). Additional deep oil and gas sources are likely to occur within this basin, but those contributions are probably unrecognised due to their great depths, and thus cannot be excluded.

## 7.3. Possible controls on coal characteristics in the Bonaparte Basin

On a global scale, the climate during the Jurassic period is reported to have been uniformly mild, leading to the peak development of similar plant communities dominated by gymnosperms including conifers, ferns and ginkgos (Thomas, 1982; Stewart and Rothwell, 1993). Collinson et al. (1994) examined the evolution of plants and selected plant compounds related to the generation of liquid hydrocarbons from coal-bearing sequences in order to explain the absence of oil-sourcing Carboniferous coals. In their review, Collinson and co-authors stated that Early Mesozoic coals are generally dominated by confers. In addition, Lapo and Drozdova (1989) concluded that bark tissue from conifers and cuticles are the dominant components of Jurassic and Lower Cretaceous coals. No detailed fossil plant investigation is available for the Lower to Middle Jurassic coals of the Plover Formation within the Bonaparte Basin. Nevertheless, further to the east in the Surat Basin, Gould and Shibaoka (1980) described the Middle Jurassic Walloon Coal as being predominantly composed of conifers. In addition, the oil potential of Jurassic coals in this latter basin was speculated to be due in part to the occurrence of liptinite, and also to be partly governed by vegetation type and biochemical changes (Saxby and Shibaoka, 1986).

The compositional kinetic models discussed in Chapter 4 and 5 reveal that at all of stages of the oil window, coals of the Plover Formation, where sampled in the Vulcan Sub-basin, have the potential to generate oils. This is also surprising since it is generally thought that even oil-prone coals generate more gas than oil in comparison to shales or other source rock facies (Macgregor, 1994). Variable amounts of liptinite macerals (e.g. liptodetrinite) were measured for sediments of the Plover Formation (Faiz et al., 1998) and could be the main precursors of the generated waxy oils, as shown by Py-GC data. Vitrinite, however, forms the main component of the hydrogen-rich coals of the Plover Formation. The oil potential of these coals could be related to the predominantly perhydrous nature of the vitrinite. A similar perhydrous nature of Jurassic vitrinite has been described in other parts of the world such as the North Sea (Bertrand et al., 1986a; Bertrand, 1989). Plant type, reducing environments and thus better preservation conditions in paralic settings where coals and shales of the

Plover Formation were deposited may explain the formation of such hydrogen-enriched coals within the Vulcan Sub-basin (Faiz et al., 1998). During diagenesis, degradation of lipids by bacteria is minimal, leading to the preservation of perhydrous vitrinite that is likely enriched in lipids. Based on data of Faiz et al. (1998), the perhydrous nature of vitrinite could account for the oil-generating potential of coals of the Plover Formation. Nevertheless, vitrinite-precursor composition and depositional environment and their varying contributions to the formation of perhydrous vitrinite, although widely documented, remain difficult to ascertain (Fermont, 1988; Diessel, 1992; Wilkins et al., 1992). Jurassic perhydrous vitrinites have good potential for liquid generation, and have vitrinite reflectance values that are generally found to be suppressed, which poses problems for accurately assessing thermal history and for basin modelling (Wilkins et al., 1992; 1994). This is well illustrated during the calibration of the 3D model constrained for the Laminaria High and Nancar Trough region of the northern Bonaparte Basin, and was discussed in Chapter 6. In this region, and others within the North West Shelf where perhydrous vitrinite is also common, substantial suppression corrections should be considered in petroleum system modelling studies.

Apart from floral control, depositional environments are considered to be important control on determining the nature of petroleum that can be generated from coals. For instance, herbaceous-dominated coals deposited in mixed swamp/marsh settings have higher petroleum potential than humic coals (Mukhopadhyay et al., 1991). Having said that, and in order to have oil potential in coals, sedimentological, environmental, and physicochemical controls need to be involved and act simultaneously to enhance preservation and expulsion of liquid hydrocarbons. Bagge et al. (1988) proposed that bacterial reworking may have enhanced the preservation of oil-prone material of either higher plant or algae material in the Jurassic coals within the Western Desert of Egypt. Sykes et al. (2014) suggested that a marine influence within a deltaic setting has no obvious effect on maceral abundance, but can enhance the preservation of the oil potential of coals. A marine influence may also be applicable to coals of the Plover Formation, as indicated by their suppressed vitrinite reflectance and the presence of pyrite. By this reasoning, the significant bitumen fraction measured for immature coals of the Plover Formation may also be used as an indication of lipid preservation due to a marine influence.

To sum up, Jurassic coals in the Bonaparte Basin are more hydrogen-enriched and thus have better potential for waxy liquid hydrocarbon generation than Upper Cretaceous-Paleocene coals of the Halibut Subgroup in the Gippsland Basin. Based on this study, it is difficult to

explain such differences and to highlight the mechanisms and precursors controlling their petroleum potential and type of these coals. Detailed microscopic study including full anatomical description of the plant materials forming the Jurassic and Cretaceous to Cenozoic coals would help reveal the plant control on their oil generating-potential. Interestingly, higher contents of the bitumen fraction were measured for coals than for associated shales in both the Gippsland and Bonaparte basins. The origin of bitumen in coals is uncertain, and can be either indigenous (original lipids; and/or generated hydrocarbons that have not been expelled), or may represent hydrocarbons that have migrated into the coals. Determining the origin of bitumen in the investigated coals is beyond the scope of this study. However, it is possible that oils generated from interbedded shales and coaly shales could migrate onto associated coals, which depending on the coal's adsorption capacity, could launch or catalyse the expulsion of the bitumen fraction from within these coals. Such a process could be further facilitated by either the proximity of coal-bearing sequences to traps or by the presence of fractures in the coal seams, as suggested by Li et al. (2001) in the Turpan Basin (NW China). As previously mentioned, this theory cannot be supported by the current study, and further research is required. If oil was trapped and incapable of being expelled from the coals, much higher amounts of gas than oil could have migrated out of these coals when the thermal maturity became sufficiently high to allow the cracking of bitumen into either gas-condensate or gas.

## 7.4. Summary of source rock characteristics in the Gippsland and Bonaparte basins

This study documents aspects of the potential source rock characteristics in both the Gippsland and Bonaparte basins. The following section briefly lists the main results and insights obtained in this study regarding the petroleum potential and petroleum generation characteristics of potential source rocks in these two basins.

The thermal maturity and quality of the organic matter in potential source rock units in both the Gippsland and Bonaparte basins were investigated by Rock-Eval pyrolysis and TOC analysis.

(1) In the Gippsland Basin, organic-rich shales, shaly coals and coals occur at various stratigraphic levels, ranging in age from the Late Cretaceous to the Paleogene. The analysis of 91 samples from the Upper Cretaceous to Paleogene Latrobe Group indicates that these sediments have variable organic richness (TOC = 1.2–73.2%) and petroleum potential ($S_2$ = 0.7–169.5 mg HC/g rock). The highest TOC and $S_2$

values are for coals from the *F. longus* and *L. balmei* biozones. Most of the samples of the Latrobe Group have $T_{max}$ values below 435°C, suggesting that they are thermally immature to marginally mature with respect to the oil window. Based on hydrogen index (HI) values, kerogens in these sediments are mainly mixed Type II/III and Type III, with the potential to generate more gas than liquid hydrocarbons. Exceptions are found within some hydrogen-rich shales (Golden Beach Subgroup) and a shale sample from the *P. mawsonii* biozone (Emperor Subgroup), where high HI values suggest Type I/II organic matter with significant potential for oil generation. Overall, the oil-generative potential is more pronounced in the shales and shaly coals than in the coals. HI values measured for coals of the Latrobe Group are generally below 200 mg HC/g TOC, implying that these sediments are gas-prone and contain mainly Type III organic matter.

(2) In the Bonaparte Basin, Mesozoic petroleum systems are widespread in both time and space; many potential source rocks have been identified in previous studies. The main and most recognised source rock units in the Vulcan Sub-basin were deposited in early syn- to early post-rift settings during the Middle Jurassic to Early Cretaceous. The analysis of 61 samples from the Lower−Middle Jurassic Plover Formation, the Upper Jurassic lower Vulcan Formation, the Upper Jurassic−Lower Cretaceous upper Vulcan Formation and the Lower Cretaceous Echuca Shoals Formation show broad variation in both organic richness (TOC = 1.1–39.9%) and petroleum potential (1.0–64.4 mg HC/g rock), with coals of the Plover Formation having the highest hydrocarbon generative potential. Rock-Eval $T_{max}$ values and equivalent vitrinite reflectance derived from the Fluorescence of Multiple Macerals (FAAM-Eq VR) data indicate that the source rock samples from the Vulcan Sub-basin lie at various stages of maturation, being marginally mature to late mature with respect to the oil window. HI values suggest that samples from both the Plover and lower Vulcan formations contain Type II and Type III kerogen, whereas Type III kerogen is predominant in samples from the upper Vulcan and Echuca Shoals formations. On the Laminaria High, the analyses of 14 solvent-extracted source rock samples from the Lower−Middle Jurassic Plover Formation, the Middle Jurassic Laminaria Formation, the Upper Jurassic Frigate Formation, and the Lower Cretaceous Flamingo and Echuca Shoals formations, show that they are generally less organic-rich (TOC = 0.6–2.8%) with lower potential for petroleum generation ($S_2$ = 0.5–9.8 mg HC/g rock) than their age-equivalents in the Vulcan Sub-basin. The source rock

sample sets from the Laminaria High are thermally immature to early mature and contain type III and Type II/III organic matter.

Open-system pyrolysis-gas chromatography was used to gain further insights into the kerogen gross molecular composition and petroleum type that can be generated from the studied source rocks. For these characterisations, the carbon chain length distribution and selected components within the kerogen pyrolysates were employed.

(3) In the Gippsland Basin, the pyrolysate composition of selected shales, coaly shales and coals from the Latrobe Group are dominated by *n*-alkane/*n*-alkene doublets, with three distribution patterns reflecting variable organic precursors. Most have relatively large amounts of phenolic compounds in the pyrolysates, indicating a derivation from ligno-cellulosic material. Exceptions are found within the oldest *T. apoxyexinus* and *P. mawsonii* biozones of the Latrobe Group, in which phenolic compounds are almost absent, suggesting minor terrigenous input. Although significant similarities in terms of molecular fingerprints exist between samples from the investigated palynological zones, the samples show the potential to generate different petroleum types. Most of the samples cluster in the P-N-A oil field with both high and low wax content. Hydrocarbons released from the hydrogen-rich shales within the *L. balmei*, *F. longus* and *T. lilliei* biozones and one shale from *P. mawsonii* biozone correspond to high wax-paraffinic oils. Samples from the *N. senectus* and *T. apoxyexinus* biozones plot in the gas-condensate field.

(4) Similarly, pyrolysates of source rock samples in the Vulcan Sub-basin are generally characterised by high concentrations of *n*-alkane/*n*-alkene doublets. However, coals of the Plover Formation are more enriched in alkylphenols and aromatic hydrocarbons as compared to the *n*-alkanes/*n*-alkenes homologues. Exceptions are the marine shale samples from the lower Vulcan Formation, which were found to be depleted in long-chain *n*-alkanes/*n*-alkenes, implying less pronounced terrigenous input material. Only some coals of the Plover Formation have the potential to generate gas-condensate, while all of the remaining samples, including other coals of the Plover Formation, plot in the P-N-A oil field with either low or high wax content, in agreement with the occurrence of mixed terrestrial- and marine-influenced organic matter. In contrast, the Py-GC traces of selected source rock samples from the Laminaria High show slightly different distribution patterns of *n*-alkyl moieties that barely extend up to *n*-$C_{23}$. Both aromatic and phenolic pyrolysis products are only present in low amounts in all of the source rock samples. Interestingly, none of these

266

pyrolysates plot in the high wax P-N-A oil field and they all either fall in the gas-condensate field or in the P-N-A oil with low wax content field.

Open-system pyrolysis experiments were applied to simulate the organic matter conversion into petroleum under geological conditions. Petroleum formation is governed by the cracking of chemical bonds that are described by bulk kinetic parameters consisting of a single frequency factor and an activation energy distribution. Timing of petroleum formation extrapolated to geological conditions was predicted assuming a constant geological heating rate of 3.3°C/Ma.

(5) In the Gippsland Basin, shale, coaly shale and coal samples from the Latrobe Group investigated by open-system pyrolysis show broad activation energy distributions and variable frequency factors, which are characteristic of the heterogeneous composition of Type II/III and Type III organic matter within these lithofacies. Exceptions are the shale sample from the *P. mawsonii* biozones, and to some extent the hydrogen-rich shales that have a more homogeneous composition as reflected by a relatively narrower activation energy distribution. Petroleum formation from each of the investigated biozones occurs over a broad temperature range, reflecting varying levels of thermal and kinetic stability. The onset of bulk petroleum generation (10% TR) ranges from 125°C for the least stable sample (a shale from the *P. mawsonii* biozone) to approximately 142°C for the most stable sample (a coal from the *F. longus* biozone).

(6) In the Vulcan Sub-basin, the most heterogeneous kerogens are those within the Plover Formation, which show broad activation energy distributions and higher frequency factors. One shale sample from the lower Vulcan Formation has a very narrow activation energy distribution, accounting for a homogeneous kerogen structure dominated with a limited variety of bond types. The remaining samples from this latter formation show intermediate distributions that tend to be narrower in the case of the Echuca Shoals and upper Vulcan formations. The onset of petroleum generation occurs at approximately 120°C for the most labile kerogens from both the upper Vulcan and Echuca Shoals formations, while petroleum formation starts at 120–158°C and 130–160°C from the most stable kerogen within the lower Vulcan and Plover formations, respectively. Compared to the Vulcan Sub-basin and with the exception of the Plover Formation, kerogens within the potential source rocks on the Laminaria High have a broader activation energy distribution. The start of bulk petroleum formation for the source rock samples is estimated to take place over a

significantly broad temperature range of 100 to 135°C. Surprisingly, the peak of petroleum formation occurs over a narrow temperature range of less than 7°C from the least to the most stable kerogen. This overall variability in terms of timing of hydrocarbon formation in both the Vulcan Sub-basin and Laminaria High is likely due to different organic matter types and degrees of preservation in these sediments.

Closed-system pyrolysis using MSSV and PVT experiments were employed to develop compositional kinetic schemes that describe the primary cracking of kerogen into petroleum and to predict the physical properties of the generated fluids. Pyrolysate compositions were simulated at a low heating rate of 0.7C/min.

(7) In the Gippsland Basin, compositional kinetic models with 14 components were developed for four selected shale samples from the Latrobe Group that were shown to generate different petroleum types and to have different orders of kinetic stability. The models show that at early stages of kerogen conversion, these shales produce black oils with relatively low GORs. In contrast, at higher levels of thermal stress, either light oil or gas and condensates are generated from shales plotting in the P-N-A field, whereas black oils continue to be generated from those plotting in the paraffinic field.

(8) In the Vulcan Sub-basin, compositional kinetic schemes were performed for samples from the upper Vulcan, lower Vulcan and Plover Formation source rocks. All of these samples produce black oil at 10 to 70% transformation ratio, whereas a broader variability within both shales and coals of the lower Vulcan and Plover formations was observed at high transformations ratios. In addition to black oil, these two formations have the capacity to generate either gas-condensate or light oil.

(9) On the Laminaria High, the Laminaria and Frigate formations generate fluids with very similar compositions and physical properties. From the onset to the late stage of petroleum generation, these two formations show the potential to produce black oils. The results from the Echuca Shoals Formation are striking, in that although this formation has been interpreted to have been deposited in an open marine environment and to potentially be the source of marine-influenced P-N-A oils in the Vulcan Sub-basin, this formation has more potential for light oil and gas-condensate generation than oils.

(10) For source rock samples from both the Vulcan Sub-basin and the Laminaria High that were subjected to compositional kinetic experiments, the carbon isotopic compositions of light methane, ethane, propane and *n*-butane were also measured under closed system conditions. Overall, these gases become isotopically heavier with increasing pyrolysis temperature, and the differences observed between gases generated from the investigated source rocks seem to be more likely a function of organic matter type and depositional environment conditions (e.g. marine versus non-marine). It can also be inferred that natural gases in these areas are unlikely to be derived from a single source, but instead are more likely the result of the mixing of gases generated at different levels of thermal stresses.

## 7.5. Implications for climate feedback

Natural hydrocarbon seeps can be used as valuable tools during early stages of petroleum exploration, as their occurrence is generally regarded as an indication of active petroleum systems (Cowley and O'Brien, 2000; Abrams, 2005). Geochemical, shallow seismic and remote sensing data have shown that potential signatures of seeps are common features in Australia's offshore basins (O'Brien and Woods, 1995; Cooper et al., 1998; Cowley and O'Brien, 2000). For instance, in the Timor Sea region, active offshore natural gas seeps have been detected and linked to proven petroleum accumulations (Jones et al., 2005; O'Brien et al., 2005; Rollet et al., 2006). Trap breach and vertical leakage of petroleum related to fault system reactivation during the late Miocene-early Pliocene have been widely documented in several areas within the North West Shelf (O'Brien and Woods, 1995; O'Brien et al., 1996; 1999; Lisk et al., 1998; Keep et al., 2002; Harrowfield and Keep, 2005).

A portion of the hydrocarbons generated during the maturation of organic matter escapes from the sedimentary basin in which it originated and can enter the atmosphere. The most important of these is methane, which is a powerful greenhouse gas, more than 20 times as effective in trapping heat in the atmosphere as carbon dioxide (e.g. Ritzkowski and Stegmann, 2007; Warmuzinski, 2008). The natural escape of methane from petroleum provinces, due partly to buoyancy associated with lithostatic pressures, is likely to be a key contributor to the global methane budget, with an enormous capacity for driving global climate. However, few climate models or atmospheric greenhouse gas inventories have quantitatively taken into account methane formed through thermal or microbial cracking of sedimentary organic matter over the geological past.

Despite the long history of petroleum exploration in the two studied Gippsland and Bonaparte basins, there is still uncertainty regarding the origin (thermogenic and/or biogenic) of some of the accumulated gases and the different processes that have contributed to the known gas reserves. Therefore, the timing of hydrocarbon generation relative to the trap formation, the potential migration paths and the possible post-charge leakage of gases within and throughout the sedimentary column should be revised and refined. The current study is a contribution toward a better definition of the potential source rocks as well as their petroleum generation characteristics within the Gippsland and Bonaparte basins.

The compilation of a range of geological data, geophysical inputs and the integration of the properties and evolution of the generated compounds derived from the established kinetic dataset into 3D numerical petroleum system models, together with subsurface, ocean and atmospheric modelling would help predict methane migration and emission from the subsurface, and so aid in the identification of potential climate feedback processes. In order to establish a valid model which describes the different scenarios, the uncertainties regarding the data need to be considered. The simulated migration models can be calibrated against the present-day distribution of mapped anomalous seismic features, such as gas chimneys, pockmarks and bright spots. The expected outputs will not only contribute toward the quantification of the methane budget, but can be further extended to estimate probabilities and test different scenarios to highlight potential factors and mechanisms that control rate and volume of methane fluxes, their variability as a function of geological time, and their effects on palaeo- and present-day climate change.

## 7.6. Most innovative outcomes from the study

The main outcomes and findings derived from this study are:

- Most of the Middle Jurassic to Lower Cretaceous source rock units in the Laminaria High area have the potential to generate either wet gases or paraffinic-naphthenic-aromatic oils with low wax content. These source rocks show the potential to generate more oil than gas. Interestingly and despite its marine source affinity, the Lower Cretaceous Echuca Shoals Formation has the potential to generate a greater proportion of gas compared to the underlying source rocks, deposited in either shallower marine or paralic settings. Another main finding is that apart from being a reservoir, the Laminaria Formation also contains organic-rich layers with the potential to generate heavy oils.

- Where sampled in the Vulcan Sub-basin, the Plover Formation and the Upper Jurassic lower Vulcan Formation are capable of generating both and oil and gas and are more likely the main source of the hydrocarbon-bearing reservoirs of the Vulcan Sub-basin. Both coals and shales of the Middle Jurassic Plover Formation have the potential to generate liquid hydrocarbons at a relatively high temperature range, due to their high levels of kinetic stability. When comparing results derived from bulk kinetic predictions to oil maturity data reported in previous biomarker analysis based works, the Plover Formation is unlikely to be the source of oils in the Laminaria and Corallina fields within the Laminaria High area.

- Definite oil-source correlations in the two basins studied are beyond the scope of this study and cannot be established based on results presented in the thesis. The analysis of extracts of the studied samples and analysis of oils from the two basins by GC-MS would complement this study and allow oil-source correlations in the two basins. Nevertheless and in the context of this study, one innovative outcome is that coals of the Halibut Subgroup, previously interpreted mainly on the basis of molecular and isotopic characteristics of both rock extracts and crude oils, to be the primary source of waxy paraffinic oil and gas in the Gippsland Basin, may not have the ability to expel liquid hydrocarbons. Thus, shales and coaly shales of the Upper Cretaceous-Paleogene Latrobe Group, rather than coals seem to have played a more significant role in sourcing oil accumulations in the Gippsland Basin. In contrast, coal facies of the Middle Jurassic Plover Formation in the Bonaparte Basin appear able to generate and expel oil at all stages of the conventional oil generation window.

- 3D petroleum system models, in which a measured compositional kinetic dataset was incorporated indicate that unlike the immature Lower Cretaceous Echuca Shoals Formation, the Jurassic Plover, Laminaria and Frigate formation source rocks are within the conventional oil window. These source rocks started generating hydrocarbons during the Early Cretaceous and their predicted present-day transformation ratios indicate ongoing petroleum generation. Oils trapped in the Laminaria and Corallina fields on the Laminaria High area were partially sourced from the Nancar Trough kitchen. Excluding in-source and in-reservoir secondary cracking, additional and preferentially retained light oil or wet gas charge, may have been provided from the Nancar Trough and other neighbouring kitchens, such as the northern Flamingo and Sahul synclines. Complete or partial loss of hydrocarbons and subsequent occurrence of under-filled and dry structures within the Nancar Trough

and Laminaria High region is very likely due to late stage fault reactivation and trap breach.

## 7.7. Conclusions

The Gippsland and Bonaparte basins are geological provinces that have undergone extensive phases of petroleum exploration. Both oil and gas discoveries have been made in these basins, indicating the occurrence of productive source rocks. The stratigraphic architecture and evolution of the source rock units within the two basins seem to be controlled to a large extent by active tectonism and associated palaeogeographical changes. However, the majority of previous geochemical studies in these two basins have focused on determining the properties of reservoired oil and gas and delineating petroleum families based on characterisation of fluids, source rock extracts and fluid inclusions. In this study, efforts were directed toward gaining insights into the bulk properties of potential source rock units and their petroleum generation characteristics. These were extended by attempts to predict the type and composition of petroleum that can be generated and to elucidate to what extent they reflect the reservoired fluids in these basins. It is important to note that this study covers only recognised potential source rock units in both the Gippsland and Bonaparte basins. It is more than likely that additional and usually deeper sources have contributed to the overall petroleum accumulations in these two basins. Each contains source rocks with the potential to generate oil and gas of the types already discovered within their boundaries. A variety of factors have influenced the generation potential, petroleum type and kinetic behaviour of their respective kerogens. The main conclusions drawn from the study are as follows:

*The Gippsland Basin*

There is no apparent age control on the organic richness and molecular characteristics of the studied source rocks in the Gippsland Basin. Where sampled, shales and coals of the Upper Cretaceous−Paleogene Latrobe Group are compositionally heterogeneous and reflect high inputs of land-plant material into their organic matter, and were deposited mainly in a delta plain environment. Although there are similarities in the waxy hydrocarbon range for most shales and coals, they show the potential to generate variable petroleum types ranging from gas-condensate to paraffinic oils. This can be explained to some extent by variability in their bulk maceral content, although samples that fall in the same petroleum organofacies field may show different bulk maceral contents. Kinetic modelling predicts a broad range for the onset and duration of petroleum formation, accounting for the large variability in the

structure of Type II/III and Type III organic matter preserved in these sediments. Overall, coals and shales exhibit prominent similarities discerned in their bulk, molecular and kinetic characteristics, indicating that the evaluation of the relative contribution from coals and interbedded shales to petroleum accumulations in the Gippsland Basin is somewhat difficult. Both of these lithofacies generate aliphatic pyrolysates that are in good agreement with the waxy nature of crude oils recovered from the Gippsland Basin.

In addition, thin hydrogen-rich shales, deposited probably in more distinct and likely restricted depositional environments, were also identified within the Latrobe Group, and these include a lacustrine shale of the *P. mawsonii* biozone and some marine-influenced shales of the *T. lilliei*, *F. longus* and *L. balmei* biozones. The petroleum potential of these shales is significant, but the properties of the discovered oils and the existing oil-source correlations do not point to discernible contributions by these organic-rich sediments to the Gippsland Basin's petroleum accumulations.

As compared to coals, the interbedded shales have higher potential for petroleum generation and expulsion, so it is likely that interbedded shales and shaly coals would have contributed significantly to petroleum accumulations in the Gippsland Basin. In contrast and based on the present data-set, the Paleocene coals of the *L. balmei* biozone have the potential to generate liquid hydrocarbons, but their low hydrogen index values (< 200 mg HC/g TOC) suggest that efficient oil expulsion is unlikely to have occurred. However, such an interpretation cannot be definitive, and the possibility that coals have provided hydrocarbon oil and/or gas charge cannot be ruled out given the limited number of analysed coals as compared to other lithofacies.

Oil fields in the Gippsland Basin may have received terrigenous-dominated charge generated by shales, shaly coals and possibly coals. Gas and condensates in the basin were likely provided by stratigraphically older formations, including the organically-lean shales of the *N. senectus* and *T. apoxyexinus* biozones of the Latrobe Group. At advanced rates of kerogen conversion, shales also show the potential to produce gas and condensates. Although definite controls on oil and gas distribution in the Gippsland Basin cannot be addressed by this study, results reported herein support to some extent the previous interpretations, in that such distributions are the result of differences in thermal maturity of the source rocks or the existence of deep source rocks. Detailed thermal maturity maps would also help identify zones of elevated temperature, and would enable the determination of whether a gas charge could have been added by secondary cracking of oil.

*The Bonaparte Basin: Vulcan Sub-basin*

In the Vulcan Sub-basin, the fluvio deltaic Lower−Middle Jurassic Plover and marine Middle−Upper lower Vulcan formations contain good but heterogeneous Type II/III organic matter with significant petroleum potential as compared to the overlying marine Upper Jurassic-Lower Cretaceous upper Vulcan and Lower Cretaceous Echuca Shoals formations. In addition to changes in depositional environment and variability in organic matter input (marine versus terrigenous), less oxic conditions at the time of deposition of the investigated source rocks have favoured the preservation of organic matter in the Plover and lower Vulcan formations. In contrast, more oxic conditions have led to the alteration of organic matter accumulated in the upper Vulcan and Echuca Shoals formations.

The Plover and lower Vulcan formations probably sourced oils that show a terrestrial geochemical signature, and those with marine affinity can be related to less oxygenated deep-water mudstones of the lower Vulcan Formation. In contrast, the upper Vulcan and Echuca Shoals formation source rocks, deposited under oxic conditions, have less potential and are not sufficiently thermally mature to generate hydrocarbons and provide additional contribution to the petroleum accumulations in the Vulcan Su-basin. Gases in the sub-basin are unlikely to have been derived from a single source rock, and they rather resemble mixtures of hydrocarbons produced from multiple source rocks at different thermal maturity levels. Apart from their capacity to generate gas-condensates, coals of the Plover Formation, although being enriched in aromatic and phenolic hydrocarbons, show the potential to generate oil-like hydrocarbons with low GORs at relatively high temperatures.

*The Bonaparte Basin: Laminaria High*

On the Laminaria High, Upper Jurassic to Lower Cretaceous source rocks also contain Type II-III organic matter and show variation in their organic richness and quality. However, compared to their age analogues in the Vulcan Sub-basin, source rocks on the Laminaria High have moderate petroleum potential and show only the potential to generate either gas-condensate or P-N-A oils with low wax content; none of the investigated source rocks produce high wax oils.

Petroleum reservoirs seem to have been filled to some extent by oils generated from the Frigate and Flamingo source rocks. An additional oil charge can be provided by organic-rich layers within the Laminaria Formation that forms the main reservoir unit in the northern Bonaparte Basin. As was the case for the Vulcan Sub-basin, gases on the Laminaria High

are most likely the result of mixing of gases generated at different maturity levels from multiple source rocks.

Despite being the most marine-influenced unit, compositional models suggest that the Echuca Shoals Formation has a greater potential for light oil and gas generation than the underlying source rock units. As was the case for the Upper Jurassic−Lower Cretaceous source rocks in the Vulcan Sub-basin, less suitable conditions for the preservation of organic matter are herein suggested to explain the moderate petroleum potential of the Flamingo and Echuca Shoals formations.

Effects of secondary alteration processes, such as water washing and vertical leakage in both the Vulcan Sub-basin and the Laminaria High make any comparison between the predicted properties of artificially generated hydrocarbons and those naturally occurring in reservoirs rather difficult.

The 3D petroleum system models implemented for the Laminaria High and Nancar Trough, a region of the northern Bonaparte Basin, represents an example of the application of compositional kinetic models developed in this study. This is an attempt toward a better understanding of the fill history through geological time, and towards elucidating the controls on the preservation of hydrocarbon accumulations in this region. The main outputs and conclusions that can be drawn are as follows:

The Plover, Laminaria and Frigate/Flamingo source rocks are mature within the Nancar Trough kitchen. Maturation of these source rocks was simulated by heating related to the Jurassic rifting event, but mainly by increasing burial during the Neogene. The peak petroleum generation from these source rocks took place during the Cenozoic (mid-Eocene) and the modelled present-day transformation ratios indicate ongoing petroleum generation and expulsion. Towards the Londonderry High, the modelled source rocks are thin compared to the Nancar Trough or the Laminaria High, and have not generated any substantial amount of hydrocarbons. The Lower Cretaceous Echuca Shoals Formation is immature with respect to the oil window across the entire Laminaria High and Nancar Trough region.

Most of the present-day filled and under-filled structures could have accessed oil-dominated charge with relatively high GORs generated from the mature Nancar Trough source rock kitchen. However, the discrepancy between the predicted physical properties of fluids and those measured in oil and gas fields on the Laminaria High (e.g. in the Laminaria and Corallina fields) may partly be accounted for by additional light oil and/or gas charge from

nearby kitchens (e.g. the Flamingo Syncline and the Sahul−Nancar Trough) that were not considered in the model due to data unavailability.

Lack of adequate hydrocarbon charge cannot be put forward as the interpretation of exploration failures in the region. The reactivation of faults during the late Miocene, combined with effects of secondary alteration processes (e.g. water washing and phase fractionation), have led to petroleum losses and the unusual properties of the remaining present-day reservoired fluids.

## 7.8.    Directions and recommendation for future work

When considering the HI value of 200 mg HC/g TOC as a threshold at which liquid hydrocarbon generation from coals occur, the Lower−Middle Jurassic coals of the Plover Formation in the Vulcan Sub-basin have higher potential for liquid hydrocarbon generation and expulsion than the Upper Cretaceous-Paleogene coals of the Latrobe Group in the Gippsland Basin. Unexpectedly, coals of the Plover Formation are phenolic-enriched, while those of the Latrobe Group contain high concentrations of long chain normal aliphatic components, indicating that there is no systematic relationship between HI values and aliphatic content. In other words, coals capable of generating and expelling liquid hydrocarbons do not necessarily contain a high concentration of aliphatic precursors. The differing behaviour of these coals seem to be governed by numerous factors, such as variations in maceral content, depositional and preservation conditions, and floral evolution (e.g. gymnosperm versus angiosperm input). Similarly, organic-rich shales in these two basins show appreciable heterogeneities and varying levels of kinetic stability. The bulk maceral composition explains to some degree these heterogeneities, but does not show a good agreement with respect to the type of petroleum that can be generated. A detailed examination of these source rocks units, in terms of sequence stratigraphy and further palaeobotanical and sedimentological investigations, is required to highlight the main controls on their organic richness and to better understand the properties and petroleum potential of coals as oil-expelling source rocks.

Compared to models with two components (oil and gas), compositional kinetics using 14 components developed in this study represent valuable inputs for future basin modelling studies. Their integration in 3D petroleum system models for both the Gippsland and Bonaparte basin would allow prediction of the timing of hydrocarbon generation/expulsion and bring new insights to their filling histories. For the Gippsland Basin, mapping of coal and shale distribution would address the extent to which coals are capable of generating and

expelling liquid hydrocarbons, and thus help correlate oil and gas accumulations to specific source rock facies.

Apart from uncertainties in the geological inputs and the thermal maturity data used for calibration, the 3D petroleum system model implemented for the Laminaria High and Nancar Trough regions was constrained based on a number of assumptions that are discussed in more detail in Chapter 6. The assigned thickness of the source rock units are somewhat speculative due to their limited penetration by wells, and thus more work is required when more data becomes available. For this region or any further region to be investigated by a 3D petroleum system modelling approach, taking into consideration source rock facies and thickness variation would allow a better understanding of the active petroleum systems and hydrocarbon charge.

In areas where hydrocarbon leakage is recognised, or is speculated to be a potential risk, such as is the case for the Bonaparte Basin and other basins of the North West Shelf of Australia, a detailed analysis of the faulting systems, their connectivity and their behaviour throughout geological time should be undertaken as a crucial task prior to any basin modelling attempts.

3D petroleum systems models that account for an accurate prediction of reservoired fluid properties and phase behaviour would depend not only on a refined definition of the extent of potential source rocks, but also on the assignation of representative kinetic datasets of each of the delineated facies and a good understanding of the in-reservoir processes.

## 7.9.    References

Abrams, M.A., 2005. Significance of hydrocarbon seepage relative to petroleum generation and entrapment. Marine and Petroleum Geology 22, 457-477.

Bagge, M., Harding, R., EL Azhary, T., SAID, M., 1988. Generation of oil from coal sequences in the Western Desert, Egypt. Proceedings of the Egyptian General Petroleum Corporation. 9th Exploration and Production Seminar, Cairo.

Bertrand, P., 1989. Microfacies and petroleum properties of coals as revealed by a study of North Sea Jurassic coals. International journal of coal geology 13, 575-595.

Bertrand, P., 1991. Coal: Formation, occurrence and related properties. Bulletin de la Société Géologique de France 162, 137-448.

Bertrand, P., Behar, F., Durand, B., 1986a. Composition of potential oil from humic coals in relation to their petrographic nature. Organic Geochemistry 10, 601-608.

Bertrand, P., Pittion, J.L., Bernaud, C., 1986b. Fluorescence of sedimentary organic matter in relation to its chemical composition. Organic Geochemistry 10, 641-647.

Clayton, C., 1991. Carbon isotope fractionation during natural gas generation from kerogen. Marine and Petroleum Geology 8, 232-240.

Collinson, M.E., Van Bergen, P.F., Scott, A.C., De Leeuw, J.W., 1994. The oil-generating potential of plants from coal and coal-bearing strata through time: a review with new evidence from Carboniferous plants. Geological Society, London, Special Publications 77, 31-70.

Cooper, G.T., Barnes, C.R., Bourne, J.D., Channon, G.J., 1998. Hydrocarbon leakage on the North West Shelf: New information from the integration of airborne laser fluorosensor (ALF) and structural data, in: Purcell, P.G., Purcell, R.R. (Eds.), The Sedimentary Basins of Western Australia 2: Proceedings of the Petroleum Exploration Society of Australia Symposium, Perth, Western Australia, pp. 255-271.

Cowley, R., O'Brien, G.W., 2000. Identification and interpretation of leaking hydrocarbons using seismic data: a comparative montage of examples from the major fields in Australia's north west shelf and Gippsland Basin. Australian Petroleum Production Exploration Association Journal 40, 121-150.

Curry, D.J., Emmett, J.K., Hunt, J.W., 1994. Geochemistry of aliphatic-rich coals in the Cooper Basin, Australia and Taranaki Basin, New Zealand: implications for the occurrence of potentially oil-generative coals. Geological Society, London, Special Publications 77, 149-181.

Dettmann, M.E., 1981. The Cretaceous flora, in: Keast, A. (Ed.), Ecological biogeography of Australia. Junk, The Hague, pp. 357-375.

Diessel, C.F.K., 1992. Coal-Bearing Depositional Systems. Springer-Verlag, Berlin, 721 p.

Durand, B., Paratte, M., 1983. Oil potential of coals: a geochemical approach. Geological Society, London, Special Publications 12, 255-265.

Faiz, M., Wilkins, R., Sherwood, N., Buckingham, C., Russell, N., Kinealy, K., 1998. Perhydrous vitrinite in the source rocks of the Western Timor Sea region. APCRC Confidential Report No.320, 223 p.

Fermont, W.J.J., 1988. Possible causes of abnormal vitrinite reflectance values in paralic deposits of the Carboniferous in the Achterhoek area, The Netherlands. Organic Geochemistry 12, 401-411.

Fielding, C.R., 1985. Coal depositional models and the distinction between alluvial and delta plain environments. Sedimentary Geology 42, 41-48.

Gould, R., Shibaoka, M., 1980. Some aspects of the formation and petrographic features of coal members in Australia, with special reference to the Tasman Orogenic Zone. Australian Coal Geology 2, 1-29.

Harrowfield, M., Keep, M., 2005. Tectonic modification of the Australian North-West Shelf: episodic rejuvenation of long-lived basin divisions. Basin Research 17, 225-239.

Hedges, J.I., Parker, P.L., 1976. Land-derived organic matter in surface sediments from the Gulf of Mexico. Geochimica et Cosmochimica Acta 40, 1019-1029.

Horne, J.C., Ferm, J.C., Caruccio, F.T., Baganz, B.P., 1978. Depositional models in coal exploration and mine planning in Appalachian region. American Association of Petroleum Geologists Bulletin 62, 2379-2411.

Horsfield, B., Yordy, K.L., Crelling, J.C., 1988. Determining the petroleum-generating potential of coal using organic geochemistry and organic petrology. Organic Geochemistry 13, 121-129.

Hunt, J.M., 1991. Generation of gas and oil from coal and other terrestrial organic matter. Organic Geochemistry 17, 673-680.

Jones, A.T., Logan, G.A., Kennard, J.M., Rollet, N., 2005. Reassessing potential origins of synthetic aperture radar (SAR) slicks from the Timor Sea region of the North West Shelf on the basis of field and ancillary data. Australian Petroleum Production and Exploration Association Journal, 311-331.

Jones, R.W., 1987. Organic facies, in: Brooks, J., Welte, D.H. (Eds.), In Advances in Petroleum Geochemistry. Academic Press, New York, pp. 1-90.

Keep, M., Clough, M., Langhi, L., 2002. Neogene tectonic and structural evolution of the Timor Sea region, NW Australia, in: Keep, M., Moss, S. (Eds.), The Sedimentary Basins of Western Australia 3: Proceedings of the Petroleum Exploration Society of Australia Symposium, Perth, Western Australia, pp. 341-353.

Lapo, A.V., Drozdova, I.N., 1989. Phyterals of humic coals in the U.S.S.R. International journal of coal geology 12, 477-510.

Li, M., Bao, J., Lin, R., Stasiuk, L.D., Yuan, M., 2001. Revised models for hydrocarbon generation, migration and accumulation in Jurassic coal measures of the Turpan basin, NW China. Organic Geochemistry 32, 1127-1151.

Lisk, M., Eadington, P.J., O'Brien, G.W., 1998. Unravelling complex filling histories by constraining the timing of events which modify oil fields after initial charge. Geological Society, London, Special Publications 144, 189-203.

Macgregor, D.S., 1994. Coal-bearing strata as source rocks—a global overview. Geological Society, London, Special Publications 77, 107-116.

Mukhopadhyay, P.K., Hatcher, P.G., Calder, J.H., 1991. Hydrocarbon generation from deltaic and intermontane fluviodeltaic coal and coaly shale from the Tertiary of Texas and Carboniferous of Nova Scotia. Organic Geochemistry 17, 765-783.

Murchison, D.G., 1987. Recent advances in organic petrology and organic geochemistry: an overview with some reference to 'oil from coal'. Geological Society, London, Special Publications 32, 257-302.

O'Brien, G.W., Woods, E.P., 1995. Hydrocarbon-related diagenetic zones (HRDZs) in the Vulcan Sub-basin, Timor Sea: recognition and exploration implications. Australian Petroleum Production and Exploration Association Journal 35, 220-220.

O'Brien, G.W., Lisk, M., Duddy, I., Eadington, P., Cadman, S., Fellows, M., 1996. Late Tertiary fluid migration in the Timor Sea: a key control on thermal and diagenetic histories. Australian Petroleum Production and Exploration Association Journal 36(1), 399-427.

O'Brien, G.W., Lisk, M., Duddy, I.R., Hamilton, J., Woods, P., Cowley, R., 1999. Plate convergence, foreland development and fault reactivation: primary controls on brine migration, thermal histories and trap breach in the Timor Sea, Australia. Marine and Petroleum Geology 16, 533-560.

O'Brien, G.W., Lawrence, G.M., Williams, A.K., Glenn, K., Barrett, A.G., Lech, M., Edwards, D.S., Cowley, R., Boreham, C.J., Summons, R.E., 2005. Yampi Shelf, Browse Basin, North-West Shelf, Australia: a test-bed for constraining hydrocarbon migration and seepage rates using combinations of 2D and 3D seismic data and multiple, independent remote sensing technologies. Marine and Petroleum Geology 22, 517-549.

Pepper, A.S., 1991. Estimating the petroleum expulsion behaviour of source rocks: a novel quantitative approach. Geological Society, London, Special Publications 59, 9-31.

Pepper, A.S., Corvi, P.J., 1995. Simple kinetic models of petroleum formation. Part III: Modelling an open system. Marine and Petroleum Geology 12, 417-452.

Petersen, H.I., Nytoft, H.P., 2006. Oil generation capacity of coals as a function of coal age and aliphatic structure. Organic Geochemistry 37, 558-583.

Powell, T.G., Boreham, C.J., 1994. Terrestrially sourced oils: where do they exist and what are our limits of knowledge?—a geochemical perspective. Geological Society, London, Special Publications 77, 11-29.

Retallack, G., Dilcher, D.L., 1981. A coastal hypothesis for the dispersal and rise to dominance of flowering plants. In: Evolution, Paleoecology and the Fossil Record, Vol. 2 (Ed. K. J. Niklas), New York: Praeger Publishers, pp. 27-77.

Ritzkowski, M., Stegmann, R., 2007. Controlling greenhouse gas emissions through landfill in situ aeration. International journal of greenhouse gas control 1, 281-288.

Rollet, N., Logan, G.A., Kennard, J.M., O'Brien, P.E., Jones, A.T., Sexton, M., 2006. Characterisation and correlation of active hydrocarbon seepage using geophysical data sets: An example from the tropical, carbonate Yampi Shelf, Northwest Australia. Marine and Petroleum Geology 23, 145-164.

Saxby, J.D., Shibaoka, M., 1986. Coal and coal macerals as source rocks for oil and gas. Applied Geochemistry 1, 25-36.

Scott, A.C., 1987. Coal and coal-bearing strata: recent advances and future prospects. Geological Society, London, Special Publications 32, 1-6.

Shanmugam, G., 1985. Significance of coniferous rain forests and related organic matter in generating commercial quantities of oil, Gippsland Basin, Australia. American Association of Petroleum Geologists Bulletin 69, 1241-1254.

Smith, G.C., Cook, A.C., 1984. Petroleum occurrence in the Gippsland Basin and its relationship to rank and organic matter type. Australian Petroleum Exploration Association Journal 24, 196-216.

Spicer, R.A., Parrish, J.T., 1986. Paleobotanical evidence for cool north polar climates in middle Cretaceous (Albian-Cenomanian) time. Geology 14, 703-706.

Stewart, W.N., Rothwell, G.W., 1993. Paleobotany and the evolution of plants. Cambridge University Press. 2nd Edition, 521 p.

Sykes, R., Snowdon, L.R., 2002. Guidelines for assessing the petroleum potential of coaly source rocks using Rock-Eval pyrolysis. Organic Geochemistry 33, 1441-1455.

Sykes, R., Volk, H., George, S.C., Ahmed, M., Higgs, K.E., Johansen, P.E., Snowdon, L.R., 2014. Marine influence helps preserve the oil potential of coaly source rocks: Eocene Mangahewa Formation, Taranaki Basin, New Zealand. Organic Geochemistry 66, 140-163.

Teichmuller, M., Teichmuller, R., 1968. Cainozoic and Mesozoic coal deposits of Germany. In Coal and Coal Bearing Strata (Edited by Murchison D. and Westoll A.), Oliver & Boyd, Edinburgh. pp. 347-379.

Thomas, B.M., 1982. Land-plant source rocks for oil and their significance in Australian basins. Australian Petroleum Exploration Association Journal 22, 164-178.

Warmuzinski, K., 2008. Harnessing methane emissions from coal mining. Process Safety and Environmental Protection 86, 315-320.

Wilkins, R.W.T., George, S.C., 2002. Coal as a source rock for oil: a review. International journal of coal geology 50, 317-361.

Wilkins, R.W.T., Wilmshurst, J.R., Russell, N.J., Hladky, G., Ellacott, M.V., Buckingham, C., 1992. Fluorescence alteration and the suppression of vitrinite reflectance. Organic Geochemistry 18, 629-640.

Wilkins, R.W.T., Russell, N.J., Ellacott, M.V., 1994. Fluorescence alteration and thermal maturity modelling of Carnarvon Basin wells, in: Purcell, P.G., Purcell, R.R. (Eds.), The Sedimentary Basins of Western

Australia: Proceedings of the Petroleum Exploration Society of Australia Symposium, Perth, Western Australia, pp. 415-432.

# 8. Appendices

**Appendix 1. List of wells used for source rock characterisation in the Vulcan Sub-basin**

| WELL NAME | LATITUDE | LONGITUDE | EASTING | NORTHING | TOTAL DEPTH | WELL TYPE |
|---|---|---|---|---|---|---|
| East Swan 1 | -12.30 | 124.58 | 672205.85 | 8639700.40 | 3038 | Exploration |
| Eclipse 1 BHP | -12.27 | 124.62 | 676203.28 | 8643047.67 | 3003 | Exploration |
| Jarrah 1A | -11.29 | 125.70 | 795263.95 | 8750827.77 | 2231 | Exploration |
| Maret 1 | -12.76 | 124.37 | 648379.00 | 8588603.57 | 3560 | Exploration |
| Montara 1 | -12.69 | 124.53 | 666455.25 | 8596880.77 | 3444 | Exploration |
| Oliver 1 | -11.64 | 125.01 | 719137.70 | 8712099.10 | 2934 | Exploration |
| Paqualin 1 | -11.98 | 124.51 | 664222.32 | 8675294.38 | 4242 | Exploration |
| Skua 1 | -12.50 | 124.43 | 655826.82 | 8617302.84 | 3048 | Exploration |
| Tahbilk 1 | -12.73 | 124.51 | 663420.85 | 8592096.51 | 3226 | Exploration |
| Taltarni 1 | -12.61 | 124.58 | 671706.53 | 8605486.60 | 3362 | Exploration |
| Vulcan 1B | -12.24 | 124.55 | 668772.52 | 8646283.10 | 3745 | Exploration |

**Appendix 2. List of wells used for source rock characterisation in the Laminaria High**

| WELL NAME | LATITUDE | LONGITUDE | EASTING | NORTHING | TOTAL DEPTH | WELL TYPE |
|---|---|---|---|---|---|---|
| Buang 1 | -10.60 | 126.07 | 179345.65 | 8826924.61 | 3712 | Exploration |
| Corallina 1 | -10.59 | 125.96 | 823638.34 | 8827783.33 | 3340 | Exploration |
| Laminaria 1 | -10.63 | 126.03 | 174962.58 | 8823757.68 | 3400 | Exploration |
| Laminaria 3 | -10.65 | 126.03 | 174771.42 | 8821701.27 | 3470 | Extension/Appraisal |
| Laminaria East 1 | -10.63 | 126.05 | 177320.94 | 8823158.99 | 3400 | Extension/Appraisal |

**Latitude:** Decimal degrees (Datum: GDA94)
**Longitude:** Decimal degrees (Datum: GDA94)
**Total depth**: mKB (Kelly bushing/rotary table)

**Appendix 3. List of wells used for source rock characterisation in the Gippsland Basin**

| WELL NAME | LATITUDE | LONGITUDE | EASTING | NORTHING | TOTAL DEPTH (mKB) | WELL TYPE |
|---|---|---|---|---|---|---|
| Anemone 1 | -38.76 | 148.33 | 615678.81 | 5708679.30 | 4609 | Exploration |
| Angler 1 | -38.66 | 148.44 | 625526.33 | 5720154.84 | 4330 | Exploration |
| Archer 1 | -38.76 | 148.31 | 613940.69 | 5708252.64 | 4051.5 | Exploration |
| Basker 1 | -38.31 | 148.70 | 648583.53 | 5758887.33 | 3991 | Exploration |
| Bignose 1 | -38.35 | 148.60 | 640044.66 | 5753646.27 | 3995 | Exploration |
| Bream 2 | -38.52 | 147.80 | 569510.77 | 5736048.31 | 3248 | Exploration |
| Helios 1 | -38.69 | 148.28 | 611090.70 | 5716513.34 | 3500 | Exploration |
| Hermes 1 | -38.60 | 148.30 | 613173.70 | 5726733.34 | 4565 | Exploration |
| Marlin A6 | -38.23 | 148.22 | 606866.86 | 5767920.51 | 3305.8 | Development |
| Omeo 1 ST1 | -38.61 | 147.71 | 562561.92 | 5726148.47 | 3379 | Exploration |
| Sawbelly 1 | -38.37 | 148.04 | 590516.93 | 5752208.48 | 3068 | Exploration |
| Selene 1 | -38.62 | 148.44 | 625160.34 | 5724176.28 | 3539 | Exploration |
| Shark 1 | -38.26 | 149.05 | 679653.00 | 5763566.59 | 3518 | Exploration |
| Tarra 1 | -38.64 | 147.70 | 561228.72 | 5722701.98 | 2905 | Exploration |
| Tuna 1A | -38.17 | 148.42 | 624274.93 | 5774142.47 | 3640.5 | Exploration |
| Turrum 3 | -38.26 | 148.25 | 609445.79 | 5764612.30 | 2995 | Extension/Appraisal |
| Veilfin 1 | -38.42 | 148.00 | 587614.68 | 5747572.31 | 3521 | Exploration |
| Volador 1 | -38.42 | 148.54 | 634848.88 | 5746123.77 | 1417 | Exploration |
| Whiting 2 | -38.25 | 147.86 | 574839.36 | 5766127.05 | 3550 | Extension/Appraisal |

**Latitude:** Decimal degrees (Datum: GDA94)
**Longitude:** Decimal degrees (Datum: GDA94)
**Total depth**: : mKB (Kelly bushing/rotary table)

**Appendix 4. Sample identity, Rock-Eval and TOC data for samples collected from the Vulcan Sub-basin**

| Sample ID | Sample Type | Well name | Upper Depth | Lower Depth | $S_1$ | $S_2$ | PP | $S_3$ | TOC | $T_{max}$ | PI | HI | OI | Formation |
|---|---|---|---|---|---|---|---|---|---|---|---|---|---|---|
| 20110049 | Cuttings | Jarrah 1A | 1854.00 | 1860.00 | 0.44 | 3.28 | 3.72 | 3.30 | 2.47 | 427 | 0.12 | 133 | 134 | |
| 20110051 | Cuttings | Maret 1 | 3158.00 | 3164.00 | 0.31 | 5.23 | 5.54 | 2.41 | 2.03 | 438 | 0.06 | 257 | 119 | **Echuca Shoals** |
| 20110065 | Cuttings | Paqualin 1 | 2517.00 | 2523.00 | 0.46 | 4.57 | 5.03 | 4.15 | 2.58 | 430 | 0.09 | 177 | 161 | |
| 20110074 | Cuttings | Skua 1 | 2410.97 | 2417.06 | 0.39 | 1.04 | 1.43 | 1.92 | 1.46 | 431 | 0.27 | 71 | 132 | |
| 20110061 | Cuttings | Oliver 1 | 2867.00 | 2873.00 | 0.20 | 2.00 | 2.20 | 4.73 | 1.78 | 435 | 0.09 | 113 | 266 | |
| 20110066 | Cuttings | Paqualin 1 | 2709.00 | 2715.00 | 0.30 | 2.86 | 3.16 | 2.50 | 1.35 | 433 | 0.09 | 212 | 185 | |
| 20110067 | Cuttings | Paqualin 1 | 2778.00 | 2787.00 | 0.44 | 2.90 | 3.34 | 5.03 | 1.27 | 433 | 0.13 | 228 | 396 | **Upper Vulcan** |
| 3848 | Cuttings | Vulcan 1B | 2438.00 | 2457.00 | 0.12 | 0.60 | 0.72 | nd | 0.75 | 425 | 0.17 | 80 | nd | |
| 3849 | Cuttings | Vulcan 1B | 2579.00 | 2597.00 | 0.39 | 1.24 | 1.63 | nd | 0.71 | 433 | 0.24 | 175 | nd | |
| 20110041 | Cuttings | East Swan 1 | 2404.87 | 2414.01 | 0.15 | 3.59 | 3.74 | 1.98 | 1.88 | 435 | 0.04 | 191 | 106 | |
| 20110042 | Cuttings | East Swan 1 | 2441.44 | 2447.54 | 1.30 | 10.17 | 11.47 | 9.98 | 4.57 | 430 | 0.11 | 223 | 218 | |
| 20110043 | Cuttings | East Swan 1 | 2478.02 | 2484.12 | 0.11 | 4.64 | 4.75 | 1.46 | 2.27 | 434 | 0.02 | 205 | 64 | |
| 20110044 | Cuttings | East Swan 1 | 2587.75 | 2593.84 | 1.18 | 29.80 | 30.98 | 3.62 | 10.13 | 434 | 0.04 | 294 | 36 | |
| 20110044 C | Cuttings | East Swan 1 | 2587.75 | 2593.84 | 13.33 | 146.70 | 160.03 | 1.72 | 33.07 | 444 | 0.08 | 444 | 5 | |
| 20110047 | Cuttings | Eclipse 1 | 2418.00 | 2421.00 | 0.37 | 4.32 | 4.69 | 3.08 | 2.82 | 431 | 0.08 | 153 | 109 | |
| 20110052 | Cuttings | Maret 1 | 3338.00 | 3344.00 | 0.44 | 4.60 | 5.04 | 3.49 | 2.20 | 434 | 0.09 | 209 | 159 | Lower Vulcan |
| 20110062 | Cuttings | Oliver 1 | 2918.00 | 2927.00 | 0.16 | 2.40 | 2.56 | 2.41 | 1.62 | 434 | 0.06 | 149 | 149 | |
| 20110068 | Cuttings | Paqualin 1 | 3399.00 | 3405.00 | 0.67 | 3.09 | 3.76 | 3.89 | 2.39 | 445 | 0.18 | 129 | 163 | |
| 20110069 | Cuttings | Paqualin 1 | 3444.00 | 3447.00 | 0.70 | 3.55 | 4.25 | 3.68 | 2.50 | 447 | 0.16 | 142 | 147 | |
| 20110070 | Cuttings | Paqualin 1 | 3501.00 | 3507.00 | 0.83 | 3.20 | 4.03 | 2.49 | 2.48 | 446 | 0.21 | 129 | 101 | |
| 20110071 | Cuttings | Paqualin 1 | 3654.00 | 3657.00 | 0.92 | 2.28 | 3.20 | 2.83 | 2.48 | 447 | 0.29 | 92 | 114 | |
| 20110072 | Cuttings | Paqualin 1 | 3861.00 | 3867.00 | 0.75 | 1.57 | 2.32 | 3.62 | 2.35 | 462 | 0.32 | 67 | 154 | |
| 20110073 | Cuttings | Paqualin 1 | 4056.00 | 4062.00 | 0.38 | 0.71 | 1.09 | 2.17 | 2.15 | 469 | 0.35 | 33 | 101 | |

**Appendix 4. (Continued) Sample identity, Rock-Eval and TOC data for samples collected from the Vulcan Sub-basin**

| Sample ID | Sample Type | Well name | Upper Depth | Lower Depth | S$_1$ | S$_2$ | PP | S$_3$ | TOC | T$_{max}$ | PI | HI | OI | Formation |
|---|---|---|---|---|---|---|---|---|---|---|---|---|---|---|
| 20110078 | Cuttings | Tahbilk 1 | 2907.00 | 2916.00 | 0.75 | 5.23 | 5.98 | 5.29 | 3.06 | 431 | 0.13 | 171 | 172 | |
| 20110079 | Cuttings | Taltarni 1 | 2931.00 | 2934.00 | 0.43 | 3.39 | 3.82 | 2.16 | 2.74 | 432 | 0.11 | 124 | 79 | |
| 20110080 | Cuttings | Taltarni 1 | 2934.00 | 2937.00 | 0.44 | 3.41 | 3.85 | 2.41 | 2.62 | 433 | 0.11 | 130 | 92 | |
| 20110081 | Cuttings | Taltarni 1 | 2937.00 | 2940.00 | 0.42 | 3.27 | 3.69 | 2.60 | 2.45 | 432 | 0.11 | 133 | 106 | |
| 20110083 | Cuttings | Vulcan 1B | 2819.40 | 2825.50 | 0.15 | 3.39 | 3.54 | 3.01 | 1.62 | 437 | 0.04 | 210 | 186 | |
| 20110084 | Cuttings | Vulcan 1B | 2944.36 | 2950.46 | 0.34 | 7.06 | 7.40 | 3.70 | 2.21 | 439 | 0.05 | 319 | 167 | |
| 20110085 | Cuttings | Vulcan 1B | 3593.59 | 3596.64 | 0.55 | 2.35 | 2.90 | 3.72 | 2.04 | 447 | 0.19 | 115 | 182 | |
| 3850 | Cuttings | Vulcan 1B | 2691.00 | 2707.00 | 0.43 | 2.17 | 2.60 | nd | 1.11 | 435 | 0.17 | 196 | nd | |
| 3851 | Cuttings | Vulcan 1B | 2926.00 | 2932.00 | 0.65 | 11.66 | 12.31 | nd | 2.32 | 431 | 0.05 | 503 | nd | **Lower Vulcan** |
| 3852 | Cuttings | Vulcan 1B | 3109.00 | 3115.00 | 0.51 | 2.65 | 3.16 | nd | 1.43 | 438 | 0.16 | 185 | nd | |
| 3853 | Cuttings | Vulcan 1B | 3246.00 | 3252.00 | 0.83 | 2.95 | 3.78 | nd | 1.58 | 443 | 0.22 | 187 | nd | |
| 3854 | Cuttings | Vulcan 1B | 3380.00 | 3386.00 | 1.14 | 2.38 | 3.52 | nd | 2.06 | 446 | 0.32 | 116 | nd | |
| 3855 | Cuttings | Vulcan 1B | 3545.00 | 3551.00 | 2.17 | 8.15 | 10.32 | nd | 3.56 | 434 | 0.21 | 229 | nd | |
| 3856 | Cuttings | Vulcan 1B | 3594.00 | 3603.00 | 0.86 | 1.58 | 2.44 | nd | 1.54 | 447 | 0.35 | 103 | nd | |
| 3857 | Core | Vulcan 1B | 3690.00 | 3690.30 | 0.60 | 0.89 | 1.49 | nd | 1.53 | 481 | 0.40 | 58 | nd | |
| 3858 | Core | Vulcan 1B | 3690.90 | 3691.00 | 0.58 | 0.66 | 1.24 | nd | 1.63 | 465 | 0.47 | 40 | nd | |
| 3859 | Core | Vulcan 1B | 3691.60 | 3692.00 | 0.49 | 0.77 | 1.26 | nd | 1.76 | 473 | 0.39 | 44 | nd | |
| 20110045 | Cuttings | East Swan 1 | 2752.34 | 2755.39 | 0.35 | 5.45 | 5.80 | 2.19 | 2.40 | 433 | 0.06 | 227 | 91 | |
| 20110046 | Cuttings | East Swan 1 | 2895.60 | 2898.64 | 0.12 | 3.57 | 3.69 | 3.56 | 2.32 | 431 | 0.03 | 154 | 154 | |
| 20110050 | Cuttings | Jarrah 1A | 1920.00 | 1923.00 | 14.41 | 184.64 | 199.05 | 9.24 | 39.94 | 428 | 0.07 | 462 | 23 | **Plover** |
| 20110053 | Cuttings | Maret 1 | 3527.00 | 3533.00 | 0.60 | 15.47 | 16.07 | 1.51 | 6.59 | 431 | 0.04 | 235 | 23 | |
| 20110053 C | Cuttings | Maret 1 | 3527.00 | 3533.00 | 7.27 | 89.46 | 96.73 | 1.46 | 26.20 | 433 | 0.08 | 341 | 6 | |

**Appendix 4. (Continued) Sample identity, Rock-Eval and TOC data for samples collected from the Vulcan Sub-basin**

| Sample ID | Sample Type | Well name | Upper Depth | Lower Depth | S₁ | S₂ | PP | S₃ | TOC | T$_{max}$ | PI | HI | OI | Formation |
|---|---|---|---|---|---|---|---|---|---|---|---|---|---|---|
| 20110054 | Cuttings | Maret 1 | 3554.00 | 3560.00 | 3.49 | 70.15 | 73.64 | 1.87 | 21.10 | 435 | 0.05 | 332 | 9 | |
| 20110054 C | Cuttings | Maret 1 | 3554.00 | 3560.00 | 15.91 | 159.61 | 175.52 | 2.08 | 33.98 | 437 | 0.09 | 470 | 6 | |
| 20110055 | Cuttings | Montara 1 | 3177.00 | 3186.00 | 2.31 | 43.36 | 45.67 | 3.81 | 15.66 | 431 | 0.05 | 277 | 24 | |
| 20110055 C | Cuttings | Montara 1 | 3177.00 | 3186.00 | 9.72 | 115.19 | 124.91 | 6.24 | 31.85 | 428 | 0.08 | 362 | 20 | |
| 20110056 | Cuttings | Montara 1 | 3201.00 | 3204.00 | 0.67 | 6.05 | 6.72 | 1.95 | 4.52 | 428 | 0.10 | 134 | 43 | |
| 20110057 | Cuttings | Montara 1 | 3306.00 | 3312.00 | 0.20 | 4.85 | 5.05 | 2.36 | 2.85 | 440 | 0.04 | 170 | 83 | |
| 20110058 | Cuttings | Montara 1 | 3315.00 | 3318.00 | 2.22 | 49.43 | 51.65 | 4.14 | 20.40 | 429 | 0.04 | 242 | 20 | |
| 20110060 | Cuttings | Montara 1 | 3417.00 | 3426.00 | 0.30 | 9.06 | 9.36 | 1.06 | 3.81 | 425 | 0.03 | 238 | 28 | Plover |
| 20110060C | Cuttings | Montara 2 | 3417.00 | 3426.00 | 9.56 | 141.82 | 151.38 | 4.93 | 31.17 | 427 | 0.06 | 455 | 16 | |
| 20110063 | Cuttings | Oliver 1 | 2979.00 | 2982.00 | 0.07 | 1.09 | 1.16 | 2.59 | 1.12 | 434 | 0.06 | 97 | 231 | |
| 20110064 | Cuttings | Oliver 1 | 3123.00 | 3129.00 | 0.09 | 0.75 | 0.84 | 2.70 | 1.19 | 436 | 0.11 | 63 | 226 | |
| 20110075 | Cuttings | Skua 1 | 2560.30 | 2563.30 | 4.14 | 72.14 | 76.28 | 5.78 | 23.28 | 426 | 0.05 | 310 | 25 | |
| 20110076 | Cuttings | Skua 1 | 2584.70 | 2587.75 | 2.78 | 44.54 | 47.32 | 4.80 | 18.93 | 422 | 0.06 | 235 | 25 | |
| 20110076 C | Cuttings | Skua 1 | 2584.70 | 2587.75 | 21.28 | 176.16 | 197.44 | 14.10 | 38.55 | 411 | 0.11 | 457 | 37 | |
| 20110077C | Cuttings | Skua 1 | 2630.40 | 2633.47 | 19.95 | 150.91 | 170.86 | 15.05 | 36.04 | 412 | 0.12 | 419 | 42 | |
| 20110082 | Cuttings | Taltarni 1 | 3294.00 | 3297.00 | 0.62 | 8.64 | 9.26 | 1.67 | 4.96 | 436 | 0.07 | 174 | 34 | |

**Sample ID:** ID allocated by Geoscience Australia
**Upper/Lower depth:** mKB (Kelly bushing/rotary Appendix)
**S₁**: Amount of free hydrocarbons in the sample in mg HC/g rock
**S₂**: Amount of hydrocarbons generated during pyrolysis in mg HC/g rock
**S₃**: Amount of oxygen containing compounds generated during pyrolysis in mg $CO_2$/g rock
**T$_{max}$**: Temperature of maximum hydrocarbon generation in °C
**HI**: Hydrogen Index (S₂*100/TOC) in mg HC/g TOC
**OI**: Oxygen Index (S₃*100/TOC) in mg $CO_2$/g TOC
**TOC**: Total Organic Carbon in %

**Appendix 5. Sample identity, Rock-Eval and TOC data for samples collected from the Laminaria High**

| Sample ID | Sample Type | Well Name | Upper Depth | Lower Depth | S$_1$ | S$_2$ | PP | S$_3$ | TOC | T$_{max}$ | PI | HI | OI | Formation |
|---|---|---|---|---|---|---|---|---|---|---|---|---|---|---|
| 20110001 | Cuttings | Buang 1 | 3110.00 | 3110.00 | 43.36 | 21.03 | 64.39 | 3.36 | 7.29 | 429 | 0.67 | 288 | 46 | |
| 20110002 | Cuttings | Buang 1 | 3120.00 | 3120.00 | 53.30 | 24.93 | 78.23 | 3.04 | 8.36 | 425 | 0.68 | 298 | 36 | |
| 20110003 | Cuttings | Buang 1 | 3110.00 | 3120.00 | 50.84 | 23.89 | 74.73 | 2.55 | 8.11 | 428 | 0.68 | 295 | 31 | **Echuca Shoals** |
| 20110010 | Cuttings | Corallina 1 | 2930.00 | 2945.00 | 0.12 | 4.03 | 4.15 | 2.06 | 2.08 | 434 | 0.03 | 194 | 99 | |
| 20110013 | Cuttings | Laminaria 1 | 2940.00 | 2950.00 | 0.12 | 5.58 | 5.70 | 0.89 | 2.17 | 435 | 0.02 | 258 | 41 | |
| 20110004 | Cuttings | Buang 1 | 3170.00 | 3170.00 | 35.77 | 23.14 | 58.91 | 3.32 | 6.32 | 430 | 0.61 | 366 | 53 | |
| 20110005 | Cuttings | Buang 1 | 3300.00 | 3300.00 | 33.59 | 18.00 | 51.59 | 4.84 | 5.41 | 430 | 0.65 | 333 | 89 | |
| 20110011 | Cuttings | Corallina 1 | 2950.00 | 2955.00 | 0.29 | 6.87 | 7.16 | 2.53 | 3.16 | 435 | 0.04 | 217 | 80 | **Flamingo** |
| 20110012 | Cuttings | Corallina 1 | 2990.00 | 3005.00 | 0.10 | 1.94 | 2.04 | 1.75 | 1.01 | 437 | 0.05 | 192 | 174 | |
| 20110018 | Cuttings | Laminaria 3 | 3110.00 | 3120.00 | 0.15 | 1.93 | 2.08 | 2.52 | 0.89 | 439 | 0.07 | 217 | 284 | |
| 20110006 | Cuttings | Buang 1 | 3500.00 | 3500.00 | 32.28 | 12.16 | 44.44 | 2.43 | 4.77 | 438 | 0.73 | 255 | 51 | |
| 20110007 | Cuttings | Buang 1 | 3580.00 | 3580.00 | 30.24 | 12.71 | 42.95 | 2.04 | 4.95 | 434 | 0.70 | 257 | 41 | |
| 20110014 | Cuttings | Laminaria 1 | 3190.00 | 3195.00 | 0.29 | 1.48 | 1.77 | 1.33 | 1.63 | 425 | 0.16 | 91 | 82 | |
| 20110015 | Cuttings | Laminaria 1 | 3195.00 | 3200.00 | 0.34 | 1.69 | 2.03 | 1.50 | 1.71 | 425 | 0.17 | 99 | 88 | **Frigate** |
| 20110019 | Cuttings | Laminaria 3 | 3230.00 | 3240.00 | 0.57 | 9.22 | 9.79 | 3.66 | 2.83 | 401 | 0.06 | 326 | 129 | |
| 20110020 | Cuttings | Laminaria 3 | 3265.00 | 3275.00 | 0.46 | 2.27 | 2.73 | 2.98 | 1.76 | 435 | 0.17 | 129 | 170 | |
| 20110021 | Cuttings | Laminaria East 1 | 3250.00 | 3255.00 | 30.91 | 21.74 | 52.65 | 8.44 | 6.57 | 402 | 0.59 | 331 | 128 | |
| 20110008 | Cuttings | Buang 1 | 3615.00 | 3615.00 | 9.66 | 13.32 | 22.98 | 2.52 | 3.42 | 427 | 0.42 | 389 | 74 | |
| 20110016 | Cuttings | Laminaria 1 | 3255.00 | 3260.00 | 0.04 | 0.92 | 0.96 | 0.84 | 0.88 | 435 | 0.04 | 105 | 95 | |
| 20110017 | Cuttings | Laminaria 1 | 3285.00 | 3290.00 | 0.37 | 1.02 | 1.39 | 0.97 | 0.95 | 431 | 0.27 | 107 | 102 | **Laminaria** |
| 20110022 | Cuttings | Laminaria East 1 | 3310.00 | 3320.00 | 7.05 | 6.87 | 13.92 | 1.53 | 2.42 | 434 | 0.51 | 284 | 63 | |
| 20110023 | Cuttings | Laminaria East 1 | 3390.00 | 3400.00 | 0.94 | 1.06 | 2.00 | 2.14 | 0.74 | 427 | 0.47 | 144 | 289 | **Plover** |

**Appendix 6. Sample identity, Rock-Eval and TOC data for samples collected from the Gippsland Basin**

| Sample ID | Sample Type | Well name | Upper Depth | Lower Depth | $S_1$ | $S_2$ | PP | $S_3$ | TOC | $T_{max}$ | PI | HI | OI | Spore/Pollen biozone |
|---|---|---|---|---|---|---|---|---|---|---|---|---|---|---|
| 20110090 | Cuttings | Bream 2 | 2724.91 | 2740.15 | 1.20 | 24.17 | 25.37 | 2.47 | 10.84 | 424 | 0.05 | 223 | 23 | |
| 20110091 | Cuttings | Bream 2 | 2743.20 | 2752.34 | 1.04 | 21.20 | 22.24 | 3.53 | 10.65 | 424 | 0.05 | 199 | 33 | |
| 20110092 | Core | Bream 2 | 2753.62 | 2753.62 | 0.53 | 16.71 | 17.24 | 1.02 | 4.38 | 438 | 0.03 | 382 | 23 | |
| 20110093 | Cuttings | Bream 2 | 2752.34 | 2758.44 | 1.73 | 34.86 | 36.59 | 1.64 | 9.83 | 422 | 0.05 | 355 | 17 | |
| 20110113 | Cuttings | Marlin A6 | 2386.58 | 2389.63 | 4.67 | 84.66 | 89.33 | 31.52 | 52.65 | 417 | 0.05 | 161 | 60 | |
| 20110114 | Cuttings | Marlin A6 | 2438.40 | 2441.45 | 2.72 | 26.37 | 29.09 | 18.70 | 18.69 | 422 | 0.09 | 141 | 100 | |
| 20110115 | Cuttings | Marlin A6 | 2499.36 | 2505.46 | 15.39 | 77.86 | 93.25 | 25.72 | 44.41 | 411 | 0.17 | 175 | 58 | |
| 20110116 | Core | Marlin A6 | 2511.86 | 2511.86 | 0.13 | 1.09 | 1.22 | 0.57 | 1.88 | 421 | 0.11 | 58 | 30 | |
| 20110117 | Core | Marlin A6 | 2518.56 | 2518.56 | 0.10 | 0.68 | 0.78 | 0.57 | 1.51 | 421 | 0.13 | 45 | 38 | |
| 20110118 | Core | Marlin A6 | 2526.79 | 2526.79 | 0.17 | 1.97 | 2.14 | 1.08 | 3.28 | 420 | 0.08 | 60 | 33 | |
| 20110119 | Cuttings | Marlin A6 | 2563.37 | 2569.46 | 30.99 | 105.01 | 136.00 | 47.97 | 73.27 | 414 | 0.23 | 143 | 65 | |
| 20110120 | Cuttings | Marlin A6 | 2615.18 | 2618.23 | 29.56 | 113.62 | 143.18 | 27.84 | 58.39 | 412 | 0.21 | 195 | 48 | *L. balmei* |
| 20110121 | Cuttings | Marlin A6 | 2624.33 | 2630.42 | 16.99 | 115.54 | 132.53 | 36.81 | 72.41 | 422 | 0.13 | 160 | 51 | |
| 20110122 | Cuttings | Marlin A6 | 2691.38 | 2694.43 | 25.24 | 110.43 | 135.67 | 58.32 | 59.21 | 416 | 0.19 | 186 | 98 | |
| 20110123 | Cuttings | Marlin A6 | 2804.16 | 2810.26 | 9.44 | 68.76 | 78.20 | 35.60 | 44.76 | 426 | 0.12 | 154 | 80 | |
| 20110124 | Cuttings | Marlin A6 | 2987.04 | 2993.14 | 7.77 | 103.80 | 111.57 | 22.90 | 60.55 | 430 | 0.07 | 171 | 38 | |
| 20110125 | Cuttings | Sawbelly 1 | 2980.00 | 2985.00 | 1.69 | 32.13 | 33.82 | 13.89 | 16.45 | 429 | 0.05 | 195 | 84 | |
| 20110126 | Cuttings | Sawbelly 1 | 3015.00 | 3015.00 | 2.23 | 29.24 | 31.47 | 9.69 | 13.84 | 431 | 0.07 | 211 | 70 | |
| 20110250 | Cuttings | Turrum 3 | 1780.00 | 1790.00 | 4.65 | 51.98 | 56.63 | 10.74 | 27.82 | 420 | 0.08 | 187 | 39 | |
| 20110138 | Cuttings | Turrum 3 | 1795.00 | 1805.00 | 1.08 | 6.83 | 7.91 | 10.63 | 8.82 | 421 | 0.14 | 77 | 120 | |
| 20110139 | Cuttings | Turrum 3 | 2385.00 | 2400.00 | 0.17 | 5.02 | 5.19 | 3.04 | 3.79 | 426 | 0.03 | 133 | 80 | |
| 20110140 | Cuttings | Turrum 3 | 2565.00 | 2580.00 | 2.57 | 41.17 | 43.74 | 9.20 | 23.18 | 425 | 0.06 | 178 | 40 | |

**Appendix 6. (Continued) Sample identity, Rock-Eval and TOC data for samples collected from the Gippsland Basin**

| Sample ID | Sample Type | Well name | Upper Depth | Lower Depth | $S_1$ | $S_2$ | PP | $S_3$ | TOC | $T_{max}$ | PI | HI | OI | Spore/Pollen biozone |
|---|---|---|---|---|---|---|---|---|---|---|---|---|---|---|
| 20110141 | Cuttings | Veilfin 1 | 2640.00 | 2650.00 | 0.09 | 5.62 | 5.71 | 6.29 | 6.86 | 427 | 0.02 | 82 | 92 | |
| 20110142 | Cuttings | Veilfin 1 | 2660.00 | 2670.00 | 0.08 | 7.99 | 8.07 | 4.94 | 7.19 | 426 | 0.01 | 111 | 69 | *L. balmei* |
| 20110152 | Cuttings | Whiting 2 | 2145.00 | 2155.00 | 0.08 | 2.76 | 2.84 | 1.88 | 2.70 | 433 | 0.03 | 102 | 70 | |
| 20110153 | Cuttings | Whiting 2 | 2325.00 | 2335.00 | 0.38 | 9.76 | 10.14 | 1.31 | 3.78 | 433 | 0.04 | 259 | 35 | |
| 20110024 | Cuttings | Anemone 1 | 3065.00 | 3075.00 | 0.24 | 13.64 | 13.88 | 11.13 | 9.40 | 416 | 0.02 | 145 | 118 | |
| 20110026 | Cuttings | Angler 1 | 3120.00 | 3130.00 | 0.24 | 16.66 | 16.90 | 9.32 | 8.77 | 419 | 0.01 | 190 | 106 | |
| 20110030 | Cuttings | Basker 1 | 2982.00 | 2985.00 | 0.19 | 14.41 | 14.60 | 5.94 | 8.38 | 425 | 0.01 | 172 | 71 | |
| 20110031 | Cuttings | Basker 1 | 3009.00 | 3024.00 | 1.05 | 44.93 | 45.98 | 8.37 | 21.97 | 421 | 0.02 | 205 | 38 | |
| 20110032 | Cuttings | Basker 1 | 3066.00 | 3072.00 | 0.80 | 37.34 | 38.14 | 6.91 | 16.74 | 427 | 0.02 | 223 | 41 | |
| 20110033 | Cuttings | Basker 1 | 3099.00 | 3105.00 | 0.95 | 22.16 | 23.11 | 3.69 | 9.02 | 428 | 0.04 | 246 | 41 | |
| 20110034 | Core | Basker 1 | 3108.80 | 3108.80 | 0.68 | 12.72 | 13.40 | 1.29 | 4.02 | 430 | 0.05 | 316 | 32 | |
| 20110036 | Cuttings | Bignose 1 | 3319.00 | 3322.00 | 0.26 | 20.39 | 20.65 | 8.31 | 13.20 | 425 | 0.01 | 154 | 63 | |
| 20110037 | Cuttings | Bignose 1 | 3331.00 | 3334.00 | 0.17 | 10.01 | 10.18 | 4.20 | 6.10 | 428 | 0.02 | 164 | 69 | |
| 20110038 | Cuttings | Bignose 1 | 3358.00 | 3364.00 | 0.15 | 8.63 | 8.78 | 3.01 | 4.68 | 428 | 0.02 | 184 | 64 | *F. longus* |
| 20110100 | Cuttings | Hermes 1 | 3175.00 | 3180.00 | 0.21 | 6.57 | 6.78 | 1.75 | 3.36 | 427 | 0.03 | 195 | 52 | |
| 20110101 | Cuttings | Hermes 1 | 3210.00 | 3215.00 | 0.16 | 6.96 | 7.12 | 1.30 | 3.13 | 426 | 0.02 | 223 | 42 | |
| 20110102 | Cuttings | Hermes 1 | 3230.00 | 3245.00 | 0.28 | 13.37 | 13.65 | 5.18 | 7.82 | 425 | 0.02 | 171 | 66 | |
| 20110103 | Cuttings | Hermes 1 | 3255.00 | 3255.00 | 3.24 | 87.64 | 90.88 | 4.90 | 24.84 | 418 | 0.04 | 353 | 20 | |
| 20110104 | Cuttings | Hermes 1 | 3295.00 | 3305.00 | 4.55 | 19.90 | 24.45 | 4.65 | 12.17 | 422 | 0.19 | 163 | 38 | |
| 20110105 | Cuttings | Hermes 1 | 3485.00 | 3500.00 | 0.62 | 19.47 | 20.09 | 3.98 | 11.41 | 427 | 0.03 | 171 | 35 | |
| 20110106 | Cuttings | Hermes 1 | 3520.00 | 3525.00 | 0.72 | 19.45 | 20.17 | 3.02 | 9.68 | 426 | 0.04 | 201 | 31 | |
| 20110107 | Cuttings | Hermes 1 | 3540.00 | 3550.00 | 0.96 | 33.45 | 34.41 | 4.70 | 17.75 | 426 | 0.03 | 188 | 26 | |

**Appendix 6. (Continued) Sample identity, Rock-Eval and TOC data for samples collected from the Gippsland Basin**

| Sample ID | Sample Type | Well name | Upper Depth | Lower Depth | S₁ | S₂ | PP | S₃ | TOC | Tmax | PI | HI | OI | Spore/Pollen biozone |
|-----------|-------------|-----------|-------------|-------------|------|--------|--------|-------|-------|------|------|-----|-----|---------------------|
| 20110129 | Cuttings | Shark 1 | 2061.00 | 2064.00 | 0.29 | 14.53 | 14.82 | 1.75 | 5.45 | 425 | 0.02 | 267 | 32 | |
| 20110130 | Cuttings | Tarra 1 | 2502.00 | 2505.00 | 0.26 | 8.78 | 9.04 | 1.18 | 3.32 | 427 | 0.03 | 265 | 36 | |
| 20110131 | Cuttings | Tarra 1 | 2517.00 | 2520.00 | 0.15 | 2.79 | 2.94 | 0.78 | 1.17 | 431 | 0.05 | 239 | 67 | |
| 20110143 | Cuttings | Veilfin 1 | 3205.00 | 3215.00 | 0.04 | 1.06 | 1.10 | 1.57 | 2.16 | 443 | 0.04 | 49 | 73 | |
| 20110144 | Cuttings | Veilfin 1 | 3355.00 | 3365.00 | 1.53 | 29.08 | 30.61 | 2.91 | 19.21 | 439 | 0.05 | 151 | 15 | |
| 20110145 | Cuttings | Veilfin 1 | 3405.00 | 3410.00 | 1.41 | 21.83 | 23.24 | 4.60 | 14.98 | 440 | 0.06 | 146 | 31 | |
| 20110146 | Cuttings | Veilfin-1 | 3430.00 | 3435.00 | 0.30 | 9.50 | 9.80 | 5.02 | 9.56 | 440 | 0.03 | 99 | 52 | |
| 20110251 | Core | Veilfin 1 | 3460.00 | 3460.10 | 0.32 | 3.50 | 3.82 | 0.08 | 1.54 | 448 | 0.08 | 228 | 5 | |
| 20110147 | Cuttings | Veilfin 1 | 3460.00 | 3470.00 | 0.30 | 21.93 | 22.23 | 5.57 | 2.62 | 445 | 0.01 | 838 | 213 | *F. longus* |
| 20110148 | Cuttings | Volador 1 | 3552.00 | 3552.00 | 1.07 | 36.16 | 37.23 | 4.88 | 19.83 | 419 | 0.03 | 182 | 25 | |
| 20110149 | Cuttings | Volador 1 | 3573.00 | 3573.00 | 0.75 | 31.86 | 32.61 | 7.66 | 17.46 | 424 | 0.02 | 182 | 44 | |
| 20110252 | Cuttings | Volador 1 | 3675.00 | 3675.00 | 0.60 | 22.79 | 23.39 | 2.56 | 11.02 | 432 | 0.03 | 207 | 23 | |
| 20110150 | Cuttings | Volador-1 | 3687.00 | 3687.00 | 0.14 | 4.43 | 4.57 | 1.17 | 3.25 | 433 | 0.03 | 136 | 36 | |
| 20110151 | Cuttings | Volador 1 | 3693.00 | 3696.00 | 0.79 | 12.69 | 13.48 | 3.72 | 6.34 | 427 | 0.06 | 200 | 59 | |
| 20110279C | Cuttings | Volador 1 | 3849.00 | 3852.00 | 7.69 | 169.55 | 177.24 | 7.70 | 68.53 | 432 | 0.04 | 247 | 11 | |
| 20110253 | Cuttings | Whiting 2 | 3015.00 | 3025.00 | 0.36 | 4.33 | 4.69 | 0.79 | 2.26 | 443 | 0.08 | 192 | 35 | |
| 20110154 | Cuttings | Whiting 2 | 3168.20 | 3180.00 | 0.24 | 2.68 | 2.92 | 0.59 | 1.82 | 443 | 0.08 | 147 | 32 | |
| 20110025 | Cuttings | Anemone 1 | 3335.00 | 3345.00 | 0.62 | 25.48 | 26.10 | 12.59 | 13.43 | 420 | 0.02 | 190 | 94 | |
| 20110027 | Cuttings | Angler 1 | 3790.00 | 3795.00 | 0.07 | 1.52 | 1.59 | 1.12 | 1.36 | 424 | 0.04 | 112 | 83 | |
| 20110028 | Cuttings | Angler 1 | 3810.00 | 3820.00 | 0.11 | 3.42 | 3.53 | 1.38 | 2.36 | 424 | 0.03 | 145 | 59 | |
| 20110029 | Cuttings | Angler 1 | 3905.00 | 3915.00 | 0.10 | 2.21 | 2.31 | 2.04 | 1.66 | 430 | 0.04 | 133 | 123 | *T. lilliei* |
| 20110267 | Cuttings | Angler 1 | 4030.00 | 4035.00 | 0.14 | 3.22 | 3.36 | 2.05 | 1.94 | 431 | 0.04 | 166 | 106 | |
| 20110035 | Cuttings | Basker 1 | 3615.00 | 3621.00 | 0.69 | 28.53 | 29.22 | 32.20 | 28.25 | 423 | 0.02 | 101 | 114 | |
| 20110039 | Cuttings | Bignose 1 | 3469.00 | 3472.00 | 0.38 | 14.94 | 15.32 | 4.64 | 8.57 | 425 | 0.02 | 174 | 54 | |

**Appendix 6. (Continued) Sample identity, Rock-Eval and TOC data for samples collected from the Gippsland Basin**

| Sample ID | Sample Type | Well name | Upper Depth | Lower Depth | S₁ | S₂ | PP | S₃ | TOC | Tmax | PI | HI | OI | Spore/Pollen biozone |
|---|---|---|---|---|---|---|---|---|---|---|---|---|---|---|
| 20110040 | Cuttings | Bignose 1 | 3544.00 | 3547.00 | 0.68 | 28.37 | 29.05 | 6.88 | 47.55 | 427 | 0.02 | 60 | 14 | |
| 20110086 | Cuttings | Bignose 1 | 3709.00 | 3712.00 | 0.59 | 18.17 | 18.76 | 3.43 | 8.15 | 430 | 0.03 | 223 | 42 | |
| 20110087 | Cuttings | Bignose 1 | 3730.00 | 3733.00 | 0.76 | 31.11 | 31.87 | 4.23 | 15.99 | 427 | 0.02 | 195 | 26 | |
| 20110088 | Cuttings | Bignose 1 | 3775.00 | 3778.00 | 0.74 | 14.21 | 14.95 | 2.58 | 6.40 | 430 | 0.05 | 222 | 40 | |
| 20110089 | Cuttings | Bignose 1 | 3811.00 | 3811.00 | 0.87 | 14.28 | 15.15 | 2.42 | 6.39 | 429 | 0.06 | 224 | 38 | |
| 20110094 | Cuttings | Bream 2 | 3096.77 | 3105.91 | 4.67 | 57.35 | 62.02 | 9.55 | 28.51 | 419 | 0.08 | 201 | 33 | |
| 20110095 | Cuttings | Bream 2 | 3145.54 | 3151.63 | 2.53 | 45.99 | 48.52 | 13.75 | 24.66 | 419 | 0.05 | 187 | 56 | |
| 20110096 | Cuttings | Bream 2 | 3166.87 | 3182.11 | 2.38 | 70.49 | 72.87 | 16.98 | 37.57 | 419 | 0.03 | 188 | 45 | |
| 20110097 | Core | Bream 2 | 3241.55 | 3241.85 | 2.45 | 27.52 | 29.97 | 1.82 | 15.42 | 442 | 0.08 | 179 | 12 | *T. lilliei* |
| 20110098 | Cuttings | Helios 1 | 3380.00 | 3380.00 | 0.76 | 45.96 | 46.72 | 16.71 | 21.13 | 419 | 0.02 | 218 | 79 | |
| 20110099 | Cuttings | Helios-1 | 3390.00 | 3390.00 | 0.10 | 13.30 | 13.40 | 10.49 | 10.45 | 421 | 0.01 | 127 | 100 | |
| 20110108 | Cuttings | Hermes 1 | 3595.00 | 3600.00 | 1.43 | 33.96 | 35.39 | 5.33 | 17.20 | 427 | 0.04 | 197 | 31 | |
| 20110109 | Cuttings | Hermes 1 | 3775.00 | 3785.00 | 1.05 | 28.06 | 29.11 | 5.13 | 16.35 | 430 | 0.04 | 172 | 31 | |
| 20110110 | Cuttings | Hermes 1 | 3845.00 | 3860.00 | 1.59 | 28.99 | 30.58 | 4.10 | 15.39 | 433 | 0.05 | 188 | 27 | |
| 20110111 | Cuttings | Hermes 1 | 4075.00 | 4080.00 | 2.85 | 28.62 | 31.47 | 7.83 | 16.31 | 435 | 0.09 | 175 | 48 | |
| 20110112 | Cuttings | Hermes 1 | 4275.00 | 4285.00 | 4.59 | 33.92 | 38.51 | 5.48 | 19.82 | 441 | 0.12 | 171 | 28 | |
| 20110127 | Core | Selene 1 | 3142.60 | 3142.60 | 0.10 | 3.48 | 3.58 | 0.37 | 2.14 | 423 | 0.03 | 163 | 17 | |
| 20110128 | Core | Selene 1 | 3148.80 | 3148.80 | 0.58 | 29.89 | 9.35 | 9.35 | 9.35 | 418 | 0.02 | 498 | 156 | |
| 20110287 | Cuttings | Volador 1 | 4335.00 | 4338.00 | 5.44 | 43.43 | 48.87 | 1.46 | 17.57 | 442 | 0.11 | 247 | 8 | |
| 20110292 | Cuttings | Volador 1 | 4527.00 | 4530.00 | 4.22 | 28.59 | 32.81 | 1.92 | 14.57 | 443 | 0.13 | 196 | 13 | |
| 20110296 | Cuttings | Archer 1 | 3915.00 | 3925.00 | 0.27 | 2.22 | 2.49 | 2.25 | 1.95 | 433 | 0.11 | 114 | 115 | *N. senectus* |
| 20110262 | Cuttings | Anemone 1 | 4390.00 | 4400.00 | 0.22 | 1.30 | 1.52 | 1.22 | 1.65 | 429 | 0.14 | 79 | 74 | *T. apoxyexinus* |
| 20110275 | Cuttings | Omeo 1 ST1 | 3363.00 | 3369.00 | 2.22 | 73.16 | 75.38 | 0.99 | 12.13 | 430 | 0.03 | 603 | 8 | *P. mawsonii* |
| 20110132 | Cuttings | Tuna A1 | 1773.94 | 1780.03 | 0.02 | 0.89 | 0.91 | 3.76 | 3.55 | 421 | 0.02 | 25 | 106 | |
| 20110133 | Core | Tuna A1 | 1887.32 | 1887.32 | 0.56 | 26.06 | 26.62 | 1.44 | 6.27 | 422 | 0.02 | 416 | 23 | **nd** |
| 20110134 | Core | Tuna A1 | 1893.42 | 1893.42 | 10.82 | 136.65 | 147.47 | 27.39 | 61.48 | 416 | 0.07 | 222 | 45 | |

**Appendix 6. (Continued) Sample identity, Rock-Eval and TOC data for samples collected from the Gippsland Basin**

| Sample ID | Sample Type | Well name | Upper Depth | Lower Depth | S₁ | S₂ | PP | S₃ | TOC | Tmax | PI | HI | OI | Spore/Pollen biozone |
|-----------|-------------|-----------|-------------|-------------|----|----|----|----|-----|------|----|----|----|----------------------|
| **20110135** | Cuttings | Tuna A1 | 1938.53 | 1944.62 | 0.69 | 28.53 | 29.22 | 32.20 | 28.25 | 423 | 0.02 | 101 | 114 | |
| **20110136** | Cuttings | Tuna A1 | 1962.91 | 1972.06 | 0.16 | 4.48 | 4.64 | 4.19 | 4.23 | 422 | 0.04 | 106 | 99 | |
| **20110137** | Cuttings | Tuna A1 | 2063.50 | 2072.64 | 0.20 | 6.89 | 7.09 | 6.66 | 6.58 | 421 | 0.03 | 105 | 101 | **nd** |

**Sample ID:** ID allocated by Geoscience Australia
**Upper/Lower depth:** mKB (Kelly bushing/rotary Appendix)
**S₁**: Amount of free hydrocarbons in the sample in mg HC/g rock
**S₂**: Amount of hydrocarbons generated during pyrolysis in mg HC/g rock
**S₃**: Amount of oxygen containing compounds generated during pyrolysis in mg $CO_2$/g rock
**Tmax**: Temperature of maximum hydrocarbon generation in °C
**HI**: Hydrogen Index (S₂*100/TOC) in mg HC/g TOC
**OI**: Oxygen Index (S₃*100/TOC) in mg $CO_2$/g TOC
**TOC**: Total Organic Carbon in %
***L. balmei***: *Lygistepollenites balmei*
***F. longus***: *Forcipites longus*
***T. lilliei***: *Tricolporites lilliei*
***N. senectus***: *Nothofagidites senectus*
***T. apoxyexinus***: *Tricolporites apoxyexinus*
***P. mawsonii***: *Phyllocladidites mawsonii*
**nd**: not determined

**Appendix 7. Pyrolysate classes and compounds in kerogens from the Vulcan Sub-basin**

| Class | Compound (mg/g TOC) | Echuca Shoals Fm | | Upper Vulcan Fm | | Lower Vulcan Fm | |
|---|---|---|---|---|---|---|---|
| | | 20110051 | 20110065 | 20110067 | 3849 | 20110042 | 20110044 |
| Aliphatic | $n\text{-}C_1$ | 10.30 | 9.51 | 9.67 | 3.56 | 5.25 | 15.68 |
| | $n\text{-}C_2$ | 8.53 | 7.71 | 8.24 | 3.74 | 4.00 | 11.05 |
| | $n\text{-}C_3$ | 7.64 | 6.44 | 7.41 | 3.70 | 3.56 | 8.05 |
| | $n\text{-}C_4$ | 8.19 | 6.06 | 6.21 | 3.35 | 2.90 | 4.76 |
| | $n\text{-}C_5$ | 3.28 | 2.39 | 3.49 | 1.42 | 1.04 | 1.96 |
| | $n\text{-}C_6$ | 2.69 | 2.04 | 2.71 | 1.41 | 1.08 | 1.72 |
| | $n\text{-}C_7$ | 2.12 | 1.60 | 2.06 | 1.04 | 0.86 | 1.53 |
| | $n\text{-}C_8$ | 1.88 | 1.35 | 1.67 | 0.87 | 0.73 | 1.31 |
| | $n\text{-}C_9$ | 1.41 | 0.95 | 1.25 | 0.57 | 0.54 | 1.13 |
| | $n\text{-}C_{10}$ | 1.23 | 0.81 | 1.12 | 0.46 | 0.45 | 1.11 |
| | $n\text{-}C_{11}$ | 1.08 | 0.75 | 0.99 | 0.39 | 0.41 | 1.12 |
| | $n\text{-}C_{12}$ | 1.12 | 0.78 | 0.91 | 0.35 | 0.46 | 1.14 |
| | $n\text{-}C_{13}$ | 1.05 | 0.63 | 0.89 | 0.29 | 0.41 | 1.32 |
| | $n\text{-}C_{14}$ | 0.95 | 0.62 | 0.78 | 0.25 | 0.35 | 1.13 |
| | $n\text{-}C_{15}$ | 0.87 | 0.55 | 0.74 | 0.21 | 0.33 | 0.95 |
| | $n\text{-}C_{16}$ | 0.75 | 0.42 | 0.60 | 0.12 | 0.29 | 1.02 |
| | $n\text{-}C_{17}$ | 0.54 | 0.30 | 0.49 | 0.07 | 0.21 | 0.88 |
| | $n\text{-}C_{18}$ | 0.48 | 0.27 | 0.44 | 0.05 | 0.19 | 0.79 |
| | $n\text{-}C_{19}$ | 0.42 | 0.26 | 0.35 | 0.04 | 0.18 | 0.87 |
| | $n\text{-}C_{20}$ | 0.33 | 0.15 | 0.28 | 0.01 | 0.14 | 0.75 |
| | $n\text{-}C_{21}$ | 0.25 | 0.11 | 0.22 | 0.00 | 0.11 | 0.71 |
| | $n\text{-}C_{22}$ | 0.21 | 0.10 | 0.19 | 0.00 | 0.09 | 0.84 |
| | $n\text{-}C_{23}$ | 0.14 | 0.06 | 0.12 | 0.00 | 0.07 | 0.81 |
| | $n\text{-}C_{24}$ | 0.16 | 0.07 | 0.14 | 0.00 | 0.09 | 0.78 |
| | $n\text{-}C_{25}$ | 0.14 | 0.00 | 0.00 | 0.00 | 0.08 | 0.80 |
| | $n\text{-}C_{26}$ | 0.14 | 0.00 | 0.00 | 0.00 | 0.03 | 0.67 |
| | $n\text{-}C_{27}$ | 0.13 | 0.00 | 0.00 | 0.00 | 0.00 | 0.61 |
| | $n\text{-}C_{28}$ | 0.05 | 0.00 | 0.00 | 0.00 | 0.00 | 0.37 |
| | $n\text{-}C_{29}$ | 0.05 | 0.00 | 0.00 | 0.00 | 0.00 | 0.23 |
| | $n\text{-}C_{30}$ | 0.05 | 0.00 | 0.00 | 0.00 | 0.00 | 0.11 |
| | $n\text{-}C_{31}$ | 0.05 | 0.00 | 0.00 | 0.00 | 0.00 | 0.00 |
| | $n\text{-}C_{32}$ | 0.05 | 0.00 | 0.00 | 0.00 | 0.00 | 0.00 |
| Mono-aromatic | Benz | 1.27 | 1.37 | 1.89 | 1.32 | 0.43 | 0.39 |
| | Tol | 1.85 | 2.01 | 2.25 | 1.23 | 0.84 | 1.57 |
| | E-Benz | 0.52 | 0.48 | 0.59 | 0.36 | 0.24 | 0.42 |
| | $m+p$ Xyl | 1.11 | 1.14 | 1.16 | 0.58 | 0.58 | 1.26 |
| | Styr | 0.31 | 0.24 | 0.34 | 0.26 | 0.10 | 0.16 |
| | $o$-Xyl | 0.55 | 0.56 | 0.62 | 0.35 | 0.27 | 0.37 |
| | PropylBenz | 0.20 | 0.13 | 0.24 | 0.04 | 0.04 | 0.05 |

**Appendix 7. (Continued) Pyrolysate classes and compounds in kerogens from the Vulcan Sub-basin**

| Class | Compound (mg/g TOC) | Echuca Shoals Fm | | Upper Vulcan Fm | | Lower Vulcan Fm | |
|---|---|---|---|---|---|---|---|
| | | 20110051 | 20110065 | 20110067 | 3849 | 20110042 | 20110044 |
| Mono-aromatic | 1M3EBenz | 0.28 | 0.45 | 0.36 | 0.13 | 0.15 | 0.27 |
| | 1M4EBenz | 0.18 | 0.27 | 0.26 | 0.08 | 0.08 | 0.14 |
| | 1,3,5TMBenz | 0.12 | 0.13 | 0.11 | 0.05 | 0.06 | 0.15 |
| | 1M2EBenz | 0.24 | 0.24 | 0.25 | 0.32 | 0.11 | 0.14 |
| | 1,2,4TMBenz | 0.48 | 0.46 | 0.47 | 0.24 | 0.23 | 0.35 |
| | 1,2,3TMBenz | 0.25 | 0.38 | 0.37 | 0.12 | 0.15 | 0.21 |
| Phenolic | Phenol | 0.71 | 0.61 | 1.04 | 0.61 | 0.43 | 1.28 |
| | 2M Phenol | 0.56 | 0.37 | 0.57 | 0.11 | 0.23 | 1.18 |
| | 3+4M Phenol | 0.44 | 0.31 | 0.52 | 0.14 | 0.29 | 2.11 |
| Naphthenic | Napht | 0.33 | 0.31 | 0.36 | 0.21 | 0.17 | 0.40 |
| | 2M Napht | 0.40 | 0.34 | 0.41 | 0.19 | 0.21 | 0.56 |
| | 1M Napht | 0.35 | 0.31 | 0.38 | 0.16 | 0.16 | 0.36 |
| | Sum DMNapht | 0.60 | 0.55 | 0.66 | 0.26 | 0.36 | 1.20 |
| | 1,3,7TMNaph | 0.05 | 0.05 | 0.05 | 0.02 | 0.01 | 0.07 |
| | 1,3,6TMNapht | 0.06 | 0.06 | 0.06 | 0.02 | 0.03 | 0.06 |
| | 1,3,5TMNapht | 0.11 | 0.08 | 0.10 | 0.03 | 0.05 | 0.16 |
| | 2,3,6TMNapht | 0.06 | 0.04 | 0.05 | 0.01 | 0.03 | 0.06 |
| | 1,2,7TMNapht | 0.16 | 0.09 | 0.13 | 0.02 | 0.06 | 0.15 |
| | 1,2,4TMNapht | 0.14 | 0.11 | 0.16 | 0.04 | 0.03 | 0.18 |

**Appendix 7. (Continued) Pyrolysate classes and compounds in kerogens from the Vulcan Sub-basin**

| Class | Compound (mg/g TOC) | Lower Vulcan Fm | | | | | |
|---|---|---|---|---|---|---|---|
| | | 20110044C | 20110047 | 20110052 | 20110062 | 20110078 | 20110081 |
| Aliphatic | $n\text{-}C_1$ | 19.18 | 8.27 | 8.06 | 7.67 | 8.53 | 6.55 |
| | $n\text{-}C_2$ | 11.56 | 6.33 | 6.39 | 6.65 | 6.06 | 5.60 |
| | $n\text{-}C_3$ | 7.92 | 5.30 | 5.79 | 5.36 | 4.58 | 5.03 |
| | $n\text{-}C_4$ | 4.08 | 4.61 | 5.34 | 4.72 | 5.81 | 4.45 |
| | $n\text{-}C_5$ | 1.66 | 2.06 | 2.69 | 2.06 | 1.55 | 1.92 |
| | $n\text{-}C_6$ | 1.53 | 1.91 | 2.05 | 1.93 | 1.60 | 1.67 |
| | $n\text{-}C_7$ | 1.34 | 1.57 | 1.62 | 1.58 | 1.36 | 1.38 |
| | $n\text{-}C_8$ | 1.13 | 1.29 | 1.52 | 1.30 | 1.10 | 1.18 |
| | $n\text{-}C_9$ | 1.02 | 0.97 | 1.10 | 0.95 | 0.86 | 0.91 |
| | $n\text{-}C_{10}$ | 0.99 | 0.85 | 1.02 | 0.76 | 0.79 | 0.77 |
| | $n\text{-}C_{11}$ | 0.92 | 0.82 | 0.86 | 0.74 | 0.77 | 0.76 |
| | $n\text{-}C_{12}$ | 1.06 | 0.80 | 0.86 | 0.75 | 0.74 | 0.71 |
| | $n\text{-}C_{13}$ | 1.36 | 0.75 | 0.85 | 0.62 | 0.69 | 0.70 |
| | $n\text{-}C_{14}$ | 1.03 | 0.63 | 0.72 | 0.60 | 0.62 | 0.59 |
| | $n\text{-}C_{15}$ | 0.92 | 0.63 | 0.68 | 0.48 | 0.60 | 0.60 |
| | $n\text{-}C_{16}$ | 1.09 | 0.48 | 0.68 | 0.39 | 0.52 | 0.49 |
| | $n\text{-}C_{17}$ | 0.87 | 0.39 | 0.50 | 0.29 | 0.41 | 0.41 |
| | $n\text{-}C_{18}$ | 0.75 | 0.33 | 0.42 | 0.25 | 0.37 | 0.32 |
| | $n\text{-}C_{19}$ | 0.86 | 0.29 | 0.40 | 0.18 | 0.34 | 0.23 |
| | $n\text{-}C_{20}$ | 0.85 | 0.24 | 0.32 | 0.12 | 0.25 | 0.18 |
| | $n\text{-}C_{21}$ | 0.83 | 0.21 | 0.28 | 0.10 | 0.25 | 0.15 |
| | $n\text{-}C_{22}$ | 0.86 | 0.17 | 0.20 | 0.09 | 0.21 | 0.13 |
| | $n\text{-}C_{23}$ | 0.82 | 0.14 | 0.18 | 0.06 | 0.19 | 0.09 |
| | $n\text{-}C_{24}$ | 0.92 | 0.12 | 0.15 | 0.08 | 0.17 | 0.10 |
| | $n\text{-}C_{25}$ | 0.73 | 0.09 | 0.12 | 0.02 | 0.14 | 0.07 |
| | $n\text{-}C_{26}$ | 0.70 | 0.07 | 0.11 | 0.00 | 0.15 | 0.00 |
| | $n\text{-}C_{27}$ | 0.65 | 0.00 | 0.00 | 0.00 | 0.08 | 0.00 |
| | $n\text{-}C_{28}$ | 0.45 | 0.00 | 0.00 | 0.00 | 0.00 | 0.00 |
| | $n\text{-}C_{29}$ | 0.22 | 0.00 | 0.00 | 0.00 | 0.00 | 0.00 |
| | $n\text{-}C_{30}$ | 0.23 | 0.00 | 0.00 | 0.00 | 0.00 | 0.00 |
| | $n\text{-}C_{31}$ | 0.00 | 0.00 | 0.00 | 0.00 | 0.00 | 0.00 |
| | $n\text{-}C_{32}$ | 0.00 | 0.00 | 0.00 | 0.00 | 0.00 | 0.00 |
| Mono-aromatic | Benz | 0.37 | 1.11 | 1.36 | 0.96 | 0.98 | 1.36 |
| | Tol | 1.66 | 1.70 | 1.74 | 1.46 | 1.51 | 1.61 |
| | E-Benz | 0.42 | 0.43 | 0.46 | 0.42 | 0.37 | 0.41 |
| | $m+p$ Xyl | 1.38 | 0.90 | 0.93 | 0.89 | 0.82 | 0.83 |
| | Styr | 0.13 | 0.19 | 0.45 | 0.24 | 0.19 | 0.20 |
| | $o$-Xyl | 0.36 | 0.49 | 0.46 | 0.47 | 0.36 | 0.46 |
| | PropylBenz | 0.00 | 0.07 | 0.18 | 0.07 | 0.05 | 0.05 |

**Appendix 7. (Continued) Pyrolysate classes and compounds in kerogens from the Vulcan Sub-basin**

| Class | Compound (mg/g TOC) | Lower Vulcan Fm | | | | | |
|---|---|---|---|---|---|---|---|
| | | 20110044C | 20110047 | 20110052 | 20110062 | 20110078 | 20110081 |
| Mono-aromatic | 1M3EBenz | 0.29 | 0.19 | 0.21 | 0.22 | 0.16 | 0.19 |
| | 1M4EBenz | 0.14 | 0.11 | 0.13 | 0.12 | 0.09 | 0.11 |
| | 1,3,5TMBenz | 0.18 | 0.10 | 0.09 | 0.10 | 0.08 | 0.08 |
| | 1M2EBenz | 0.14 | 0.25 | 0.22 | 0.21 | 0.17 | 0.23 |
| | 1,2,4TMBenz | 0.32 | 0.33 | 0.30 | 0.33 | 0.26 | 0.26 |
| | 1,2,3TMBenz | 0.21 | 0.23 | 0.12 | 0.17 | 0.18 | 0.18 |
| Phenolic | Phenol | 1.35 | 0.75 | 0.95 | 0.51 | 0.95 | 0.72 |
| | 2M Phenol | 1.27 | 0.36 | 0.66 | 0.23 | 0.46 | 0.40 |
| | 3+4M Phenol | 2.16 | 0.48 | 0.53 | 0.26 | 0.61 | 0.41 |
| Naphthenic | Napht | 0.42 | 0.28 | 0.33 | 0.29 | 0.27 | 0.28 |
| | 2M Napht | 0.65 | 0.32 | 0.36 | 0.32 | 0.31 | 0.33 |
| | 1M Napht | 0.37 | 0.27 | 0.31 | 0.25 | 0.24 | 0.28 |
| | Sum DMNapht | 1.14 | 1.15 | 1.47 | 0.77 | 0.44 | 1.07 |
| | 1,3,7TMNaph | 0.06 | 0.02 | 0.03 | 0.05 | 0.03 | 0.05 |
| | 1,3,6TMNapht | 0.07 | 0.05 | 0.05 | 0.05 | 0.04 | 0.05 |
| | 1,3,5TMNapht | 0.16 | 0.08 | 0.10 | 0.07 | 0.08 | 0.07 |
| | 2,3,6TMNapht | 0.06 | 0.03 | 0.05 | 0.03 | 0.03 | 0.03 |
| | 1,2,7TMNapht | 0.14 | 0.09 | 0.14 | 0.08 | 0.09 | 0.10 |
| | 1,2,4TMNapht | 0.19 | 0.09 | 0.08 | 0.05 | 0.08 | 0.09 |

**Appendix 7. (Continued) Pyrolysate classes and compounds in kerogens from the Vulcan Sub-basin**

| Class | Compound (mg/g TOC) | Lower Vulcan Fm | | | Plover Fm | | |
|---|---|---|---|---|---|---|---|
| | | 20110084 | 3851 | 3853 | 20110045 | 20110050 | 20110054 |
| Aliphatic | $n\text{-}C_1$ | 12.23 | 10.36 | 8.19 | 10.65 | 2.04 | 15.58 |
| | $n\text{-}C_2$ | 12.37 | 14.11 | 5.15 | 7.82 | 1.27 | 9.64 |
| | $n\text{-}C_3$ | 12.38 | 14.72 | 3.95 | 6.24 | 0.90 | 6.72 |
| | $n\text{-}C_4$ | 9.98 | 10.85 | 3.32 | 4.73 | 0.57 | 3.57 |
| | $n\text{-}C_5$ | 4.37 | 5.40 | 1.71 | 2.01 | 0.27 | 1.64 |
| | $n\text{-}C_6$ | 4.46 | 5.82 | 1.69 | 2.06 | 0.26 | 1.51 |
| | $n\text{-}C_7$ | 3.63 | 4.58 | 1.37 | 1.73 | 0.21 | 1.35 |
| | $n\text{-}C_8$ | 2.76 | 3.37 | 1.18 | 1.41 | 0.17 | 1.20 |
| | $n\text{-}C_9$ | 2.21 | 2.71 | 0.90 | 1.05 | 0.13 | 1.03 |
| | $n\text{-}C_{10}$ | 1.51 | 1.93 | 0.81 | 0.88 | 0.14 | 1.01 |
| | $n\text{-}C_{11}$ | 1.52 | 1.92 | 0.75 | 0.85 | 0.13 | 0.98 |
| | $n\text{-}C_{12}$ | 1.22 | 1.44 | 0.71 | 0.87 | 0.16 | 1.09 |
| | $n\text{-}C_{13}$ | 0.92 | 1.13 | 0.65 | 0.80 | 0.15 | 1.30 |
| | $n\text{-}C_{14}$ | 0.78 | 1.13 | 0.66 | 0.75 | 0.14 | 1.10 |
| | $n\text{-}C_{15}$ | 0.77 | 0.91 | 0.59 | 0.67 | 0.11 | 0.86 |
| | $n\text{-}C_{16}$ | 0.67 | 0.69 | 0.49 | 0.62 | 0.12 | 0.99 |
| | $n\text{-}C_{17}$ | 0.39 | 0.48 | 0.35 | 0.47 | 0.10 | 0.83 |
| | $n\text{-}C_{18}$ | 0.34 | 0.40 | 0.28 | 0.35 | 0.10 | 0.72 |
| | $n\text{-}C_{19}$ | 0.33 | 0.39 | 0.25 | 0.34 | 0.10 | 0.79 |
| | $n\text{-}C_{20}$ | 0.25 | 0.27 | 0.16 | 0.25 | 0.09 | 0.73 |
| | $n\text{-}C_{21}$ | 0.24 | 0.28 | 0.14 | 0.23 | 0.09 | 0.75 |
| | $n\text{-}C_{22}$ | 0.22 | 0.25 | 0.17 | 0.23 | 0.11 | 0.75 |
| | $n\text{-}C_{23}$ | 0.15 | 0.18 | 0.12 | 0.20 | 0.11 | 0.74 |
| | $n\text{-}C_{24}$ | 0.15 | 0.20 | 0.11 | 0.16 | 0.13 | 0.77 |
| | $n\text{-}C_{25}$ | 0.16 | 0.17 | 0.08 | 0.13 | 0.13 | 0.68 |
| | $n\text{-}C_{26}$ | 0.20 | 0.22 | 0.08 | 0.13 | 0.14 | 0.57 |
| | $n\text{-}C_{27}$ | 0.18 | 0.21 | 0.06 | 0.05 | 0.12 | 0.53 |
| | $n\text{-}C_{28}$ | 0.00 | 0.00 | 0.06 | 0.05 | 0.07 | 0.28 |
| | $n\text{-}C_{29}$ | 0.00 | 0.00 | 0.00 | 0.00 | 0.04 | 0.16 |
| | $n\text{-}C_{30}$ | 0.00 | 0.00 | 0.00 | 0.00 | 0.00 | 0.00 |
| | $n\text{-}C_{31}$ | 0.00 | 0.00 | 0.00 | 0.00 | 0.00 | 0.00 |
| | $n\text{-}C_{32}$ | 0.00 | 0.00 | 0.00 | 0.00 | 0.00 | 0.00 |
| Mono-aromatic | Benz | 1.18 | 1.13 | 1.17 | 0.76 | 0.14 | 0.36 |
| | Tol | 1.82 | 1.82 | 1.44 | 1.48 | 0.21 | 1.45 |
| | E-Benz | 0.77 | 0.74 | 0.39 | 0.42 | 0.05 | 0.40 |
| | $m+p$ Xyl | 1.56 | 1.50 | 0.91 | 1.03 | 0.15 | 1.17 |
| | Styr | 0.36 | 0.31 | 0.19 | 0.15 | 0.04 | 0.13 |
| | $o$-Xyl | 0.71 | 0.66 | 0.39 | 0.47 | 0.05 | 0.33 |
| | PropylBenz | 0.13 | 0.20 | 0.08 | 0.10 | 0.01 | 0.07 |

| Class | Compound (mg/g TOC) | Lower Vulcan Fm | | | Plover Fm | | |
|---|---|---|---|---|---|---|---|
| | | 20110084 | 3851 | 3853 | 20110045 | 20110050 | 20110054 |
| Mono-aromatic | 1M3EBenz | 0.49 | 0.43 | 0.17 | 0.27 | 0.03 | 0.25 |
| | 1M4EBenz | 0.45 | 0.55 | 0.14 | 0.14 | 0.02 | 0.13 |
| | 1,3,5TMBenz | 0.26 | 0.27 | 0.12 | 0.14 | 0.01 | 0.16 |
| | 1M2EBenz | 0.84 | 0.34 | 0.20 | 0.22 | 0.02 | 0.14 |
| | 1,2,4TMBenz | 0.71 | 0.59 | 0.32 | 0.43 | 0.04 | 0.30 |
| | 1,2,3TMBenz | 0.25 | 0.41 | 0.21 | 0.28 | 0.03 | 0.16 |
| Phenolic | Phenol | 0.73 | 0.96 | 1.74 | 0.71 | 0.21 | 1.10 |
| | 2M Phenol | 0.44 | 0.55 | 0.76 | 0.43 | 0.11 | 1.04 |
| | 3+4M Phenol | 0.55 | 0.64 | 0.75 | 0.57 | 0.19 | 1.68 |
| Naphthenic | Napht | 0.92 | 1.03 | 0.27 | 0.31 | 0.05 | 0.35 |
| | 2M Napht | 0.50 | 0.46 | 0.27 | 0.38 | 0.06 | 0.55 |
| | 1M Napht | 0.41 | 0.45 | 0.25 | 0.30 | 0.05 | 0.36 |
| | Sum DMNapht | 1.31 | 1.52 | 0.97 | 1.32 | 0.35 | 2.78 |
| | 1,3,7TMNaph | 0.07 | 0.05 | 0.05 | 0.06 | 0.01 | 0.05 |
| | 1,3,6TMNapht | 0.11 | 0.09 | 0.07 | 0.05 | 0.01 | 0.06 |
| | 1,3,5TMNapht | 0.34 | 0.39 | 0.09 | 0.10 | 0.02 | 0.12 |
| | 2,3,6TMNapht | 0.14 | 0.15 | 0.04 | 0.04 | 0.01 | 0.06 |
| | 1,2,7TMNapht | 0.24 | 0.34 | 0.09 | 0.12 | 0.02 | 0.13 |
| | 1,2,4TMNapht | 0.17 | 0.13 | 0.05 | 0.07 | 0.03 | 0.16 |

**Appendix 7. (Continued) Pyrolysate classes and compounds in kerogens from the Vulcan Sub-basin**

| Class | Compound (mg/g TOC) | Plover Fm | | | | | |
|---|---|---|---|---|---|---|---|
| | | 20110054C | 20110055 | 20110058 | 20110076 | 20110076C | 20110077C |
| Aliphatic | $n\text{-}C_1$ | 16.14 | 11.43 | 10.43 | 6.42 | 15.85 | 27.01 |
| | $n\text{-}C_2$ | 11.08 | 7.31 | 5.54 | 3.89 | 8.11 | 12.84 |
| | $n\text{-}C_3$ | 7.98 | 5.18 | 3.56 | 2.65 | 4.91 | 7.80 |
| | $n\text{-}C_4$ | 4.35 | 3.11 | 1.68 | 1.81 | 2.63 | 3.15 |
| | $n\text{-}C_5$ | 1.84 | 1.48 | 0.42 | 0.60 | 0.75 | 0.64 |
| | $n\text{-}C_6$ | 1.65 | 1.41 | 0.25 | 0.54 | 0.62 | 0.36 |
| | $n\text{-}C_7$ | 1.45 | 1.23 | 0.19 | 0.49 | 0.59 | 0.28 |
| | $n\text{-}C_8$ | 1.32 | 1.05 | 0.13 | 0.42 | 0.43 | 0.14 |
| | $n\text{-}C_9$ | 1.13 | 0.93 | 0.11 | 0.34 | 0.38 | 0.11 |
| | $n\text{-}C_{10}$ | 1.13 | 0.85 | 0.15 | 0.30 | 0.34 | 0.12 |
| | $n\text{-}C_{11}$ | 1.07 | 0.81 | 0.19 | 0.28 | 0.32 | 0.46 |
| | $n\text{-}C_{12}$ | 1.21 | 0.86 | 0.43 | 0.33 | 0.61 | 0.00 |
| | $n\text{-}C_{13}$ | 1.46 | 0.96 | 0.40 | 0.37 | 0.65 | 1.69 |
| | $n\text{-}C_{14}$ | 1.21 | 0.85 | 0.12 | 0.30 | 0.42 | 0.61 |
| | $n\text{-}C_{15}$ | 0.95 | 0.65 | 0.26 | 0.24 | 0.42 | 0.35 |
| | $n\text{-}C_{16}$ | 1.14 | 0.71 | 0.51 | 0.25 | 0.59 | 0.40 |
| | $n\text{-}C_{17}$ | 1.00 | 0.62 | 0.52 | 0.20 | 0.56 | 1.43 |
| | $n\text{-}C_{18}$ | 0.82 | 0.58 | 0.39 | 0.17 | 0.28 | 1.14 |
| | $n\text{-}C_{19}$ | 0.93 | 0.61 | 0.00 | 0.19 | 0.58 | 0.80 |
| | $n\text{-}C_{20}$ | 0.85 | 0.57 | 0.00 | 0.14 | 0.23 | 0.00 |
| | $n\text{-}C_{21}$ | 0.88 | 0.59 | 0.00 | 0.13 | 0.26 | 0.00 |
| | $n\text{-}C_{22}$ | 0.89 | 0.63 | 0.00 | 0.14 | 0.25 | 0.00 |
| | $n\text{-}C_{23}$ | 0.86 | 0.65 | 0.00 | 0.12 | 0.22 | 0.00 |
| | $n\text{-}C_{24}$ | 0.94 | 0.71 | 0.00 | 0.13 | 0.21 | 0.00 |
| | $n\text{-}C_{25}$ | 0.85 | 0.65 | 0.00 | 0.16 | 0.18 | 0.00 |
| | $n\text{-}C_{26}$ | 0.71 | 0.58 | 0.00 | 0.17 | 0.16 | 0.00 |
| | $n\text{-}C_{27}$ | 0.73 | 0.63 | 0.00 | 0.09 | 0.17 | 0.00 |
| | $n\text{-}C_{28}$ | 0.43 | 0.33 | 0.00 | 0.09 | 0.12 | 0.00 |
| | $n\text{-}C_{29}$ | 0.19 | 0.20 | 0.00 | 0.00 | 0.00 | 0.00 |
| | $n\text{-}C_{30}$ | 0.10 | 0.18 | 0.00 | 0.00 | 0.00 | 0.00 |
| | $n\text{-}C_{31}$ | 0.09 | 0.11 | 0.00 | 0.00 | 0.00 | 0.00 |
| | $n\text{-}C_{32}$ | 0.00 | 0.00 | 0.00 | 0.00 | 0.00 | 0.00 |
| Mono-aromatic | Benz | 0.33 | 0.40 | 0.53 | 0.28 | 0.52 | 1.00 |
| | Tol | 1.48 | 1.10 | 1.77 | 0.88 | 2.21 | 3.43 |
| | E-Benz | 0.31 | 0.30 | 0.23 | 0.20 | 0.43 | 0.46 |
| | $m+p$ Xyl | 1.22 | 0.78 | 1.74 | 0.53 | 1.56 | 3.41 |
| | Styr | 0.16 | 0.12 | 0.11 | 0.10 | 0.19 | 0.14 |
| | $o\text{-}$Xyl | 0.35 | 0.30 | 0.20 | 0.17 | 0.26 | 0.34 |
| | PropylBenz | 0.04 | 0.12 | 0.03 | 0.05 | 0.04 | 0.00 |

**Appendix 7. (Continued) Pyrolysate classes and compounds in kerogens from the Vulcan Sub-basin**

| Class | Compound (mg/g TOC) | Plover Fm | | | | | |
|---|---|---|---|---|---|---|---|
| | | 20110054C | 20110055 | 20110058 | 20110076 | 20110076C | 20110077C |
| Mono-aromatic | 1M3EBenz | 0.25 | 0.17 | 0.33 | 0.10 | 0.28 | 0.57 |
| | 1M4EBenz | 0.14 | 0.12 | 0.09 | 0.07 | 0.19 | 0.28 |
| | 1,3,5TMBenz | 0.16 | 0.11 | 0.03 | 0.04 | 0.05 | 0.05 |
| | 1M2EBenz | 0.14 | 0.14 | 0.07 | 0.07 | 0.12 | 0.08 |
| | 1,2,4TMBenz | 0.33 | 0.20 | 0.23 | 0.13 | 0.35 | 0.49 |
| | 1,2,3TMBenz | 0.21 | 0.13 | 0.06 | 0.14 | 0.14 | 0.11 |
| Phenolic | Phenol | 1.11 | 1.09 | 6.79 | 0.91 | 4.65 | 14.58 |
| | 2M Phenol | 1.16 | 0.76 | 4.45 | 0.55 | 3.00 | 9.23 |
| | 3+4M Phenol | 1.95 | 1.25 | 11.62 | 1.04 | 9.02 | 31.12 |
| Naphthenic | Napht | 0.41 | 0.28 | 0.47 | 0.18 | 0.63 | 0.83 |
| | 2M Napht | 0.57 | 0.35 | 0.56 | 0.20 | 0.46 | 0.55 |
| | 1M Napht | 0.37 | 0.27 | 0.47 | 0.15 | 0.39 | 0.83 |
| | Sum DMNapht | 3.22 | 2.14 | 0.00 | 0.44 | 0.79 | 0.00 |
| | 1,3,7TMNaph | 0.07 | 0.04 | 0.00 | 0.02 | 0.09 | 0.00 |
| | 1,3,6TMNapht | 0.08 | 0.03 | 0.00 | 0.03 | 0.09 | 0.00 |
| | 1,3,5TMNapht | 0.17 | 0.09 | 0.00 | 0.05 | 0.10 | 0.00 |
| | 2,3,6TMNapht | 0.07 | 0.02 | 0.00 | 0.02 | 0.05 | 0.00 |
| | 1,2,7TMNapht | 0.16 | 0.09 | 0.00 | 0.05 | 0.08 | 0.00 |
| | 1,2,4TMNapht | 0.18 | 0.15 | 0.00 | 0.07 | 0.07 | 0.00 |

**Appendix 8. Pyrolysate classes and compounds in kerogens from the Laminaria High**

| Class | Compound (mg/g TOC) | Echuca Shoals Fm | | | Flamingo Fm | | |
|---|---|---|---|---|---|---|---|
| | | 20110002 | 20110010 | 20110013 | 20110004 | 20110011 | 20110018 |
| Aliphatic | $n$-C$_1$ | 12.30 | 12.36 | 15.85 | 9.86 | 11.07 | 7.20 |
| | $n$-C$_2$ | 15.81 | 9.46 | 11.75 | 14.36 | 9.16 | 7.25 |
| | $n$-C$_3$ | 13.77 | 7.94 | 10.44 | 13.95 | 7.84 | 6.11 |
| | $n$-C$_4$ | 12.99 | 10.03 | 9.07 | 13.79 | 5.62 | 5.26 |
| | $n$-C$_5$ | 4.95 | 2.40 | 2.78 | 6.47 | 2.49 | 2.93 |
| | $n$-C$_6$ | 4.44 | 2.22 | 2.45 | 6.22 | 2.42 | 2.74 |
| | $n$-C$_7$ | 3.60 | 1.79 | 2.01 | 5.16 | 1.97 | 2.29 |
| | $n$-C$_8$ | 2.84 | 1.37 | 1.56 | 4.28 | 1.57 | 1.75 |
| | $n$-C$_9$ | 2.20 | 0.98 | 1.15 | 3.31 | 1.23 | 1.32 |
| | $n$-C$_{10}$ | 1.75 | 0.82 | 0.97 | 2.83 | 1.01 | 1.14 |
| | $n$-C$_{11}$ | 1.68 | 0.77 | 0.96 | 2.63 | 0.94 | 1.05 |
| | $n$-C$_{12}$ | 1.46 | 0.67 | 0.97 | 2.23 | 0.90 | 0.97 |
| | $n$-C$_{13}$ | 1.40 | 0.59 | 0.67 | 2.03 | 0.87 | 0.80 |
| | $n$-C$_{14}$ | 1.12 | 0.50 | 0.54 | 1.59 | 0.83 | 0.68 |
| | $n$-C$_{15}$ | 0.94 | 0.43 | 0.63 | 1.32 | 0.64 | 0.56 |
| | $n$-C$_{16}$ | 0.92 | 0.30 | 0.41 | 1.18 | 0.51 | 0.31 |
| | $n$-C$_{17}$ | 0.72 | 0.20 | 0.31 | 0.86 | 0.37 | 0.16 |
| | $n$-C$_{18}$ | 0.91 | 0.00 | 0.25 | 1.03 | 0.30 | 0.00 |
| | $n$-C$_{19}$ | 0.49 | 0.00 | 0.21 | 0.54 | 0.28 | 0.00 |
| | $n$-C$_{20}$ | 0.25 | 0.00 | 0.13 | 0.27 | 0.22 | 0.00 |
| | $n$-C$_{21}$ | 0.25 | 0.00 | 0.08 | 0.22 | 0.16 | 0.00 |
| | $n$-C$_{22}$ | 0.25 | 0.00 | 0.06 | 0.27 | 0.15 | 0.00 |
| | $n$-C$_{23}$ | 0.13 | 0.00 | 0.04 | 0.16 | 0.12 | 0.00 |
| | $n$-C$_{24}$ | 0.16 | 0.00 | 0.03 | 0.16 | 0.09 | 0.00 |
| | $n$-C$_{25}$ | 0.12 | 0.00 | 0.00 | 0.13 | 0.07 | 0.00 |
| | $n$-C$_{26}$ | 0.08 | 0.00 | 0.00 | 0.09 | 0.06 | 0.00 |
| | $n$-C$_{27}$ | 0.06 | 0.00 | 0.00 | 0.08 | 0.06 | 0.00 |
| | $n$-C$_{28}$ | 0.04 | 0.00 | 0.00 | 0.08 | 0.00 | 0.00 |
| | $n$-C$_{29}$ | 0.03 | 0.00 | 0.00 | 0.00 | 0.00 | 0.00 |
| | $n$-C$_{30}$ | 0.00 | 0.00 | 0.00 | 0.00 | 0.00 | 0.00 |
| | $n$-C$_{31}$ | 0.00 | 0.00 | 0.00 | 0.00 | 0.00 | 0.00 |
| | $n$-C$_{32}$ | 0.00 | 0.00 | 0.00 | 0.00 | 0.00 | 0.00 |
| Mono-aromatic | Benz | 0.87 | 0.88 | 0.75 | 1.58 | 0.72 | 2.06 |
| | Tol | 1.69 | 1.65 | 1.87 | 2.05 | 1.45 | 1.83 |
| | E-Benz | 1.12 | 0.55 | 0.60 | 0.89 | 0.43 | 0.57 |
| | $m+p$ Xyl | 1.70 | 1.29 | 1.65 | 1.53 | 1.18 | 0.99 |
| | Styr | 0.50 | 0.21 | 0.23 | 0.72 | 0.25 | 0.43 |
| | $o$-Xyl | 0.85 | 0.64 | 0.80 | 1.03 | 0.55 | 0.62 |
| | PropylBenz | 0.34 | 0.08 | 0.18 | 0.27 | 0.10 | 0.10 |

**Appendix 8. (Continued) Pyrolysate classes and compounds in kerogens from the Laminaria High**

| Class | Compound (mg/g TOC) | Echuca Shoals Fm | | | Flamingo Fm | | |
|---|---|---|---|---|---|---|---|
| | | 20110002 | 20110010 | 20110013 | 20110004 | 20110011 | 20110018 |
| Mono-aromatic | 1M3EBenz | 0.54 | 0.41 | 0.58 | 0.52 | 0.32 | 0.28 |
| | 1M4EBenz | 0.36 | 0.22 | 0.31 | 0.33 | 0.23 | 0.19 |
| | 1,3,5TMBenz | 0.28 | 0.13 | 0.19 | 0.26 | 0.13 | 0.11 |
| | 1M2EBenz | 0.60 | 0.32 | 0.45 | 0.79 | 0.31 | 0.34 |
| | 1,2,4TMBenz | 0.91 | 0.62 | 0.82 | 1.22 | 0.47 | 0.39 |
| | 1,2,3TMBenz | 0.28 | 0.30 | 0.44 | 0.44 | 0.23 | 0.19 |
| Phenolic | Phenol | 1.63 | 0.27 | 0.36 | 1.27 | 0.33 | 0.52 |
| | 2M Phenol | 0.50 | 0.24 | 0.32 | 0.60 | 0.28 | 0.30 |
| | 3+4M Phenol | 0.42 | 0.23 | 0.38 | 0.48 | 0.31 | 0.20 |
| Naphthenic | Napht | 0.39 | 0.33 | 0.44 | 0.46 | 0.29 | 0.36 |
| | 2M Napht | 0.50 | 0.41 | 0.54 | 0.56 | 0.36 | 0.35 |
| | 1M Napht | 0.41 | 0.31 | 0.40 | 0.52 | 0.31 | 0.31 |
| | Sum DMNapht | 0.93 | 0.67 | 0.74 | 1.16 | 0.62 | 0.48 |
| | 1,3,7TMNaph | 0.03 | 0.05 | 0.07 | 0.22 | 0.03 | 0.05 |
| | 1,3,6TMNapht | 0.09 | 0.07 | 0.10 | 0.12 | 0.07 | 0.05 |
| | 1,3,5TMNapht | 0.18 | 0.09 | 0.14 | 0.25 | 0.11 | 0.06 |
| | 2,3,6TMNapht | 0.09 | 0.05 | 0.08 | 0.12 | 0.06 | 0.03 |
| | 1,2,7TMNapht | 0.23 | 0.10 | 0.09 | 0.31 | 0.12 | 0.10 |
| | 1,2,4TMNapht | 0.09 | 0.04 | 0.06 | 0.39 | 0.03 | 0.04 |

Appendix 8. (Continued) Pyrolysate classes and compounds in kerogens from the Laminaria High

| Class | Compound (mg/g TOC) | Frigate Fm | | | | Laminaria Fm | |
|---|---|---|---|---|---|---|---|
| | | 20110007 | 20110015 | 20110019 | 20110021 | 20110008 | 20110017 |
| Aliphatic | $n$-$C_1$ | 8.52 | 1.81 | 4.67 | 17.41 | 11.06 | 6.17 |
| | $n$-$C_2$ | 9.14 | 3.98 | 4.40 | 9.11 | 11.70 | 4.65 |
| | $n$-$C_3$ | 8.63 | 4.20 | 4.15 | 9.36 | 12.28 | 4.20 |
| | $n$-$C_4$ | 6.95 | 3.76 | 14.27 | 8.30 | 9.98 | 2.92 |
| | $n$-$C_5$ | 3.35 | 1.66 | 1.79 | 4.38 | 5.35 | 0.94 |
| | $n$-$C_6$ | 3.18 | 1.53 | 1.65 | 4.24 | 4.89 | 0.67 |
| | $n$-$C_7$ | 2.62 | 1.24 | 1.40 | 3.56 | 4.00 | 0.52 |
| | $n$-$C_8$ | 2.06 | 1.05 | 1.07 | 3.06 | 3.23 | 0.42 |
| | $n$-$C_9$ | 1.56 | 0.75 | 0.73 | 2.26 | 2.29 | 0.29 |
| | $n$-$C_{10}$ | 1.31 | 0.60 | 0.60 | 1.90 | 1.93 | 0.21 |
| | $n$-$C_{11}$ | 1.20 | 0.54 | 0.56 | 1.79 | 1.77 | 0.16 |
| | $n$-$C_{12}$ | 1.03 | 0.47 | 0.46 | 1.42 | 1.52 | 0.10 |
| | $n$-$C_{13}$ | 0.97 | 0.37 | 0.34 | 1.24 | 1.12 | 0.05 |
| | $n$-$C_{14}$ | 0.79 | 0.24 | 0.24 | 0.96 | 0.93 | 0.00 |
| | $n$-$C_{15}$ | 0.74 | 0.16 | 0.16 | 0.88 | 0.84 | 0.00 |
| | $n$-$C_{16}$ | 0.60 | 0.05 | 0.05 | 0.65 | 0.60 | 0.00 |
| | $n$-$C_{17}$ | 0.45 | 0.04 | 0.04 | 0.37 | 0.45 | 0.00 |
| | $n$-$C_{18}$ | 0.46 | 0.00 | 0.00 | 0.50 | 0.33 | 0.00 |
| | $n$-$C_{19}$ | 0.35 | 0.00 | 0.00 | 0.24 | 0.28 | 0.00 |
| | $n$-$C_{20}$ | 0.20 | 0.00 | 0.00 | 0.15 | 0.17 | 0.00 |
| | $n$-$C_{21}$ | 0.19 | 0.00 | 0.00 | 0.13 | 0.13 | 0.00 |
| | $n$-$C_{22}$ | 0.19 | 0.00 | 0.00 | 0.14 | 0.10 | 0.00 |
| | $n$-$C_{23}$ | 0.12 | 0.00 | 0.00 | 0.07 | 0.03 | 0.00 |
| | $n$-$C_{24}$ | 0.12 | 0.00 | 0.00 | 0.07 | 0.00 | 0.00 |
| | $n$-$C_{25}$ | 0.09 | 0.00 | 0.00 | 0.03 | 0.00 | 0.00 |
| | $n$-$C_{26}$ | 0.06 | 0.00 | 0.00 | 0.00 | 0.00 | 0.00 |
| | $n$-$C_{27}$ | 0.04 | 0.00 | 0.00 | 0.00 | 0.00 | 0.00 |
| | $n$-$C_{28}$ | 0.00 | 0.00 | 0.00 | 0.00 | 0.00 | 0.00 |
| | $n$-$C_{29}$ | 0.00 | 0.00 | 0.00 | 0.00 | 0.00 | 0.00 |
| | $n$-$C_{30}$ | 0.00 | 0.00 | 0.00 | 0.00 | 0.00 | 0.00 |
| | $n$-$C_{31}$ | 0.00 | 0.00 | 0.00 | 0.00 | 0.00 | 0.00 |
| | $n$-$C_{32}$ | 0.00 | 0.00 | 0.00 | 0.00 | 0.00 | 0.00 |
| Mono-aromatic | Benz | 0.84 | 1.66 | 3.63 | 2.98 | 2.04 | 1.25 |
| | Tol | 1.42 | 1.37 | 1.62 | 3.28 | 2.32 | 1.28 |
| | E-Benz | 0.59 | 0.35 | 0.45 | 1.06 | 0.82 | 0.25 |
| | $m$+$p$ Xyl | 1.13 | 0.56 | 0.72 | 1.36 | 1.53 | 0.52 |
| | Styr | 0.36 | 0.32 | 0.31 | 0.95 | 0.57 | 0.17 |
| | $o$-Xyl | 0.67 | 0.38 | 0.46 | 0.99 | 0.92 | 0.34 |
| | PropylBenz | 0.19 | 0.05 | 0.00 | 0.19 | 0.17 | 0.00 |

| Class | Compound (mg/g TOC) | Frigate Fm | | | | Laminaria Fm | |
|---|---|---|---|---|---|---|---|
| | | 20110007 | 20110015 | 20110019 | 20110021 | 20110008 | 20110017 |
| Mono-aromatic | 1M3EBenz | 0.42 | 0.12 | 0.19 | 0.43 | 0.53 | 0.11 |
| | 1M4EBenz | 0.22 | 0.09 | 0.12 | 0.29 | 0.30 | 0.05 |
| | 1,3,5TMBenz | 0.15 | 0.06 | 0.07 | 0.21 | 0.29 | 0.02 |
| | 1M2EBenz | 0.45 | 0.19 | 0.26 | 0.76 | 0.71 | 0.14 |
| | 1,2,4TMBenz | 0.67 | 0.22 | 0.32 | 0.87 | 0.96 | 0.15 |
| | 1,2,3TMBenz | 0.17 | 0.12 | 0.15 | 0.20 | 0.28 | 0.11 |
| Phenolic | Phenol | 0.55 | 0.10 | 0.24 | 1.16 | 0.63 | 0.06 |
| | 2M Phenol | 0.36 | 0.06 | 0.00 | 0.54 | 0.35 | 0.00 |
| | 3+4M Phenol | 0.32 | 0.03 | 0.00 | 0.57 | 0.37 | 0.00 |
| Naphthenic | Napht | 0.35 | 0.31 | 0.39 | 0.62 | 0.43 | 0.26 |
| | 2M Napht | 0.50 | 0.19 | 0.21 | 0.60 | 0.53 | 0.05 |
| | 1M Napht | 0.36 | 0.18 | 0.21 | 0.56 | 0.39 | 0.06 |
| | Sum DMNapht | 0.81 | 0.14 | 0.24 | 0.88 | 0.94 | 0.00 |
| | 1,3,7TMNaph | 0.06 | 0.01 | 0.01 | 0.11 | 0.10 | 0.00 |
| | 1,3,6TMNapht | 0.08 | 0.02 | 0.02 | 0.08 | 0.09 | 0.00 |
| | 1,3,5TMNapht | 0.14 | 0.02 | 0.02 | 0.12 | 0.13 | 0.00 |
| | 2,3,6TMNapht | 0.08 | 0.01 | 0.01 | 0.06 | 0.08 | 0.00 |
| | 1,2,7TMNapht | 0.18 | 0.02 | 0.02 | 0.14 | 0.18 | 0.00 |
| | 1,2,4TMNapht | 0.07 | 0.01 | 0.02 | 0.17 | 0.13 | 0.00 |

| Class | Compound (mg/g TOC) | Laminaria Fm 20110022 | Plover Fm 20110023 |
|---|---|---|---|
| Aliphatic | $n$-$C_1$ | 8.80 | 2.89 |
| | $n$-$C_2$ | 6.80 | 3.77 |
| | $n$-$C_3$ | 7.26 | 3.90 |
| | $n$-$C_4$ | 7.49 | 5.64 |
| | $n$-$C_5$ | 2.27 | 1.47 |
| | $n$-$C_6$ | 1.78 | 1.20 |
| | $n$-$C_7$ | 1.29 | 1.08 |
| | $n$-$C_8$ | 0.95 | 0.96 |
| | $n$-$C_9$ | 0.64 | 0.68 |
| | $n$-$C_{10}$ | 0.48 | 0.56 |
| | $n$-$C_{11}$ | 0.48 | 0.50 |
| | $n$-$C_{12}$ | 0.36 | 0.38 |
| | $n$-$C_{13}$ | 0.25 | 0.18 |
| | $n$-$C_{14}$ | 0.16 | 0.09 |
| | $n$-$C_{15}$ | 0.13 | 0.06 |
| | $n$-$C_{16}$ | 0.04 | 0.01 |
| | $n$-$C_{17}$ | 0.02 | 0.02 |
| | $n$-$C_{18}$ | 0.00 | 0.00 |
| | $n$-$C_{19}$ | 0.00 | 0.00 |
| | $n$-$C_{20}$ | 0.00 | 0.00 |
| | $n$-$C_{21}$ | 0.00 | 0.00 |
| | $n$-$C_{22}$ | 0.00 | 0.00 |
| | $n$-$C_{23}$ | 0.00 | 0.00 |
| | $n$-$C_{24}$ | 0.00 | 0.00 |
| | $n$-$C_{25}$ | 0.00 | 0.00 |
| | $n$-$C_{26}$ | 0.00 | 0.00 |
| | $n$-$C_{27}$ | 0.00 | 0.00 |
| | $n$-$C_{28}$ | 0.00 | 0.00 |
| | $n$-$C_{29}$ | 0.00 | 0.00 |
| | $n$-$C_{30}$ | 0.00 | 0.00 |
| | $n$-$C_{31}$ | 0.00 | 0.00 |
| | $n$-$C_{32}$ | 0.00 | 0.00 |
| Mono-aromatic | Benz | 1.82 | 2.05 |
| | Tol | 1.82 | 1.48 |
| | E-Benz | 0.46 | 0.36 |
| | $m+p$ Xyl | 0.82 | 0.53 |
| | Styr | 0.23 | 0.44 |
| | $o$-Xyl | 0.51 | 0.37 |
| | PropylBenz | 0.00 | 0.05 |

**Appendix 8. (Continued) Pyrolysate classes and compounds in kerogens from the Laminaria High**

| Class | Compound (mg/g TOC) | Laminaria Fm 20110022 | Plover Fm 20110023 |
|---|---|---|---|
| Mono-aromatic | 1M3EBenz | 0.25 | 0.12 |
| | 1M4EBenz | 0.12 | 0.10 |
| | 1,3,5TMBenz | 0.07 | 0.07 |
| | 1M2EBenz | 0.24 | 0.19 |
| | 1,2,4TMBenz | 0.34 | 0.14 |
| | 1,2,3TMBenz | 0.18 | 0.12 |
| Phenolic | Phenol | 0.35 | 0.17 |
| | 2M Phenol | 0.12 | 0.00 |
| | 3+4M Phenol | 0.11 | 0.00 |
| Naphthenic | Napht | 0.30 | 0.40 |
| | 2M Napht | 0.24 | 0.12 |
| | 1M Napht | 0.20 | 0.12 |
| | Sum DMNapht | 0.22 | 0.06 |
| | 1,3,7TMNaph | 0.01 | 0.00 |
| | 1,3,6TMNapht | 0.02 | 0.00 |
| | 1,3,5TMNapht | 0.02 | 0.00 |
| | 2,3,6TMNapht | 0.01 | 0.00 |
| | 1,2,7TMNapht | 0.02 | 0.00 |
| | 1,2,4TMNapht | 0.01 | 0.00 |

**Appendix 9. Pyrolysate classes and compounds in kerogens from the Gippsland Basin**

| Class | Compound (mg/g TOC) | *L. balmei* biozone | | | | | |
|---|---|---|---|---|---|---|---|
| | | 20110092 | 20110113 | 20110121 | 20110126 | 20110140 | 20110153 |
| Aliphatic | $n$-$C_1$ | 14.72 | 16.41 | 15.98 | 19.26 | 17.09 | 22.64 |
| | $n$-$C_2$ | 11.07 | 6.67 | 5.88 | 9.04 | 7.75 | 11.33 |
| | $n$-$C_3$ | 9.55 | 4.51 | 4.05 | 6.10 | 4.87 | 7.12 |
| | $n$-$C_4$ | 5.83 | 2.55 | 2.13 | 3.27 | 2.58 | 4.52 |
| | $n$-$C_5$ | 3.35 | 1.11 | 0.90 | 1.44 | 1.09 | 2.64 |
| | $n$-$C_6$ | 3.41 | 0.97 | 0.79 | 1.26 | 0.97 | 2.62 |
| | $n$-$C_7$ | 3.00 | 0.87 | 0.70 | 1.09 | 0.84 | 2.26 |
| | $n$-$C_8$ | 2.74 | 0.74 | 0.59 | 0.95 | 0.72 | 1.95 |
| | $n$-$C_9$ | 2.38 | 0.64 | 0.49 | 0.78 | 0.58 | 1.77 |
| | $n$-$C_{10}$ | 2.16 | 0.60 | 0.47 | 0.71 | 0.53 | 1.55 |
| | $n$-$C_{11}$ | 2.02 | 0.61 | 0.44 | 0.67 | 0.49 | 1.47 |
| | $n$-$C_{12}$ | 2.07 | 0.73 | 0.54 | 0.73 | 0.56 | 1.80 |
| | $n$-$C_{13}$ | 2.08 | 0.65 | 0.48 | 0.69 | 0.52 | 1.72 |
| | $n$-$C_{14}$ | 2.13 | 0.75 | 0.49 | 0.73 | 0.54 | 1.64 |
| | $n$-$C_{15}$ | 1.97 | 0.69 | 0.49 | 0.67 | 0.52 | 1.58 |
| | $n$-$C_{16}$ | 1.75 | 0.63 | 0.44 | 0.60 | 0.50 | 1.39 |
| | $n$-$C_{17}$ | 1.44 | 0.52 | 0.40 | 0.46 | 0.42 | 1.26 |
| | $n$-$C_{18}$ | 1.42 | 0.42 | 0.35 | 0.45 | 0.35 | 1.22 |
| | $n$-$C_{19}$ | 1.41 | 0.38 | 0.35 | 0.41 | 0.32 | 1.24 |
| | $n$-$C_{20}$ | 1.37 | 0.40 | 0.37 | 0.45 | 0.36 | 1.17 |
| | $n$-$C_{21}$ | 1.37 | 0.36 | 0.35 | 0.37 | 0.34 | 1.12 |
| | $n$-$C_{22}$ | 1.39 | 0.39 | 0.37 | 0.35 | 0.32 | 1.23 |
| | $n$-$C_{23}$ | 1.37 | 0.38 | 0.37 | 0.33 | 0.29 | 1.15 |
| | $n$-$C_{24}$ | 1.37 | 0.41 | 0.38 | 0.34 | 0.29 | 1.22 |
| | $n$-$C_{25}$ | 1.22 | 0.39 | 0.37 | 0.27 | 0.24 | 1.10 |
| | $n$-$C_{26}$ | 1.10 | 0.36 | 0.32 | 0.25 | 0.21 | 0.93 |
| | $n$-$C_{27}$ | 0.91 | 0.32 | 0.27 | 0.19 | 0.14 | 0.81 |
| | $n$-$C_{28}$ | 0.73 | 0.27 | 0.19 | 0.15 | 0.12 | 0.62 |
| | $n$-$C_{29}$ | 0.59 | 0.21 | 0.14 | 0.12 | 0.08 | 0.53 |
| | $n$-$C_{30}$ | 0.41 | 0.14 | 0.10 | 0.07 | 0.05 | 0.34 |
| | $n$-$C_{31}$ | 0.28 | 0.09 | 0.06 | 0.06 | 0.04 | 0.21 |
| | $n$-$C_{32}$ | 0.16 | 0.00 | 0.00 | 0.00 | 0.00 | 0.08 |
| Mono-aromatic | Benz | 0.48 | 0.83 | 0.48 | 0.51 | 0.44 | 13.66 |
| | Tol | 1.23 | 1.84 | 1.27 | 1.51 | 1.24 | 19.46 |
| | E-Benz | 0.46 | 0.39 | 0.27 | 0.34 | 0.26 | 5.46 |
| | $m$+$p$ Xyl | 0.99 | 1.01 | 0.87 | 1.09 | 0.98 | 13.86 |
| | Styr | 0.14 | 0.09 | 0.05 | 0.10 | 0.07 | 2.04 |
| | $o$-Xyl | 0.47 | 0.43 | 0.33 | 0.35 | 0.32 | 6.32 |
| | PropylBenz | 0.12 | 0.04 | 0.03 | 0.06 | 0.04 | 0.00 |

**Appendix 9. (Continued) Pyrolysate classes and compounds in kerogens from the Gippsland Basin**

| Class | Compound (mg/g TOC) | *L. balmei* biozone | | | | | |
|---|---|---|---|---|---|---|---|
| | | 20110092 | 20110113 | 20110121 | 20110126 | 20110140 | 20110153 |
| Mono-aromatic | 1M3EBenz | 0.23 | 0.18 | 0.12 | 0.21 | 0.18 | 2.81 |
| | 1M4EBenz | 0.17 | 0.14 | 0.13 | 0.14 | 0.13 | 1.96 |
| | 1,3,5TMBenz | 0.12 | 0.09 | 0.08 | 0.13 | 0.11 | 1.11 |
| | 1M2EBenz | 0.23 | 0.15 | 0.16 | 0.15 | 0.15 | 3.37 |
| | 1,2,4TMBenz | 0.36 | 0.28 | 0.22 | 0.30 | 0.31 | 4.52 |
| | 1,2,3TMBenz | 0.20 | 0.28 | 0.20 | 0.14 | 0.16 | 4.29 |
| Phenolic | Phenol | 0.38 | 1.24 | 1.38 | 0.77 | 0.95 | 17.00 |
| | 2M Phenol | 0.36 | 0.73 | 0.77 | 0.77 | 0.68 | 7.87 |
| | 3+4M Phenol | 0.63 | 1.91 | 1.59 | 1.25 | 1.41 | 16.17 |
| | Alkylphenol | 1.10 | 1.40 | 1.59 | 1.91 | 1.72 | 24.60 |
| Naphthenic | Napht | 0.23 | 0.23 | 0.12 | 0.28 | 0.20 | 2.39 |
| | 2M Napht | 0.40 | 0.29 | 0.25 | 0.60 | 0.40 | 5.03 |
| | 1M Napht | 0.23 | 0.21 | 0.20 | 0.35 | 0.25 | 4.61 |
| | Sum DMNapht | 1.00 | 0.62 | 0.58 | 1.02 | 0.74 | 11.79 |
| | 1,3,7TMNaph | 0.08 | 0.11 | 0.08 | 0.10 | 0.09 | 0.59 |
| | 1,3,6TMNapht | 0.07 | 0.03 | 0.03 | 0.06 | 0.04 | 1.09 |
| | 1,3,5TMNapht | 0.13 | 0.06 | 0.07 | 0.10 | 0.08 | 1.93 |
| | 2,3,6TMNapht | 0.08 | 0.02 | 0.03 | 0.06 | 0.04 | 0.78 |
| | 1,2,7TMNapht | 0.12 | 0.12 | 0.07 | 0.09 | 0.07 | 1.31 |
| | 1,2,4TMNapht | 0.14 | 0.29 | 0.20 | 0.11 | 0.09 | 5.57 |

**Appendix 9. (Continued) Pyrolysate classes and compounds in kerogens from the Gippsland Basin**

| Class | Compound (mg/g TOC) | *F. longus* biozone | | | | | |
|---|---|---|---|---|---|---|---|
| | | 20110034 | 20110103 | 20110149 | 20110130 | 20110251 | 20110252 |
| Aliphatic | $n$-$C_1$ | 14.72 | 21.70 | 14.09 | 19.12 | 20.27 | 24.50 |
| | $n$-$C_2$ | 9.01 | 10.48 | 6.82 | 9.95 | 11.03 | 9.67 |
| | $n$-$C_3$ | 7.38 | 7.35 | 5.07 | 6.64 | 8.47 | 6.30 |
| | $n$-$C_4$ | 4.70 | 3.79 | 2.84 | 3.96 | 5.10 | 3.57 |
| | $n$-$C_5$ | 2.43 | 1.65 | 1.43 | 1.77 | 2.61 | 1.81 |
| | $n$-$C_6$ | 2.50 | 1.46 | 1.36 | 1.65 | 2.59 | 1.66 |
| | $n$-$C_7$ | 2.13 | 1.28 | 1.18 | 1.44 | 2.11 | 1.46 |
| | $n$-$C_8$ | 1.85 | 1.14 | 1.03 | 1.22 | 1.78 | 1.30 |
| | $n$-$C_9$ | 1.58 | 0.95 | 0.84 | 1.02 | 1.45 | 1.00 |
| | $n$-$C_{10}$ | 1.58 | 0.94 | 0.81 | 0.88 | 1.29 | 0.92 |
| | $n$-$C_{11}$ | 1.52 | 0.86 | 0.80 | 0.88 | 1.25 | 0.90 |
| | $n$-$C_{12}$ | 1.70 | 1.02 | 0.84 | 1.13 | 1.36 | 1.13 |
| | $n$-$C_{13}$ | 1.64 | 0.91 | 0.85 | 1.07 | 1.20 | 1.11 |
| | $n$-$C_{14}$ | 1.55 | 0.95 | 0.87 | 0.97 | 1.15 | 1.01 |
| | $n$-$C_{15}$ | 1.47 | 0.89 | 0.77 | 0.93 | 1.12 | 0.97 |
| | $n$-$C_{16}$ | 1.47 | 0.89 | 0.69 | 1.02 | 1.07 | 0.90 |
| | $n$-$C_{17}$ | 1.18 | 0.83 | 0.60 | 0.69 | 0.88 | 0.79 |
| | $n$-$C_{18}$ | 1.07 | 0.83 | 0.62 | 0.62 | 0.75 | 0.71 |
| | $n$-$C_{19}$ | 1.06 | 0.76 | 0.61 | 0.63 | 0.77 | 0.73 |
| | $n$-$C_{20}$ | 1.08 | 0.85 | 0.61 | 0.56 | 0.58 | 0.67 |
| | $n$-$C_{21}$ | 1.12 | 0.78 | 0.62 | 0.53 | 0.51 | 0.66 |
| | $n$-$C_{22}$ | 1.18 | 0.81 | 0.62 | 0.50 | 0.49 | 0.67 |
| | $n$-$C_{23}$ | 1.18 | 0.80 | 0.61 | 0.47 | 0.39 | 0.65 |
| | $n$-$C_{24}$ | 1.18 | 0.79 | 0.61 | 0.50 | 0.33 | 0.63 |
| | $n$-$C_{25}$ | 1.13 | 0.74 | 0.49 | 0.43 | 0.25 | 0.54 |
| | $n$-$C_{26}$ | 0.95 | 0.61 | 0.40 | 0.34 | 0.22 | 0.41 |
| | $n$-$C_{27}$ | 0.80 | 0.54 | 0.34 | 0.27 | 0.11 | 0.32 |
| | $n$-$C_{28}$ | 0.57 | 0.37 | 0.23 | 0.21 | 0.07 | 0.21 |
| | $n$-$C_{29}$ | 0.41 | 0.26 | 0.15 | 0.16 | 0.05 | 0.15 |
| | $n$-$C_{30}$ | 0.24 | 0.15 | 0.09 | 0.11 | 0.04 | 0.06 |
| | $n$-$C_{31}$ | 0.17 | 0.13 | 0.06 | 0.05 | 0.02 | 0.04 |
| | $n$-$C_{32}$ | 0.06 | 0.00 | 0.00 | 0.03 | 0.00 | 0.02 |
| Mono-aromatic | Benz | 0.76 | 0.70 | 0.56 | 1.38 | 1.12 | 1.13 |
| | Tol | 1.63 | 1.70 | 1.19 | 1.99 | 1.64 | 1.92 |
| | E-Benz | 0.44 | 0.39 | 0.30 | 0.41 | 0.36 | 0.48 |
| | $m$+$p$ Xyl | 1.17 | 1.15 | 0.76 | 1.27 | 1.24 | 1.26 |
| | Styr | 0.16 | 0.12 | 0.09 | 0.19 | 0.23 | 0.12 |
| | $o$-Xyl | 0.53 | 0.46 | 0.33 | 0.52 | 0.48 | 0.50 |
| | PropylBenz | 0.12 | 0.12 | 0.06 | 0.00 | 0.00 | 0.00 |

**Appendix 9. (Continued) Pyrolysate classes and compounds in kerogens from the Gippsland Basin**

| Class | Compound (mg/g TOC) | *F. longus* biozone | | | | | |
|---|---|---|---|---|---|---|---|
| | | 20110034 | 20110103 | 20110149 | 20110130 | 20110251 | 20110252 |
| Mono-aromatic | 1M3EBenz | 0.26 | 0.23 | 0.15 | 0.28 | 0.37 | 0.25 |
| | 1M4EBenz | 0.19 | 0.18 | 0.11 | 0.18 | 0.18 | 0.16 |
| | 1,3,5TMBenz | 0.16 | 0.15 | 0.09 | 0.11 | 0.09 | 0.07 |
| | 1M2EBenz | 0.29 | 0.23 | 0.17 | 0.26 | 0.26 | 0.26 |
| | 1,2,4TMBenz | 0.39 | 0.34 | 0.23 | 0.34 | 0.45 | 0.36 |
| | 1,2,3TMBenz | 0.26 | 0.27 | 0.15 | 0.32 | 0.16 | 0.27 |
| Phenolic | Phenol | 0.87 | 1.46 | 1.01 | 1.88 | 0.68 | 2.04 |
| | 2M Phenol | 0.51 | 1.00 | 0.65 | 0.83 | 0.35 | 0.98 |
| | 3+4M Phenol | 0.95 | 2.47 | 1.33 | 1.86 | 0.43 | 2.03 |
| | Alkylphenol | 1.10 | 2.76 | 1.74 | 2.11 | 1.10 | 2.35 |
| Naphthenic | Napht | 0.30 | 0.29 | 0.19 | 0.37 | 0.43 | 0.49 |
| | 2M Napht | 0.41 | 0.48 | 0.28 | 0.62 | 0.61 | 0.43 |
| | 1M Napht | 0.25 | 0.31 | 0.23 | 0.43 | 0.35 | 0.36 |
| | Sum DMNapht | 0.93 | 0.94 | 0.64 | 0.90 | 0.75 | 0.76 |
| | 1,3,7TMNaph | 0.09 | 0.17 | 0.09 | 0.04 | 0.10 | 0.07 |
| | 1,3,6TMNapht | 0.07 | 0.06 | 0.02 | 0.09 | 0.08 | 0.05 |
| | 1,3,5TMNapht | 0.14 | 0.10 | 0.06 | 0.13 | 0.12 | 0.12 |
| | 2,3,6TMNapht | 0.08 | 0.06 | 0.03 | 0.09 | 0.09 | 0.06 |
| | 1,2,7TMNapht | 0.13 | 0.11 | 0.08 | 0.09 | 0.06 | 0.09 |
| | 1,2,4TMNapht | 0.19 | 0.19 | 0.10 | 0.21 | 0.10 | 0.21 |

| Class | Compound | T. lilliei biozone | | | | | | |
|---|---|---|---|---|---|---|---|---|
| | | 20110025 | 20110086 | 201100098 | 20110128 | 20110267 | 20110287 | 20110292 |
| Aliphatic | $n$-$C_1$ | 12.77 | 22.55 | 20.64 | 13.22 | 13.72 | 20.82 | 18.83 |
| | $n$-$C_2$ | 6.69 | 10.45 | 9.23 | 8.80 | 7.67 | 9.92 | 8.54 |
| | $n$-$C_3$ | 4.87 | 6.66 | 6.28 | 7.17 | 5.43 | 6.39 | 5.32 |
| | $n$-$C_4$ | 3.06 | 4.01 | 3.56 | 4.37 | 3.38 | 4.07 | 3.32 |
| | $n$-$C_5$ | 1.42 | 2.08 | 1.47 | 2.45 | 1.83 | 1.95 | 1.75 |
| | $n$-$C_6$ | 1.36 | 1.89 | 1.31 | 2.52 | 1.63 | 1.79 | 1.53 |
| | $n$-$C_7$ | 1.15 | 1.63 | 1.15 | 2.19 | 1.35 | 1.50 | 1.29 |
| | $n$-$C_8$ | 1.03 | 1.45 | 1.03 | 1.95 | 1.12 | 1.27 | 1.07 |
| | $n$-$C_9$ | 0.81 | 1.14 | 0.79 | 1.63 | 0.79 | 1.08 | 0.90 |
| | $n$-$C_{10}$ | 0.81 | 1.11 | 0.77 | 1.73 | 0.77 | 0.99 | 0.80 |
| | $n$-$C_{11}$ | 0.75 | 1.06 | 0.75 | 1.63 | 0.72 | 0.94 | 0.76 |
| | $n$-$C_{12}$ | 0.86 | 1.17 | 0.90 | 1.79 | 0.74 | 1.11 | 0.86 |
| | $n$-$C_{13}$ | 0.83 | 1.15 | 0.79 | 1.76 | 0.64 | 1.07 | 0.80 |
| | $n$-$C_{14}$ | 0.85 | 1.18 | 0.87 | 1.93 | 0.71 | 0.00 | 0.71 |
| | $n$-$C_{15}$ | 0.81 | 1.08 | 0.88 | 1.58 | 0.73 | 0.00 | 0.62 |
| | $n$-$C_{16}$ | 0.70 | 1.00 | 0.74 | 1.65 | 0.64 | 0.00 | 0.61 |
| | $n$-$C_{17}$ | 0.60 | 0.84 | 0.65 | 1.59 | 0.54 | 0.00 | 0.55 |
| | $n$-$C_{18}$ | 0.57 | 0.78 | 0.59 | 1.62 | 0.42 | 0.00 | 0.51 |
| | $n$-$C_{19}$ | 0.57 | 0.77 | 0.59 | 1.63 | 0.41 | 0.00 | 0.49 |
| | $n$-$C_{20}$ | 0.59 | 0.80 | 0.63 | 1.75 | 0.33 | 0.00 | 0.44 |
| | $n$-$C_{21}$ | 0.59 | 0.76 | 0.59 | 1.80 | 0.30 | 0.00 | 0.43 |
| | $n$-$C_{22}$ | 0.63 | 0.74 | 0.62 | 1.94 | 0.30 | 0.00 | 0.43 |
| | $n$-$C_{23}$ | 0.63 | 0.74 | 0.61 | 2.03 | 0.24 | 0.00 | 0.38 |
| | $n$-$C_{24}$ | 0.66 | 0.75 | 0.61 | 2.11 | 0.22 | 0.00 | 0.35 |
| | $n$-$C_{25}$ | 0.65 | 0.64 | 0.58 | 2.02 | 0.19 | 0.00 | 0.29 |
| | $n$-$C_{26}$ | 0.61 | 0.53 | 0.48 | 1.74 | 0.14 | 0.00 | 0.22 |
| | $n$-$C_{27}$ | 0.54 | 0.41 | 0.42 | 1.58 | 0.09 | 0.00 | 0.17 |
| | $n$-$C_{28}$ | 0.40 | 0.26 | 0.31 | 1.16 | 0.05 | 0.00 | 0.11 |
| | $n$-$C_{29}$ | 0.30 | 0.17 | 0.23 | 0.86 | 0.04 | 0.00 | 0.08 |
| | $n$-$C_{30}$ | 0.18 | 0.09 | 0.16 | 0.52 | 0.01 | 0.00 | 0.05 |
| | $n$-$C_{31}$ | 0.14 | 0.07 | 0.11 | 0.36 | 0.01 | 0.00 | 0.03 |
| | $n$-$C_{32}$ | 0.05 | 0.00 | 0.04 | 0.13 | 0.00 | 0.00 | 0.02 |
| Mono-aromatic | Benz | 0.87 | 0.89 | 0.97 | 0.68 | 1.67 | 0.88 | 0.95 |
| | Tol | 1.57 | 1.89 | 1.90 | 1.43 | 1.79 | 1.45 | 1.39 |
| | E-Benz | 0.37 | 0.47 | 0.45 | 0.38 | 0.38 | 0.30 | 0.36 |
| | m+p Xyl | 0.85 | 1.21 | 1.09 | 0.84 | 0.93 | 1.06 | 0.89 |
| | Styr | 0.13 | 0.11 | 0.13 | 0.14 | 0.27 | 2.75 | 0.21 |
| | o-Xyl | 0.43 | 0.47 | 0.49 | 0.42 | 0.50 | 0.32 | 0.28 |
| | PropylBenz | 0.10 | 0.12 | 0.22 | 0.22 | 0.00 | 0.00 | 0.00 |

**Appendix 9. (Continued) Pyrolysate classes and compounds in kerogens from the Gippsland Basin**

| Class | Compound | *T. lilliei* biozone | | | | | | |
|---|---|---|---|---|---|---|---|---|
| | | 20110025 | 20110086 | 201100098 | 20110128 | 20110267 | 20110287 | 20110292 |
| Mono-aromatic | 1M3EBenz | 0.17 | 0.22 | 0.20 | 0.19 | 0.23 | 0.20 | 0.19 |
| | 1M4EBenz | 0.15 | 0.17 | 0.16 | 0.16 | 0.15 | 0.11 | 0.10 |
| | 1,3,5TMBenz | 0.10 | 0.14 | 0.10 | 0.12 | 0.08 | 0.06 | 0.04 |
| | 1M2EBenz | 0.21 | 0.24 | 0.25 | 0.22 | 0.29 | 0.19 | 0.13 |
| | 1,2,4TMBenz | 0.27 | 0.34 | 0.31 | 0.31 | 0.35 | 0.28 | 0.25 |
| | 1,2,3TMBenz | 0.23 | 0.21 | 0.31 | 0.23 | 0.20 | 0.11 | 0.09 |
| Phenolic | Phenol | 1.58 | 1.20 | 1.84 | 1.30 | 1.00 | 0.80 | 0.51 |
| | 2M Phenol | 0.65 | 0.78 | 0.85 | 0.65 | 0.38 | 0.62 | 0.30 |
| | 3+4M Phenol | 1.48 | 1.30 | 2.35 | 1.54 | 0.66 | 0.88 | 0.51 |
| | Alkylphenol | 1.58 | 1.88 | 2.37 | 1.95 | 1.10 | 1.81 | 1.03 |
| Naphthenic | Napht | 0.25 | 0.27 | 0.30 | 0.22 | 0.35 | 0.36 | 0.33 |
| | 2M Napht | 0.30 | 0.41 | 0.40 | 0.38 | 0.33 | 0.43 | 0.36 |
| | 1M Napht | 0.24 | 0.32 | 0.29 | 0.20 | 0.27 | 0.32 | 0.26 |
| | Sum DMNapht | 0.74 | 1.01 | 0.73 | 0.83 | 0.71 | 0.10 | 0.55 |
| | 1,3,7TMNaph | 0.12 | 0.13 | 0.16 | 0.19 | 0.03 | 0.00 | 0.05 |
| | 1,3,6TMNapht | 0.04 | 0.07 | 0.04 | 0.02 | 0.07 | 0.00 | 0.06 |
| | 1,3,5TMNapht | 0.09 | 0.12 | 0.09 | 0.07 | 0.11 | 0.00 | 0.09 |
| | 2,3,6TMNapht | 0.05 | 0.06 | 0.05 | 0.05 | 0.07 | 0.00 | 0.05 |
| | 1,2,7TMNapht | 0.08 | 0.14 | 0.11 | 0.17 | 0.10 | 0.00 | 0.04 |
| | 1,2,4TMNapht | 0.22 | 0.18 | 0.22 | 0.19 | 0.16 | 0.00 | 0.05 |

**Appendix 9. (Continued) Pyrolysate classes and compounds in kerogens from the Gippsland Basin**

| Class | Compound | *N. senectus* biozone<br>20110296 | *T. apoxyexinus* biozone<br>20110262 | *P. mawsonii* biozone<br>20110275 |
|---|---|---|---|---|
| Aliphatic | $n\text{-}C_1$ | 9.27 | 6.09 | 5.78 |
| | $n\text{-}C_2$ | 5.35 | 4.20 | 4.33 |
| | $n\text{-}C_3$ | 3.91 | 3.33 | 4.25 |
| | $n\text{-}C_4$ | 2.98 | 1.63 | 3.15 |
| | $n\text{-}C_5$ | 1.54 | 0.74 | 1.60 |
| | $n\text{-}C_6$ | 1.16 | 0.56 | 1.62 |
| | $n\text{-}C_7$ | 0.94 | 0.46 | 1.34 |
| | $n\text{-}C_8$ | 0.79 | 0.36 | 1.11 |
| | $n\text{-}C_9$ | 0.56 | 0.25 | 0.99 |
| | $n\text{-}C_{10}$ | 0.52 | 0.19 | 0.92 |
| | $n\text{-}C_{11}$ | 0.51 | 0.18 | 0.82 |
| | $n\text{-}C_{12}$ | 0.44 | 0.16 | 0.81 |
| | $n\text{-}C_{13}$ | 0.36 | 0.10 | 0.79 |
| | $n\text{-}C_{14}$ | 0.32 | 0.09 | 0.71 |
| | $n\text{-}C_{15}$ | 0.32 | 0.08 | 0.61 |
| | $n\text{-}C_{16}$ | 0.18 | 0.05 | 0.56 |
| | $n\text{-}C_{17}$ | 0.15 | 0.04 | 0.51 |
| | $n\text{-}C_{18}$ | 0.13 | 0.03 | 0.47 |
| | $n\text{-}C_{19}$ | 0.12 | 0.02 | 0.49 |
| | $n\text{-}C_{20}$ | 0.07 | 0.01 | 0.43 |
| | $n\text{-}C_{21}$ | 0.06 | 0.01 | 0.41 |
| | $n\text{-}C_{22}$ | 0.04 | 0.00 | 0.38 |
| | $n\text{-}C_{23}$ | 0.02 | 0.00 | 0.36 |
| | $n\text{-}C_{24}$ | 0.01 | 0.00 | 0.33 |
| | $n\text{-}C_{25}$ | 0.00 | 0.00 | 0.26 |
| | $n\text{-}C_{26}$ | 0.00 | 0.00 | 0.21 |
| | $n\text{-}C_{27}$ | 0.00 | 0.00 | 0.17 |
| | $n\text{-}C_{28}$ | 0.00 | 0.00 | 0.14 |
| | $n\text{-}C_{29}$ | 0.00 | 0.00 | 0.12 |
| | $n\text{-}C_{30}$ | 0.00 | 0.00 | 0.09 |
| | $n\text{-}C_{31}$ | 0.00 | 0.00 | 0.06 |
| | $n\text{-}C_{32}$ | 0.00 | 0.00 | 0.03 |
| Mono-aromatic | Benz | 1.64 | 1.14 | 0.53 |
| | Tol | 1.71 | 1.15 | 0.74 |
| | E-Benz | 0.40 | 0.22 | 0.32 |
| | m+p Xyl | 0.78 | 0.47 | 0.66 |
| | Styr | 0.34 | 0.13 | 0.17 |
| | o-Xyl | 0.44 | 0.28 | 0.29 |
| | PropylBenz | 0.00 | 0.00 | 0.00 |

**Appendix 9. (Continued) Pyrolysate classes and compounds in kerogens from the Gippsland Basin**

| Class | Compound | *N. senectus* biozone 20110296 | *T. apoxyexinus* biozone 20110262 | *P. mawsonii* biozone 20110275 |
|---|---|---|---|---|
| Mono-aromatic | 1M3EBenz | 0.17 | 0.10 | 0.15 |
| | 1M4EBenz | 0.11 | 0.05 | 0.14 |
| | 1,3,5TMBenz | 0.04 | 0.02 | 0.10 |
| | 1M2EBenz | 0.23 | 0.11 | 0.19 |
| | 1,2,4TMBenz | 0.26 | 0.15 | 0.27 |
| | 1,2,3TMBenz | 0.17 | 0.13 | 0.17 |
| Phenolic | Phenol | 0.96 | 0.08 | 0.23 |
| | 2M Phenol | 0.51 | 0.02 | 0.13 |
| | 3+4M Phenol | 0.35 | 0.02 | 0.15 |
| | Alkylphenol | 0.79 | 0.00 | 0.00 |
| Naphthenic | Napht | 0.35 | 0.20 | 0.17 |
| | 2M Napht | 0.28 | 0.09 | 0.21 |
| | 1M Napht | 0.23 | 0.07 | 0.20 |
| | Sum DMNapht | 0.44 | 0.11 | 0.45 |
| | 1,3,7TMNaph | 0.02 | 0.00 | 0.03 |
| | 1,3,6TMNapht | 0.05 | 0.01 | 0.04 |
| | 1,3,5TMNapht | 0.05 | 0.01 | 0.06 |
| | 2,3,6TMNapht | 0.02 | 0.00 | 0.03 |
| | 1,2,7TMNapht | 0.03 | 0.00 | 0.05 |
| | 1,2,4TMNapht | 0.06 | 0.01 | 0.05 |

**Appendix 10. Py-GC boiling ranges in pyrolysates from the Vulcan Sub-basin**

| Formation | Echuca Shoals | | Upper Vulcan | | Lower Vulcan | | | | | |
|---|---|---|---|---|---|---|---|---|---|---|
| Sample ID | 20110051 | 20110065 | 20110067 | 3849 | 20110042 | 20110044 | 20110044C | 20110047 | 20110052 | 20110062 |
| *TOC (%) | 1.75 | 2.19 | 1.08 | 0.79 | 2.12 | 12.80 | 20.80 | 2.52 | 1.81 | 1.44 |
| Range (mg/g sample) | | | | | | | | | | |
| $n$-$C_1$*1.1 | 0.20 | 0.24 | 0.12 | 0.03 | 0.23 | 1.54 | 6.16 | 0.23 | 0.17 | 0.12 |
| $C_1$-$C_5$ Total | 0.87 | 0.91 | 0.51 | 0.18 | 0.87 | 4.36 | 15.19 | 0.82 | 0.71 | 0.48 |
| $C_2$-$C_5$ Total | 0.66 | 0.67 | 0.39 | 0.15 | 0.64 | 2.82 | 9.03 | 0.60 | 0.54 | 0.36 |
| $C_6$-$C_{14}$ Total | 1.57 | 1.57 | 0.96 | 0.32 | 1.42 | 6.11 | 18.66 | 1.40 | 1.30 | 0.76 |
| $C_{15+}$ Total | 9.41 | 9.20 | 7.19 | 8.00 | 11.12 | 24.26 | 85.00 | 5.00 | 6.82 | 3.95 |
| Range (mg/g TOC) | | | | | | | | | | |
| $n$-$C_1$*1.1 | 11.61 | 10.89 | 11.06 | 4.38 | 11.00 | 12.06 | 29.64 | 8.99 | 9.52 | 8.39 |
| $C_1$-$C_5$ Total | 49.54 | 41.70 | 47.16 | 22.74 | 41.04 | 34.06 | 73.05 | 32.74 | 39.08 | 33.65 |
| $C_2$-$C_5$ Total | 37.93 | 30.81 | 36.10 | 18.36 | 30.04 | 22.00 | 43.41 | 23.74 | 29.56 | 25.27 |
| $C_6$-$C_{14}$ Total | 89.53 | 71.81 | 89.20 | 40.50 | 67.09 | 47.76 | 89.70 | 55.71 | 71.58 | 52.64 |
| $C_{15+}$ Total | 537.56 | 420.32 | 665.93 | 1013.05 | 524.39 | 189.53 | 408.66 | 198.27 | 376.68 | 274.36 |
| Gas:oil ratio ($C_1$-$C_5$/$C_{6+}$) | 0.08 | 0.08 | 0.06 | 0.02 | 0.07 | 0.14 | 0.15 | 0.13 | 0.09 | 0.10 |
| Gas wetness ($C_2$-$C_5$/$C_1$-$C_5$) | 0.77 | 0.74 | 0.77 | 0.81 | 0.73 | 0.65 | 0.59 | 0.73 | 0.76 | 0.75 |

**\*TOC:** TOC measured on solvent extracted sample

Appendix 10. (Continued) Py-GC boiling ranges in pyrolysates from the Vulcan Sub-basin

| Formation | Lower Vulcan | | | | | Plover | | | | |
|---|---|---|---|---|---|---|---|---|---|---|
| Sample ID | 20110078 | 20110081 | 20110084 | 3851 | 3853 | 20110045 | 20110050 | 20110054 | 20110054C | 20110055 |
| *TOC (%) | 2.50 | 2.03 | 2.03 | 2.38 | 3.30 | 2.03 | 6.95 | 19.80 | 41.70 | 14.00 |
| Range (mg/g sample) | | | | | | | | | | |
| $n$-$C_1$*1.1 | 0.25 | 0.16 | 0.26 | 0.23 | 0.28 | 0.25 | 0.79 | 3.19 | 5.33 | 1.74 |
| $C_1$-$C_5$ Total | 0.86 | 0.65 | 1.28 | 1.42 | 0.91 | 0.86 | 2.19 | 8.16 | 14.66 | 4.72 |
| $C_2$-$C_5$ Total | 0.61 | 0.49 | 1.01 | 1.19 | 0.62 | 0.61 | 1.40 | 4.96 | 9.33 | 2.98 |
| $C_6$-$C_{14}$ Total | 1.37 | 1.10 | 2.61 | 3.22 | 1.60 | 1.36 | 3.09 | 10.15 | 18.96 | 6.65 |
| $C_{15+}$ Total | 6.59 | 5.57 | 8.45 | 11.90 | 5.16 | 5.81 | 43.14 | 33.17 | 69.12 | 28.88 |
| Range (mg/g TOC) | | | | | | | | | | |
| $n$-$C_1$*1.1 | 10.14 | 7.68 | 12.94 | 9.82 | 8.58 | 12.24 | 11.40 | 57.57 | 12.78 | 12.43 |
| $C_1$-$C_5$ Total | 34.35 | 31.91 | 62.84 | 59.73 | 27.46 | 42.34 | 31.53 | 159.24 | 35.16 | 33.74 |
| $C_2$-$C_5$ Total | 24.21 | 24.23 | 49.89 | 49.91 | 18.88 | 30.10 | 20.13 | 101.67 | 22.37 | 21.31 |
| $C_6$-$C_{14}$ Total | 54.95 | 54.33 | 128.57 | 135.11 | 48.42 | 67.23 | 44.39 | 224.20 | 45.46 | 47.52 |
| $C_{15+}$ Total | 263.43 | 274.45 | 416.24 | 499.83 | 156.33 | 286.29 | 620.75 | 3135.11 | 165.77 | 206.29 |
| Gas:oil ratio ($C_1$-$C_5$/$C_{6+}$) | 0.11 | 0.10 | 0.12 | 0.09 | 0.13 | 0.12 | 0.05 | 0.19 | 0.17 | 0.13 |
| Gas wetness ($C_2$-$C_5$/$C_1$-$C_5$) | 0.70 | 0.76 | 0.79 | 0.84 | 0.69 | 0.71 | 0.64 | 0.64 | 0.64 | 0.63 |

*TOC: TOC measured on solvent extracted sample

320

| Formation | Plover | | | |
|---|---|---|---|---|
| Sample ID | 20110058 | 20110076 | 20110076C | 20110077C |
| *TOC (%) | 17.50 | 10.90 | 31.90 | 51.40 |
| **Range (mg/g sample)** | | | | |
| $n$-$C_1$*1.1 | 2.07 | 1.18 | 5.94 | 9.46 |
| $C_1$-$C_5$ Total | 4.59 | 3.08 | 12.90 | 19.20 |
| $C_2$-$C_5$ Total | 2.52 | 1.90 | 6.96 | 9.74 |
| $C_6$-$C_{14}$ Total | 12.02 | 4.50 | 23.67 | 51.21 |
| $C_{15+}$ Total | 32.47 | 29.45 | 57.85 | 87.04 |
| **Range (mg/g TOC)** | | | | |
| $n$-$C_1$*1.1 | 11.82 | 10.84 | 18.61 | 18.41 |
| $C_1$-$C_5$ Total | 26.23 | 28.28 | 40.44 | 37.36 |
| $C_2$-$C_5$ Total | 14.41 | 17.44 | 21.83 | 18.96 |
| $C_6$-$C_{14}$ Total | 68.70 | 41.25 | 74.20 | 99.63 |
| $C_{15+}$ Total | 185.57 | 270.21 | 181.36 | 169.34 |
| **Gas:oil ratio ($C_1$-$C_5$/$C_{6+}$)** | 0.10 | 0.09 | 0.16 | 0.14 |
| **Gas wetness ($C_2$-$C_5$/$C_1$-$C_5$)** | 0.55 | 0.62 | 0.54 | 0.51 |

**\*TOC:** TOC measured on solvent extracted sample

**Appendix 11. Py-GC boiling ranges in pyrolysates from the Laminaria High**

| Formation | Echuca Shoals | | | Flamingo | | | Frigate | | | |
|---|---|---|---|---|---|---|---|---|---|---|
| Sample ID | 20110002 | 20110010 | 20110013 | 20110004 | 20110011 | 20110018 | 20110007 | 20110015 | 20110019 | 20110021 |
| *TOC (%) | 2.67 | 1.75 | 1.89 | 1.78 | 2.82 | 1.00 | 2.51 | 1.54 | 1.43 | 2.07 |
| **Range (mg/g sample)** | | | | | | | | | | |
| $n$-$C_1$*1.1 | 0.32 | 0.21 | 0.29 | 0.19 | 0.30 | 0.07 | 0.21 | 0.03 | 0.06 | 0.35 |
| $C_1$-$C_5$ Total | 1.87 | 0.81 | 1.04 | 1.35 | 1.11 | 0.35 | 1.06 | 0.27 | 0.46 | 1.20 |
| $C_2$-$C_5$ Total | 1.56 | 0.60 | 0.75 | 1.16 | 0.80 | 0.28 | 0.85 | 0.24 | 0.40 | 0.85 |
| $C_6$-$C_{14}$ Total | 3.54 | 1.03 | 1.40 | 3.17 | 1.82 | 0.63 | 2.08 | 0.43 | 0.59 | 2.25 |
| $C_{15+}$ Total | 6.50 | 3.10 | 3.53 | 5.93 | 5.23 | 2.97 | 4.77 | 2.68 | 3.21 | 4.61 |
| **Range (mg/g TOC)** | | | | | | | | | | |
| $n$-$C_1$*1.1 | 11.96 | 12.01 | 15.41 | 10.77 | 10.76 | 7.00 | 8.28 | 1.76 | 4.54 | 16.93 |
| $C_1$-$C_5$ Total | 70.22 | 46.57 | 54.87 | 75.92 | 39.28 | 34.74 | 42.30 | 17.22 | 32.33 | 57.79 |
| $C_2$-$C_5$ Total | 58.26 | 34.55 | 39.46 | 65.15 | 28.52 | 27.74 | 34.02 | 15.46 | 27.78 | 40.87 |
| $C_6$-$C_{14}$ Total | 132.70 | 58.94 | 74.10 | 178.31 | 64.55 | 63.33 | 82.81 | 27.94 | 41.01 | 108.86 |
| $C_{15+}$ Total | 243.47 | 176.91 | 186.92 | 333.01 | 185.36 | 296.58 | 190.09 | 173.79 | 224.82 | 222.81 |
| **Gas:oil ratio ($C_1$-$C_5$/$C_{6+}$)** | 0.19 | 0.20 | 0.21 | 0.15 | 0.16 | 0.10 | 0.15 | 0.09 | 0.12 | 0.17 |
| **Gas wetness ($C_2$-$C_5$/$C_1$-$C_5$)** | 0.83 | 0.74 | 0.72 | 0.86 | 0.73 | 0.80 | 0.80 | 0.90 | 0.86 | 0.71 |

**\*TOC:** TOC measured on solvent extracted sample

322

**Appendix 11. (Continued) Py-GC boiling ranges in pyrolysates from the Laminaria High**

| Formation | Laminaria | | | Plover |
|---|---|---|---|---|
| Sample ID | 20110008 | 20110017 | 20110022 | 20110023 |
| **\*TOC (%)** | 1.56 | 0.95 | 1.14 | 0.62 |
| **Range (mg/g sample)** | | | | |
| $n$-$C_1$\*1.1 | 0.17 | 0.06 | 0.10 | 0.02 |
| $C_1$-$C_5$ Total | 0.98 | 0.20 | 0.46 | 0.12 |
| $C_2$-$C_5$ Total | 0.81 | 0.14 | 0.37 | 0.10 |
| $C_6$-$C_{14}$ Total | 1.96 | 0.15 | 0.51 | 0.18 |
| $C_{15+}$ Total | 4.35 | 2.36 | 2.15 | 2.61 |
| **Range (mg/g TOC)** | | | | |
| $n$-$C_1$\*1.1 | 10.75 | 6.00 | 8.55 | 2.81 |
| $C_1$-$C_5$ Total | 62.92 | 21.08 | 40.71 | 19.50 |
| $C_2$-$C_5$ Total | 52.17 | 15.08 | 32.15 | 16.69 |
| $C_6$-$C_{14}$ Total | 125.65 | 15.29 | 44.84 | 29.69 |
| $C_{15+}$ Total | 278.58 | 248.48 | 188.21 | 421.09 |
| **Gas:oil ratio ($C_1$-$C_5$/$C_{6+}$)** | 0.16 | 0.08 | 0.17 | 0.04 |
| **Gas wetness ($C_2$-$C_5$/$C_1$-$C_5$)** | 0.83 | 0.72 | 0.79 | 0.86 |

**\*TOC:** TOC measured on solvent extracted sample

**Appendix 12. Py-GC boiling ranges in pyrolysates from the Gippsland Basin**

| Biozone | *L. balmei* | | | | | | *F. longus* | | | |
|---|---|---|---|---|---|---|---|---|---|---|
| Sample ID | 20110092 | 20110113 | 20110121 | 20110126 | 20110140 | 20110153 | 20110034 | 20110103 | 20110149 | 20110130 |
| TOC (%) | 4.38 | 52.65 | 72.41 | 13.84 | 23.18 | 3.78 | 4.02 | 24.84 | 17.46 | 3.32 |
| **Range mg/g sample** | | | | | | | | | | |
| $n$-$C_1$*1.1 | 0.63 | 8.40 | 11.24 | 2.59 | 3.85 | 0.83 | 0.57 | 5.24 | 2.39 | 0.62 |
| $C_1$-$C_5$ Total | 2.04 | 17.30 | 21.66 | 5.58 | 8.03 | 1.90 | 1.61 | 11.51 | 5.51 | 1.45 |
| $C_2$-$C_5$ Total | 1.42 | 8.90 | 10.41 | 2.99 | 4.18 | 1.07 | 1.03 | 6.27 | 3.12 | 0.83 |
| $C_6$-$C_{14}$ Total | 3.04 | 21.99 | 21.76 | 5.77 | 8.04 | 2.59 | 2.50 | 13.37 | 6.82 | 1.95 |
| $C_{15+}$ Total | 6.92 | 29.21 | 29.24 | 10.52 | 13.34 | 3.39 | 5.31 | 23.84 | 9.85 | 2.06 |
| **Range mg/g TOC** | | | | | | | | | | |
| $n$-$C_1$*1.1 | 14.30 | 15.95 | 15.53 | 18.72 | 16.61 | 22.00 | 14.30 | 21.09 | 13.69 | 18.58 |
| $C_1$-$C_5$ Total | 46.64 | 32.86 | 29.91 | 40.34 | 34.64 | 50.33 | 39.99 | 46.35 | 31.56 | 43.55 |
| $C_2$-$C_5$ Total | 32.34 | 16.91 | 14.38 | 21.62 | 18.03 | 28.33 | 25.69 | 25.25 | 17.87 | 24.96 |
| $C_6$-$C_{14}$ Total | 69.47 | 41.76 | 30.05 | 41.72 | 34.70 | 68.60 | 62.26 | 53.82 | 39.08 | 58.66 |
| $C_{15+}$ Total | 158.03 | 55.49 | 40.38 | 75.98 | 57.53 | 89.62 | 132.07 | 95.96 | 56.42 | 62.16 |
| **Gas:oil ratio ($C_1$-$C_5$/$C_{6+}$)** | 0.21 | 0.34 | 0.42 | 0.34 | 0.38 | 0.32 | 0.21 | 0.31 | 0.33 | 0.36 |
| **Gas wetness ($C_2$-$C_5$/$C_1$-$C_5$)** | 0.69 | 0.51 | 0.48 | 0.54 | 0.52 | 0.56 | 0.64 | 0.54 | 0.57 | 0.57 |

**Appendix 12. (Continued) Py-GC boiling ranges in pyrolysates from the Gippsland Basin**

| Biozone | *F. longus* | | *T. lilliei* | | | | | | |
|---|---|---|---|---|---|---|---|---|---|
| Sample ID | 20110251 | 20110252 | 20110025 | 20110086 | 201100098 | 20110128 | 20110267 | 20110287 | 20110292 |
| TOC (%) | 1.54 | 11.02 | 13.43 | 8.15 | 21.13 | 9.35 | 1.94 | 17.57 | 14.57 |
| **Range mg/g sample** | | | | | | | | | |
| $n$-C$_1$*1.1 | 0.30 | 2.62 | 1.67 | 1.79 | 4.24 | 1.20 | 0.29 | 4.02 | 3.02 |
| C$_1$-C$_5$ Total | 0.77 | 5.23 | 4.11 | 3.86 | 9.10 | 3.53 | 7.76 | 0.29 | 0.69 |
| C$_2$-C$_5$ Total | 0.47 | 2.61 | 2.44 | 2.07 | 4.86 | 2.33 | 0.43 | 4.20 | 2.95 |
| C$_6$-C$_{14}$ Total | 0.87 | 5.46 | 6.14 | 4.13 | 10.78 | 6.67 | 0.94 | 7.88 | 4.92 |
| C$_{15+}$ Total | 0.98 | 5.34 | 9.62 | 6.18 | 15.11 | 14.74 | 0.70 | 10.47 | 5.06 |
| **Range mg/g TOC** | | | | | | | | | |
| $n$-C$_1$*1.1 | 19.70 | 23.82 | 12.41 | 21.91 | 20.06 | 12.85 | 15.09 | 22.90 | 20.71 |
| C$_1$-C$_5$ Total | 50.16 | 47.50 | 30.59 | 47.36 | 43.06 | 37.73 | 399.93 | 1.65 | 4.70 |
| C$_2$-C$_5$ Total | 30.46 | 23.69 | 18.18 | 25.44 | 23.00 | 24.89 | 21.99 | 23.93 | 20.27 |
| C$_6$-C$_{14}$ Total | 56.69 | 49.55 | 45.70 | 50.62 | 51.03 | 71.30 | 48.42 | 44.87 | 33.78 |
| C$_{15+}$ Total | 63.90 | 48.42 | 71.67 | 75.86 | 71.53 | 157.62 | 35.92 | 59.61 | 34.75 |
| **Gas:oil ratio (C$_1$-C$_5$/C$_{6+}$)** | 0.42 | 0.48 | 0.26 | 0.37 | 0.35 | 0.16 | 4.74 | 0.02 | 0.07 |
| **Gas wetness (C$_2$-C$_5$/C$_1$-C$_5$)** | 0.61 | 0.50 | 0.59 | 0.54 | 0.53 | 0.66 | 0.05 | 14.52 | 4.31 |

**Appendix 12. (Continued) Py-GC boiling ranges in pyrolysates from the Gippsland Basin**

| Biozone | *N. senectus* | *T. apoxyexinus* | *P. mawsonii* |
|---|---|---|---|
| Sample ID | 20110296 | 20110262 | 20110275 |
| TOC (%) | 1.95 | 1.65 | 12.13 |
| Range mg/g sample | | | |
| $n$-$C_1$*1.1 | 0.20 | 0.11 | 0.77 |
| $C_1$-$C_5$ Total | 0.54 | 5.62 | 2.45 |
| $C_2$-$C_5$ Total | 0.36 | 0.19 | 1.76 |
| $C_6$-$C_{14}$ Total | 0.67 | 0.24 | 4.42 |
| $C_{15+}$ Total | 0.30 | 0.17 | 6.39 |
| Range mg/g TOC | | | |
| $n$-$C_1$*1.1 | 10.20 | 6.70 | 6.36 |
| $C_1$-$C_5$ Total | 27.65 | 340.56 | 20.16 |
| $C_2$-$C_5$ Total | 18.64 | 11.62 | 14.54 |
| $C_6$-$C_{14}$ Total | 34.46 | 14.74 | 36.40 |
| $C_{15+}$ Total | 15.14 | 10.12 | 52.65 |
| **Gas:oil ratio ($C_1$-$C_5$/$C_{6+}$)** | 0.56 | 13.70 | 0.23 |
| **Gas wetness ($C_2$-$C_5$/$C_1$-$C_5$)** | 0.67 | 0.03 | 0.72 |

**Appendix 13. Kinetic parameters, activation energies (Ea) and frequency factors (A) measured for samples from the Vulcan Sub-basin (heating rates: 0.7, 2.0 and 5.0 k/min)**

| Formation | Echuca Shoals | Upper Vulcan | Lower Vulcan | | | |
|---|---|---|---|---|---|---|
| Sample ID | 20110051 | 20110067 | 20110044C | 20110047 | 20110078 | 3851 |
| Pre-exponential Factor A ($S^{-1}$) | 1.38E+13 | 3.36E+13 | 3.56E+15 | 6.03E+13 | 1.69E+13 | 1.72E+16 |
| Activation Energy (kcal/mol) | | | | | | |
| 39 | 0.00 | 0.00 | 0.00 | 0.00 | 0.36 | 0.00 |
| 40 | 1.02 | 0.34 | 0.00 | 0.00 | 0.21 | 0.00 |
| 41 | 0.00 | 0.38 | 0.00 | 0.00 | 0.63 | 0.00 |
| 42 | 1.23 | 0.67 | 0.00 | 0.55 | 0.56 | 0.00 |
| 43 | 0.43 | 0.52 | 0.00 | 0.04 | 0.61 | 0.00 |
| 44 | 1.02 | 0.78 | 0.00 | 0.72 | 0.62 | 0.00 |
| 45 | 0.54 | 0.59 | 0.00 | 0.29 | 0.75 | 0.00 |
| 46 | 0.93 | 0.81 | 0.00 | 0.75 | 0.74 | 0.00 |
| 47 | 0.99 | 1.33 | 0.00 | 0.58 | 1.14 | 0.00 |
| 48 | 0.66 | 1.05 | 0.14 | 1.12 | 2.38 | 0.00 |
| 49 | 2.94 | 3.58 | 0.00 | 1.18 | 0.20 | 0.00 |
| 50 | 0.00 | 0.46 | 0.20 | 3.34 | 7.76 | 0.00 |
| 51 | 48.19 | 10.05 | 0.04 | 1.76 | 32.53 | 0.00 |
| 52 | 19.31 | 38.44 | 0.46 | 17.79 | 23.96 | 0.00 |
| 53 | 14.46 | 18.60 | 0.00 | 32.70 | 10.93 | 0.00 |
| 54 | 1.86 | 12.54 | 0.90 | 18.51 | 6.60 | 0.00 |
| 55 | 3.41 | 3.10 | 0.34 | 9.16 | 3.61 | 0.00 |
| 56 | 0.21 | 3.39 | 0.00 | 4.49 | 2.77 | 0.00 |
| 57 | 1.21 | 0.44 | 9.57 | 4.42 | 1.65 | 0.00 |
| 58 | 0.39 | 1.19 | 17.22 | 0.17 | 0.00 | 0.00 |
| 59 | 0.06 | 0.00 | 18.90 | 0.74 | 1.02 | 0.00 |
| 60 | 0.70 | 0.65 | 16.15 | 0.26 | 0.00 | 0.00 |
| 61 | 0.00 | 0.36 | 8.53 | 0.00 | 0.00 | 81.70 |
| 62 | 0.00 | 0.00 | 7.09 | 0.68 | 0.00 | 0.00 |
| 63 | 0.00 | 0.00 | 4.50 | 0.01 | 0.97 | 12.80 |
| 64 | 0.44 | 0.72 | 4.10 | 0.00 | 0.00 | 5.50 |
| 65 | 0.00 | 0.00 | 2.20 | 0.00 | 0.00 | 0.00 |
| 66 | 0.00 | 0.00 | 3.56 | 0.74 | 0.00 | 0.00 |
| 67 | 0.00 | 0.00 | 0.00 | 0.00 | 0.00 | 0.00 |
| 68 | 0.00 | 0.00 | 1.58 | 0.00 | 0.00 | 0.00 |
| 69 | 0.00 | 0.00 | 1.61 | 0.00 | 0.00 | 0.00 |
| 70 | 0.00 | 0.00 | 0.00 | 0.00 | 0.00 | 0.00 |
| 71 | 0.00 | 0.00 | 0.00 | 0.00 | 0.00 | 0.00 |
| 72 | 0.00 | 0.00 | 2.91 | 0.00 | 0.00 | 0.00 |

**Appendix 13. (Continued) Kinetic parameters, activation energies (Ea) and frequency factors (A) measured for samples from the Vulcan Sub-basin (heating rates: 0.7, 2.0 and 5.0 k/min)**

| Formation | Plover | | | | | |
|---|---|---|---|---|---|---|
| Sample ID | 20110050 | 20110054C | 20110058 | 20110076 | 20110076C | 20110077C |
| Pre-exponential Factor A (S$^{-1}$) | 1.56E+14 | 9.90E+15 | 7.91E+16 | 5.13E+14 | 1.22E+16 | 9.07E+16 |
| Activation Energy (kcal/mol) | | | | | | |
| 44 | 0.02 | 0.00 | 0.00 | 0.00 | 0.00 | 0.00 |
| 45 | 0.28 | 0.00 | 0.00 | 0.18 | 0.00 | 0.00 |
| 46 | 0.07 | 0.00 | 0.00 | 0.00 | 0.00 | 0.00 |
| 47 | 0.58 | 0.00 | 0.00 | 0.20 | 0.00 | 0.00 |
| 48 | 0.11 | 0.00 | 0.00 | 0.11 | 0.00 | 0.00 |
| 49 | 1.16 | 0.00 | 0.00 | 0.31 | 0.00 | 0.00 |
| 50 | 0.03 | 0.22 | 0.00 | 0.22 | 0.00 | 0.00 |
| 51 | 2.18 | 0.00 | 0.00 | 0.36 | 0.32 | 0.00 |
| 52 | 2.39 | 0.21 | 0.00 | 0.66 | 0.00 | 0.00 |
| 53 | 15.69 | 0.16 | 0.00 | 3.17 | 0.44 | 0.00 |
| 54 | 25.09 | 0.35 | 0.21 | 8.35 | 0.36 | 0.32 |
| 55 | 17.16 | 0.36 | 0.00 | 19.32 | 1.24 | 0.15 |
| 56 | 13.98 | 0.80 | 0.13 | 19.43 | 0.87 | 0.06 |
| 57 | 5.25 | 0.00 | 0.20 | 15.02 | 3.12 | 1.39 |
| 58 | 3.21 | 4.50 | 0.29 | 9.33 | 12.39 | 0.04 |
| 59 | 6.52 | 10.52 | 0.00 | 6.65 | 16.11 | 0.00 |
| 60 | 0.00 | 22.04 | 0.00 | 2.61 | 15.97 | 7.64 |
| 61 | 1.82 | 14.45 | 3.10 | 4.95 | 11.60 | 19.51 |
| 62 | 0.58 | 14.24 | 19.83 | 1.75 | 9.51 | 16.23 |
| 63 | 1.16 | 6.37 | 17.74 | 1.27 | 6.12 | 13.96 |
| 64 | 0.00 | 6.52 | 18.25 | 1.42 | 5.05 | 9.37 |
| 65 | 1.41 | 4.19 | 8.67 | 0.29 | 3.47 | 7.75 |
| 66 | 0.07 | 3.58 | 11.13 | 1.86 | 2.89 | 5.08 |
| 67 | 0.00 | 2.28 | 2.43 | 0.00 | 2.44 | 4.66 |
| 68 | 1.24 | 2.41 | 7.14 | 0.00 | 1.26 | 2.80 |
| 69 | 0.00 | 0.98 | 4.11 | 2.54 | 1.57 | 3.70 |
| 70 | 0.00 | 1.29 | 0.35 | 0.00 | 0.95 | 0.73 |
| 71 | 0.00 | 1.73 | 1.63 | 0.00 | 0.68 | 2.04 |
| 72 | 0.00 | 0.00 | 0.79 | 0.00 | 1.50 | 0.45 |
| 73 | 0.00 | 0.00 | 0.30 | 0.00 | 0.00 | 1.25 |
| 74 | 0.00 | 2.80 | 0.89 | 0.00 | 0.00 | 0.22 |
| 75 | 0.00 | 0.00 | 0.90 | 0.00 | 2.14 | 1.18 |
| 76 | 0.00 | 0.00 | 0.00 | 0.00 | 0.00 | 0.00 |
| 77 | 0.00 | 0.00 | 0.00 | 0.00 | 0.00 | 0.00 |
| 78 | 0.00 | 0.00 | 1.91 | 0.00 | 0.00 | 1.47 |

**Appendix 14. Kinetic parameters, activation energies (Ea) and frequency factors (A) measured for samples from the Laminaria High (heating rates: 0.7, 2.0 and 5.0 k/min)**

| Formation | Echuca Shoals | | Flamingo | | Frigate | | Laminaria |
|---|---|---|---|---|---|---|---|
| Sample ID | 20110002 | 20110013 | 20110004 | 20110011 | 20110007 | 20110021 | 20110008 |
| Pre-exponential Factor A (S⁻¹) | 9.82E + 13 | 7.75E + 13 | 4.19E + 13 | 4.86E + 13 | 2.83E + 13 | 1.65E + 14 | 8.10E + 13 |
| Activation Energy (kcal/mol) | | | | | | | |
| 40 | 0.00 | 0.00 | 0.59 | 0.00 | 0.66 | 0.00 | 0.00 |
| 41 | 0.28 | 0.00 | 0.45 | 0.00 | 0.22 | 0.00 | 0.90 |
| 42 | 0.12 | 0.32 | 0.99 | 0.27 | 1.00 | 0.92 | 0.10 |
| 43 | 0.54 | 0.00 | 0.97 | 0.00 | 0.74 | 0.31 | 1.15 |
| 44 | 0.42 | 0.22 | 1.43 | 0.16 | 1.24 | 1.46 | 0.86 |
| 45 | 0.91 | 0.29 | 1.45 | 0.28 | 1.61 | 1.06 | 1.47 |
| 46 | 0.67 | 0.00 | 2.45 | 0.06 | 1.77 | 2.03 | 1.78 |
| 47 | 1.91 | 0.49 | 2.63 | 0.67 | 2.66 | 2.75 | 2.07 |
| 48 | 1.45 | 0.58 | 3.63 | 0.00 | 2.66 | 3.27 | 3.26 |
| 49 | 3.67 | 0.00 | 4.50 | 0.00 | 4.70 | 4.64 | 2.35 |
| 50 | 2.32 | 0.00 | 5.27 | 0.00 | 0.00 | 4.05 | 5.39 |
| 51 | 5.26 | 0.00 | 8.31 | 0.00 | 6.16 | 6.55 | 3.10 |
| 52 | 8.36 | 0.00 | 17.58 | 23.26 | 32.17 | 4.67 | 8.28 |
| 53 | 18.80 | 34.54 | 22.08 | 37.14 | 21.97 | 10.07 | 23.43 |
| 54 | 19.56 | 27.32 | 13.05 | 19.16 | 9.85 | 18.31 | 19.89 |
| 55 | 18.25 | 18.84 | 7.01 | 6.76 | 7.47 | 17.03 | 8.35 |
| 56 | 5.24 | 5.18 | 6.12 | 9.13 | 3.84 | 10.08 | 12.55 |
| 57 | 10.58 | 8.26 | 0.00 | 0.00 | 0.00 | 5.81 | 0.39 |
| 58 | 0.00 | 0.00 | 0.34 | 1.34 | 0.26 | 3.92 | 2.17 |
| 59 | 0.18 | 2.19 | 0.51 | 0.48 | 0.45 | 0.89 | 0.70 |
| 60 | 0.80 | 0.17 | 0.00 | 0.00 | 0.13 | 0.62 | 0.00 |
| 61 | 0.00 | 0.70 | 0.25 | 0.47 | 0.00 | 0.38 | 0.92 |
| 62 | 0.25 | 0.34 | 0.04 | 0.00 | 0.00 | 0.13 | 0.00 |
| 63 | 0.00 | 0.00 | 0.00 | 0.00 | 0.00 | 0.48 | 0.00 |
| 64 | 0.00 | 0.48 | 0.35 | 0.00 | 0.43 | 0.00 | 0.00 |
| 65 | 0.43 | 0.00 | 0.00 | 0.00 | 0.00 | 0.00 | 0.87 |
| 66 | 0.00 | 0.08 | 0.00 | 0.82 | 0.00 | 0.57 | 0.00 |

**Appendix 15. Kinetic parameters, activation energies (Ea) and frequency factors (A) measured for samples from the Gippsland Basin (heating rates: 0.7, 2.0 and 5.0 k/min)**

| Biozone | *L. balmei* | | | *F. longus* | | | |
|---|---|---|---|---|---|---|---|
| Sample ID | 20110092 | 20110126 | 20110153 | 20110034 | 20110149 | 20110130 | 20110251 |
| Pre-exponential Factor A (S$^{-1}$) | 2.61E +14 | 9.13E+13 | 1.58E+14 | 1.11E+14 | 4.82E+14 | 4.78E+13 | 9.13E+13 |
| Activation Energy (kcal/mol) | | | | | | | |
| 40 | 0.00 | 0.00 | 0.00 | 0.00 | 0.00 | 0.00 | 0.00 |
| 41 | 0.00 | 0.00 | 0.00 | 0.00 | 0.00 | 0.00 | 0.00 |
| 42 | 0.00 | 0.00 | 0.00 | 0.00 | 0.00 | 0.00 | 0.00 |
| 43 | 0.00 | 0.03 | 0.00 | 0.00 | 0.00 | 0.08 | 0.03 |
| 44 | 0.00 | 0.07 | 0.10 | 0.03 | 0.00 | 0.06 | 0.07 |
| 45 | 0.07 | 0.12 | 0.00 | 0.04 | 0.00 | 0.07 | 0.12 |
| 46 | 0.04 | 0.12 | 0.24 | 0.11 | 0.08 | 0.36 | 0.12 |
| 47 | 0.10 | 0.34 | 0.00 | 0.16 | 0.00 | 0.00 | 0.34 |
| 48 | 0.14 | 0.00 | 0.50 | 0.26 | 0.17 | 0.49 | 0.00 |
| 49 | 0.08 | 0.72 | 0.00 | 0.35 | 0.11 | 0.06 | 0.72 |
| 50 | 0.33 | 0.39 | 0.91 | 0.00 | 0.38 | 2.18 | 0.39 |
| 51 | 0.00 | 0.00 | 0.97 | 2.35 | 0.40 | 5.15 | 0.00 |
| 52 | 0.00 | 0.00 | 1.88 | 1.65 | 0.84 | 22.64 | 0.00 |
| 53 | 0.00 | 0.00 | 4.35 | 21.59 | 2.11 | 22.46 | 0.00 |
| 54 | 3.86 | 25.85 | 27.35 | 32.22 | 6.20 | 20.23 | 25.85 |
| 55 | 35.69 | 23.93 | 22.29 | 20.24 | 17.32 | 6.42 | 23.93 |
| 56 | 26.40 | 20.10 | 18.79 | 8.37 | 21.77 | 6.46 | 20.10 |
| 57 | 15.97 | 5.20 | 4.04 | 1.67 | 17.39 | 3.98 | 5.20 |
| 58 | 7.15 | 6.66 | 5.99 | 6.02 | 10.22 | 1.48 | 6.66 |
| 59 | 1.03 | 2.36 | 1.92 | 0.00 | 5.10 | 1.75 | 2.36 |
| 60 | 4.53 | 3.92 | 2.48 | 1.24 | 3.95 | 0.98 | 3.92 |
| 61 | 1.76 | 1.15 | 1.42 | 0.83 | 2.93 | 1.41 | 1.15 |
| 62 | 0.00 | 2.84 | 1.24 | 0.29 | 2.22 | 0.00 | 2.84 |
| 63 | 0.79 | 0.83 | 1.32 | 0.97 | 1.64 | 1.43 | 0.83 |
| 64 | 0.30 | 1.61 | 0.57 | 0.00 | 1.30 | 0.68 | 1.61 |
| 65 | 0.19 | 1.44 | 1.03 | 0.29 | 1.52 | 0.07 | 1.44 |
| 66 | 0.53 | 0.00 | 0.82 | 1.32 | 0.22 | 0.00 | 0.00 |
| 67 | 0.30 | 2.32 | 0.00 | 0.00 | 1.87 | 1.56 | 2.32 |
| 68 | 0.00 | 0.00 | 1.79 | 0.00 | 0.00 | 0.00 | 0.00 |
| 69 | 0.74 | 0.00 | 0.00 | 0.00 | 0.00 | 0.00 | 0.00 |
| 70 | 0.00 | 0.00 | 0.00 | 0.00 | 2.26 | 0.00 | 0.00 |
| 71 | 0.00 | 0.00 | 0.00 | 0.00 | 0.00 | 0.00 | 0.00 |
| 72 | 0.00 | 0.00 | 0.00 | 0.00 | 0.00 | 0.00 | 0.00 |

**Appendix 15. (Continued) Kinetic parameters, activation energies (Ea) and frequency factors (A) measured for samples from the Gippsland Basin (heating rates: 0.7, 2.0 and 5.0 k/min)**

| Biozone | *F. longus* | *T. lilliei* | | | *P. mawsonii* |
|---|---|---|---|---|---|
| Sample ID | 20110279C | 20110086 | 20110128 | 20110292 | 20110275 |
| Pre-exponential Factor A (S⁻¹) | 6.70E+14 | 2.22E+14 | 4.32E+14 | 5.80E+14 | 2.13E+13 |
| **Activation Energy (kcal/mol)** | | | | | |
| 40 | 0.00 | 0.00 | 0.00 | 0.00 | 0.00 |
| 41 | 0.00 | 0.00 | 0.00 | 0.00 | 0.09 |
| 42 | 0.00 | 0.00 | 0.00 | 0.00 | 0.10 |
| 43 | 0.00 | 0.00 | 0.00 | 0.00 | 0.21 |
| 44 | 0.00 | 0.00 | 0.00 | 0.00 | 0.20 |
| 45 | 0.00 | 0.05 | 0.12 | 0.00 | 0.36 |
| 46 | 0.05 | 0.02 | 0.00 | 0.07 | 0.48 |
| 47 | 0.04 | 0.08 | 0.22 | 0.04 | 0.65 |
| 48 | 0.09 | 0.17 | 0.20 | 0.09 | 1.03 |
| 49 | 0.27 | 0.08 | 0.57 | 0.11 | 1.60 |
| 50 | 0.13 | 0.56 | 0.88 | 0.09 | 3.09 |
| 51 | 0.75 | 0.16 | 1.96 | 0.28 | 24.78 |
| 52 | 0.40 | 1.87 | 3.66 | 0.10 | 32.68 |
| 53 | 1.94 | 1.19 | 7.20 | 0.34 | 17.80 |
| 54 | 2.44 | 15.35 | 14.03 | 0.68 | 7.18 |
| 55 | 9.00 | 21.94 | 20.69 | 1.44 | 3.55 |
| 56 | 18.02 | 19.04 | 18.19 | 11.11 | 1.48 |
| 57 | 15.02 | 11.91 | 15.57 | 18.61 | 1.24 |
| 58 | 14.62 | 5.62 | 5.20 | 20.73 | 0.48 |
| 59 | 8.03 | 5.18 | 3.58 | 12.75 | 0.98 |
| 60 | 6.48 | 2.72 | 1.07 | 8.06 | 0.00 |
| 61 | 4.90 | 2.61 | 2.61 | 4.25 | 0.74 |
| 62 | 3.38 | 2.09 | 0.42 | 7.56 | 0.54 |
| 63 | 3.42 | 1.31 | 0.71 | 1.04 | 0.00 |
| 64 | 1.33 | 2.31 | 0.87 | 3.16 | 0.00 |
| 65 | 2.82 | 0.03 | 0.08 | 1.51 | 0.74 |
| 66 | 0.00 | 2.79 | 0.93 | 1.12 | 0.00 |
| 67 | 3.22 | 0.00 | 0.09 | 2.82 | 0.00 |
| 68 | 0.00 | 0.00 | 0.00 | 0.00 | 0.00 |
| 69 | 0.00 | 2.92 | 1.15 | 0.00 | 0.00 |
| 70 | 3.65 | 0.00 | 0.00 | 4.04 | 0.00 |
| 71 | 0.00 | 0.00 | 0.00 | 0.00 | 0.00 |
| 72 | 0.00 | 0.00 | 0.00 | 0.00 | 0.00 |

**Appendix 16. MSSV individual compound yields of samples from the Vulcan Sub-basin**

| Formation/Sample ID | Upper Vulcan: 20110067 | | | | |
|---|---|---|---|---|---|
| Transformation ratio (%) | 10 | 30 | 50 | 70 | 90 |
| End Temperature (°C) | 357 | 389 | 406 | 420 | 442 |
| **Resolved (µg/g sample)** | | | | | |
| $n$-$C_1$ * 1.1 | 5.83 | 38.97 | 85.56 | 111.36 | 184.23 |
| $n$-$C_2$ | 2.38 | 24.45 | 49.27 | 79.86 | 133.91 |
| $n$-$C_3$ | 3.08 | 21.43 | 40.75 | 64.33 | 104.97 |
| $i$-$C_4$ | 1.71 | 3.78 | 6.78 | 10.67 | 20.56 |
| $n$-$C_4$ | 28.73 | 22.14 | 37.87 | 51.02 | 67.31 |
| $i$-$C_5$ | 16.60 | 20.93 | 28.50 | 34.99 | 45.61 |
| $n$-$C_5$ | 6.46 | 10.40 | 19.38 | 29.56 | 47.75 |
| $C_6$ | 21.59 | 39.61 | 70.71 | 86.02 | 106.29 |
| $C_7$ | 16.52 | 41.30 | 68.36 | 89.67 | 101.88 |
| $C_8$ | 31.09 | 55.04 | 79.00 | 101.64 | 112.22 |
| $C_9$ | 18.12 | 41.09 | 65.16 | 82.54 | 96.29 |
| $C_{10}$ | 10.03 | 28.29 | 45.41 | 58.38 | 69.43 |
| $C_{11}$ | 9.32 | 23.89 | 38.23 | 49.14 | 55.06 |
| $C_{12}$ | 7.02 | 20.86 | 35.24 | 43.75 | 44.28 |
| $C_{13}$ | 5.59 | 17.71 | 30.93 | 36.04 | 32.10 |
| $C_{14}$ | 3.25 | 10.63 | 18.75 | 20.43 | 15.58 |
| $C_{15}$ | 2.72 | 9.19 | 16.52 | 18.03 | 16.49 |
| $C_{16}$ | 1.84 | 6.53 | 11.30 | 11.51 | 9.42 |
| $C_{17}$ | 0.93 | 3.65 | 5.75 | 5.82 | 3.44 |
| $C_{18}$ | 1.07 | 3.26 | 4.82 | 3.69 | 1.82 |
| $C_{19}$ | 0.66 | 2.12 | 3.29 | 1.89 | 0.73 |
| $C_{20}$ | 0.46 | 1.28 | 2.51 | 1.12 | 0.49 |
| $C_{21}$ | 0.46 | 1.12 | 2.15 | 0.62 | 0.22 |
| $C_{22}$ | 0.27 | 0.65 | 1.56 | 0.33 | 0.11 |
| $C_{23}$ | 0.18 | 0.31 | 0.81 | 0.15 | 0.03 |
| $C_{24}$ | 0.12 | 0.21 | 0.56 | 0.09 | 0.02 |
| $C_{25}$ | 0.06 | 0.09 | 0.20 | 0.04 | 0.02 |
| $C_{26}$ | 0.07 | 0.06 | 0.15 | 0.03 | 0.02 |
| $C_{27}$ | 0.02 | 0.03 | 0.05 | 0.02 | 0.02 |
| $C_{28}$ | 0.04 | 0.02 | 0.02 | 0.02 | 0.03 |
| $C_{29}$ | 0.07 | 0.03 | 0.04 | 0.03 | 0.06 |
| $C_{30+}$ | 2.03 | 0.52 | 0.57 | 0.34 | 0.42 |

**Appendix 16. (Continued) MSSV individual compound yields of samples from the Vulcan Sub-basin**

| Formation/Sample ID | Upper Vulcan: 20110067 | | | | |
|---|---|---|---|---|---|
| Transformation ratio (%) | 10 | 30 | 50 | 70 | 90 |
| End Temperature (°C) | 357 | 389 | 406 | 420 | 442 |
| **Total (µg/g sample)** | | | | | |
| $C_6$ | 22.47 | 40.13 | 72.17 | 88.15 | 107.71 |
| $C_7$ | 19.14 | 42.61 | 71.63 | 93.41 | 104.76 |
| $C_8$ | 34.05 | 57.54 | 85.06 | 105.58 | 114.37 |
| $C_9$ | 21.46 | 45.59 | 74.10 | 90.03 | 99.47 |
| $C_{10}$ | 14.38 | 34.33 | 57.32 | 68.28 | 74.84 |
| $C_{11}$ | 14.57 | 31.55 | 51.94 | 60.96 | 62.01 |
| $C_{12}$ | 11.63 | 29.04 | 47.92 | 56.21 | 51.02 |
| $C_{13}$ | 10.47 | 26.92 | 44.73 | 49.51 | 39.33 |
| $C_{14}$ | 8.13 | 20.85 | 36.03 | 34.90 | 22.15 |
| $C_{15}$ | 7.19 | 19.91 | 33.86 | 30.97 | 22.62 |
| $C_{16}$ | 6.10 | 16.25 | 27.04 | 21.85 | 14.29 |
| $C_{17}$ | 4.89 | 11.60 | 20.14 | 13.91 | 7.17 |
| $C_{18}$ | 4.17 | 9.51 | 16.88 | 9.16 | 3.95 |
| $C_{19}$ | 3.87 | 7.81 | 14.07 | 6.00 | 2.29 |
| $C_{20}$ | 3.37 | 6.21 | 11.86 | 4.06 | 1.48 |
| $C_{21}$ | 3.13 | 4.96 | 10.23 | 2.84 | 0.95 |
| $C_{22}$ | 2.71 | 3.71 | 8.26 | 2.08 | 0.59 |
| $C_{23}$ | 2.38 | 2.77 | 6.07 | 1.53 | 0.34 |
| $C_{24}$ | 2.46 | 1.96 | 5.05 | 1.14 | 0.21 |
| $C_{25}$ | 2.17 | 1.14 | 3.13 | 0.63 | 0.13 |
| $C_{26}$ | 2.23 | 0.76 | 2.15 | 0.43 | 0.14 |
| $C_{27}$ | 2.30 | 0.49 | 1.41 | 0.35 | 0.17 |
| $C_{28}$ | 1.69 | 0.26 | 0.70 | 0.22 | 0.14 |
| $C_{29}$ | 2.57 | 0.31 | 0.80 | 0.32 | 0.22 |
| $C_{30+}$ | 40.27 | 1.94 | 8.16 | 6.54 | 4.82 |

**Appendix 16. (Continued) MSSV individual compound yields of samples from the Vulcan Sub-basin**

| Formation/Sample ID | Lower Vulcan: 20110044C | | | | |
|---|---|---|---|---|---|
| Transformation ratio (%) | 10 | 30 | 50 | 70 | 90 |
| End Temperature (°C) | 382 | 405 | 421 | 440 | 484 |
| **Resolved (µg/g sample)** | | | | | |
| $n\text{-}C_1 * 1.1$ | 352.44 | 1032.55 | 1956.78 | 3632.31 | 9993.21 |
| $n\text{-}C_2$ | 187.97 | 713.77 | 1441.23 | 2629.66 | 6221.55 |
| $n\text{-}C_3$ | 216.71 | 716.56 | 1398.37 | 2467.51 | 5901.99 |
| $i\text{-}C_4$ | 113.13 | 89.73 | 191.19 | 354.45 | 884.57 |
| $n\text{-}C_4$ | 144.30 | 365.88 | 707.94 | 1268.96 | 2969.41 |
| $i\text{-}C_5$ | 48.18 | 133.74 | 255.17 | 453.92 | 670.01 |
| $n\text{-}C_5$ | 49.84 | 181.87 | 383.00 | 737.04 | 1260.16 |
| $C_6$ | 229.46 | 521.91 | 930.24 | 1514.85 | 1317.33 |
| $C_7$ | 248.25 | 707.32 | 1231.72 | 1897.97 | 1608.37 |
| $C_8$ | 281.95 | 782.50 | 1367.80 | 2100.82 | 2217.95 |
| $C_9$ | 259.67 | 734.39 | 1298.91 | 1954.20 | 2229.90 |
| $C_{10}$ | 228.55 | 704.98 | 1238.97 | 1872.32 | 2298.59 |
| $C_{11}$ | 280.76 | 961.42 | 1680.36 | 2459.03 | 2704.62 |
| $C_{12}$ | 268.53 | 954.98 | 1593.89 | 2309.21 | 1914.03 |
| $C_{13}$ | 247.28 | 814.70 | 1292.40 | 1822.25 | 1531.09 |
| $C_{14}$ | 158.07 | 526.57 | 831.62 | 1049.33 | 633.19 |
| $C_{15}$ | 191.42 | 544.56 | 885.85 | 1069.68 | 902.91 |
| $C_{16}$ | 175.56 | 497.69 | 762.52 | 829.42 | 537.32 |
| $C_{17}$ | 103.98 | 337.28 | 519.48 | 520.45 | 351.28 |
| $C_{18}$ | 107.12 | 328.13 | 502.76 | 443.55 | 370.45 |
| $C_{19}$ | 93.68 | 270.28 | 451.25 | 356.95 | 398.36 |
| $C_{20}$ | 80.84 | 242.21 | 419.02 | 239.69 | 260.56 |
| $C_{21}$ | 84.57 | 256.32 | 407.87 | 172.92 | 280.17 |
| $C_{22}$ | 77.08 | 204.40 | 305.26 | 72.98 | 173.74 |
| $C_{23}$ | 68.27 | 198.48 | 298.70 | 43.37 | 206.75 |
| $C_{24}$ | 68.46 | 212.24 | 292.24 | 32.89 | 201.65 |
| $C_{25}$ | 53.35 | 168.46 | 209.69 | 18.54 | 140.20 |
| $C_{26}$ | 44.42 | 144.48 | 185.75 | 12.76 | 119.90 |
| $C_{27}$ | 35.53 | 120.83 | 162.02 | 8.36 | 60.05 |
| $C_{28}$ | 26.11 | 85.21 | 107.31 | 4.66 | 29.53 |
| $C_{29}$ | 16.96 | 57.16 | 61.79 | 2.87 | 15.39 |
| $C_{30+}$ | 45.44 | 125.17 | 156.26 | 8.36 | 21.21 |

**Appendix 16. (Continued) MSSV individual compound yields of samples from the Vulcan Sub-basin**

| Formation/Sample ID | Lower Vulcan: 20110044C | | | | |
|---|---|---|---|---|---|
| Transformation ratio (%) | 10 | 30 | 50 | 70 | 90 |
| End Temperature (°C) | 382 | 405 | 421 | 440 | 484 |
| Total (μg/g sample) | | | | | |
| $C_6$ | 232.53 | 523.86 | 932.36 | 1518.42 | 1321.65 |
| $C_7$ | 255.63 | 715.43 | 1239.99 | 1906.06 | 1610.28 |
| $C_8$ | 295.95 | 804.35 | 1393.75 | 2135.09 | 2232.68 |
| $C_9$ | 287.26 | 798.45 | 1385.32 | 2040.66 | 2250.72 |
| $C_{10}$ | 270.23 | 798.96 | 1402.24 | 2060.55 | 2325.13 |
| $C_{11}$ | 335.98 | 1079.25 | 1887.63 | 2706.41 | 2749.60 |
| $C_{12}$ | 338.14 | 1119.06 | 1877.41 | 2602.89 | 1984.57 |
| $C_{13}$ | 349.58 | 1087.99 | 1708.84 | 2217.69 | 1619.81 |
| $C_{14}$ | 299.02 | 920.79 | 1376.99 | 1551.23 | 743.24 |
| $C_{15}$ | 346.37 | 966.72 | 1481.22 | 1614.27 | 1028.02 |
| $C_{16}$ | 329.23 | 926.63 | 1377.23 | 1360.36 | 654.16 |
| $C_{17}$ | 271.77 | 785.86 | 1164.00 | 1024.44 | 471.32 |
| $C_{18}$ | 275.23 | 789.77 | 1167.70 | 896.68 | 505.52 |
| $C_{19}$ | 253.43 | 732.48 | 1084.07 | 729.61 | 549.24 |
| $C_{20}$ | 240.53 | 714.00 | 1040.86 | 544.99 | 440.94 |
| $C_{21}$ | 243.48 | 745.80 | 1072.38 | 424.01 | 489.94 |
| $C_{22}$ | 236.98 | 710.61 | 996.51 | 266.65 | 375.10 |
| $C_{23}$ | 223.31 | 690.00 | 938.68 | 175.55 | 418.33 |
| $C_{24}$ | 222.07 | 661.50 | 888.91 | 122.14 | 431.03 |
| $C_{25}$ | 208.66 | 632.88 | 802.43 | 88.99 | 378.62 |
| $C_{26}$ | 185.00 | 565.60 | 728.72 | 66.88 | 317.80 |
| $C_{27}$ | 172.24 | 535.24 | 678.25 | 55.03 | 210.95 |
| $C_{28}$ | 144.95 | 452.80 | 555.49 | 42.72 | 126.13 |
| $C_{29}$ | 123.86 | 387.69 | 459.47 | 35.90 | 73.12 |
| $C_{30+}$ | 608.15 | 1943.87 | 2214.17 | 376.13 | 233.19 |

**Appendix 16. (Continued) MSSV individual compound yields of samples from the Vulcan Sub-basin**

| Formation/Sample ID | Plover: 20110076 (shale) | | | | |
|---|---|---|---|---|---|
| Transformation ratio (%) | 10 | 30 | 50 | 70 | 90 |
| End Temperature (°C) | 373 | 396 | 415 | 430 | 441 |
| **Resolved (µg/g sample)** | | | | | |
| $n\text{-}C_1 * 1.1$ | 127.79 | 281.72 | 445.36 | 934.42 | 2256.31 |
| $n\text{-}C_2$ | 56.76 | 160.78 | 275.52 | 588.80 | 1222.58 |
| $n\text{-}C_3$ | 58.48 | 137.51 | 233.57 | 519.55 | 1108.99 |
| $i\text{-}C_4$ | 7.49 | 23.61 | 41.73 | 96.25 | 212.86 |
| $n\text{-}C_4$ | 33.68 | 76.75 | 124.63 | 272.76 | 582.38 |
| $i\text{-}C_5$ | 34.29 | 75.90 | 98.09 | 182.38 | 253.41 |
| $n\text{-}C_5$ | 12.70 | 35.09 | 64.15 | 159.78 | 303.02 |
| $C_6$ | 119.66 | 217.02 | 255.18 | 438.31 | 410.88 |
| $C_7$ | 78.23 | 167.96 | 235.81 | 455.56 | 418.79 |
| $C_8$ | 104.54 | 221.68 | 311.16 | 588.90 | 676.91 |
| $C_9$ | 95.52 | 200.39 | 284.24 | 515.95 | 588.88 |
| $C_{10}$ | 132.33 | 265.11 | 374.19 | 644.32 | 734.68 |
| $C_{11}$ | 180.27 | 355.99 | 533.98 | 893.27 | 829.91 |
| $C_{12}$ | 140.24 | 305.45 | 483.74 | 790.47 | 542.47 |
| $C_{13}$ | 94.07 | 207.86 | 328.62 | 540.85 | 349.08 |
| $C_{14}$ | 58.60 | 122.38 | 183.73 | 300.41 | 149.02 |
| $C_{15}$ | 69.10 | 136.49 | 188.99 | 292.59 | 208.50 |
| $C_{16}$ | 72.11 | 126.51 | 143.11 | 222.59 | 113.34 |
| $C_{17}$ | 33.23 | 68.51 | 90.92 | 139.60 | 50.60 |
| $C_{18}$ | 37.24 | 76.89 | 92.22 | 132.58 | 48.94 |
| $C_{19}$ | 27.26 | 59.52 | 71.81 | 108.91 | 42.82 |
| $C_{20}$ | 18.71 | 41.03 | 50.20 | 79.97 | 23.25 |
| $C_{21}$ | 19.82 | 39.70 | 51.18 | 76.16 | 19.93 |
| $C_{22}$ | 14.31 | 29.00 | 39.12 | 54.32 | 10.81 |
| $C_{23}$ | 13.52 | 25.77 | 34.54 | 48.66 | 8.73 |
| $C_{24}$ | 12.76 | 22.06 | 30.51 | 41.61 | 5.01 |
| $C_{25}$ | 9.85 | 14.54 | 23.12 | 29.20 | 2.29 |
| $C_{26}$ | 9.03 | 11.45 | 19.09 | 23.16 | 1.61 |
| $C_{27}$ | 9.41 | 8.83 | 17.16 | 18.49 | 0.75 |
| $C_{28}$ | 6.77 | 5.47 | 13.29 | 13.22 | 0.41 |
| $C_{29}$ | 3.98 | 4.18 | 8.58 | 7.53 | 0.47 |
| $C_{30+}$ | 12.18 | 17.02 | 14.78 | 9.71 | 1.08 |

| Formation/Sample ID | Plover: 20110076 (shale) | | | | |
|---|---|---|---|---|---|
| Transformation ratio (%) | 10 | 30 | 50 | 70 | 90 |
| End Temperature (°C) | 373 | 396 | 415 | 430 | 441 |
| Total (µg/g sample) | | | | | |
| $C_6$ | 120.26 | 217.84 | 256.06 | 438.95 | 411.33 |
| $C_7$ | 79.85 | 171.52 | 238.80 | 460.25 | 420.53 |
| $C_8$ | 108.56 | 231.34 | 320.87 | 601.16 | 681.16 |
| $C_9$ | 104.96 | 221.48 | 311.47 | 550.50 | 596.65 |
| $C_{10}$ | 148.03 | 299.23 | 411.05 | 702.78 | 748.51 |
| $C_{11}$ | 200.43 | 400.45 | 577.78 | 966.81 | 851.16 |
| $C_{12}$ | 166.24 | 365.28 | 538.91 | 879.40 | 569.95 |
| $C_{13}$ | 132.55 | 298.43 | 413.27 | 668.37 | 382.07 |
| $C_{14}$ | 110.05 | 247.00 | 308.17 | 473.95 | 185.91 |
| $C_{15}$ | 126.22 | 274.25 | 325.45 | 473.22 | 242.50 |
| $C_{16}$ | 129.16 | 257.36 | 270.08 | 387.32 | 143.01 |
| $C_{17}$ | 90.29 | 195.29 | 212.81 | 303.18 | 77.66 |
| $C_{18}$ | 93.80 | 197.70 | 210.45 | 286.58 | 73.98 |
| $C_{19}$ | 76.66 | 168.30 | 181.18 | 244.16 | 64.97 |
| $C_{20}$ | 65.52 | 143.53 | 152.20 | 202.21 | 45.19 |
| $C_{21}$ | 62.78 | 135.08 | 144.54 | 189.84 | 37.92 |
| $C_{22}$ | 54.00 | 116.34 | 123.44 | 155.91 | 24.55 |
| $C_{23}$ | 51.11 | 105.58 | 110.26 | 133.93 | 19.42 |
| $C_{24}$ | 46.30 | 93.60 | 96.03 | 113.24 | 13.57 |
| $C_{25}$ | 41.39 | 82.16 | 83.45 | 94.29 | 9.46 |
| $C_{26}$ | 36.34 | 70.68 | 71.42 | 77.06 | 6.53 |
| $C_{27}$ | 34.38 | 63.04 | 63.16 | 64.16 | 4.69 |
| $C_{28}$ | 28.43 | 50.45 | 49.98 | 47.86 | 2.95 |
| $C_{29}$ | 23.46 | 42.56 | 39.46 | 34.42 | 1.99 |
| $C_{30+}$ | 88.72 | 171.24 | 130.62 | 96.44 | 10.58 |

**Appendix 16. (Continued) MSSV individual compound yields of samples from the Vulcan Sub-basin**

| Formation/Sample ID | Plover: 20110076C (coal) | | | | |
|---|---|---|---|---|---|
| Transformation ratio (%) | 10 | 30 | 50 | 70 | 90 |
| End Temperature (°C) | 368 | 393 | 410 | 432 | 479 |
| **Resolved (µg/g sample)** | | | | | |
| $n$-$C_1$ * 1.1 | 512.47 | 1363.34 | 2025.68 | 3793.11 | 10316.56 |
| $n$-$C_2$ | 187.07 | 661.84 | 1066.74 | 2108.09 | 4656.01 |
| $n$-$C_3$ | 139.17 | 443.39 | 796.74 | 1666.51 | 3693.48 |
| $i$-$C_4$ | 44.04 | 11.69 | 168.70 | 348.28 | 697.05 |
| $n$-$C_4$ | 112.28 | 64.58 | 369.68 | 787.02 | 1681.74 |
| $i$-$C_5$ | 105.78 | 227.67 | 296.59 | 505.79 | 626.35 |
| $n$-$C_5$ | 26.20 | 92.71 | 175.26 | 409.57 | 734.78 |
| $C_6$ | 849.06 | 1009.83 | 957.22 | 1190.46 | 851.60 |
| $C_7$ | 183.97 | 414.43 | 614.80 | 1066.94 | 1007.95 |
| $C_8$ | 296.16 | 587.79 | 859.00 | 1433.11 | 1944.28 |
| $C_9$ | 224.56 | 544.16 | 835.52 | 1363.57 | 2128.48 |
| $C_{10}$ | 747.70 | 2120.87 | 2352.66 | 3770.41 | 5283.08 |
| $C_{11}$ | 1261.68 | 3535.14 | 4224.04 | 6288.02 | 6506.47 |
| $C_{12}$ | 744.48 | 2308.11 | 3058.25 | 4498.70 | 3409.94 |
| $C_{13}$ | 463.47 | 1382.91 | 1938.20 | 2829.22 | 1650.80 |
| $C_{14}$ | 200.43 | 583.75 | 801.32 | 1133.97 | 502.44 |
| $C_{15}$ | 186.61 | 463.80 | 653.30 | 962.28 | 701.28 |
| $C_{16}$ | 165.81 | 404.61 | 495.45 | 746.00 | 435.90 |
| $C_{17}$ | 115.66 | 335.03 | 395.97 | 626.74 | 358.31 |
| $C_{18}$ | 123.17 | 411.37 | 456.84 | 751.03 | 404.87 |
| $C_{19}$ | 94.77 | 322.81 | 328.02 | 629.76 | 319.43 |
| $C_{20}$ | 55.77 | 185.84 | 168.42 | 339.52 | 142.83 |
| $C_{21}$ | 50.94 | 185.05 | 144.68 | 315.48 | 123.92 |
| $C_{22}$ | 27.72 | 114.55 | 84.39 | 228.79 | 69.17 |
| $C_{23}$ | 30.28 | 100.56 | 70.17 | 203.27 | 66.32 |
| $C_{24}$ | 24.17 | 69.34 | 45.45 | 144.37 | 42.74 |
| $C_{25}$ | 15.38 | 42.24 | 24.14 | 87.26 | 23.34 |
| $C_{26}$ | 11.78 | 36.94 | 20.51 | 74.99 | 17.03 |
| $C_{27}$ | 12.30 | 30.06 | 16.79 | 49.49 | 6.52 |
| $C_{28}$ | 7.33 | 21.96 | 12.94 | 30.96 | 3.99 |
| $C_{29}$ | 4.16 | 18.10 | 8.83 | 25.24 | 3.75 |
| $C_{30+}$ | 18.36 | 39.40 | 16.09 | 45.49 | 7.56 |

| Formation/Sample ID | Plover: 20110076C (coal) | | | | |
|---|---|---|---|---|---|
| Transformation ratio (%) | 10 | 30 | 50 | 70 | 90 |
| End Temperature (°C) | 368 | 393 | 410 | 432 | 479 |
| Total (µg/g sample) | | | | | |
| $C_6$ | 851.07 | 1029.39 | 958.75 | 1191.25 | 852.98 |
| $C_7$ | 194.39 | 476.88 | 621.77 | 1076.21 | 1011.58 |
| $C_8$ | 316.74 | 686.19 | 879.94 | 1461.46 | 1955.42 |
| $C_9$ | 255.10 | 668.61 | 903.75 | 1456.45 | 2148.44 |
| $C_{10}$ | 790.49 | 2263.54 | 2468.73 | 3936.22 | 5317.51 |
| $C_{11}$ | 1318.77 | 3712.72 | 4363.76 | 6503.71 | 6570.36 |
| $C_{12}$ | 816.92 | 2541.53 | 3268.28 | 4799.53 | 3530.81 |
| $C_{13}$ | 570.66 | 1648.18 | 2239.13 | 3195.53 | 1807.86 |
| $C_{14}$ | 340.77 | 907.05 | 1171.36 | 1615.67 | 636.34 |
| $C_{15}$ | 353.36 | 851.99 | 1104.34 | 1517.11 | 821.76 |
| $C_{16}$ | 337.62 | 793.26 | 963.93 | 1278.94 | 557.93 |
| $C_{17}$ | 286.81 | 740.05 | 873.57 | 1163.50 | 486.37 |
| $C_{18}$ | 286.74 | 854.94 | 945.87 | 1337.03 | 550.92 |
| $C_{19}$ | 247.67 | 759.41 | 790.84 | 1233.75 | 479.32 |
| $C_{20}$ | 203.73 | 615.43 | 585.82 | 967.34 | 298.60 |
| $C_{21}$ | 195.95 | 604.56 | 512.93 | 931.08 | 263.87 |
| $C_{22}$ | 167.54 | 525.23 | 398.41 | 799.82 | 187.77 |
| $C_{23}$ | 149.40 | 462.71 | 314.07 | 721.34 | 154.53 |
| $C_{24}$ | 126.78 | 390.67 | 246.84 | 610.36 | 118.60 |
| $C_{25}$ | 107.73 | 337.44 | 196.94 | 519.58 | 88.02 |
| $C_{26}$ | 90.56 | 297.71 | 159.32 | 451.45 | 66.34 |
| $C_{27}$ | 81.40 | 265.11 | 132.41 | 385.93 | 46.33 |
| $C_{28}$ | 63.64 | 214.37 | 100.63 | 295.04 | 31.24 |
| $C_{29}$ | 51.00 | 181.87 | 78.28 | 225.90 | 20.54 |
| $C_{30+}$ | 184.15 | 880.51 | 381.49 | 756.97 | 122.79 |

**Appendix 17. MSSV individual compound yields of samples from the Laminaria High**

| Formation/Sample ID | Echuca Shoals: 20110013 | | | | |
|---|---|---|---|---|---|
| Transformation ratio (%) | 10 | 30 | 50 | 70 | 90 |
| End Temperature (°C) | 379 | 401 | 414 | 427 | 450 |
| **Resolved (µg/g sample)** | | | | | |
| $n\text{-}C_1 * 1.1$ | 88.46 | 149.05 | 317.00 | 458.03 | 740.43 |
| $n\text{-}C_2$ | 39.48 | 85.22 | 170.00 | 248.00 | 356.14 |
| $n\text{-}C_3$ | 35.46 | 77.64 | 149.73 | 211.12 | 299.12 |
| $i\text{-}C_4$ | 191.05 | 35.08 | 56.90 | 65.48 | 81.60 |
| $n\text{-}C_4$ | 339.58 | 99.99 | 114.76 | 121.86 | 162.42 |
| $i\text{-}C_5$ | 14.75 | 31.85 | 50.32 | 67.97 | 87.24 |
| $n\text{-}C_5$ | 9.23 | 25.46 | 43.51 | 65.73 | 92.39 |
| $C_6$ | 101.20 | 159.14 | 277.05 | 279.11 | 217.07 |
| $C_7$ | 43.10 | 86.10 | 116.60 | 152.01 | 138.87 |
| $C_8$ | 55.33 | 103.53 | 144.04 | 164.25 | 138.12 |
| $C_9$ | 37.89 | 85.22 | 112.65 | 140.38 | 133.20 |
| $C_{10}$ | 28.30 | 69.02 | 96.28 | 120.00 | 109.23 |
| $C_{11}$ | 21.83 | 53.51 | 75.86 | 95.31 | 76.61 |
| $C_{12}$ | 24.13 | 59.22 | 90.55 | 112.25 | 74.30 |
| $C_{13}$ | 19.05 | 47.34 | 71.02 | 83.61 | 39.69 |
| $C_{14}$ | 11.04 | 27.91 | 41.75 | 48.13 | 13.79 |
| $C_{15}$ | 8.70 | 20.54 | 34.11 | 40.04 | 15.72 |
| $C_{16}$ | 5.65 | 13.67 | 24.72 | 31.51 | 9.42 |
| $C_{17}$ | 3.39 | 8.37 | 17.00 | 20.69 | 2.62 |
| $C_{18}$ | 2.15 | 4.25 | 9.52 | 10.15 | 1.43 |
| $C_{19}$ | 1.05 | 1.36 | 5.03 | 4.81 | 0.72 |
| $C_{20}$ | 0.36 | 0.40 | 1.71 | 1.89 | 0.42 |
| $C_{21}$ | 0.27 | 0.34 | 1.22 | 1.41 | 0.51 |
| $C_{22}$ | 0.18 | 0.15 | 0.53 | 0.53 | 0.49 |
| $C_{23}$ | 0.09 | 0.02 | 0.11 | 0.15 | 0.23 |
| $C_{24}$ | 0.04 | 0.03 | 0.07 | 0.11 | 0.20 |
| $C_{25}$ | 0.02 | 0.02 | 0.03 | 0.05 | 0.09 |
| $C_{26}$ | 0.02 | 0.02 | 0.02 | 0.03 | 0.03 |
| $C_{27}$ | 0.02 | 0.02 | 0.02 | 0.02 | 0.02 |
| $C_{28}$ | 0.01 | 0.02 | 0.01 | 0.02 | 0.02 |
| $C_{29}$ | 0.02 | 0.02 | 0.02 | 0.02 | 0.02 |
| $C_{30+}$ | 0.26 | 0.27 | 0.36 | 0.36 | 0.43 |

**Appendix 17. (Continued) MSSV individual compound yields of samples from the Laminaria High**

| Formation/Sample ID | Echuca Shoals: 20110013 | | | | |
|---|---|---|---|---|---|
| Transformation ratio (%) | 10 | 30 | 50 | 70 | 90 |
| End Temperature (°C) | 379 | 401 | 414 | 427 | 450 |
| **Total (µg/g sample)** | | | | | |
| $C_6$ | 105.61 | 160.93 | 280.14 | 280.63 | 219.74 |
| $C_7$ | 47.54 | 89.95 | 124.08 | 158.08 | 144.11 |
| $C_8$ | 61.43 | 109.61 | 149.91 | 170.02 | 142.21 |
| $C_9$ | 45.81 | 94.98 | 122.58 | 150.61 | 138.65 |
| $C_{10}$ | 39.04 | 83.08 | 112.74 | 135.47 | 117.90 |
| $C_{11}$ | 33.10 | 70.32 | 94.89 | 113.16 | 86.70 |
| $C_{12}$ | 33.66 | 75.43 | 110.91 | 131.23 | 82.85 |
| $C_{13}$ | 28.53 | 65.35 | 94.06 | 106.08 | 48.09 |
| $C_{14}$ | 21.28 | 48.45 | 68.99 | 74.45 | 21.92 |
| $C_{15}$ | 18.26 | 40.49 | 61.06 | 65.63 | 22.16 |
| $C_{16}$ | 13.73 | 30.22 | 46.84 | 52.63 | 14.41 |
| $C_{17}$ | 9.63 | 21.07 | 35.65 | 37.96 | 6.77 |
| $C_{18}$ | 6.85 | 14.23 | 24.93 | 23.73 | 3.72 |
| $C_{19}$ | 4.73 | 8.18 | 17.24 | 15.38 | 2.67 |
| $C_{20}$ | 3.17 | 4.69 | 10.33 | 8.82 | 1.85 |
| $C_{21}$ | 2.61 | 2.79 | 6.86 | 5.83 | 1.69 |
| $C_{22}$ | 2.23 | 1.51 | 3.99 | 3.21 | 1.46 |
| $C_{23}$ | 1.68 | 0.76 | 2.00 | 1.51 | 0.87 |
| $C_{24}$ | 1.08 | 0.38 | 0.99 | 0.79 | 0.65 |
| $C_{25}$ | 0.57 | 0.21 | 0.48 | 0.44 | 0.45 |
| $C_{26}$ | 0.30 | 0.16 | 0.29 | 0.31 | 0.37 |
| $C_{27}$ | 0.19 | 0.15 | 0.22 | 0.26 | 0.36 |
| $C_{28}$ | 0.11 | 0.10 | 0.14 | 0.17 | 0.25 |
| $C_{29}$ | 0.14 | 0.15 | 0.20 | 0.24 | 0.39 |
| $C_{30+}$ | 2.14 | 3.00 | 4.14 | 4.42 | 7.88 |

| Formation/Sample ID | Frigate: 20110021 | | | | |
|---|---|---|---|---|---|
| Transformation ratio (%) | 10 | 30 | 50 | 70 | 90 |
| End Temperature (°C) | 321 | 370 | 396 | 415 | 441 |
| **Resolved (µg/g sample)** | | | | | |
| $n$-$C_1$ * 1.1 | 6.93 | 34.53 | 80.32 | 197.76 | 349.16 |
| $n$-$C_2$ | 11.94 | 42.29 | 81.21 | 156.09 | 313.15 |
| $n$-$C_3$ | 9.21 | 38.27 | 82.26 | 160.04 | 328.80 |
| $i$-$C_4$ | 1.19 | 4.35 | 11.54 | 27.72 | 70.18 |
| $n$-$C_4$ | 129.76 | 83.17 | 95.87 | 154.96 | 265.84 |
| $i$-$C_5$ | 63.65 | 67.00 | 77.11 | 101.28 | 146.37 |
| $n$-$C_5$ | 16.42 | 33.65 | 63.71 | 108.81 | 200.15 |
| $C_6$ | 57.79 | 121.89 | 173.65 | 294.42 | 409.09 |
| $C_7$ | 56.90 | 138.18 | 198.84 | 317.09 | 403.75 |
| $C_8$ | 58.32 | 142.29 | 202.84 | 279.57 | 350.20 |
| $C_9$ | 54.30 | 128.13 | 169.65 | 242.78 | 302.30 |
| $C_{10}$ | 43.68 | 104.96 | 139.15 | 198.28 | 245.67 |
| $C_{11}$ | 42.05 | 95.38 | 127.82 | 170.53 | 196.57 |
| $C_{12}$ | 36.31 | 85.23 | 112.12 | 146.33 | 163.26 |
| $C_{13}$ | 27.11 | 67.25 | 98.77 | 120.65 | 129.92 |
| $C_{14}$ | 21.78 | 56.97 | 78.48 | 80.70 | 75.32 |
| $C_{15}$ | 16.72 | 51.33 | 69.05 | 65.70 | 61.98 |
| $C_{16}$ | 25.90 | 66.56 | 67.31 | 48.60 | 39.47 |
| $C_{17}$ | 13.58 | 43.42 | 45.49 | 32.85 | 21.93 |
| $C_{18}$ | 17.08 | 46.40 | 44.93 | 21.71 | 11.08 |
| $C_{19}$ | 7.14 | 18.67 | 21.37 | 7.84 | 4.20 |
| $C_{20}$ | 2.48 | 15.68 | 17.31 | 2.82 | 2.36 |
| $C_{21}$ | 0.93 | 6.65 | 9.74 | 1.09 | 1.63 |
| $C_{22}$ | 0.50 | 2.95 | 6.50 | 0.61 | 0.75 |
| $C_{23}$ | 0.33 | 3.32 | 5.12 | 0.23 | 0.28 |
| $C_{24}$ | 0.11 | 1.65 | 3.33 | 0.15 | 0.17 |
| $C_{25}$ | 0.10 | 0.73 | 1.86 | 0.23 | 0.08 |
| $C_{26}$ | 0.03 | 0.51 | 1.63 | 0.06 | 0.02 |
| $C_{27}$ | 0.05 | 0.30 | 1.00 | 0.04 | 0.02 |
| $C_{28}$ | 0.05 | 0.12 | 0.24 | 0.02 | 0.02 |
| $C_{29}$ | 0.03 | 0.20 | 0.52 | 0.06 | 0.04 |
| $C_{30+}$ | 0.68 | 0.99 | 1.40 | 0.37 | 0.40 |

**Appendix 17. (Continued) MSSV individual compound yields of samples from the Laminaria High**

| Formation/Sample ID | Frigate: 20110021 | | | | |
|---|---|---|---|---|---|
| Transformation ratio (%) | 10 | 30 | 50 | 70 | 90 |
| End Temperature (°C) | 321 | 370 | 396 | 415 | 441 |
| **Total (µg/g sample)** | | | | | |
| $C_6$ | 62.90 | 125.29 | 178.10 | 298.88 | 416.77 |
| $C_7$ | 65.22 | 149.21 | 210.66 | 330.42 | 417.46 |
| $C_8$ | 68.42 | 157.27 | 216.99 | 291.87 | 360.18 |
| $C_9$ | 65.09 | 146.72 | 188.21 | 260.88 | 314.92 |
| $C_{10}$ | 55.71 | 128.54 | 162.58 | 226.88 | 264.48 |
| $C_{11}$ | 54.66 | 122.20 | 155.95 | 203.99 | 219.74 |
| $C_{12}$ | 49.05 | 113.38 | 143.52 | 181.11 | 187.72 |
| $C_{13}$ | 39.80 | 96.04 | 132.67 | 155.92 | 155.65 |
| $C_{14}$ | 34.01 | 87.81 | 118.93 | 120.75 | 103.57 |
| $C_{15}$ | 29.68 | 87.81 | 116.61 | 109.69 | 88.26 |
| $C_{16}$ | 40.66 | 111.27 | 119.88 | 88.37 | 61.66 |
| $C_{17}$ | 28.52 | 92.80 | 98.64 | 67.55 | 40.99 |
| $C_{18}$ | 30.97 | 92.10 | 94.52 | 49.58 | 24.82 |
| $C_{19}$ | 18.28 | 57.17 | 64.72 | 27.45 | 12.69 |
| $C_{20}$ | 10.44 | 49.49 | 55.12 | 14.19 | 7.56 |
| $C_{21}$ | 7.09 | 35.18 | 42.61 | 7.56 | 5.25 |
| $C_{22}$ | 5.40 | 26.48 | 34.94 | 4.19 | 3.33 |
| $C_{23}$ | 3.68 | 25.47 | 29.56 | 2.35 | 1.76 |
| $C_{24}$ | 3.01 | 19.88 | 25.20 | 1.56 | 1.05 |
| $C_{25}$ | 2.60 | 15.84 | 20.52 | 1.16 | 0.65 |
| $C_{26}$ | 2.34 | 12.73 | 16.97 | 0.69 | 0.44 |
| $C_{27}$ | 2.33 | 10.13 | 13.67 | 0.50 | 0.35 |
| $C_{28}$ | 1.57 | 5.46 | 7.37 | 0.27 | 0.20 |
| $C_{29}$ | 2.25 | 6.20 | 8.68 | 0.34 | 0.27 |
| $C_{30+}$ | 37.51 | 35.08 | 33.94 | 3.06 | 3.47 |

**Appendix 17. (Continued) MSSV individual compound yields of samples from the Laminaria High**

| Formation/Sample ID | Laminaria: 20110008 | | | | |
|---|---|---|---|---|---|
| Transformation ratio (%) | 10 | 30 | 50 | 70 | 90 |
| End Temperature (°C) | 331 | 380 | 402 | 420 | 448 |
| **Resolved (µg/g sample)** | | | | | |
| $n$-$C_1$ * 1.1 | 7.73 | 54.47 | 153.91 | 253.51 | 352.89 |
| $n$-$C_2$ | 12.09 | 46.24 | 97.15 | 167.78 | 284.77 |
| $n$-$C_3$ | 11.48 | 48.70 | 112.04 | 189.78 | 298.41 |
| $i$-$C_4$ | 27.64 | 6.32 | 27.57 | 51.48 | 88.17 |
| $n$-$C_4$ | 279.27 | 152.17 | 149.75 | 135.80 | 235.13 |
| $i$-$C_5$ | 14.39 | 29.85 | 52.06 | 86.91 | 153.51 |
| $n$-$C_5$ | 6.93 | 25.50 | 47.75 | 80.22 | 144.01 |
| $C_6$ | 52.42 | 120.44 | 218.85 | 291.16 | 309.74 |
| $C_7$ | 54.03 | 128.60 | 185.09 | 252.49 | 300.82 |
| $C_8$ | 55.29 | 127.72 | 178.72 | 230.20 | 228.59 |
| $C_9$ | 57.97 | 121.34 | 157.27 | 199.39 | 216.23 |
| $C_{10}$ | 44.13 | 98.64 | 127.09 | 163.62 | 175.40 |
| $C_{11}$ | 37.41 | 87.49 | 111.88 | 141.70 | 140.85 |
| $C_{12}$ | 35.09 | 80.17 | 112.10 | 146.63 | 115.82 |
| $C_{13}$ | 25.89 | 62.22 | 86.39 | 117.00 | 82.44 |
| $C_{14}$ | 24.34 | 46.79 | 57.96 | 72.21 | 46.45 |
| $C_{15}$ | 18.89 | 39.25 | 50.08 | 70.49 | 50.08 |
| $C_{16}$ | 34.96 | 45.45 | 47.49 | 72.64 | 36.87 |
| $C_{17}$ | 18.16 | 27.99 | 29.90 | 39.09 | 20.21 |
| $C_{18}$ | 25.78 | 27.96 | 19.83 | 25.38 | 12.80 |
| $C_{19}$ | 8.77 | 15.41 | 11.99 | 19.67 | 10.44 |
| $C_{20}$ | 8.01 | 11.03 | 4.93 | 11.55 | 8.20 |
| $C_{21}$ | 3.72 | 7.58 | 3.85 | 9.95 | 8.39 |
| $C_{22}$ | 1.95 | 4.77 | 2.42 | 8.56 | 5.75 |
| $C_{23}$ | 1.15 | 3.51 | 1.01 | 5.17 | 2.71 |
| $C_{24}$ | 0.90 | 2.96 | 0.51 | 3.72 | 2.36 |
| $C_{25}$ | 0.67 | 2.05 | 0.35 | 2.60 | 1.23 |
| $C_{26}$ | 0.51 | 1.66 | 0.17 | 1.69 | 0.60 |
| $C_{27}$ | 0.27 | 1.18 | 0.05 | 1.25 | 0.24 |
| $C_{28}$ | 0.24 | 0.82 | 0.03 | 0.66 | 0.14 |
| $C_{29}$ | 0.22 | 0.75 | 0.06 | 0.64 | 0.08 |
| $C_{30+}$ | 1.08 | 2.32 | 1.11 | 1.06 | 0.70 |

| Formation/Sample ID | Laminaria: 20110008 | | | | |
|---|---|---|---|---|---|
| Transformation ratio (%) | 10 | 30 | 50 | 70 | 90 |
| End Temperature (°C) | 331 | 380 | 402 | 420 | 448 |
| **Total (µg/g sample)** | | | | | |
| $C_6$ | 53.63 | 122.84 | 220.31 | 293.03 | 313.54 |
| $C_7$ | 57.80 | 134.70 | 187.69 | 255.98 | 303.51 |
| $C_8$ | 60.22 | 137.48 | 183.53 | 238.28 | 234.87 |
| $C_9$ | 65.08 | 139.76 | 169.80 | 217.01 | 227.73 |
| $C_{10}$ | 52.14 | 123.90 | 148.34 | 190.21 | 188.78 |
| $C_{11}$ | 46.15 | 111.30 | 136.14 | 172.36 | 153.75 |
| $C_{12}$ | 44.91 | 110.19 | 142.89 | 181.05 | 130.61 |
| $C_{13}$ | 35.35 | 95.08 | 122.08 | 155.68 | 100.42 |
| $C_{14}$ | 34.95 | 83.64 | 99.72 | 128.53 | 64.05 |
| $C_{15}$ | 31.36 | 82.59 | 97.09 | 133.31 | 65.96 |
| $C_{16}$ | 50.48 | 90.38 | 92.01 | 127.48 | 52.27 |
| $C_{17}$ | 35.74 | 73.52 | 66.99 | 88.76 | 34.45 |
| $C_{18}$ | 42.90 | 73.23 | 52.37 | 70.55 | 24.62 |
| $C_{19}$ | 23.92 | 54.14 | 36.52 | 56.57 | 20.03 |
| $C_{20}$ | 21.04 | 45.94 | 24.12 | 43.15 | 16.19 |
| $C_{21}$ | 14.90 | 39.23 | 17.80 | 38.09 | 15.83 |
| $C_{22}$ | 11.95 | 33.47 | 12.18 | 34.18 | 12.91 |
| $C_{23}$ | 10.12 | 29.46 | 7.95 | 28.84 | 9.31 |
| $C_{24}$ | 9.35 | 27.86 | 5.40 | 25.88 | 8.60 |
| $C_{25}$ | 7.95 | 24.07 | 3.34 | 21.41 | 6.66 |
| $C_{26}$ | 6.85 | 20.84 | 2.15 | 17.18 | 5.35 |
| $C_{27}$ | 6.20 | 18.89 | 1.70 | 14.18 | 4.43 |
| $C_{28}$ | 5.97 | 16.50 | 2.20 | 11.15 | 4.39 |
| $C_{29}$ | 5.05 | 13.99 | 1.77 | 7.98 | 3.58 |
| $C_{30+}$ | 94.04 | 135.73 | 34.40 | 41.92 | 78.38 |

**Appendix 18. MSSV individual compound yields of samples from the Gippsland Basin**

| Biozone/Sample ID | *L. balmei*: 20110126 | | | | |
|---|---|---|---|---|---|
| Transformation ratio (%) | 10 | 30 | 50 | 70 | 90 |
| End Temperature (°C) | 385 | 409 | 425 | 445 | 493 |
| **Resolved (µg/g sample)** | | | | | |
| $n\text{-}C_1 * 1.1$ | 165.93 | 381.18 | 753.12 | 1237.68 | 2749.99 |
| $n\text{-}C_2$ | 82.00 | 225.98 | 504.08 | 802.37 | 1373.02 |
| $n\text{-}C_3$ | 90.09 | 224.44 | 458.75 | 713.15 | 1068.70 |
| $i\text{-}C_4$ | 10.70 | 32.23 | 73.88 | 124.16 | 199.70 |
| $n\text{-}C_4$ | 55.02 | 121.14 | 242.82 | 387.31 | 394.60 |
| $i\text{-}C_5$ | 28.60 | 54.95 | 106.60 | 163.57 | 75.93 |
| $n\text{-}C_5$ | 24.48 | 62.60 | 142.76 | 233.64 | 66.91 |
| $C_6$ | 67.25 | 154.88 | 289.08 | 407.06 | 52.79 |
| $C_7$ | 95.64 | 202.22 | 374.42 | 487.08 | 143.57 |
| $C_8$ | 118.13 | 232.40 | 417.87 | 544.80 | 412.52 |
| $C_9$ | 97.37 | 206.28 | 388.07 | 517.76 | 415.64 |
| $C_{10}$ | 83.71 | 192.25 | 375.58 | 477.03 | 327.05 |
| $C_{11}$ | 93.33 | 234.80 | 464.41 | 530.86 | 223.64 |
| $C_{12}$ | 81.23 | 217.21 | 441.34 | 451.05 | 151.20 |
| $C_{13}$ | 72.78 | 191.54 | 371.30 | 371.59 | 184.16 |
| $C_{14}$ | 59.93 | 141.54 | 267.74 | 243.38 | 101.85 |
| $C_{15}$ | 52.85 | 121.72 | 204.76 | 235.08 | 71.68 |
| $C_{16}$ | 53.59 | 109.25 | 197.01 | 171.40 | 45.16 |
| $C_{17}$ | 28.43 | 65.51 | 117.80 | 103.48 | 29.28 |
| $C_{18}$ | 29.43 | 63.83 | 105.29 | 80.81 | 44.10 |
| $C_{19}$ | 28.14 | 61.47 | 117.46 | 83.70 | 37.63 |
| $C_{20}$ | 17.24 | 41.39 | 83.59 | 56.97 | 16.98 |
| $C_{21}$ | 19.18 | 47.15 | 81.62 | 57.48 | 18.77 |
| $C_{22}$ | 15.75 | 41.09 | 63.33 | 37.58 | 11.71 |
| $C_{23}$ | 12.63 | 39.03 | 60.09 | 29.57 | 9.95 |
| $C_{24}$ | 12.33 | 39.91 | 64.04 | 26.55 | 9.26 |
| $C_{25}$ | 7.12 | 29.20 | 44.67 | 14.53 | 5.40 |
| $C_{26}$ | 4.86 | 24.55 | 34.43 | 9.62 | 3.86 |
| $C_{27}$ | 2.63 | 18.73 | 25.40 | 6.18 | 1.72 |
| $C_{28}$ | 1.46 | 15.59 | 22.28 | 4.27 | 2.05 |
| $C_{29}$ | 1.13 | 12.04 | 17.71 | 3.37 | 1.95 |
| $C_{30+}$ | 6.38 | 20.81 | 33.69 | 11.03 | 7.56 |

**Appendix 18. (Continued) MSSV individual compound yields of samples from the Gippsland Basin**

| Biozone/Sample ID | _L. balmei_: 20110126 | | | | |
|---|---|---|---|---|---|
| Transformation ratio (%) | 10 | 30 | 50 | 70 | 90 |
| End Temperature (°C) | 385 | 409 | 425 | 445 | 493 |
| **Total (µg/g sample)** | | | | | |
| $C_6$ | 67.96 | 156.11 | 295.43 | 411.51 | 57.63 |
| $C_7$ | 100.32 | 207.58 | 383.76 | 484.90 | 146.59 |
| $C_8$ | 125.85 | 247.96 | 435.24 | 558.78 | 416.86 |
| $C_9$ | 112.31 | 232.49 | 423.87 | 551.24 | 420.96 |
| $C_{10}$ | 106.48 | 232.19 | 428.97 | 527.00 | 335.19 |
| $C_{11}$ | 118.46 | 283.14 | 528.66 | 595.96 | 234.75 |
| $C_{12}$ | 110.23 | 278.21 | 526.63 | 542.80 | 164.11 |
| $C_{13}$ | 111.54 | 268.10 | 487.70 | 477.92 | 197.37 |
| $C_{14}$ | 113.64 | 252.90 | 437.42 | 368.24 | 117.48 |
| $C_{15}$ | 110.02 | 233.73 | 366.41 | 351.86 | 86.72 |
| $C_{16}$ | 105.27 | 213.19 | 344.39 | 269.79 | 62.22 |
| $C_{17}$ | 78.95 | 174.19 | 284.31 | 202.87 | 42.30 |
| $C_{18}$ | 75.04 | 168.09 | 268.60 | 178.75 | 57.86 |
| $C_{19}$ | 67.25 | 155.54 | 252.95 | 168.38 | 52.42 |
| $C_{20}$ | 54.32 | 131.38 | 213.36 | 136.33 | 32.60 |
| $C_{21}$ | 53.66 | 131.10 | 212.79 | 130.55 | 32.99 |
| $C_{22}$ | 46.15 | 118.40 | 188.89 | 99.80 | 24.25 |
| $C_{23}$ | 39.23 | 107.43 | 169.28 | 79.01 | 20.05 |
| $C_{24}$ | 34.58 | 100.56 | 155.99 | 66.91 | 17.70 |
| $C_{25}$ | 27.13 | 87.60 | 134.16 | 52.10 | 14.00 |
| $C_{26}$ | 21.05 | 76.32 | 116.35 | 41.33 | 11.34 |
| $C_{27}$ | 15.23 | 63.60 | 96.54 | 30.58 | 7.37 |
| $C_{28}$ | 11.39 | 54.70 | 81.76 | 23.56 | 5.23 |
| $C_{29}$ | 7.92 | 42.07 | 61.74 | 16.63 | 3.31 |
| $C_{30+}$ | 26.24 | 104.20 | 167.36 | 88.91 | 1.07 |

**Appendix 18. (Continued) MSSV individual compound yields of samples from the Gippsland Basin**

| Biozone/Sample ID | *F. longus*: 20110034 | | | | |
|---|---|---|---|---|---|
| Transformation ratio (%) | 10 | 30 | 50 | 70 | 90 |
| End Temperature (°C) | 374 | 397 | 411 | 425 | 453 |
| **Resolved (µg/g sample)** | | | | | |
| $n$-$C_1$ * 1.1 | 36.37 | 93.71 | 150.81 | 240.55 | 570.73 |
| $n$-$C_2$ | 23.46 | 65.32 | 111.52 | 185.04 | 437.78 |
| $n$-$C_3$ | 31.12 | 75.27 | 122.52 | 194.95 | 452.99 |
| $i$-$C_4$ | 5.63 | 14.40 | 22.49 | 33.80 | 75.35 |
| $n$-$C_4$ | 20.85 | 45.17 | 69.39 | 111.28 | 273.71 |
| $i$-$C_5$ | 14.37 | 25.28 | 34.40 | 46.83 | 95.84 |
| $n$-$C_5$ | 7.74 | 24.23 | 42.75 | 73.63 | 186.03 |
| $C_6$ | 28.25 | 65.07 | 105.83 | 167.48 | 321.83 |
| $C_7$ | 41.19 | 94.40 | 139.57 | 207.97 | 353.27 |
| $C_8$ | 46.37 | 102.08 | 147.85 | 217.01 | 395.13 |
| $C_9$ | 43.66 | 97.78 | 141.66 | 210.66 | 359.54 |
| $C_{10}$ | 40.95 | 93.20 | 136.93 | 203.64 | 315.75 |
| $C_{11}$ | 39.89 | 100.38 | 148.67 | 225.73 | 318.32 |
| $C_{12}$ | 34.32 | 88.10 | 138.01 | 210.44 | 278.72 |
| $C_{13}$ | 31.31 | 76.44 | 121.43 | 182.86 | 215.70 |
| $C_{14}$ | 24.37 | 60.90 | 89.28 | 143.27 | 139.66 |
| $C_{15}$ | 21.97 | 58.72 | 83.45 | 121.52 | 115.40 |
| $C_{16}$ | 26.53 | 61.29 | 84.06 | 115.46 | 97.08 |
| $C_{17}$ | 16.94 | 40.77 | 57.37 | 84.53 | 55.80 |
| $C_{18}$ | 13.87 | 37.06 | 52.05 | 72.66 | 40.54 |
| $C_{19}$ | 11.51 | 33.54 | 50.94 | 67.80 | 39.21 |
| $C_{20}$ | 8.20 | 26.45 | 43.57 | 56.40 | 24.95 |
| $C_{21}$ | 9.92 | 29.38 | 43.09 | 55.72 | 26.01 |
| $C_{22}$ | 9.65 | 30.46 | 44.38 | 55.53 | 17.78 |
| $C_{23}$ | 8.00 | 29.52 | 42.81 | 53.58 | 12.74 |
| $C_{24}$ | 8.04 | 30.71 | 43.00 | 52.58 | 9.47 |
| $C_{25}$ | 6.38 | 28.52 | 38.01 | 45.04 | 4.95 |
| $C_{26}$ | 4.70 | 27.88 | 35.03 | 38.43 | 4.03 |
| $C_{27}$ | 2.72 | 26.23 | 31.74 | 32.87 | 3.29 |
| $C_{28}$ | 1.01 | 18.62 | 22.96 | 23.35 | 2.37 |
| $C_{29}$ | 0.43 | 13.25 | 19.67 | 18.02 | 1.30 |
| $C_{30+}$ | 3.07 | 18.78 | 23.95 | 22.63 | 2.61 |

**Appendix 18. (Continued) MSSV individual compound yields of samples from the Gippsland Basin**

| Biozone/Sample ID | *F. longus*: 20110034 | | | | |
|---|---|---|---|---|---|
| Transformation ratio (%) | 10 | 30 | 50 | 70 | 90 |
| End Temperature (°C) | 374 | 397 | 411 | 425 | 453 |
| **Total (µg/g sample)** | | | | | |
| $C_6$ | 30.42 | 69.51 | 110.51 | 173.33 | 325.80 |
| $C_7$ | 44.52 | 100.56 | 146.77 | 215.82 | 361.13 |
| $C_8$ | 50.12 | 109.49 | 158.80 | 229.23 | 399.31 |
| $C_9$ | 51.46 | 109.88 | 159.28 | 233.25 | 379.85 |
| $C_{10}$ | 50.82 | 113.54 | 161.98 | 233.66 | 346.19 |
| $C_{11}$ | 50.89 | 121.94 | 174.86 | 255.06 | 351.67 |
| $C_{12}$ | 47.40 | 113.93 | 171.06 | 252.56 | 316.15 |
| $C_{13}$ | 47.03 | 110.30 | 164.74 | 236.81 | 262.90 |
| $C_{14}$ | 45.47 | 109.06 | 153.07 | 221.68 | 210.05 |
| $C_{15}$ | 44.72 | 111.53 | 147.06 | 198.79 | 173.31 |
| $C_{16}$ | 45.14 | 107.03 | 137.89 | 181.48 | 144.23 |
| $C_{17}$ | 37.42 | 87.67 | 119.55 | 157.29 | 104.22 |
| $C_{18}$ | 33.90 | 83.48 | 115.15 | 148.21 | 86.48 |
| $C_{19}$ | 28.33 | 75.41 | 106.00 | 136.41 | 76.90 |
| $C_{20}$ | 23.23 | 65.92 | 95.04 | 121.27 | 58.36 |
| $C_{21}$ | 23.22 | 67.29 | 92.22 | 118.44 | 55.69 |
| $C_{22}$ | 21.38 | 64.30 | 86.13 | 108.35 | 41.41 |
| $C_{23}$ | 19.34 | 61.04 | 80.47 | 100.45 | 32.57 |
| $C_{24}$ | 17.99 | 60.02 | 77.10 | 94.96 | 27.22 |
| $C_{25}$ | 15.33 | 56.65 | 70.88 | 86.05 | 21.29 |
| $C_{26}$ | 12.17 | 53.75 | 64.48 | 75.83 | 16.95 |
| $C_{27}$ | 8.89 | 50.60 | 58.41 | 66.58 | 13.53 |
| $C_{28}$ | 5.98 | 41.38 | 48.11 | 53.69 | 9.69 |
| $C_{29}$ | 3.97 | 30.91 | 39.07 | 41.57 | 6.67 |
| $C_{30+}$ | 30.49 | 90.36 | 103.52 | 107.79 | 36.53 |

Appendix 18. (Continued) MSSV individual compound yields of samples from the Gippsland Basin

| Biozone/Sample ID | F. longus: 20110149 | | | | |
|---|---|---|---|---|---|
| Transformation ratio (%) | 10 | 30 | 50 | 70 | 90 |
| End Temperature (°C) | 375 | 399 | 415 | 433 | 481 |
| **Resolved (µg/g sample)** | | | | | |
| $n\text{-}C_1$ * 1.1 | 185.26 | 486.36 | 807.34 | 1396.05 | 3564.78 |
| $n\text{-}C_2$ | 79.41 | 257.52 | 493.66 | 898.87 | 2120.89 |
| $n\text{-}C_3$ | 94.47 | 269.22 | 469.54 | 851.46 | 1808.94 |
| $i\text{-}C_4$ | 10.91 | 42.77 | 78.97 | 138.57 | 290.88 |
| $n\text{-}C_4$ | 63.28 | 138.95 | 250.38 | 471.22 | 922.93 |
| $i\text{-}C_5$ | 50.90 | 113.39 | 160.79 | 236.18 | 287.94 |
| $n\text{-}C_5$ | 24.93 | 82.17 | 160.30 | 314.50 | 486.82 |
| $C_6$ | 87.36 | 214.65 | 335.37 | 645.96 | 564.37 |
| $C_7$ | 108.10 | 274.91 | 445.64 | 642.59 | 584.31 |
| $C_8$ | 127.88 | 305.98 | 479.15 | 741.73 | 763.35 |
| $C_9$ | 107.78 | 285.07 | 449.75 | 711.17 | 764.94 |
| $C_{10}$ | 126.01 | 345.57 | 536.67 | 809.65 | 748.81 |
| $C_{11}$ | 150.00 | 415.33 | 683.80 | 1020.83 | 739.62 |
| $C_{12}$ | 115.66 | 342.27 | 603.91 | 928.39 | 467.97 |
| $C_{13}$ | 92.23 | 265.80 | 473.51 | 719.72 | 333.04 |
| $C_{14}$ | 69.75 | 170.93 | 311.07 | 455.62 | 154.50 |
| $C_{15}$ | 83.19 | 190.47 | 335.71 | 425.19 | 186.18 |
| $C_{16}$ | 98.25 | 194.09 | 279.07 | 372.43 | 119.07 |
| $C_{17}$ | 51.40 | 111.81 | 184.62 | 250.88 | 68.68 |
| $C_{18}$ | 56.75 | 121.65 | 202.65 | 252.26 | 60.03 |
| $C_{19}$ | 41.73 | 105.39 | 179.75 | 223.89 | 56.37 |
| $C_{20}$ | 38.02 | 93.52 | 171.29 | 193.68 | 34.15 |
| $C_{21}$ | 40.71 | 98.32 | 148.96 | 191.77 | 38.85 |
| $C_{22}$ | 40.41 | 92.57 | 147.71 | 163.51 | 21.17 |
| $C_{23}$ | 42.52 | 88.57 | 147.84 | 148.67 | 20.67 |
| $C_{24}$ | 41.92 | 84.11 | 137.58 | 127.38 | 17.81 |
| $C_{25}$ | 39.83 | 74.41 | 117.93 | 101.32 | 10.24 |
| $C_{26}$ | 33.44 | 59.79 | 95.25 | 75.13 | 6.98 |
| $C_{27}$ | 31.03 | 52.43 | 84.08 | 56.25 | 3.60 |
| $C_{28}$ | 23.42 | 40.01 | 66.60 | 37.96 | 3.17 |
| $C_{29}$ | 19.76 | 32.76 | 74.05 | 27.16 | 2.58 |
| $C_{30+}$ | 45.30 | 62.98 | 117.08 | 44.91 | 6.03 |

**Appendix 18. (Continued) MSSV individual compound yields of samples from the Gippsland Basin**

| Biozone/Sample ID | *F. longus*: 20110149 | | | | |
|---|---|---|---|---|---|
| Transformation ratio (%) | 10 | 30 | 50 | 70 | 90 |
| End Temperature (°C) | 375 | 399 | 415 | 433 | 481 |
| Total (µg/g sample) | | | | | |
| $C_6$ | 92.13 | 222.51 | 347.94 | 658.09 | 575.90 |
| $C_7$ | 117.13 | 285.79 | 459.86 | 663.65 | 598.44 |
| $C_8$ | 142.76 | 326.43 | 504.25 | 789.98 | 781.65 |
| $C_9$ | 128.30 | 319.59 | 497.02 | 782.29 | 784.06 |
| $C_{10}$ | 155.09 | 399.30 | 612.80 | 904.97 | 779.76 |
| $C_{11}$ | 180.97 | 485.74 | 769.96 | 1128.37 | 778.61 |
| $C_{12}$ | 153.63 | 439.72 | 734.34 | 1065.06 | 518.21 |
| $C_{13}$ | 142.88 | 385.86 | 645.42 | 906.65 | 377.06 |
| $C_{14}$ | 141.22 | 350.65 | 550.18 | 738.68 | 193.74 |
| $C_{15}$ | 155.25 | 364.09 | 560.65 | 684.25 | 232.63 |
| $C_{16}$ | 170.93 | 343.25 | 491.21 | 605.49 | 154.88 |
| $C_{17}$ | 133.46 | 270.43 | 418.47 | 509.12 | 104.81 |
| $C_{18}$ | 132.21 | 270.48 | 423.84 | 482.76 | 94.13 |
| $C_{19}$ | 108.05 | 233.89 | 377.20 | 425.47 | 91.01 |
| $C_{20}$ | 100.32 | 212.64 | 373.41 | 380.27 | 68.67 |
| $C_{21}$ | 101.34 | 213.13 | 348.28 | 372.68 | 71.49 |
| $C_{22}$ | 95.80 | 201.50 | 324.37 | 332.06 | 52.53 |
| $C_{23}$ | 94.07 | 192.34 | 307.61 | 297.61 | 53.45 |
| $C_{24}$ | 90.13 | 176.11 | 281.11 | 254.66 | 49.58 |
| $C_{25}$ | 86.35 | 160.46 | 255.77 | 215.83 | 40.85 |
| $C_{26}$ | 76.60 | 137.85 | 220.89 | 173.91 | 32.36 |
| $C_{27}$ | 71.58 | 121.72 | 194.19 | 141.46 | 23.48 |
| $C_{28}$ | 62.59 | 102.45 | 166.41 | 110.72 | 18.62 |
| $C_{29}$ | 54.61 | 84.41 | 159.71 | 83.00 | 13.86 |
| $C_{30+}$ | 279.63 | 346.83 | 568.51 | 316.81 | 67.90 |

**Appendix 18. (Continued) MSSV individual compound yields of samples from the Gippsland Basin**

| Biozone/Sample ID | *P. mawsonii*: 20110275 | | | | |
|---|---|---|---|---|---|
| Transformation ratio (%) | 10 | 30 | 50 | 70 | 90 |
| End Temperature (°C) | 370 | 395 | 409 | 424 | 447 |
| **Resolved (µg/g sample)** | | | | | |
| $n\text{-}C_1 * 1.1$ | 44.90 | 110.49 | 197.02 | 330.53 | 701.62 |
| $n\text{-}C_2$ | 30.46 | 82.84 | 153.05 | 270.15 | 587.64 |
| $n\text{-}C_3$ | 36.78 | 101.47 | 187.35 | 317.02 | 674.50 |
| $i\text{-}C_4$ | 3.86 | 14.15 | 32.35 | 57.49 | 128.70 |
| $n\text{-}C_4$ | 33.20 | 77.03 | 125.77 | 199.28 | 416.26 |
| $i\text{-}C_5$ | 15.60 | 27.44 | 46.44 | 72.86 | 152.53 |
| $n\text{-}C_5$ | 15.09 | 39.09 | 71.26 | 124.19 | 270.75 |
| $C_6$ | 45.20 | 101.71 | 164.85 | 278.47 | 532.59 |
| $C_7$ | 56.50 | 140.82 | 246.61 | 375.27 | 674.06 |
| $C_8$ | 56.22 | 147.55 | 252.19 | 386.97 | 702.84 |
| $C_9$ | 53.90 | 147.26 | 250.05 | 383.93 | 632.08 |
| $C_{10}$ | 45.35 | 120.95 | 208.76 | 312.12 | 530.14 |
| $C_{11}$ | 42.71 | 108.24 | 184.90 | 287.80 | 493.18 |
| $C_{12}$ | 36.31 | 102.21 | 185.84 | 292.57 | 485.26 |
| $C_{13}$ | 33.69 | 103.18 | 181.65 | 296.59 | 493.51 |
| $C_{14}$ | 27.43 | 86.15 | 144.09 | 240.68 | 379.64 |
| $C_{15}$ | 26.33 | 74.33 | 117.26 | 191.88 | 252.99 |
| $C_{16}$ | 25.73 | 70.50 | 113.11 | 169.50 | 249.04 |
| $C_{17}$ | 14.51 | 42.62 | 72.99 | 111.72 | 157.37 |
| $C_{18}$ | 13.08 | 40.05 | 67.14 | 110.73 | 138.59 |
| $C_{19}$ | 12.13 | 39.87 | 67.44 | 110.35 | 147.06 |
| $C_{20}$ | 8.47 | 29.53 | 47.91 | 84.32 | 98.37 |
| $C_{21}$ | 9.68 | 32.00 | 61.34 | 80.64 | 108.15 |
| $C_{22}$ | 8.94 | 30.68 | 53.53 | 80.16 | 96.25 |
| $C_{23}$ | 6.96 | 25.40 | 45.65 | 69.51 | 73.83 |
| $C_{24}$ | 6.06 | 24.35 | 42.99 | 63.05 | 73.41 |
| $C_{25}$ | 4.37 | 19.42 | 32.81 | 48.39 | 52.77 |
| $C_{26}$ | 3.31 | 15.50 | 26.44 | 35.93 | 35.94 |
| $C_{27}$ | 3.11 | 13.48 | 21.82 | 30.98 | 27.45 |
| $C_{28}$ | 2.67 | 12.28 | 22.15 | 32.91 | 25.49 |
| $C_{29}$ | 2.98 | 13.89 | 23.17 | 44.70 | 22.67 |
| $C_{30+}$ | 11.05 | 38.08 | 80.18 | 123.58 | 80.70 |

**Appendix 18. (Continued) MSSV individual compound yields of samples from the Gippsland Basin**

| Biozone/Sample ID | *P. mawsonii*: 20110275 | | | | |
|---|---|---|---|---|---|
| Transformation ratio (%) | 10 | 30 | 50 | 70 | 90 |
| End Temperature (°C) | 370 | 395 | 409 | 424 | 447 |
| **Total (µg/g sample)** | | | | | |
| $C_6$ | 48.17 | 106.09 | 174.89 | 287.86 | 541.12 |
| $C_7$ | 61.84 | 147.61 | 252.66 | 386.98 | 683.34 |
| $C_8$ | 65.20 | 159.47 | 266.46 | 404.23 | 716.02 |
| $C_9$ | 67.29 | 171.80 | 285.90 | 431.45 | 693.30 |
| $C_{10}$ | 64.76 | 162.74 | 268.31 | 395.52 | 618.35 |
| $C_{11}$ | 63.51 | 158.35 | 262.02 | 388.69 | 604.53 |
| $C_{12}$ | 60.24 | 156.27 | 269.83 | 405.13 | 627.57 |
| $C_{13}$ | 61.18 | 160.85 | 277.02 | 417.44 | 641.14 |
| $C_{14}$ | 61.21 | 167.46 | 290.40 | 418.53 | 591.89 |
| $C_{15}$ | 62.33 | 170.13 | 285.02 | 379.23 | 475.47 |
| $C_{16}$ | 61.51 | 162.98 | 254.25 | 351.87 | 435.68 |
| $C_{17}$ | 50.93 | 134.27 | 222.86 | 311.59 | 362.60 |
| $C_{18}$ | 48.39 | 132.10 | 219.80 | 310.83 | 336.31 |
| $C_{19}$ | 46.80 | 132.59 | 216.85 | 303.37 | 328.33 |
| $C_{20}$ | 41.68 | 121.07 | 192.92 | 278.18 | 270.93 |
| $C_{21}$ | 40.93 | 122.87 | 196.92 | 270.11 | 268.20 |
| $C_{22}$ | 37.95 | 116.47 | 186.04 | 252.56 | 236.02 |
| $C_{23}$ | 34.85 | 109.07 | 175.33 | 235.00 | 201.71 |
| $C_{24}$ | 31.82 | 104.30 | 168.82 | 225.63 | 186.09 |
| $C_{25}$ | 29.74 | 99.76 | 161.52 | 212.64 | 167.34 |
| $C_{26}$ | 26.80 | 92.38 | 149.81 | 194.74 | 147.13 |
| $C_{27}$ | 24.87 | 87.89 | 142.94 | 183.43 | 131.28 |
| $C_{28}$ | 23.60 | 85.77 | 140.65 | 182.24 | 121.65 |
| $C_{29}$ | 21.45 | 77.66 | 128.18 | 176.64 | 102.91 |
| $C_{30+}$ | 151.40 | 507.36 | 1087.60 | 1229.63 | 590.28 |

**Appendix 19. MSSV boiling ranges in pyrolysates from the Vulcan Sub-basin**

| Formation/Sample ID | Upper Vulcan: 20110067 | | | | |
|---|---|---|---|---|---|
| Transformation ratio (%) | 10 | 30 | 50 | 70 | 90 |
| End Temperature (°C) | 357 | 389 | 406 | 420 | 442 |
| *TOC (%): 1.08 | | | | | |
| Range (mg/g sample) | | | | | |
| $n$-C$_1$ * 1.1 | 0.01 | 0.04 | 0.09 | 0.11 | 0.18 |
| C$_1$-C$_5$ Total | 0.06 | 0.14 | 0.27 | 0.38 | 0.60 |
| C$_2$-C$_5$ Total | 0.06 | 0.10 | 0.18 | 0.27 | 0.42 |
| C$_6$-C$_{14}$ Total | 0.16 | 0.33 | 0.54 | 0.65 | 0.68 |
| C$_{15+}$ Total | 0.09 | 0.09 | 0.17 | 0.10 | 0.06 |
| Range (mg/g TOC) | | | | | |
| $n$-C$_1$ * 1.1 | 0.54 | 3.61 | 7.92 | 10.31 | 17.06 |
| C$_1$-C$_5$ Total | 6.00 | 13.16 | 24.83 | 35.35 | 55.96 |
| C$_2$-C$_5$ Total | 5.46 | 9.55 | 16.90 | 25.04 | 38.90 |
| C$_6$-C$_{14}$ Total | 14.47 | 30.42 | 50.08 | 59.91 | 62.56 |
| C$_{15+}$ Total | 8.47 | 8.30 | 15.72 | 9.45 | 5.51 |
| Gas:oil ratio (C$_1$-C$_5$/C$_{6+}$) | 0.26 | 0.34 | 0.38 | 0.51 | 0.82 |
| Gas wetness (C$_2$-C$_5$/C$_1$-C$_5$) | 0.91 | 0.73 | 0.68 | 0.71 | 0.70 |

**Appendix 19. (Continued) MSSV boiling ranges in pyrolysates from the Vulcan Sub-basin**

| Formation/Sample ID | Lower Vulcan: 20110044C | | | | |
|---|---|---|---|---|---|
| Transformation ratio (%) | 10 | 30 | 50 | 70 | 90 |
| End Temperature (°C) | 382 | 405 | 421 | 440 | 484 |
| *TOC (%): 20.80 | | | | | |
| Range (mg/g sample) | | | | | |
| $n$-C$_1$ * 1.1 | 0.35 | 1.03 | 1.96 | 3.63 | 9.99 |
| C$_1$-C$_5$ Total | 1.11 | 3.23 | 6.33 | 11.54 | 27.90 |
| C$_2$-C$_5$ Total | 0.76 | 2.20 | 4.38 | 7.91 | 17.91 |
| C$_6$-C$_{14}$ Total | 2.66 | 7.85 | 13.20 | 18.74 | 16.84 |
| C$_{15+}$ Total | 4.09 | 12.24 | 16.65 | 7.82 | 6.70 |
| Range (mg/g TOC) | | | | | |
| $n$-C$_1$ * 1.1 | 1.69 | 4.96 | 9.41 | 17.46 | 48.04 |
| C$_1$-C$_5$ Total | 5.35 | 15.55 | 30.45 | 55.50 | 134.14 |
| C$_2$-C$_5$ Total | 3.65 | 10.58 | 21.04 | 38.04 | 86.09 |
| C$_6$-C$_{14}$ Total | 12.81 | 37.73 | 63.48 | 90.09 | 80.95 |
| C$_{15+}$ Total | 19.64 | 58.85 | 80.05 | 37.62 | 32.23 |
| Gas:oil ratio (C$_1$-C$_5$/C$_{6+}$) | 0.16 | 0.16 | 0.21 | 0.43 | 1.19 |
| Gas wetness (C$_2$-C$_5$/C$_1$-C$_5$) | 0.68 | 0.68 | 0.69 | 0.69 | 0.64 |

*TOC: TOC measured on solvent extracted sample

**Appendix 19. (Continued) MSSV boiling ranges in pyrolysates from the Vulcan Sub-basin**

| Formation/Sample ID | Plover: 20110076 (shale) | | | | |
|---|---|---|---|---|---|
| Transformation ratio (%) | 10 | 30 | 50 | 70 | 90 |
| End Temperature (°C) | 373 | 396 | 415 | 430 | 441 |
| *TOC (%): 10.90 | | | | | |
| Range (mg/g sample) | | | | | |
| $n$-C$_1$ * 1.1 | 0.13 | 0.28 | 0.45 | 0.93 | 2.26 |
| C$_1$-C$_5$ Total | 0.33 | 0.79 | 1.28 | 2.75 | 5.94 |
| C$_2$-C$_5$ Total | 0.20 | 0.51 | 0.84 | 1.82 | 3.68 |
| C$_6$-C$_{14}$ Total | 1.17 | 2.45 | 3.38 | 5.74 | 4.85 |
| C$_{15+}$ Total | 1.05 | 2.17 | 2.26 | 2.90 | 0.78 |
| Range (mg/g TOC) | | | | | |
| $n$-C$_1$ * 1.1 | 1.17 | 2.58 | 4.09 | 8.57 | 20.70 |
| C$_1$-C$_5$ Total | 3.04 | 7.26 | 11.77 | 25.27 | 54.49 |
| C$_2$-C$_5$ Total | 1.87 | 4.68 | 7.69 | 16.69 | 33.79 |
| C$_6$-C$_{14}$ Total | 10.74 | 22.50 | 30.98 | 52.68 | 44.47 |
| C$_{15+}$ Total | 9.62 | 19.88 | 20.78 | 26.64 | 7.15 |
| Gas:oil ratio (C$_1$-C$_5$/C$_{6+}$) | 0.15 | 0.17 | 0.23 | 0.32 | 1.06 |
| Gas wetness (C$_2$-C$_5$/C$_1$-C$_5$) | 0.61 | 0.64 | 0.65 | 0.66 | 0.62 |

**Appendix 19. (Continued) MSSV boiling ranges in pyrolysates from the Vulcan Sub-basin**

| Formation/Sample ID | Plover: 20110076C (coal) | | | | |
|---|---|---|---|---|---|
| Transformation ratio (%) | 10 | 30 | 50 | 70 | 90 |
| End Temperature (°C) | 368 | 393 | 410 | 432 | 479 |
| *TOC (%): 31.90 | | | | | |
| Range (mg/g sample) | | | | | |
| $n$-C$_1$ * 1.1 | 0.51 | 1.36 | 2.03 | 3.79 | 10.32 |
| C$_1$-C$_5$ Total | 1.13 | 2.87 | 4.90 | 9.62 | 22.41 |
| C$_2$-C$_5$ Total | 0.61 | 1.50 | 2.87 | 5.83 | 12.09 |
| C$_6$-C$_{14}$ Total | 5.45 | 13.93 | 16.88 | 25.24 | 23.83 |
| C$_{15+}$ Total | 2.93 | 8.78 | 7.79 | 13.20 | 4.29 |
| Range (mg/g TOC) | | | | | |
| $n$-C$_1$ * 1.1 | 1.61 | 4.27 | 6.35 | 11.89 | 32.34 |
| C$_1$-C$_5$ Total | 3.53 | 8.98 | 15.36 | 30.15 | 70.24 |
| C$_2$-C$_5$ Total | 1.93 | 4.71 | 9.01 | 18.26 | 37.90 |
| C$_6$-C$_{14}$ Total | 17.10 | 43.68 | 52.90 | 79.11 | 74.71 |
| C$_{15+}$ Total | 9.20 | 27.51 | 24.41 | 41.36 | 13.46 |
| Gas:oil ratio (C$_1$-C$_5$/C$_{6+}$) | 0.13 | 0.13 | 0.20 | 0.25 | 0.80 |
| Gas wetness (C$_2$-C$_5$/C$_1$-C$_5$) | 0.55 | 0.52 | 0.59 | 0.61 | 0.54 |

**\*TOC:** TOC measured on solvent extracted sample

**Appendix 20. MSSV boiling ranges in pyrolysates from the Laminaria High**

| Formation/Sample ID | Echuca Shoals: 20110013 | | | | |
|---|---|---|---|---|---|
| Transformation ratio (%) | 10 | 30 | 50 | 70 | 90 |
| End Temperature (°C) | 379 | 401 | 414 | 427 | 450 |
| *TOC (%): 1.89 | | | | | |
| Range (mg/g sample) | | | | | |
| $n$-$C_1$ * 1.1 | 0.09 | 0.15 | 0.32 | 0.46 | 0.74 |
| $C_1$-$C_5$ Total | 0.72 | 0.50 | 0.90 | 1.24 | 1.82 |
| $C_2$-$C_5$ Total | 0.63 | 0.36 | 0.59 | 0.78 | 1.08 |
| $C_6$-$C_{14}$ Total | 0.42 | 0.80 | 1.16 | 1.32 | 1.00 |
| $C_{15+}$ Total | 0.07 | 0.13 | 0.22 | 0.22 | 0.07 |
| Range (mg/g TOC) | | | | | |
| $n$-$C_1$ * 1.1 | 4.68 | 7.89 | 16.77 | 24.23 | 39.18 |
| $C_1$-$C_5$ Total | 37.99 | 26.68 | 47.74 | 65.51 | 96.26 |
| $C_2$-$C_5$ Total | 33.31 | 18.80 | 30.96 | 41.28 | 57.09 |
| $C_6$-$C_{14}$ Total | 22.01 | 42.23 | 61.29 | 69.83 | 53.02 |
| $C_{15+}$ Total | 3.57 | 6.78 | 11.39 | 11.71 | 3.49 |
| Gas:oil ratio ($C_1$-$C_5$/$C_{6+}$) | 1.49 | 0.54 | 0.66 | 0.80 | 1.70 |
| Gas wetness ($C_2$-$C_5$/$C_1$-$C_5$) | 0.88 | 0.70 | 0.65 | 0.63 | 0.59 |

**Appendix 20. (Continued) MSSV boiling ranges in pyrolysates from the Laminaria High**

| Formation/Sample ID | Frigate: 20110021 | | | | |
|---|---|---|---|---|---|
| Transformation ratio (%) | 10 | 30 | 50 | 70 | 90 |
| End Temperature (°C) | 321 | 370 | 396 | 415 | 441 |
| *TOC (%): 2.07 | | | | | |
| Range (mg/g sample) | | | | | |
| $n$-$C_1$ * 1.1 | 0.01 | 0.03 | 0.08 | 0.20 | 0.35 |
| $C_1$-$C_5$ Total | 0.24 | 0.30 | 0.49 | 0.91 | 1.67 |
| $C_2$-$C_5$ Total | 0.23 | 0.27 | 0.41 | 0.71 | 1.32 |
| $C_6$-$C_{14}$ Total | 0.49 | 1.13 | 1.51 | 2.07 | 2.44 |
| $C_{15+}$ Total | 0.23 | 0.68 | 0.78 | 0.38 | 0.25 |
| Range (mg/g TOC) | | | | | |
| $n$-$C_1$ * 1.1 | 0.33 | 1.67 | 3.88 | 9.55 | 16.87 |
| $C_1$-$C_5$ Total | 11.55 | 14.65 | 23.77 | 43.80 | 80.85 |
| $C_2$-$C_5$ Total | 11.22 | 12.98 | 19.89 | 34.25 | 63.99 |
| $C_6$-$C_{14}$ Total | 23.91 | 54.42 | 72.83 | 100.03 | 117.90 |
| $C_{15+}$ Total | 10.93 | 33.00 | 37.82 | 18.28 | 12.21 |
| Gas:oil ratio ($C_1$-$C_5$/$C_{6+}$) | 0.33 | 0.17 | 0.21 | 0.37 | 0.62 |
| Gas wetness ($C_2$-$C_5$/$C_1$-$C_5$) | 0.97 | 0.89 | 0.84 | 0.78 | 0.79 |

*TOC: TOC measured on solvent extracted sample

**Appendix 20. (Continued) MSSV boiling ranges in pyrolysates from the Laminaria High**

| Formation/Sample ID | Laminaria: 20110008 | | | | |
|---|---|---|---|---|---|
| Transformation ratio (%) | 10 | 30 | 50 | 70 | 90 |
| End Temperature (°C) | 331 | 380 | 402 | 420 | 448 |
| **\*TOC (%): 1.56** | | | | | |
| **Range (mg/g sample)** | | | | | |
| $n$-$C_1$ * 1.1 | 0.01 | 0.05 | 0.15 | 0.25 | 0.35 |
| $C_1$-$C_5$ Total | 0.36 | 0.36 | 0.64 | 0.97 | 1.56 |
| $C_2$-$C_5$ Total | 0.35 | 0.31 | 0.49 | 0.71 | 1.20 |
| $C_6$-$C_{14}$ Total | 0.45 | 1.06 | 1.41 | 1.83 | 1.72 |
| $C_{15+}$ Total | 0.38 | 0.78 | 0.46 | 0.76 | 0.36 |
| **Range (mg/g TOC)** | | | | | |
| $n$-$C_1$ * 1.1 | 0.50 | 3.49 | 9.87 | 16.25 | 22.62 |
| $C_1$-$C_5$ Total | 23.05 | 23.28 | 41.04 | 61.89 | 99.80 |
| $C_2$-$C_5$ Total | 22.55 | 19.79 | 31.17 | 45.64 | 77.18 |
| $C_6$-$C_{14}$ Total | 28.86 | 67.88 | 90.42 | 117.44 | 110.08 |
| $C_{15+}$ Total | 24.22 | 49.99 | 29.36 | 48.76 | 23.27 |
| **Gas:oil ratio ($C_1$-$C_5$/$C_{6+}$)** | 0.43 | 0.20 | 0.34 | 0.37 | 0.75 |
| **Gas wetness ($C_2$-$C_5$/$C_1$-$C_5$)** | 0.98 | 0.85 | 0.76 | 0.74 | 0.77 |

**\*TOC:** TOC measured on solvent extracted sample

**Appendix 21. MSSV boiling ranges in pyrolysates from the Gippsland Basin**

| Biozone/Sample ID | *L. balmei*: 20110126 | | | | |
|---|---|---|---|---|---|
| Transformation ratio (%) | 10 | 30 | 50 | 70 | 90 |
| End Temperature (°C) | 385 | 409 | 425 | 445 | 493 |
| **TOC (%): 13.84** | | | | | |
| **Range (mg/g sample)** | | | | | |
| *n*-$C_1$ * 1.1 | 0.17 | 0.38 | 0.75 | 1.24 | 2.75 |
| $C_1$-$C_5$ Total | 0.46 | 1.10 | 2.28 | 3.66 | 5.93 |
| $C_2$-$C_5$ Total | 0.29 | 0.72 | 1.53 | 2.42 | 3.18 |
| $C_6$-$C_{14}$ Total | 0.97 | 2.16 | 3.95 | 4.52 | 2.09 |
| $C_{15+}$ Total | 0.77 | 1.96 | 3.11 | 1.94 | 0.47 |
| **Range (mg/g TOC)** | | | | | |
| *n*-$C_1$ * 1.1 | 1.20 | 2.75 | 5.44 | 8.94 | 19.87 |
| $C_1$-$C_5$ Total | 3.30 | 7.97 | 16.49 | 26.46 | 42.84 |
| $C_2$-$C_5$ Total | 2.10 | 5.21 | 11.05 | 17.52 | 22.97 |
| $C_6$-$C_{14}$ Total | 6.99 | 15.60 | 28.52 | 32.65 | 15.11 |
| $C_{15+}$ Total | 5.59 | 14.18 | 22.51 | 14.00 | 3.41 |
| **Gas:oil ratio ($C_1$-$C_5$/$C_{6+}$)** | 0.26 | 0.27 | 0.32 | 0.57 | 2.31 |
| **Gas wetness ($C_2$-$C_5$/$C_1$-$C_5$)** | 0.64 | 0.65 | 0.67 | 0.66 | 0.54 |

**Appendix 21. (Continued) MSSV boiling ranges in pyrolysates from the Gippsland Basin**

| Biozone/Sample ID | *F. longus*: 20110034 | | | | |
|---|---|---|---|---|---|
| Transformation ratio (%) | 10 | 30 | 50 | 70 | 90 |
| End Temperature (°C) | 374 | 397 | 411 | 425 | 453 |
| **TOC (%): 4.02** | | | | | |
| **Range (mg/g sample)** | | | | | |
| *n*-$C_1$ * 1.1 | 0.04 | 0.09 | 0.15 | 0.24 | 0.57 |
| $C_1$-$C_5$ Total | 0.14 | 0.34 | 0.55 | 0.89 | 2.09 |
| $C_2$-$C_5$ Total | 0.10 | 0.25 | 0.40 | 0.65 | 1.52 |
| $C_6$-$C_{14}$ Total | 0.42 | 0.96 | 1.40 | 2.05 | 2.95 |
| $C_{15+}$ Total | 0.37 | 1.11 | 1.44 | 1.80 | 0.91 |
| **Range (mg/g TOC)** | | | | | |
| *n*-$C_1$ * 1.1 | 0.90 | 2.33 | 3.75 | 5.98 | 14.20 |
| $C_1$-$C_5$ Total | 3.47 | 8.54 | 13.78 | 22.04 | 52.05 |
| $C_2$-$C_5$ Total | 2.57 | 6.21 | 10.03 | 16.06 | 37.85 |
| $C_6$-$C_{14}$ Total | 10.40 | 23.84 | 34.85 | 51.03 | 73.46 |
| $C_{15+}$ Total | 9.24 | 27.55 | 35.85 | 44.71 | 22.51 |
| **Gas:oil ratio ($C_1$-$C_5$/$C_{6+}$)** | 0.18 | 0.17 | 0.19 | 0.23 | 0.54 |
| **Gas wetness ($C_2$-$C_5$/$C_1$-$C_5$)** | 0.74 | 0.73 | 0.73 | 0.73 | 0.73 |

**Appendix 21. (Continued) MSSV boiling ranges in pyrolysates from the Gippsland Basin**

| Biozone/Sample ID | *F. longus*: 20110149 | | | | |
|---|---|---|---|---|---|
| Transformation ratio (%) | 10 | 30 | 50 | 70 | 90 |
| End Temperature (°C) | 375 | 399 | 415 | 433 | 481 |
| **TOC (%): 17.46** | | | | | |
| **Range (mg/g sample)** | | | | | |
| *n*-$C_1$ * 1.1 | 0.19 | 0.49 | 0.00 | 1.40 | 3.56 |
| $C_1$-$C_5$ Total | 1.11 | 3.23 | 0.00 | 11.54 | 27.90 |
| $C_2$-$C_5$ Total | 0.76 | 2.20 | 0.00 | 7.91 | 17.91 |
| $C_6$-$C_{14}$ Total | 2.66 | 7.85 | 0.01 | 18.74 | 16.84 |
| $C_{15+}$ Total | 4.09 | 12.24 | 0.01 | 7.82 | 6.70 |
| **Range (mg/g TOC)** | | | | | |
| *n*-$C_1$ * 1.1 | 1.06 | 2.79 | 0.00 | 8.00 | 20.42 |
| $C_1$-$C_5$ Total | 6.37 | 18.52 | 0.02 | 66.12 | 159.80 |
| $C_2$-$C_5$ Total | 4.35 | 12.61 | 0.01 | 45.31 | 102.56 |
| $C_6$-$C_{14}$ Total | 15.26 | 44.95 | 0.04 | 107.33 | 96.44 |
| $C_{15+}$ Total | 23.40 | 70.11 | 0.07 | 44.81 | 38.39 |
| **Gas:oil ratio ($C_1$-$C_5$/$C_{6+}$)** | 0.16 | 0.16 | 0.21 | 0.43 | 1.19 |
| **Gas wetness ($C_2$-$C_5$/$C_1$-$C_5$)** | 0.68 | 0.68 | 0.69 | 0.69 | 0.64 |

**Appendix 21. (Continued) MSSV boiling ranges in pyrolysates from the Gippsland Basin**

| Biozone/Sample ID | *P. mawsonii*: 20110275 | | | | |
|---|---|---|---|---|---|
| Transformation ratio (%) | 10 | 30 | 50 | 70 | 90 |
| End Temperature (°C) | 370 | 395 | 409 | 424 | 447 |
| **TOC (%): 12.13** | | | | | |
| **Range (mg/g sample)** | | | | | |
| *n*-$C_1$ * 1.1 | 0.04 | 0.11 | 0.20 | 0.33 | 0.70 |
| $C_1$-$C_5$ Total | 0.18 | 0.45 | 0.81 | 1.37 | 2.93 |
| $C_2$-$C_5$ Total | 0.13 | 0.34 | 0.62 | 1.04 | 2.23 |
| $C_6$-$C_{14}$ Total | 0.55 | 1.39 | 2.35 | 3.54 | 5.72 |
| $C_{15+}$ Total | 0.74 | 2.26 | 3.93 | 5.10 | 4.36 |
| **Range (mg/g TOC)** | | | | | |
| *n*-$C_1$ * 1.1 | 0.37 | 0.91 | 1.62 | 2.72 | 5.78 |
| $C_1$-$C_5$ Total | 1.48 | 3.73 | 6.70 | 11.31 | 24.17 |
| $C_2$-$C_5$ Total | 1.11 | 2.82 | 5.08 | 8.58 | 18.39 |
| $C_6$-$C_{14}$ Total | 4.56 | 11.46 | 19.35 | 29.15 | 47.13 |
| $C_{15+}$ Total | 6.06 | 18.60 | 32.39 | 42.03 | 35.96 |
| **Gas:oil ratio ($C_1$-$C_5$/$C_{6+}$)** | 0.14 | 0.12 | 0.13 | 0.16 | 0.29 |
| **Gas wetness ($C_2$-$C_5$/$C_1$-$C_5$)** | 0.75 | 0.76 | 0.76 | 0.76 | 0.76 |

**Appendix 22. Molar composition at different MSSV-pyrolysis end temperatures of samples from the Vulcan Sub-basin**

| Formation/Sample ID | Upper Vulcan: 20110067 | | | | |
|---|---|---|---|---|---|
| Transformation ratio (%) | 10 | 30 | 50 | 70 | 90 |
| End Temperature (°C) | 357 | 389 | 406 | 420 | 442 |
| Mol% | | | | | |
| $n\text{-}C_1$ | 30.88 | 39.68 | 44.01 | 46.96 | 55.21 |
| $n\text{-}C_2$ | 1.84 | 9.11 | 10.20 | 10.66 | 10.67 |
| $n\text{-}C_3$ | 1.63 | 5.44 | 5.75 | 5.86 | 5.70 |
| $i\text{-}C_4$ | 0.68 | 0.73 | 0.73 | 0.74 | 0.85 |
| $n\text{-}C_4$ | 11.52 | 4.27 | 4.05 | 3.52 | 2.76 |
| $i\text{-}C_5$ | 5.36 | 3.25 | 2.46 | 1.95 | 1.53 |
| $n\text{-}C_5$ | 2.09 | 1.61 | 1.67 | 1.64 | 1.59 |
| $n\text{-}C_6$ | 10.63 | 6.80 | 6.45 | 5.82 | 4.87 |
| $C_7\text{-}C_{15}$ | 19.23 | 22.34 | 18.18 | 18.55 | 13.79 |
| $C_{16}\text{-}C_{25}$ | 9.41 | 5.43 | 5.02 | 3.62 | 2.57 |
| $C_{26}\text{-}C_{35}$ | 3.94 | 1.07 | 1.14 | 0.57 | 0.38 |
| $C_{36}\text{-}C_{45}$ | 1.65 | 0.21 | 0.26 | 0.09 | 0.06 |
| $C_{46}\text{-}C_{55}$ | 0.69 | 0.04 | 0.06 | 0.01 | 0.01 |
| $C_{56}\text{-}C_{80}$ | 0.44 | 0.01 | 0.02 | 0.00 | 0.00 |

**Appendix 22. (Continued) Molar composition at different MSSV-pyrolysis end temperatures of samples from the Vulcan Sub-basin**

| Formation/Sample ID | Lower Vulcan: 20110044C | | | | |
|---|---|---|---|---|---|
| Transformation ratio (%) | 10 | 30 | 50 | 70 | 90 |
| End Temperature (°C) | 382 | 405 | 421 | 440 | 484 |
| Mol% | | | | | |
| $n\text{-}C_1$ | 37.55 | 37.62 | 40.36 | 47.18 | 65.05 |
| $n\text{-}C_2$ | 9.29 | 11.52 | 11.93 | 11.85 | 10.67 |
| $n\text{-}C_3$ | 7.30 | 7.89 | 7.89 | 7.59 | 6.91 |
| $i\text{-}C_4$ | 2.89 | 0.75 | 0.82 | 0.83 | 0.79 |
| $n\text{-}C_4$ | 3.69 | 3.06 | 3.03 | 2.96 | 2.64 |
| $i\text{-}C_5$ | 0.99 | 0.90 | 0.88 | 0.85 | 0.48 |
| $n\text{-}C_5$ | 1.03 | 1.22 | 1.32 | 1.38 | 0.90 |
| $n\text{-}C_6$ | 4.57 | 3.48 | 3.37 | 3.28 | 1.35 |
| $C_7\text{-}C_{15}$ | 17.18 | 17.12 | 16.04 | 16.38 | 5.97 |
| $C_{16}\text{-}C_{25}$ | 8.76 | 9.03 | 8.14 | 5.53 | 3.00 |
| $C_{26}\text{-}C_{35}$ | 3.84 | 4.10 | 3.55 | 1.56 | 1.29 |
| $C_{36}\text{-}C_{45}$ | 1.68 | 1.86 | 1.55 | 0.44 | 0.56 |
| $C_{46}\text{-}C_{55}$ | 0.74 | 0.85 | 0.67 | 0.12 | 0.24 |
| $C_{56}\text{-}C_{80}$ | 0.50 | 0.61 | 0.46 | 0.05 | 0.16 |

**Appendix 22. (Continued) Molar composition at different MSSV-pyrolysis end temperatures of samples from the Vulcan Sub-basin**

| Formation/Sample ID | Plover: 20110076 (shale) | | | | |
|---|---|---|---|---|---|
| Transformation ratio (%) | 10 | 30 | 50 | 70 | 90 |
| End Temperature (°C) | 373 | 396 | 415 | 430 | 441 |
| Mol% | | | | | |
| $n$-$C_1$ | 32.91 | 35.59 | 38.20 | 42.59 | 62.41 |
| $n$-$C_2$ | 9.64 | 11.05 | 11.68 | 11.78 | 10.36 |
| $n$-$C_3$ | 6.77 | 6.44 | 6.75 | 7.09 | 6.41 |
| $i$-$C_4$ | 0.66 | 0.84 | 0.92 | 1.00 | 0.93 |
| $n$-$C_4$ | 2.96 | 2.73 | 2.73 | 2.82 | 2.55 |
| $i$-$C_5$ | 2.43 | 2.17 | 1.73 | 1.52 | 0.89 |
| $n$-$C_5$ | 0.90 | 1.01 | 1.13 | 1.33 | 1.07 |
| $n$-$C_6$ | 6.63 | 5.48 | 4.21 | 3.66 | 1.89 |
| $C_7$-$C_{15}$ | 21.75 | 20.70 | 19.92 | 18.21 | 9.59 |
| $C_{16}$-$C_{25}$ | 9.61 | 8.90 | 8.26 | 6.85 | 2.91 |
| $C_{26}$-$C_{35}$ | 3.61 | 3.25 | 2.90 | 2.16 | 0.73 |
| $C_{36}$-$C_{45}$ | 1.36 | 1.19 | 1.02 | 0.68 | 0.18 |
| $C_{46}$-$C_{55}$ | 0.51 | 0.43 | 0.36 | 0.22 | 0.05 |
| $C_{56}$-$C_{80}$ | 0.28 | 0.23 | 0.18 | 0.09 | 0.02 |

**Appendix 22. (Continued) Molar composition at different MSSV-pyrolysis end temperatures of samples from the Vulcan Sub-basin**

| Formation/Sample ID | Plover: 20110076C (coal) | | | | |
|---|---|---|---|---|---|
| Transformation ratio (%) | 10 | 30 | 50 | 70 | 90 |
| End Temperature (°C) | 368 | 393 | 410 | 432 | 479 |
| Mol% | | | | | |
| $n$-$C_1$ | 29.01 | 30.70 | 35.47 | 39.52 | 58.53 |
| $n$-$C_2$ | 9.58 | 13.06 | 12.37 | 12.79 | 12.66 |
| $n$-$C_3$ | 4.86 | 5.97 | 6.30 | 6.89 | 6.85 |
| $i$-$C_4$ | 1.17 | 0.12 | 1.01 | 1.09 | 0.98 |
| $n$-$C_4$ | 2.97 | 0.66 | 2.22 | 2.47 | 2.37 |
| $i$-$C_5$ | 2.26 | 1.87 | 1.43 | 1.28 | 0.71 |
| $n$-$C_5$ | 0.56 | 0.76 | 0.85 | 1.04 | 0.83 |
| $n$-$C_6$ | 11.53 | 5.40 | 3.61 | 2.54 | 0.93 |
| $C_7$-$C_{15}$ | 22.71 | 23.65 | 22.74 | 18.55 | 10.09 |
| $C_{16}$-$C_{25}$ | 9.76 | 10.86 | 9.22 | 8.47 | 4.03 |
| $C_{26}$-$C_{35}$ | 3.56 | 4.25 | 3.16 | 3.29 | 1.36 |
| $C_{36}$-$C_{45}$ | 1.30 | 1.67 | 1.08 | 1.28 | 0.46 |
| $C_{46}$-$C_{55}$ | 0.48 | 0.65 | 0.37 | 0.50 | 0.15 |
| $C_{56}$-$C_{80}$ | 0.25 | 0.38 | 0.18 | 0.29 | 0.07 |

**Appendix 23. Molar composition at different MSSV-pyrolysis end temperatures of samples from the Laminaria High**

| Formation/Sample ID | Echuca Shoals: 20110013 | | | | |
|---|---|---|---|---|---|
| Transformation ratio (%) | 10 | 30 | 50 | 70 | 90 |
| End Temperature (°C) | 379 | 401 | 414 | 427 | 450 |
| **Mol%** | | | | | |
| $n\text{-}C_1$ | 64.29 | 48.79 | 54.44 | 58.81 | 73.00 |
| $n\text{-}C_2$ | 2.20 | 8.65 | 9.58 | 9.85 | 7.48 |
| $n\text{-}C_3$ | 1.35 | 5.38 | 5.76 | 5.72 | 4.29 |
| $i\text{-}C_4$ | 5.51 | 1.84 | 1.66 | 1.35 | 0.89 |
| $n\text{-}C_4$ | 9.80 | 5.25 | 3.35 | 2.50 | 1.77 |
| $i\text{-}C_5$ | 0.34 | 1.35 | 1.18 | 1.13 | 0.76 |
| $n\text{-}C_5$ | 0.21 | 1.08 | 1.02 | 1.09 | 0.81 |
| $n\text{-}C_6$ | 6.12 | 8.36 | 7.97 | 5.94 | 3.34 |
| $C_7\text{-}C_{15}$ | 0.59 | 16.32 | 12.28 | 11.23 | 6.25 |
| $C_{16}\text{-}C_{25}$ | 0.91 | 2.60 | 2.34 | 2.04 | 1.19 |
| $C_{26}\text{-}C_{35}$ | 1.17 | 0.33 | 0.36 | 0.30 | 0.18 |
| $C_{36}\text{-}C_{45}$ | 1.33 | 0.04 | 0.05 | 0.04 | 0.03 |
| $C_{46}\text{-}C_{55}$ | 1.36 | 0.01 | 0.01 | 0.01 | 0.00 |
| $C_{56}\text{-}C_{80}$ | 1.26 | 0.00 | 0.00 | 0.00 | 0.00 |

**Appendix 23. (Continued) Molar composition at different MSSV-pyrolysis end temperatures of samples from the Laminaria High**

| Formation/Sample ID | Frigate: 20110021 | | | | |
|---|---|---|---|---|---|
| Transformation ratio (%) | 10 | 30 | 50 | 70 | 90 |
| End Temperature (°C) | 321 | 370 | 396 | 415 | 441 |
| **Mol%** | | | | | |
| $n\text{-}C_1$ | 30.63 | 24.72 | 29.65 | 37.58 | 46.24 |
| $n\text{-}C_2$ | 2.28 | 5.29 | 7.07 | 8.24 | 8.81 |
| $n\text{-}C_3$ | 1.20 | 3.26 | 4.88 | 5.76 | 6.31 |
| $i\text{-}C_4$ | 0.12 | 0.28 | 0.52 | 0.76 | 1.02 |
| $n\text{-}C_4$ | 12.79 | 5.38 | 4.32 | 4.23 | 3.87 |
| $i\text{-}C_5$ | 5.05 | 3.49 | 2.80 | 2.23 | 1.72 |
| $n\text{-}C_5$ | 1.30 | 1.75 | 2.31 | 2.39 | 2.35 |
| $n\text{-}C_6$ | 8.66 | 9.08 | 8.27 | 8.18 | 7.08 |
| $C_7\text{-}C_{15}$ | 25.47 | 31.05 | 26.56 | 25.51 | 19.32 |
| $C_{16}\text{-}C_{25}$ | 8.87 | 11.03 | 9.53 | 4.41 | 2.90 |
| $C_{26}\text{-}C_{35}$ | 2.58 | 3.28 | 2.87 | 0.60 | 0.34 |
| $C_{36}\text{-}C_{45}$ | 0.75 | 0.98 | 0.86 | 0.08 | 0.04 |
| $C_{46}\text{-}C_{55}$ | 0.22 | 0.29 | 0.26 | 0.01 | 0.01 |
| $C_{56}\text{-}C_{80}$ | 0.09 | 0.12 | 0.11 | 0.00 | 0.00 |

Appendix 23. (Continued) Molar composition at different MSSV-pyrolysis end temperatures of samples from the Laminaria High

| Formation/Sample ID | Laminaria: 20110008 | | | | |
|---|---|---|---|---|---|
| Transformation ratio (%) | 10 | 30 | 50 | 70 | 90 |
| End Temperature (°C) | 331 | 380 | 402 | 420 | 448 |
| **Mol%** | | | | | |
| $n$-$C_1$ | 37.80 | 30.56 | 38.55 | 41.79 | 50.29 |
| $n$-$C_2$ | 1.65 | 5.65 | 7.67 | 9.03 | 9.27 |
| $n$-$C_3$ | 1.07 | 4.06 | 6.03 | 6.97 | 6.62 |
| $i$-$C_4$ | 1.95 | 0.40 | 1.13 | 1.43 | 1.48 |
| $n$-$C_4$ | 19.68 | 9.63 | 6.12 | 3.78 | 3.96 |
| $i$-$C_5$ | 0.82 | 1.52 | 1.71 | 1.95 | 2.08 |
| $n$-$C_5$ | 0.39 | 1.30 | 1.57 | 1.80 | 1.95 |
| $n$-$C_6$ | 6.10 | 8.29 | 8.57 | 7.69 | 6.04 |
| $C_7$-$C_{15}$ | 16.33 | 22.41 | 20.58 | 16.90 | 10.72 |
| $C_{16}$-$C_{25}$ | 8.16 | 10.03 | 6.09 | 6.06 | 4.74 |
| $C_{26}$-$C_{35}$ | 3.50 | 3.82 | 1.49 | 1.82 | 1.78 |
| $C_{36}$-$C_{45}$ | 1.50 | 1.46 | 0.36 | 0.55 | 0.67 |
| $C_{46}$-$C_{55}$ | 0.64 | 0.56 | 0.09 | 0.17 | 0.25 |
| $C_{56}$-$C_{80}$ | 0.42 | 0.31 | 0.03 | 0.07 | 0.14 |

**Appendix 24. Molar composition at different MSSV-pyrolysis end temperatures of samples from the Gippsland Basin**

| Biozone/Sample ID | *L. balmei*: 20110126 | | | | |
|---|---|---|---|---|---|
| Transformation ratio (%) | 10 | 30 | 50 | 70 | 90 |
| End Temperature (°C) | 385 | 409 | 425 | 445 | 493 |
| Mol% | | | | | |
| $n$-$C_1$ | 43.54 | 44.08 | 45.79 | 53.12 | 78.58 |
| $n$-$C_2$ | 10.53 | 11.54 | 12.09 | 11.68 | 8.30 |
| $n$-$C_3$ | 7.89 | 7.81 | 7.50 | 7.08 | 4.41 |
| $i$-$C_4$ | 0.71 | 0.85 | 0.92 | 0.93 | 0.62 |
| $n$-$C_4$ | 3.66 | 3.20 | 3.01 | 2.92 | 1.23 |
| $i$-$C_5$ | 1.53 | 1.17 | 1.07 | 0.99 | 0.19 |
| $n$-$C_5$ | 1.31 | 1.33 | 1.43 | 1.42 | 0.17 |
| $n$-$C_6$ | 3.38 | 3.29 | 3.09 | 2.93 | 0.24 |
| $C_7$-$C_{15}$ | 18.15 | 16.47 | 15.32 | 12.57 | 4.17 |
| $C_{16}$-$C_{25}$ | 6.51 | 6.73 | 6.35 | 4.47 | 1.47 |
| $C_{26}$-$C_{35}$ | 1.96 | 2.32 | 2.23 | 1.33 | 0.43 |
| $C_{36}$-$C_{45}$ | 0.59 | 0.80 | 0.78 | 0.40 | 0.13 |
| $C_{46}$-$C_{55}$ | 0.18 | 0.28 | 0.28 | 0.12 | 0.04 |
| $C_{56}$-$C_{80}$ | 0.07 | 0.14 | 0.14 | 0.05 | 0.02 |

**Appendix 24. (Continued) Molar composition at different MSSV-pyrolysis end temperatures of samples from the Gippsland Basin**

| Biozone/Sample ID | *F. longus*: 20110034 | | | | |
|---|---|---|---|---|---|
| Transformation ratio (%) | 10 | 30 | 50 | 70 | 90 |
| End Temperature (°C) | 374 | 397 | 411 | 425 | 453 |
| Mol% | | | | | |
| $n$-$C_1$ | 33.76 | 34.04 | 35.76 | 37.41 | 48.58 |
| $n$-$C_2$ | 8.23 | 9.31 | 9.91 | 10.37 | 10.58 |
| $n$-$C_3$ | 7.44 | 7.31 | 7.42 | 7.45 | 7.47 |
| $i$-$C_4$ | 1.02 | 1.06 | 1.03 | 0.98 | 0.94 |
| $n$-$C_4$ | 3.78 | 3.33 | 3.19 | 3.23 | 3.42 |
| $i$-$C_5$ | 2.10 | 1.50 | 1.27 | 1.09 | 0.97 |
| $n$-$C_5$ | 1.13 | 1.44 | 1.58 | 1.72 | 1.87 |
| $n$-$C_6$ | 4.44 | 4.08 | 4.24 | 4.33 | 4.17 |
| $C_7$-$C_{15}$ | 24.02 | 22.53 | 21.52 | 20.30 | 15.11 |
| $C_{16}$-$C_{25}$ | 9.43 | 9.75 | 9.06 | 8.48 | 4.99 |
| $C_{26}$-$C_{35}$ | 3.12 | 3.59 | 3.23 | 3.00 | 1.37 |
| $C_{36}$-$C_{45}$ | 1.03 | 1.32 | 1.15 | 1.06 | 0.38 |
| $C_{46}$-$C_{55}$ | 0.34 | 0.49 | 0.41 | 0.38 | 0.10 |
| $C_{56}$-$C_{80}$ | 0.16 | 0.26 | 0.21 | 0.19 | 0.04 |

Appendix 24. (Continued) Molar composition at different MSSV-pyrolysis end temperatures of samples from the Gippsland Basin

| Biozone/Sample ID | *F. longus*: 20110149 | | | | |
|---|---|---|---|---|---|
| Transformation ratio (%) | 10 | 30 | 50 | 70 | 90 |
| End Temperature (°C) | 375 | 399 | 415 | 433 | 481 |
| **Mol%** | | | | | |
| $n\text{-}C_1$ | 38.04 | 39.80 | 40.68 | 44.54 | 68.91 |
| $n\text{-}C_2$ | 9.42 | 10.66 | 11.38 | 11.47 | 9.76 |
| $n\text{-}C_3$ | 7.64 | 7.60 | 7.38 | 7.41 | 5.68 |
| $i\text{-}C_4$ | 0.67 | 0.92 | 0.94 | 0.91 | 0.69 |
| $n\text{-}C_4$ | 3.88 | 2.98 | 2.99 | 3.11 | 2.20 |
| $i\text{-}C_5$ | 2.52 | 1.96 | 1.55 | 1.26 | 0.55 |
| $n\text{-}C_5$ | 1.23 | 1.42 | 1.54 | 1.67 | 0.93 |
| $n\text{-}C_6$ | 3.67 | 3.41 | 3.15 | 3.64 | 1.69 |
| $C_7\text{-}C_{15}$ | 18.30 | 18.48 | 17.50 | 16.16 | 6.07 |
| $C_{16}\text{-}C_{25}$ | 8.71 | 8.06 | 7.93 | 6.50 | 2.36 |
| $C_{26}\text{-}C_{35}$ | 3.54 | 2.99 | 3.07 | 2.21 | 0.78 |
| $C_{36}\text{-}C_{45}$ | 1.44 | 1.11 | 1.19 | 0.75 | 0.25 |
| $C_{46}\text{-}C_{55}$ | 0.59 | 0.41 | 0.46 | 0.26 | 0.08 |
| $C_{56}\text{-}C_{80}$ | 0.36 | 0.22 | 0.26 | 0.12 | 0.04 |

Appendix 24. (Continued) Molar composition at different MSSV-pyrolysis end temperatures of samples from the Gippsland Basin

| Biozone/Sample ID | *P. mawsonii*: 20110275 | | | | |
|---|---|---|---|---|---|
| Transformation ratio (%) | 10 | 30 | 50 | 70 | 90 |
| End Temperature (°C) | 370 | 395 | 409 | 424 | 447 |
| **Mol%** | | | | | |
| $n\text{-}C_1$ | 34.60 | 33.29 | 34.15 | 35.57 | 40.65 |
| $n\text{-}C_2$ | 8.43 | 8.72 | 9.03 | 9.52 | 9.99 |
| $n\text{-}C_3$ | 6.94 | 7.29 | 7.54 | 7.62 | 7.82 |
| $i\text{-}C_4$ | 0.55 | 0.77 | 0.99 | 1.05 | 1.13 |
| $n\text{-}C_4$ | 4.75 | 4.20 | 3.84 | 3.63 | 3.66 |
| $i\text{-}C_5$ | 1.80 | 1.20 | 1.14 | 1.07 | 1.08 |
| $n\text{-}C_5$ | 1.74 | 1.72 | 1.75 | 1.82 | 1.92 |
| $n\text{-}C_6$ | 5.75 | 4.98 | 4.58 | 4.72 | 4.65 |
| $C_7\text{-}C_{15}$ | 19.60 | 19.63 | 18.63 | 17.93 | 16.74 |
| $C_{16}\text{-}C_{25}$ | 9.38 | 10.16 | 9.96 | 9.41 | 7.59 |
| $C_{26}\text{-}C_{35}$ | 3.84 | 4.52 | 4.59 | 4.25 | 2.93 |
| $C_{36}\text{-}C_{45}$ | 1.57 | 2.01 | 2.11 | 1.92 | 1.13 |
| $C_{46}\text{-}C_{55}$ | 0.64 | 0.90 | 0.97 | 0.87 | 0.44 |
| $C_{56}\text{-}C_{80}$ | 0.40 | 0.62 | 0.71 | 0.62 | 0.25 |

**Appendix 25. 14 component kinetic data for samples from the Vulcan Sub-basin**

| Sample ID/Formation | | | | | | | Upper Vulcan: 20110067 | | | | | | | |
|---|---|---|---|---|---|---|---|---|---|---|---|---|---|---|
| Component | $n$-$C_1$ | $n$-$C_2$ | $n$-$C_3$ | $i$-$C_4$ | $n$-$C_4$ | $i$-$C_5$ | $n$-$C_5$ | $n$-$C_6$ | $C_7$-$C_{15}$ | $C_{16}$-$C_{25}$ | $C_{26}$-$C_{35}$ | $C_{36}$-$C_{45}$ | $C_{46}$-$C_{55}$ | $C_{56}$-$C_{80}$ |
| **Activation Energy (kcal/mol)** | | | | | | | | | | | | | | |
| 40 | 0.13 | 0.04 | 0.06 | 0.18 | 0.56 | 0.45 | 0.25 | 0.34 | 0.22 | 0.43 | 0.80 | 1.31 | 1.88 | 2.51 |
| 41 | 0.15 | 0.04 | 0.07 | 0.20 | 0.63 | 0.50 | 0.28 | 0.38 | 0.24 | 0.48 | 0.89 | 1.47 | 2.10 | 2.81 |
| 42 | 0.26 | 0.07 | 0.11 | 0.35 | 1.10 | 0.89 | 0.49 | 0.67 | 0.43 | 0.84 | 1.57 | 2.59 | 3.71 | 4.95 |
| 43 | 0.20 | 0.06 | 0.09 | 0.27 | 0.86 | 0.69 | 0.38 | 0.52 | 0.33 | 0.65 | 1.22 | 2.01 | 2.88 | 3.84 |
| 44 | 0.30 | 0.08 | 0.13 | 0.41 | 1.28 | 1.04 | 0.57 | 0.78 | 0.50 | 0.98 | 1.83 | 3.01 | 4.31 | 5.76 |
| 45 | 0.23 | 0.06 | 0.10 | 0.31 | 0.97 | 0.78 | 0.43 | 0.59 | 0.38 | 0.74 | 1.38 | 2.28 | 3.26 | 4.36 |
| 46 | 0.31 | 0.09 | 0.14 | 0.42 | 1.33 | 1.08 | 0.59 | 0.81 | 0.52 | 1.02 | 1.90 | 3.13 | 4.48 | 5.98 |
| 47 | 0.51 | 0.14 | 0.23 | 0.69 | 2.19 | 1.77 | 0.97 | 1.33 | 0.85 | 1.67 | 3.12 | 5.13 | 7.36 | 9.82 |
| 48 | 0.40 | 0.11 | 0.18 | 0.55 | 1.73 | 1.40 | 0.76 | 1.05 | 0.67 | 1.32 | 2.46 | 4.05 | 5.81 | 7.75 |
| 49 | 1.37 | 0.39 | 0.61 | 1.86 | 5.89 | 4.76 | 2.60 | 3.58 | 2.29 | 4.49 | 8.40 | 13.82 | 19.80 | 26.44 |
| 50 | 0.18 | 0.05 | 0.08 | 0.24 | 0.76 | 0.61 | 0.33 | 0.46 | 0.29 | 0.58 | 1.08 | 1.78 | 2.54 | 3.40 |
| 51 | 7.47 | 8.14 | 8.72 | 8.39 | 9.25 | 12.22 | 8.52 | 9.71 | 11.26 | 10.99 | 9.70 | 7.56 | 5.10 | 2.53 |
| 52 | 34.41 | 37.86 | 38.26 | 34.81 | 36.52 | 38.40 | 36.63 | 38.22 | 38.08 | 42.20 | 42.77 | 38.17 | 29.74 | 17.87 |
| 53 | 19.95 | 21.51 | 21.18 | 19.20 | 17.25 | 16.52 | 19.58 | 18.75 | 21.10 | 16.54 | 11.54 | 7.05 | 3.83 | 1.14 |
| 54 | 19.12 | 17.55 | 16.81 | 17.99 | 11.02 | 10.57 | 15.47 | 12.78 | 12.79 | 9.57 | 6.35 | 3.72 | 1.79 | 0.47 |
| 55 | 4.73 | 4.34 | 4.16 | 4.45 | 2.72 | 2.61 | 3.83 | 3.16 | 3.16 | 2.37 | 1.57 | 0.92 | 0.44 | 0.12 |
| 56 | 5.17 | 4.74 | 4.55 | 4.86 | 2.98 | 2.86 | 4.18 | 3.45 | 3.46 | 2.59 | 1.72 | 1.01 | 0.48 | 0.13 |
| 57 | 0.67 | 0.62 | 0.59 | 0.63 | 0.39 | 0.37 | 0.54 | 0.45 | 0.45 | 0.34 | 0.22 | 0.13 | 0.06 | 0.02 |
| 58 | 1.81 | 1.67 | 1.60 | 1.71 | 1.05 | 1.00 | 1.47 | 1.21 | 1.21 | 0.91 | 0.60 | 0.35 | 0.17 | 0.04 |
| 59 | 0.00 | 0.00 | 0.00 | 0.00 | 0.00 | 0.00 | 0.00 | 0.00 | 0.00 | 0.00 | 0.00 | 0.00 | 0.00 | 0.00 |
| 60 | 0.99 | 0.91 | 0.87 | 0.93 | 0.57 | 0.55 | 0.80 | 0.66 | 0.66 | 0.50 | 0.33 | 0.19 | 0.09 | 0.02 |
| 61 | 0.55 | 0.50 | 0.48 | 0.52 | 0.32 | 0.30 | 0.44 | 0.37 | 0.37 | 0.27 | 0.18 | 0.11 | 0.05 | 0.01 |
| 62 | 0.00 | 0.00 | 0.00 | 0.00 | 0.00 | 0.00 | 0.00 | 0.00 | 0.00 | 0.00 | 0.00 | 0.00 | 0.00 | 0.00 |
| 63 | 0.00 | 0.00 | 0.00 | 0.00 | 0.00 | 0.00 | 0.00 | 0.00 | 0.00 | 0.00 | 0.00 | 0.00 | 0.00 | 0.00 |
| 64 | 1.10 | 1.01 | 0.97 | 1.03 | 0.63 | 0.61 | 0.89 | 0.73 | 0.73 | 0.55 | 0.36 | 0.21 | 0.10 | 0.03 |
| **Potential (%)** | **11.35** | **4.48** | **3.67** | **0.67** | **3.57** | **2.56** | **1.82** | **8.05** | **36.62** | **17.88** | **6.05** | **2.07** | **0.76** | **0.46** |

**Appendix 25. (Continued) 14 component kinetic data for samples from the Vulcan Sub-basin**

| Sample ID/Formation | | | | | | Lower Vulcan: 20110044C | | | | | | | | |
|---|---|---|---|---|---|---|---|---|---|---|---|---|---|---|
| Component | $n$-$C_1$ | $n$-$C_2$ | $n$-$C_3$ | $i$-$C_4$ | $n$-$C_4$ | $i$-$C_5$ | $n$-$C_5$ | $n$-$C_6$ | $C_7$-$C_{15}$ | $C_{16}$-$C_{25}$ | $C_{26}$-$C_{35}$ | $C_{36}$-$C_{45}$ | $C_{46}$-$C_{55}$ | $C_{56}$-$C_{80}$ |
| **Activation Energy (kcal/mol)** | | | | | | | | | | | | | | |
| 48 | 0.08 | 0.08 | 0.10 | 0.30 | 0.13 | 0.13 | 0.09 | 0.16 | 0.13 | 0.15 | 0.17 | 0.19 | 0.20 | 0.20 |
| 49 | 0.00 | 0.00 | 0.00 | 0.00 | 0.00 | 0.00 | 0.00 | 0.00 | 0.00 | 0.00 | 0.00 | 0.00 | 0.00 | 0.00 |
| 50 | 0.11 | 0.12 | 0.14 | 0.42 | 0.18 | 0.19 | 0.12 | 0.23 | 0.19 | 0.22 | 0.24 | 0.26 | 0.28 | 0.29 |
| 51 | 0.02 | 0.02 | 0.03 | 0.08 | 0.04 | 0.04 | 0.02 | 0.05 | 0.04 | 0.04 | 0.05 | 0.05 | 0.06 | 0.06 |
| 52 | 0.25 | 0.27 | 0.32 | 0.98 | 0.41 | 0.43 | 0.29 | 0.53 | 0.43 | 0.50 | 0.56 | 0.61 | 0.64 | 0.67 |
| 53 | 0.00 | 0.00 | 0.00 | 0.00 | 0.00 | 0.00 | 0.00 | 0.00 | 0.00 | 0.00 | 0.00 | 0.00 | 0.00 | 0.00 |
| 54 | 0.49 | 0.53 | 0.63 | 1.91 | 0.81 | 0.84 | 0.56 | 1.04 | 0.83 | 0.97 | 1.09 | 1.19 | 1.26 | 1.31 |
| 55 | 0.18 | 0.20 | 0.24 | 0.72 | 0.31 | 0.32 | 0.21 | 0.39 | 0.32 | 0.37 | 0.41 | 0.45 | 0.48 | 0.50 |
| 56 | 0.00 | 0.00 | 0.00 | 0.00 | 0.00 | 0.00 | 0.00 | 0.00 | 0.00 | 0.00 | 0.00 | 0.00 | 0.00 | 0.00 |
| 57 | 5.16 | 5.66 | 6.73 | 20.30 | 8.59 | 8.97 | 5.98 | 11.08 | 8.88 | 10.32 | 11.64 | 12.65 | 13.37 | 13.96 |
| 58 | 9.06 | 12.29 | 12.73 | 9.21 | 12.46 | 14.24 | 12.48 | 14.79 | 15.49 | 18.63 | 21.76 | 24.53 | 26.89 | 29.53 |
| 59 | 11.76 | 15.39 | 15.41 | 12.18 | 14.95 | 16.85 | 16.30 | 17.30 | 17.56 | 20.33 | 22.79 | 24.64 | 25.91 | 26.87 |
| 60 | 16.42 | 18.27 | 17.69 | 14.69 | 17.44 | 19.50 | 20.41 | 20.14 | 21.42 | 16.49 | 11.94 | 8.34 | 5.66 | 3.24 |
| 61 | 8.67 | 9.65 | 9.34 | 7.76 | 9.21 | 10.30 | 10.78 | 10.64 | 11.32 | 8.71 | 6.31 | 4.41 | 2.99 | 1.71 |
| 62 | 7.21 | 8.02 | 7.77 | 6.45 | 7.66 | 8.56 | 8.96 | 8.84 | 9.41 | 7.24 | 5.24 | 3.66 | 2.48 | 1.42 |
| 63 | 8.93 | 6.49 | 6.35 | 5.50 | 6.12 | 4.32 | 5.23 | 3.26 | 3.08 | 3.53 | 3.91 | 4.18 | 4.35 | 4.45 |
| 64 | 8.13 | 5.91 | 5.78 | 5.01 | 5.58 | 3.94 | 4.77 | 2.97 | 2.80 | 3.21 | 3.56 | 3.81 | 3.97 | 4.05 |
| 65 | 4.36 | 3.17 | 3.10 | 2.69 | 2.99 | 2.11 | 2.56 | 1.59 | 1.50 | 1.72 | 1.91 | 2.05 | 2.13 | 2.18 |
| 66 | 7.06 | 5.13 | 5.02 | 4.35 | 4.84 | 3.42 | 4.14 | 2.58 | 2.44 | 2.79 | 3.10 | 3.31 | 3.44 | 3.52 |
| 67 | 0.00 | 0.00 | 0.00 | 0.00 | 0.00 | 0.00 | 0.00 | 0.00 | 0.00 | 0.00 | 0.00 | 0.00 | 0.00 | 0.00 |
| 68 | 3.13 | 2.28 | 2.23 | 1.93 | 2.15 | 1.52 | 1.84 | 1.14 | 1.08 | 1.24 | 1.37 | 1.47 | 1.53 | 1.56 |
| 69 | 3.19 | 2.32 | 2.27 | 1.97 | 2.19 | 1.55 | 1.87 | 1.17 | 1.10 | 1.26 | 1.40 | 1.50 | 1.56 | 1.59 |
| 70 | 0.00 | 0.00 | 0.00 | 0.00 | 0.00 | 0.00 | 0.00 | 0.00 | 0.00 | 0.00 | 0.00 | 0.00 | 0.00 | 0.00 |
| 71 | 0.00 | 0.00 | 0.00 | 0.00 | 0.00 | 0.00 | 0.00 | 0.00 | 0.00 | 0.00 | 0.00 | 0.00 | 0.00 | 0.00 |
| 72 | 5.77 | 4.19 | 4.11 | 3.56 | 3.96 | 2.79 | 3.39 | 2.11 | 1.99 | 2.28 | 2.53 | 2.71 | 2.81 | 2.88 |
| **Potential (%)** | **10.81** | **4.57** | **4.43** | **0.77** | **2.31** | **0.74** | **1.15** | **3.29** | **24.84** | **21.35** | **12.53** | **6.77** | **3.52** | **2.91** |

| Sample ID/Formation | | | | | | | Plover: 20110076 (shale) | | | | | | | |
|---|---|---|---|---|---|---|---|---|---|---|---|---|---|---|
| Component | $n\text{-}C_1$ | $n\text{-}C_2$ | $n\text{-}C_3$ | $i\text{-}C_4$ | $n\text{-}C_4$ | $i\text{-}C_5$ | $n\text{-}C_5$ | $n\text{-}C_6$ | $C_7\text{-}C_{15}$ | $C_{16}\text{-}C_{25}$ | $C_{26}\text{-}C_{35}$ | $C_{36}\text{-}C_{45}$ | $C_{46}\text{-}C_{55}$ | $C_{56}\text{-}C_{80}$ |
| **Activation Energy (kcal/mol)** | | | | | | | | | | | | | | |
| 45 | 0.09 | 0.11 | 0.13 | 0.09 | 0.14 | 0.20 | 0.10 | 0.23 | 0.17 | 0.20 | 0.22 | 0.25 | 0.28 | 0.31 |
| 46 | 0.00 | 0.00 | 0.00 | 0.00 | 0.00 | 0.00 | 0.00 | 0.00 | 0.00 | 0.00 | 0.00 | 0.00 | 0.00 | 0.00 |
| 47 | 0.10 | 0.12 | 0.14 | 0.10 | 0.15 | 0.23 | 0.11 | 0.26 | 0.19 | 0.22 | 0.25 | 0.28 | 0.31 | 0.34 |
| 48 | 0.05 | 0.07 | 0.08 | 0.06 | 0.08 | 0.13 | 0.06 | 0.14 | 0.11 | 0.12 | 0.14 | 0.15 | 0.17 | 0.19 |
| 49 | 0.15 | 0.19 | 0.22 | 0.16 | 0.24 | 0.35 | 0.18 | 0.40 | 0.30 | 0.34 | 0.39 | 0.43 | 0.47 | 0.53 |
| 50 | 0.11 | 0.14 | 0.16 | 0.11 | 0.17 | 0.25 | 0.13 | 0.28 | 0.21 | 0.24 | 0.27 | 0.31 | 0.34 | 0.38 |
| 51 | 0.18 | 0.22 | 0.26 | 0.18 | 0.28 | 0.41 | 0.20 | 0.46 | 0.35 | 0.40 | 0.45 | 0.50 | 0.55 | 0.62 |
| 52 | 0.32 | 0.41 | 0.47 | 0.34 | 0.51 | 0.75 | 0.38 | 0.85 | 0.63 | 0.72 | 0.82 | 0.92 | 1.01 | 1.13 |
| 53 | 1.55 | 1.97 | 2.27 | 1.62 | 2.44 | 3.61 | 1.80 | 4.08 | 3.04 | 3.48 | 3.95 | 4.41 | 4.85 | 5.43 |
| 54 | 4.09 | 5.19 | 5.98 | 4.28 | 6.43 | 9.50 | 4.75 | 10.74 | 8.01 | 9.17 | 10.40 | 11.61 | 12.78 | 14.30 |
| 55 | 10.98 | 14.78 | 14.14 | 13.56 | 14.73 | 21.14 | 13.18 | 22.01 | 18.94 | 21.09 | 23.23 | 25.19 | 26.95 | 28.92 |
| 56 | 12.71 | 16.84 | 15.98 | 15.94 | 15.91 | 18.17 | 16.03 | 18.23 | 19.65 | 21.10 | 22.37 | 23.33 | 24.02 | 24.51 |
| 57 | 12.65 | 15.15 | 14.96 | 15.47 | 14.65 | 14.22 | 16.80 | 14.17 | 16.03 | 15.61 | 14.89 | 13.98 | 12.93 | 11.42 |
| 58 | 7.86 | 9.41 | 9.29 | 9.61 | 9.10 | 8.84 | 10.44 | 8.80 | 9.96 | 9.69 | 9.25 | 8.68 | 8.03 | 7.10 |
| 59 | 14.01 | 10.08 | 10.23 | 10.96 | 10.02 | 6.32 | 10.21 | 5.51 | 6.38 | 5.02 | 3.81 | 2.84 | 2.08 | 1.38 |
| 60 | 5.50 | 3.96 | 4.02 | 4.30 | 3.93 | 2.48 | 4.01 | 2.16 | 2.50 | 1.97 | 1.50 | 1.12 | 0.82 | 0.54 |
| 61 | 10.43 | 7.50 | 7.62 | 8.16 | 7.46 | 4.71 | 7.60 | 4.10 | 4.75 | 3.74 | 2.84 | 2.12 | 1.55 | 1.03 |
| 62 | 3.69 | 2.65 | 2.69 | 2.89 | 2.64 | 1.66 | 2.69 | 1.45 | 1.68 | 1.32 | 1.00 | 0.75 | 0.55 | 0.36 |
| 63 | 2.68 | 1.93 | 1.95 | 2.09 | 1.91 | 1.21 | 1.95 | 1.05 | 1.22 | 0.96 | 0.73 | 0.54 | 0.40 | 0.26 |
| 64 | 2.99 | 2.15 | 2.18 | 2.34 | 2.14 | 1.35 | 2.18 | 1.18 | 1.36 | 1.07 | 0.81 | 0.61 | 0.44 | 0.29 |
| 65 | 0.61 | 0.44 | 0.45 | 0.48 | 0.44 | 0.28 | 0.45 | 0.24 | 0.28 | 0.22 | 0.17 | 0.12 | 0.09 | 0.06 |
| 66 | 3.92 | 2.82 | 2.86 | 3.07 | 2.80 | 1.77 | 2.86 | 1.54 | 1.79 | 1.40 | 1.07 | 0.79 | 0.58 | 0.39 |
| 67 | 0.00 | 0.00 | 0.00 | 0.00 | 0.00 | 0.00 | 0.00 | 0.00 | 0.00 | 0.00 | 0.00 | 0.00 | 0.00 | 0.00 |
| 68 | 0.00 | 0.00 | 0.00 | 0.00 | 0.00 | 0.00 | 0.00 | 0.00 | 0.00 | 0.00 | 0.00 | 0.00 | 0.00 | 0.00 |
| 69 | 5.35 | 3.85 | 3.91 | 4.19 | 3.83 | 2.41 | 3.90 | 2.11 | 2.44 | 1.92 | 1.46 | 1.09 | 0.80 | 0.53 |
| **Potential (%)** | **10.18** | **4.40** | **3.94** | **0.70** | **2.11** | **1.45** | **1.08** | **4.20** | **29.66** | **22.44** | **11.24** | **5.08** | **2.17** | **1.36** |

**Appendix 25. (Continued) 14 component kinetic data for samples from the Vulcan Sub-basin**

| Sample ID/Formation | | | | | | | Plover: 20110076C (coal) | | | | | | | |
|---|---|---|---|---|---|---|---|---|---|---|---|---|---|---|
| Component | $n$-$C_1$ | $n$-$C_2$ | $n$-$C_3$ | $i$-$C_4$ | $n$-$C_4$ | $i$-$C_5$ | $n$-$C_5$ | $n$-$C_6$ | $C_7$-$C_{15}$ | $C_{16}$-$C_{25}$ | $C_{26}$-$C_{35}$ | $C_{36}$-$C_{45}$ | $C_{46}$-$C_{55}$ | $C_{56}$-$C_{80}$ |
| **Activation Energy (kcal/mol)** | | | | | | | | | | | | | | |
| 51 | 0.17 | 0.20 | 0.19 | 0.31 | 0.33 | 0.43 | 0.17 | 0.76 | 0.33 | 0.33 | 0.32 | 0.32 | 0.32 | 0.31 |
| 52 | 0.00 | 0.00 | 0.00 | 0.00 | 0.00 | 0.00 | 0.00 | 0.00 | 0.00 | 0.00 | 0.00 | 0.00 | 0.00 | 0.00 |
| 53 | 0.23 | 0.27 | 0.26 | 0.43 | 0.46 | 0.59 | 0.23 | 1.05 | 0.45 | 0.45 | 0.45 | 0.44 | 0.44 | 0.43 |
| 54 | 0.19 | 0.22 | 0.22 | 0.35 | 0.37 | 0.48 | 0.19 | 0.86 | 0.37 | 0.37 | 0.37 | 0.36 | 0.36 | 0.35 |
| 55 | 0.66 | 0.76 | 0.74 | 1.22 | 1.29 | 1.67 | 0.65 | 2.96 | 1.27 | 1.27 | 1.26 | 1.25 | 1.23 | 1.20 |
| 56 | 0.46 | 0.54 | 0.52 | 0.85 | 0.90 | 1.17 | 0.46 | 2.08 | 0.89 | 0.89 | 0.88 | 0.87 | 0.86 | 0.84 |
| 57 | 1.66 | 1.92 | 1.87 | 3.06 | 3.24 | 4.20 | 1.64 | 7.44 | 3.19 | 3.19 | 3.17 | 3.14 | 3.09 | 3.02 |
| 58 | 6.59 | 7.63 | 7.42 | 12.14 | 12.86 | 16.67 | 6.52 | 29.57 | 12.69 | 12.66 | 12.58 | 12.45 | 12.29 | 11.99 |
| 59 | 8.61 | 12.83 | 11.24 | 1.53 | 3.52 | 17.06 | 10.97 | 17.07 | 16.30 | 17.37 | 18.52 | 19.66 | 20.81 | 22.34 |
| 60 | 11.54 | 14.10 | 13.78 | 15.08 | 13.72 | 15.16 | 14.14 | 13.23 | 18.19 | 17.10 | 15.96 | 14.83 | 13.74 | 12.31 |
| 61 | 9.74 | 11.04 | 11.42 | 12.33 | 11.58 | 10.24 | 13.09 | 7.06 | 11.24 | 11.90 | 12.60 | 13.30 | 13.97 | 14.86 |
| 62 | 7.98 | 9.05 | 9.36 | 10.11 | 9.49 | 8.40 | 10.73 | 5.79 | 9.22 | 9.76 | 10.33 | 10.90 | 11.45 | 12.19 |
| 63 | 5.14 | 5.82 | 6.02 | 6.51 | 6.11 | 5.40 | 6.91 | 3.73 | 5.93 | 6.28 | 6.65 | 7.01 | 7.37 | 7.84 |
| 64 | 10.82 | 8.20 | 8.50 | 8.30 | 8.32 | 4.26 | 7.89 | 1.93 | 4.59 | 4.25 | 3.89 | 3.56 | 3.24 | 2.84 |
| 65 | 7.43 | 5.63 | 5.84 | 5.70 | 5.71 | 2.93 | 5.42 | 1.33 | 3.15 | 2.92 | 2.67 | 2.44 | 2.23 | 1.95 |
| 66 | 6.19 | 4.69 | 4.87 | 4.75 | 4.76 | 2.44 | 4.52 | 1.11 | 2.62 | 2.43 | 2.23 | 2.04 | 1.85 | 1.62 |
| 67 | 5.23 | 3.96 | 4.11 | 4.01 | 4.02 | 2.06 | 3.81 | 0.93 | 2.22 | 2.05 | 1.88 | 1.72 | 1.57 | 1.37 |
| 68 | 2.70 | 2.04 | 2.12 | 2.07 | 2.07 | 1.06 | 1.97 | 0.48 | 1.14 | 1.06 | 0.97 | 0.89 | 0.81 | 0.71 |
| 69 | 3.36 | 2.55 | 2.64 | 2.58 | 2.59 | 1.32 | 2.45 | 0.60 | 1.43 | 1.32 | 1.21 | 1.11 | 1.01 | 0.88 |
| 70 | 2.04 | 1.54 | 1.60 | 1.56 | 1.56 | 0.80 | 1.49 | 0.36 | 0.86 | 0.80 | 0.73 | 0.67 | 0.61 | 0.53 |
| 71 | 1.46 | 1.10 | 1.15 | 1.12 | 1.12 | 0.57 | 1.06 | 0.26 | 0.62 | 0.57 | 0.52 | 0.48 | 0.44 | 0.38 |
| 72 | 3.21 | 2.43 | 2.53 | 2.46 | 2.47 | 1.27 | 2.34 | 0.57 | 1.36 | 1.26 | 1.16 | 1.06 | 0.96 | 0.84 |
| 73 | 0.00 | 0.00 | 0.00 | 0.00 | 0.00 | 0.00 | 0.00 | 0.00 | 0.00 | 0.00 | 0.00 | 0.00 | 0.00 | 0.00 |
| 74 | 0.00 | 0.00 | 0.00 | 0.00 | 0.00 | 0.00 | 0.00 | 0.00 | 0.00 | 0.00 | 0.00 | 0.00 | 0.00 | 0.00 |
| 75 | 4.58 | 3.47 | 3.60 | 3.52 | 3.52 | 1.81 | 3.35 | 0.82 | 1.94 | 1.80 | 1.65 | 1.51 | 1.37 | 1.20 |
| **Potential (%)** | **8.00** | **4.28** | **3.27** | **0.63** | **1.52** | **1.11** | **0.70** | **3.81** | **28.12** | **23.75** | **13.18** | **6.52** | **3.03** | **2.08** |

**Appendix 26. 14 component kinetic data for samples from the Laminaria High**

| Sample ID/Formation | Echuca Shoals: 20110013 | | | | | | | | | | | | | |
| --- | --- | --- | --- | --- | --- | --- | --- | --- | --- | --- | --- | --- | --- | --- |
| Component | $n\text{-}C_1$ | $n\text{-}C_2$ | $n\text{-}C_3$ | $i\text{-}C_4$ | $n\text{-}C_4$ | $i\text{-}C_5$ | $n\text{-}C_5$ | $n\text{-}C_6$ | $C_7\text{-}C_{15}$ | $C_{16}\text{-}C_{25}$ | $C_{26}\text{-}C_{35}$ | $C_{36}\text{-}C_{45}$ | $C_{46}\text{-}C_{55}$ | $C_{56}\text{-}C_{80}$ |
| **Activation Energy (kcal/mol)** | | | | | | | | | | | | | | |
| 42 | 0.23 | 0.06 | 0.06 | 0.94 | 0.74 | 0.08 | 0.05 | 0.26 | 0.01 | 0.12 | 1.01 | 5.70 | 13.39 | 16.03 |
| 43 | 0.00 | 0.00 | 0.00 | 0.00 | 0.00 | 0.00 | 0.00 | 0.00 | 0.00 | 0.00 | 0.00 | 0.00 | 0.00 | 0.00 |
| 44 | 0.16 | 0.04 | 0.04 | 0.65 | 0.51 | 0.05 | 0.04 | 0.18 | 0.01 | 0.08 | 0.70 | 3.92 | 9.20 | 11.02 |
| 45 | 0.21 | 0.05 | 0.06 | 0.86 | 0.67 | 0.07 | 0.05 | 0.23 | 0.01 | 0.10 | 0.92 | 5.17 | 12.13 | 14.53 |
| 46 | 0.00 | 0.00 | 0.00 | 0.00 | 0.00 | 0.00 | 0.00 | 0.00 | 0.00 | 0.00 | 0.00 | 0.00 | 0.00 | 0.00 |
| 47 | 0.35 | 0.09 | 0.10 | 1.45 | 1.14 | 0.12 | 0.08 | 0.39 | 0.02 | 0.18 | 1.55 | 8.73 | 20.50 | 24.55 |
| 48 | 0.42 | 0.11 | 0.11 | 1.71 | 1.34 | 0.14 | 0.09 | 0.47 | 0.02 | 0.21 | 1.83 | 10.33 | 24.26 | 29.05 |
| 49 | 0.00 | 0.00 | 0.00 | 0.00 | 0.00 | 0.00 | 0.00 | 0.00 | 0.00 | 0.00 | 0.00 | 0.00 | 0.00 | 0.00 |
| 50 | 0.00 | 0.00 | 0.00 | 0.00 | 0.00 | 0.00 | 0.00 | 0.00 | 0.00 | 0.00 | 0.00 | 0.00 | 0.00 | 0.00 |
| 51 | 0.00 | 0.00 | 0.00 | 0.00 | 0.00 | 0.00 | 0.00 | 0.00 | 0.00 | 0.00 | 0.00 | 0.00 | 0.00 | 0.00 |
| 52 | 0.00 | 0.00 | 0.00 | 0.00 | 0.00 | 0.00 | 0.00 | 0.00 | 0.00 | 0.00 | 0.00 | 0.00 | 0.00 | 0.00 |
| 53 | 20.58 | 27.52 | 29.04 | 36.97 | 46.58 | 35.50 | 30.24 | 41.20 | 42.70 | 38.67 | 32.82 | 20.57 | 5.75 | 1.49 |
| 54 | 24.13 | 30.46 | 30.04 | 26.25 | 21.60 | 28.82 | 29.70 | 28.48 | 28.58 | 29.55 | 28.98 | 20.98 | 6.71 | 1.43 |
| 55 | 28.03 | 21.66 | 21.08 | 16.20 | 14.25 | 18.31 | 20.67 | 14.97 | 14.89 | 16.17 | 16.73 | 12.79 | 4.19 | 0.99 |
| 56 | 7.71 | 5.96 | 5.80 | 4.45 | 3.92 | 5.04 | 5.68 | 4.12 | 4.09 | 4.44 | 4.60 | 3.52 | 1.15 | 0.27 |
| 57 | 12.29 | 9.50 | 9.24 | 7.10 | 6.25 | 8.03 | 9.06 | 6.56 | 6.53 | 7.09 | 7.34 | 5.61 | 1.84 | 0.43 |
| 58 | 0.00 | 0.00 | 0.00 | 0.00 | 0.00 | 0.00 | 0.00 | 0.00 | 0.00 | 0.00 | 0.00 | 0.00 | 0.00 | 0.00 |
| 59 | 3.26 | 2.52 | 2.45 | 1.88 | 1.66 | 2.13 | 2.40 | 1.74 | 1.73 | 1.88 | 1.95 | 1.49 | 0.49 | 0.11 |
| 60 | 0.25 | 0.20 | 0.19 | 0.15 | 0.13 | 0.17 | 0.19 | 0.14 | 0.13 | 0.15 | 0.15 | 0.12 | 0.04 | 0.01 |
| 61 | 1.04 | 0.80 | 0.78 | 0.60 | 0.53 | 0.68 | 0.77 | 0.56 | 0.55 | 0.60 | 0.62 | 0.48 | 0.16 | 0.04 |
| 62 | 0.51 | 0.39 | 0.38 | 0.29 | 0.26 | 0.33 | 0.37 | 0.27 | 0.27 | 0.29 | 0.30 | 0.23 | 0.08 | 0.02 |
| 63 | 0.00 | 0.00 | 0.00 | 0.00 | 0.00 | 0.00 | 0.00 | 0.00 | 0.00 | 0.00 | 0.00 | 0.00 | 0.00 | 0.00 |
| 64 | 0.71 | 0.55 | 0.54 | 0.41 | 0.36 | 0.47 | 0.53 | 0.38 | 0.38 | 0.41 | 0.43 | 0.33 | 0.11 | 0.03 |
| 65 | 0.00 | 0.00 | 0.00 | 0.00 | 0.00 | 0.00 | 0.00 | 0.00 | 0.00 | 0.00 | 0.00 | 0.00 | 0.00 | 0.00 |
| 66 | 0.12 | 0.09 | 0.09 | 0.07 | 0.06 | 0.08 | 0.09 | 0.06 | 0.06 | 0.07 | 0.07 | 0.05 | 0.02 | 0.00 |
| **Potential (%)** | **22.98** | **5.71** | **4.93** | **1.75** | **3.96** | **1.66** | **1.55** | **10.57** | **32.00** | **11.03** | **2.45** | **0.66** | **0.36** | **0.36** |

**Appendix 26. (Continued) 14 component kinetic data for samples from the Laminaria High**

| Sample ID/Formation | | | | | | | | Frigate: 20110021 | | | | | | |
|---|---|---|---|---|---|---|---|---|---|---|---|---|---|---|
| Component | $n\text{-}C_1$ | $n\text{-}C_2$ | $n\text{-}C_3$ | $i\text{-}C_4$ | $n\text{-}C_4$ | $i\text{-}C_5$ | $n\text{-}C_5$ | $n\text{-}C_6$ | $C_7\text{-}C_{15}$ | $C_{16}\text{-}C_{25}$ | $C_{26}\text{-}C_{35}$ | $C_{36}\text{-}C_{45}$ | $C_{46}\text{-}C_{55}$ | $C_{56}\text{-}C_{80}$ |
| **Activation Energy (kcal/mol)** | | | | | | | | | | | | | | |
| 42 | 0.60 | 0.23 | 0.17 | 0.12 | 1.74 | 1.41 | 0.44 | 0.79 | 0.76 | 1.15 | 1.52 | 1.76 | 1.87 | 1.91 |
| 43 | 0.20 | 0.08 | 0.06 | 0.04 | 0.59 | 0.47 | 0.15 | 0.27 | 0.26 | 0.39 | 0.51 | 0.59 | 0.63 | 0.64 |
| 44 | 0.95 | 0.36 | 0.28 | 0.20 | 2.76 | 2.23 | 0.70 | 1.25 | 1.21 | 1.82 | 2.41 | 2.79 | 2.97 | 3.04 |
| 45 | 0.69 | 0.26 | 0.20 | 0.14 | 2.00 | 1.62 | 0.51 | 0.91 | 0.88 | 1.32 | 1.75 | 2.02 | 2.16 | 2.21 |
| 46 | 1.32 | 0.51 | 0.39 | 0.28 | 3.84 | 3.10 | 0.97 | 1.74 | 1.69 | 2.53 | 3.35 | 3.87 | 4.13 | 4.22 |
| 47 | 1.79 | 0.69 | 0.52 | 0.37 | 5.20 | 4.21 | 1.31 | 2.36 | 2.28 | 3.43 | 4.54 | 5.25 | 5.60 | 5.72 |
| 48 | 2.13 | 0.82 | 0.62 | 0.44 | 6.18 | 5.00 | 1.56 | 2.80 | 2.72 | 4.08 | 5.39 | 6.24 | 6.66 | 6.80 |
| 49 | 3.02 | 1.16 | 0.88 | 0.63 | 8.77 | 7.10 | 2.22 | 3.97 | 3.86 | 5.79 | 7.65 | 8.85 | 9.45 | 9.65 |
| 50 | 1.86 | 2.05 | 1.83 | 1.15 | 2.81 | 3.74 | 2.27 | 3.18 | 3.59 | 5.49 | 7.42 | 8.78 | 9.58 | 10.02 |
| 51 | 3.01 | 3.32 | 2.96 | 1.86 | 4.55 | 6.05 | 3.68 | 5.14 | 5.80 | 8.89 | 12.00 | 14.19 | 15.49 | 16.20 |
| 52 | 2.14 | 2.37 | 2.11 | 1.33 | 3.24 | 4.31 | 2.62 | 3.67 | 4.14 | 6.34 | 8.56 | 10.12 | 11.05 | 11.55 |
| 53 | 6.19 | 7.61 | 7.61 | 5.91 | 6.27 | 8.32 | 8.32 | 8.04 | 8.52 | 13.18 | 17.99 | 21.50 | 23.67 | 25.20 |
| 54 | 19.97 | 22.59 | 22.85 | 21.91 | 15.64 | 16.87 | 21.94 | 20.26 | 20.82 | 15.53 | 9.63 | 5.27 | 2.56 | 1.21 |
| 55 | 18.57 | 21.01 | 21.25 | 20.38 | 14.55 | 15.69 | 20.41 | 18.84 | 19.37 | 14.44 | 8.96 | 4.90 | 2.38 | 1.13 |
| 56 | 16.55 | 16.28 | 16.86 | 19.92 | 9.64 | 8.76 | 14.49 | 11.80 | 10.62 | 6.88 | 3.67 | 1.71 | 0.78 | 0.22 |
| 57 | 9.54 | 9.38 | 9.72 | 11.48 | 5.55 | 5.05 | 8.35 | 6.80 | 6.12 | 3.97 | 2.12 | 0.99 | 0.45 | 0.12 |
| 58 | 6.44 | 6.33 | 6.56 | 7.75 | 3.75 | 3.40 | 5.64 | 4.59 | 4.13 | 2.68 | 1.43 | 0.67 | 0.30 | 0.08 |
| 59 | 1.46 | 1.44 | 1.49 | 1.76 | 0.85 | 0.77 | 1.28 | 1.04 | 0.94 | 0.61 | 0.32 | 0.15 | 0.07 | 0.02 |
| 60 | 1.02 | 1.00 | 1.04 | 1.23 | 0.59 | 0.54 | 0.89 | 0.73 | 0.65 | 0.42 | 0.23 | 0.11 | 0.05 | 0.01 |
| 61 | 0.62 | 0.61 | 0.64 | 0.75 | 0.36 | 0.33 | 0.55 | 0.44 | 0.40 | 0.26 | 0.14 | 0.06 | 0.03 | 0.01 |
| 62 | 0.21 | 0.21 | 0.22 | 0.26 | 0.12 | 0.11 | 0.19 | 0.15 | 0.14 | 0.09 | 0.05 | 0.02 | 0.01 | 0.00 |
| 63 | 0.79 | 0.78 | 0.80 | 0.95 | 0.46 | 0.42 | 0.69 | 0.56 | 0.51 | 0.33 | 0.17 | 0.08 | 0.04 | 0.01 |
| 64 | 0.00 | 0.00 | 0.00 | 0.00 | 0.00 | 0.00 | 0.00 | 0.00 | 0.00 | 0.00 | 0.00 | 0.00 | 0.00 | 0.00 |
| 65 | 0.00 | 0.00 | 0.00 | 0.00 | 0.00 | 0.00 | 0.00 | 0.00 | 0.00 | 0.00 | 0.00 | 0.00 | 0.00 | 0.00 |
| 66 | 0.94 | 0.92 | 0.95 | 1.13 | 0.54 | 0.50 | 0.82 | 0.67 | 0.60 | 0.39 | 0.21 | 0.10 | 0.04 | 0.01 |
| **Potential (%)** | **7.40** | **2.69** | **2.73** | **0.49** | **3.86** | **2.34** | **1.93** | **8.53** | **41.62** | **18.91** | **6.30** | **2.13** | **0.73** | **0.35** |

| Sample ID/Formation | | | | | | Laminaria: 20110008 | | | | | | | | |
|---|---|---|---|---|---|---|---|---|---|---|---|---|---|---|
| Component | $n\text{-}C_1$ | $n\text{-}C_2$ | $n\text{-}C_3$ | $i\text{-}C_4$ | $n\text{-}C_4$ | $i\text{-}C_5$ | $n\text{-}C_5$ | $n\text{-}C_6$ | $C_7\text{-}C_{15}$ | $C_{16}\text{-}C_{25}$ | $C_{26}\text{-}C_{35}$ | $C_{36}\text{-}C_{45}$ | $C_{46}\text{-}C_{55}$ | $C_{56}\text{-}C_{80}$ |
| **Activation Energy (kcal/mol)** | | | | | | | | | | | | | | |
| 41 | 0.64 | 0.16 | 0.14 | 1.02 | 1.93 | 0.34 | 0.18 | 0.61 | 0.72 | 0.93 | 1.17 | 1.41 | 1.65 | 1.96 |
| 42 | 0.07 | 0.02 | 0.02 | 0.11 | 0.21 | 0.04 | 0.02 | 0.07 | 0.08 | 0.10 | 0.13 | 0.16 | 0.18 | 0.22 |
| 43 | 0.82 | 0.21 | 0.18 | 1.31 | 2.47 | 0.44 | 0.24 | 0.78 | 0.93 | 1.19 | 1.49 | 1.80 | 2.11 | 2.51 |
| 44 | 0.62 | 0.15 | 0.13 | 0.98 | 1.84 | 0.33 | 0.18 | 0.58 | 0.69 | 0.89 | 1.12 | 1.35 | 1.58 | 1.88 |
| 45 | 1.05 | 0.26 | 0.23 | 1.67 | 3.15 | 0.56 | 0.30 | 1.00 | 1.18 | 1.52 | 1.91 | 2.30 | 2.70 | 3.21 |
| 46 | 1.28 | 0.32 | 0.28 | 2.02 | 3.82 | 0.67 | 0.36 | 1.21 | 1.43 | 1.84 | 2.31 | 2.79 | 3.26 | 3.88 |
| 47 | 1.48 | 0.37 | 0.32 | 2.35 | 4.44 | 0.78 | 0.42 | 1.40 | 1.67 | 2.14 | 2.69 | 3.25 | 3.80 | 4.52 |
| 48 | 2.34 | 0.58 | 0.51 | 3.70 | 6.99 | 1.23 | 0.67 | 2.21 | 2.62 | 3.37 | 4.23 | 5.11 | 5.98 | 7.11 |
| 49 | 1.68 | 0.42 | 0.37 | 2.67 | 5.04 | 0.89 | 0.48 | 1.59 | 1.89 | 2.43 | 3.05 | 3.68 | 4.31 | 5.13 |
| 50 | 3.86 | 0.96 | 0.84 | 6.12 | 11.55 | 2.04 | 1.10 | 3.66 | 4.34 | 5.57 | 6.99 | 8.45 | 9.88 | 11.76 |
| 51 | 1.62 | 1.72 | 1.66 | 0.65 | 2.94 | 1.97 | 1.90 | 2.58 | 3.10 | 3.56 | 3.98 | 4.28 | 4.44 | 4.50 |
| 52 | 4.34 | 4.59 | 4.43 | 1.75 | 7.85 | 5.27 | 5.06 | 6.90 | 8.27 | 9.52 | 10.62 | 11.42 | 11.87 | 12.02 |
| 53 | 21.90 | 24.95 | 26.34 | 19.68 | 19.98 | 23.79 | 24.52 | 28.56 | 30.42 | 23.14 | 16.57 | 11.41 | 7.61 | 4.32 |
| 54 | 20.73 | 25.65 | 26.56 | 21.87 | 10.79 | 23.64 | 24.52 | 22.37 | 21.81 | 20.11 | 17.70 | 15.00 | 12.31 | 9.02 |
| 55 | 12.08 | 12.74 | 12.22 | 10.97 | 5.47 | 12.22 | 12.88 | 8.51 | 6.70 | 7.61 | 8.37 | 8.87 | 9.11 | 9.00 |
| 56 | 18.15 | 19.16 | 18.37 | 16.48 | 8.22 | 18.37 | 19.36 | 12.79 | 10.07 | 11.44 | 12.59 | 13.33 | 13.69 | 13.52 |
| 57 | 0.56 | 0.60 | 0.57 | 0.51 | 0.26 | 0.57 | 0.60 | 0.40 | 0.31 | 0.36 | 0.39 | 0.41 | 0.43 | 0.42 |
| 58 | 3.14 | 3.31 | 3.18 | 2.85 | 1.42 | 3.18 | 3.35 | 2.21 | 1.74 | 1.98 | 2.18 | 2.30 | 2.37 | 2.34 |
| 59 | 1.01 | 1.07 | 1.02 | 0.92 | 0.46 | 1.02 | 1.08 | 0.71 | 0.56 | 0.64 | 0.70 | 0.74 | 0.76 | 0.75 |
| 60 | 0.00 | 0.00 | 0.00 | 0.00 | 0.00 | 0.00 | 0.00 | 0.00 | 0.00 | 0.00 | 0.00 | 0.00 | 0.00 | 0.00 |
| 61 | 1.33 | 1.40 | 1.35 | 1.21 | 0.60 | 1.35 | 1.42 | 0.94 | 0.74 | 0.84 | 0.92 | 0.98 | 1.00 | 0.99 |
| 62 | 0.00 | 0.00 | 0.00 | 0.00 | 0.00 | 0.00 | 0.00 | 0.00 | 0.00 | 0.00 | 0.00 | 0.00 | 0.00 | 0.00 |
| 63 | 0.00 | 0.00 | 0.00 | 0.00 | 0.00 | 0.00 | 0.00 | 0.00 | 0.00 | 0.00 | 0.00 | 0.00 | 0.00 | 0.00 |
| 64 | 0.00 | 0.00 | 0.00 | 0.00 | 0.00 | 0.00 | 0.00 | 0.00 | 0.00 | 0.00 | 0.00 | 0.00 | 0.00 | 0.00 |
| 65 | 1.26 | 1.33 | 1.27 | 1.14 | 0.57 | 1.27 | 1.34 | 0.89 | 0.70 | 0.79 | 0.87 | 0.92 | 0.95 | 0.94 |
| **Potential (%)** | **8.36** | **2.74** | **2.99** | **0.98** | **5.27** | **1.54** | **1.37** | **7.66** | **27.75** | **21.16** | **10.92** | **5.20** | **2.39** | **1.68** |

**Appendix 27. 14 component kinetic data for samples from the Gippsland Basin**

| Sample ID/Biozone | | | | | | | | | | | | | | |
|---|---|---|---|---|---|---|---|---|---|---|---|---|---|
| | | | | | | | | *L. balmei*: 20110126 | | | | | | |
| Component | $n\text{-}C_1$ | $n\text{-}C_2$ | $n\text{-}C_3$ | $i\text{-}C_4$ | $n\text{-}C_4$ | $i\text{-}C_5$ | $n\text{-}C_5$ | $n\text{-}C_6$ | $C_7\text{-}C_{15}$ | $C_{16}\text{-}C_{25}$ | $C_{26}\text{-}C_{35}$ | $C_{36}\text{-}C_{45}$ | $C_{46}\text{-}C_{55}$ | $C_{56}\text{-}C_{80}$ |
| **Activation Energy (kcal/mol)** | | | | | | | | | | | | | | |
| 47 | 0.08 | 0.10 | 0.12 | 0.09 | 0.14 | 0.18 | 0.13 | 0.15 | 0.15 | 0.15 | 0.14 | 0.13 | 0.12 | 0.11 |
| 48 | 0.00 | 0.00 | 0.00 | 0.00 | 0.00 | 0.00 | 0.00 | 0.00 | 0.00 | 0.00 | 0.00 | 0.00 | 0.00 | 0.00 |
| 49 | 0.08 | 0.11 | 0.13 | 0.09 | 0.15 | 0.19 | 0.14 | 0.16 | 0.17 | 0.16 | 0.15 | 0.14 | 0.13 | 0.11 |
| 50 | 0.10 | 0.13 | 0.16 | 0.11 | 0.19 | 0.23 | 0.17 | 0.19 | 0.20 | 0.19 | 0.18 | 0.17 | 0.15 | 0.14 |
| 51 | 0.11 | 0.14 | 0.17 | 0.13 | 0.21 | 0.26 | 0.18 | 0.22 | 0.22 | 0.21 | 0.20 | 0.19 | 0.17 | 0.15 |
| 52 | 0.24 | 0.32 | 0.39 | 0.28 | 0.46 | 0.58 | 0.41 | 0.48 | 0.50 | 0.47 | 0.44 | 0.41 | 0.38 | 0.34 |
| 53 | 0.24 | 0.31 | 0.38 | 0.28 | 0.45 | 0.56 | 0.40 | 0.47 | 0.48 | 0.46 | 0.43 | 0.40 | 0.37 | 0.33 |
| 54 | 0.23 | 0.30 | 0.36 | 0.26 | 0.42 | 0.53 | 0.38 | 0.44 | 0.46 | 0.44 | 0.41 | 0.38 | 0.35 | 0.32 |
| 55 | 0.00 | 0.00 | 0.00 | 0.00 | 0.00 | 0.00 | 0.00 | 0.00 | 0.00 | 0.00 | 0.00 | 0.00 | 0.00 | 0.00 |
| 56 | 6.44 | 8.38 | 10.16 | 7.46 | 12.07 | 15.18 | 10.77 | 12.62 | 13.09 | 12.40 | 11.62 | 10.83 | 10.04 | 8.96 |
| 57 | 11.37 | 16.02 | 17.56 | 15.59 | 18.43 | 20.23 | 19.11 | 21.43 | 20.72 | 22.34 | 24.07 | 25.76 | 27.41 | 29.52 |
| 58 | 11.50 | 16.36 | 16.42 | 16.35 | 16.91 | 17.96 | 19.94 | 19.56 | 18.78 | 20.55 | 22.50 | 24.49 | 26.49 | 29.17 |
| 59 | 13.03 | 15.42 | 15.12 | 16.28 | 15.97 | 16.32 | 19.33 | 18.09 | 15.05 | 14.11 | 13.09 | 12.08 | 11.10 | 9.70 |
| 60 | 7.40 | 8.76 | 8.59 | 9.24 | 9.07 | 9.27 | 10.98 | 10.27 | 8.54 | 8.01 | 7.43 | 6.86 | 6.30 | 5.51 |
| 61 | 5.43 | 6.43 | 6.31 | 6.79 | 6.66 | 6.81 | 8.06 | 7.54 | 6.27 | 5.88 | 5.46 | 5.04 | 4.63 | 4.04 |
| 62 | 11.40 | 6.48 | 5.56 | 6.43 | 4.00 | 1.86 | 1.36 | 0.88 | 2.95 | 2.74 | 2.51 | 2.29 | 2.06 | 1.83 |
| 63 | 11.47 | 6.52 | 5.60 | 6.47 | 4.02 | 1.87 | 1.37 | 0.89 | 2.97 | 2.76 | 2.53 | 2.31 | 2.07 | 1.84 |
| 64 | 4.82 | 2.74 | 2.35 | 2.72 | 1.69 | 0.79 | 0.57 | 0.37 | 1.25 | 1.16 | 1.06 | 0.97 | 0.87 | 0.77 |
| 65 | 5.10 | 2.90 | 2.49 | 2.88 | 1.79 | 0.83 | 0.61 | 0.39 | 1.32 | 1.23 | 1.13 | 1.03 | 0.92 | 0.82 |
| 66 | 4.48 | 2.55 | 2.19 | 2.53 | 1.57 | 0.73 | 0.53 | 0.35 | 1.16 | 1.08 | 0.99 | 0.90 | 0.81 | 0.72 |
| 67 | 1.04 | 0.59 | 0.51 | 0.58 | 0.36 | 0.17 | 0.12 | 0.08 | 0.27 | 0.25 | 0.23 | 0.21 | 0.19 | 0.17 |
| 68 | 6.29 | 3.58 | 3.07 | 3.55 | 2.21 | 1.03 | 0.75 | 0.49 | 1.63 | 1.51 | 1.39 | 1.26 | 1.14 | 1.01 |
| 69 | 0.00 | 0.00 | 0.00 | 0.00 | 0.00 | 0.00 | 0.00 | 0.00 | 0.00 | 0.00 | 0.00 | 0.00 | 0.00 | 0.00 |
| 70 | 0.00 | 0.00 | 0.00 | 0.00 | 0.00 | 0.00 | 0.00 | 0.00 | 0.00 | 0.00 | 0.00 | 0.00 | 0.00 | 0.00 |
| 71 | 7.80 | 4.43 | 3.81 | 4.40 | 2.73 | 1.27 | 0.93 | 0.60 | 2.02 | 1.87 | 1.72 | 1.57 | 1.41 | 1.25 |
| **Potential (%)** | **15.59** | **5.43** | **4.92** | **0.80** | **2.53** | **1.05** | **1.26** | **3.32** | **27.61** | **20.50** | **9.93** | **4.30** | **1.75** | **1.01** |

**Appendix 27. (Continued) 14 component kinetic data for samples from the Gippsland Basin**

| Sample ID/Biozone | | | | | | | *F. longus*: 20110034 | | | | | | | |
| Component | $n\text{-}C_1$ | $n\text{-}C_2$ | $n\text{-}C_3$ | $i\text{-}C_4$ | $n\text{-}C_4$ | $i\text{-}C_5$ | $n\text{-}C_5$ | $n\text{-}C_6$ | $C_7\text{-}C_{15}$ | $C_{16}\text{-}C_{25}$ | $C_{26}\text{-}C_{35}$ | $C_{36}\text{-}C_{45}$ | $C_{46}\text{-}C_{55}$ | $C_{56}\text{-}C_{80}$ |
|---|---|---|---|---|---|---|---|---|---|---|---|---|---|---|
| **Activation Energy (kcal/mol)** | | | | | | | | | | | | | | |
| 44 | 0.02 | 0.02 | 0.03 | 0.03 | 0.03 | 0.05 | 0.02 | 0.03 | 0.03 | 0.03 | 0.03 | 0.03 | 0.03 | 0.03 |
| 45 | 0.03 | 0.03 | 0.04 | 0.04 | 0.04 | 0.06 | 0.02 | 0.04 | 0.04 | 0.04 | 0.04 | 0.04 | 0.04 | 0.03 |
| 46 | 0.08 | 0.08 | 0.10 | 0.10 | 0.11 | 0.17 | 0.07 | 0.10 | 0.12 | 0.12 | 0.11 | 0.11 | 0.10 | 0.09 |
| 47 | 0.12 | 0.12 | 0.14 | 0.14 | 0.16 | 0.24 | 0.10 | 0.15 | 0.17 | 0.17 | 0.16 | 0.16 | 0.15 | 0.14 |
| 48 | 0.20 | 0.19 | 0.23 | 0.23 | 0.26 | 0.39 | 0.16 | 0.24 | 0.28 | 0.27 | 0.26 | 0.25 | 0.24 | 0.22 |
| 49 | 0.27 | 0.25 | 0.31 | 0.32 | 0.35 | 0.53 | 0.21 | 0.33 | 0.38 | 0.37 | 0.36 | 0.34 | 0.32 | 0.30 |
| 50 | 0.00 | 0.00 | 0.00 | 0.00 | 0.00 | 0.00 | 0.00 | 0.00 | 0.00 | 0.00 | 0.00 | 0.00 | 0.00 | 0.00 |
| 51 | 1.79 | 1.71 | 2.09 | 2.12 | 2.38 | 3.56 | 1.43 | 2.19 | 2.53 | 2.48 | 2.39 | 2.29 | 2.18 | 2.02 |
| 52 | 1.25 | 1.20 | 1.47 | 1.49 | 1.67 | 2.50 | 1.01 | 1.54 | 1.78 | 1.74 | 1.68 | 1.61 | 1.53 | 1.42 |
| 53 | 15.96 | 17.16 | 18.18 | 19.55 | 18.53 | 22.53 | 16.12 | 17.83 | 21.05 | 22.70 | 24.37 | 25.93 | 27.37 | 29.11 |
| 54 | 26.56 | 28.95 | 29.24 | 30.17 | 28.13 | 30.30 | 28.11 | 29.40 | 31.86 | 33.41 | 34.79 | 35.91 | 36.75 | 37.58 |
| 55 | 18.32 | 19.97 | 19.34 | 18.85 | 18.75 | 17.15 | 20.12 | 19.78 | 19.81 | 20.62 | 21.31 | 21.82 | 22.16 | 22.42 |
| 56 | 14.11 | 12.08 | 11.50 | 10.75 | 11.80 | 8.98 | 13.01 | 11.31 | 8.75 | 7.19 | 5.77 | 4.59 | 3.64 | 2.65 |
| 57 | 2.82 | 2.41 | 2.29 | 2.14 | 2.35 | 1.79 | 2.60 | 2.26 | 1.75 | 1.44 | 1.15 | 0.92 | 0.73 | 0.53 |
| 58 | 10.15 | 8.69 | 8.27 | 7.73 | 8.48 | 6.46 | 9.35 | 8.13 | 6.29 | 5.17 | 4.15 | 3.30 | 2.62 | 1.90 |
| 59 | 0.00 | 0.00 | 0.00 | 0.00 | 0.00 | 0.00 | 0.00 | 0.00 | 0.00 | 0.00 | 0.00 | 0.00 | 0.00 | 0.00 |
| 60 | 2.09 | 1.79 | 1.70 | 1.59 | 1.75 | 1.33 | 1.93 | 1.68 | 1.30 | 1.07 | 0.86 | 0.68 | 0.54 | 0.39 |
| 61 | 1.40 | 1.20 | 1.14 | 1.07 | 1.17 | 0.89 | 1.29 | 1.12 | 0.87 | 0.71 | 0.57 | 0.46 | 0.36 | 0.26 |
| 62 | 0.49 | 0.42 | 0.40 | 0.37 | 0.41 | 0.31 | 0.45 | 0.39 | 0.30 | 0.25 | 0.20 | 0.16 | 0.13 | 0.09 |
| 63 | 1.64 | 1.40 | 1.33 | 1.25 | 1.37 | 1.04 | 1.51 | 1.31 | 1.01 | 0.83 | 0.67 | 0.53 | 0.42 | 0.31 |
| 64 | 0.00 | 0.00 | 0.00 | 0.00 | 0.00 | 0.00 | 0.00 | 0.00 | 0.00 | 0.00 | 0.00 | 0.00 | 0.00 | 0.00 |
| 65 | 0.49 | 0.42 | 0.40 | 0.37 | 0.41 | 0.31 | 0.45 | 0.39 | 0.30 | 0.25 | 0.20 | 0.16 | 0.13 | 0.09 |
| 66 | 2.23 | 1.91 | 1.81 | 1.69 | 1.86 | 1.42 | 2.05 | 1.78 | 1.38 | 1.13 | 0.91 | 0.72 | 0.57 | 0.42 |
| **Potential (%)** | **7.04** | **3.35** | **3.65** | **0.65** | **2.15** | **0.99** | **1.32** | **4.05** | **30.50** | **23.99** | **12.42** | **5.76** | **2.52** | **1.60** |

**Appendix 27. (Continued) 14 component kinetic data for samples from the Gippsland Basin**

| Sample ID/Biozone | | | | | | | | | | | | | | |
|---|---|---|---|---|---|---|---|---|---|---|---|---|---|
| | | | | | | | *F. longus*: 20110149 | | | | | | |
| Component | $n$-$C_1$ | $n$-$C_2$ | $n$-$C_3$ | $i$-$C_4$ | $n$-$C_4$ | $i$-$C_5$ | $n$-$C_5$ | $n$-$C_6$ | $C_7$-$C_{15}$ | $C_{16}$-$C_{25}$ | $C_{26}$-$C_{35}$ | $C_{36}$-$C_{45}$ | $C_{46}$-$C_{55}$ | $C_{56}$-$C_{80}$ |

Activation Energy (kcal/mol)

| Component | $n$-$C_1$ | $n$-$C_2$ | $n$-$C_3$ | $i$-$C_4$ | $n$-$C_4$ | $i$-$C_5$ | $n$-$C_5$ | $n$-$C_6$ | $C_7$-$C_{15}$ | $C_{16}$-$C_{25}$ | $C_{26}$-$C_{35}$ | $C_{36}$-$C_{45}$ | $C_{46}$-$C_{55}$ | $C_{56}$-$C_{80}$ |
|---|---|---|---|---|---|---|---|---|---|---|---|---|---|---|
| 46 | 0.04 | 0.05 | 0.06 | 0.05 | 0.08 | 0.11 | 0.05 | 0.07 | 0.08 | 0.09 | 0.10 | 0.11 | 0.12 | 0.14 |
| 47 | 0.00 | 0.00 | 0.00 | 0.00 | 0.00 | 0.00 | 0.00 | 0.00 | 0.00 | 0.00 | 0.00 | 0.00 | 0.00 | 0.00 |
| 48 | 0.09 | 0.11 | 0.13 | 0.10 | 0.17 | 0.24 | 0.11 | 0.16 | 0.17 | 0.19 | 0.21 | 0.23 | 0.26 | 0.29 |
| 49 | 0.06 | 0.07 | 0.09 | 0.06 | 0.11 | 0.16 | 0.07 | 0.10 | 0.11 | 0.12 | 0.13 | 0.15 | 0.17 | 0.19 |
| 50 | 0.20 | 0.24 | 0.30 | 0.22 | 0.37 | 0.54 | 0.25 | 0.35 | 0.37 | 0.41 | 0.46 | 0.52 | 0.57 | 0.66 |
| 51 | 0.21 | 0.25 | 0.32 | 0.23 | 0.39 | 0.57 | 0.26 | 0.37 | 0.39 | 0.44 | 0.49 | 0.55 | 0.60 | 0.69 |
| 52 | 0.44 | 0.53 | 0.66 | 0.48 | 0.82 | 1.20 | 0.55 | 0.77 | 0.82 | 0.92 | 1.03 | 1.14 | 1.27 | 1.45 |
| 53 | 1.10 | 1.32 | 1.67 | 1.21 | 2.06 | 3.02 | 1.39 | 1.93 | 2.06 | 2.30 | 2.58 | 2.88 | 3.19 | 3.64 |
| 54 | 3.22 | 3.89 | 4.89 | 3.56 | 6.06 | 8.87 | 4.09 | 5.68 | 6.05 | 6.76 | 7.58 | 8.45 | 9.37 | 10.69 |
| 55 | 10.27 | 13.42 | 14.83 | 14.86 | 14.16 | 21.01 | 14.36 | 16.09 | 18.62 | 19.07 | 19.47 | 19.77 | 19.97 | 20.05 |
| 56 | 13.25 | 18.09 | 18.19 | 19.28 | 17.94 | 20.94 | 19.68 | 18.75 | 22.26 | 23.71 | 25.24 | 26.73 | 28.16 | 30.01 |
| 57 | 13.57 | 17.04 | 17.07 | 17.51 | 17.47 | 15.92 | 19.99 | 20.28 | 19.23 | 18.17 | 17.00 | 15.83 | 14.67 | 13.07 |
| 58 | 7.97 | 10.02 | 10.03 | 10.29 | 10.27 | 9.36 | 11.75 | 11.92 | 11.30 | 10.68 | 9.99 | 9.30 | 8.62 | 7.68 |
| 59 | 11.64 | 8.04 | 7.25 | 7.35 | 6.84 | 3.88 | 6.19 | 5.23 | 4.00 | 3.66 | 3.31 | 2.97 | 2.65 | 2.26 |
| 60 | 9.01 | 6.23 | 5.62 | 5.69 | 5.30 | 3.01 | 4.79 | 4.05 | 3.10 | 2.83 | 2.56 | 2.30 | 2.05 | 1.75 |
| 61 | 6.68 | 4.62 | 4.17 | 4.22 | 3.93 | 2.23 | 3.55 | 3.00 | 2.30 | 2.10 | 1.90 | 1.71 | 1.52 | 1.30 |
| 62 | 5.06 | 3.50 | 3.16 | 3.20 | 2.98 | 1.69 | 2.69 | 2.28 | 1.74 | 1.59 | 1.44 | 1.29 | 1.15 | 0.98 |
| 63 | 3.74 | 2.59 | 2.33 | 2.36 | 2.20 | 1.25 | 1.99 | 1.68 | 1.29 | 1.18 | 1.06 | 0.96 | 0.85 | 0.73 |
| 64 | 2.97 | 2.05 | 1.85 | 1.87 | 1.74 | 0.99 | 1.58 | 1.33 | 1.02 | 0.93 | 0.84 | 0.76 | 0.67 | 0.58 |
| 65 | 3.47 | 2.40 | 2.16 | 2.19 | 2.04 | 1.16 | 1.84 | 1.56 | 1.19 | 1.09 | 0.99 | 0.89 | 0.79 | 0.67 |
| 66 | 0.50 | 0.35 | 0.31 | 0.32 | 0.30 | 0.17 | 0.27 | 0.23 | 0.17 | 0.16 | 0.14 | 0.13 | 0.11 | 0.10 |
| 67 | 4.27 | 2.95 | 2.66 | 2.69 | 2.51 | 1.42 | 2.27 | 1.92 | 1.47 | 1.34 | 1.21 | 1.09 | 0.97 | 0.83 |
| 68 | 0.00 | 0.00 | 0.00 | 0.00 | 0.00 | 0.00 | 0.00 | 0.00 | 0.00 | 0.00 | 0.00 | 0.00 | 0.00 | 0.00 |
| 69 | 0.00 | 0.00 | 0.00 | 0.00 | 0.00 | 0.00 | 0.00 | 0.00 | 0.00 | 0.00 | 0.00 | 0.00 | 0.00 | 0.00 |
| 70 | 5.16 | 3.56 | 3.21 | 3.26 | 3.03 | 1.72 | 2.74 | 2.32 | 1.77 | 1.62 | 1.47 | 1.32 | 1.17 | 1.00 |
| **Potential (%)** | **11.82** | **4.54** | **4.29** | **0.68** | **2.32** | **1.28** | **1.35** | **3.47** | **26.13** | **21.79** | **11.95** | **5.85** | **2.69** | **1.83** |

**Appendix 27. (Continued) 14 component kinetic data for samples from the Gippsland Basin**

| Sample ID/Biozone | | | | | | | | | | | | | | |
|---|---|---|---|---|---|---|---|---|---|---|---|---|---|
| Component | $n\text{-}C_1$ | $n\text{-}C_2$ | $n\text{-}C_3$ | $i\text{-}C_4$ | $n\text{-}C_4$ | $i\text{-}C_5$ | $n\text{-}C_5$ | $n\text{-}C_6$ | $C_7\text{-}C_{15}$ | $C_{16}\text{-}C_{25}$ | $C_{26}\text{-}C_{35}$ | $C_{36}\text{-}C_{45}$ | $C_{46}\text{-}C_{55}$ | $C_{56}\text{-}C_{80}$ |

*P. mawsonii*: 20110275

**Activation Energy (kcal/mol)**

| Component | $n\text{-}C_1$ | $n\text{-}C_2$ | $n\text{-}C_3$ | $i\text{-}C_4$ | $n\text{-}C_4$ | $i\text{-}C_5$ | $n\text{-}C_5$ | $n\text{-}C_6$ | $C_7\text{-}C_{15}$ | $C_{16}\text{-}C_{25}$ | $C_{26}\text{-}C_{35}$ | $C_{36}\text{-}C_{45}$ | $C_{46}\text{-}C_{55}$ | $C_{56}\text{-}C_{80}$ |
|---|---|---|---|---|---|---|---|---|---|---|---|---|---|---|
| 41 | 0.08 | 0.08 | 0.08 | 0.05 | 0.11 | 0.13 | 0.08 | 0.10 | 0.09 | 0.09 | 0.09 | 0.09 | 0.08 | 0.08 |
| 42 | 0.09 | 0.09 | 0.09 | 0.05 | 0.12 | 0.15 | 0.09 | 0.12 | 0.11 | 0.10 | 0.10 | 0.09 | 0.09 | 0.08 |
| 43 | 0.19 | 0.18 | 0.19 | 0.11 | 0.25 | 0.31 | 0.19 | 0.24 | 0.22 | 0.22 | 0.21 | 0.20 | 0.19 | 0.18 |
| 44 | 0.18 | 0.17 | 0.18 | 0.11 | 0.24 | 0.30 | 0.18 | 0.23 | 0.21 | 0.20 | 0.20 | 0.19 | 0.18 | 0.17 |
| 45 | 0.32 | 0.31 | 0.32 | 0.20 | 0.43 | 0.54 | 0.33 | 0.41 | 0.38 | 0.37 | 0.36 | 0.34 | 0.33 | 0.30 |
| 46 | 0.43 | 0.41 | 0.42 | 0.26 | 0.57 | 0.72 | 0.44 | 0.55 | 0.51 | 0.49 | 0.47 | 0.46 | 0.44 | 0.41 |
| 47 | 0.59 | 0.56 | 0.58 | 0.35 | 0.77 | 0.97 | 0.60 | 0.75 | 0.69 | 0.67 | 0.64 | 0.62 | 0.59 | 0.55 |
| 48 | 0.93 | 0.89 | 0.91 | 0.56 | 1.23 | 1.54 | 0.95 | 1.19 | 1.09 | 1.05 | 1.02 | 0.98 | 0.93 | 0.87 |
| 49 | 1.44 | 1.38 | 1.42 | 0.87 | 1.91 | 2.40 | 1.47 | 1.84 | 1.69 | 1.64 | 1.58 | 1.52 | 1.45 | 1.35 |
| 50 | 2.79 | 2.66 | 2.73 | 1.68 | 3.68 | 4.63 | 2.84 | 3.56 | 3.26 | 3.16 | 3.05 | 2.93 | 2.80 | 2.61 |
| 51 | 19.70 | 20.23 | 21.08 | 17.18 | 23.88 | 22.78 | 20.53 | 22.61 | 23.96 | 25.17 | 26.41 | 27.57 | 28.66 | 30.04 |
| 52 | 29.23 | 30.65 | 30.60 | 32.43 | 28.70 | 28.10 | 30.30 | 29.78 | 30.40 | 32.40 | 34.51 | 36.57 | 38.60 | 41.31 |
| 53 | 22.56 | 21.73 | 21.22 | 23.66 | 19.54 | 19.17 | 21.53 | 19.79 | 19.17 | 17.64 | 16.07 | 14.58 | 13.15 | 11.30 |
| 54 | 9.10 | 8.76 | 8.56 | 9.54 | 7.88 | 7.73 | 8.68 | 7.98 | 7.73 | 7.12 | 6.48 | 5.88 | 5.30 | 4.56 |
| 55 | 4.50 | 4.33 | 4.23 | 4.72 | 3.90 | 3.82 | 4.29 | 3.95 | 3.82 | 3.52 | 3.21 | 2.91 | 2.62 | 2.25 |
| 56 | 1.88 | 1.81 | 1.76 | 1.97 | 1.62 | 1.59 | 1.79 | 1.65 | 1.59 | 1.47 | 1.34 | 1.21 | 1.09 | 0.94 |
| 57 | 1.57 | 1.51 | 1.48 | 1.65 | 1.36 | 1.34 | 1.50 | 1.38 | 1.34 | 1.23 | 1.12 | 1.02 | 0.92 | 0.79 |
| 58 | 0.61 | 0.59 | 0.57 | 0.64 | 0.53 | 0.52 | 0.58 | 0.53 | 0.52 | 0.48 | 0.43 | 0.39 | 0.35 | 0.30 |
| 59 | 1.24 | 1.20 | 1.17 | 1.30 | 1.08 | 1.06 | 1.19 | 1.09 | 1.06 | 0.97 | 0.88 | 0.80 | 0.72 | 0.62 |
| 60 | 0.00 | 0.00 | 0.00 | 0.00 | 0.00 | 0.00 | 0.00 | 0.00 | 0.00 | 0.00 | 0.00 | 0.00 | 0.00 | 0.00 |
| 61 | 0.94 | 0.90 | 0.88 | 0.98 | 0.81 | 0.80 | 0.89 | 0.82 | 0.80 | 0.73 | 0.67 | 0.61 | 0.55 | 0.47 |
| 62 | 0.68 | 0.66 | 0.64 | 0.72 | 0.59 | 0.58 | 0.65 | 0.60 | 0.58 | 0.54 | 0.49 | 0.44 | 0.40 | 0.34 |
| 63 | 0.00 | 0.00 | 0.00 | 0.00 | 0.00 | 0.00 | 0.00 | 0.00 | 0.00 | 0.00 | 0.00 | 0.00 | 0.00 | 0.00 |
| 64 | 0.00 | 0.00 | 0.00 | 0.00 | 0.00 | 0.00 | 0.00 | 0.00 | 0.00 | 0.00 | 0.00 | 0.00 | 0.00 | 0.00 |
| 65 | 0.94 | 0.90 | 0.88 | 0.98 | 0.81 | 0.80 | 0.89 | 0.82 | 0.80 | 0.73 | 0.67 | 0.61 | 0.55 | 0.47 |
| **Potential (%)** | **5.77** | **2.76** | **3.24** | **0.55** | **2.17** | **0.81** | **1.28** | **4.04** | **24.14** | **23.31** | **14.93** | **8.54** | **4.59** | **3.86** |

**Appendix 28. Predicted GOR, $B_o$, $P_{sat}$ and ($C_1/C_2$-$C_5$) from the PVT simulation of samples from the Vulcan Sub-basin**

| End. Temperature (°C) | TR (%) | GOR (Sm³/Sm³) | $B_o$ (m³/Sm³) | $P_{sat}$ (bar) | $C_1/C_2$-$C_5$ |
|---|---|---|---|---|---|
| **Formation: Upper Vulcan** | | | | | |
| **Sample ID: 20110067** | | | | | |
| 357 | 10 | 87.90 | 1.34 | 128.33 | 1.34 |
| 389 | 30 | 188.10 | 1.74 | 147.84 | 1.63 |
| 406 | 50 | 238.00 | 1.90 | 175.47 | 1.77 |
| 420 | 70 | 291.80 | 2.13 | 177.67 | 1.93 |
| 442 | 90 | 451.30 | 2.71 | 215.18 | 2.39 |
| **Formation: Lower Vulcan** | | | | | |
| **Sample ID: 20110044C** | | | | | |
| 382 | 10 | 141.60 | 1.47 | 205.04 | 1.49 |
| 405 | 30 | 139.50 | 1.44 | 222.12 | 1.48 |
| 421 | 50 | 165.40 | 1.53 | 235.97 | 1.56 |
| 440 | 70 | 266.50 | 1.93 | 216.34 | 1.85 |
| 484 | 90 | 629.80 | | 580.45 | 2.91 |
| **Formation: Plover (shale)** | | | | | |
| **Sample ID: 20110076** | | | | | |
| 373 | 10 | 113.60 | 1.41 | 150.47 | 1.41 |
| 396 | 30 | 133.70 | 1.47 | 166.60 | 1.47 |
| 412 | 50 | 155.40 | 1.54 | 181.00 | 1.53 |
| 430 | 70 | 202.80 | 1.70 | 197.86 | 1.67 |
| 471 | 90 | 595.80 | 2.97 | 303.99 | 2.81 |
| **Formation: Plover (coal)** | | | | | |
| **Sample ID: 20110076C** | | | | | |
| 368 | 10 | 95.10 | 1.36 | 124.45 | 1.36 |
| 393 | 30 | 99.20 | 1.35 | 149.60 | 1.37 |
| 410 | 50 | 133.30 | 1.47 | 164.48 | 1.47 |
| 432 | 70 | 160.70 | 1.53 | 208.74 | 1.55 |
| 479 | 90 | 455.10 | 2.39 | 348.32 | 2.40 |

**TR:** Transformation ratio

**GOR:** Gas:oil ratio

**$B_o$:** Formation volume factor

**$P_{sat}$:** Saturation pressure

**$C_1/C_2$-$C_5$:** Gas wetness

**Appendix 29. Predicted GOR, B$_o$, P$_{sat}$ and (C$_1$/C$_2$-C$_5$) from the PVT simulation of samples from the Laminaria High**

| End. Temperature (°C) | TR (%) | GOR (Sm$^3$/Sm$^3$) | B$_o$ (m$^3$/Sm$^3$) | P$_{sat}$ (bar) | C$_1$/C$_2$-C$_5$ |
|---|---|---|---|---|---|
| **Formation: Echuca Shoals** | | | | | |
| **Sample ID: 20110013** | | | | | |
| 379 | 10 | 769.20 | 4.10 | 223.00 | 3.31 |
| 401 | 30 | 341.90 | 2.37 | 173.75 | 2.07 |
| 414 | 50 | 460.00 | 2.79 | 205.34 | 2.41 |
| 427 | 70 | 565.10 | 3.15 | 228.39 | 2.72 |
| 450 | 90 | 1201.40 | | 309.99 | 4.56 |
| **Formation: Frigate** | | | | | |
| **Sample ID: 20110021** | | | | | |
| 321 | 10 | 92.10 | 1.39 | 108.56 | 1.35 |
| 370 | 30 | 65.70 | 1.29 | 90.17 | 1.27 |
| 396 | 50 | 94.40 | 1.38 | 114.26 | 1.35 |
| 415 | 70 | 176.30 | 1.73 | 129.97 | 1.59 |
| 441 | 90 | 289.90 | 2.17 | 163.67 | 1.92 |
| **Formation: Laminaria** | | | | | |
| **Sample ID: 20110008** | | | | | |
| 331 | 10 | 137.80 | 1.50 | 174.02 | 1.48 |
| 380 | 30 | 94.60 | 1.36 | 129.64 | 1.35 |
| 402 | 50 | 176.00 | 1.69 | 147.45 | 1.59 |
| 420 | 70 | 204.70 | 1.75 | 177.51 | 1.67 |
| 448 | 90 | 311.00 | 2.04 | 262.69 | 1.98 |

**TR:** Transformation ratio

**GOR:** Gas:oil ratio

**B$_o$:** Formation volume factor

**P$_{sat}$:** Saturation pressure

**C$_1$/C$_2$-C$_5$:** Gas wetness

**Appendix 30. Predicted GOR, B₀, P_sat and (C₁/C₂-C₅) from the PVT simulation of samples from the Gippsland Basin**

| End. Temperature (°C) | TR (%) | GOR (Sm³/Sm³) | $B_o$ (m³/Sm³) | $P_{sat}$ (bar) | $C_1/C_2$-$C_5$ |
|---|---|---|---|---|---|
| **Biozone:** *L. balmei* | | | | | |
| **Sample ID: 20110126** | | | | | |
| | 10 | 213.40 | 1.75 | 197.00 | 1.70 |
| | 30 | 214.30 | 1.73 | 213.20 | 1.70 |
| | 50 | 234.30 | 1.78 | 226.90 | 1.76 |
| | 70 | 359.70 | 2.22 | 254.20 | 2.12 |
| | 90 | 1443.20 | | 410.00 | 5.27 |
| **Biozone:** *F. longus* | | | | | |
| **Sample ID: 20110034** | | | | | |
| | 10 | 118.60 | 1.44 | 145.40 | 1.42 |
| | 30 | 117.70 | 1.42 | 154.80 | 1.42 |
| | 50 | 132.50 | 1.47 | 163.40 | 1.46 |
| | 70 | 146.90 | 1.51 | 172.90 | 1.51 |
| | 90 | 291.00 | 2.02 | 218.00 | 1.92 |
| **Biozone:** *F. longus* | | | | | |
| **Sample ID: 20110149** | | | | | |
| | 10 | 144.70 | 1.49 | 194.50 | 1.50 |
| | 30 | 165.00 | 1.56 | 195.80 | 1.56 |
| | 50 | 171.60 | 1.57 | 209.90 | 1.58 |
| | 70 | 222.22 | 1.75 | 218.00 | 1.72 |
| | 90 | 826.70 | | 457.50 | 3.48 |
| **Biozone:** *P. mawsonii* | | | | | |
| **Sample ID: 20110275** | | | | | |
| | 10 | 120.20 | 1.42 | 168.40 | 1.43 |
| | 30 | 107.90 | 1.37 | 174.30 | 1.39 |
| | 50 | 112.50 | 1.37 | 189.30 | 1.41 |
| | 70 | 123.90 | 1.41 | 196.50 | 1.44 |
| | 90 | 175.00 | 1.59 | 205.10 | 1.59 |

**TR:** Transformation ratio

**GOR:** Gas:oil ratio

**B₀:** Formation volume factor

**P_sat:** Saturation pressure

**C₁/C₂-C₅:** Gas wetness